# 2009
# Office of Fossil Energy
# Fuel Cell Program Annual Report

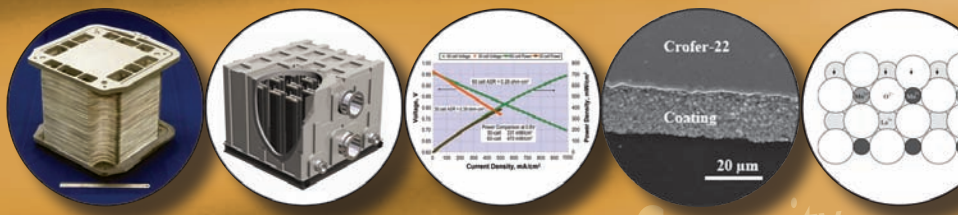


Increase Energy Security
Eliminate Carbon Footprint
Enhance Water Conservation

SECA
Solid State Energy Conversion Alliance

U.S. DEPARTMENT OF ENERGY

NETL

DOE/NETL-2009/1379

# 2009
# OFFICE OF FOSSIL ENERGY
# FUEL CELL PROGRAM ANNUAL REPORT

November 2009

# Table of Contents

# I. INTRODUCTION

# I. Introduction

## Competitive Innovation: Accelerating Technology Development

The U.S. Department of Energy (DOE) Office of Fossil Energy, through the National Energy Technology Laboratory (NETL) and in collaboration with private industry, educational institutions and national laboratories, has forged Government-industry partnerships under the Solid State Energy Conversion Alliance (SECA) to reduce the cost of solid oxide fuel cells (SOFCs) and to develop integrated gasification fuel cell (IGFC) systems utilizing coal for clean and efficient central power generation. These goals equate to removing environmental, climate change, and water concerns associated with fossil fuel use while simultaneously establishing a foundation for a secure energy future in the United States. With the successful completion of the first phase of the SECA Cost Reduction program element in 2006, SECA moved one step closer to realizing its vision of cost-effective, near-zero-emission fuel cell technology for commercial applications. SECA moved another step closer in 2009, with two of the Industry Teams successfully completing the first phase of Coal-Based Systems testing - metric tests for 10 kilowatt (kW) stacks in accordance with the SECA minimum requirements of greater than 5,000 hours of operation and degradation of less than 4.0 percent per 1,000 hours (<4%/1,000 h). The other two Industry Teams will test their coal-based systems in 2010.

Successful phase testing reflects the excellent progress being made toward the SECA goals. A coal-based SOFC power generation system that meets the goals will achieve environmental regulations compliance with effectively no carbon footprint, near-zero water requirements, and the lowest available cost of electricity. This technology makes substantial strides in realizing clean, economic energy production from coal in any state in the United States.

The Administration's Office of Management and Budget previously cited the SECA program as leading the way in Government-industry partnerships.

*"The SECA program leverages private-sector ingenuity by providing Government funding to Industry Teams developing fuel cells, as long as the Teams continue to exceed a series of stringent technical performance hurdles. This novel incentive structure has generated a high level of competition between the Teams and an impressive array of technical approaches. The SECA program also develops certain core technologies that can be used by all the Industry Teams to avoid duplication of effort. The program exceeded its 2005 performance targets, and it is on track to meet its goal for an economically competitive technology by 2010."*

The SECA Fuel Cell Program is a critical element of the DOE's Office of Fossil Energy technology portfolio. From an energy security perspective, coal is a primary resource for reducing dependence on imported oil and natural gas. More than half of the nation's electricity supply is generated from coal - developing technology to ensure its environmentally clean and climate friendly use is of crucial national importance. SECA technology offers greater than 99 percent carbon capture, less than 0.5 ppm NOx emission, reduced water requirements, and a coal-to-electricity efficiency exceeding 50 percent on a higher heating value (HHV) basis. The SECA cost goal of $700/kW (2007 U.S. dollar basis) pursued under the SECA Cost Reduction program element will ensure that the cost of electricity to the user will not exceed what is typical today. Concurrently, the SECA Coal-Based Systems program element will scale and integrate SECA SOFC technology for use in large IGFC systems. Cross-cutting research and development (R&D) and testing support are provided by SECA's Core Technology program element.

SECA is comprised of three groups: Industry Teams, Core Technology participants, and federal government management. The Industry Teams within the SECA Cost Reduction and Coal-Based Systems program elements design the fuel cells and handle most hardware and market penetration issues. The Core Technology program element, made up of universities, national laboratories, small businesses, and other R&D organizations, addresses applied technological issues common to all Industry Teams. Findings and inventions under the Core Technology program are made available to all Industry Teams under unique intellectual property provisions that serve to accelerate development. The federal government management facilitates interaction between Industry Teams and the Core Technology

program element as well as establishes technical priorities and approaches.

Across the United States, SECA Core Technology participants are working on dozens of fuel cell projects, led by the brightest minds from leading universities, national laboratories and businesses. These competitively-selected projects provide vital R&D and testing in support of the Industry Teams.

In the same spirit of healthy competition, the Industry Teams leverage the collective ingenuity of the Core Technology participants to independently pursue innovations in fuel cell design that can be mass-produced at lower cost. Focusing on Cost Reduction and Coal-Based Systems, the Industry Teams are working to solve the challenges of fuel cell technology, each using different design and manufacturing approaches. As a result, the SECA program is rich in innovation, allowing it to reach its goals much faster.

## Fuel Cell Research and Development

The Office of Fossil Energy and NETL are pleased to present this FY 2009 Office of Fossil Energy Fuel Cell Program Annual Report, a compilation of abstracts from the fuel cell projects managed through these offices. These abstracts are divided into subsections as detailed in the following.

### SECA Industry Teams – Coal-Based Systems

Through its Coal-Based Systems program element, SECA seeks to leverage successes in the Cost Reduction program element; scale SOFC cells and stacks to sizes appropriate for central power generation applications; and integrate the SOFC, associated balance of plant, and coal gasification technology to create an IGFC system. Industry Teams will focus on developing large megawatt (MW)-scale systems while continuing SECA Cost Reduction activities through 2010. It is anticipated that the best technology from any Industry Team will be available for incorporation into one or more of the SECA Coal-Based Systems projects. Key R&D topics include coal contaminants, pressurization, failure analysis, system integration, balance of plant, materials, manufacturing, and controls and instrumentation.

### SECA Industry Teams – Cost Reduction

To achieve cost targets, Industry Teams are refining and validating advanced technology in 3-10 kW SOFC modules that can be mass produced, aggregated, and scaled to meet a broad range of applications. This development activity is blending established manufacturing processes with state-of-the-art fuel cell technology advancements in order to leverage the advantages of economies of production (high-volume

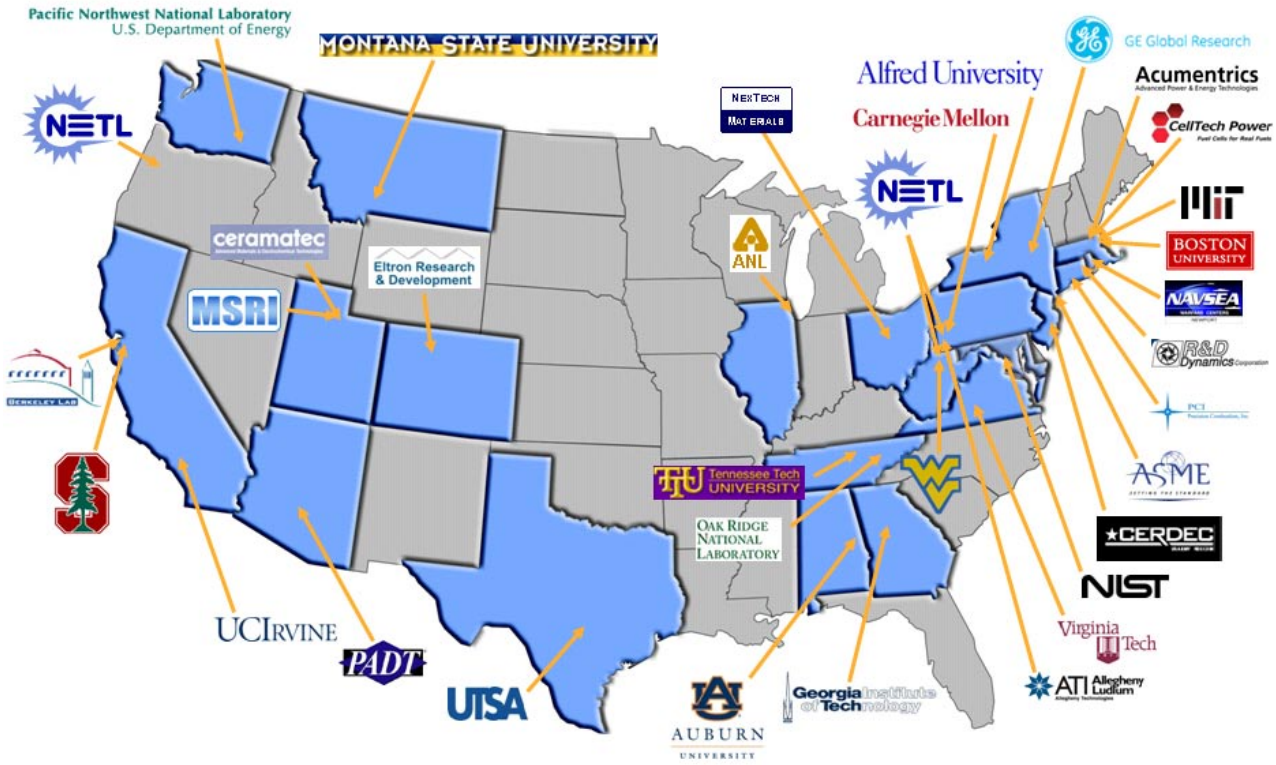


SECA Core Technology and Advanced Research Participants

mass production) and scale to reduce fuel cell costs. Achieving the cost targets requires reaching a full spectrum of large markets, such as auxiliary power units (APUs) for trucks and recreational vehicles, and other markets such as residential-commercial-industrial power, a wide range of distributed generation, and specialized applications for the military. Producing a common module for these vast markets will create the opportunity for the high-volume production required to reduce cost to the necessary level.

### SECA Core Technology

The Core Technology program element provides comprehensive applied research support in nine focus areas. This structure and special intellectual property provisions reduce cost by leveraging resources so that all Industry Teams do not engage in separate applied research programs, paying multiple times for the same research. This approach also ensures that only major issues are addressed. SECA's goal is to raise the technology bar in large strides rather than small steps. Core Technology program element areas of research are also funded by special topics under DOE Science Initiatives, Small Business Innovation Research (SBIR), Small Business Technology Transfer (STTR), Basic Energy Sciences, and Historically Black Colleges and Universities. The Core Technology focus areas include the following:

- **Cathodes** – Improve the stability and performance of fuel cell cathodes, using state-of-the-art concepts and methodologies.
- **Anodes and Coal Contaminants** – Determine potential coal syngas contaminants and their impact on anode performance.
- **Interconnects and Contact Materials** – Develop stable, low-cost metallic interconnects and interconnect contact materials operating in the temperature range of 650 to 850°C with acceptably low area-specific resistance (ASR) and stability over the service lifetime.
- **Seals** – Develop materials and designs exhibiting adequate sealing performance with the requisite chemical and phase stability in long-term service.
- **Cross-Cutting Materials and Manufacturing** – Develop materials and manufacturing technologies that improve fuel cell reliability, performance, and ability to tolerate any fuel or air contaminants, and that achieve cost reductions.
- **Fuel Processing** – Develop fuel processing technologies that will meet application requirements such as zero water consumption, space and volume constraints, and transient capability.
- **Power Electronics** – Optimize efficiency and cost in conversion of fuel cell output to usable DC (direct current) and AC (alternating current) power.
- **Modeling and Simulation** – Create models to determine a reliable operating space and to guide manufacturing.
- **Balance of Plant** – Develop high temperature heat exchangers and blowers to enable high system efficiency and low cost.

### Innovative Concepts

SECA Innovative Concepts will assess the feasibility of a coal power plant based upon a direct coal SOFC and will validate the performance, robustness, cost and scalability of metallic-supported cell designs for use in coal-based SOFC power systems.

### Advanced Research

The SECA Advanced Research program element provides cross-cutting, multidisciplinary research that leads to advanced electrochemical technologies minimizing the environmental consequences of using fossil fuels in energy generation. This program element supports future advances in the SECA and Office of Fossil Energy Coal and Power programs by developing novel electrochemical energy-conversion and integrated technologies that advance the efficiency, reliability, and cost goals of fuel cell systems.

## Key Program Accomplishments

### SECA Industry Teams – Coal-Based Systems

- **Progress Achieved in Next Generation of SOFC Scaled-up Stacks for Coal-Based Systems.** FuelCell Energy, Inc. and its technology partner, Versa Power Systems, Inc., validated the production methods planned for building SOFC stacks that will be incorporated in power plants, expanded the range of stack operating temperature, and passed an independent audit of the anticipated costs to manufacture systems on a commercial scale. In February 2009, two 10 kW stacks passed 5,000 hours of continuous operation while producing rated power, successfully completing metric tests that demonstrated the longevity and robustness of the SOFC stack technology. These tests were implemented using 550 $cm^2$ active area cells based on a manufacturing process that ensures quality and repeatability in high volume manufacturing. Also, the next generation of larger cells with an active area of 961 $cm^2$ were successfully tested. Increasing the active area of

the fuel cell, while maintaining cell performance, contributes to reduced fuel cell stack and system costs due to fewer components and improved manufacturability. Performance of the 10 kW metric stack formed the basis for the design of a 527 MW coal-based SOFC power plant integrated with a gasification island, resulting in a system that reduced greenhouse gas emissions by more than 90 percent, while generating electricity with an efficiency approaching 52 percent of coal HHV. The new stack being developed will serve as the building block for 250 kW to 1 MW fuel cell power modules to be used to power a 5 MW proof-of-concept (POC) power plant system. The module and POC system are to be designed, fabricated and tested in subsequent SECA program phases.

- **Power Density Increased for Solid Oxide Fuel Cells Targeted for Centralized Coal-Based Power Plants.** Rolls-Royce Fuel Cell Systems has demonstrated higher power densities for its integrated planar SOFC reducing the cost of the fuel cell power block modules for an IGFC combined cycle plant that is projected to allow sequestration of 90 percent of carbon dioxide ($CO_2$) and achieve an overall efficiency of greater than 50 percent. Power density at normal system operating conditions has been increased 40 percent primarily through improved performance of the active layers of the cell and through the lower electrical resistance achieved by decreasing the size (area) of individual cells printed onto the ceramic substrates through which the fuel is distributed. These increased power levels have been achieved while substituting the active cell layers with lower cost materials. Operation of fuel cells at higher power densities allows smaller overall fuel cell systems at equivalent power ratings, which cascades into an overall lower cost for the power plant and lower cost of electricity. System modeling studies have resulted in selection of a cycle for operation of the pressurized Rolls-Royce SOFC system as part of an advanced IGFC plant that is predicted to achieve the DOE's plant efficiency target.

## SECA Industry Teams – Cost Reduction

- **SOFCs Successfully Scaled for Large-scale Stationary Applications.** Delphi, in partnership with Battelle Memorial Institute under the SECA Cost Reduction program element, developed cost-effective 3-5 kW SOFC power systems for a range of fuels and applications. The Delphi team was able to demonstrate test cells with power density greater than that required to meet SECA goals. In Fiscal Year 2009, Delphi successfully fabricated cells with 403 $cm^2$ active area for its Generation 4 stack. This represents an increase in the cell active area of 284 percent from the Generation 3.2 cell (105 $cm^2$).

## SECA Core Technology – Cathodes

- **SOFC Cathode Surface Chemistry Characterized with Synchrotron X-Rays.** Researchers at Argonne National Laboratory (ANL), Carnegie Mellon University, Massachusetts Institute of Technology, and Stanford University are gaining unique insight into the chemistry and structure of SOFC cathodes. ANL researchers are using the Advanced Photon Source, one of the world's brightest X-ray sources, to probe the atomic and chemical structure of model cathodes under conditions closely approximating those of operating fuel cells. Recent results of these studies show that in strontium-containing cathodes such as $La_{0.7}Sr_{0.7}MnO_3$, strontium segregates to the surface. For epitaxial films, the degree of surface segregation varies with crystalline orientation, composition, and oxygen activity. In cathode/electrolyte half-cells, electrochemical-loading leads to strontium-rich surface particles, whose coverage can be tuned by control of field strength and temperature. Other near-surface charge compensating mechanisms associated with the B- and O-sites of $ABO_3$ perovskites used in SOFC cathodes are also being explored. When the transition metal B-site contains more than one elemental species, reduction in these mixed-composition perovskites is found to become highly preferential as temperature increases, favoring the minority cobalt species over iron in $La_{0.6}Sr_{0.4}Co_{0.2}Fe_{0.8}O_{3-\delta}$, for instance. When coupled with in situ characterization studies such as these, complementary ultra-high vacuum techniques, known for their spatial and energetic sensitivities, permit direct access to the electronic structure of the cathodes and establish accurate descriptions of the local chemical and structural landscape. The new insight arising from this study is guiding theoreticians and engineers in their understanding of the role of surfaces in fuel cell cathode performance.
- **Low Degradation, High Performance of LSCF-based SOFCs Successfully Demonstrated.** GE Global Research made significant progress in mitigating performance degradation of lanthanum strontium cobalt ferrite (LSCF)-based SOFCs. A high-performance LSCF-based cathode architecture and processing route was demonstrated to have no measurable performance degradation over 1,000 hours at 800°C measured at 0.7 V using a gold cathode current collector. Subsequent test

results using 441HP ferritic stainless steel current collectors with protective spinel coatings, operating at ~1 W/cm$^2$, yielded a 1.9%/1,000 h power density degradation rate that decreased with time and approached an asymptotic value over the 1,500-hour test. The observed resistance increase was purely ohmic, with no loss in catalytic activity. Further, the resistance change could be directly attributed to the resistance associated with the anticipated growth of chromium oxide on the stainless steel current collector. This accomplishment contributes to the overall SECA degradation goal of < 2%/1,000 h and cost goal of < $700/kW for the system power block by 2010.

- **SOFC Cathode Performance Significantly Enhanced by Infiltration of Nanocatalyst.** Lawrence Berkeley National Laboratory (LBNL) has developed a low-cost technique for infiltrating a continuous coating of nanocatalyst into porous SOFC electrodes. The technique involves flooding the pores of the electrode with highly concentrated molten salt precursor material at low temperature (<120°C). Because of the high concentration, a single infiltration step is sufficient to create a well-connected nanocatalyst network, in contrast to traditional infiltration techniques that require many steps to build up sufficient catalyst loading. The LBNL technique has been used to dramatically improve the performance of SOFC cathodes, especially at the lower end of the operating temperature window, 700°C. Traditional anode-supported lanthanum strontium manganite (LSM)-yttria-stabilized zirconia (YSZ) composite cathodes were operated at 700°C with and without infiltration of YDC ($Y_{0.2}Ce_{0.8}O_{2-\delta}$) nanocatalyst. Addition of a single YDC infiltration step increased the performance about 2.5 times, from 210 to 525 mW/cm$^2$. Sintering traditional composite cathodes requires that the catalyst and electrolyte materials be non-reactive at the sintering temperature. This severely constrains the choice of catalyst materials. The LBNL infiltration technique alleviates this restriction and enables the preparation of novel electrode architectures. Catalyst-free porous zirconia electrode backbones were prepared at high temperature, followed by infiltration of the entire catalyst content at low temperature. Competitive performance was achieved for this electrode architecture. Anode-supported cells with YSZ-infiltrated LSM and YSZ-infiltrated lanthanum strontium cobaltite cathodes achieved 490 and 700 mW/cm$^2$, respectively, at 700°C. These improvements in cathode performance and design flexibility are expected to improve current distribution in the presence of thermal gradients and contribute to lower cell and stack costs.
- **Synchrotron Investigations of LSCF Cathode Degradation Conducted.** Montana State University (MSU) has observed Ni transport and depletion of the anode with the presence of $H_2S$ in the fuel stream. This depletion was shown to occur at exposed grain surfaces. MSU has conducted depth-sensitive synchrotron investigations of Ni versus YSZ concentration in anodes that were exposed to $H_2S$ during operation have confirmed and clarified the spatial selectivity of $H_2S$ induced degradation (depletion). Hydrogen sulfide is found to attack exposed Ni surfaces by promoting migration of Ni, presumably in the gas phase. Using a surface sensitive detection technique, very little Ni is observed. However, using a bulk sensitive technique it was found that most of the Ni remains intact. Though surface Ni consists of a small portion of the entire Ni content, this Ni is critical in achieving interconnection in cermet's Ni network. Its depletion renders anodes electrically insulating and useless.

## SECA Core Technology – Anodes and Coal Contaminants

- **Low Cost Coating Method Developed for SOFC Interconnects.** Successful deposition of Mn/Co alloys onto low-cost T441 stainless steel interconnects was achieved by research work performed at NETL. Electrodeposition using pulse plating methods was investigated and showed lower degradation using on-cell tests than for interconnects without a coating. Separately, tests for ASR measurements showed stable performance for over 1,200 hours. From the present work on button cells, it is concluded that pulse plating methods can be a low-cost option for coating stainless steels with Mn/Co alloys so as to achieve low degradation performance. Future work will examine the performance at larger commercial scale interconnect sizes.
- **Coal Syngas Impurities are the Focus of Experiments and Simulations at WVU.** Researchers from National Institute for Fuel-cell Technology at West Virginia University (WVU) have combined multiple expertise in experimentation and modeling to address the problems associated with impurities in coal syngas and other complex fuels. One identified volatile impurity, phosphine, has been shown to cause immediate and irreversible degradation of SOFC performance. Analysis of the Ni/YSZ anode reveals migration of nickel to the surface and into voids in the composite anode,

and the presence of both phosphide and phosphate species at various locations. Computational modeling of the SOFC has been used to address numerous questions, such as effects of multiple reactions, reactions rates, and chemical equilibria for complex fuels passing through the anode and reacting at the active layer.

## SECA Core Technology – Interconnects and Contact Materials

- **SOFC Interconnect-Coating Reaction Product Identified.** Auburn University has evaluated the interaction between chromia and the promising coating material $(Mn,Co)_3O_4$ at 1,000-1,200°C. Chromium can dissolve in the spinel coating and form a reaction layer with the general composition of $(Mn,Co)Cr_2O_4$. During SOFC operation, this phase could form at the interface between the alloy oxidation scale and the protective coating, which would reduce the amount of chromium reaching the coating surface and thus inhibit the associated chromium poisoning of the cathode. However, this reaction layer would be part of the fuel cell circuit, so its presence could affect fuel cell performance. Thus, the composition, and associated properties, of this compound should be considered in selection of the optimal coating composition for long-time SOFC operation
- **Improved Materials Developed for SOFC Interconnects.** SOFC interconnect materials based on inexpensive ferritic stainless steel with a manganese-cobalt oxide spinel coating were validated at Pacific Northwest National Laboratory (PNNL) through long-term (1 year) testing. Overall, these tests indicated excellent performance and stability in terms of both oxidation resistance and electrical conductivity. Ce-modified MnCo spinel coatings resulted in improved oxide scale adhesion compared to baseline (Ce-free) spinel compositions. In addition, optimization of the spinel coating composition (i.e., Ce content) and processing procedures (e.g., powder calcination temperature, conditions for reduction, and oxidation heat treatments) were performed, and development of a spray-based fabrication process for the spinel coatings was initiated. Spray-based fabrication techniques will allow for selective application of the spinel coatings to full-size interconnects being utilized by SECA industry teams in their SOFC stacks.
- **Ag-Perovskite Composites Offer Improved Performance as SOFC Cathode-Interconnect Contact.** Tennessee Technological University developed a composite material system consisting of low-cost noble metal silver (Ag) and a conductive perovskite such as doped $LaCoO_3$ and $LaMnO_3$ for the SOFC cathode-interconnect contact application. By selecting the right perovskite material and optimizing its distribution, volume fraction and sintering parameters, a new composite material system was achieved that combined the Cr-absorbing characteristics of the perovskite with the excellent electrical and mechanical properties of Ag, while maintaining the overall relatively low cost of the contact material. Under typical SOFC thermal conditions (i.e. cyclic and isothermal exposures), the composite contact outperformed Ag or the perovskite phase alone. The composite contact material was able to maintain acceptably low ASR during harsh thermal exposure conditions and inhibit chromium migration from the interconnect into the cathode layer. The utilization of such composite contact materials in the SOFC stack is expected to reduce the material cost and improve the stack performance stability.

## SECA Core Technology – Seals

- **New Viscous Glass Sealants May Improve SOFC Stack Lifetime.** Two new glass composition regimes have been identified by Alfred University that show promise for improved viscous glass SOFC sealants. Initial glass sealant candidates in the galliosilicate and germanosilicate compositions show promising behavior for sealing to YSZ and stainless steels in SOFC stacks. The galliosilicate glasses exhibit excellent resistance to crystallization in bulk or fritted form at 850°C for 504 hours. These glasses also meet the desired thermal expansion target, with values of 11 to 12 ppm/K, while exhibiting low glass transition temperatures, and rather low softening temperatures. Germanosilicate compositions exhibit excellent flow below 850°C with minimal alkali content and moderate crystallization behavior after running at 850°C for 504 hours. Further compositional adjustments should allow improved properties for the SOFC application.
- **Glass-to-Metal Seal and Nb-$LaCrO_3$ Coating Improve Thermal Cycling Performance in SOFC Stack.** Materials & Systems Research Inc. (MSRI) investigated the effect of adding varying amounts of nano-MgO powder into a Ba-Ca-Al-B silicate (BCAS) base-glass composition. The addition of appropriate amounts of nano-MgO was found to prevent the formation of the undesirable hexa-celsian phase and to stabilize the coefficeient of thermal expansion at 12.4 x $10^{-6}$/°C for 900 hours at 800°C. A niobium-doped $LaCrO_3$ coating was successfully applied to the sealing area of the

metallic interconnect by a technique of spraying and curing. The Nb-$LaCrO_3$ coating functioned as an effective barrier layer against chromium migration and prevented undesirable reaction between the metallic interconnect and the glass-based seal after 675 hours at 800°C. Sealing gaskets of glass-MgO composites were fabricated by tape-casting. It was conclusively shown by helium leak testing at 800°C that the addition of MgO nanopowder to the BCAS glass significantly enhances the thermal cycling capability of the glass-to-metal seal. The performance of the glass-MgO seal and Nb-$LaCrO_3$ coating combination performed satisfactorily in a five-cell SOFC stack even after thermal cycling. The results suggest that the sealing technology developed by MSRI significantly improves the long-term chemical and thermal stability of rigid seals, thereby enabling longer duration of stable SOFC operation.

## SECA Core Technology – Fuel Processing

- **On-board Reforming of Volatile Components Distilled from Diesel Fuel May Find Application for Regeneration of $NO_X$ Traps.** Researchers in Boulder, Colorado, working to reform diesel fuel into a mixture of hydrogen and CO for powering mobile SOFCs, have shown that volatile compounds distilled from diesel fuel heated below 200°C are relatively easily reformed - somewhat similar to reforming gasoline. Although considerable effort will be required to produce a practical device, preliminary results at Eltron Research and Development, Inc. indicate that the hydrogen and CO produced by dry partial oxidation of the most volatile components extracted from diesel fuel may be adequate for regeneration of $NO_X$ traps developed by automotive companies to control emissions of nitrogen oxides from diesel engines. Conversion of the relatively easy-to-reform most volatile components of diesel fuel into $H_2$ + CO greatly simplifies diesel-fuel reformers, otherwise requiring complex and expensive liquid-fuel injectors and air mixers, plasma discharge, or addition of water to raise steam. Use of $H_2$ and CO from an on-board fuel reformer could eliminate need to store and use ammonia or urea for regeneration of $NO_X$ traps. Production of $H_2$ and CO for automotive pollution control devices by reforming components of diesel fuel is one side benefit of the SECA program.
- **Fuel Reformer Operation Demonstrated for Water Neutrality.** Precision Combustion, Inc. has successfully demonstrated the feasibility of using a recycle approach for water recovery for diesel fuel processor operation under a water neutral condition. Several POC tests were performed using a Microlith®-based reformer with Tier II diesel. In these preliminary tests, the reformer was operated using fuel, air, and a surrogate gas mixture that simulated a typical anode recycle gas composition. This gas mixture contained sufficient moisture to achieve stable reformer operation without external water addition. During these short-term tests, <20 $ppm_v$ of coke precursors (e.g., ethane, ethylene) were measured in the reformate stream. Additionally, ASPEN modeling and simulation studies were carried out to determine the heat and mass balance requirements, overall system efficiency, and expected product composition for the reformer-anode gas recycle configuration. The reformate gas composition obtained experimentally was in good agreement with that obtained via ASPEN thermodynamic analysis. This demonstrates the potential of a water-neutral system concept utilizing anode recycle approach. More rigorous tests will be performed to confirm these preliminary results.

## SECA Core Technology – Modeling and Simulation

- **SOFC Design Guide Developed.** In a collaborative effort among NETL, the American Society of Mechanical Engineers, PNNL, and Oak Ridge National Laboratory, a SOFC design guide has been prepared. The objective of the guide is to provide recommended design practices and associated modeling and analysis procedures for use by U.S. designers and fabricators of SOFCs to optimize design of durable and reliable SOFCs. The guide is based on past successful usage and advances in the state of knowledge. It describes suggested analytical procedures developed by the SECA Core Technology Program to model electrochemical and thermo-mechanical performance of SOFCs, as well as how these tools and other simulation tools can be used in designing a structurally-reliable and durable SOFC stack. The recommended modeling procedures contained in the guide attempt to quantify the variability in material properties and design parameters of all elements in the SOFC structure. These modeling procedures address the coupled electro-chemical and thermo-mechanical nature of SOFCs by quantifying the electro-chemistry activities and the associated thermal-mechanical behaviors of various SOFC components, for different design configurations. The guide is intended to facilitate development of cost-effective, reliable, SOFC designs, and it will be made available to SOFC developers in 2009. The guide will be a living document, to be updated and expanded on

a regular basis and maintained electronically for access via the internet.

- **Effects of Surface Quality on Interfacial Strength of Oxide Scale and Ferritic Interconnect Evaluated by Integrated Experimental/Modeling Method.** PNNL developed an integrated experimental/analytical methodology for quantifying the interfacial strength between the oxide scale and the different metallic interconnect candidates. This approach was applied to investigate the effect of the interconnect substrate surface quality on the interfacial strength. It was found that the surface quality influences the interfacial strength of the oxide scale and metallic interconnects. As-received SS441 with an $R_a$ surface roughness of 0.3 has a high tendency for oxide scale spallation during cooling. Polishing the surface to a $R_a$ of 0.02 reduces the tendency for scale spallation. Surface modification through mechanical shot peening also dramatically reduces the tendency for oxide scale spallation during cooling. The influence of the thickness of the protective spinel coating layer on the interfacial stresses was studied for SS441 using finite element analyses. It was found that for the same oxide-scale thickness, the cooling-induced interfacial stresses slightly increase with coating thickness for the SS441 interconnect candidate.
- **Effects of In-Stack Contact Paste Densification Evaluated by Modeling.** PNNL has developed modeling tools to evaluate the effects of material volumetric changes during SOFC stack assembly on load distribution and component stresses. Volumetric changes (resulting from processes such as contact paste sintering, glass-ceramic seal devitrification, and anode reduction) have not been included in thermal-mechanical stack models previously, but are important to determine residual stresses in the cells and their effect on reliability. The densification of the cathode contact paste layer in a prototypical stack was simulated, and the contact layer was shown to be beneficial for distributing thermal mismatch loads to the metallic interconnect and reducing the load requirements for cell perimeter seals. The model can be used in stack simulations to optimize the load path, reduce residual stresses, and improve strength and reliability of the contact layer.
- **Modeling and Simulation Tools Assist SOFC Stack Designers.** The SECA Core Technology program element and PNNL have made it their goal to develop and validate multi-physics modeling tools to simulate SOFC stack performance for optimization of modular SOFC stack designs with mitigation of performance degradation, and to disseminate/transfer modeling tools to SECA industry teams and Core participants. During the past year, the modeling team has developed models that extend the range of physical phenomena that can be examined numerically. These include the ability to examine the densification and strength of cathode contact materials and creep within stack components such that structural analyses can more accurately predict and optimize the distribution of mechanical load within a stack design. The simulation tools can now examine the improved electrical efficiency and modified on-cell methane reforming behavior due to pressurized operation. This capability enables researchers to explore a broad range of fuel composition and operating pressure combinations without the need for costly and time consuming experiments.

## SECA Core Technology – Balance of Plant

- **Low Cost and High Temperature Blowing Systems Completed**. Phoenix Analysis and Design Technologies (PADT) completed an SBIR project to develop blowing systems for the SOFC industry. The industry needs low-cost systems and systems that can pump very high temperature gases. As part of the work, PADT developed two technologies: first, a small multi-stage blowing system that can be manufactured at low cost in high volumes; and second, a very high temperature (up to ~800°C) blower that would enable anode recycle as a system option. PADT completed 11 iterations on the aerodynamic development for the small multi-stage technology and demonstrated efficiencies that are 50 percent better than existing off-the-shelf solutions. PADT also designed and tested a first prototype of the high-temperature blower for anode recycle. This first prototype was made from stainless steel and is capable of 500°C operation. Higher temperatures are capable with the same design by using more exotic materials.
- **SOFC Anode Gas Recycling Is Now Possible Using High-Temperature Foil Bearing Supported Blower.** R&D Dynamics made significant progress in developing a high-temperature, centrifugal type, foil bearing supported anode gas recycle blower (FBS-AGRB) for SOFC systems. The high-temperature AGRB is used in an SOFC system for recycling the water-saturated anode exhaust gas and mixing it with fresh incoming fuel. The blower is designed to sustain the high SOFC system temperature and the high humidity of the anode gas. The FBS-AGRB has been tested up to 718°C inlet temperature and successfully met the following requirements set by SECA: high-temperature applicability, high efficiency, high reliability, low

power consumption, compact design, maintenance-free, low cost, and scalable. No such blower was previously available in the market to meet these targets. A prototype unit was successfully tested by the U.S. Navy at the Naval Undersea Warfare Center in Newport, Rhode Island. Testing results have been very encouraging and demonstrated the viability of the technology; however, some improvements were required in order for the blower to reach the inlet temperature goal of 850°C. The following required improvements were made:

- Analyzed and optimized design
- Upgraded blower materials to achieve 850°C
- Designed and manufactured motor capable of handling high temperature
- Improved sealing design to eliminate anode gas leakage at high temperature
- Manufactured parts

This FBS-AGRB accomplishment substantially contributes to achievement of the SECA goal to commercialize 3-10 kW low-cost SOFCs by 2010.

- **Efficient Low-Cost Air Blower Being Developed for 3 to 10 kW SOFC Systems.** R&D Dynamics Corporation is developing a low-cost cathode air blower which will cost less than $100 at a production volume of 50,000 units per year. The blower being developed is efficient, reliable, oil-free, maintenance-free and compact. Design for Manufacturing and Assembly techniques are used to reduce the cost of the blower. The blower is designed with only 16 parts. A low-cost controller was developed and tested for the blower. Cooperation and support has been obtained from SECA members and the prototype blower is planned to be tested in an actual fuel cell system in year 2010. The low-cost and efficient blower will help DOE and SECA meet its cost target goals for small SOFC systems.
- **Reliable High-Temperature Recycle Blower Made Possible for Large SOFC Power Plants.** R&D Dynamics Corporation has proved the feasibility of a reliable high-temperature recycle blower. The blower is designed such that it can be used as a cathode or anode recycle blower. The recycle blower will increase the overall plant efficiency of large size SOFC power plants. Significant progress has been made during Phase I. A high temperature capable (up to 850°C), efficient, reliable, oil-free, maintenance-free and easily scalable blower was designed. A 6-inch diameter foil journal bearing suitable for this application was manufactured and successfully tested. The blower will be designed, manufactured, and tested as both an anode and cathode recycle blower during Phase II.

## Innovative Concepts

- **Liquid Tin Demonstrated as a Purification Mechanism for Coal Reaction.** CellTech Power, LLC (CellTech) evaluated the reaction of liquid tin with coal as part of a broader study of a direct coal fuel cell based on the liquid tin anode (LTA) SOFC. Mixtures of tin and coal were processed in a coal/tin reactor to assess the fate of coal contaminants. Contaminants of interest were spiked into an operating liquid tin fuel cell to evaluate their potential impact on fuel cell life. In the coal/tin reactor tests, West Virginia coal samples were reacted with tin oxide at the target operating temperature of 1,000°C to obtain tin samples representative of an operating direct coal fuel cell. Among the elements of interest, only arsenic and selenium were found to be present in the chemical analysis of coal-tin samples after reaction. In the fuel cell testing, five elements of interest were spiked at 1,600 ppm, far in excess of the contaminant levels expected during operation. At this high level, fuel cell degradation was observed; however, the cell was still functional when the test was terminated at 420 hours. Postmortem analysis of the fuel cell tin indicated that the spatial distribution of contaminants is complex and highly variable. The results of this work provide promising evidence of the viability of the LTA SOFC as a high efficiency direct coal conversion device.
- **Liquid Tin Anode Fuel Cell Developed as a Direct Coal Generator.** Electrochemical looping[1] (ECL) is a new concept for direct generation of power from a variety of fuels including coal and biomass. Direct conversion is more efficient. ECL combines multiple processes, reducing inefficiency and lowering capital cost compared to other advanced baseload technologies. For instance, there is no oxygen plant or gasifier required. The enabling technology for ECL is a new type of fuel cell that uses an LTA. LTA has been demonstrated at CellTech in small scale, and commercialization for small power applications provides an important link to commercialization of large-scale generation technologies. A plan of action to accelerate ECL development includes further work on key risk items, including durability, demonstration of a bench scale system, and scale up of the enabling technology components. The commercialization

[1] The electrochemical aspect refers to the highly efficient production of power without combustion while the looping concept refers to the shuttling or "looping" of oxygen by the liquid tin anode.

path incorporates early revenue from markets such as portable power and distributed generation, providing near-term reliability improvement while reducing the time and risk associated with development of baseload applications.

### Advanced Research

- **Composite Electrolyte Improves Chemical Stability in Proton SOFC.** One of the prime attractions of fuel cells is the opportunity for achieving energy conversion efficiencies much higher than possible with the thermal cycle systems. Materials have been developed which function as high temperature solid electrolytes in fuel cell applications. Two of the most widely considered materials are YSZ, which transports oxygen ions, and yttria-doped $BaCeO_3$ (BCY), which transports protons. The thermodynamic difference between proton and oxygen ion cells is manifest in reversible potential variation with reactant utilization as a function of product water location. Excess air flow, used to remove the heat generated by cell operation, results in a lower water concentration in the cathode stream of a proton cell than in the anode stream of an $O_2$ cell. This results in proton cells having higher driving potential at a given fuel utilization than an oxygen cell, thus enabling higher voltage and consequently higher efficiency operation. Ceramatec is addressing a critical technical hurdle, the chemical stability of $BaCeO_3$ in $CO_2$ containing fuel compositions, to make proton SOFCs a technical reality. A ceramic composite containing a mixture of $BaCeO_3$ and doped ceria has been shown to improve the chemical stability. Stable cell performance using the composite electrolyte was demonstrated in high $CO_2$-containing fuel gas. Anode-supported proton cells have been demonstrated to show a power density of 230 mW/cm$^2$ at 700°C. Cell scale up is in progress, and testing of stacks is planned.
- **SECA Fuel Cells Tested by Navy under Extreme Conditions.** The Naval Undersea Warfare Center, Division Newport (NUWCDIVNPT) is collaborating with DOE to examine the effect of pure oxygen on SOFC stacks and to provide POC system demonstrations. NUWCDIVNPT's role is to provide independent testing and evaluation of SOFC stacks being developed under the DOE's SECA program. System demonstrations have consisted of a SOFC stack integrated with fuel processor, high-temperature anode recycle blower, and carbon dioxide sorbent. This system has attained an overall fuel utilization over 75 percent, oxygen utilization over 95 percent, and fuel efficiency over 50 percent (lower heating value). These pure oxygen studies have shown up to 10 percent efficiency gains by using pure oxygen instead of air; however, long-term stack stability under pure oxygen is still under investigation.

### SECA Adds Core Technology and Other Projects

The University of Cincinnati will engineer and demonstrate innovative sealing concepts for SOFCs using a promising viscous glass. This project was selected in 2008, but the award occurred 2009. A number of other projects were selected in 2009 under various solicitations. Under SBIR grants, TDA Research will assess sorbents for warm temperature removal of arsenic and phosphorous from coal-derived synthesis gas, Eltron Research & Development will study perovskite adsorbents for warm-gas and phosphorus removal and first principles identification of new cathode electrocatalysts for fuel cells, and Materials and Systems Research will assess novel SOFC anodes with enhanced tolerance to coal contaminants. Through a STTR project, Faraday Technology will assess electrodeposited Mn-Co alloy coatings for SOFC interconnects.

### 2009 Annual SECA Workshop in Pittsburgh, Pennsylvania

The SECA program held its 10$^{th}$ annual workshop July 14–16, 2009, in Pittsburgh, Pennsylvania. Principal investigators of projects provided presentations. The findings and recommendations will be used by the DOE Project Managers to guide their future work and by the Technology Manager to make programmatic and funding decisions for the upcoming fiscal years. The workshop proceedings will be found on the program's Web site at http://www.netl.doe.gov/seca/.

## Summary

In light of the substantial technical progress realized in FY 2009, ongoing cell performance and scaling improvements will undoubtedly result in additional cost reduction and the testing of larger SOFC stacks. The maximum obtainable performance of cathode materials is limited by stability and activity, and results show that both are directly related to surface chemistry and structure where characterization is more appropriate. Technological spinoffs of SOFCs into a variety of other applications, especially APUs for heavy-duty trucks and related military power applications for the Department of Defense, will add to market penetration, increase manufacturing production volume, and lower SOFC cost.

By developing fuel cells to operate cost effectively on coal gas as well as natural gas, bio-fuels, diesel, and hydrogen, SECA is solving today's environmental, climate change, fuel availability, and energy security issues. SECA fuel cells are ideal for use in central generation applications, enabling high efficiency, diverse opportunities for carbon capture (e.g., post-power block), lower criteria pollutant emissions (e.g., less than 0.5 ppm $NO_X$, regardless of fuel), and water conservation. IGFC system configurations utilizing near-term gasification and syngas cleaning technologies will generate power from coal with overall efficiencies of greater than 45 to 50 percent (HHV, coal to AC power), including the coal gasification and $CO_2$ capture processes. Advanced systems are capable of efficiencies of greater than 50 percent, approaching 60 percent for some configurations. In conjunction with SECA-driven fuel cell cost reduction, these IGFC systems will enable the clean, efficient and cost-effective use of the nation's most abundant fossil fuel. The once distant vision of using clean, low-cost fuel cell technology for everyday applications is now within reach.

# II. SECA INDUSTRY TEAMS

## A. Coal-Based Systems

# II.A.1 FuelCell Energy Inc. (FCE) Solid State Energy Conversion Alliance (SECA) Coal-Based Solid Oxide Fuel Cell (SOFC) Power Plant Development Project

Hossein Ghezel-Ayagh
FuelCell Energy, Inc.
3 Great Pasture Road
Danbury, CT 06813
Phone: (203) 825-6048; Fax: (203) 825-6273
E-mail: hghezel@fce.com

DOE Project Manager: Travis Shultz
Phone: (304) 285-1370
E-mail: Travis.Shultz@netl.doe.gov

Subcontractors:
- Versa Power Systems, Inc., Littleton, CO
- WorleyParsons Group, Inc., Reading, PA

Contract Number: 41837

Start Date: February 27, 2004
End Date: September 30, 2010

## FY 2009 Objectives

- Improve anode supported SOFC components to increase cell performance, lower performance degradation rate, and decrease cost.
- Scale up the fuel cell size to 33 cm x 33 cm.
- Design, build and test a 30 kW SOFC stack tower to validate the concept for incorporation in megawatt scale modules.
- Demonstrate cell/stack size, design and material improvements to reduce cost of the SOFC stack to $165/kW (2002 United States dollar [USD]).
- Develop a MW-scale stack module design concept suitable for incorporation in large-scale centralized coal power plants.
- Develop the design of a Module Demonstration Unit (MDU) for validation of the MW-scale SOFC module performance and endurance.
- Develop a coal-based >100 MW baseline integrated gasification fuel cell (IGFC) system with electrical efficiency >50% (coal higher heating value [HHV] to net alternating current) and capability for >90% of carbon capture (as $CO_2$) from coal syngas.
- Verify the baseline system power block factory cost of <$600/kW (2002 USD) and a power density of >250 mW/cm$^2$ based on 5,000-hr metric test of a 10 kW scaled-up stack.
- Demonstrate that a steady state degradation of <4%/1,000 hr is achievable by a 10 kW scaled-up stack after completion of 5,000-hr metric test.

## Accomplishments

- Single cell testing of improved cell components showed a performance gain of up to 15%. A very low degradation rate of 0.75% per 1,000 hr (at 500 mA/cm$^2$ and 750°C) has been observed in a 25 cm x 25 cm single cell test during a 4,500-hr period. The performance of the cell was also quantified at fuel utilizations up to 85% with a small voltage loss due to the increase in utilization.
- Fuel cell manufacturing processes were developed to support the new scaled-up baseline cell (25 cm x 25 cm). The accomplishments included: commissioning of new manufacturing equipment, re-tooling of existing equipment, and application of statistical process control and optimization for yield improvements. More than 1,500 cells were produced with a high level of process control. Production yield of >95% was established inline with the fuel cell factory cost reduction goals.
- The scale up of the SOFC to a 33 cm x 33 cm cell (active area of 961 cm$^2$) has shown a peak power of 880 W (915 mW/cm$^2$) and a degradation rate of 1.3% per 1,000 hr (at 520 mA/cm$^2$) during the 1,900-hr test period.
- Manufacturing of the scaled-up 10 kW stacks with baseline 25 cm x 25 cm cells was accomplished to establish the building block foundation for multi-MW coal-based power plants. An improved stack design with advanced components was developed to meet the objectives of performance and endurance criteria.
- In accordance with the SECA minimum requirements, the Phase I metric tests were completed by fabricating and running two 10 kW stacks for >5,000 hr of operation. The two stacks operated with degradation of <2.7%/1,000 hr, which was significantly better than the 4%/1,000/hr target for the Phase I project.
- The peak power of 11 kW in two metric test stacks, and 14.8 kW in a third stack was demonstrated. The metric tests also verified stack cost of $197/kW (2002 USD) and a power density of 314 mW/cm$^2$ at the peak power rating of 11 kW. The stack cost is further decreased to $146/kW at 14.8 kW peak power corresponding to 420 mW/cm$^2$ power density which is about 12% lower than the targeted value of $165/kW.
- The operation of a 10 kW stack in a module configuration was demonstrated for >5,000 hr to simulate the operational environment of a fuel cell stack module.

- MW-scale SOFC module concept was developed, including 20 stack towers. The flow distribution piping, base structure, insulation, and electrical bus-bar connections were designed for the 1 MW fuel cell module.
- An advanced 527 MW baseline IGFC system was developed utilizing a catalytic gasifier and warm gas clean-up subsystem, achieving an electrical efficiency of 52% (HHV coal) while removing greater than 90% carbon (as $CO_2$) from syngas. The independently audited factory cost of the coal-based baseline SOFC power block was estimated to be $597/kW (2002 USD) for a production rate of two power plants/year meeting the Phase I target.

## Introduction

FCE is in Phase II of a three-phase project to develop SOFC stack modules and power blocks for application in coal-based IGFC power plants. The primary objective of the project is to develop affordable and highly efficient multi-MW SOFC systems that have near-zero emissions of SOx and NOx, low water consumption, and amenability to greenhouse gas (carbon dioxide) capture. IGFC systems are projected to achieve electrical efficiencies greater than 50% based on the HHV of coal, while separating carbon dioxide to capture at least 90 percent of the carbon in the syngas for environmentally secure storage.

FCE utilizes the SOFC technology of its partner, Versa Power Systems (VPS), in the development of IGFC power plants. VPS has well established processes, quality control procedures, and equipment for the manufacturing of fuel cells. Key research and development activities for the project include: cell and stack size scale up, SOFC performance optimization, increased stack manufacturing capacity development, and MW-class conceptual design.

## Approach

Fuel cell development work has been focused on key cell issues related to cost reduction, endurance enhancement and performance improvement. The main technical approach includes extension of the operating temperature window, reduction of average operating temperature, thermo-mechanical strength improvement, and scaled-up cell fabrication process development. The emphasis is placed on the development of an anode substrate with increased thermo-mechanical strength. Material solutions with enhanced mechanical and electrochemical properties are being evaluated with considerations for endurance and cost. Laboratory process and equipment retooling have been utilized to support the cell scale up process development to 33 cm x 33 cm size. Various cell component design considerations, such as anode substrate thickness and porosity, have been evaluated to identify the optimum cell configuration for operation at high power density on coal syngas. Parameters such as performance (power, thermal management, and efficiency), design simplicity, technical risk, manufacturability, and cost have been considered in the design selection process.

Baseline power plant conceptual design focuses on evaluation of process alternatives that will increase power plant efficiency, meet carbon capture requirements, and minimize cost of the power plant's power island. Various process configuration analyses and parametric studies were conducted considering voltage, current density, fuel utilization, stream recycle levels, and process components. Concurrent with the baseline power plant design work, conceptual design of a 1 MW module demonstration unit is continued with process configuration evaluations and operating parameter studies.

## Results

In Fiscal Year 2009, FCE completed Phase I of the project, meeting the SECA program intermediate targets for system cost, fuel cell performance degradation, power plant efficiency, and percent carbon capture. The SOFC technology advancement included cell area scale up and stack building block validation testing. Figure 1 shows the picture of a 10 kW stack building block consisting of 64 cells with 550 $cm^2$ cell active area. A key success story of the year was the completion of the 5,000-hr 10 kW stack block metric test. The FCE-VPS team exceeded the SECA goals by achieving a degradation rate of ≤2.7%/1,000 hr in the stack metric test. Figure 2 shows metric test results for one of the two metric tests conducted. In parallel, the coal-based IGFC baseline power plant system development and cost analysis were continued. The power plant was designed utilizing

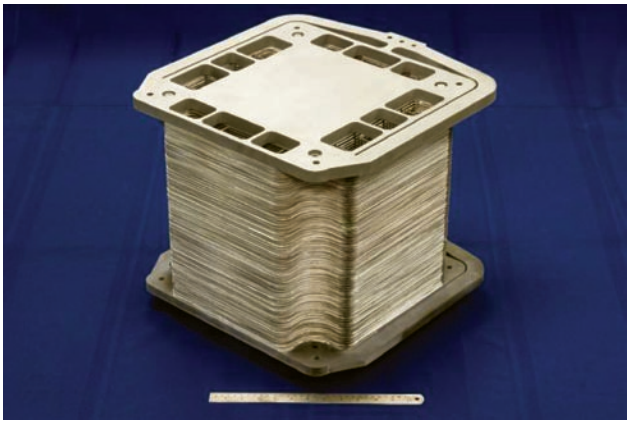

**FIGURE 1.** 10 kW Stack Block

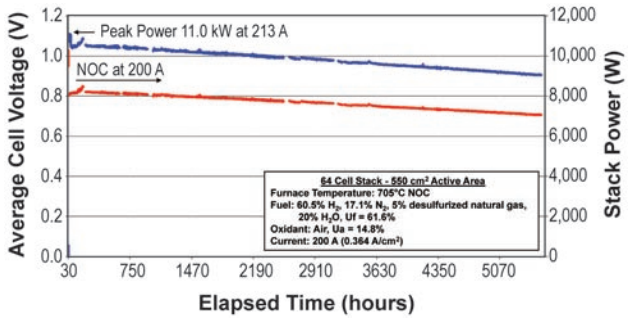


**FIGURE 2.** 10 kW Stack Performance during 5,000-hr Metric Test

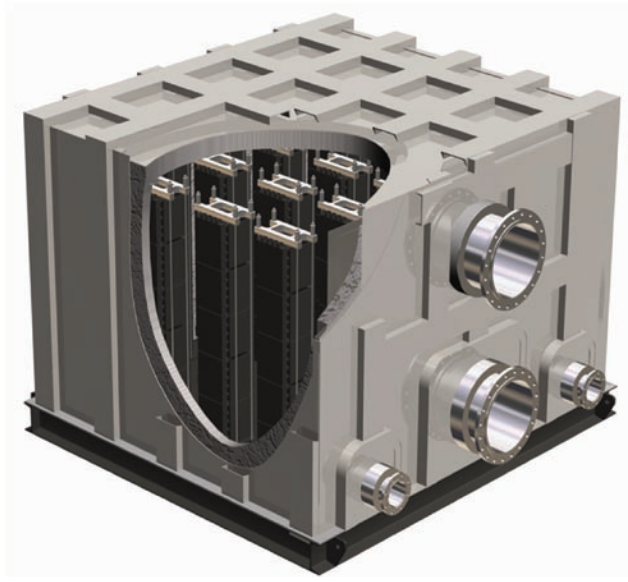

**FIGURE 3.** 1 MW SOFC Stack Module

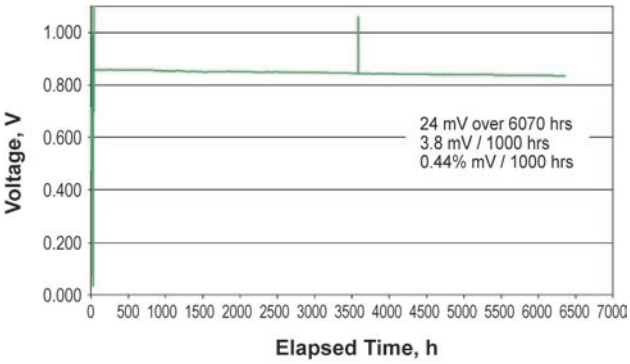


**FIGURE 4.** Long-Term Degradation Test of an Advanced Cell

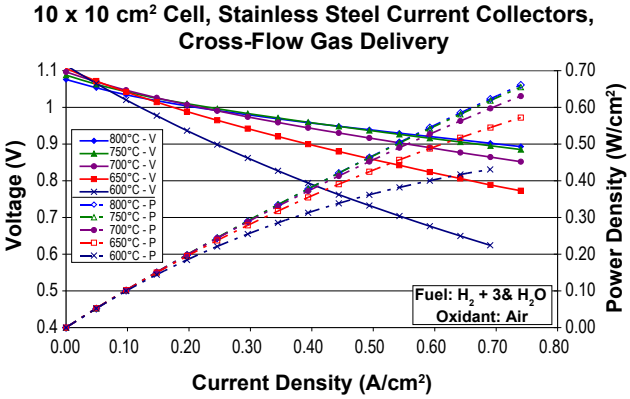


**FIGURE 5.** Performance Data Representative of Advanced Cells

MW-scale fuel cell modules. Figure 3 shows a schematic of the module concept developed. The module consists of 20 stack towers, each assembled with five 10 kW stack building blocks. The system design was based on fuel cell stack data generated during the Phase I metric test. The cost analysis of the baseline system indicated that an SOFC power island cost of $597/kW is achievable for a manufacturing production of two plants per year. The factory assembled SOFC cost of $197/kW is the key in making a measurable contribution to the cost-competitiveness of IGFC systems relative to other power generation technologies operating on coal.

Phase II development activities have been initiated. Material research efforts are focused on improving cell performance, lowering operating temperature, reducing performance degradation rate and cell area scale up. Cell performance degradation is one of the major technical challenges in SOFC development. Progress was made in investigation of cell degradation mechanisms at various operating conditions using a reliable electrochemical testing method for separating over-potential and resistance losses during the steady-state and transient operation. An improved cell with advanced cathode was developed with significantly lower degradation rate. Figure 4 shows long-term single cell test results of the cell, with degradation rate of $< 0.5\%/1{,}000$ hr over a 6,000-hr period. The advanced cells have been further improved by modifying anodes. These advanced cells offer the combination of high cell performance and low performance degradation rate. Figure 5 shows the performance characteristics of one such cell, at operating temperatures from 600 to 800°C. Power densities of greater than 500 mW/cm$^2$ are observed even at a low temperature of 650°C while maintaining a cell voltage of 0.8 V. The cell improvements have multiple benefits related to the cost and efficiency of the fuel cell power module. To investigate the preferred operating conditions in a stack, cells have been extensively tested to study long-term degradation in the 650 to 800°C temperature range. Currently, 750°C is the optimum operating temperature with the lowest degradation rate. In order to incorporate the advanced cell in stack, efforts are being made to reduce the degradation rate at lower operating temperatures of 700°C and 650°C.

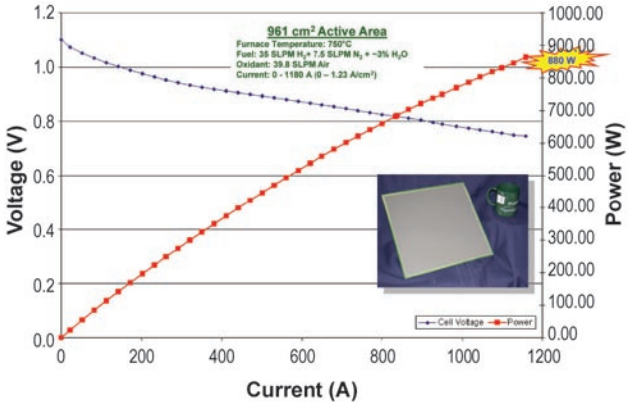


**FIGURE 6.** Large Area Cell (33 cm x 33 cm) Performance

The new advanced cathode was incorporated in large area cells for further validation. The performance degradation rate of 0.75%/1,000 hr over a 4,500-hr period observed in the 25 cm x 25 cm cell is similar to that demonstrated in 10 cm x 10 cm size cells earlier. The cell was also operated at higher fuel utilizations up to 85% with a relatively small voltage drop from increased utilization. Cell area scale up activities are being continued in Phase II, with 33 cm x 33 cm cells (961 $cm^2$ cell active area) produced using the standard TSC (Tape casting–Screen printing–Co-firing) manufacturing process. All the functional layers were screen-printed onto the green substrates, punch cut to size and single step co-fired to the final cell dimension. Figure 6 shows the performance characteristics of the scaled-up cell. The cell produced a power of 880 W (915 $mW/cm^2$) in characterization tests. The cell has operated for more than 4,000 hr at 500 $mA/cm^2$ and testing continues.

A 10 kW SOFC stack was successfully tested in a module environment. Stack performance data provided valuable information for design of the stack towers and stack module configuration. Subsequently, a 30 kW stack tower has been assembled to validate the operability of the multiple stack blocks. This test represents a crucial step in the development of SOFC modules for DOE's goal of an SOFC-based platform suitable for coal-fueled MW-scale central power plant systems.

System analysis for the baseline power plant resulted in an advanced 527 MW IGFC system, meeting the goals of >90% carbon capture from coal syngas. This system utilizes the unique characteristics of the fuel cell including internal reforming, and separated anode and cathode gas streams to achieve the superior efficiencies of greater than 52%.

## Conclusions and Future Directions

Major breakthroughs in cell materials development led to cell performance enhancement of up to 15% and performance degradation rate reduction of 50% in single cell operation. The TSC cell process has been shown to be capable of making large area cells with very good process control and high yields. Stack development used both modeling and iterative stack testing to achieve repeatability and good performance in scaled-up 10 kW stacks. Stack block tests both in the metric test facility as well as in the module configuration validated SOFC scalability, and the suitability of the approach for the large MW-scale coal-based power generation applications.

In the second half of Phase II, the following areas will be emphasized:

- Continue cell and stack performance development while increasing endurance.
- Continue stack tower development, specifically developing stacks into a stack tower which will be the building block for a MW module.
- Complete an endurance test for the Phase II generation stacks and stack tower.
- Complete at least 1,500 hr of metric tests for a ≥25 kW stack tower.
- Complete the baseline power plant system analysis and cost estimate. Compare the cost estimate against the 2010 SECA SOFC cost goal of $700/kW (2007 USD).
- Complete the conceptual design for a >250 kW module demonstration unit and complete an MDU cost estimate.

## FY 2009 Publications/Presentations

**1.** Brian Borglum, "Development of Solid Oxide Fuel Cells at Versa Power Systems," Electrochemical Society Transaction, Editor(s): M. Williams, K. Krist, N. Garland, Volume 17, pp. 9-13.

**2.** Hossein Ghezel-Ayagh, Jody Doyon, Jim Walzak, Stephen Jolly, Dilip Patel, Allen Adriani, Peng Huang, Keith E. Davis, David Stauffer, Vladimir Vaysman, Sunitha Asapu, Brian Borglum, Eric Tang, Randy Petri, and Chakravarthy Sishtla, "Coal-Based Solid Oxide Fuel Cell Systems," Electrochemical Society Transaction, Editor(s): M. Williams, K. Krist, N. Garland, Volume 17, pp. 15-22.

# II.A.2 SECA Coal-Based Systems – Rolls-Royce


Richard Goettler (Primary Contact), Greg Rush, Ted Ohrn, Mark Scotto, Zhien Liu
Rolls-Royce Fuel Cell Systems (U.S.) Inc. (RRFCS)
6065 Strip Avenue NW
North Canton, OH 44720
Phone: (330) 491-4821; Fax: (330) 491-4808
E-mail: richard.goettler@us.rrfcs.com

DOE Project Manager: Travis Shultz
Phone: (304) 285-1370
E-mail: Travis.Shultz@netl.doe.gov

Subcontractors:
- Rolls-Royce Fuel Cell Systems Limited, Loughborough and Derby, United Kingdom
- Case Western Reserve University, Cleveland, OH
- University of Connecticut, Storrs, CT
- Matrix Innovations, Lynchburg, VA
- Oak Ridge National Laboratory, Oak Ridge, TN
- Pacific Northwest National Laboratory, Richland, WA



Contract Number: NT0003893

Start Date: Contract in negotiation
End Date: September 30, 2010


## FY 2009 Objectives

- Select a solid oxide fuel cell (SOFC) power block cycle for executing the 15 kWe stack milestone test, and which achieves the design goals for the integrated coal gasification fuel cell (IGFC) combined cycle power plant.
- Complete a redesign of the RRFCS stack test rigs to allow simulation of a coal-derived syngas composition of an IGFC plant.
- Demonstrate lower cost active cell layers able to achieve lower area specific resistance (ASR).

## Accomplishments

- A SOFC power block cycle has been selected which based on preliminary system modeling studies achieves the DOE's target of >50% efficiency (higher heating value) for an IGFC plant.
- The pressurized stack test rig has been redesigned to include a catalytic partial oxidation (CPOX) reactor to supply a fuel composition to the SOFC stack that replicates the output from an oxygen fed catalytic coal gasifier.
- A 40% increase in power density has been demonstrated for the RRFCS integrated-planar (IP)-SOFC using lower cost active cell materials.
- An electrochemical model has been combined with the output of a gaseous counter diffusion model to predict voltage-current density curves as a function of tube permeability values to provide guidelines for a refined substrate specification.

## Introduction

The RRFCS Solid State Energy Conversion Alliance (SECA) project is aimed at demonstrating the viability of the RRFCS IP-SOFC technology, which is being developed for the distributed energy market, for eventual scale-up to a megawatt-scale system suitable for incorporation into centralized power generation facilities employing coal gasification and carbon sequestration. The RRFCS stack concept is based on thin planar cells which are series-connected on a fuel-carrying porous ceramic support substrate [1]. These active substrates are the elemental building block of the fuel cell stack and are grouped together to form a megawatt-scale IP-SOFC system as shown in Figure 1. Figure 2 shows the pre-project advancement of the IP-SOFC from 15 cells to the latest standard of 60 cells per side of each substrate. These cells are applied onto the substrates using well established thick film screen printing techniques. Contrary to other SOFC developers who seek ever larger single cell active areas, RRFCS desires smaller cells to reduce current levels and achieve lower ohmic ($I^2R$) losses. This represents a switch in design philosophy from a low voltage, high current fuel cell to a high voltage, low current approach in a similar

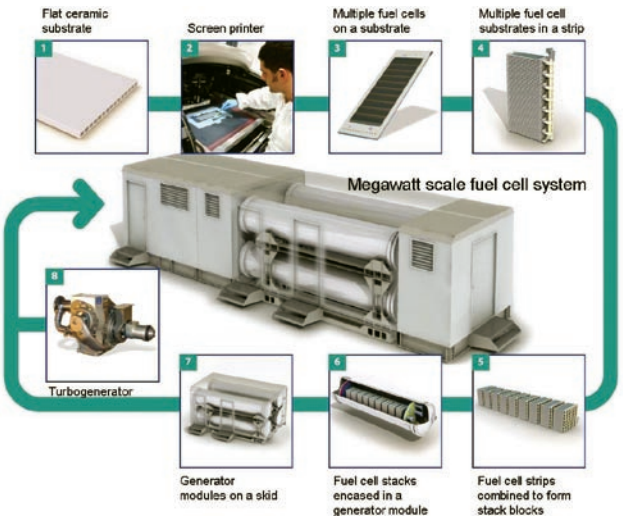


**FIGURE 1.** Schematic of the Planned RRFCS 1 MW Distributed Energy Fuel Cell System

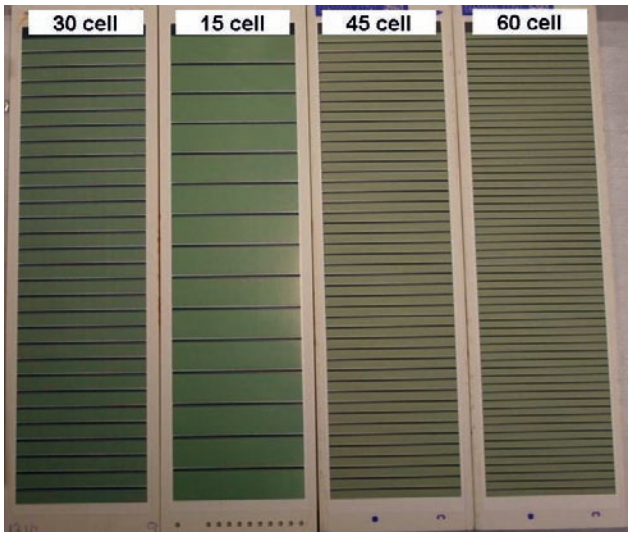


**FIGURE 2.** Evolution of the RRFCS Substrate Design to the Current 60 Cells per Side

manner to conventional electrical devices, including transformers, motors, and generators. These 60-cell active substrates allow the use of new sets of current collecting materials as a result of the lower conductance requirements necessary to achieve similar area specific resistances associated with the in-plane ohmic losses. These new material sets are necessary for meeting the DOE 2010 cost target of <$700/kWe (in 2007$), and testing under this project is validating performance benefits of the new substrate design plus active layers and its long-term durability to the system conditions selected for the RRFCS IP-SOFC power block module of the IGFC plant.

## Approach

Achieving a successful 5,000-hour end-of-phase 15 kWe stack test requires thorough screening of the latest active cell layers at the full system operating conditions to verify the ability to meet the 2%/1,000-hour degradation targets prior to commencement of the milestone test. RRFCS has recently commissioned five pressurized test stands capable of testing either multiple subscale substrates containing single cells or five cells/four interconnections or a single full-scale substrate, and at conditions representative of the designed IGFC power block and the Phase 1 milestone stack test. The subscale test samples are highly instrumented to allow analysis by impedance spectroscopy to identify degradation sources and guide the materials selection and optimization for the active layers. A second level of testing at the bundle level (multiple substrates in series), also at system relevant conditions, will be performed prior to the milestone test to qualify this next generation cell technology.

Contaminant carryover from the coal gasification cycle will be removed prior to entering the fuel cell power block of the IGFC plant, and future phases of a RRFCS SECA project will evaluate the tolerance of the fuel cell to the residual contaminant levels expected [2]. A known additional SOFC contaminant, beyond that expected from the coal gasification process, is volatile chromium species originating from the balance-of-plant metallic components of the fuel cell power block [3]. The electrochemical impact of the chromium contaminants evolved under the RRFCS cycle conditions are being investigated, and chromium mitigation schemes will be quantified by the University of Connecticut, and adopted as necessary to insure the ability to meet the SECA degradation target.

Not only must the fuel cell stack meet electrochemical performance and durability targets, it must demonstrate structural integrity for the full duration of the test. Stack mechanical reliability is being investigated in collaboration with Oak Ridge National Laboratory where detailed mechanical characterization of the substrate and fully processed and tested active substrates will be performed. Studies of the long-term interactions between the substrate material and the glass used to seal the inactive regions will be performed by Pacific Northwest National Laboratory, as reactivity and evolving thermal stress states could impact substrate strength. A detailed understanding of the requirements for substrate diffusivity, based on modeling and validated with electrochemical testing, is being performed to achieve a substrate microstructure that provides sufficient transport of reactant and product gases, while maximizing structural properties.

## Results

The combination of the new 60-cell/side active substrate design plus new anode and cathode current collecting layers has achieved repeat unit ASR at 900°C of 0.26 ohm-cm$^2$ under SECA IGFC system relevant conditions, and a roughly 40% increase in power density (Figure 3). System modeling results indicate that these ASR levels will allow lowering of the stack operating temperature from a peak of 970°C to 900°C compared to the stacks incorporating active substrates of the 30-cell design. This will positively impact the degradation rate of the stack as well as improve durability of the balance-of-plant components making up the stack test rig. Additional reduction in ASR is anticipated upon further optimization of the active cell layers.

A gaseous counter diffusion model has been utilized to extend the understanding of how key tube characteristics such as porosity, tortuosity and mean pore radius, as determined through accurate permeability measurements, influence the electrochemical performance of the RRFCS active substrate [4]. Substrates exhibiting low permeability

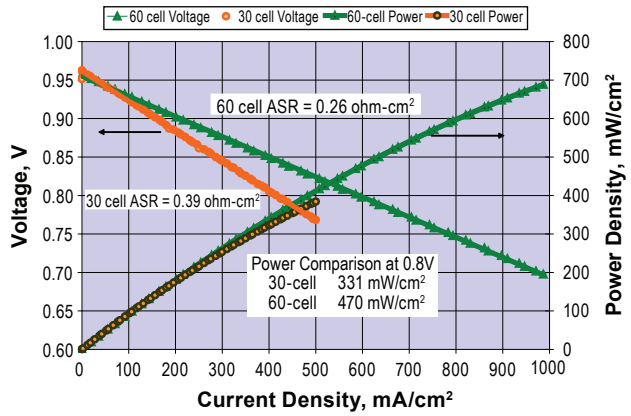


**FIGURE 3.** ASR and Power Density Improvement Between 30-Cell and 60-Cell Designs (900°C, 6 $bar_a$, stack inlet fuel composition, 12% $O_2$)

show diffusional electrochemical resistance at lower than desired current densities. Electrochemical characterization of tubes with a range of permeabilities has been performed. The experimental results have been analyzed with models developed by RRFCS that combine the gaseous counter diffusion model with an electrochemical model to provide a more fundamental understanding of the physical requirements for the substrates. These results are guiding the substrate supply for the SECA stack test.

System modeling employing Aspen Plus® has been performed to investigate system designs to accommodate coal-derived synthesis gas and separate air and fuel gas streams as required for $CO_2$ capture. In order to meet the challenge for achieving 50% overall plant efficiency, an advanced low temperature catalytic coal gasification process is assumed. In addition, the arrangement of components in the fuel cell plant was modified, relative to the current natural gas-based RRFCS power plant design shown in Figure 4. In order to sustain the required fuel cell performance, integrating anode-side recycle into the fuel-reforming step was eliminated. Instead, the coal-derived synthesis gas is reformed and converted in the fuel cell in a single pass. The anode ejector that was applied to generate the anode recycle stream in the current natural gas-based design is now applied to generate a heat source to reform the coal-derived synthesis gas. The motive fluid for the ejector uses a portion of the pressurized $CO_2$ and $O_2$, two of the available streams in coal gasification plants designed for $CO_2$ sequestration and/or recovery. The cathode recycle loop no longer functions as the heat source for reforming, or the oxidation gas to burn out the unspent fuel exiting the fuel cell. These design changes are significant and necessary modifications to yield a stream of relatively pure $CO_2$. The modified fuel cell power plant still operates at moderate pressures up to 6 bar with an integrated turbo-generator, and can yield efficiencies that reach 50% if the overall fuel cell fuel utilization reaches

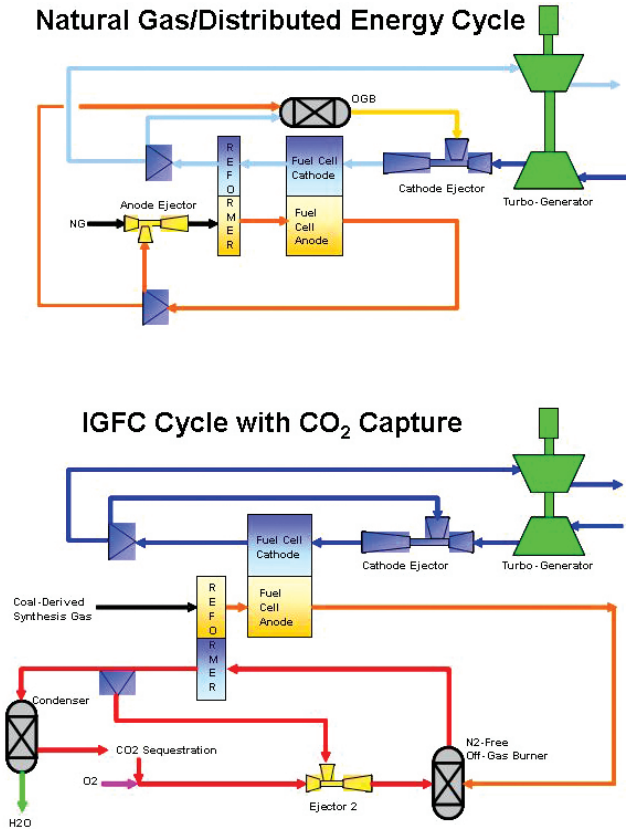


**FIGURE 4.** Modification of the Roll-Royce System Cycle to Meet the SECA IGFC Requirements

roughly 80%. High fuel cell fuel utilization in a single-pass arrangement is one of the major challenges with the Rolls-Royce technology in that fuel cell performance must be sustained as reactant concentrations drop to relatively low levels toward the exit of the fuel cell stacks. The combined substrate gaseous diffusion and electrochemical model will be a valuable tool for designing a stack for high single pass fuel utilization.

A pressurized test-rig being assembled at the RRFCS Canton, Ohio facility, funded through a combination of RRFCS capital and funding from Ohio's Third Frontier, has been redesigned to enable testing the fuel cell for the milestone stack test under conditions that match the modified cycle described above as closely as possible. In order to continuously supply a coal-derived synthesis gas through practical means, a catalytic oxygen-based CPOX reactor will be fabricated. This effort is possible given the previous experience and expertise in CPOX at RRFCS. The reactor will provide a replica of the nominal coal-derived synthesis gas composition that is expected to exit the coal gasifier of the IGFC plant, and which feeds the fuel cell stack inlet. The stack test will assess the fuel cell and cathode recycle loop under conditions that closely represent the SECA IGFC cycle. The stack test will employ an air compressor in place of the turbo-generator.

## Conclusions and Future Directions

Lower cell ASRs have been demonstrated utilizing next generation, lower cost current collecting layers made possible through the adoption of a new active substrate design having a smaller cell area, and less stringent in-plane conductance requirements. Further optimization of the active cell layers is on-going, being driven by degradation trends resulting from the subscale testing at full pressurized system operating conditions and at the extremes of stack temperature and high fuel utilization to provide accelerated durability testing to validate the next generation cell technology prior to commencement of the 5,000-hour stack test. Redesigned stack fuel manifold components, to optimize flow distribution through the substrate channels, will be qualified prior to the milestone stack test. Two commissioning tests of the new pressurized stack rig will be performed within the first two quarters of 2010. In addition to the 15 kWe stack test, a six substrate bundle test, at full IGFC system conditions, is planned which will incorporate the latest cell and stack technology advances, including operating at peak single-pass fuel utilization. Development of the cost model required to support an independent audit of the ability to achieve the targeted <$700/kWe SOFC system high volume manufacturing continues.

## FY 2009 Publications/Presentations

**1.** Presentation at 2009 SECA Workshop, Pittsburgh, Pennsylvania, July 14–16, 2009.

## References

**1.** US Patent 7,422,820.

**2.** J. Trembly, R. Gemmen, and D. Bayless, "The Effect of UGFC Warm Gas Cleanup System Conditions on the Gas-Solid Partitioning and Form of Trace Species in Coal Syngas and Their Interactions with SOF Anodes," J. Power Sources, 163 (2) 2007.

**3.** E. Konysheva et. al., "Chromium Poisoning of the Porous Composite Cathode – Effect of Cathode Thickness and Current Density," J. Electrochemical Soc., 154 (12) B1252-B1264 (2007).

**4.** J.B. Young and B. Todd, "Modeling of Multi-Component Gas Flows in Capillaries and Porous Solids," Int'l Journal of Heat and Mass Transfer, 48 5338-5353 (2005).

# II.A.3 Coal Gas-Fueled SOFC Hybrid Power Systems with $CO_2$ Separation

Joseph F. Pierre
Siemens Energy, Inc.
Stationary Fuel Cells
1310 Beulah Road
Pittsburgh, PA 15235
Phone: (412) 256-5313; Fax: (412) 256-2012
E-mail: joseph.pierre@siemens.com

DOE Project Manager: Travis Shultz
Phone: (304) 285-1370
E-mail: Travis.Shultz@netl.doe.gov

Contract Number: 42613

Start Date: October 1, 2005
End Date: September 30, 2009

### FY 2009 Objectives

- Identify and resolve barrier issues relative to the Delta8 cell geometry.
- Complete the end-of-Phase I stack test.
- Continue the evolution and optimization of the Delta8 cell geometry with respect to performance, cost, integrity, and manufacturability.
- Develop process conditions for the manufacturing of 100 cm Delta8 air electrodes which improve quality and cost.
- Develop process conditions for the electrolyte, fuel electrode, and interconnection using plasma spray.
- Increase the power density and power per cell.
- Develop high quality, low cost process for the bundling of Delta8 cells.
- Continue the design of the Advanced Module.
- Manufacture 100 cm Delta8 cells and bundles.
- Design and build end-of-Phase II stack test article (100 cm Delta8 cells).
- Initiate the end-of-Phase II Delta8 stack test (≥25 kWe).
- Update the performance and cost estimate of the baseline power system based on experimental performance data obtained from the end-of-Phase II stack test.

### Accomplishments

- Met or exceeded all Phase I milestones and successfully moved into Phase II.
- Successfully completed the end-of-Phase I Delta8 stack test.
- Achieved or exceeded all end-of-phase stack test performance criteria, including operation for more than 5,000 hrs.
- Demonstrated significantly higher power density and higher power per cell for the Delta8 cell.
- Demonstrated the voltage stability of the Delta8 cells.
- Developed lower cost and scalable manufacturing processes for the Delta8 cell.
- Demonstrated seamless closed end extrusion for Delta8 cells.
- Increased the Delta8 cell length from 75 to 100 cm (active area = 2,570 $cm^2$).
- Manufactured cells and bundles with 100 cm Delta8 cells.
- Continued the development of the Advanced Module concept.
- Validated the stack performance and baseline system performance models based using experimental performance data obtained from the end-of-phase stack test.
- Validated a stack cost that achieves and exceeds the $225/kWe milestone.
- Verified via independent audit that the conceptualized baseline power system meets: the power and electric efficiency goals, the carbon separation goals, and the Phase I cost target.

## Introduction

The Stationary Fuel Cell (SFC) Division of Siemens Energy, Inc. and the U.S. Department of Energy are presently entered into Cooperative Agreement No. DE-FC26-05NT42613, titled SECA Coal-based Systems – Siemens. The overall goal of this project is the development of solid oxide fuel cell (SOFC) cell and stack technology suitable for use in a highly-efficient, economically competitive central station power plant fuel by coal-derived synthesis gas. Siemens will develop a MWe-class SOFC power system to operate on coal-derived synthesis gas and demonstrate operation at greater than 50% electrical efficiency (basis higher heating value [HHV] coal) with greater that 90% $CO_2$ capture. The system will be scalable to sizes greater than 100 MWe output and, when offered in commercial quantities, will have a target cost (at end of Phase III) of $400/kWe including any extraordinary costs of integration to the balance of plant. Corroboration of the technical and economic feasibility of the SOFC power system will be achieved through the conceptual design

of a large (>100 MWe) baseline power plant and the subsequent design, development, fabrication, and test of a proof-of-concept (POC) system. The POC will be representative of the baseline system, have multi-MWe capacity, and demonstrate an electrical efficiency >50% (coal HHV).

The coal-fueled SOFC baseline power system will generate ~128 MWe net alternating current (AC) power at >50% efficiency (net AC/coal HHV) while separating for sequestration 90% of the $CO_2$. A maximum power output of ~170 MWe can be achieved by firing the gas turbine combustor, albeit at an efficiency of <50%. The baseline power system includes an oxygen-blown gasification system selected for its relatively high cold gas efficiency and ability to meet the 90% $CO_2$ separation requirement when coupled in series with a SELEXOL™ $CO_2$ removal process. Oxygen for the coal gasification process will be provided by an ion transport membrane (ITM). The SOFC system incorporates the high power density Delta8 cell configuration. The Delta8 cells are packaged into a pressurized module, rated at approximately 1.2 MWe per module. To achieve the baseline system power rating, the modules are arranged in two banks of 40 modules per bank. Centrally located between the two banks of modules is the gas turbine-generator and heat recovery system. The gas turbine delivers the air oxidant/coolant to the SOFC system and in return receives the high temperature, high pressure SOFC exhaust. During normal operation the gas turbine is not fired. Following expansion, the lower grade heat remaining in the gas turbine exhaust is delivered to a dual pressure heat recovery steam generator. The steam produced herein is supplied to a steam turbine cycle, generating additional electric power.

## Approach

Siemens continuously evaluates, updates, and corroborates the technical and economic feasibility of the baseline power system. As presently configured, the baseline power system meets all Phase I objectives:

- >100 MWe net AC power
- >50% efficiency (net AC/coal HHV)
- A $CO_2$ effluent stream suitable for sequestration and containing 90% of the $CO_2$
- A projected factory cost of $600/kWe (target at end of Phase I)

Thus, Siemens focused effort on the continued optimization of the Delta8 cell, bundle, stack, and module designs, respectively. Analytical modeling was employed to optimize effect of cell height, cell wall thickness, and cell length to determine their collective influence on performance, cost, integrity, and manufacturability. It was expected that the cell length would be increased from 75 cm to 100 cm, resulting in an active area of 2,750 $cm^2$.

In addition to longer cells, further increases in cell power were expected to be achieved by reducing the two dominant voltage loss mechanisms, activation polarization and ohmic resistance. The use of a porous, mixed electronic and ionic conducting interlayer between the cathode and the electrolyte was evaluated in an attempt to reduce the activation polarization at the cathode. A composite interlayer consisting of cathode material (electrocatalyst) and electrolyte material (ionic conductor) was used at the cathode/electrolyte interface. Different combinations of electrocatalyst and ionic conductors were screened to identify a composite that yields maximum power.

The Delta8 cell design lends itself to reduced current path lengths (versus the cylindrical tube geometry) due to the planar cathode and the presence of multiple ribs that serve as current paths. Additionally, by optimizing the plasma spray process for the electrolyte and lowering the electrolyte densification temperature, the presence of insulating phases at the cathode-electrolyte interface can be avoided, thereby reducing the ohmic resistance. Cathode compositions with increased electrical conductivity were evaluated to further increase cell power. Good cell performance over a wide operating temperature (800°-1,000°C) is desirable because the SOFC generator operates with a significant temperature distribution both axially and transversely within the module. An alternate electrolyte which has significantly higher conductivity than the present electrolyte, especially at lower temperatures, was utilized to improve cell performance over a wider temperature range.

With the implementation of the cell power enhancements initiatives mentioned above, the cell performance was improved. Furthermore, Siemens continues to evolve the Delta8 cell manufacturing processes as yield improvements are necessary. Delta8 cell testing was performed at atmospheric and elevated pressure to verify cell voltage stability, cell constituent chemistry, and structural morphology.

The Delta8 stack concept was refined with the emphasis on manufacturability and acceptable cost. The key technical features of the stack design were validated via mathematical analysis and testing of key components and substacks (bundles). Select critical components were optimized, designs refined, analyzed, and bench tested.

A major objective of Phase II was a 1,500-hr test of a Delta8 cell stack with a rating of greater than 25 kWe. Siemens manufactured the Delta8 cells, assembled the bundles and test article, and constructed a test facility. The end-of-phase stack test was initiated.

The baseline power system performance analysis and cost estimate, respectively, were updated and revised

based on cell performance data obtained from the end-of-Phase I stack test.

## Results

The end-of-Phase I stack test successfully achieved more than 5,300 hrs of operation. The POC Delta8 system (POCD8R0) tested was comprised of two main subassemblies, the SOFC module and the balance of plant (BOP). The module contained cell stack, recuperative air preheater, prereformer, and external insulation. The fuel cell stack, shown in Figure 1, consisted of 24 75 cm active length (1,950 $cm^2$ active area) Delta8 cells arranged in an array of four bundles, with each bundle containing six Delta8 cells. The BOP contained the electrical load, fuel and air delivery systems, and control hardware.

The stack test met or exceeded all the performance criteria. It achieved a maximum power of ~10 kWe. Fueled by simulated coal-derived synthesis gas the system operated in a thermally self-sustaining mode for more than 5,300 hrs and displayed no detectable voltage degradation. Operation was marked by seven open circuit conditions, caused by BOP and/or control issues. Despite the interruptions, the test demonstrated an availability factor of 85% at 50% power or greater. An operational summary of the end-of-Phase I stack test is shown in Figure 2.

Cell manufacturing process parameters were developed, qualified, and subsequently employed to manufacture 100 cm active length (representing

**FIGURE 1.** Delta8 Cell Stack

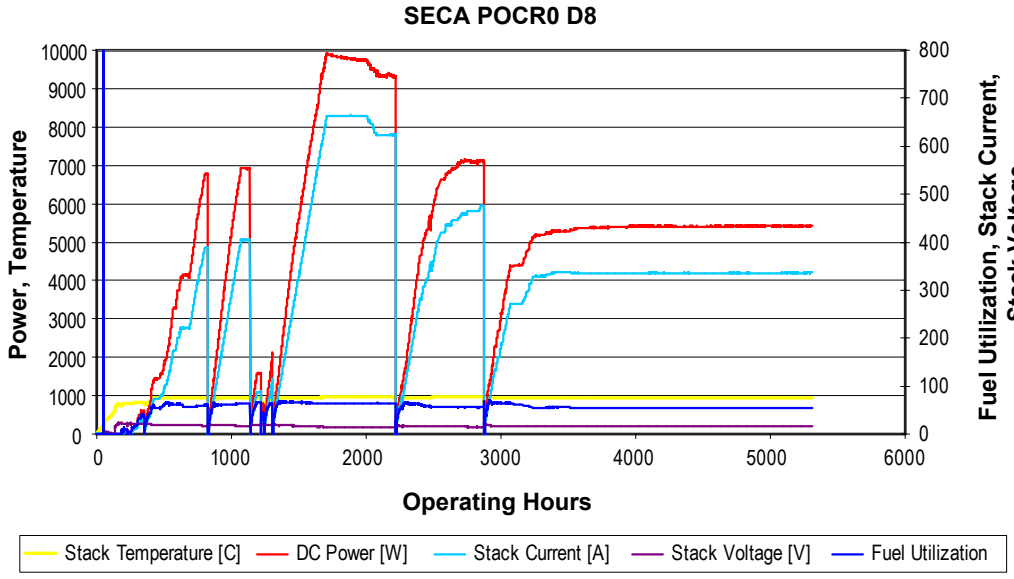


**FIGURE 2.** Operating History of the End-of-Phase I Stack Test

an active area of 2,570 $cm^2$) Delta8 cells. The cell manufacturing emphasis has shifted from 75 cm active length cells to 100 cm active length cells. Bundles, incorporating eight Delta8 cells have been fabricated and will be tested in a 25 kWe-class Delta8 cell stack test during Phase II.

The increased active length (to 100 cm from 75 cm) coupled with additional advancements in cell manufacturing processes, materials, and design enhancements resulted in significantly higher power per cell and higher power density. Figure 3 illustrates the increase in surface area and the power enhancement achieved. Compared to the standard cylindrical SOFC, the 100 cm Delta8 cell is projected to produce approximately 6.5 times the power with only three times the active area. Extrapolating this performance to an eight-cell Delta8 bundle, Figure 4, results in 120% increase in bundle power and a 5% reduction in weight compared to a 24-cell 150 cm active length cylindrical SOFC bundle.

Additional cell development activities are focused on lowering the electrolyte densification temperature and reducing the electrolyte thickness. Preliminary results are encouraging as a 50% power enhancement in cylindrical cells was measured via single cell testing.

The reference baseline pressurized integrated gasification SOFC (IGSOFC) power system will generate ~128 MWe at 50% efficiency (net AC/coal HHV), have a maximum-power capacity of ~170 MWe, and satisfy the 90% $CO_2$ separation requirement. The baseline plant closely approaches the end-of-Phase I cost target of $600/kWe (2002$). The reference power system cycle is illustrated schematically in Figure 5. The main systems in the baseline IGSOFC power system include the pressurized SOFC power block, an oxygen-blown transport gasifier, an ITM oxygen system, a Siemens SGT-800 industrial gas turbine, a commercially-available SELEXOL™ gas clean-up system, and a steam turbine system. The power and electrical performance estimates are presented in Table 1. Two operating scenarios are presented, a high efficiency case and a high power case. The high efficiency case produces approximately 128 MWe net AC at an efficiency of ~51%. The alternative high power case generates maximum net AC albeit at a reduced efficiency of approximately 49%. The SOFC performance basis was validated using experimental performance obtained from the end-of-Phase I stack test. The conceptual-level cost estimate excludes the cost of the coal gasification system, synthesis gas clean-up, $CO_2$ separation and isolation systems, step-up transformer, and AC grid connection switchgear. Cost forecasts were made for production volume of three systems per year in an automated factory and a volume of 25 systems. Adjusted to 2002$ this yielded a cost of ~$600/kWe (based on the high power scenario) for an IGSOFC power system producing 128 MWe net AC at high efficiency operation and capable of producing ~168 MWe net AC at high power operation. An alternate concept was evaluated that was based on the same quantity of fuel cells, but used additional gas turbine generators to allow operation of the fuel cells at higher current densities and additional heat recovery steam generators and steam turbine capacity to handle the increased heat load. The adjusted cost was calculated based on the new total cost that accounted for the additional BOP components. This produced a cost of ~$413/kWe (2002$) from a system

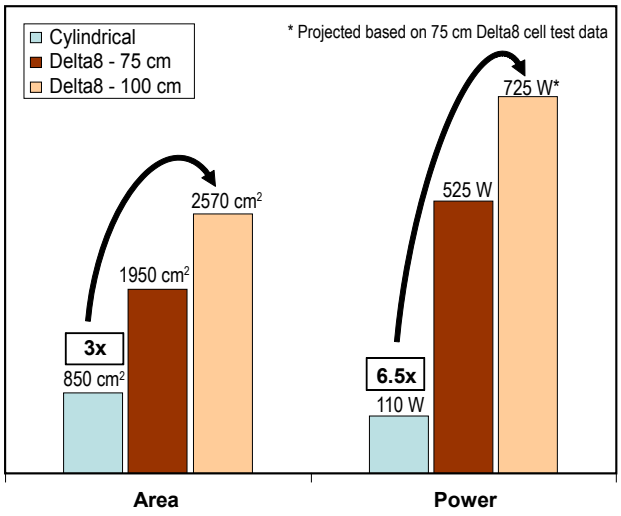


**FIGURE 3.** Cell Performance Comparison

| 24 cylindrical cells | 8, 100 cm Delta8 cells |
|---|---|
| DC power: 2.6 kWe | DC power: 5.8 kWe* |
| Weight: 34 kg | Weight: 32 kg |

* Projected based on 75 cm Delta8 cell test data

**FIGURE 4.** Bundle Performance Comparison

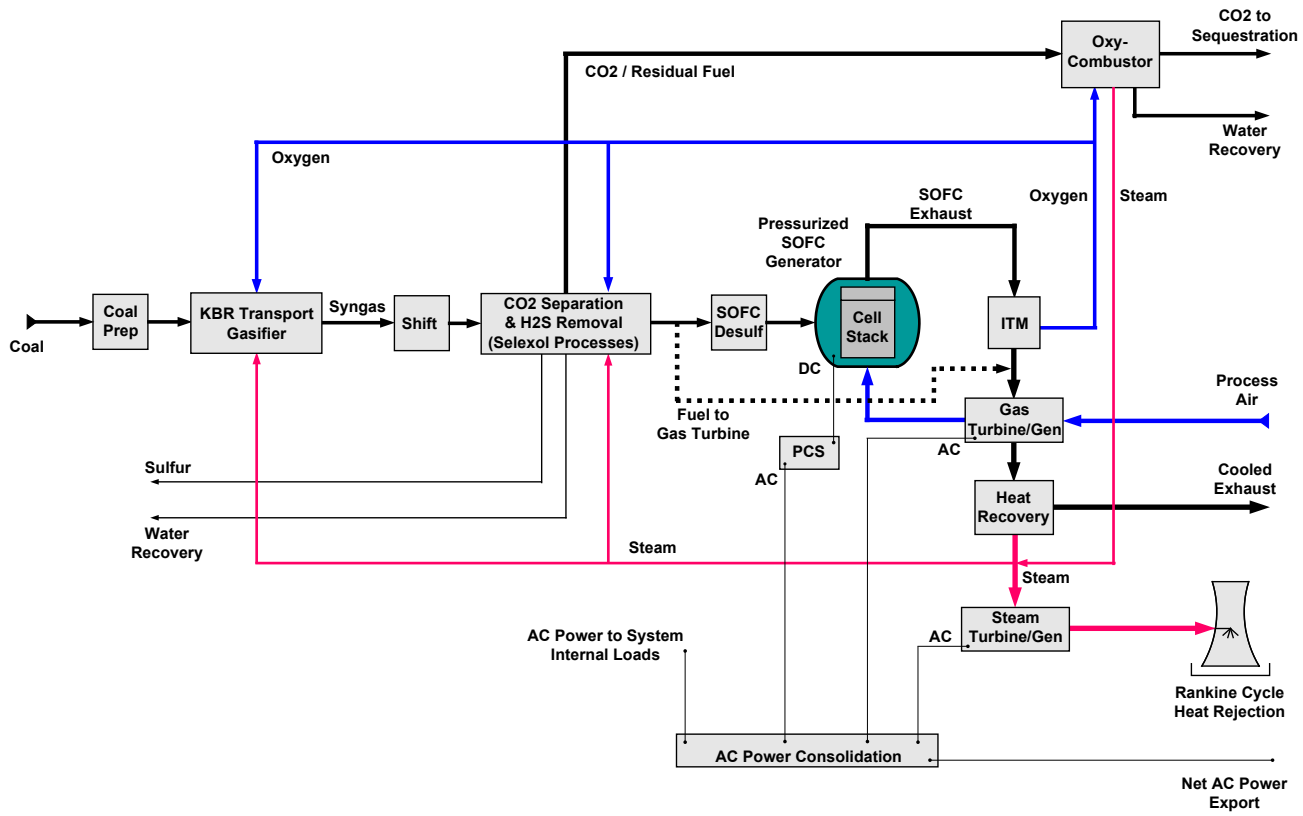


**FIGURE 5.** Reference Baseline IGSOFC Power System with $CO_2$ Separation

**TABLE 1.** Baseline System Performance Analysis

| | High Efficiency | High Power |
|---|---|---|
| Coal Energy Input (HHV), MW | 251.4 | 341.4 |
| Turbine Inlet Temperature, C | 877 | 1,200 |
| AC Power Generated, MWe | | |
| Gross SOFC AC Power, MWe | 100.4 | 100.4 |
| Gas Turbine AC Power, MWe | 26.1 | 53.6 |
| Steam Turbine AC Power, MWe | 7.5 | 21.4 |
| Gross AC Power Generated, MWe | 134.0 | 175.4 |
| Parasitic AC Power, Mwe | | |
| I&C Allowance | 0.25 | 0.45 |
| Feed/Condensate Pumps | 0.3 | 0.7 |
| OxyCombustor $O_2$ Compressor AC Power | 0.04 | 0.1 |
| Gasifier $O_2$ Compressor AC Power | 2.8 | 3.8 |
| Selexol Process AC Power | 2.5 | 3.4 |
| Other Gasifier AC Power | 0.2 | 0.3 |
| Total Parasitic AC Power, MWe | 6.1 | 8.8 |
| Net AC Power Generated, MWe | 127.9 | 166.6 |
| Net AC Efficiency (Coal HHV), % | 50.9 | 48.8 |

I&C - instrumentation & controls

producing ~350 MWe net AC with an efficiency of ~45%. Performance and cost estimates were reviewed and validated by an independent DOE-approved auditor.

## Conclusions

The end-of-Phase I Stack test requirements were satisfied as demonstrated by the 10 kWe POCD8R0 stack test that accumulated more than 5,300 hrs of operation with no detectable voltage degradation. The active length of the Delta8 SOFC has been increased to 100 cm with an active area 2,570 $cm^2$. The increased active area coupled with cell performance enhancements have increased the power per Delta8 cell to a projected 725 W/cell. Based on existing cell and stack testing, systems analysis indicate the performance, $CO_2$ separation, and cost targets, respectively, for the baseline IGSOFC power system can be achieved. SFC expects to exceed the performance and cost targets via the implementation of advanced cell materials and manufacturing processes, and improvements in SOFC module and BOP component technologies.

# II.A.4 SECA Coal-Based Systems - UTC Power

David D. Brengel (Primary Contact),
Gary Blake (Delphi), Larry Chick (Delphi),
John Ferro (Project Director),
Karl Haltiner (Delphi), Toby Junker (UTRC),
Subhasish Mukerjee (Delphi), Ellen Sun (UTRC)
UTC Power
195 Governors Highway
South Windsor, CT 06074
Phone: (860) 727-2478; Fax: (860) 353-4135
E-mail: david.brengel@utcpower.com

DOE Project Manager: Travis Shultz
Phone: (304) 285-1370
E-mail: Travis.Shultz@netl.doe.gov

Subcontractors:
- Delphi, West Henrietta, NY
- United Technologies Research Center (UTRC), East Hartford, CT
- Battelle/Pacific Northwest National Laboratory, Richland, WA

Contract Number: NT0003894

Start Date: October 1, 2008
End Date: September 30, 2010

## FY 2009 Objectives

- Scale up cell area to a size suitable for use in a 25 to 50 kW stack.
- Modify an existing manufacturing facility to enable construction of large area single cells.
- Assemble large area cells into 25 to 50 kW stacks for use in Phase I of the project.
- Receive a 25 to 50 kW stack from Delphi for verification testing.
- Develop a durable cathode, anode and electrolyte with increased tolerance to low levels of sulfur and other contaminates in the fuel gas.
- Develop improved cell fabrication techniques leading to lower cell/stack costs in high production.
- Fabricate and test a large number of cells, varying in size, to ensure consistency of size and performance from cell-to-cell.
- Evaluate coated alloys for the fabrication of cost-effective stack components via long-term oxidation, rapid thermal cycling, and area-specific electric resistance (ASR) measurement as well as detailed material characterization.
- Develop and evaluate self healing glass seal concepts and materials.
- Develop and optimize coating material composition and coating processes for multiple components in the stack with a focus on meeting durability and cost requirements.
- Complete conceptual and detailed designs of a test stand capable of testing a stack up to 50 kW.
- Initiate construction of the test stand capable of testing a stack up to 50 kW.
- Develop preliminary design of a 250-1,000 kW solid oxide fuel cell (SOFC) power module operating on either pre-reformed natural gas or coal syngas.
- Develop conceptual design of a >100 MW baseload SOFC power plant operating on coal syngas with a target efficiency of 50 percent (higher heating value [HHV]) that separates greater than 90 percent of the carbon in the coal feedstock.

## Accomplishments

- Fabricated multiple cells with 400 $cm^2$ active area for the Generation 4 stack.
- Demonstrated an average voltage of 0.85 volts per cell at a 570 mA/$cm^2$ current density for a 30-cell Generation 3.2 stack on 48.5% $H_2$, 3% $H_2O$, rest $N_2$ fuel at 750°C.
- Demonstrated a cassette-to-cassette voltage variation of 0.03 volts at a 570 mA/$cm^2$ current density for a 30-cell Generation 3.2 stack on 48.5% $H_2$, 3% $H_2O$, rest $N_2$ fuel.
- Demonstrated power densities equal to or greater than 450 mW/$cm^2$ at fuel utilizations up to 80 percent for a 30-cell Generation 3.2 stack on 48.5% $H_2$, 3% $H_2O$, rest $N_2$ fuel.
- Acquired a new facility in Fenton, Michigan for cell development and manufacturing development.
- Installed new equipment and test stands in the Rochester, New York facility for stack development and testing to meet Solid State Energy Conversion Alliance (SECA) targets.
- Completed long-term oxidation tests, thermal cycling tests, ASR measurements and post-test characterization of $(MnCo)_3O_4$ (MCO) spinel coated Crofer 22 APU, Pleasee ITM and Haynes 230 alloys.
- Completed characterization and thermal cycling tests of two self healing glass seal material candidates. Both candidates exhibited self healing behavior.
- Demonstrated a cost-effective aluminizing process and MCO coating process suitable for complex shaped stack components at the coupon level.
- Completed the conceptual design of a test stand capable of testing a stack up to 50 kW.

- Completed the conceptual design of a 400 kW power module operating on syngas and achieving an efficiency of 55 percent (lower heating value [LHV]).
- Completed conceptual designs of three integrated gasification fuel cell (IGFC) systems meeting the desired efficiency and carbon separation targets: an atmospheric SOFC/steam turbine (ST) cycle; an atmospheric SOFC/gas turbine (GT)/ST cycle; and a pressurized SOFC/GT/ST cycle.

## Introduction

UTC Power is a world leader in developing and producing fuel cells that generate energy for buildings and for transportation, space and defense applications. UTC Power has recently developed and begun shipments of its newest generation fuel cell system for the commercial combined heat and power (CHP) market. Delphi has been developing SOFC systems since 1999. After demonstrating its first generation SOFC power system in 2001, Delphi teamed with Battelle under the SECA program to improve the basic cell and stack technology, while Delphi developed the system integration, system packaging and assembly.

In addition to its high power density, another key advantage of the SOFC is its high system efficiency, particularly when its high temperature co-product heat can be used in combination with its electrical output. For example, the addition of a bottoming cycle with a steam turbine-generator can increase the overall efficiency to greater than 50 percent, significantly higher than the 35-40 percent efficiency for a typical coal-fired power plant.

UTC Power is developing conceptual process designs of a wide range of power systems ranging from 250 kW up to 100+ MW with a focus on meeting the system efficiency and carbon separation targets specified in the SECA minimum requirements. Designs for a sub-MW system for distributed power generation and a 5 MW proof-of-concept system will be developed, as well as a conceptual design and costing for a baseload power plant that separates greater than 90 percent of the carbon from the coal feedstock at an efficiency of 50 percent (HHV). In support of the design of a 250-1,000 kW SOFC power module, UTC Power will develop and build a test stand capable of testing a stack up to 50 kW, and will subsequently test a >25 kW Delphi stack for at least 1,500 hours in Phase I on a simulated coal syngas.

United Technologies Research Center (UTRC) is developing stack materials and processes in support of the stack development effort led by Delphi. UTRC is focusing on key technical challenges for stack scale-up and durability, including the evaluation of coated alloys, the development and evaluation of advanced seal concepts and materials, and the development of coating materials and processes for multiple stack components.

## Approach

Delphi utilized a staged approach to develop a modular SOFC system for a range of fuels and applications. Major subsystems and individual components were developed and tested as building blocks for applications in targeted markets. These were then integrated into a "close-coupled" architecture for integrated bench testing, as well as a stationary power unit and an auxiliary power unit for the stationary and transportation markets, respectively.

UTC Power is using first principles-based models developed from performance data to prepare mass and energy balances (M&EBs) and to predict the performance of the concept designs. Results from the M&EBs are used for trade studies, component sizing and costing. To design highly efficient SOFC/GT hybrid systems, UTC Power is working closely with Pratt & Whitney to establish turbine performance models. Using these models, both atmospheric and pressurized SOFC designs are being developed. Final designs are selected to meet the desired cost and performance targets.

UTC Power is using a well-defined work process with multiple, gated reviews to develop the 50 kW test stand from the conceptual design phase through the readiness phase, with an emphasis on reliability and simplicity. Key challenges include ensuring chromia is properly mitigated and unintended shutdowns are minimized during the duration of the stack test.

UTRC is conducting long-term oxidation, rapid thermal cycling, and ASR measurements for coated alloy evaluation, utilizing advanced material characterization techniques including high resolution transmission electron microscopy and focused ion beam. Seal performance is evaluated via thermal cycling tests. Coating processes are being developed with an emphasis on both performance and cost, optimized at the coupon level and scaled up for stack components.

## Results

The SECA Coal-Based Systems (CBS) project is a continuation of the core hardware development activities begun in the SECA Cost Reduction project. The efforts in SECA CBS are more application-driven as Delphi and UTC Power move this technology closer to pilot and production releases. The SECA CBS program will support and address the development of fuel cells for central generation applications. This market has unique demands, and development tasks must address specific issues that are economic drivers of the design and application.

Stack design efforts have focused on optimizing the current design and adding features such as a cassette containing thermocouples in the center of the stack to get better temperature feedback. Development also focused on investigating different concepts for scaling up the active area footprint. Work on stack models has focused on developing algorithms that describe the current-voltage (I-V) response of an SOFC cell at a particular temperature and fuel composition. Such algorithms are essential to detailed stack models, such as the MARC-SECA code, which are used to predict the temperature, current, gas composition and, indirectly, the mechanical stress distributions within a large-scale, multi-cell stack. The algorithm is used by the model to predict the I-V response of each localized node within the mesh based on the local temperature and local anode gas composition. The cathode gas composition could also have a significant effect on the I-V response if the cathode air is allowed to become appreciably depleted in oxygen.

Delphi continues to make progress with improved cell fabrication techniques by focusing on material and process improvements. Battelle Pacific Northwest Division and Delphi continue to partner in the area of cathode powder and paste development to develop cell material sets that lead to improved electrochemical performance while being robust to potential failures such as cathode layer delamination. Delphi continues to work closely with commercial suppliers of production materials to develop a consistent supply of production grade material and optimize the material properties to provide robust performance in the SOFC stack and ultimately the fuel cell system. Figure 1 shows an I-V curve from a typical 30-cell stack on 48.5% $H_2$, 3% $H_2O$, rest $N_2$ fuel at 750°C. The data shows an average voltage of 0.85 volts per cell at 570 mA/cm$^2$ of current density.

The principles of the Delphi Manufacturing System Design are being applied to develop control and quality standards for each step of the manufacturing process. By focusing efforts in these areas early in the development process, Delphi has been able to scale up the fabrication process to mass quantities while maintaining the highest quality standards. Figure 2 shows a cassette-to-cassette voltage variation of 0.03 volts at a 570 mA/cm² current density for a 30-cell Generation 3.2 stack on 48.5% $H_2$, 3% $H_2O$, rest $N_2$ fuel.

UTC Power has developed a library of models for simple-cycle SOFC power plants and used them to model a previously designed power plant concept (Figure 3). The power plant desulfurizes natural gas and pre-reforms hydrocarbons higher than methane to eliminate the risk of carbon formation in the stack. Anode recycle provides water to the steam reformer and ensures a high system efficiency of greater than 55 percent (LHV). To date, conceptual designs of three IGFC systems meeting the desired efficiency and carbon separation targets have been completed. UTC Power also successfully completed the conceptual design phase review for the 50 kW test stand and moved into the preliminary design phase.

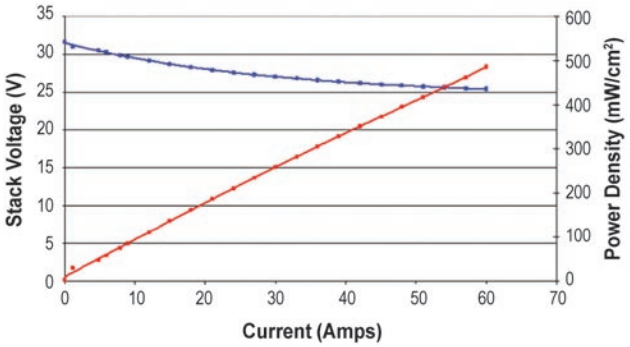


**FIGURE 1.** Generation 3.2 30-Cell Stack Performance (I-V Curves)

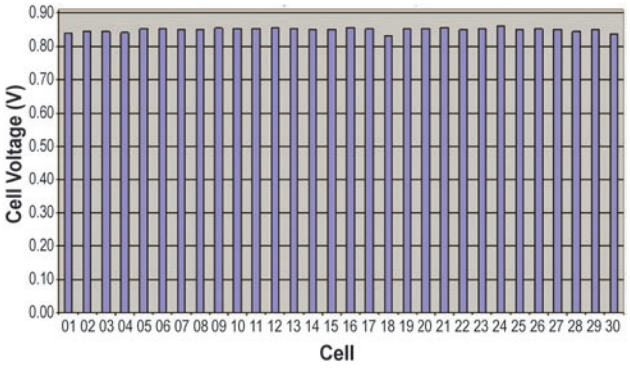


**FIGURE 2.** Generation 3.2 30-Cell Stack Performance (Stack Cell Voltages for Polarization)

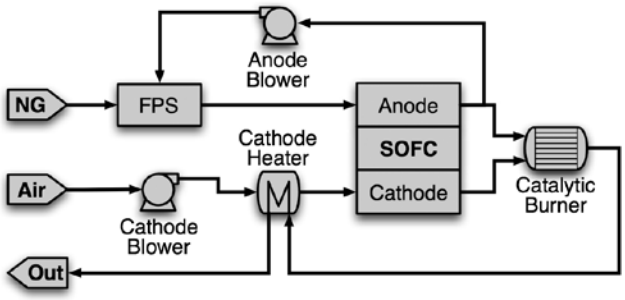


**FIGURE 3.** Process flow diagram of conceptual 400 kW NG-fueled SOFC power module. In the fuel processing system (FPS), NG is desulfurized and pre-reformed. Anode recycle provides water to the pre-reformer and ensures high plant efficiency.

UTRC has characterized the effectiveness of MCO for both ferritic stainless steels and Ni-based superalloys. MCO is effective in improving oxidation resistance of ferritic stainless steels, but does not influence oxidation

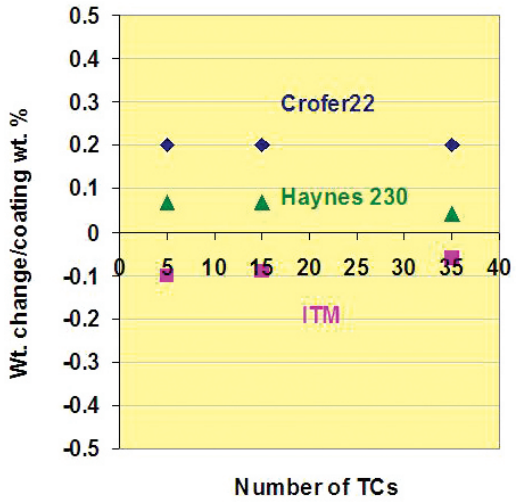


**FIGURE 4.** MCO Adherence on Alloy Coupons Were Validated Via Rapid Thermal Cycling Tests (TCs)

behavior of Ni-based superalloys such as Haynes 230. MCO adheres well to the alloy substrates during rapid thermal cycling tests using a "drop bottom" furnace and no coating spallation has been observed (Figure 4). Glass candidates consistently exhibit self-healing behavior at temperatures above 300°C. Thin uniform MCO and aluminide coatings have been obtained on coupons and processes are being scaled up for stack components.

## Conclusions and Future Directions

SECA CBS is focused on the stationary markets, with Delphi leading the development of the stack for a coal syngas based MW-scale power module. Product and process improvements were initiated for the current stack design, and for the development of the next generation stack design. Development of the large active area footprint stack will continue for stationary applications.

The present sub-MW power module design meets all design specifications. Current and future work efforts are directed at developing a packaged system design with improved reliability and cost. Study of the IGFC systems shows that the GT-based hybrid systems have superior performance compared to systems employing only a steam bottoming cycle. In Fiscal Year 2010, a 5 MW proof-of-concept power plant will be designed based on the selected IGFC system (>100 MW) that meets the $700/kW (2007 U.S. dollar) power block cost target. The test of a >25 kW Delphi stack for at least 1,500 hours in Phase I on a simulated coal syngas will serve to validate the models used to design the 250-1,000 kW SOFC power module.

MCO is effective in both containing chromia and improving oxidation resistance for stainless steels. MCO coating applied at UTRC adheres well to alloy substrates during thermal cycling. Two material candidates have been identified as self healing glass seals. Progress has been made in developing cost effective coating processes. Areas warranting continuation during FY 2009 include evaluation of coated stack components, evaluation of self healing glass seals and validation of coating processes via stack testing, and optimization of self healing glass seals to minimize interaction between glass and the metal frame alloys.

## FY 2009 Publications/Presentations

**1.** "Evaluation of Protective Coatings on Nickel Based Superalloy and Ferritic Stainless Steels for SOFC Interconnect Applications," Oral Presentation at the 6th International Symposium of Solid Oxide Fuel Cells (SOFC): Materials, Science, and Technology, American Ceramic Society, Daytona, Florida, January 18–23, 2009.

# II. SECA INDUSTRY TEAMS
## B. Cost Reduction

# II.B.1 Solid State Energy Conversion Alliance Delphi SOFC


Steven Shaffer (Primary Contact),
Gary Blake, Sean Kelly, Karl Haltiner,
Subhasish Mukerjee, David Schumann,
Gail Geiger, Larry Chick, Ellen Sun
Delphi Automotive Systems LLC
5725 Delphi Drive
Troy, MI 48098
Phone: (585) 359-6615; Fax: (585) 359-6061
E-mail: steven.shaffer@delphi.com

DOE Project Manager: Maria Reidpath
Phone: (304) 285-4140
E-mail: Maria.Reidpath@netl.doe.gov

Subcontractors:
- Battelle/Pacific Northwest National Laboratory, Richland, WA
- Electricore, Inc., Valencia, CA
- United Technologies Research Center, East Hartford, CT



Contract Number: 41246

Start Date: July 1, 2002
End Date: December 31, 2011


## Objectives

- Develop and test major subsystems and individual components as building blocks for applications in targeted markets of heavy-duty truck and military.
- Develop a 3-5 kW auxiliary power unit (APU) for heavy-duty trucks and military power applications (Figure 1).
- Develop system modeling and cell evaluation for high efficiency coal-based solid oxide fuel cell (SOFC) gas turbine hybrid system.


**FIGURE 1.** Next Generation SOFC System

## Accomplishments

- Successfully demonstrated the diesel-fueled SOFC APU on Class 8 truck at several customer locations.
- Continued development of thermal cycle capability on a natural gas-powered and diesel-fueled SOFC systems.
- Completed integration and test of a diesel-fueled SOFC system to support a heavy-duty commercial vehicle application including SOFC system, 12 V direct current (DC)/DC converter, lead-acid battery and software and controls.
- Designed and procured a heavy-duty vehicle application development chassis.
- Developed and analyzed system mechanizations for both SPU 1 and DPS3000D diesel systems.
- Developed a novel heat exchanger that allows for cooling of the reformate stream with the cathode air feed stream to the stack.
- Performed system analysis on both SPU 1E (present) and DPS3000 (future) diesel SOFC systems.
- Completed power architecture and electronics design.
- Successfully completed Solid State Energy Conversion Alliance (SECA) Core Technology Program collaboration between Delphi and Virginia Tech.
- Progress was made in the development of Delphi's next-generation diesel SOFC APU design, including stack, reformer, heat exchangers, and desulfurizer designs.
- Delphi is developing a larger footprint repeating unit design which is a developmental platform for the Generation 4 concept. Initial design and analysis for this design is complete and parts are being fabricated for the stack build.
- Development has continued on the partial oxidation reformers and endothermic reformer designs. The next generation endothermic reformer for use in the heavy-duty truck application is also being finalized.
- Development of the various next generation components for the diesel-fueled SOFC APU has continued, and development of liquid diesel fuel desulfurization was completed.
- United Technologies Research Center has concluded the development effort that started in August 2006, as part of Delphi's SECA project, to investigate SOFC system configurations utilizing coal gas and develop stack technologies for MW-scale power generation.

## Introduction

Delphi has been developing SOFC systems since 1999. After demonstrating its first generation SOFC power system in 2001, Delphi teamed with Battelle under the SECA program to improve the basic cell and stack technology, while Delphi developed the system integration, system packaging and assembly, heat exchanger, fuel reformer, and power conditioning and control electronics, along with other component technologies. Compared to its first generation system in 2001, the Delphi-led team has reduced system volume and mass by 75 percent. By January 2005, the Delphi team was able to demonstrate test cells with power density more than required to meet the SECA 2011 goals.

In addition to its compactness, another key advantage of the SOFC is its high system fuel efficiency, particularly when its high temperature co-product heat can be used in combination with its electrical output. For example, SOFCs can be teamed with gas turbines driven by the SOFC's co-product heat to potentially generate power at 55 percent to 80 percent thermal efficiency (depending on scale and fuel used). This is significantly more efficient than today's typical coal-fueled power plant thermal efficiency of 35 percent to 40 percent. By co-generating power on-site at industrial facilities, commercial businesses, or even residences, the SOFC's high-grade co-product heat will enable up to 90 percent efficiency in distributed, combined heat and electrical power generation. Similarly, heavy-duty trucks will be able to utilize SOFC auxiliary power systems for both heat and electrical power when parked, to save 85 percent of the fuel that today they consume when idling their main engine, and likewise reduce idling emissions.

While size and efficiency advantages are important for many potential applications, the SOFC's most significant advantage overall is its very broad applicability due to its inherent fuel-flexibility. With relatively small changes, SOFC systems can potentially operate on a full range of conventional and alternative fuels. This includes natural gas and conventional petroleum-based fuels like low-sulfur gasoline, diesel and propane; high-sulfur military fuels like JP-8 and jet fuel; low-$CO_2$ renewable fuels from biomass like ethanol, methanol and bio-diesel; synthetic fuels from coal and natural gas; and non-hydrocarbon fuels such as hydrogen and ammonia. This will be critical for future development to make SOFC scalable for large coal gas power plants.

## Approach

Delphi utilized a staged approach to develop a modular SOFC system for a range of fuels and applications including:

- Develop and test major subsystems and individual components as building blocks for applications in targeted markets.
- Integrate major subsystems and individual components into a "close-coupled" architecture for integrated bench testing.
- Integrate major subsystems and individual components into a stationary power unit (SPU) for the stationary market.
- Integrate major subsystems and individual components into an APU for the transportation market.
- Demonstrate large-scale hybrid stack module using simulated coal gas.

## Results

SECA Phase II is a continuation of the core hardware development activities begun in Phase I. The systems efforts in Phase II are more application-driven as Delphi moves this technology closer to pilot and production releases. The Phase II project will support and address two market opportunities. The stationary market and the transportation market have unique demands, and development tasks must address specific values that are economic drivers of the design and application.

For SECA Phase II, Delphi is aggressively pursuing performance targets which drive SOFC stack, subsystem performance, and cost reduction. Delphi is also utilizing technical progress and market research to focus effort on development of a diesel commercial vehicle SOFC APU. In the first half of SECA Phase II, emphasis has been placed on achieving Phase II performance metrics on natural gas. Progress has been made toward Phase II system targets: specifically, thermal cycling and power degradation rate. Current results on natural gas stationary systems are on target. Reduced efficiency and power, and increased degradation rate is anticipated when using diesel fuel. This is due in part to reduced efficiency and stack thermal management capability between internal reforming (natural gas) and catalytic partial oxidation/endothermic reforming (diesel).

Stack design efforts have focused on optimizing the current design and adding features such as a cassette containing thermocouples in the center of the stack to get better temperature feedback. Development also focused on investigating different concepts for scaling up the active area footprint. Work on stack models

has focused on developing algorithms that describe the current-voltage (I-V) response of an SOFC cell at a particular temperature and fuel composition. Such algorithms are essential to detailed stack models, such as the MARC-SECA code, which are used to predict the temperature, current, gas composition and, indirectly, the mechanical stress distributions within a large-scale, multi-cell stack. The algorithm is used by the model to predict the I-V response of each localized node within the mesh based on the local temperature and local anode gas composition. The cathode gas composition could also have a significant effect on the I-V response if the cathode air is allowed to become appreciably depleted in oxygen.

Delphi continues to make progress with improved cell fabrication techniques by focusing on material and process improvements. Battelle Pacific Northwest Division and Delphi continue to partner in the area of cathode powder and paste development to develop cell material sets that lead to improved electrochemical performance while being robust to potential failures such as cathode layer delamination. Delphi continues to work closely with commercial suppliers of production materials to develop a consistent supply of production grade material and optimize the material properties to provide robust performance in the SOFC stack and ultimately the fuel cell system. The principles of the Delphi Manufacturing System Design are being applied to develop control and quality standards for each step of the manufacturing process. By focusing efforts in these areas early in the development process, Delphi will be able to scale-up the fabrication process to mass quantities while maintaining the highest quality standards.

A platinum-based mixed-metal oxide catalyst formulation was found to be very effective for natural gas hydrogenolysis. This formulation reduced ethane and propane content to almost undetectable levels and provided similar levels of performance as previously tested Rh-based catalysts, but at different operating conditions. Some supplier catalysts can match the performance of the best internally developed benchmark catalysts. The use of honeycomb substrates at higher cell counts results in better performing catalysts for partial oxidation reactions while foam substrates are not useful for partial oxidation. A novel FeCrAlY-based thick wall honeycomb monolith was prepared which may be useful for chemical reactions requiring significant heat input.

Development of balance of plant components continued with the main efforts focused on sourcing process air blowers and new recycle pumps for the next generation system. A new set of requirements for a 12 VDC air pump were created. A sourcing study was completed and R&D Dynamics of Bloomfield, Connecticut was selected as a supplier. Their proposal includes the use of air foil bearings and claims a service life of over 100,000 hours with greater than 30,000 start/stop cycles. The delivery of the first units was completed in early 2008, with later integration into a diesel-fueled SOFC APU enclosure.

## Conclusions

- SECA Phase II is focused on two markets, stationary and transportation, with additional emphasis on developing the system and stack requirements for a coal gas-based MW-scale hybrid power system.
- Product and process improvements were initiated for the current stack design with the initial requirements and development for the next generation stack design.
- Initiated and developed a tubular diesel endothermic reformer. In addition, developed a natural gas cracking reactor.
- Customer demonstrations on Class 8 heavy-duty trucks using low sulfur diesel fuel in our current generation SOFC power plant have been completed.

## Future Directions

The project is currently on hold.

## FY 2009 Publications/Presentations

1. January 2008: SOFC Technology R&D Needs; Golden, Colorado: FUEL CELL DEVELOPMENT: DOE PRE-SOLICITATION WORKSHOP Steven Shaffer, Delphi Corporation

# III. SECA CORE RESEARCH & DEVELOPMENT

## A. Cathodes

# III.A.1 Synchrotron X-Ray Studies of SOFC Cathodes

P.H. Fuoss (Primary Contact), J.A. Eastman, T.T. Fister, D.D. Fong, K.-C. Chang, H. You
Argonne National Laboratory (ANL)
9700 S. Cass Ave.
Argonne, IL 60439
Phone: (630) 252-3289; Fax: (630) 252-7777
E-mail: fuoss@anl.gov

DOE Project Manager: Briggs White
Phone: (304) 285-5437
E-mail: Briggs.White@netl.doe.gov

Contract Number: 49071

Start Date: June 2007
End Date: May 2010

### FY 2009 Objectives

- Determine the structure of, and composition gradients in $La_{1-x}Sr_xMnO_3$ (LSM), $La_{1-x}Sr_xCoO_3$ (LSC) and $La_{1-x}Sr_xCo_{1-y}FeO_3$ (LSCF) thin films as a function of oxygen partial pressure and temperature.
- Study the chemical and atomic structure of LSM, LSC and LSCF thin film cathodes on yttria-stabilized zirconia (YSZ) electrolytes in a solid oxide fuel cell (SOFC) half-cell configuration as functions of operating temperature and electrochemical potential.
- Correlate the in situ measurements of the first and second bullets with ex situ measurements.
- Integrate the electrochemical measurements into the controlled environment system.
- Study the operation of the cathode side of a fuel cell and correlate the structure and chemical state with those determined by ex situ measurements from the literature and supplemental measurements performed at ANL, Carnegie Mellon University, and the Massachusetts Institute of Technology.

### Accomplishments

- Determined trends for strontium surface segregation in LSM, LSC and LSCF as a function of temperature and oxygen partial pressure.
- Constructed an integrated electrochemical and X-ray analysis system with controlled temperature and gas environment (e.g. controlled oxygen partial pressure).
- Demonstrated the utility of resonant X-ray scattering techniques and inelastic X-ray measurements for probing the chemical state of materials under conditions approximating those of operating SOFCs.
- Completed X-ray scattering and spectroscopy experiments comparing LSM(011) on YSZ(111) that were electrochemically conditioned in situ and ex situ. Ex situ conditioned samples were found to be more electrochemically stable when subject to the same applied potential for further experiments.
- Demonstrated that surface Sr segregation on LSM(011) on YSZ(111) is dependent on the distance from the contract wires under cathodic potential. Sr was found to segregate in areas of the LSM thin film that is less active under potential.
- Found that LSC (011) without a GdC buffer layer reacts with YSZ(111) forming a resistive layer. LSC(001) on a GdC(001) buffer film was found to decompose if the GdC film is less than 60 nm thick.

## Introduction

The performance of SOFCs is strongly influenced by the nanoscale structure and chemistry of electrode materials under operating conditions. However, because SOFCs are operated at elevated temperatures and at near-atmospheric pressure, the utilization of traditional surface science techniques, which typically involve vacuum conditions near room temperature, requires validation. The studies being performed in this program provide the needed understanding of in situ-ex situ correlations. The results also enable the development of molecular-level models for stimulating the rational design and development of high-performance cathode materials.

## Approach

We employ in situ X-ray scattering and spectroscopy technologies developed at ANL to both measure equilibrium structures of SOFC cathode materials at elevated temperatures and controlled oxygen partial pressures, and to examine the dynamic structural changes that occur at the cathode side of a fuel cell under conditions that simulate actual operating conditions. This work is performed in collaboration with P. Salvador's group at Carnegie Mellon University, which grows the sample materials with pulsed laser deposition, and B. Yildiz's group at the Massachusetts Institute of Technology which uses scanning tunneling microscopy and scanning tunneling spectroscopy to develop spatial images of electronic, topological, and electrochemical properties of cathode materials.

## Results

### Equilibrium Structures in Active Atmospheres

By controlling the penetration of the incident X-ray beam by its incident angle, we are able to depth profile the composition of thin films at high temperature (25-900°C) and variable $pO_2$ (0.05-150 Torr) using total reflection X-ray fluorescence and X-ray scattering techniques. Building from last year's study of strontium surface segregation in $La_{0.7}Sr_{0.3}MnO_3$ as a function of oxygen partial pressure ($pO_2$), temperature, and epitaxial strain, we have expanded our research to $La_{0.8}Sr_{0.2}MnO_3$, mixed conductors ($La_{0.6}Sr_{0.4}CoO_3$ and $La_{0.6}Sr_{0.4}Co_{0.2}Fe_{0.8}O_3$), and crystalline orientation. The combined results are summarized in Table 1. In general, we find evidence for strontium surface segregation in most epitaxial thin films. As shown for LSM/YSZ, surface segregation is reduced with the increase in grain boundaries in the film. In contrast to the $pO_2$-dependence found in the strontium surface concentration of LSM, the ionic conductors LSC and LSCF exhibited no $pO_2$-dependence at 700°C. Surprisingly, no evidence of strontium surface segregation was found in $La_{0.8}Sr_{0.2}MnO_3$ and (110)-oriented $La_{0.7}Sr_{0.3}MnO_3$.

**TABLE 1.** A summary of strontium segregation on film composition and substrate at elevated temperature in controlled atmospheres. The segregation was determined by measuring X-ray fluorescence in a grazing incidence geometry. The fluorescence was excited with 24 keV photons and detected using a silicon drift detector.

| Sample | Observed segregation (700°C) |
|---|---|
| 20 nm (100)-$La_{0.7}Sr_{0.3}MnO_3$/YSZ (textured) | weak, $pO_2$-dependent |
| 20 nm (110)-$La_{0.7}Sr_{0.3}MnO_3$/YSZ (textured) | weak, $pO_2$-dependent |
| 6, 20 nm (100)- $La_{0.7}Sr_{0.3}MnO_3$/$DyScO_3$ (epitaxial) | strong, $pO_2$-dependent |
| 6, 20 nm (100)- $La_{0.7}Sr_{0.3}MnO_3$/$NdGaO_3$ (epitaxial) | strong, $pO_2$-dependent |
| 20 nm (110)- $La_{0.7}Sr_{0.3}MnO_3$/$NdGaO_3$ (epitaxial) | none |
| 20 nm (100)-$La_{0.8}Sr_{0.2}MnO_3$/$DyScO_3$ (epitaxial) | none |
| 20 nm (100)-$La_{0.6}Sr_{0.4}CoO_3$/$DyScO_3$ (relaxed) | strong, no $pO_2$-dependence |
| 20 nm (100)-$La_{0.6}Sr_{0.4}Co_{0.2}Fe_{0.8}$/$NdGaO_3$ (epitaxial) | strong, no $pO_2$-dependence |

Based on grazing incidence X-ray diffraction and reflectivity, the increase in strontium surface concentration in LSM and LSC was observed to occur without any change in surface structure. In LSCF, however, quarter-order, in-plane diffraction peaks indicated a surface reconstruction, which could possibly be linked to the segregation or reduction of the atmospheric oxygen itself.

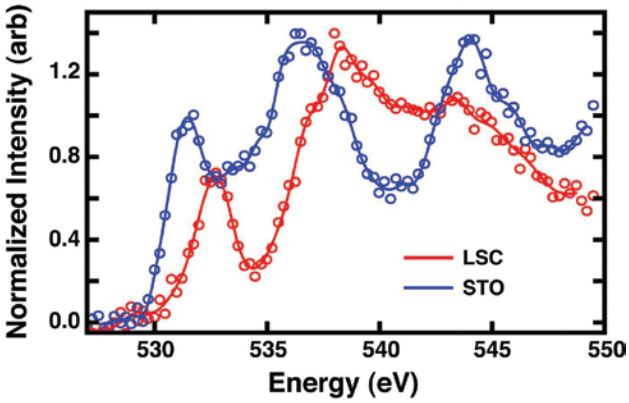


**FIGURE 1.** Oxygen K-edge spectra taken X-rays with an incident energy of 10 keV. At grazing incidence, the bulk signal is suppressed revealing the $La_{0.6}Sr_{0.4}CoO_3$ spectrum.

Using a modified environmental chamber for lower energy measurements, we have begun studying changes in B-site valence state in the samples that exhibit strong surface segregation using various spectroscopy techniques. Changes in valence can be correlated with features in an element's X-ray absorption near edge (XANES) spectrum. In addition to standard, fluorescence-mode XANES, we have begun using resonant techniques that can be used to depth profile changes in composition and electronic structure. Finally, we recently completed grazing incidence core-shell inelastic X-ray scattering measurements on an LSC thin film grown on $SrTiO_3$. As an X-ray analogue to electron energy loss spectroscopy, this technique can be used as an in situ counterpart to electron and soft X-ray measurements of the oxygen K-edge and the d-shell spectra from the cation species. A comparison between the grazing incidence LSC oxygen spectra and the $SrTiO_3$ spectrum is shown in Figure 1.

### In Situ X-ray Studies of SOFC Cathodes

Thin films of LSM and LSC on YSZ were studied as model SOFC cathodes under applied potential, simulating operating conditions in a half-cell configuration. We compared ex situ and in situ electrochemically conditioned LSM samples and found that their electrochemical behavior (e.g. conductivity) is similar at high temperature. Ex situ samples were found to have similar electrochemical behavior when the experiment was resumed after cooling to room temperature.

In order to better correlate our model cathode results to operating fuel cell conditions, we also used total reflection X-ray fluorescence to measure the

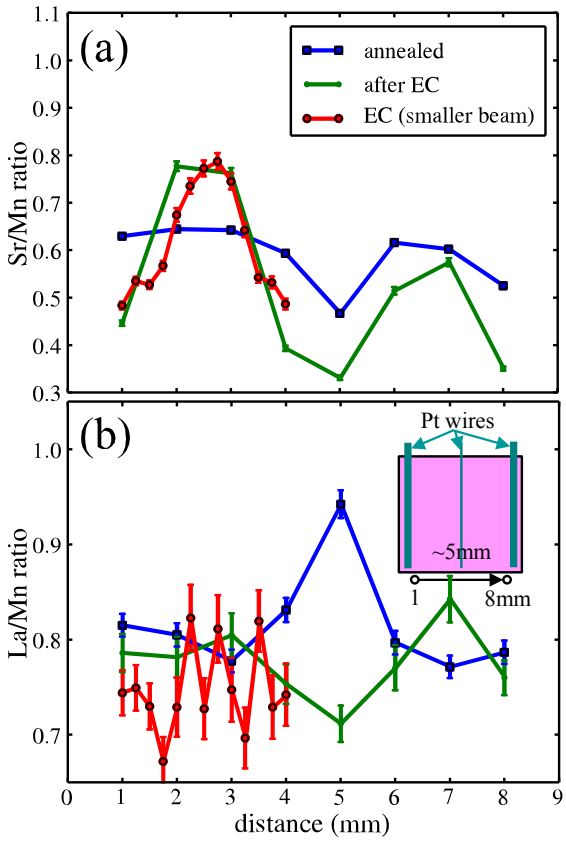


**FIGURE 2.** (a) Sr/Mn and (b) La/Mn ratios from X-ray fluorescence of an LSM thin film on YSZ averaged over signals measured under surface sensitive conditions. The Sr/Mn and La/Mn ratios were calibrated to be 0.3 and 0.7 in the bulk respectively. An annealed sample was compared to an electrochemically conditioned sample with 1 mm and 0.1 mm (smaller) beam size. The inset in the bottom graph shows the geometry of the Pt wires on the samples relative to the distance in the graph.

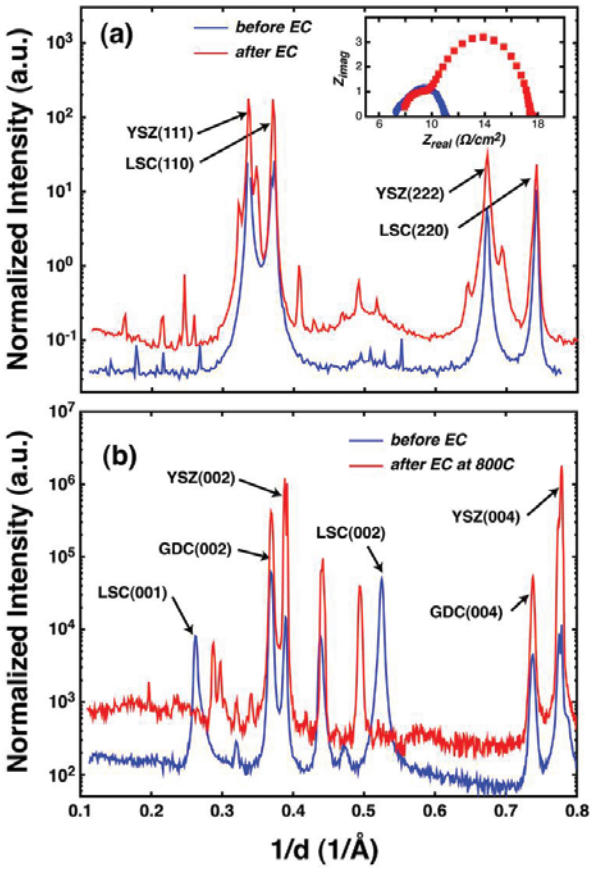


**FIGURE 3.** X-ray diffraction from a (a) 60 nm LSC(011) on YSZ(111) and (b) 60 nm LSC(001) / 60 nm GdC(001) on YSZ(001). LSC under an applied potential shows a different type of instability for both substrates. The LSC/YSZ interface reacts to form tetragonal zirconia at the interface as shown in (a). The inset shows impedance results suggesting the formation of a resistive layer during applied potential. LSC on GdC decomposes to form $Co_3O_4$ if the GdC film is thinner than 60 nm as shown in (b).

strontium surface segregation as a function of distance from the contact wires on the LSM, as shown Figure 2. Electrochemical measurements beforehand indicated that showed only 70% of a 60 nm thick LSM film is activated due to the thin film's high sheet resistance. We found the largest strontium segregation in the least active regions (i.e. away from platinum contact wires) when the cathode was under -0.3 V applied potential for 72 hours at 800°C. In contrast, annealing the sample at 800°C for just 24 hours yielded a uniform strontium segregation in the area between the contacts. This result demonstrates that the strontium surface segregation is affected by the long-term applied potential.

We also found that LSC thin films have limited stability at high temperature and/or under applied potential depending on choice of substrates (see Figure 3). Epitaxial LSC(011)/YSZ(111) interfaces reacts to form tetragonal zirconia at high temperature which roughens the interface. When a buffer layer of GdC(001) on YSZ(001) is used, LSC(001) can decompose into $Co_3O_4$ if the GdC film is thinner than 60 nm. We determined that a 100 nm or thicker layer of GdC is needed to prevent LSC decomposition.

## Conclusions and Future Directions

- Significant differences in strontium surface segregation are found in LSM, LSC and LSCF. Notably, there appears to be a significant dependence on the average La/Sr ratio in LSM films.
- For LSM(011) thin films on YSZ(111), cation segregation is dependent on the cathodic potential with high Sr segregation correlated with areas of low potential.
- LSC(001) thin films on a GdC(001) buffer layer decompose into $Co_3O_4$ if the GdC film is less than 60 nm thick.

We plan to extend our investigations of LSCF including detailed examination of surface structure, La/Sr and Fe/Co composition gradients, and oxygen chemical state. These studies will be performed as a function of electrochemical state, $pO_2$, temperature and film composition. The results of these measurements will be used to relate and validate ex situ measurements as a probe of structural changes in SOFC materials.

## FY 2009 Publications/Presentations

**1.** T.T. Fister, D.D. Fong, J.A. Eastman, P.M. Baldo, M.J. Highland, P.H. Fuoss, K.R. Balasubramaniam, J.C. Meador, and P.A. Salvador, "In situ Characterization of Strontium Surface Segregation in Epitaxial $La_{0.7}Sr_{0.3}MnO_3$ Thin Films as a Function of Oxygen Partial Pressure," Appl. Phys. Lett., **93**, 151904 (2008).

**2.** Kee-Chul Chang, Brian Ingram, Bilge Yildiz, Daniel Hennessy, Balasubramaniam Kavaipatti, Paul Salvador, and Hoydoo You, "In situ Synchrotron X-ray Studies of Dense Thin-Film Perovskite Solid Oxide Fuel Cell Cathode Materials," Electrochemical Transactions for Solid State Ionic Devices - Nano Ionics, the 214th Meeting of the Electrochemical Society, in press.

**3.** Kee-Chul Chang, Brian Ingram, Balasubramaniam Kavaipatti, Bilge Yildiz, Daniel Hennessy, Nadia Leyarovska, Paul Salvador, and Hoydoo You, "In situ Synchrotron X-ray Studies of Dense Thin-Film Strontium-Doped Lanthanum Manganite Solid Oxide Fuel Cell Cathodes," MRS Proceedings Volume 1126, S08-10 (2008).

**4.** P.H. Fuoss, "Synchrotron X-ray Studies of SOFC Cathode Materials," 9th Annual SECA Workshop, Pittsburgh, Pennsylvania, August 5–7, 2008.

**5.** T.T. Fister, M.J. Highland, M.-I. Richard, D.D. Fong, J.A. Eastman, P.M. Baldo, P.H. Fuoss, K.R. Balasubramaniam, J.C. Meador, and P.A. Salvador, "In situ Measurement of Strontium Surface Segregation in Epitaxial $La_{0.7}Sr_{0.3}MnO_3$ with Variable $pO_2$," 2008 MRS Fall Meeting, Symposium S: Solid-State Ionics, Boston, Massachusetts, December 1–5, 2008.

**5.** T.T. Fister, M.J. Highland, M.-I. Richard, D.D. Fong, J.A. Eastman, P.M. Baldo, P.H. Fuoss, K.R. Balasubramaniam, J.C. Meador, and P.A. Salvador, "In situ Synchrotron Measurements of Equilibrium Strontium Surface Segregation in $La_{0.7}Sr_{0.3}MnO_3$ as a Function of Oxygen Partial Pressure: Implications for SOFC Performance and Growth," 33rd International Conference and Exposition on Advanced Ceramics and Composites, January 18–23, 2009.

# III.A.2 Solid Oxide Fuel Cell Cathodes: Unraveling the Relationship Between Structure, Surface Chemistry and Oxygen Reduction

Srikanth Gopalan[1] (Primary Contact), Uday Pal[1], and Soumendra Basu[1], Karl Ludwig[2] and Kevin Smith[2]
[1]Department of Mechanical Engineering & Division of Materials Science and Engineering
[2]Department of Physics
Boston University
15 St. Mary's Street
Boston, MA 02215
Phone: (617) 358-2297
E-mail: sgopalan@bu.edu

DOE Project Manager: Briggs White
Phone: (304) 285-5437
E-mail: Briggs.White@netl.doe.gov

Contract Number: NT0004104

Phase I Start Date: October 1, 2008
Phase I End Date: September 30, 2009

### FY 2009 Objectives

- Obtain heteroepitaxial thin films of strontium-doped lanthanum manganite (LSM) and strontium-doped lanthanum cobalt iron oxide (LSCF) on single crystal substrates of lanthanum aluminate (LAO) and yttria-stabilized zirconia (YSZ).
- Build a chamber to characterize the kinetics of oxygen surface exchange by simultaneously employing two tools: X-ray fluorescence (XRF) using synchrotron X-rays and electrical conductivity relaxation.
- Employ X-ray photoelectron spectroscopy (XPS) as a characterization tool to probe the surfaces of the thin film heteroepitaxial cathodes.

### Accomplishments

- The process conditions to deposit thin films up to 250 Å in thickness of LSM cathodes on various single crystal substrates have been identified.
- A chamber to perform in situ synchrotron X-ray experiments simultaneously with electrical conductivity relaxation has been built.
- XPS measurements have been performed on as-deposited LSM thin films on LAO. The results indicate that no surface enhancement of Sr occurs in the as-deposited films.
- Transmission electron microscopy (TEM) characterization of the LSM thin films on LAO substrates show well-adhered films with excellent in-plane registry and epitaxy.

## Introduction

Many of the specific details of the oxygen reduction reaction in a solid oxide fuel cell (SOFC) remain poorly understood. Surface chemistry directly influences the nature of oxygen reduction reaction pathways on the SOFC cathodes and the rates at which the individual processes proceed. From semi-empirical correlations between the chemistry and structure of oxide surfaces and their electrocatalytic performance, the true cause-and-effect relationships in the oxygen reduction processes at the cathode could be elucidated. This would provide valuable guidance in improving cathode performance.

## Approach

In the proposed work, we aim to acquire such surface-specific chemical and structural data on heteroepitaxial thin films of LSM and LSCF cathodes on single-crystals of YSZ and YSZ coated with a barrier layer of rare-earth doped ceria (e.g. $Y_2O_3$ doped $CeO_2$ or YDC) electrolytes. This will be accomplished using a combination of analytical spectroscopic techniques and TEM. Further, we also aim to employ simultaneously, synchrotron-based X-ray techniques (specifically XRF and X-ray diffraction [XRD]) and electrical conductivity relaxation to measure and correlate the kinetics of oxygen surface exchange to the details of the surface structure of the oxide thin films. Finally, the thin film films will be subjected to direct current cathodic polarization and its effect on surface structure and chemistry will be characterized.

## Results

We have been able to deposit films of varying thicknesses up to 350 Å. A number of samples have been fabricated. The Sr/(Sr+La) ratio was determined to be 0.21. The target composition was a ratio of 0.20. Likewise, the Mn/(Sr+La) was determined to be 0.95. Thus, the composition of the film appears to be slightly A-site excess.

XRD patterns were obtained at Boston University of the films deposited at the Environmental Molecular Sciences Laboratory. The XRD pattern clearly shows the presence of an epitaxial film on the LAO substrate.

XPS analysis of as-prepared thin films of LSM on LAO substrates revealed no surface enrichment of strontium. However, significant surface enrichment of strontium occurs upon annealing the films in oxygen.

High resolution TEM (HRTEM) analysis shows that the film is uniform (~25 nm thick) and adherent with the substrate. The electron diffraction pattern clearly reveals the heteroepitaxial nature of the film. The appearance of split diffraction spots in the [001] (growth) direction, but not in the [100] direction indicates that the two lattices match up very well along the interface due to the heteroepitaxy constraints, but the film relaxes to its original lattice parameter in the growth direction due to lack of constraint. The HRTEM image and the selected area electron diffraction pattern shows that the epitaxial quality of the films is sufficiently good to perform surface chemistry and electrochemical characterization experiments.

## Conclusions and Future Directions

Thus far we have been able to demonstrate that high quality films of LSM on various single crystal substrates can be obtained at Pacific Northwest National Laboratory consistently. We have also built a high temperature chamber to conduct simultaneous XRD and electrical conductivity measurements. We have also obtained baseline XPS data on the LSM films.

In future, we expect to accomplish the following.

1. Synchrotron X-ray experiments will be repeated at Brookhaven National Laboratory using the redesigned and modified X-ray chamber. In situ simultaneous electrical conductivity relaxation and X-ray experiments will be performed at the synchrotron after equilibrating the thin film sample between two different $pO_2$s.
2. Produce clean well-ordered surfaces for low energy electron diffraction (LEED) studies. Once we have such a surface we can begin monitoring the effects on the cathode interface following exposure to $O_2$ and operational temperatures using XPS. From angular core-level XPS, we shall be able to determine compositional changes. In combination with LEED we may also be able to determine structural changes at the cathode/gas interface.

# III.A.3 SOFC Cathode Surface Chemistry and Optimization Studies

Paul A. Salvador (Primary Contact), Lu Yan, Shanling Wang, K.R. Balasubramaniam, and Hui Du
Carnegie Mellon University (CMU)
Department of Materials Science and Engineering
5000 Forbes Avenue
Pittsburgh, PA 15206
Phone: (412) 268-2703; Fax: (412) 268-3113
E-mail: paul7@andrew.cmu.edu

Collaborators: Drs. Paul Fuoss,[a] Jeff Eastman,[a] Dillon Fong,[a] Tim Fister,[a] Peter Baldo,[a] Hoydoo You,[a] Kee-Chul Chang,[a] Bilge Yildez,[b] K. Katsiev,[b] C. Heske,[c] and S. Krause[c]
[a] Argonne National Laboratory (ANL)
9700 South Cass Avenue
Argonne, IL 60439-4837
[b] Massachusetts Institute of Technology (MIT)
Department of Nuclear Science and Engineering
77 Massachusetts Avenue, Rm: 24-210
Cambridge, MA 02139
[c] University of Nevada, Las Vegas (UNLV)
Department of Chemistry
4505 Maryland Parkway, Box 454003
Las Vegas, NV 89154

DOE Project Manager: Briggs White
Phone: (304) 285-5437
E-mail: Briggs.White@netl.doe.gov

Contract Number: NT0004105

Start Date: September 1, 2008
End Date: February 28, 2010

## FY 2009 Objectives

- Develop samples of cathode materials having specific surface structures and chemistries using thin film preparation methods.
- Provide lanthanum strontium manganese oxide (LSM), lanthanum strontium cobalt oxide (LSC), and lanthanum strontium cobalt iron oxide (LSCF) samples for surface characterization to collaborators at the ANL-Advanced Photon Source (APS), MIT, UNLV, and the National Energy Technology Laboratory (NETL).
- Determine the key correlations between surface features and electrochemical performance for solid oxide fuel cell (SOFC) cathodes.
- Develop further experimental tools that provide a sensitive measure of activity/stability in operational conditions, including Kelvin probe spectroscopy (KPS).
- Determine the effects of engineered surface chemistries on oxygen uptake kinetics in thin film samples, specifically LSM (100), (110), and (111).
- Correlate electrical conductivity relaxation (ECR) and transient piezoelectric crystal microbalance (PCM) measurements using lanthanum nickel oxide (LNO).

## Accomplishments

- Developed single-crystal, epitaxial, textured, and polycrystalline thin films of LSM, LSC, and LSCF with low roughness values on both insulating and electrolytic substrates that were used in both in-house and collaborators' experimental facilities to understand the nature of the surface chemistry/reactivity of cathode materials.
- Thin film samples were characterized at the APS as a function of temperature (T), pressure (P), and electrochemistry for their surface compositions, structures, and charge states; at MIT for their local electronic properties using scanning tunneling spectroscopy (STS) and electrochemical properties with electrochemical impedance spectroscopy; at UNLV with Auger electron spectroscopy (AES) and X-ray photoelectron spectroscopy (XPS); and at CMU with X-ray diffraction (XRD), atomic force microscopy (AFM), ECR, KPS, and PCM.
- Developed a simultaneous ECR/KPS testing method for thin film characterization in atmospheric pressure using mixed gases to control the $pO_2$.
- Demonstrated that epitaxial thin film samples of LSM having different surface orientations exhibit anisotropies in ECR between 2 and 50% (referenced to the orientation with the maximum activity in a given condition).

## Introduction

The cathode in SOFCs is responsible for the reduction of $O_2$ gas and its incorporation into the electrolyte. When SOFCs are operated at specific current densities/voltages, the oxygen incorporation (or uptake) process can contribute significantly to the losses of the cell, thereby limiting the performance of the SOFC system. Two major options exist for improving the cathode performance by specifically targeting the oxygen incorporation process: changing the component solid materials or adding yet another material (a catalyst) to the existing frameworks [1,2]. We aim to address both approaches in this work by (1) developing an

experimental project that allows us to probe the nature of atomic scale surface chemistry and its role in oxygen incorporation in LSM, LSC, lanthanum strontium ferrite, and LSCF (and related cathode materials) and (2) determining the optimal catalyst chemistry from both an activity and stability perspective [3-7]. Realizing these goals will lead to improved cathode performance in SOFCs and an acceleration of introduction of new materials into SOFCs to allow for the DOE Solid State Energy Conversion Alliance (SECA) program to meet performance metrics.

Generally speaking, the limitations in designing highly active cathodes for oxygen incorporation arise from the general lack of direct correlations between surface/interface chemistry/structure and performance of SOFC cathode materials over the appropriate ranges SOFC operational conditions [8]. In this work, we aim to fill this need by (1) developing experimental protocols that will provide a sensitive measure of activity/stability in operational conditions and by (2) determining key correlations between structure (solid state atomic, electronic, crystallographic, and chemical) and electrochemical performance (mass and charge transfer) parameters in surface engineered samples. At CMU, we are generating surface engineered samples and providing them to a range of collaborators who characterize the samples. Several groups at ANL have investigated samples using high-energy synchrotron X-ray techniques at the APS [4,9]. A group at MIT uses STS and electrochemical impedance spectroscopy are carried out to determine electrical characteristics of the films [7]. Two new collaborations involve (1) a group at NETL to carry out scanning tunneling microscopy (STM), XPS, and AES to determine surface structures/compositions and (2) a group at UNLV to carry out experimental electronic structure determination of thin film surfaces. Separate reports will be provided by these collaborators. In this report, we describe the progress at CMU on sample preparation, especially surface engineered epitaxial structures for STM/STS, and on measurement of the oxygen uptake kinetics using ECR and transient PCM.

## Approach

A key part of an experimental project that can address the above-stated goals is the development of samples that allow both for controlled changes in surface chemistry and for detailed experiments to be carried out upon them. Epitaxial and textured thin films are ideal samples for these experiments. To screen for structure-performance correlations, we are producing single-crystal and textured thin film samples using pulsed laser deposition (PLD) to produce thin, flat films that can be used to characterize the structure, chemistry, and physical properties of surfaces [4-6,9]. For the current year, we have continued to focus on understanding the *native* surface on LSM, LSC, and LSCF, as well as establishing measurement techniques that allow for the determination of surface kinetic parameters.

To establish a baseline in understanding the bulk and surface structure of LSM, LSC, and LSCF, epitaxial thin films of each were grown using PLD on different single crystal perovskite substrates ($SrTiO_3$ [STO], $NdGaO_3$ [NGO], $DyScO_3$ [DSO]) as well as electrolytes (yttria-stabilized zirconia [YSZ] and gadolinia doped ceria [GDC]-buffered YSZ) [4-6,9]. The films were characterized for their growth rate, surface roughness, and structural characteristics at CMU using X-ray techniques and AFM. Representative samples were sent to ANL and were characterized at the APS using in situ X-ray scattering observations, while the films were exposed to various T, P, and electrochemical environments [4,9]. A low-pressure ECR measurement was used at CMU to determine the chemical surface exchange coefficient ($k_{chem}$) at operational temperatures. A PCM was used at CMU to measure mass uptake in $LaNiO_{3-x}$ to demonstrate the utility of this direct measurement technique in determining mass changes and exchange kinetics. An atmospheric KPS/ECR system was installed at CMU and initial studies were carried out on LSC films.

## Results

In all depositions, LSM, LSC, and LSCF followed cube-on-cube epitaxy on all perovskite substrates (STO, NGO, DSO, $LaAlO_3$), as expected and observed in earlier work [4-6,9]; they exhibited low surface roughness values (on the order of unit-cell roughness), using most deposition conditions. By using YSZ(111) substrates, we generated epitaxial (110)-oriented perovskites having low surface roughnesses [6-9]. To compare directly the perovskite-perovskite and perovskite-fluorite film-substrate combinations it is ideal to have similar surfaces exposed on both. Using a cube-on-cube epitaxial GDC(100)-buffer on YSZ(100), LSM, LSC, and LSCF films showed only (100) orientations [6,9]. (Note the GDC(100) overlaps with the perovskite (110), but through more detailed XRD analysis the existence of the (110) orientations were ruled out as a major phase.) The root mean square roughness values of most epitaxial perovskite-fluorite films were on the unit-cell values. Direct correlations between the perovskite-perovskite and perovskite-fluorite film-substrate combinations allow for the effects of microstructure and surface crystallography to be de-convoluted, which is a focus on next year's work.

For more sensitive surface sensitive measurements, such as STM or STS [7], surface flatness should be atomically smooth over hundreds to thousands of angstroms. To achieve such surfaces, stricter growth conditions are required that allow for 2-dimensional (2D) growth (either by step-flow growth or by terrace

nucleation/2D island coalescence) and improved substrate surfaces [10]. Figure 1(a) shows the AFM image of a Nb-doped $SrTiO_3$(100) single crystal after being chemically etched and thermally treated at 1,000°C. The contrast shows unit-cell high steps separated by ≈200 nm terraces. These large terraces make 2D step-flow growth challenging, owing to the large diffusion lengths. By depositing at a low laser energy frequency of 1Hz (typical value ≈3 Hz) to allow for diffusion time, a low oxygen pressure of 1 mTorr $O_2$ (typical value of ≈50-200 mTorr) to increase the kinetic energy of arriving species, at a low laser energy of 1 J/cm$^2$ (typical value of 2-4 J/cm$^2$) to lower the supersaturation, and at a higher temperature of 850°C (typical value of 750-850°C) to increase thermal energy, films were observed to grow in the 2D island nucleation/coalescence mode. Figure 1(b) shows the AFM image of an ≈11 nm thick film. The step structure of Figure 1(a) is still evident after growth of >25 unit cells. On those terraces, 1 unit cell high islands are observed, with some evidence of a second layer forming prior to coalescence. These surfaces are already useful to use STM and other surface sensitive measurements that are perturbed by local surface roughness, though we will continue to improve the 2D growth mode in the future. Such samples are being provided to MIT, NETL, and ANL.

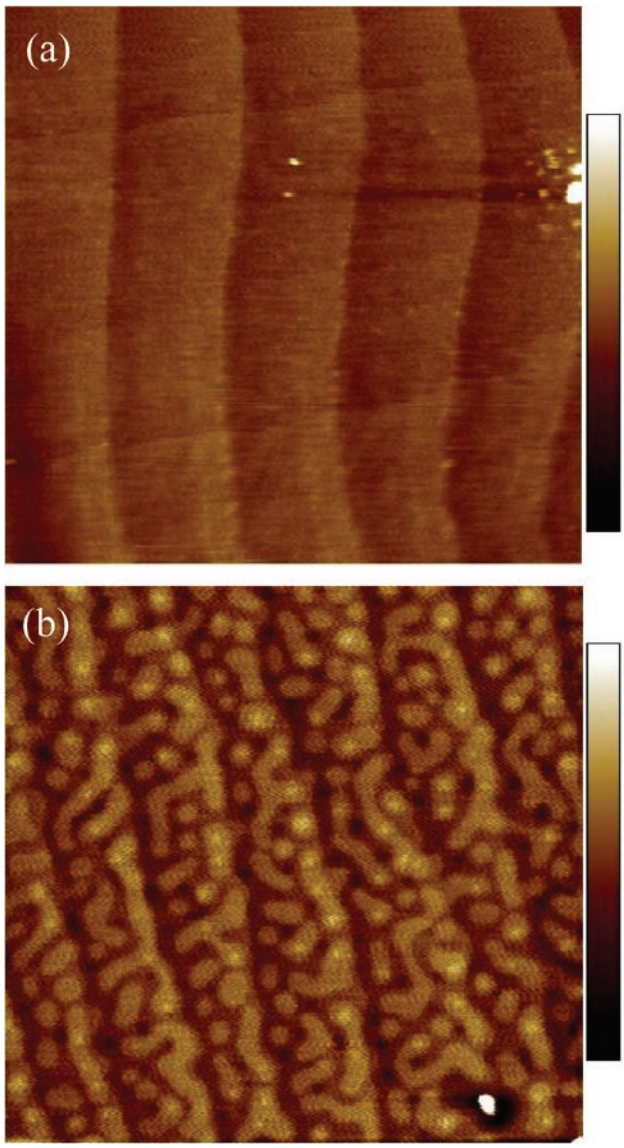


**FIGURE 1.** AFM images of (a) an etched and annealed STO(100) substrate prior to growth and (b) an ≈11 nm thick film of LSM(100) deposited on STO(100). Each image has linear dimensions of 1x1 μm$^2$ and the full-scale contrast (key given on the right) is 3 nm. The steps in (a) correspond to unit cell high step of ≈0.4 nm. The contrast in (b) correspond largely to 2D islands (≈0.4 nm high) nucleated on the 2D terraces of the film grown below it.

Over the course of the past year, we have used the well-known ECR technique to explore the variation in activity of different crystallographic surfaces of LSM. Epitaxial thin films of the three low-index orientations were deposited on STO(100), (110), and (111) [4-6]. A van der Pauw set-up was used to measure the conductivity of the films. The differences between the geometrical configurations of the voltage and current probes were <1%, indicating the good homogeneity of the films and allowing for the use of a single configuration to determine the conductivity of the films. To ensure that the films were similar to bulk materials, the conductivity was measured at different thicknesses over a range of temperature (≈650°C-900°C). Figure 2(a) shows the temperature dependence (as 1/T) of the conductivity (as ln σT) for the three orientations of 100 nm thick films. All three show the same conductivity and is in reasonable agreement with expectations [11,12]. The activation energy extracted from these graphs is ≈ 0.1 eV, in agreement with reports on polaron conductivity of LSM [11,12]. Figure 2(b) shows a similar graph for (110)-oriented films of three thicknesses. The minor disagreement for the 100 nm thick film is likely a result of inaccuracies in the thickness value. Generally, the three samples exhibit similar conductivity values and activation energies (≈0.1 eV). Finally, Figure 3(a) shows the $pO_2$ dependence of the conductivity (in log-log form) as a function of temperature. Again, this functional form is in agreement with the expected values from defect chemistry (see discussion in ref. 2) transitioning from an oxygen stoichiometric regime at low $pO_2$ to an oxygen excess regime at higher $pO_2$. All of these results indicate that the films are capable of being compared to one another.

Figure 3 shows the normalized conductivity,

$$g(t) = \frac{\sigma(t) - \sigma(0)}{\sigma(\infty) - \sigma(0)},$$

where $\sigma(t)$ is the conductivity at a given time $t$, measured on changing the oxygen pressure from 50 mTorr to 500 mTorr at T≈1,190 K for the LSM(110) 100 nm-thick

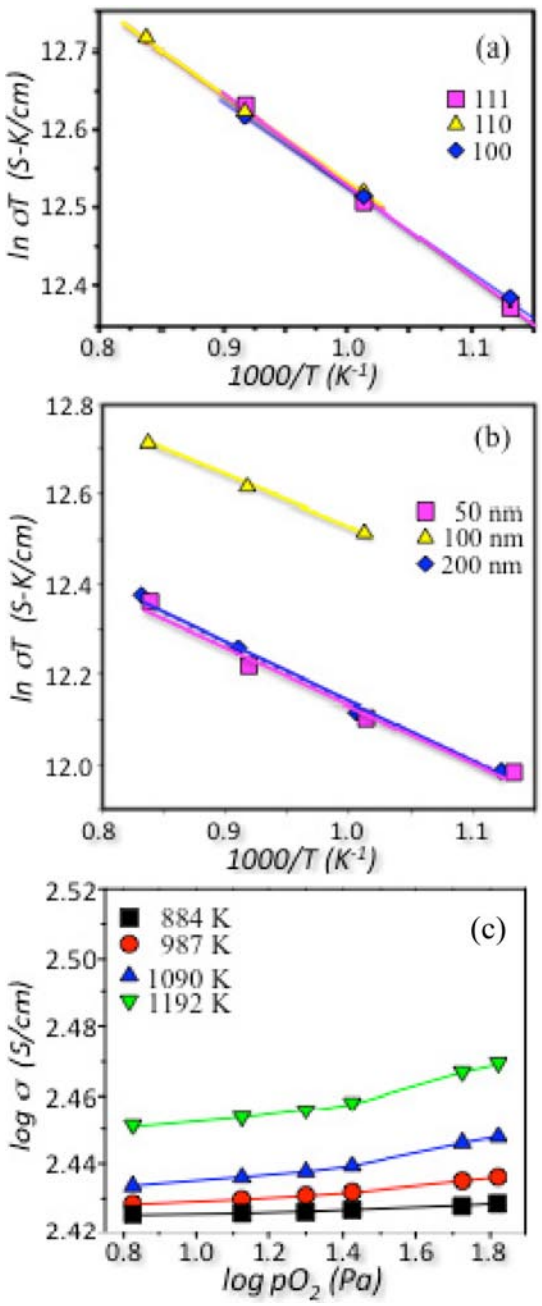


**FIGURE 2.** Baseline characterization of thin films to ensure appropriateness of thin film measurements to bulk characteristics: temperature dependent conductivity (plotted as ln σT vs. $10^3$/T) as a function of (a) orientation for the 100 nm thick films and (b) thickness for the (110)-oriented films; and (c) oxygen pressure dependence of conductivity (plotted as log σ vs log $pO_2$) for the 100 nm thick (111)-oriented films.

film. At this thickness, the response is expected to be surface controlled [13]. Though this pressure change is an order of magnitude, the overall kinetics can be fit reasonably well with a simple exponential:

$$g(t) = 1 - e^{-\left(\frac{k_{chem} t}{l}\right)},$$

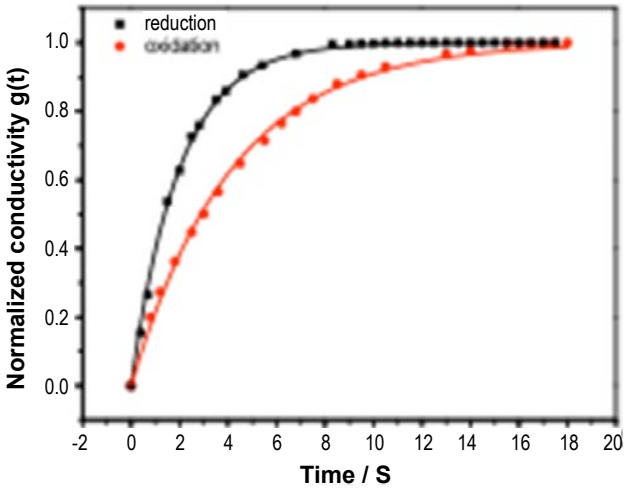


**FIGURE 3.** Typical ECR plot of films measured in this study. Taken from a (110) film of 100 nm thickness at T≈1,190 K on changing the $pO_2$ between 50 and 500 mTorr.

where $l$ is the thickness of the film and $k_{chem}$ is the chemical surface exchange coefficient. The value of $k_{chem}$ on reduction is $5.02 \times 10^{-6}$ cm/s and on oxidation is $2.41 \times 10^{-6}$ cm/s. Values were extracted from similar curves for LSM(100), LSM(110), and LSM(111). At T=1,192 K, the reduction (oxidation) $k_{chem}$ values were respectively $6.31 \times 10^{-6}$ cm/s ($2.57 \times 10^{-6}$ cm/s), $6.3 \times 10^{-6}$ cm/s ($2.49 \times 10^{-6}$ cm/s), and $7.09 \times 10^{-6}$ cm/s ($2.62 \times 10^{-6}$ cm/s). In each case, the reduction was faster than the oxidation by a factor of ≈2.5. The (111) surface exhibited the highest rate, followed by the (100) surface and then the (110). The observed anisotropy as a function of orientation according to the oxidation (reduction) $k_{chem}$ values are: (100)/(111) ≈0.89 (0.98) and (110)/(111) ≈0.73 (0.95). Further experiments are required to verify the anisotropic nature of the oxidation and reduction process, as well as to determine the temperature dependence of this observation. These $k_{chem}$ values are similar to those reported for other epitaxial films of LSC and other perovskites [14]. Further work is necessary to understand the nature of $k_{chem}$ as a function of T, P, thickness, and orientation. Crystallographic anisotropies of the surface exchange have been reported and are important to understanding the overall performance of complex microstructures in cathodes.

Using a $GaPO_4$ piezoelectric microbalance, the oxygen uptake in LNO was measured for polycrystalline films deposited on the PCM electrode and ECR was measured for LNO films deposited on glass. Figure 4(a) shows the normalized conductivity change for the LNO film on a glass slide, measured at T = 300°C on changing from 3 mTorr $O_2$ to 10 mTorr $O_2$ in a total pressure of 220 mTorr ($N_2$ balance). (This situation avoided measurement drift in temperature or pressure that affected sensitivity.) Figure 4(b) shows the normalized mass change measured using the PCM (in the same

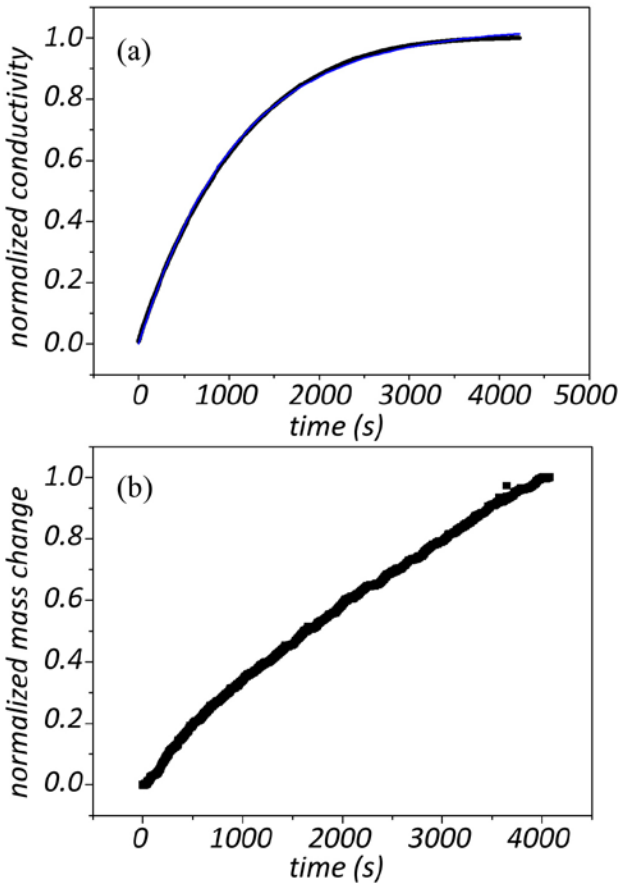


**FIGURE 4.** Plots of transient (a) conductivity and (b) mass change for polycrystalline films of LNO on (a) a glass slide and (b) a Pt electrode on a $GaPO_4$ PCM. The film thickness was ≈130. The pressure change in both conditions is from 3 mTorr $O_2$ to 10 mTorr $O_2$ in a total pressure of 220 mTorr (nitrogen balance).

chamber and experimental conditions as the ECR measurements). The data in Figure 4(a) can be fit well to a simple exponential function *g(t)* (line overdrawn in image), and $k_{chem}$ was determined to be $1x10^{-9}$ cm/s. This value is very low compared to the LSM (and other perovskite films) but not outside of expectations at the low temperature of T = 300°C. The same exponential function cannot be used to model the PCM data, though the early stages do exhibit a similar exponential behavior and the latter stages have a nearly linear behavior. In the ECR data, the conductivity has changed by 90% by $t = 2{,}000$ s but the mass uptake has only changed by 50%. Using a simple combination of an exponential function and a linear region

$$g(t) = 1 - Ae^{-\left(\frac{k_{chem}t}{l}\right)} + Ct,$$

the data could be fit using the same $k_{chem}$ as ECR and $A$ (the fraction of the mass response from the exponential portion) was ≈20-30 percent. Further work is necessary to deconvolute the two effects and to isolate the nature of the linear oxygen uptake in the mass balance, though the initial uptake could be correlated to the ECR data. By combining mass uptake with ECR, it should be possible to deconvolute mass adsorption steps (affecting PCM) from electron transfer steps (affecting ECR).

## Conclusions and Future Directions

We have demonstrated that surface engineered films of cathode materials can be produce and characterized in detail for the structural and chemical properties, including atomically smooth surfaces for use in STM and STS measurements. Crystallographic anisotropies were observed for epitaxial LSM single crystal films in their oxygen uptake kinetics. Both ECR and PCM equipment can be used to simultaneously measure oxygen uptake. We will continue to produce a series of surface engineered films and will investigate (1) their structural properties, (2) their stabilities, and (3) their oxygen uptake kinetics using ECR, PCM, and KPS measurements (now operational). By fabricating a matrix of related materials and carrying out these measurements, we will be able to provide a large amount of data to determine the key parameters that correlate surface structure to surface activity, with the aim of providing information to the DOE-SECA program to improve cathode activity by design.

## FY 2009 Publications/Presentations

**1.** K.R. Balasubramanian, L. Yan, S. Wang, and P.A. Salvador, "Synthesis and Electrical Conductivity Relaxation Studies of Epitaxial/Textured Cathode Thin Films on Single Crystal Substrates," Presented at 33rd International Conference & Exposition on Advanced Ceramics and Composites, Daytona Beach, Florida, January 2009.

**2.** K.R. Balasubramanian, L. Yan, S. Wang, and P.A. Salvador, "Synthesis of Epitaxial/Textured Cathode Thin Films on Single Crystal Electrolyte Substrates," Presented at the MS&T Conference 2008, Pittsburgh, Pennsylvania, October 2008.

**3.** P.A. Salvador, K.R. Balasubramaniam, S. Wang, L. Yan, J. Eastman, P. Fuoss, D. Fong, P. Baldo, B. Ingram, M. Krumpelt, K.-C. Chang, B. Misirlioglu, and B. Yildiz, "Structure and Properties of Thin Films of SOFC Cathode Materials," Presented at the MS&T Conference 2008, Pittsburgh, Pennsylvania, October 2008.

**4.** T.T. Fister, D.D. Fong, J.A. Eastman, P.M. Baldo, M.J. Highland, P.H. Fuoss, K.R. Balasubramaniam, J.C. Meador, and P.A. Salvador, "*In situ* Characterization of Strontium Surface Segregation in Epitaxial $La_{0.7}Sr_{0.3}MnO_3$ Thin Films as a Function of Oxygen Partial Pressure," *Applied Physics Letters*, **93**, 151904 (2008).

**5.** K.-C. Chang, B. Ingram, K.R. Balasubramaniam, B. Yildiz, D. Hennessy, P.A. Salvador, N. Leyarovska, and H. You, "In situ Synchrotron X-ray Studies of Dense Thin-

Film Strontium-Doped Lanthanum Manganite Solid Oxide Fuel Cell Cathodes," to be published in *Mat. Res. Soc. Symp. Proc.* (2009).

## References


**1.** E. Maguire, B. Gharbage, and F.M.B. Marques, "Cathode Materials for Intermediate Temperature SOFCs," *Solid State Ionics* 2000.

**2.** N.Q. Minh, Science and Technology of Ceramic Fuel Cells, Elsevier Science: 1995.

**3.** K.-C. Chang, B. Ingram, K.R. Balasubramaniam, B. Yildiz, D. Hennessy, P.A. Salvador, N. Leyarovska, and H. You, "In situ Synchrotron X-ray Studies of Dense Thin-Film Strontium-Doped Lanthanum Manganite Solid Oxide Fuel Cell Cathodes," *Mat. Res. Soc. Symp. Proc* 2009, *1126*, 1126-S08-10.1-6.

**4.** T.T. Fister, D.D. Fong, J.A. Eastman, P.M. Baldo, M.J. Highland, P.H. Fuoss, K.R. Balasubramaniam, J.C. Meador, and P.A. Salvador, "In situ Characterization of Strontium Surface Segregation in Epitaxial $La_{0.7}Sr_{0.3}MnO_3$ Thin Films as a Function of Oxygen Partial Pressure," *Applied Physics Letters* 2008, *93* (15), 151904.

**5.** P.A. Salvador, J. Meador, K.R. Balasubramaniam, P. Fuoss, J. Eastman, D. Fong, and P. Baldo, "SOFC Cathode Surface Chemistry and Optimization Studies," FY 2007 Office of Fossil Energy Fuel Cell Program Annual Report, U.S. Department of Energy 2007, Paper IV.A.4, 1-5.

**6.** P.A. Salvador, L. Yan, S. Wang, K.R. Balasubramaniam, P. Fuoss, J. Eastman, D. Fong, T. Fister, P. Baldo, H. You, K.-C. Chang, B. Yildiz, and I.B. Misirlioglu, "SOFC Cathode Chemistry and Optimization Studies," FY 2008 Office of Fossil Energy Fuel Cell Program Annual Report, U.S. Department of Energy 2008, Paper III.A.2, 1-5.

**7.** K. Katsiev, B. Yildiz, P.A. Salvador, and K.R. Balasubramaniam, "Electron Tunneling Characteristics on $La_{0.7}Sr_{0.3}MnO_3$ Thin-Film Surfaces at High Temperature," *Applied Physics Letters* 2009 in press.

**8.** J. Fleig, H. Kim, J. Jamnik, and J. Maier, "Oxygen Reduction Kinetics of Lanthanum Manganite (LSM) Model Cathodes: Partial Pressure Dependence and Rate-Limiting Steps," *Fuel Cells* 2008, *8*, 330-337.

**9.** K.-C. Chang, B. Ingram, K.R. Balasubramaniam, B. Yildiz, D. Hennessy, P.A. Salvador, N. Leyarovska, and H. You, "In situ Synchrotron X-ray Studies of Dense Thin-Film Strontium-Doped Lanthanum Manganite Solid Oxide Fuel Cell Cathodes," *Mat. Res. Soc. Symp. Proc* in press 2009.

**10.** H. Du, P.J. Fisher, M. Skowronski, P.A. Salvador, and O. Maksimov, "Growth and Structural Characterization of Epitaxial $Ba_{0.6}Sr_{0.4}TiO_3$ Films Deposited on $REScO_3(110)$ (RE = Dy, Gd) Substrates Using Pulsed Laser Deposition," *Journal of Crystal Growth* 2008, *310* (7-9), 1991-1998.

**11.** T. Suzuki, M. Awano, V. Petrovsky, and H. Anderson, "Optical and Electrical Properties of Amorphous and Nanocrystalline $(La_{0.8}Sr_{0.2})_{0.9}MnO_3$ Thin Films Prepared from Low-Temperature Processing Technique," *J American Ceramic Society* 2006, *89* (12), 3854-3857.

**12.** H. Taguchi, S. Matsu-ura, M. Nagao, and H. Kido, "Electrical Properties of Perovskite-Type $La(Cr_{1-x}Mn_x)O_{3+\delta}$," *Physica B* 1999, *270*, 325-331.

**13.** I. Yasuda and M. Hishinuma, "Electrical Conductivity and Chemical Diffusion Coefficient of Strontium-Doped Lanthanum Manganites," *J Solid State Chem* 1996, *123*, 382-390.

**14.** X. Chen, S. Wang, Y. Yang, L. Smith, N. Wu, B. Kim, S. Perry, A. Jacobson, and A. Ignatiev, "Electrical Conductivity Relaxation Studies of an Epitaxial $La_{0.5}Sr_{0.5}CoO_{3-\delta}$ Thin Film," *Solid State Ionics* 2002, *146*, 405-413.

# III.A.4 TEM Investigations of SOFCs: Stability of LSCF-based Cathodes

Paul A. Salvador (Primary Contact), Rumyana Petrova, and Shanling Wang
Carnegie Mellon University (CMU)
5000 Forbes Avenue
Pittsburgh, PA 15206
Phone: (412) 268-2703; Fax: (412) 268-3113
E-mail: paul7@andrew.cmu.edu

Collaborators: Dr. Subhasish Mukerjee (Primary Contact)
Delphi Corporation, Fuel Cells
5500 West Henrietta Road
West Henrietta, NY 14586
Phone: (585) 359-6465; Fax: (585) 359-6061
E-mail: subhasish.mukerjee@delphi.com

DOE Project Manager: Briggs White
Phone: (304) 285-5437
E-mail: Briggs.White@netl.doe.gov

Contract Number: 41817

Start Date: October 1, 2008
Project End Date: September 30, 2009

## FY 2009 Objectives

- Support solid oxide fuel cell (SOFC) development in the Solid State Energy Conversion Alliance (SECA) program by carrying out transmission electron microscope (TEM) investigations on SOFCs provided by SECA collaborators to determine the effects of processing or operational conditions on local microstructure/chemistry.
- Example projects include:
  - Understand better the stability of $La_{1-x}Sr_xCo_{1-y}Fe_yO_{3-\delta}$ (LSCF) in operational SOFCs by comparing stoichiometry of LSCF at different stages of SOFC production/operation;
  - Analyze the Cr-interaction in LSCF cathodes;
  - Characterize the stability/evolution of metallic interconnects in SOFCs using LSCF cathodes;
  - Characterize anode microstructures after exposure to different contaminants/operational conditions;
  - Characterize cathode microstructures infiltrated with catalysts; and
  - Characterize glasses used for seals based on composition and processing history.

## Accomplishments

- Used focused ion beam (FIB) technique to produce reliably TEM specimens (on the order of 50 specimens) from specific locations inside SOFCs.
- Used TEM, scanning transmission electron microscopy (STEM), scanning electron microscopy (SEM), select area electron diffraction (SAED), electron energy loss spectroscopy (EELS), and energy dispersive spectroscopy (EDS) techniques to quantify local compositions and local microstructures of anodes, cathodes, interconnects, and glass seals of SOFCs for SECA members.
- Demonstrated that the local composition of LSCF cathodes was stable in long-term SOFC stack operation: the average composition was identical from powder to 3,600-hr operation.
- Located minor microstructural variations at interfaces of LSCF cathodes: slightly higher compositional variations near LSCF/doped ceria (DC) interface and minor Sr-Zr-O phases at the yttria-stabilized zirconia (YSZ)/DC layer after 3,600 hrs of stack operation.
- Demonstrated Cr-poisoning was absent in LSCF cathodes in SOFC stacks after 3,600-hr operation.
- Provided detailed microstructural characterization of Ni-YSZ anodes in SOFC stacks that exhibited both good and bad performance characteristics showing little obvious differences.
- Provided detailed microstructural characterization of scales on interconnects of SOFCs.

## Introduction

This project continues to support SECA research efforts by providing TEM characterization to other groups [1,2]. Overall, this project enables SECA to meet technical targets by providing advanced materials characterization to industrial and national laboratory groups [1-4]. While a variety of projects were completed this year (see FY 2009 Objectives/Accomplishments), this report focuses on the effort to characterize the stability of LSCF cathodes used in operational fuel cell stacks. LSCF is currently being pursued as the cathode material in some SOFC stacks under development in the SECA program. Though a variety of reports have focused on the interaction of LSCF with YSZ or DC (primarily gadolinia DC [GDC]) in powder compacts [5-8] or in single cells [9-13], there have only been a few efforts to characterize SOFC stacks carried out in operational conditions for extended

periods of time [14-17]. The reported stability of LSCF (or lanthanum strontium ferrite/lanthanum strontium cobaltite) varies with composition [5-8,10,13,17,18], atmospheric conditions [5-8,10-12,18], the nature of other solid phases in its proximity [5,6,8,9,13,15,17], and time [10-12,14,15,17]. While some reports indicate that LSCF could be stable in anode-supported SOFCs using a DC (generally GDC) interlayer between the YSZ electrolyte and LSCF cathode [14,17], three primary degradation mechanisms have been reported as harmful to SOFC operation: direct interaction with YSZ or DC components [5,6,8,10,16], indirect interaction with YSZ through a DC interlayer [9,13,15-17], and LSCF compositional or morphological instability [7,10-12,15,17]. It is therefore essential to characterize operational SOFCs based on LSCF cathodes to establish the appropriateness of LSCF use for long-term (>10,000-40,000-hr) operation.

This report focuses on LSCF compositional and morphological stability and the direct interaction with a DC interlayer. To determine the long-term stability of LSCF in SOFC cathodes and to better understand the nanoscale microstructural/chemical properties at different stages of cell life, TEM investigations of LSCF powders and LSCF cathodes from an SOFC stack operated at Delphi for 3,600 hrs, which in addition to electrochemical loads included heated stainless steel components containing Cr. (The precise details of the cells, stacks, and balance of plant are proprietary.) A secondary focus was to determine if Cr poisoning could be avoided [19,20]. At Delphi, powders, cells, and stacks were characterized electrochemically as well as microstructurally using SEM, EDS, and X-ray diffraction. TEM complements these spatially averaging techniques by allowing location of nanosized grains and interrogation of their precise chemistry/structure; isolation of low levels or the initial stages of contamination/degradation; and identification of the spatial variation of microstructural evolution [1-4,9]. These results will ultimately allow determination of how SOFC cathodes can be optimized to meet DOE goals.

## Approach

LSCF powders were prepared at Delphi nominally of the 6428 composition and were characterized with TEM and EDS at CMU to determine the initial phase and composition of LSCF as a baseline for comparison. Anode (Ni/YSZ) supported cells (8YSZ electrolyte, DC interlayer, and LSCF 6428 active cathode) were also prepared at Delphi and integrated into SOFC stacks. A fabricated but untested cell was taken as a second baseline comparison for the electrochemically treated cell. Stacks were operated under normal operating conditions (V = 0.8 Volts per cell, T = 750°C, fuel = 28% $H_2$, 30% CO, 6% $H_2O$, 2.5 ppmv $H_2S$) for 3,600 hrs. After the initial lowering of power due to $H_2S$ [21], the stack showed less than 1% degradation during the course of this long-term durability test, indicating the stable performance of the stacks based on LSCF cathodes. This report focuses on the stability of the LSCF cathode in such operational environments. A single cell was taken from the stack and characterized with TEM as a function of location in the cathode, including nearby to and away from the DC interface and at the air inlet or air outlet region of the cell. Cross-sectional TEM specimens fabricated using a FIB [3,4,22] method that enables location and later imaging of precise positions in the SOFC were used. TEM, STEM, EDS, chemical mapping, EELS, and SAED techniques (described elsewhere [4,22-24]) were used to analyze chemical composition and crystal structures of the cathode materials.

## Results

Figure 1(a) shows a bright-field TEM image of an agglomerate in the initial LSCF powder. Most primary particle sizes are on the order of 50-100 nm in linear dimension. The SAED pattern of this agglomerate is shown in Figure 1(b). The pattern is best described

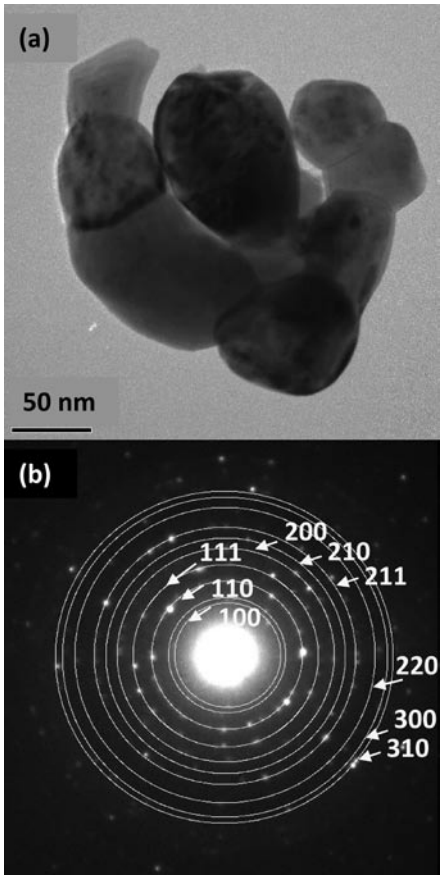


**FIGURE 1.** (a) Bright field TEM image of the initial LSCF powder. (b) SAED pattern of the powder in (a) with the cubic perovskite rings overlayed and indexed.

as spots on rings. These rings can be indexed to a perovskite pattern, as expected and as marked in the figure. EDS analysis (using standard correction techniques) of the cation composition was carried out in the STEM on many individual particles (including the particles shown in Figure 1(a)). The composition of the individual particles determined by EDS was always similar to the nominal composition, though the actual values varied significantly around the average compositions. The average elemental compositions and compositional ratios are given in Figure 2 (for this powder and for several cells) and the important cation ratios are listed in Table 1 (again for this powder and the cells discussed later). It should be mentioned that a few grains could be found in the initial powder whose compositions fell well outside the error bars shown in Figure 2 and Table 1. The general trend in such grains was to be B-site deficient and cobalt enriched relative to the average, even to the point of Fe:Co ≈1 and A:B ≈2.

Figure 3(a) shows the STEM image taken from the active anode region (>1 micron away from the DC interface) of the cell that was fabricated but untested, illustrating the baseline morphology of the as-prepared cell. Figures 3(b) and 3(c) show similar images (again taken from the active anode region >1 micron away from the DC interface) of the cell tested for 3,600 hrs near (a) the air inlet and (b) the air outlet. No obvious morphological variation was observed for the cathode microstructure anywhere in the active cathode. Again EDS analysis was carried out on the STEM by collecting information from many local particles (whose sizes are on the order of 100-250 nm in linear dimension). The average elemental compositions and compositional ratios are in Figure 2 and in Table 1. One can see that both the averages and the variations are similar in these three areas and in the initial powder. Averages from two different regions of the tested cell near the air inlet are reported in Figure 2, illustrating the local variation within a given cell is similar to variations between cells. (A few outlier grains were again observed to be Co-rich and B-site poor, similar to the initial powder.) These results illustrate that the local composition of LSCF in the bulk cathode does not vary significantly from the powder to the cell operated for 3,600 hrs.

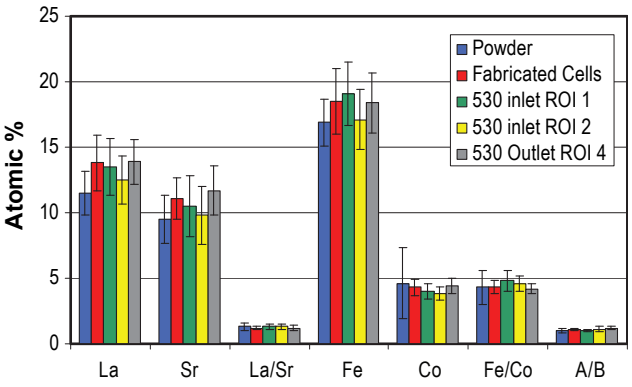


**FIGURE 2.** Bar graphs of the average compositions for LSCF given as elemental composition in atomic% of La, Sr, Fe, and Co and as the important ratios of these values, including La/Sr, Fe/Co, and A/B (or La+Sr/Fe+Co). Each group is broken down into the values for the initial powders (blue), the fabricated untested cell (red), two similar regions of interest (ROIs) of the tested cell near the inlet (green and yellow), and the tested cell near the outlet. For the cells, these regions are away from the LSCF/DC interface. The lines at the top of each bar represent the deviation in the values.

**TABLE 1.** Average values of the ratios of the elemental compositions of LSCF for the initial powder, the untested cell, the tested cell near the inlet, and the tested cell near the outlet. For the latter three, values are given for bulk regions away from (>1 micron) and interface regions nearby to (<0.5 micron) the LSCF/DC interface.

| LSCF Sample | Composition Ratio (at%/at%) | | |
|---|---|---|---|
| | La:Sr | Fe:Co | (La+Sr): (Fe+Co) |
| Powder | 1.3±0.3 | 4.3±1.3 | 1.0±0.2 |
| Untested Bulk | 1.3±0.2 | 4.2±0.4 | 1.1±0.1 |
| Tested Bulk Inlet | 1.3±0.2 | 4.8±0.8 | 1.0±0.1 |
| Tested Bulk Outlet | 1.2±0.2 | 4.2±0.4 | 1.2±0.1 |
| Untested Interface | 1.2±0.4 | 4.4±0.9 | 1.0±0.1 |
| Tested Interface Inlet | 1.6±0.6 | 5.4±2.9 | 0.9±0.3 |
| Tested Interface Outlet | 1.3±0.2 | 5±0.8 | 1.1±0.2 |

Figure 4(a) shows the STEM image taken from the LSCF cathode/DC interlayer interfacial region of the cell that was fabricated but untested, illustrating the baseline morphology of the as-prepared cell. Figures 4(b) and 4(c) show similar images (again taken from the LSCF cathode/DC interlayer interfacial region) of the cell tested for 3,600 hrs near (a) the air inlet and (b) the air outlet. The approximate interface is marked with a dashed line in each image. No obvious morphological variation was observed for either the LSCF or the DC, indicating the stability of this interface in agreement with the performance data. EDS analysis was carried out on the STEM by collecting information from many individual LSCF particles within a 1 micron distance from the interface. The average elemental compositions and compositional ratios are given in Table 1. One can see that the averages remain similar to the initial powder and bulk cathode. Near the air-inlet, the variations in the composition increased compared to the initial powders in a significant fashion, even though no morphological variation occurred and SAED showed only perovskite rings. Further work is necessary to determine whether or not this variation is: consistent

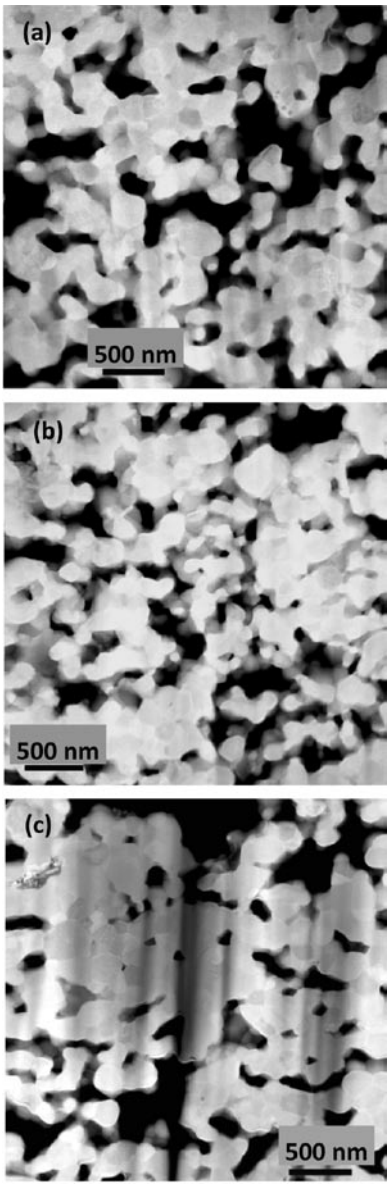


**FIGURE 3.** STEM images of the bulk LSCF cathode away from (>1 micron) the LSCF/DC interface in (a) the untested fabricated cell, (b) the tested cell near the air inlet, and (c) the tested cell near the air outlet. The morphologies are very similar and the microstructure has undergone little evolution after 3,600-hr operation.

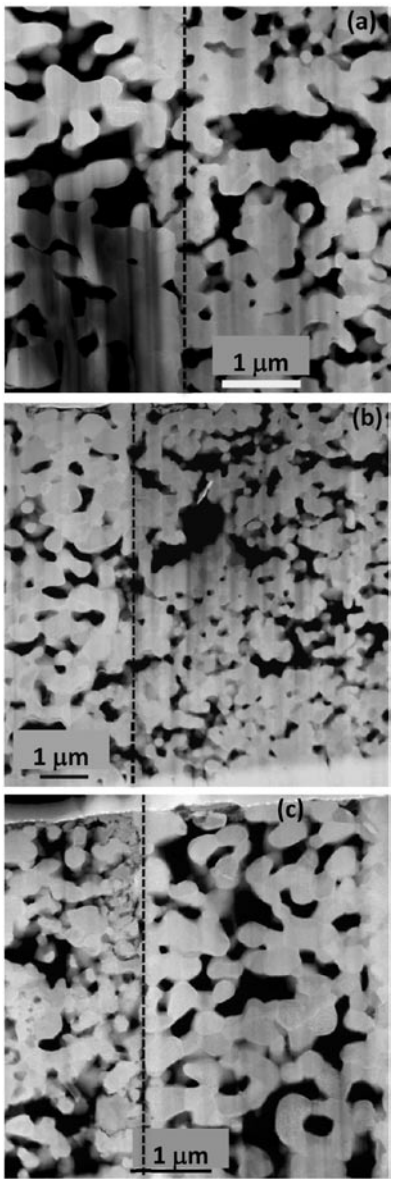


**FIGURE 4.** STEM images of the LSCF cathode at the LSCF/DC interface (whose approximate location is indicated by the dashed line) in (a) the untested cell, (b) the tested cell near the air inlet, and (c) the tested cell near the air outlet. The morphologies are similar to each other and to those shown in Figure 3, indicating the morphological stability of the LSCF in contact with the DC layer after 3,600-hr operation.

between cells, related to local operational variations, and/or relevant to performance.

Of the three reported degradation mechanisms, these results indicate that the perovskite LSCF 6428 is compositionally and morphologically stable in SOFC operational conditions and in contact with DC layers. Further work is necessary to investigate the nature of the interaction of the DC/LSCF cathode with YSZ, though initial observations in the tested cell are noted here. The last reported reaction mechanism in YSZ/DC/LSCF cathodes (tested in laboratory conditions) is the formation of Sr-Zr-O phases, even at the YSZ/DC interface [9,13,15-17]. It should be mentioned that Zr was found throughout the DC layer in the tested cell, but not in the LSCF layer. Furthermore, no minor phases were observed at the LSCF/DC interface (as discussed above) even when Zr was found in the neighboring DC grains. Though the morphology of the YSZ/DC layer appeared unchanged from the fabricated cell to the tested cell, the occurrence of Sr at the YSZ/DC interfaces was observed and a few minor grains having compositions close to Sr:Zr = 1:1 were identified (similar

to other observations [9,13,15-17]). Further work is necessary to investigate the amount of this phase with processing and operational time, as well as its relation to performance. Finally, it should be noted that no Cr was found in the cathode, indicating that Cr-poisoning [19,20] can be avoided in long-term stack operation.

## Conclusions and Future Directions

These results illustrate that the local morphology and composition of LSCF in the bulk cathode and at the LSCF/DC interface does not vary significantly from the powder to the cell operated in a real stack for 3,600 hrs. This result is important to SECA because it demonstrates that the reported benefits of using LSCF as a cathode can be realized in real stacks operated for at least 3,600 hrs; the low performance degradation and microstructural degradation imply that the lifetime of LSCF is significantly longer and within the SECA lifetime goals. Of the three reported degradation mechanisms, these results indicate that the perovskite LSCF 6428 is compositionally and morphologically stable in SOFC operational conditions and in contact with DC layers. Further work is necessary to determine the long-term interactions of YSZ and LSCF through the DC layers used in SOFC stacks.

## References


**1.** P.A. Salvador, R. Petrova, S. Wang, M. Krumpelt, T.A. Cruse, and B. Ingram, "TEM Investigations of Cr-Contamination in SOFC Cathodes," 2008, Paper III.A.3, pp. 1-5.

**2.** P.A. Salvador, S. Wang, M. Krumpelt, and T.A. Cruse, "Investigations of Cr-Contamination in SOFC Cathodes Using TEM," 2007, Paper IV.A.5, pp. 1-5.

**3.** T.A. Cruse, M. Krumpelt, B. Ingram, S. Wang, and P.A. Salvador, "Examination of Chromium's Effects on a LSM/YSZ Solid Oxide Fuel Cell Cathode," In *Advances in Solid Oxide Fuel Cells IV*, P. Singh, N.P. Bansal, Eds. Wiley-Interscience: 2008, pp. 147-158.

**4.** T.A. Cruse, M. Krumpelt, B. Ingram, S. Wang, and P.A. Salvador, "Effects of Cell Operating Conditions on Degradation by Chromium," In *TMS 2008 Annual Meeting Supplemental Proceedings Volume 1: Materials Processing and Properties*, 2008, pp. 571-580.

**5.** N. Sakai, H. Kishimoto, K. Yamaji, T. Horita, M.E. Brito, and H. Yokokawa, "Interface Stability of Perovskite Cathodes and Rare-Earth Doped Ceria Interlayer in SOFCs," In *J. Electrochem Soc*, 2007, Vol. 154, pp. B1331-B1337.

**6.** S.P. Simner, J.P. Shelton, and M.D. Anderson, "Interaction between La (Sr) $FeO_3$ SOFC cathode and YSZ electrolyte," *Solid State Ionics*, 2003.

**7.** S. Li, N. Xu, J. Shi, M.Z.C. Hu, and E.A. Payzant, "In Situ High-Temperature X-ray Diffraction Studies of Mixed-Conducting Perovskite-Type Oxides," *Journal of Materials Science Letters*, 2001.

**8.** G.C. Kostogloudis, G. Tsiniarakis, and C. Ftikos, "Chemical Reactivity of Perovskite Oxide SOFC Cathodes and Yttria Stabilized Zirconia," *Solid State Ionics*, 2000.

**9.** S. Uhlenbruck, T. Moskalewicz, and N. Jordan, "Element Interdiffusion at Electrolyte–Cathode Interfaces in Ceramic High-Temperature Fuel," *Solid State Ionics*, 2009.

**10.** W. Wang, M.D. Gross, J.M. Vohs, R.J. Gorte, "The Stability of LSF-YSZ Electrodes Prepared by Infiltration," *J. Electrochem Soc*, 2007.

**11.** P. Hjalmarsson, M. Sogaard, and M. Mogensen, "Electrochemical Performance and Degradation of $(La_{0.6}Sr_{0.4})(0.99)CoO_{3-\delta}$ as Porous SOFC-Cathode," In *Solid State Ionics*, 2008, Vol. 179, pp. 1422-1426.

**12.** F. Tietz, A. Mai, and D. Stoever, "From Powder Properties to Fuel Cell Performance - A Holistic Approach for SOFC Cathode Development," In *Solid State Ionics*, 2008, Vol. 179, pp. 1509-1515.

**13.** S.P. Simner, J.R. Bonnett, N.L. Canfield, K.D. Meinhardt, J.P. Shelton, V.L. Sprenkle, and J.W. Stevenson, "Development of Lanthanum Ferrite SOFC Cathodes," In *Journal of Power Sources*, 2003, Vol. 113, pp. 1-10.

**14.** S.P. Simner, M.D. Anderson, and J.E. Coleman, "Performance of a Novel La (Sr) Fe (Co) $O_3$–Ag SOFC Cathode," *Journal of Power Sources*, 2006.

**15.** S.P. Simner, M.D. Anderson, M.H. Engelhard, and J.W. Stevenson, "Degradation Mechanisms of La-Sr-Co-Fe-$O_3$ SOFC Cathodes," In *Electrochem Solid St*, 2006, Vol. 9, pp. A478-A481.

**16.** A. Mai, M. Becker, W. Assenmacher, F. Tietz, D. Hathiramani, E. Ivers-Tiffee, D. Stoever, and W. Mader, "Time-Dependent Performance of Mixed-Conducting SOFC Cathodes," In *Solid State Ionics*, 2006, Vol. 177, pp. 1965-1968.

**17.** A. Mai, V.A.C. Haanappel, S. Uhlenbruck, and F. Tietz, "Ferrite-Based Perovskites as Cathode Materials for Anode-Supported Solid Oxide Fuel Cells," *Solid State Ionics*, 2005.

**18.** S.J. Xu and W.J. Thomson, "Stability of $La_{0.6}Sr_{0.4}Co_{0.2}Fe_{0.8}O_{3-\delta}$ Perovskite Membranes in Reducing and Nonreducing Environments," In *Ind Eng Chem Res*, 1998, Vol. 37, pp. 1290-1299.

**19.** J. Kim, V.L. Sprenkle, N.L. Canfield, K.D. Meinhardt, and L.A. Chick, "Effects of Chrome Contamination on the Performance of $La_{0.6}Sr_{0.4}Co_{0.2}Fe_{0.8}O_3$ Cathode Used in Solid Oxide Fuel Cells," In *J. Electrochem Soc*, 2006, Vol. 153, pp. A880-A886.

**20.** X. Li, J. Lee, and B.N. Popov, "Performance Studies of Solid Oxide Fuel Cell Cathodes in the Presence of Bare and Cobalt Coated E-brite Alloy Interconnects," In *Journal of Power Sources*, 2009, Vol. 187, pp. 356-362.

**21.** K. Sasaki, K. Susuki, A. Iyoshi, M. Uchimura, N. Imamura, H. Kusaba, Y. Teraoka, H. Fuchino, K. Tsujimoto, Y. Uchida, and N. Jingod, "$H_2S$ Poisoning of Solid Oxide Fuel Cells," *Journal of The Electrochemical Society*, 2006, Vol. 153 (11), pp. A2023-A2029.

**22.** P. Fisher, S. Wang, M. Skowronski, P.A. Salvador, M. Snyder, O. Maksimov, "A Series of Layered Intergrowth Phases Grown by Molecular Beam Epitaxy: $Sr_mTiO_{2+m}$ (m=1-5)," *Applied Physics Letters*, 2007, Vol. 91 (25), 252901.

**23.** A.J. Francis, C.G. Roberts, Y. Cao, A.D. Rollett, and P.A. Salvador, "Monte Carlo Simulations and Experimental Observations of Templated Grain Growth in Thin Platinum Films," *Acta Materialia*, 2007, Vol. 55 (18), pp. 6159-6169.

**24.** S. Havelia, S. Wang, K.R. Balasubramaniam, and P.A. Salvador, "Epitaxial Stabilization of (110)-Layered Perovskites of the $RE_2Ti_2O_7$ (RE = La, Nd, Sm, Gd) Family," *Journal of Solid State Chemistry*, 2009, Vol. 182, pp. 1603-1610.

# III.A.5 Performance Degradation of LSCF Cathodes

Matthew Alinger (Primary Contact), James Ruud
GE Global Research
1 Research Circle, MB277
Niskayuna, NY 12309
Phone: (518) 387-5124; Fax: (518) 387-5576
E-mail: alinger@ge.com

DOE Project Manager: Joseph Stoffa
Phone: (304) 285-0285
E-mail: Joseph.Stoffa@netl.doe.gov

Subcontractors:
Rensselaer Polytechnic Institute, Troy, NY
NexTech Materials, Lewis Center, OH

Contract Number: NT0004109

Start Date: October 1, 2008
End Date: September 30, 2010

### FY 2009 Objectives

- Identify fundamental cathode degradation mechanisms and cost-effective mitigation strategies.
- Validate degradation mechanisms and mitigation solutions on representative area cells.
- Evaluate operational condition-specific (temperature, voltage, current) performance degradation.
- Evaluate alternative cell manufacturing approaches to address barrier layer contact degradation.
- Investigate interconnect chromium evaporation to optimize coating structure to mitigate chromium transport.

### Accomplishments

- Identified high-impact fundamental degradation mechanisms and developed cost-effective mitigation solutions.
- Demonstrated high, stable performance of lanthanum strontium cobalt ferrite (LSCF)-based cathode solid oxide fuel cells (SOFCs) with gold current collectors.
- Demonstrated parabolic power density degradation behavior with ferritic stainless steel current collectors that are indicative of chromia scale growth.
- Validated 441HP stainless steel as a viable, low-cost, current collector alloy during a 1,500-hour electrochemical test.
- Designed, constructed and validated a novel approach to real time measurement of chromium volatilization from interconnect alloys using solution conductivity.

## Introduction

Through research and development efforts conducted within the Department of Energy's Solid State Energy Conversion Alliance fuel cell program, considerable progress has been made towards the realization of current SOFC stack cost goals. However, performance degradation of high-performance SOFC cathodes, in particular $La_{1-x}Sr_xCo_{1-y}Fe_yO_{3-\delta}$ (LSCF), remains a technical barrier to the commercial viability of SOFC technology. The objective of this project is to identify the dominant degradation mechanisms, and to develop and implement cost-effective mitigation strategies to retain high electrochemical performance in LSCF-based cathodes over the operational lifetime of an SOFC stack (>40,000 hours). The project goal is to reduce power density degradation rates to less than 1% per 1,000 hours, while maintaining high initial power densities (>0.75 W/cm$^2$).

## Approach

The LSCF-based cathode degradation mechanisms will be identified and evaluated using the state-of-the-art SOFC characterization laboratory at the GE Global Research Center, Niskayuna, New York. The approach relies on the electrochemical testing of SOFCs under realistic operating conditions. However, given the complexity of SOFCs, off-line laboratory testing including sintering studies, contact resistance, and diffusion couples will be leveraged to isolate and understand specific mechanisms under representative conditions. The structural and chemical degradation components will be identified using advanced characterization techniques such as high-resolution transmission electron microscopy, scanning electron microscope microprobe, and high-angular resolution synchrotron X-ray diffraction.

As the contact integrity of critical interfaces has been recently identified as a major degradation mechanism, alternative cell manufacturing approaches will also be evaluated. In particular, approaches will be evaluated for improved barrier layers to provide enhanced cathode interfacial strength. In addition, interconnect chromium barrier coatings will be evaluated and optimized, focusing on $(Mn,Co)_3O_4$ spinel, for thin and dense coatings to mitigate the well-

known chromium poisoning degradation mechanism. Combined, these results will enable the development of structure-property-performance correlations. These will be used to guide the identification and development of cost-effective path(s) for reduced degradation of high-performance LSCF-based SOFCs.

## Results

Cathode-side degradation mechanisms comprise contributions of various ohmic (e.g., oxide scale growth and interaction/reaction layers between the metal interconnect and cathode) and non-ohmic (destruction of catalytically active sites and diffusion pathways for oxygen reduction within the cathode) mechanisms. A summary of potential mechanisms is presented in Figure 1. A combination of electrochemical cell testing and electrical contact resistance experiments have been employed to simulate the configuration and conditions of operating SOFCs. A quantitative comparison of the results from the experiments, in conjunction with existing models, will furnish understanding of the degradation processes that contribute to the performance degradation of LSCF-based SOFCs.

In order to isolate and study specific degradation mechanisms, idealized testing configurations are useful. For example, gold can be used as a cathode current collector to remove the potentially confounding effects of using ferritic stainless steel (FSS) current collectors. Figure 2 shows the evolution of power density and area specific resistance (ASR) as a function of time for cell testing using gold current collectors. These tests were conducted at 800°C and operated at 1.25 A/cm$^2$ for ~1,000 hours and the data were collected from periodic power curves at 0.7 V. The power density degradation rate is ~0%/1,000 h and the ASR rate is ~1 mΩ-cm$^2$/1,000 h.

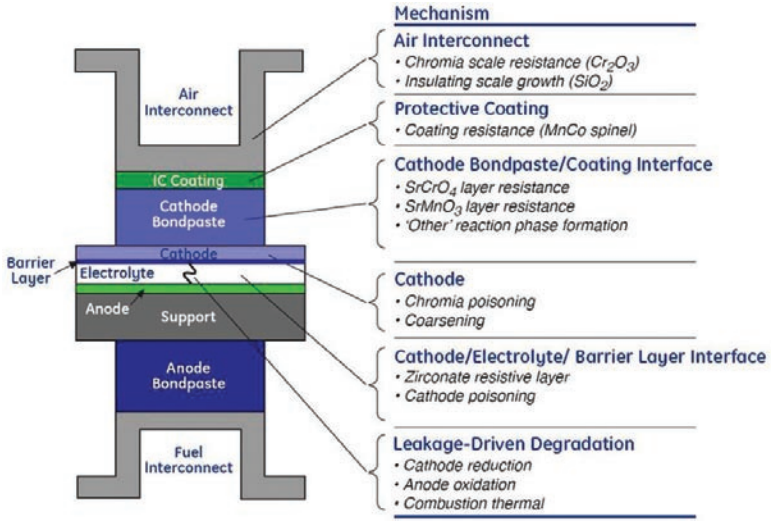


**FIGURE 1.** Schematic of an SOFC Highlighting Potential Degradation Mechanisms

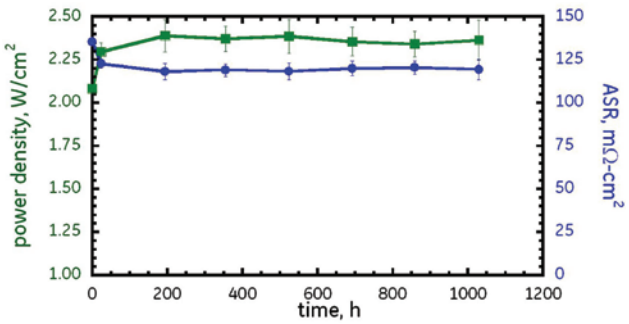


**FIGURE 2.** Evolution of Power Density (green) and ASR (blue) for Three Cells Averaged over 1,000 Hours at 0.7 V and 800°C with Gold Cathode Current Collectors

Thus, there is no observable degradation of the cells with gold current collectors. In addition, the electrochemical performance, >2.3 W/cm$^2$, is very high indicating that high performance does not necessarily correlate to high degradation. The results indicate that properly optimized LSCF-based cathodes are inherently stable, and that the electrical and electrochemical paths of the LSCF-based system, using gold current collectors, are durable and robust over time.

Upon the introduction of a FSS interconnect, however, the degradation behavior is altered. Figure 3 shows the effect of the stable LSCF-based cathode system, using 441HP FSS current collectors with protective spinel coatings. The linear power density degradation rate is ~1.9%/1,000 h. The corresponding linear ASR increase is ~12 mΩ-cm$^2$/1,000 h. Most interesting is that the curve shape of the degradation behavior is non-linear, and gradually decreases with time, as would be anticipated from a diffusion limited growth process (i.e. chromia growth on the current collector). Through impedance spectroscopy, the measured degradation is determined to be entirely ohmic. The ohmic degradation is consistent with the expected resistance increase resulting from the thermally grown chromia on the FSS current collector. Extrapolation of this curve leads to a linear power density degradation rate of ~0.24%/1,000 h, or <10% over a 40,000-hour lifetime. However, in order to meet targeted performances at end of life (40,000 hours), this degradation mechanism must be better understood.

There are several significant risks to the extrapolation of the data shown in Figure 3. First, late-blooming degradation mechanisms may not be accounted for, including detrimental secondary phase formation. And, second, these results are largely made possible through the implementation of a protective

coating on the cathode interconnect that is capable of suppressing the volatilization of Cr and subsequent cathode poisoning. Thus, the ability of this coating to suppress Cr volatilization for the life of the cell must be determined. One approach is to directly measure the Cr evaporation rate in the experimental setup shown schematically in Figure 4. These measurements utilize a novel method where a de-ionized water solution captures the vaporized chromium ions and the real-time change in solution conductivity is converted to a vaporization rate. Initial experiments were performed to measure the effect of chromium concentration on solution conductivity and results indicate that the solution conductivity method will provide the accuracy necessary for measuring the concentrations of chromium volatilized. Detailed knowledge of the coating compositions and structures capable of suppressing chromium volatilization will enable optimization of the cathode interconnect coating.

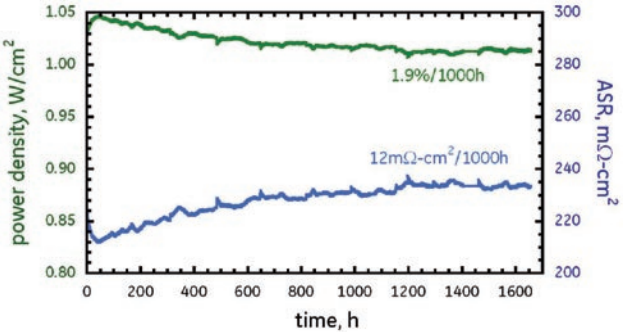


**FIGURE 3.** Evolution of Power Density (green) and ASR (blue) for Two Cells Averaged over 1,600 Hours at 1.25 A/cm$^2$ and 800°C with Spinel Coated 441SS Cathode Current Collectors

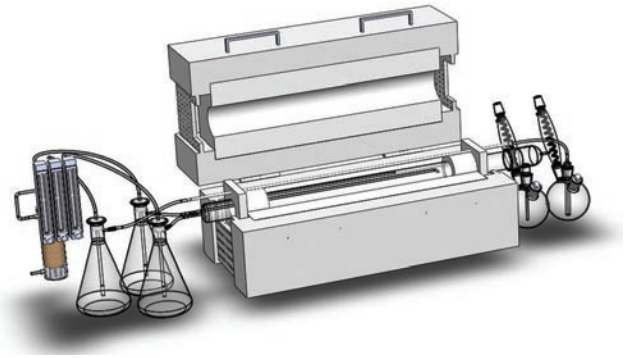

**FIGURE 4.** Schematic of Chromium Volatilization Measurement Apparatus

## Conclusions and Future Directions

The inherent stability and high electrochemical performance entitlement of LSCF cathode-based SOFCs has been demonstrated. The high performance of this material system plays a major role in decreasing the cost per kilowatt of SOFCs. However, a reliable solution to the degradation behavior requires more detailed knowledge of the kinetics of the dominant mechanisms, requiring additional investigation. Ultimately, a degradation mitigation solution for high performance (>0.75 W/cm$^2$) SOFCs with ferritic steel interconnects, having a repeatable performance degradation of <1%/1,000 h , will be demonstrated.

## FY 2009 Publications/Presentations

**1.** Quarterly Report for 1st calendar quarter 2009, January 30, 2009.

**2.** Quarterly Report for 2nd calendar quarter 2009, April 30, 2009.

# III.A.6 Characterization of Atomic and Electronic Structure of Electrochemically Active SOFC Cathode Surfaces

Meilin Liu (Primary Contact), Kevin Blinn, and Harry Abernathy
Georgia Institute of Technology
771 Ferst Drive
Atlanta, GA 30332
Phone: (404) 894-6114; Fax: (404) 894-9140
E-mail: meilin.liu@mse.gatech.edu

DOE Project Manager: Briggs White
Phone: (304) 285-5437
E-mail: Briggs.White@netl.doe.gov

Contract Number: 42735

Start Date: February 13, 2006
End Date: August 12, 2009

### FY 2009 Objectives

- Use simple modification techniques on solid oxide fuel cell (SOFC) cathode material surfaces to achieve surface-enhanced Raman scattering (SERS) and increase detection sensitivity for pertinent species, such as adsorbed and reduced oxygen.
- Demonstrate Raman spectroscopy as a versatile tool for characterizing inhomogeneities in cathode material surfaces that can occur under operating conditions.

### Accomplishments

- Evidence of adsorbed and reduced oxygen species on cathode surfaces has been shown by SERS techniques.
- Signal enhancement of one or more orders of magnitude was achieved for species adsorbed on cathode surfaces, with up to 15-20% incidence of SERS for one modification technique.
- Changes in stoichiometry of the cathode surface before and after exposure to simulated SOFC operating conditions were detected by Raman spectroscopy.

## Introduction

Unraveling the mechanisms of oxygen reduction is a critical step toward the rational design of more efficient SOFC cathode materials. One step towards improving the understanding of oxygen reduction is the development of a tool for detecting oxygen species on cathode surfaces as well as the chemical and structural properties of the cathode in situ, or under its operating conditions. Conventional surface analysis methods are ill-suited for this task, as they tend to require high vacuum environments for successful application. We report Raman spectroscopy as a viable route to experimentally characterizing various $ABO_3$ perovskite SOFC cathode materials by species adsorbed on their surfaces as well as their surface chemistry. In addition, we have demonstrated methods for increasing signal of these surface species through SERS.

## Approach

For SERS experiments, the candidate cathode materials SSC ($Sm_{0.5}Sr_{0.5}CoO_{3-\delta}$), LSM ($La_{0.8}Sr_{0.2}O_{3-\delta}$), and LSCF ($La_{1-x}Sr_xCo_{0.2}Fe_{0.8}O_{3-\delta}$) were studied. Dense cathode surfaces were modified by nanoscale metal structures either through dropwise application of 20 nm colloidal silver or gold nanoparticles or direct current (DC) sputtering of discontinuous silver thin films on surfaces. Samples for which the colloidal methods were used were fired to ~300°C in order to modify the structure of the surface nanoparticles. Surfaces were analyzed by Raman microscope either in ambient air or in a chamber capable of inducing different atmospheres and temperatures on the sample. Due to the tendency for favorable nanoscale metal structures on the surface to form "hot spots" where signal enhancement was highest but were not optically observable, spectra were collected from different spots in large rectangular grids up to 100 µm in length. Some peaks in these spectra were assigned to possible adsorbed species.

Additionally, conventional Raman spectroscopy was used to analyze LSCF before and after it was held under an intermediate SOFC operating temperature and high DC polarization. Its spectra were compared to powders of different stoichiometries to show changes in its surface chemistry following such treatment.

## Results

For any of our SERS experiments, most spectra collected consisted of a fluorescence signal, likely produced by the surface metal nanoparticles themselves, which dominated over any other type of signal that might otherwise be observed. In the case of samples treated with silver, however, spectra collected from some spots displayed signals attributable to SERS effects. Such spectra, which were collected from SSC samples

modified by silver colloids, are shown in Figure 1. Typically, only about 5-10% of the points sampled from any one area treated with silver colloid generated a spectrum with a number of peaks comparable to the spectrum in Figure 1. The relative scarcity of these spots supports the theory that the effect only occurs in certain "hot spots" where the metal nanostructures happen to be in a favorable configuration. While there are many peaks in these spectra that require identification, the spectra show evidence of adsorbed molecular oxygen (near 1,530 $cm^{-1}$) and adsorbed reduced oxygen (800-1,100 $cm^{-1}$ range) [1]. The ability to observe how these peaks change under SOFC operating conditions would help elucidate the oxygen reduction process. It should be noted that these spectra only came from silver-treated samples, however. The samples treated with gold nanoparticles did not produce a surface-specific SERS signal in any one spot measured, possibly due to the fact that 514 nm, our Raman spectrometer's wavelength, is below the absorption maximum of the gold nanoparticles.

Samples treated by sputtering showed slightly different behavior. Figure 2 displays spectra collected from LSCF and LSM sample surfaces with discontinuous silver films. While the spectra show indication of signal enhancement, the potential reduced oxygen species features are typically not as apparent as with some of the spectra with signal enhanced by colloids. That being said, a larger percentage (~10-20%) of the sample points collected from the sputtered samples show signs of SERS than those collected from colloidal samples. The enhanced adsorbed molecular oxygen peak is usually present with the sputtered samples, as well. As can be seen above, the same features in general can be found in spectra from LSCF and LSM samples, but with slight shifts and varying degrees of enhancement, suggesting that the signals originate from the surface of the cathode samples rather than the enhancing nanoparticles themselves.

We have also analyzed sputter-treated cathode samples under atmospheres that contain only oxygen and inert gas (Ar) to examine the effects on the spectra and isolate oxygen peaks. Figure 3 shows these effects. As can be observed in the figure, some peaks in the 800-1,100 $cm^{-1}$ range change upon exposure, supporting the claim that at least some of these features correspond to reduced oxygen species. In addition, the features marked with asterisks, which may correspond to disordered carbon and graphite [2], disappear in the spectrum from the oxygen-exposed sample. This may happen due to oxidation of carbon.

Some of our other work has involved the use of Raman spectroscopy to characterize the degradation of LSCF under polarization. One possible reason

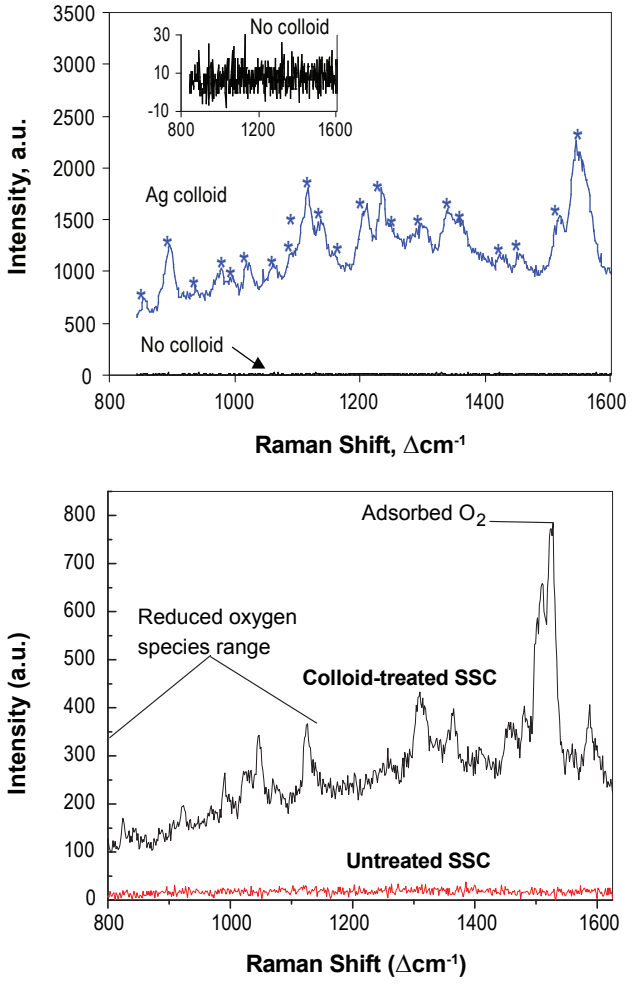


**FIGURE 1.** Raman spectra collected from various SSC samples modified with 20 nm Ag colloid in air. Different SERS "hot spots" may enhance different species signals and thus different peaks.

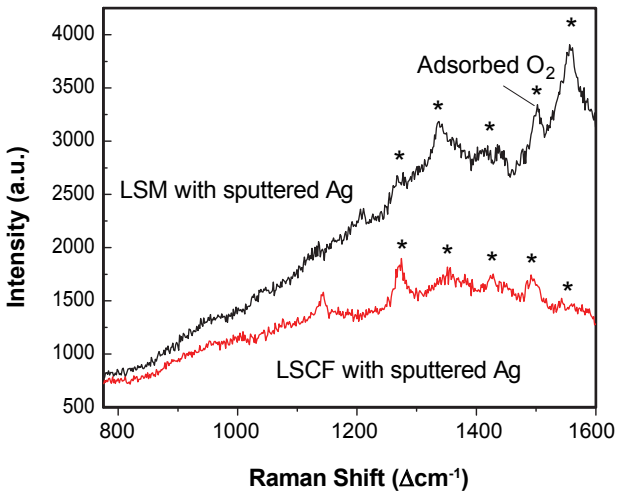


**FIGURE 2.** Raman spectra for LSM and LSCF samples in air after DC sputtering of Ag.

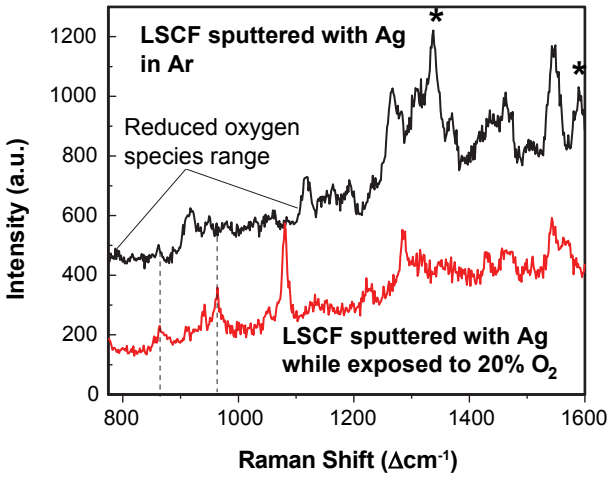


**FIGURE 3.** Raman spectra collected at room temperature from LSCF with sputtered Ag under various controlled atmosphere conditions (argon and oxygen gases).

for degradation from polarization is the transport of strontium from the lattice to the surface, forming a layer of SrO. This layer would reduce the catalytic activity on the surface of the material, and increase the ohmic resistance of the cathode due to the poor electronic conductivity of SrO. Figure 4a shows spectra collected from a 1 µm LSCF film on a gadolinium-doped ceria (GDC) substrate before and after exposure to 0.8 V DC polarization at 700°C. A shift in the peaks can be observed, as well as an increase in the ratio of the right peak to the left. According to LSCF powders of various stoichiometries that were also measured by Raman spectroscopy (Figure 4b), this change possibly corresponds to an increase in the La/Sr ratio in the lattice, suggesting the migration of Sr out of the lattice that may form its own oxide on the surface.

## Conclusions and Future Work

While we have potentially located the pertinent oxygen species peaks needed to understand the oxygen reduction process using SERS, we need to further analyze the spectra and correlate them with chemical calculations already made earlier in the project as well as further ones that might be necessary. We will further examine the effects of DC polarization and oxygen partial pressure on pure cathode pellet samples treated for SERS as we have described previously (colloidal and sputter deposition of metal nanoparticles). We will also evaluate sputtered cathode thin films on other substrates, similar to the one described previously, by SERS methods.

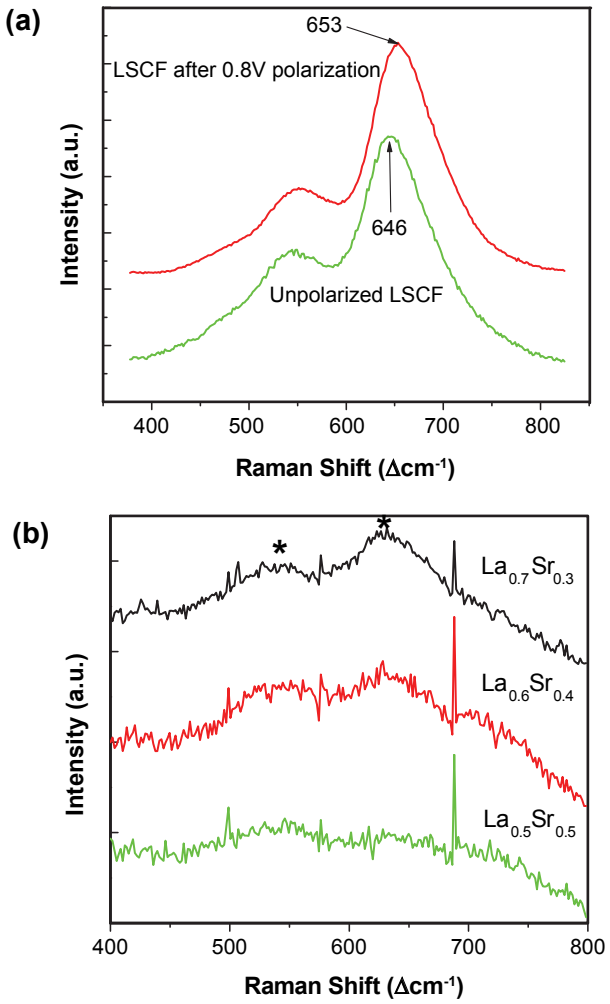


**FIGURE 4.** (a) Raman spectrum collected from surface of LSCF film on GDC pellet in air before and after application of 0.8 V DC polarization. A shift in the wave-numbers of the peaks can be seen, and the ratio of the larger peak to the smaller one also increases. (b) Raman spectra collected from powders of different LSCF ($La_{1-x}Sr_xCo_{0.2}Fe_{0.8}O_{3-\delta}$) compositions. The two marked peaks vary with change in La/Sr ratio.

## FY 2009 Publications

**1.** K.S. Blinn, H.W. Abernathy, and M. Liu, "Surface Enhanced Raman Spectroscopy for Investigation of SOFC Cathodes," *33rd International Conference on Advanced Ceramics and Composites (ICACC)*, presented at conference and accepted for publication in proceedings, 2009.

**2.** H. Abernathy, E. Koep, C. Compson, Z. Cheng, and M. Liu, "Monitoring Ag-Cr Interactions in SOFC Cathodes Using Raman Spectroscopy," *Journal of Physical Chemistry C,* 112(34), 13299-13303, 2008.

**3.** H. Chen, A. Aleksandrov, M. Liu, and T. Orlando, "Electron Stimulated Desorption of O2+ from Gadolinia-Doped Ceria Surfaces," *Applied Surface Science*, 254(16), 4965-4969, 2008.

**4.** Y.M. Choi, M.E. Lynch, M.C. Lin, and M. Liu, "Prediction of $O_2$ Dissociation Kinetics on $LaMnO_3$-Based Cathode Materials for Solid Oxide Fuel Cells," *Journal of Physical Chemistry C,* 113(17), 7290-7297, 2009.

**5.** J.H. Wang, Y.M. Choi, and M. Liu, "Quantum Chemical Calculations of Surface and Interfacial Reactions in Solid Oxide Fuel Cells," In Quantum Chemical Calculations of Surfaces and Interfaces of Materials (Editors: V.A. Basiuk and P. Ugliengo), Chapter 14, p. 289-304, American Scientific Publishers, Los Angeles 2008.

## FY 2009 Presentations

**1.** M. Liu, "Modeling and Simulation of Electrode Materials for SOFC," Presented to International Conference on Clean Energy, NRC, Vancouver, Canada, March 15, 2008.

**2.** M. Liu, "Recent Development in New Materials for Solid Oxide Fuel Cells," Presented to the International Symposium on Renewable Energies, South Korea, December 2–6, 2008.

**3.** M. Liu, "Modeling, Simulation, and In-situ Characterization of Electrode Materials for Solid Oxide Fuel Cells," Columbia University, New York, New York, April 18, 2008.

**4.** M. Liu, "Probing and Mapping Electrode Reactions Using Raman Spectroscopy," University of West Virginia, Morgantown, West Virginia, July 8, 2008.

## References

**1.** Y.M. Choi, H. Abernathy, H.-T. Chen, M.C. Lin, and M. Liu, "Characterization of $O_2$-$CeO_2$ Interactions Using in Situ Raman Spectroscopy and First-Principle Calculations," *ChemPhysChem*, 7, 1957-1963, 2006.

**2.** M. Pomfret, J.C. Owrutsky, and R.A. Walker, "In Situ Studies of Fuel Oxidation in Solid Oxide Fuel Cells," *Analytical Chemistry*, 79, 2367-2372, 2007.

# III.A.7 Theory, Investigation and Stability of Cathode Electro-Catalytic Activity

Meilin Liu (Primary Contact), Mingfei Liu, Ze Liu, Lei Yang, Lifang Nie
Georgia Institute of Technology
School of Materials Science and Engineering
771 Ferst Drive
Atlanta, GA 30332-0245
Phone: (404) 894-6114; Fax: (404) 894-9140
E-mail: meilin.liu@mse.gatech.edu

DOE Project Manager: Briggs White
Phone: (304) 285-5437
E-mail: Briggs.White@netl.doe.gov

Contract Number: NT0006557

Start Date: September 1, 2008
End Date: August 31, 2011

## Objectives

- Characterize the surface composition, morphology, and electro-catalytic properties of catalysts coated on $La_xSr_{1-x}Co_yFe_{1-y}O_{3-\delta}$ (LSCF).
- Establish the scientific basis for rational design of high-performance cathodes by combining a porous backbone (such as LSCF) with a thin catalyst coating.

## Accomplishments

- Developed a methodology for optimizing the morphology and thickness of infiltrated catalyst coatings.
- Developed a standard procedure to fabricate anode-supported yttria-stabilized zirconia (YSZ) electrolyte solid oxide fuel cells (SOFCs) utilizing an LSCF cathode.
- Demonstrated that the initial performance of a single cell with an LSCF cathode can be improved by infiltration of a proper amount of $La_xSr_{1-x}MnO_{3-\delta}$ (LSM).
- Demonstrated that LSCF cathodes infiltrated with a thin coating of LSM have improved performance stability.

## Introduction

One of the reasons that LSCF-based cathodes show much better performance than those based on LSM is that LSCF has a much higher ionic and electronic conductivity than LSM, significantly extending the active sites beyond the triple-phase boundaries [1]. One obvious downfall for LSCF is that it reacts adversely with YSZ, which can be mitigated by the use of a buffer layer of doped-$CeO_2$ between the LSCF and YSZ [2]. However, the catalytic activity of the stand-alone LSCF cathodes is likely to be limited by the surface catalytic properties. Further, the surface properties of LSCF cathodes may change during operation, which presents an opportunity to improve the stability of LSCF cathode performance even further. Thus, it is hypothesized that the *performance* and *stability* of a porous LSCF cathode may be improved by the application of a catalytically active coating though infiltration. The selection of the catalytic materials as well as the detailed microstructures of the porous LSCF and the catalyst layer may critically impact the performance of the proposed cathodes. The objective of this project is to optimize the composition and morphology of the catalyst layer and microstructure of the LSCF backbone for better performance.

## Approach

The proposed cathode consists of a porous LSCF backbone with a thin-film coating of LSM. In order to control the microstructure and thickness of the LSCF backbone, we developed a tape-casting process for fabrication of the LSCF layer. Then, a solution infiltration process was used to deposit a thin LSM coating on the LSCF backbone [3]. Initial studies were focused on the optimization of the fabrication process for anode-supported cells and the LSM infiltration process to achieve reproducible and consistent results. Finally, the electro-chemical performances of the LSCF cathode with and without the LSM coating were examined in symmetric cells as well as anode-supported button cells by analyzing impedance response, current-voltage characteristics, and long-term stability.

## Results

**Deposition of LSM films on a dense LSCF surface:** Thin-film coatings of LSM were deposited on the LSCF backbone by a nitrite solution infiltration process. In order to facilitate the characterization of the phase, morphology, and thickness of the LSM films derived from the LSM nitrite solutions, the LSM coatings were first deposited to dense LSCF substrates. The chemistry of the LSM solution (e.g., solvents, surfactant, chelating agents, and LSM concentration) and heating rate were investigated to obtain an uniform LSM coating on a dense LSCF surface.

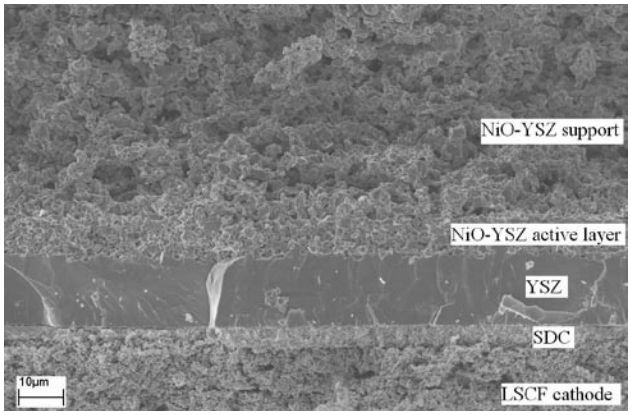


**FIGURE 1.** A Typical Cross-Sectional View of a Home-Fabricated Anode-Supported Single Cell

**Optimization of the cell fabrication processes**: We have developed a reproducible process for fabrication of button cells. Both the Ni-YSZ anode support layers (~800 μm) and the LSCF cathode layers were fabricated using a tape-casting process. The NiO-YSZ active layer, YSZ electrolyte layer, and samaria-doped ceria (SDC) or gadolinium-doped ceria buffer layer were fabricated by a suspension coating process. The thicknesses and microstructure of each layer can be easily controlled using these processes. The fabrication processes, including firing temperature and schedule as well as thickness of each layer, were optimized to produce high-performance cells. Shown in Figure 1 is a typical cross-sectional view of a home-prepared button cell, demonstrating peak power densities of 1.43, 0.81, and 0.53 W/cm$^2$ at 800, 750, and 700°C, respectively.

**Infiltration of LSM into porous LSCF backbone:** A solution infiltration process has been developed for deposition of a thin LSM layer on porous LSCF backbones. To control the thickness and morphology, an LSM solution with different concentrations of precursors was used for infiltration, including 0.005, 0.01, 0.03 and 0.06 mol/L. An appropriate amount of $La(NO_3)_3$, $Sr(NO_3)_2$ and $Mn(NO_3)_2$ was dissolved in a mixture of water and ethanol (1:1, vol/vol) to prepare these solutions. Glycine was added as the chelating agent (the molar ratio of glycine to metal was ~1.3:1). Polyvinyl pyrrolidone was used as a surfactant to improve the wetting property of the solution onto the LSCF backbone. A 5 μl LSM solution was infiltrated into the porous LSCF electrode (superficial area of ~0.24 cm$^2$) using a micro-liter syringe in order to accurately control the amount of solution. Vacuum was then used to facilitate the penetration of the LSM solution into the pores of the LSCF cathodes. The infiltrated cells were fired at 900°C for 1 hour to obtain the desired phase of LSM. Shown in Figure 2(a) is a typical view of a blank LSCF backbone (without LSM infiltration); the surface is clean and the grain boundaries are clear. Shown in Figure 2(b) is an image of the porous LSCF backbone infiltrated with a 0.03 mol/L LSM solution. An LSM film was uniformly coated on LSCF grains. The thickness of the film appears to be about 20 nm.

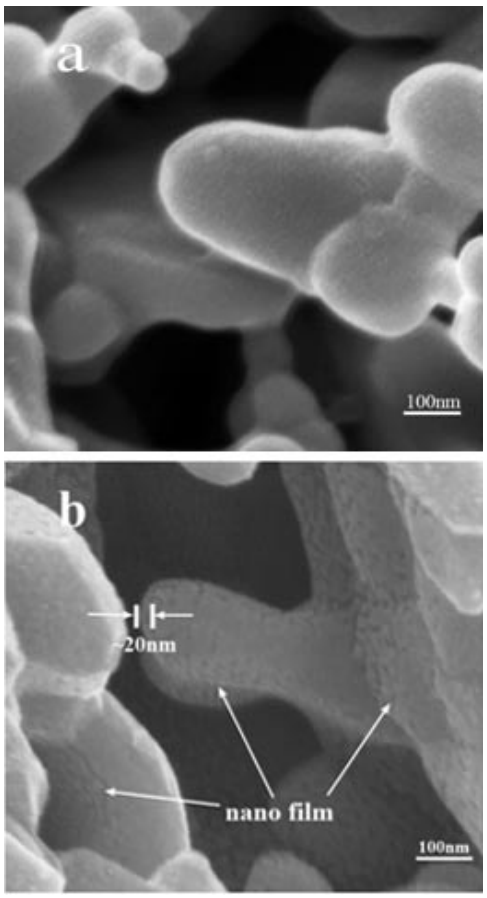


**FIGURE 2.** Scanning Electron Microscope Images of the Porous LSCF Backbone (a) without LSM Infiltration (blank) and (b) Infiltrated with 0.0312 mol/L LSM Solution

**Cell performance of LSCF cathode with and without LSM infiltration:** The performance and the stability of the cells with and without LSM infiltration have been evaluated under typical fuel cell operating conditions. Shown in Figure 3 is the comparison of the peak power densities for the cells with and without LSM infiltration. Clearly, cell performance has been improved by infiltration of an appropriate amount of LSM. With 0.03 mol/L LSM solution infiltration, peak power densities of 1.58 and 0.6 W/cm$^2$ have been achieved at 800 and 700°C, respectively, representing ~10% enhancement. However, further increasing the concentration of the LSM solution to 0.06 mol/L resulted in a lower power density of 0.42 W/cm$^2$ at 700°C, due most likely to the poor performance of a thick LSM coating at low temperatures. Figure 4 shows the current densities of two test cells, with and without infiltration of LSM, as a function of time under a constant cell voltage of 0.7 V at 750°C. The cell infiltrated with LSM showed higher current density

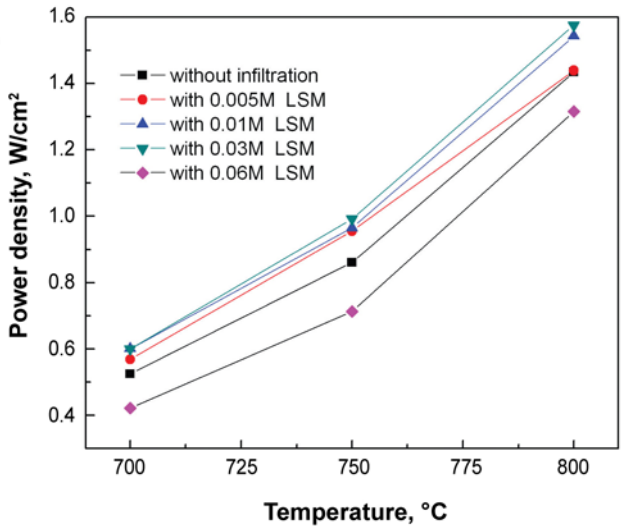


**FIGURE 3.** Typical Peak Power Densities of Home-Fabricated Cells with and without LSM Infiltration (Humidified Hydrogen as Fuel and Stationary Air as Oxidant)

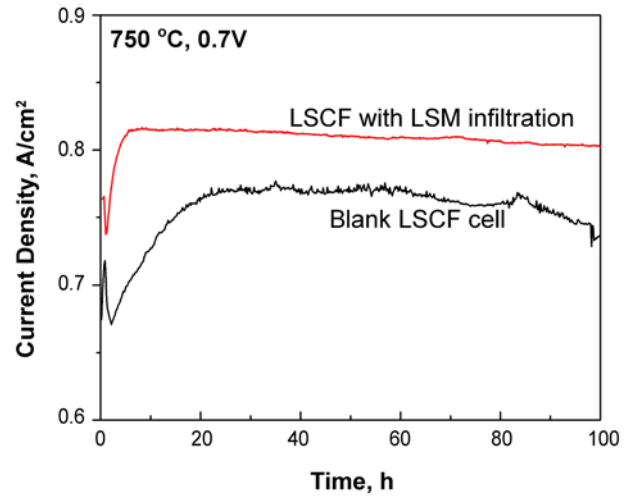


**FIGURE 4.** Performances of Two Test Cells Based on LSCF Cathodes (with and without LSM Infiltration) as Measured under a Constant Cell Voltage of 0.7 V at 750°C (Humidified Hydrogen as Fuel and Stationary Air as Oxidant)

and better stability than the blank cell without LSM infiltration.

## Conclusions

We have developed a reliable process to fabricate anode-supported cells with an LSCF cathode for evaluating the catalytic properties of a thin coating on the LSCF backbone. Results suggest that 1) home-fabricated button cells show high cell performance at 700-800°C; 2) the stability and performance of LSCF porous electrodes can be improved by infiltrating the proper amount of LSM. LSM-coated LSCF offers better performance and stability. However, several fundamental questions still remain; it is still not clear what happens at the interface between the LSM and LSCF and why an LSM coating improves the stability of LSCF cathodes. We plan to investigate the mechanistic details, including characterization of both continuous and discontinuous LSM films on dense LSCF backbones under various operating conditions. While the concept feasibility of the electrode architecture is demonstrated, other catalytically more active catalysts and more conductive matrixes are yet to be identified or developed for further enhancement of the performance and stability of SOFC cathodes.

## Patents Issued

**1.** D. Mebane, M. Liu, L. Wilson, and W. Surdoval, "Novel cathode design for solid oxide fuel cells using particle infiltration technology," Provisional Patent Application.

## FY 2009 Publications

**1.** M.E. Lynch, D.S. Mebane, Y. Liu and M. Liu, "Triple Phase Boundary and Surface Transport in Mixed Conducting Patterned Electrodes," *Journal of the Electrochemical Society*, 155(6): B635-B643, 2008.

**2.** D.S. Mebane, Y.J. Liu, and M. Liu, "Refinement of the Bulk Defect Model for $La_xSr_{1-x}MnO_{3\pm\delta}$," *Solid State Ionics*, 178(39-40): 1950-1957, 2008.

**3.** M. Lynch, D. Mebane, and M. Liu, "Numerical Continuum Modeling and Simulation of Mixed-Conducting Thin-Film and Patterned Electrodes," *Ceramic Engineering and Science Proceedings* (Advances in Solid Oxide Fuel Cells III), accepted, 2009.

## References

**1.** S.P. Jiang, "A Comparison of O-2 Reduction Reactions on Porous (La,Sr)$MnO_3$ and (La,Sr)(Co,Fe)O-3 Electrodes," *Solid State Ionics*, 146(1-2): p. 1-22, 2002.

**2.** S.P. Simner, M.D. Anderson, M.H. Engelhard, and J.W. Stevenson, "Degradation Mechanisms of La–Sr–Co–Fe–O SOFC Cathodes," *Electrochemical and Solid-State Letters*, 9(10): A478-A481, 2006.

**3.** T.Z. Sholklapper, C. Lu, C.P. Jacobson, S.J. Visco, and L.C. De Jonghe, "LSM-Infiltrated Solid Oxide Fuel Cell Cathodes," *Electrochemical and Solid-State Letters*, 9(8): A376–A378, 2006.

# III.A.8 Catalyst Infiltration in Support of Anode Support Cell Development

Lutgard C. DeJonghe (Primary Contact), Michael C. Tucker, Tal Z. Sholklapper, and Steven J. Visco
Lawrence Berkeley National Laboratory (LBNL)
Materials Sciences Division
1 Cyclotron Rd.
MS 62-203
Berkeley, CA 94720
Phone: (510) 486-6138; Fax: (510) 486-4881
E-mail: lcdejonghe@lbl.gov

DOE Project Manager: Joseph Stoffa
Phone: (304) 285-0285
E-mail: Joseph.Stoffa@netl.doe.gov

Contract Number: MSD-NETL-01

Start Date: October 1, 2008
End Date: September 30, 2009

## FY 2009 Objectives

- Development of technologies enabling improvement of solid oxide fuel cell (SOFC) performance at equivalent (or lower cost) relative to existing SOFC components.
- Target high risk/high benefit strategies and basic science (rather than incremental engineering advances that are better suited to industrial developers).
- Characterization of performance improvement.
- Transfer of technology to industrial teams, national labs, and/or university teams.

## Accomplishments

- Worked closely with ESL (Electroscience Laboratories), enabling them to produce an anode-support cell (ASC) that provides 700 mA/cm$^2$ at 0.7 V and 700°C.
- Demonstrated significant boost in power upon infiltrating standard lanthanum strontium manganite-yttria-stabilized zirconia (LSM-YSZ) cathode with YDC ($Y_{0.2}Ce_{0.8}O_{2-d}$). Maximum power improved about 2.5x from 210 mW/cm$^2$ to 525 mW/cm$^2$ at 700°C.
- Achieved very high performance for novel cathode architecture consisting of sintered porous YSZ backbone infiltrated at low temperature with catalyst nanoparticles. ASCs with YSZ-LSM and YSZ-lanthanum strontium cobaltite (LSC) cathodes achieved 490 and 700 mW/cm$^2$, respectively at 700°C.
- Demonstrated improved performance upon cathode infiltration using commercial 5 cm x 5 cm anode-supported cells tested in a two-cell stack configuration.
- Observed extent of reaction with chromium and reaction mode for various popular cathode materials.

## Introduction

The main focus of the LBNL project is to support industrial Solid State Energy Conversion Alliance (SECA) teams in their effort to commercialize SOFC technology that meets the SECA performance and cost targets. In order to achieve this goal, it is necessary to improve the performance of SOFC components through the introduction of novel yet inexpensive techniques such as infiltration to improve the low temperature performance of conventional air cathodes and improve the sulfur and carbon tolerance of the fuel electrode. Such innovations may allow the industrial developers to lower the operating temperature of SOFC systems and/or tolerate larger thermal gradients while maintaining high system efficiency. Over the last decade, many SOFC developers have focused on replacing ceramic components with metallic ones (particularly interconnect plates) in an effort to further reduce SOFC stack costs and improve system reliability. If successful, this approach could lead to a cost-competitive system and penetration of the clean energy market. Among the various commercial (and specialty) alloys studied, it is relatively clear that the ferritic steels (particularly the 400 series) are the best option due to the slow growth (and reasonable electronic conductivity) of the $Cr_2O_3$ scale, and the close match of the thermal expansion coefficient with that of the other stack components. The introduction of stainless steel into the SOFC stack also constrains the operating temperature range to about 600-800ºC. We use fundamental studies to assess the compatibility of various cathode materials with low-cost chromia-forming stainless steel interconnects.

## Approach

Accordingly, in fiscal year 2009 the LBNL core effort has been focused on the following issues:

- Infiltration of perovskites and other appropriate catalysts into composite cathodes and porous zirconia backbone structures to form an interconnected network nanoparticulate coating;

- Determination of baseline performance and long-term stability of infiltrated and non-infiltrated commercial and novel electrodes;
- Determination of processes that accompany infiltrated electrode aging, and using this knowledge to predict long-term stability and improve longevity;
- Infiltration of ceria and other appropriate materials into Ni-zirconia anodes to improve sulfur and coking tolerance in the presence of coal gas;
- Developing fundamental understanding of cathode-Cr interaction.

## Results

### Development of Standard Commercial Anode-Supported Cell

The LBNL team has been working with developers at ESL in order to establish a United States (U.S.) company that can produce consistent ASCs to the SECA industrial developer and the Core Technology Program participants. We believe that a U.S. developer that can supply a "standard" ASC along with a LBNL "standard" stack would accelerate research efforts at the university and lab level and so move SOFCs closer to a commercial reality. Such a standard cell and stack would allow researchers to focus on a particular component (seals, contact pastes, coatings, etc.) and compare the performance of their material with a baseline. For example, a researcher with a new contact paste could assemble a standard two-cell stack and compare the performance to the baseline. They would not have to develop the processing skills needed to make 5 cm x 5 cm cells, seals, etc.

To this end the LBNL team has been working closely with ESL to develop what we call a "777" cell. That is an ASC operating at 700°C that attains 700 mA/cm$^2$ at 700 mV. This is ~500 mW/cm$^2$ at 0.7 V. We have gone through several iterations with ESL and they were successful in manufacturing a "777" button cell (~3 cm$^2$ active area). The potential and power data are shown in Figure 1 for both the initial performance and after activation under 700 mA/cm$^2$ overnight.

### Improving Composite Cathodes by Infiltration

The use of catalyst infiltration as developed at LBNL provides a simple, cost-effective means of boosting fuel cell performance at reduced operating temperatures. In the case of LSM-YSZ cathodes infiltrated with $Y_{0.2}Ce_{0.8}O_{2-\delta}$ (YDC), the improvement in performance can be as high as 174% at 700°C, Figure 2. This improvement is not limited to electrodes with poor low-temperature performance, but also improves high performing electrodes, as can be seen in the impedance characteristic of lanthanum strontium cobalt ferrite (LSCF) with YDC, Figure 2. Assuming the LBNL group can demonstrate long-term stability (projected to 40,000 hours) for such cathodes, this technology will be a clear candidate for technology transfer.

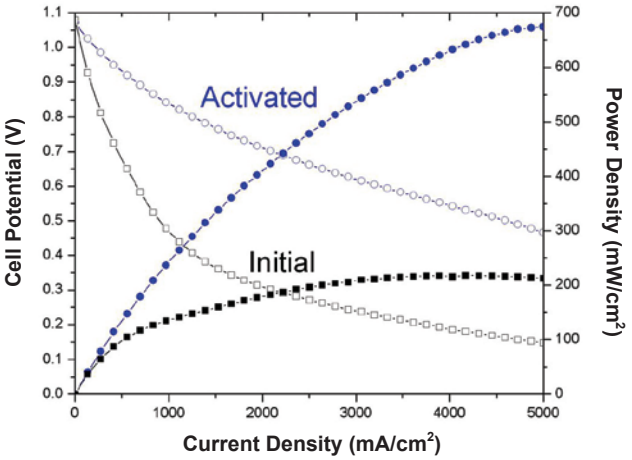


**FIGURE 1.** ESL anode supported cells as initially tested and after a 24 hour activation period.

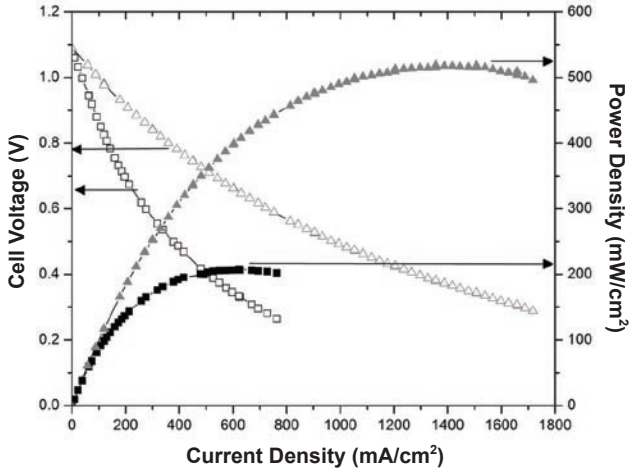


**FIGURE 2.** Enhancement of anode supported LSM-YSZ cathode before (■) and after (▲) infiltration of YDC, at 700°C.

LBNL has conducted stack tests of ASCs with and without cathode infiltrations. 5 cm by 5 cm anode-supported membranes with LSM-YSZ cathodes were purchased from H.C. Starck, while the stack fixture was manufactured by McAlister, following the now standard LBNL design. The sealing material was a glass. One of the membranes in the two-cell series stack was tested unmodified, while the other was infiltrated with scandia-doped ceria (SDC). The stack was heated to bond the glass seals, and then tested at 700°C, at a constant current density of 200 mA/cm$^2$. The corresponding voltage for the unmodified Starck membrane cell was 0.81 V, while the voltage over the SDC infiltrated cathode membrane was significantly higher: 0.92 V. The performance over the first 100 hours is shown in Figure 3. The cell performance was relatively stable.

A decline in performance may be seen, particularly for the infiltrated cell. This decline actually parallels an open circuit voltage loss for the infiltrated cell which, in a post-mortem analysis, this could be attributed to a progressive failure of the glass seal. Unfortunately, catastrophic seal failure after 100 hours of operation prevented collection of data for more extended times.

### Performance of Cathode Nanocatalysts Infiltrated into Porous Zirconia Backbone Structure

The LBNL team has developed a process whereby a porous electrolyte matrix can be infiltrated in a single processing step to form the entire air electrode structure; this unique result offers tremendous flexibility in electrode design. The performance of the single-step infiltrated electrodes is quite good as shown in Figure 4, where a traditional LSM electrocatalyst is compared to a typically reactive lanthanum strontium ferrite (LSF) electrocatalyst. The availability of air electrodes with low overpotential at reduced temperatures supports the trend toward lowering the operating temperature of the SOFC stack with the key benefit of greatly reduced stack cost enabled through the use of inexpensive metal components.

### Compatibility of Cathode Materials with Cr-Containing Interconnects

Pellets of LSM, LSCF, and lanthanum nickel ferrite (LNF) were aged in contact with Cr blocks for 150 hours in moist, Cr-saturated air. After this aging, the extent of reaction between the pellet and Cr block by solid-state processes, and the extent of reaction by vapor-deposition processes (away from the area of direct block-pellet contact) were determined using scanning electron microscopy/energy dispersive spectrometer. Pellets composed of physical mixtures of $Cr_2O_3$ and the individual cathode materials were also reacted in the same conditions. Extent of reaction was determined using X-ray diffraction. The results are tabulated in Table 1. It was found that LSCF is the most reactive towards Cr contamination, whereas LNF is the most Cr-tolerant. These results provide guidance for cathode selection for a system where imperfect Cr barrier layers are expected.

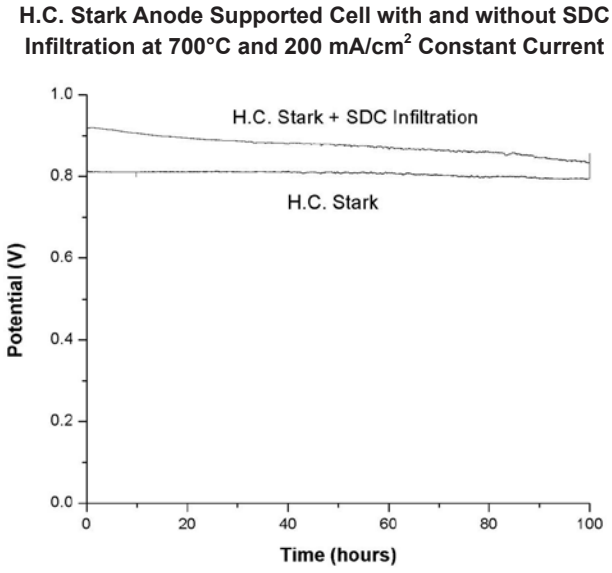


**FIGURE 3.** 700°C performance of anode supported cell with porous YSZ air electrode infiltrated with LSM (■) or LSF (▲). The power density at 0.7 V is about 15% higher for LSF compared to LSM infiltrated backbones.

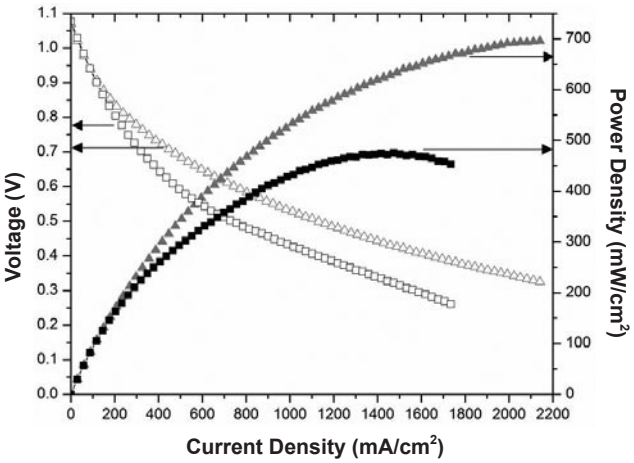


**FIGURE 4.** LBNL two-cell stack with 5 cm by 5 cm H.C. Starck anode-supported cells. One cell was tested as-is and the other cell's cathode was infiltrated with SDC. Test performed at 700°C and 200 mA/cm².

**TABLE 1.** Observations from reaction of cathode materials in contact with Cr source and Cr-saturated air atmosphere.

| Sample Name | Cr Vapor Deposition | Cr Solid State Deposition | Reaction with Cathode Materials |
|---|---|---|---|
| LSCF | Significant | Significant | Severe |
| LSM | Minor | Observed | Observed |
| LNF | None | Significant | No |

## Conclusions and Future Directions

- The LBNL approach specifically targets low-cost alternatives and/or modifications to existing SOFC technology.
- Improvement of low-temperature performance of air electrodes through infiltration could improve current distribution in the stack, reduce thermal stresses and improve stack lifetime.
- Infiltration process technology should be inexpensive to implement in a commercial product

and raw materials costs are low. The technology has been transferred to a number of labs and companies.

- Infiltration can significantly improve performance of traditional LSM-YSZ composite cathodes.
- Novel electrodes consisting of porous YSZ backbone and infiltrated catalyst show competitive performance and offer significantly improved flexibility in choice of catalyst composition.
- Future anode work will focus on demonstrating improved C,S-tolerance using ceria-infiltrated Ni-YSZ anodes.
- Future cathode work will focus on determining the aging mechanisms for infiltrated structures and using this knowledge to design improved electrodes and predict long-term electrode stability.

## Special Recognitions and Awards/Patents

**1.** Masters of Science Degree, San Jose State University, May 2009 awarded to Grace Lau.

## FY 2009 Publications/Presentations

**1.** (Invited) Tal Z. Sholklapper, Craig P. Jacobson, Steven J. Visco, and Lutgard C. De Jonghe, Synthesis of Dispersed and Contiguous Nanoparticles in Solid Oxide Fuel Cell Electrodes, Fuel Cells – From Fundamentals to System topical issue on Fuel Cell Novel Ceramic Materials for Fuel Cells, Volume 8, Issue 5, pp. 303-312 (2008).

**2.** T. Sholklapper, M. Tucker, G. Lau, C. Jacobson, L. De Jonghe, S. Visco, "Metal-Supported Solid Oxide Fuel Cells", presentation at 214th Meeting of ECS, Honolulu, HI, October 12–17, 2008.

**3.** T. Shoklapper, M. Tucker, G. Lau, C. Jacobson, L. DeJonghe, S. Visco, "Longevity of Metal-Supported SOFCs", presentation at the 33rd International Conference & Exposition on Advanced Ceramics and Composites, Daytona Beach, FL, January 18–23, 2009.

**4.** T. Sholklapper, C. Jacobson, S. Visco, L. De Jonghe, "Stability of Nanoparticle Infiltrated Solid Oxide Fuel Cells", presentation at the 236th ACS National Meeting in Philadelphia, PA, August 17–21, 2008.

**5.** Michael Tucker, Tal Sholklapper, Grace Lau, Liming Yang, Velimir Radmilovic, Steve Visco, and Lutgard De Jonghe, "Cathode Infiltration", presentation at SECA Cathode Workshop, Pittsburgh, PA, March 25, 2009.

**6.** Michael Tucker, Tal Sholklapper, Grace Lau, Steve Visco, and Lutgard De Jonghe, "Progress in Metal-Supported SOFCs", presentation at European SOFC Forum, Lucerne, Switzerland, July 2009.

# III.A.9 Correlations of Electronic and Chemical State on $La_{0.7}Sr_{0.3}MnO_3$ Dense Thin-Film Cathode Surfaces


Bilge Yildiz (Primary Contact) and Khabiboulakh Katsiev
Massachusetts Institute of Technology
Nuclear Science & Engineering Department
77 Massachusetts Avenue, 24-210
Cambridge, MA 02139
Phone: (617) 324-4009; Fax: (617) 258-8863
E-mail: byildiz@mit.edu

Subcontractors:
Clemens Heske (Primary Contact) and Stefan Krause
University of Nevada, Las Vegas (UNLV)
Department of Chemistry
4505 Maryland Parkway, Box 454003
Las Vegas, NV 89154-4003
Phone: (702) 895-2694; Fax: (702) 895-4072
E-mail: heske@unlv.nevada.edu

DOE Project Manager: Briggs White
Phone: (304) 285-5437
E-mail: Briggs.White@netl.doe.gov



Contract Number: NT0004117

Phase I Start Date: October 1, 2008
Phase I End Date: March 31, 2010


### FY 2009 Objectives

- Investigate the surface topography, electron tunneling properties, and chemical characteristics on $La_{0.7}Sr_{0.3}MnO_3$ (LSM) dense thin-film model cathodes.
- Identify the role of the structural inhomogeneities, such as grain boundaries, on the electronic properties of the surface of LSM.
- Identify correlations between the surface chemical composition and the surface electronic and ionic exchange characteristics on LSM.

### Accomplishments

- Significantly higher electron tunneling on select grain boundaries compared to the grain surface was revealed using scanning tunneling spectroscopy (STS). This result suggests a higher rate of the electocatalytic activity at the grain boundaries of LSM. This information is particularly important for tailoring the properties of infiltrated LSM cathodes.
- Thickness dependence of LSM thin-film grain coarsening during heat treatment was observed in situ using scanning tunneling microscopy (STM).
- A thickness dependence of the chemical composition in surface-sensitive ex situ X-ray photoelectron spectroscopy (XPS) was observed, resulting in a Mn-enrichment for thinner films and an associated A/B-ratio decrease.
- A threshold-like drop in the tunneling current was found at positive bias in STS and suggested as a unique indicator of the activation polarization in cation-oxygen bonding on the LSM surface.
- Sr-enrichment and a relative reduction in Mn content on the surface at high temperature was found by auger electron spectroscopy. This chemical change was accompanied by a reduction in tunneling conductance in STS, suggesting that the Mn-terminated surfaces are more active for electron exchange in oxygen reduction compared to the (La,Sr)-terminated surfaces on LSM.

## Introduction

Perovskite type mixed ionic-electronic conductor (MIEC) oxides are widely used as solid oxide fuel cell (SOFC) cathodes [1]. It is well-known that their surface structure plays an important role in the electrocatalytic activity for oxygen reduction (OR) [2,3]. A particularly interesting material in this context is LSM [4,5] – an MIEC with poor ionic conductivity. The main obstacles to a widespread use of SOFCs thus far are materials degradation at the high operating temperatures or poor activity of the cathode if lowering of temperatures attempted. A major limitation of the cathode performance at lowered temperatures is the slow kinetics of the oxygen exchange on the perovskite oxide surfaces. The underlying OR mechanisms involving electronic and ionic charge transport on SOFC cathodes are not fully understood, and the impact of the different metal cations on the catalytic properties of the surface remains unclear. Thus, a fundamental understanding of the surface electronic and chemical state and its relation to the oxygen reduction at the atomistic level is essential for the development of cathodes with enhanced electrocatalytic activity.

## Experimental Approach

A new in situ approach was deployed which combines surface sensitive probes of electronic structure and chemical state on the dense thin film cathodes – STM/STS and Auger electron spectroscopy (AES). Utilizing these surface sensitive probes, particularly

the STM/STS, at high temperature and non-ultra-high vacuum (UHV) conditions is unique, and makes it possible to relate the chemical and electronic state of the model cathode surfaces closely to the reacting environment of operational SOFC cathodes.

$La_{0.7}Sr_{0.3}MnO_3$ polycrystalline dense thin films with thicknesses of 10-100 nm were grown on single crystal (111) yttrium-stabilized zirconia (YSZ) by pulsed laser deposition at 800°C in 50 mTorr of $O_2$, and subsequently cooled to room temperature in 300 Torr $O_2$ [6]. The results on the 10 nm and 50 nm-thick LSM films are reported here.

The in situ structural, electronic, and compositional characterization was performed in the commercial UHV system (Omicron GmbH) at Harvard University's Center for Nanoscale Systems.

Complementary room-temperature X-ray emission spectroscopy (XES), X-ray absorption spectroscopy (XAS), and XPS measurements were performed at UNLV and the Advanced Light Source, Lawrence Berkeley National Laboratory, in order to investigate chemical composition and electronic structure in different probing depths in an ex situ (UHV) environment.

## Results and Discussion

The STM performed on the 10 and 50 nm-thick LSM dense thin-films at room temperature (Figure 1(a-d)) showed a textured surface structure. Two types of grains coexist without an apparent crystallographic orientation. First are the large flat island-type grains, with an average size of 100 nm and 70 nm on the 10 nm- and 50 nm-thick films, respectively, exhibiting clearly distinguishable step edges even at high-temperature imaging. The second type comprises the smaller grains, with an average size of 20 nm and 35 nm. The overall peak-to-valley height difference is 4 nm for the 10 nm and 6 nm for the 50 nm-thick films. Grain coarsening occurred on the 10 nm-thick LSM film upon annealing at 580°C in oxygen pressure of $10^{-3}$ mbar during STM/STS experiments lasting up to 24 hours. The coarsening resulted in the significantly increased fraction of the island-type grains (Figure 1(b)). Contrary to this, the structure of the 50 nm film did not evidently change via grain coarsening or surface roughening upon heating (Figure 1(d)).

The fine-resolution mapping of the tunneling current on the LSM surface obtained with STS at room temperature demonstrate a clear correlation between the surface topography (Figure 2(a)) and the electron tunneling characteristics (Figure 2(b)). The dark regions in Figure 2(b) that are associated with the higher tunneling conductance mainly correspond to select grain boundaries in Figure 2(a). Considerably higher tunneling conductance at select grain boundaries compared to grain surfaces can be explained by the possible changes in the chemical composition due to segregation or structural distortions at the boundaries.

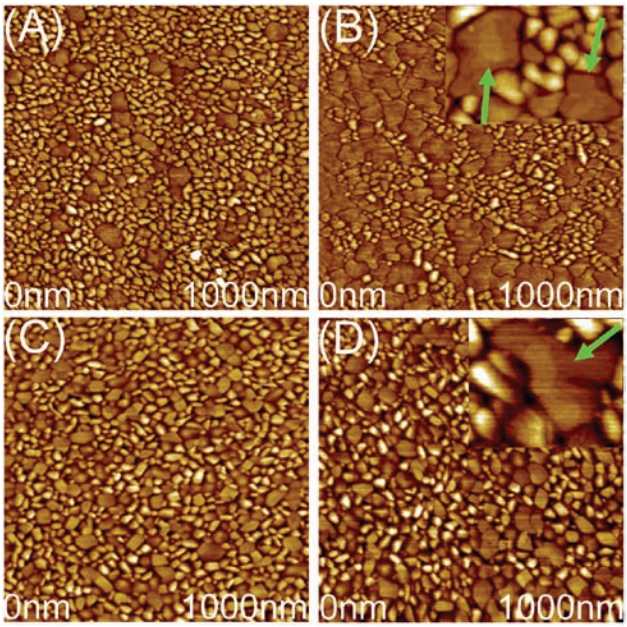


**FIGURE 1.** 1 x 1 $\mu m^2$ topography of the (a,b) 10 nm- and (c,d) 50 nm-thick thin-film LSM surface, imaged with tunneling conditions of 2 V and 1 nA, at (a,c) room temperature, and (b,d) 580°C, $P_{02}=10^{-3}$ mbar. The insets in (b,d), 195 x 130 $nm^2$ and 164 x 137 $nm^2$, respectively, show the step-edge resolution (marked with arrows) on the island-type flat grains at high temperature.

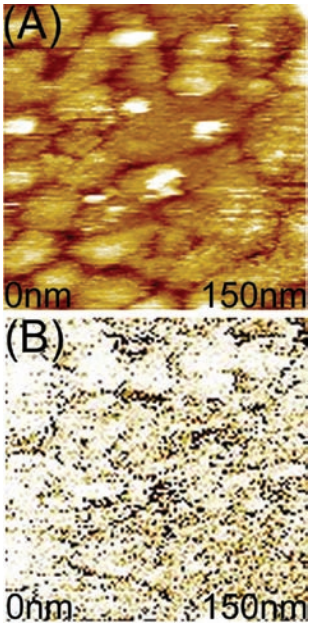


**FIGURE 2.** (a) Constant current STM image of 10 nm LSM film surface (2 V and 0.2 nA) taken simultaneously with the tunneling spectroscopy map, and (b) the corresponding tunneling current map (on the same area in A) at -2.2 V. Dark regions in (b), visible at some grain boundaries, represent higher tunneling current, and thus imply higher activity in electron exchange at select interfaces.

The temperature-dependent AES measurement in $10^{-6}$ mbar oxygen pressure revealed enrichment of Sr and depletion of Mn and La on the surface (Figure 3(a)), resulting in an overall 15-27% increase in the (La+Sr)/Mn ratio at 600-700°C (Figure 3(b)). This evolution is attributed to a thermodynamically favored A-site cation-rich phase on the LSM surface during the AES experiment conditions.

Complementary to the temperature-dependent AES investigation, area-integrating room temperature XPS measurements were performed to monitor the surface (<10 nm information depth) chemical composition with increasing thickness. For this purpose, the same set of samples (10, 50, and 100 nm) were investigated at UNLV and the relative change of element-specific signals with increasing thickness was derived (Figure 3(c)). A clear decrease in the A/B ratio with increasing thickness can be observed (Figure 3(d)). A thickness-dependent trend is also found in the La XES and the O-K XAS (not shown here).

The tunneling current measurements on LSM surface showed a semiconductor-like band-gap behavior at room temperature and a metallic nature at 400-580°C, when the STS was collected with the acquisition time of 0.6 ms per voltage step. An increase in the tunneling conductance was found as the temperature increased to 400°C and 500°C, followed by its decrease at 580°C.

Electronic conductance of the LSM is associated with the Mn cation and its oxidation state. A p-type conductivity in LSM arises as a result of hole-doping through the increase in $Mn^{4+}/Mn^{3+}$ ratio [7], which depends on the A-site cation substitution and oxygen non-stoichiometry. The decreasing tunneling conductance measured by STS at 580°C is attributed to the depletion of Mn on the surface at comparable conditions (Figure 3). This result suggests that the A-site rich and Mn-poor surfaces are less active for electron exchange in oxygen reduction on LSM.

The STS measured within the -/+3 V range with the 20 ms acquisition time per voltage step at $10^{-3}$ mbar oxygen pressure and elevated temperatures revealed a sudden drop in the tunneling current at a positive threshold bias (Figure 4(a)). This differs from STS spectra acquired with the acquisition time of 0.6 ms (Figure 4(a)). The threshold bias decrease with increasing temperature is observed and estimated to 2.6,

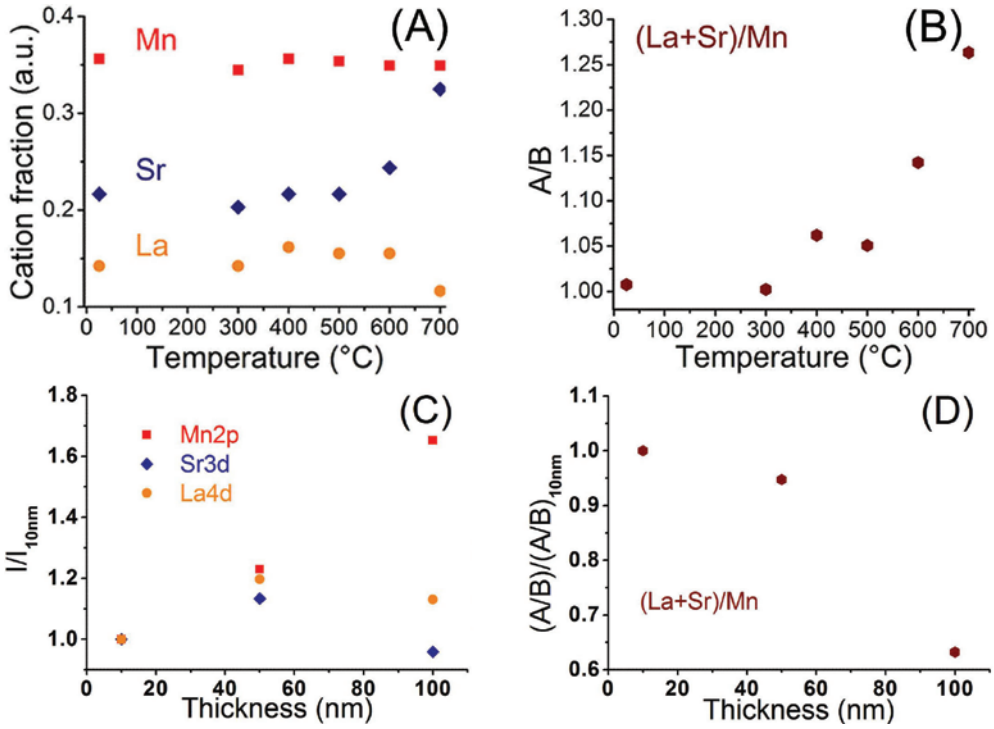


**FIGURE 3.** Temperature-dependent AES in $10^{-6}$ mbar oxygen pressure revealed (a) Sr enrichment, accompanied by a decrease in La at the surface above 500°C, while Mn remains unchanged. (b) (La+Sr)/Mn ratio showed an overall increase of the A site cations. The quantification in the AES data was performed based on the $La_{MNN}$, $Sr_{LMM}$, $Mn_{LMM}$, and $O_{KLL}$ transitions. The percentage error on the experiments was estimated to <2%. (c) Intensity of Mn 2p, Sr 3d, and La 4d XPS signals as a function of thickness, normalized to the 10 nm value. A significant increase of the Mn 2p signal with increasing thickness was found, which leads to a decrease of the A/B ratio, plotted in (d). The XPS spectra were recorded in UHV and at room temperature with an estimated error of <5%.

2.3, and 1.5 V at 400°C, 500°C, and 580°C, respectively (Figure 4(b)). Similar threshold behavior was also observed on the 10 and 100 nm-thick LSM films (not shown here). STM imaging and STS with the 0.6 ms acquisition-time was fully recovered following the tunneling current drop, thus proving that the tip was not altered.

The acquisition time-, temperature-, and bias-dependent character of the tunneling drop on LSM suggests that the underlying phenomenon is an activated chemical reaction. On the LSM surface, positive bias leads to an upward bending of the electronic bands [11] to higher energy levels, as schematically shown in inset of Figure 4(b). The bias-induced band bending could be then responsible for the oxygen chemisorption localized at the tip – LSM surface at high temperature. The resulting formation of oxidized sites is a possible mechanism explaining the tunneling drop in STS. This mechanism suggests that the threshold bias can serve as a unique probe of the activation polarization in cation-oxygen bonding on LSM cathode surface.

A broad distribution of the STS spectra was observed on the surface regardless of the grain boundaries at room temperature. On the 50 nm-thick LSM film, the band-gap variation extended from 1.9 to 3.6 eV, which goes far beyond the instrument-related data dispersion [8]. The broad range of band-gap on the LSM surface is tentatively attributed to two main mechanisms: 1) the abovementioned coexistence of the (Sr,La)O- and $MnO_2$-terminated surfaces. This is consistent with topographic and spectroscopic atomic-scale study of $Bi_{0.24}Ca_{0.76}MnO_3$, on which the phase separation into metallic and insulating surface regions were resolved in real space with STM/STS at atomic-scale resolution [9]. And 2) presence of electronic inhomogeneities on the surface due to defect ordering on perovskite-type oxides. This behavior was recently shown by imaging the $Mn^{3+}$ and $Mn^{+4}$ sites using STM at ambient temperature on $(La_{5/8-0.3}Pr_{0.3})Ca_{3/8}MnO_3$ [10]. The surface defects were reported to form strong short-range correlation with clear preference to exist as nanoscale charge-order-like clusters with varying electronic tunneling characteristics. While these two mechanisms could control the broad distribution of the current/voltage spectra on LSM reported here, the exact reasons are not yet fully identified.

## Conclusion and Future Directions

The surface topography, electron tunneling and chemical characteristics of 10 nm- and 50 nm-thick LSM thin-films at temperatures up to 580°C in $10^{-3}$ mbar oxygen pressure using in situ STM/STS are reported. Coarsening of the grains was found on the 10 nm-thick LSM film. Additional ex situ XPS measurements on 10 nm-, 50 nm- and 100 nm-thick films show a thickness dependence of the surface chemical composition, corroborated by trends in the XES and XAS spectra. High resolution mapping of the tunneling spectra onto the surface topography showed a higher electron exchange rate at select grain boundaries compared to grain surfaces. A threshold-like drop in the tunneling current was observed at positive bias in STS, and is suggested as a unique indicator to the activation polarization in cation-oxygen bonding on LSM. Sr-enrichment and Mn-depletion were found on the surface at high temperature using AES accompanied by a reduction in tunneling conductance in STS. This suggests that the Mn-terminated surfaces are more active for electron exchange in oxygen reduction compared to the (La,Sr)-terminated surfaces on LSM. The chemical nature of the enhanced activity at the grain boundaries is the subject of our ongoing investigation.

Integrating our results from the enhanced tunneling conductance on the grain boundaries with the thickness

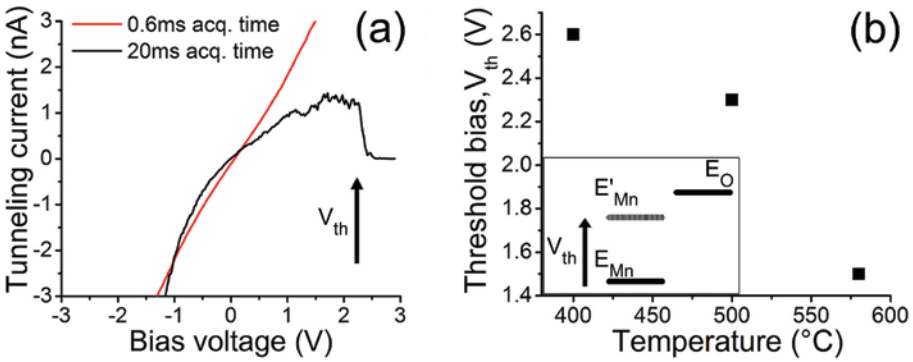


**FIGURE 4.** (a) Tunneling conductance spectra acquired on the surface of the 50 nm LSM at 580°C (acquisition time of 0.6 and 20 ms per voltage step), and (b) the threshold bias as a function of temperature. The inset in (b) schematically shows the cation energy levels ($E_{Mn}$) shifting upward ($E'_{Mn}$) at positive bias, and approaching the oxygen electronic levels ($E_0$).

dependence of the grain growth due to heat treatment can provide valuable insights for the design of the infiltrated LSM cathodes [12]. Based on these results, the infiltrated cathode film electrocatalytic activity and its durability could favor the presence of large number of the grain boundaries with a film thickness above few tens of nanometers.

## FY 2009 Publications

**1.** K. Katsiev, B. Yildiz*, K. Balasubramaniam, P.A. Salvador, "Electron Tunneling Characteristics on $La_{0.7}Sr_{0.3}MnO_3$ Thin-Film Surfaces at High Temperature," accepted to Applied Physics Letters, July 2009.

**2.** K. Katsiev, B. Yildiz*, K. Balasubramaniam, P.A. Salvador, "Correlations of Electronic and Chemical State on $La_{0.7}Sr_{0.3}MnO_3$ Dense Thin-Film Cathode Surfaces," accepted to the Proceedings of the 216th Meeting of the Electrochemical Society, Solid Oxide Fuel Cells 11th International Symposium, Vienna, Austria, October 2009.

## References

**1.** S.C. Singhal, *Sol. St. Ionics*, **135** 305 (2000).

**2.** S.B. Adler, *Chem. Rev.,* **104** (10) 4791 (2004).

**3.** F.S. Baumann, J. Fleig, M. Konuma, U. Starke, H.-U. Habermeier, and J. Maier, *J. Electrochem. Soc.*, **152** (10) A2074 (2005).

**4.** V. Brichzin, J. Fleig, H.-U. Habermeier, G. Cristiani, and J. Maier, *Sol. St. Ionics*, **499** 152 (2002).

**5.** G.J. la O', B. Yildiz, S. McEuen, and Y. Shao-Horn, *J. Electrochem. Soc.*, **154** (4) B427 (2007).

**6.** K.R. Balasubramaniam, S. Havlia, P.A. Salvador, H. Zheng, and J. Mitchell, *Appl. Phys. Lett.*, **91** 232901 (2007).

**7.** C. Zender, *Phys. Rev.,* **82** 403 (1951).

**8.** N. Severin, S. Groeper, R. Kniprath, H. Glowatzki, N. Koch, I.M. Sokolov, and J.P. Rabe, *Ultramicrosc.*, **109** 85 (2008).

**9.** Ch. Renner, G. Aeppli, B.-G. Kim, Yeong-Ah Soh, and S.-W. Cheong, *Nature,* **416** 518 (2002).

**10.** J.X. Ma, D.T. Gillaspie, E.W. Plummer, and J. Shen, *Phys. Rev. Lett.,* **95** 237210 (2005).

**11.** R.M. Feenstra, Y. Dong, M.P. Semtsiv and W.T. Masselink, *Nanotech.*, **18** 044015 (7pp) (2007).

**12.** T.Z. Sholklapper, V. Radmilovic, C.P. Jacobson, St. J. Visco, and L.C. De Jonghe, *Electrochem. and Sol. St. Lett.*, **10** (4) B74 (2007).

# III.A.10 Synchrotron Investigations of LSCF Cathode Degradation

Prof. Yves Idzerda
Montana State University
Department of Physics
Bozeman, MT 59717
Phone: (406) 994-7838; Fax: (406) 994-4452
E-mail: Idzerda@physics.montana.edu

DOE Project Manager: Joseph Stoffa
Phone: (304) 285-0285
E-mail: Joseph.Stoffa@netl.doe.gov

Contract Number: NT0004115

Start Date: September 3, 2008
End Date: September 2, 2011

### FY 2009 Objective

Investigate and characterize nano-scale variations of the solid oxide fuel cell (SOFC) cathode/electrolyte interface region and correlate these variations with operating parameters.

### Accomplishments

- The baseline soft-X-ray absorption spectroscopy (XAS) spectra for each element of $La_{0.5}Sr_{0.5}FeO_3$, $La_{0.5}Sr_{0.5}CoO_3$, $La_{0.5}Sr_{0.5}NiO_3$, and $La_{0.5}Sr_{0.5}Fe_{0.5}Co_{0.5}O_3$ materials up to 1000°C have been measured.
- The effect of overlayer stress from lattice mismatch on the transition metal L23-edge XAS spectra near the interface for $La_{0.5}Sr_{0.5}FeO_3$, $La_{0.5}Sr_{0.5}CoO_3$, and $La_{0.5}Sr_{0.5}Fe_{0.5}Co_{0.5}O_3$ as a function of $LaAlO_3$ overlayer thickness has been measured to determine the change in transition metal valence in response to the stress. Due to increasing interfacial stress energy, the ionic Sr in the interface is found to migrate away from the interfacial region and into the bulk.

## Introduction

One poorly understood area of SOFC systems is the interfacial region between the electrolyte and the cathode and/or anode. As the electrodes become increasingly nanostructured, this interfacial behavior becomes the dominant contributor to SOFC performance. If the material properties of the electrolyte/cathode/anode at the interface significantly differ from the bulk properties, these buried regions, which are difficult to probe, may become the dominant inhibitor of electron or oxygen vacancy transport. Fortunately, X-rays have a significant penetration depth and have been shown to be sensitive to the electronic and crystalline structure of these interfacial regions [1].

Manganite compounds in general exhibit physical properties that depend upon a strong coupling between the structural, charge, and even spin degrees of freedom [2,3]. The complex interplay between these coupled motions leads to fascinating and potentially useful electron and oxygen ion transport properties associated with any LaSrTMO systems (TM is a transition metal), especially those that have shown promise as cathode materials for solid oxide fuel cells. This interplay also makes the transport properties sensitive to external perturbations. In the case of ultra thin films (a few nanometers thick), it is possible to control the film's in-plane lattice constant if the film is epitaxial (i.e., grows in crystalline registry with the underlying substrate). For thicker films, the lattice constant relaxes to the bulk value with a modified region present at the interface, but the method of strain relaxation at the interface is not known a priori. The general idea is that by controlling the in-plane structure of the interface, it may be possible to either tune the SOFC properties of the various components or create a system with improved operational performance. At the very least, understanding of how these strain effects could modify the structure and transport properties is needed.

## Approach

Interfacial stress is a straightforward method of generating interfacial disruption. This interfacial disruption leads to a modification of the electronic structure of the cathode material that can be quantified and interpreted in a mechanistic way. It is important to stress that these measurements simply allow demonstration of the electronic modifications that interfacial disruption can create, acting as a surrogate for interface degradation due to SOFC operation. If similar variations in the X-ray absorption spectra are observed in degraded performance SOFC structures, successful interface disruption studies will allow identification of the mechanism for disruption.

## Results

As one example, the interfacial stress generated by depositing lanthanum aluminum oxide (LAO) on a thick pulsed laser deposition film of lanthanum strontium cobaltite (LSC) is examined in Figure 1. By varying the thickness of the overlayer, the large interfacial

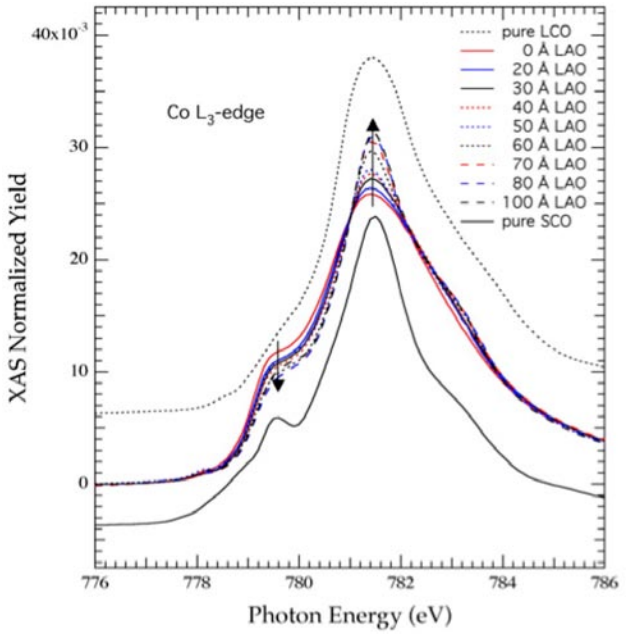


**FIGURE 1.** The Co $L_3$-edge XAS spectra as a function of LAO overlayer coverage (increasing compressive strain energy). Also shown are the XAS spectra of pure LCO and SCO.

stress energy that increases with the volume (thickness) of the film can be controllably altered. When the overlayer thickness is changed from 0 to 10 nm (100 Å), a variation in the Co L3-edge XAS spectra from the interfacial region of the buried LSC film is observed. The lower energy shoulder is observed to diminish while the higher energy peak is observed to grow. Also shown on the figure are the XAS spectra for pure lanthanum cobalt oxide (LCO) and strontium cobalt oxide (SCO). It can be concluded that the interfacial stress is modifying the LSC and generating a region of La-rich material by driving the Sr from the region.

Since the lattice constant of LAO is much closer to SCO than to LCO, the interfacial strain energy results in a thermodynamic generalized force which drives Sr from the interfacial region, essentially creating a buffer layer of more closely lattice matched phase that gradually changes to LSC away from the interface. This new relaxation mechanism needs to be better understood.

This relaxation method is found to occur for lanthanum strontium ferrite (LSF) films as well. The XAS spectra for the Fe L3-edge of a LSF film and for a buried LSF film capped by 8 nm (80 Å) of strontium ruthenate (SRO) are very different, suggesting that a similar modification of the LSF occurs as is observed for the LSC films. In this case, additional studies with varying thickness of SRO are needed, as are the XAS spectra for the standard films of lanthanum iron oxide (LFO) and strontium iron oxide (SFO). These will be obtained in the near future, although the conceptual understanding of the interfacial degradation is firmly established without additional data.

For completeness, the variation of the XAS for lanthanum strontium nickelate (LSN) (Ni transition metal) films with stress has also been examined. Although LSN is not a superior performance SOFC cathode, the behavior of this material may generate insight into the behavior of the related LSF and LSC materials. Figure 2 shows the Ni L3-edge XAS spectra as a function of LAO thickness. Analysis of this data is complicated by an accidental overlap of the Ni L3 edge with the La M5 edge. Interestingly, in this case no variation in the Ni spectra is observed with stress, suggesting that LSN does not relax in the same manner as LSF or LSC films.

Finally, Figure 3 shows the ability to generate XAS scans at high temperature in the vacuum system for in-situ measurements. These simple spectra show that the Mn L-edge spectra of lanthanum cobalt manganese oxide (LCMO) are not affected by temperature cycling to 1000°C.

## Conclusions

These studies show that interfacial stress can be used as a controllable variable to generate interfacial disruption as a surrogate to degradation. In addition, the XAS is a sensitive method to quantify the disruption that occurs and can be used to suggest a concrete mechanism for the degradation. For LSC and LSF films, the interfacial stress generates a single valence buffer region which undoubtedly has lower oxygen ion mobility. If high ion currents generate similar thermodynamic generalized forces, a similar mechanism

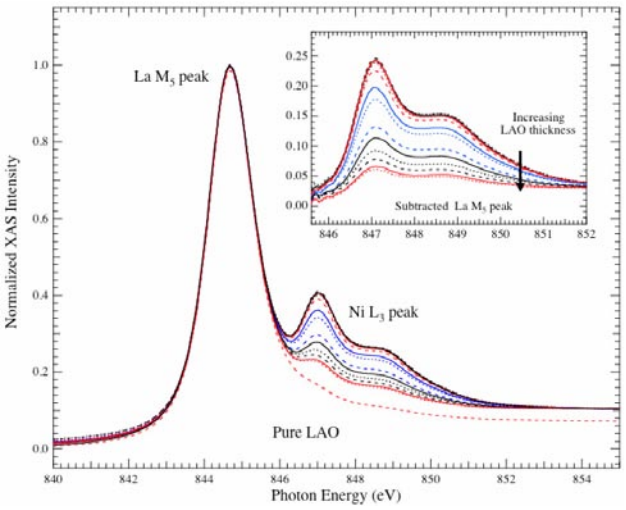


**FIGURE 2.** Ni $L_3$ XAS spectra for LSNO films capped by various thicknesses of an LAO overlayer. The major peak is the La M5 edge. The inset is the LSNO spectra after removal of the La M5 peak.

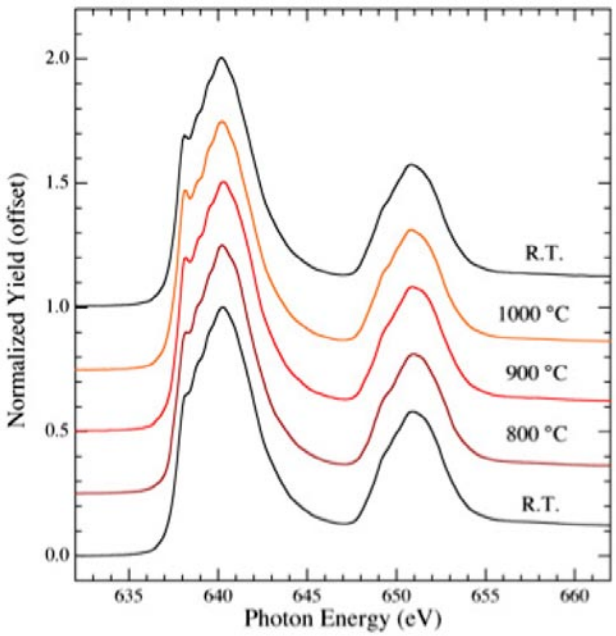


**FIGURE 3.** Temperature dependent XAS spectra of the Mn L-edge for LCMO showing both the high temperature spectra and the reproducibility with temperature cycling.

of cation migration away from triple phase regions can now be identified and quantified. X-ray resonant scattering measurements can be used to quantify the thickness of these buffer layers and to quantify the cation migration. Preliminary measurements show a systematic trend with stress energy.

## FY 2009 Publications

**1.** A. Lussier, J. Dvorak, S. Stadler, J. Holroyd, M. Liberati, E. Arenholz, S.B. Ogale, T. Wu, T. Venkatesan, and Y.U. Idzerda, "Stress Relaxation of $La_{1/2}Sr_{1/2}MnO_3$ and $La_{2/3}Ca_{1/3}MnO_3$ at Solid Oxide Fuel Cell Interfaces", Thin Solid Films 516, 880 (2008).

**2.** A. Lussier, S. Sophie, J. Dvorak, and Y.U. Idzerda, "Mechanism for SOFC Anode Degradation from Hydrogen Sulfide Exposure," Int. J. of Hydrogen Energy 33, 3945 (2008).

**3.** Submitted: A. Lussier, J. Dvorak, S. Sofie, and Y.U. Idzerda, "Hydrogen Sulfide Induced Nickel Depletion of SOFC Anodes," Proceedings of the Sixth International Fuel Cell Science, Engineering and Technology Conference (2008) 65189.

## References

**1.** S. Stadler, Y.U. Idzerda, Z. Chen, S.B. Ogale, and T. Venkatesan, Appl. Phys. Lett. 75 (1999) 3384.

**2.** M.B. Salamon and M. Jaime, Rev. of Modern Phys. 73 (2001) 583.

**3.** A.J. Millis, Nature 392 (1998) 147 (and references therein).

# III.A.11 Development of SOFC Cathodes

X.D. Zhou (Primary Contact), J.W. Templeton, J.W. Stevenson
Pacific Northwest National Laboratory (PNNL)
P.O. Box 999, MS K2-44
Richland, WA 99352
Phone: (509) 372-4468; Fax: (509) 375-2186
E-mail: xiaodong.zhou@pnl.gov

DOE Project Manager: Briggs White
Phone: (304) 285-5437
E-mail: Briggs.White@netl.doe.gov

Contract Number: 40552

Start Date: October 1, 2008
End Date: September 30, 2009

### FY 2009 Objectives

- Develop solid oxide fuel cell (SOFC) electrodes offering high performance and long-term stability at intermediate SOFC operating temperatures (650-850°C).
- Investigate the effects of potential volatile seal constituents (such as B, Na, K) on SOFC cathode performance.

### Accomplishments

- Evaluated stability and performance of a novel cathode material, $Pr_2NiO_4$.
- Studied effects of volatilized K species on SOFC cathode electrochemical performance.

## Introduction

Minimization of electrode polarization processes at intermediate temperatures represents one of the greatest challenges in obtaining high, stable power densities from SOFCs. Cathodic polarization exhibits high activation energy relative to the other internal power losses (e.g., anodic polarization and electrolyte ohmic losses), so the need to improve cathode performance becomes increasingly important as the targeted SOFC operating temperature is reduced. The contacting phases and the environmental conditions experienced by the cathode during cell operation greatly reduce the number of likely candidate materials. In particular, the cathode material must be stable at the SOFC operating temperature in air; and it must have high electronic conductivity, high catalytic activity for oxygen molecule dissociation and oxygen reduction, and a thermal expansion compatible with the SOFC electrolyte (usually yttria-stabilized zirconia, YSZ). Chemical interactions with the electrolyte, interconnect, and contact materials must be minimal. In addition, the cathode material must have a porous microstructure so that gaseous oxygen can readily diffuse through the cathode to the cathode/electrolyte interface. This porous morphology must remain stable during SOFC operation over the lifetime of the cell. In general, a simple materials system with relatively few cationic elements may lead to better compatibility and high stability than materials with many elemental constituents (e.g., four cations in $(La,Sr)(Fe,Co)O_3$ [LSCF]). During Fiscal Year 2009, PNNL investigated a non-perovskite rare earth nickelate $Pr_2NiO_4$ (P2NO), which has only two cations. The study focused on improving the understanding of the relationships between composition, processing conditions, and performance (including chemical stability, electrical stability, and compatibility with contact materials).

Another potential cathode-related challenge facing stack developers is degradation of cathode performance over time due to interaction between the cathode material and gas species volatilized from other stack components, such as alloy interconnects (e.g., Cr) and/or glass seals (e.g., B, Na, K). The potentially deleterious effects of volatile Cr species on cathode performance have been the subject of numerous studies, while effects of volatile seal constituents have received very limited attention to date. During FY 2009, PNNL continued to study the possible impact of seal constituent evaporation on the performance and stability of intermediate temperature SOFC cathodes. Information gained in this study will assist Solid State Energy Conversion Alliance (SECA) industrial developers in identifying and optimizing seal materials and designs consistent with the SECA cost and performance targets. (Due to space constraints, only results from the P2NO study will be discussed in this report.)

## Approach

Anode-supported electrolyte bilayers were fabricated through a non-aqueous tape-casting and lamination process. Green tapes of the electrolyte (YSZ), functional anode layer and bulk anode layer were laminated together and then co-sintered in air. After sintering, the thickness and diameter of the bilayers were approximately 1 mm and 25 mm, respectively, with a dense electrolyte membrane (~8 μm thick). Samarium-

doped ceria (SDC) interlayers were applied to the anode-supported YSZ membranes via screen printing, and co-sintered with the anode current collector (Ni mesh embedded in NiO paste) at 1,200°C for 2 hours. Inks containing the cathode powder were applied by screen-printing (1.6 cm diameter print) and then sintered at 1,200°C. The cathode area after sintering, 2 $cm^2$, was used as the active cell area to calculate power density and area specific resistance (ASR). The cathode contact material was Sr-doped lanthanum cobaltite. The cells were sealed to alumina test fixtures using a glass sealing material. Current-voltage (I-V) and electrochemical impedance spectroscopy (EIS) data were recorded at various temperatures from 600 to 800°C using a Solartron 1480 Multistat and 1255 Frequency Response Analyzer. During EIS measurements, cells were subjected to different *dc* current densities (e.g., from 0.025 to 1.0 A/$cm^2$). The typical *ac* amplitude was 20 mA. The fuel side gas ($H_2$-3% $H_2O$) was supplied to the anode at 200 sccm. The oxidant was supplied to the cathode at 400 sccm.

## Results

Results from recent anode-supported cell tests at PNNL are shown in Figure 1. Stable performance has been observed for SOFCs with (La,Sr)$MnO_3$ (LSM)-based cathodes, but the cell power density tends to be relatively low. For example, Figure 1 shows data for an LSM/SDC-based cell, which had a low power density (~0.3 W/$cm^2$), but was stable over the 2,000-hour testing period. Higher cathode activity can be obtained using mixed oxygen-ion/electron conductors, such as LSCF and (Ba,Sr)(Co,Fe)$O_3$ (BSCF). As shown in Figure 1, LSCF was very active at T >650°C, resulting in a power density of ~0.9 W/$cm^2$ at 750°C. BSCF, an even more active material, yielded a peak power density of ~1 W/$cm^2$ at 650°C. However, the cells with either LSCF or BSCF cathodes were found to degrade rapidly during operation. The degradation mechanism is unknown, but may be related to segregation of Sr and demixing of cations under electrochemical potential. On the other hand, cells with a P2NO cathode exhibited similar initial power density to the LSCF-based cells, but considerably better stability during the 2,000-hour test. As can be seen in the figure, reasonably reproducible behavior was observed in three cells with the P2NO cathode. The degradation rate for those cells was 1-3% per 1,000 hours, whereas the degradation rate of LSCF-based cells was in the range of 10-20% per 1,000 hours, while BSCF-based cells degraded even more rapidly.

The electrochemical performance of the cathode determines the rate of conversion of oxygen molecules to oxygen ions and the transport of the oxygen ions into the electrolyte membrane. Hence, understanding these processes and finding strategies for circumventing their limitations are important in developing improved SOFC materials. In the search for new cathode materials, two physical properties believed to be critical to the cathodic oxygen reduction reaction in an SOFC are oxygen surface exchange coefficient (k) and oxygen diffusion coefficient (D). Based on previous studies, k and D of P2NO, BSCF and LSCF are close to each other, and substantially greater than those of LSM, which is consistent with the observed initial cell performances.

In order to evaluate the electrochemistry of P2NO, a systematic EIS analysis was carried out. Shown in Figure 2 are impedance spectra of a P2NO-based cell measured at 750°C under five current densities: 1.0, 0.75, 0.5, 0.25 and 0.025 A/$cm^2$. It will be noted that EIS measurements under constant current density allow for direct comparison of cathodic behavior of various compositions at a constant anodic polarization, since, regardless of the cathode composition under test, the

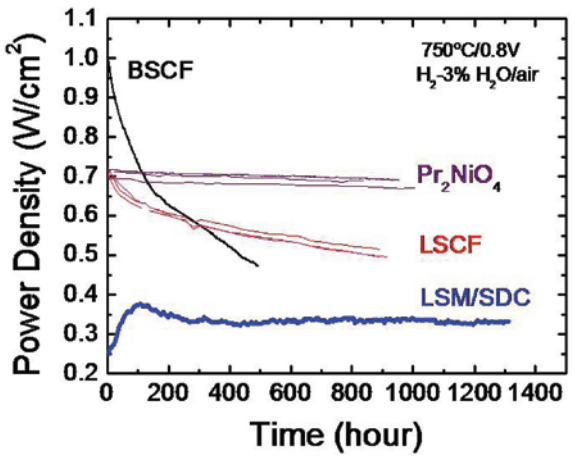


**FIGURE 1.** Electrochemical Performance of Cells Based on the Indicated Cathodes as a Function of Time at 750°C and 0.8 V

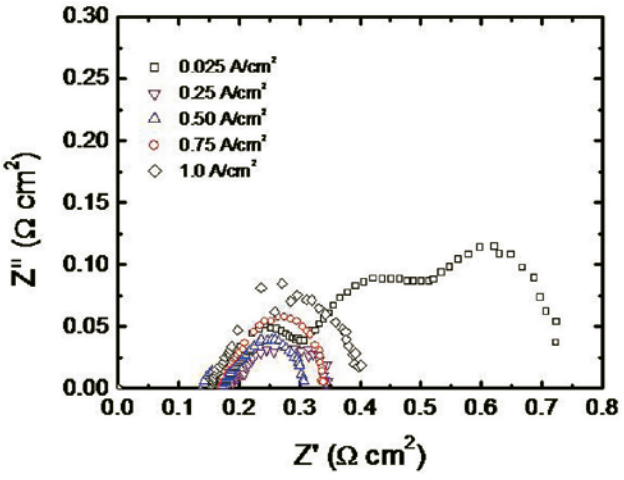


**FIGURE 2.** EIS Analysis of a Cell with P2NO Cathode at the Indicated Current Densities Using Air as the Oxidant

anodic component of the impedance should be constant at a given current density and temperature. It is clear that the impedance spectrum is dynamic, as the shape of the spectrum changes with current density. These results illustrate the fact that impedance spectra measured at or near the open circuit condition cannot be expected to accurately represent the cathode performance.

ASR calculations were used to cross-validate results from *ac* EIS and *dc* I-V sweep measurements. Figure 3 shows the total ASR vs. current density of the cell measured at 750°C in air. The total ASR from the *ac* EIS measurement, designated $ASR_{t,ac}$, was obtained from the low frequency intercept of the impedance spectrum. The total ASR from the *dc* I-V measurement, designated $ASR_{t,dc}$, was derived from dV/dI – the tangential slope of the I-V curve – at the given current density. Clearly, constant ASR was not observed over the range of current density investigated. However, for any specific cell current density, the $ASR_{t,ac}$ was nearly identical with that calculated from the tangent of the comparable I-V curve, $ASR_{t,dc}$. This observation held for other testing conditions (e.g., various temperatures and oxygen partial pressure), indicating that $ASR_t$ is a measurable cell parameter (for a given set of operating conditions) that can be obtained self-consistently from either a *dc* I-V sweep or *ac* EIS results. These results also demonstrate that $ASR_t$ is a dynamic property, dependent upon the current density of the cell under test.

The above measurements only provided direct information regarding the total cell performance. It is, of course, of interest to know how much of the observed ASR was attributable to cathodic polarization. In an effort to obtain that information, the cell performance was also evaluated using oxygen instead of air as the oxidant. For the measurements in air and in oxygen,

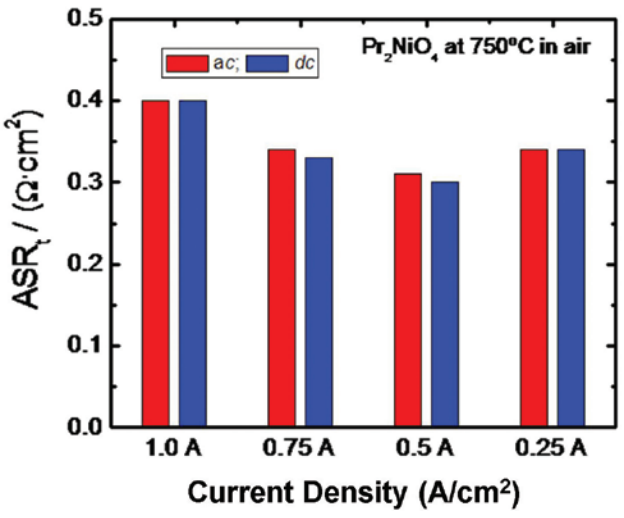


**FIGURE 3.** ASR Calculated from Both *ac* and *dc* Measurements at the Indicated Current Densities

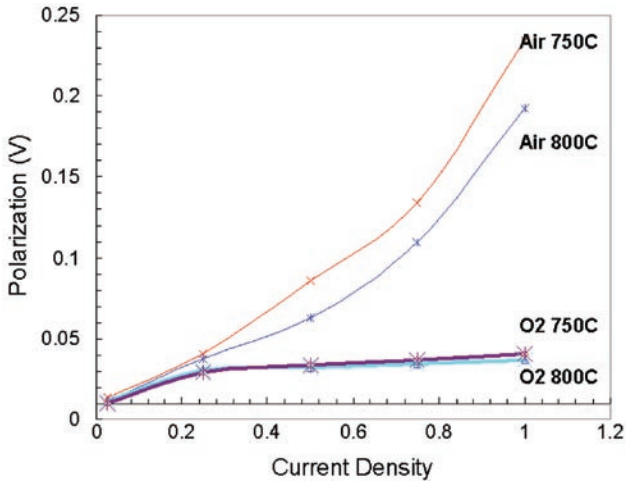


**FIGURE 4.** Calculated Total Electrode Polarization vs. Current Density ($A/cm^2$) Using Air or Oxygen as the Oxidant

total electrode polarization (η) at a specific current density (J) was calculated using: $\eta = J \times ASR_e$, where $ASR_e$ is the areal specific resistance of the electrodes, which is the diameter of the depressed semi-circle measured via EIS. The polarization magnitudes, which include the contribution from both the anode and the cathode, are shown in Figure 4. If these magnitudes represent the summation of both anodic and cathodic polarization, then clearly the anodic polarization at a given current density must be less than or, in the limiting case, equal to this total polarization measured in oxygen. Also, the anodic polarization should be a function of the current density, but not a function of the choice of oxidant. Thus, the substantially higher polarizations measured at higher current densities in air instead of oxygen must be attributed to increased cathodic polarization resulting from the fact that, in air, the active red-ox species, oxygen, is present in diluted form. Hence, in developing high performance cells, the cathode concentration polarization may not be overlooked. These results suggest that future efforts to improve cell performance should focus on optimization of the cathode composition and microstructure to reduce this high polarization observed during cell operation in air.

## Conclusions and Future Directions

P2NO appears to be a promising SOFC cathode material, as demonstrated by the high power density and reasonable stability obtained from anode-supported cells containing P2NO cathodes. Future optimization of cathode composition and microstructure may allow for further reduction in cathode polarization and cell degradation rates.

## FY 2009 Publications/Presentations

**1.** X.D. Zhou, J.D. Templeton, Z. Nie, P. Singh, L.R. Pederson, and J.W. Stevenson, "Recent Research and Development on SOFC Cathodes at PNNL," 33rd International Conference on Advanced Ceramics and Composites, Daytona Beach, Florida, January 18–23, 2009.

# III.A.12 Electronic Structure of Cathode Materials

Walter A. Harrison
GLAM/McCullough Bldg.
Stanford University
Stanford, CA 94305-4045
Phone: (650) 723-4224
E-mail: walt@stanford.edu

DOE Project Manager: Briggs White
Phone: (304) 285-5437
E-mail: Briggs.White@netl.doe.gov

Contract Number: 41817

Start Date: January 7, 2008
End Date: October 31, 2009

### FY 2009 Objectives

- Incorporate Madelung energies into the theory of manganite elastic constants.
- Extend the approach to the surfaces of $SrMnO_3$ and $LaMnO_3$.
- Predict the lattice relaxations at these surfaces.

### Accomplishments

- Successfully extended the theory to include Madelung energies.
- Gained insight into the nature and effect of cohesive contributions to surface energy.
- Completed calculation of surface energies and relaxation in $SrMnO_3$ and $LaMnO_3$.

## Introduction

During the Fiscal Year 2008 an understanding of the electronic structure of oxide systems such as the manganites was sought using a theory which assumed cancellation between intra-atomic and inter-atomic (Madelung) Coulomb interactions which would otherwise require intricate calculation. This approximation had proven adequate for a range of properties of simpler ionic solids such as the alkali halides and chalcogenides in the text, Elementary Electronic Structure [1]. The approach was extended to the elastic constants of the transition-metal oxides and finally to those of the manganites. However, when it was used to describe the surface relaxation, spontaneous distortions were found which were far from those obtained in full LDA (local-density-approximation) calculations carried out at the University of Wisconsin [Yueh-Lin Lee and Dane Morgan, private communication], calculations which could be expected to be reliable for these questions. It became clear that the simplification of the electrostatic energies was not going to be adequate for studies of the manganite surfaces and oxygen incorporation. The general tight-binding approach which was in itself both a simplification and a valid representation of the localized electronic states which occur in the manganites could be continued, but calculations of the Madelung energies would need to be explicitly incorporated.

## Approach

Fortunately, a simplified method for such Madelung calculations [2] had already been developed, in which direct sums were carried to large radial distances, and then corrected for non-neutrality by adding corrections at the surface of the corresponding sphere. This avoided use of the well-known but cumbersome Ewald method for such calculations. The values for such Madelung sums were not even known for the elastic constants of perovskite structures, so those needed to be calculated first. Once that was accomplished, the electronic structure terms and a single form of $1/d^6$ repulsion were added, with a scale factor fit to give the observed equilibrium spacing, for each compound. The resulting total energy as a function of elastic distortions allowed the prediction of the elastic constants for both compounds of interest, in adequate accord with experiment. This provided all of the features needed to again address the energies and relaxations of the surfaces of these oxides.

## Results

The surface energies were systematically calculated, now with the more complete theory. The first term considered was a cohesive contribution, obtained by imagining a plane within the crystal where a surface is to be formed, and associating individual terms in the cohesive energy with ions on a particular side, leading to contributions shown in parentheses at the bottom in Table 1. These terms would enter in a thermodynamic study of the formation of different surfaces, depending upon the thermodynamic states of the constituents forming the crystal. However, they cancel in the cleavage energy associated with splitting the crystal and simultaneously forming surfaces of both types (e.g., a (100) SrO surface and a $MnO_2$ surface in $SrMnO_3$). Furthermore, they do not appear in the LDA surface-energy calculations of workers such as Evarestov, et al.

[3], who calculated the energies of slabs with even numbers of (100) planes so that surfaces of both types occurred. Finally, they are seen to be rather large on the scale of the other terms which enter. Thus, they are listed separately in Table 1. The remaining totals are on the scale of the cleavage energy, which is taken as the sum of the two surface energies prior to relaxation. (That energy must be supplied to cleave the crystal, and the subsequent relaxation would become thermal energy in the separated crystals.) This new insight provides a very useful, though perhaps arbitrary, way to divide the surface energies to the two subcrystals, a separation not available with other approaches.

**TABLE 1.** Contributions to the Surface Energy [in eV per area $(2d)^2$, with $d$ the Mn-O distance] for the Two (100) Surfaces

| | $SrMnO_3(MnO_2)$ | $SrMnO_3(SrO)$ | $LaMnO_3(MnO_2)$ | $LaMnO_3(LaO)$ |
|---|---|---|---|---|
| Madelung | 2.28 | 2.28 | 1.59 | 1.59 |
| Repulsive | −2.75 | −2.75 | −2.02 | −2.02 |
| *sp* bond | 1.13 | 1.58 | 1.11 | 1.63 |
| *pd* bond | 0.64 | – | 0 | – |
| Relaxation | −0.32 | −0.41 | –0.13 | −0.32 |
| Total | 0.98 | 0.70 | 0.55 | 0.88 |
| Cohesive cont. | (4.31) | (−4.31) | (7.79) | (−7.79) |

The second step in the calculations was to obtain the Madelung sums, the sums of Coulomb interactions between ions near the surface and the half-crystals which are to be removed in forming the crystal. This was straight-forward in $SrMnO_3$ in which each of the (100) planes of ions was formally neutral (e.g., $Sr^{2+}O^{2-}$), and local charge redistributions leave this essentially true. However, in $LaMnO_3$ the individual planes are formally charged (e.g., $La^{3+}O^{2-}$), giving an electric field between the separated half-crystals, or in the bulk, and a divergent crystal energy. This difficulty is *real* (as discussed extensively for surface energies in Ref. 1) and the crystals are expected to avoid the divergence by replacing half of the surface $Mn^{3+}$ ions on the $MnO_2$ side by $Mn^{4+}$ and replacing half of the $Mn^{3+}$ ions on the plane below the LaO surface by $Mn^{2+}$. This important symmetry-breaking transition should be observable experimentally, but it has not been found. It is absent in the LDA calculations of Evarestov, et al. [3], which accomplish the same result by artificially forming partly-filled bands and a fictitious metallic state. This feature requires extra steps in the Madelung calculation, which itself is based upon ion charges modified by local charge rearrangements. In Figure 1, modifications of the charges which occur near the surfaces in $LaMnO_3$ are listed. The calculations were performed, including these modifications, and the results appear as the first line in Table 1.

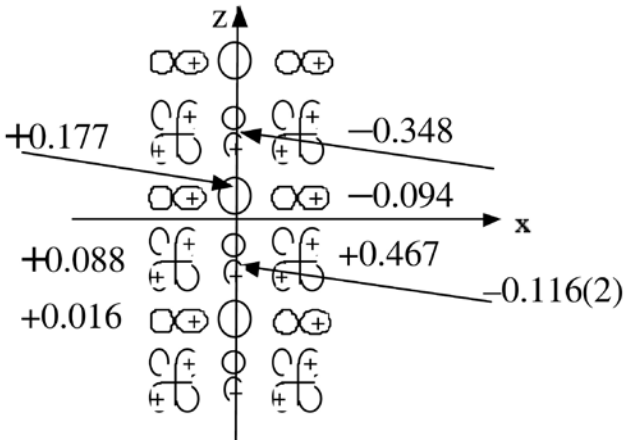


**FIGURE 1.** Changes in effective charges near the interface in $LaMnO_3$ arising from the removal of coupling across the $z=0$ plane, plus the formation of $Mn^{2+}$ and $Mn^{4+}$ ions, indicated. Charges on other ions are taken to be unchanged at their bulk values of $Z^*(Mn) = 1.98$ (shown as clover leaves), $Z^*(O) = -1.115$ (shown as figure eights), and $Z^*(La) = 1.36$ (shown as circles).

The third step is much simpler, removing the overlap repulsions, proportional to the inverse sixth power of distance, between ions on the two half crystals, with the result appearing as the second line in Table 1. Similarly, the effects of coupling between the *s* states on the surface Mn and Sr or La ions and the oxygen ions on the other side are removed, appearing as the third line in Table 1. The effects of the coupling between the Mn *d* states and the oxygen *p* states on the other face are more intricate, and more important. They involve recalculating the associated $MnO_6$ cluster states for the reduced number of neighbors, and the contributions are different for the surface ions which have been converted from $Mn^{3+}$ to $Mn^4$. These effects appear as the fourth line in Table 1.

When the surface ions are finally allowed to move from their starting positions relative to the substrate, all of the above effects come into play and all must be included in the energy as a function of these displacements. Positions are chosen which minimize the total energy, giving a prediction of the relaxation of the surface ions and the relaxation contribution to the surface energy, the fifth line in Table 1. The displacement of ions at the LaO surface of $LaMnO_3$ is shown in Figure 2.

It was an important step in the end to compare calculated relaxation displacements and surface energies with those calculated in LDA by Evarestov, et al. [3], since these quantities seem not to be available from experiment. The comparison offers some form of test of the approach, and quite interesting insights into the differences between the two approaches. In particular, as we see in Figure 2, the displacement of different oxygen ions in the same plane can be different, and

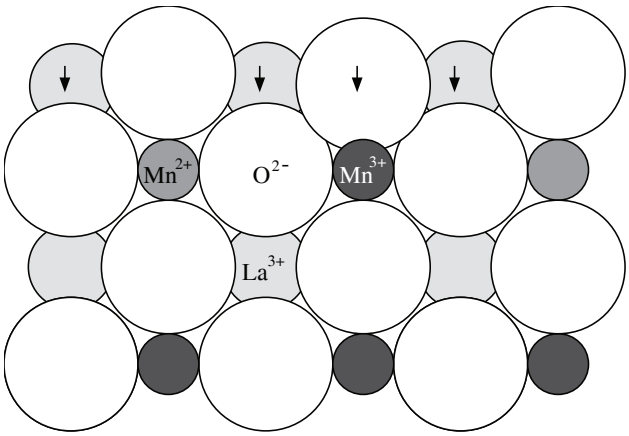


**FIGURE 2.** $LaMnO_3$ with a LaO surface at the top. The large white circles are oxygen. The small darker circles are $Mn^{3+}$, and half the subsurface manganese become $Mn^{2+}$. The oxygens above these $Mn^{2+}$ displace little, but the other surface oxygens move downward by 0.11*d* and the surface $La^{3+}$ move downward by 0.14*d* in the calculations here.

while the differences are real and observable, they are not present in the LDA calculations, as has been indicated. In order to compare with the Evarestov, et al. results, the positions of the different predicted ions must be averaged for the different valences, and the energies of the different clusters must be averaged. This symmetry-breaking did not occur for the treatment of the $SrMnO_3$ surfaces, but other such theoretical calculations with which to compare for those surfaces were not available. For the $LaMnO_3$ surfaces, the averaged unrelaxed surface energies summed to a value very close to the cleavage energies obtained by Evarestov, et al [3]. Indeed, such local-density calculations as theirs have often proven reliable for total energies even in systems where strong localization is believed to occur. Their calculation of relaxation led to quite large displacements deep below the surface, which are not understood. The calculations performed here restricted displacement to the surface ions alone, and gave displacements only similar to the changes in distance that Evarestov, et al. found between ions in the last two planes. Correspondingly, the relaxation energy is about half of that found by Evarestov, et al. It is not clear which is more likely to be correct. The approximate agreement of surface energies supports both approaches.

## Conclusions and Future Directions

This study has provided a reasonable description of the surfaces of these complicated materials, and an approach which can be extended directly to oxygen molecules interacting with these surfaces. It is not as simple as hoped because it is necessary to include the Madelung terms. However, it is clear that these terms are important in the properties of the surfaces and it has been essential to carry out their detailed treatment and to be sure that they are properly included. Oxygen molecules can now be introduced near these surfaces to understand their behavior.

## FY 2009 Publications/Presentations

**1.** Walter A. Harrison, "Tight-Binding Theory of the Oxides of Manganese and Iron," arXiv:0803.0994, Phys. Rev. B77.130001 (2008).

**2.** Walter A. Harrison, "Tight-Binding Theory of Lanthanum Strontium Manganate," arXiv:0807.2248, and submitted to Phys. Rev.

## References

**1.** Walter A. Harrison, Elementary Electronic Structure, World Scientific (Singapore, 1999), revised edition (2004).

**2.** Walter A. Harrison, "Simple Calculation of Madelung Constants," Phys. Rev. B **73**, 212103 (2006).

**3.** R.A. Evarestov, E.A. Kotomin, Yu. A. Mastrikov, D. Gryaznov, E. Heifets, and J. Maier, Phys. Rev. *B* **72**, 2014411 (2007).

# III. SECA CORE RESEARCH & DEVELOPMENT

## B. Anodes and Coal Contaminants

# III.B.1 Novel Sulfur-Tolerant Anodes for Solid Oxide Fuel Cells

Meilin Liu (Primary Contact), Lei Yang
Georgia Institute of Technology
School of Materials Science and Engineering
771 Ferst Drive NW
Atlanta, GA 30332-0245
Phone: (404) 894-6114; Fax: (404) 894-9140
E-mail: meilin.liu@mse.gatech.edu

DOE Project Manager: Briggs White
Phone: (304) 285-5437
E-mail: Briggs.White@netl.doe.gov

Contract Number: 42219

Start Date: October 1, 2004
End Date: December 31, 2008

### FY 2009 Objectives

- Characterize the sulfur-poisoning effect on anode-supported solid oxide fuel cells (SOFCs) under practical operation conditions.
- Investigate the effect of sealant on second-stage sulfur poisoning behaviors.

### Accomplishments

- Characterized sulfur poisoning behavior of state-of-the-art anode-supported SOFC button cells under various operating conditions, including the concentration of $H_2S$ and cell current density.
- Improved second-stage stability of cells in $H_2S$ by application of new sealant.

## Introduction

One of the unique advantages of SOFCs over other types of fuel cells is the fuel flexibility. SOFCs have the potential of direct utilization of hydrocarbon fuels. Compared with pure hydrogen, hydrocarbon fuels have higher energy density and are readily available and easier to transport and store based on current infrastructure. To use them, hydrocarbon fuels are reformed externally or internally into CO and $H_2$ on catalysts such as nickel. However, one problem with all hydrocarbon fuels is that they all contain contaminants such as sulfur compounds. For example, sulfur concentration in pipeline natural gas is usually several ppm by volume while sulfur concentration in liquid fuels such as gasoline, jet propellant and diesel could be as high as ~100-1,000 ppm by volume. The sulfur compounds would transform into gaseous hydrogen sulfide ($H_2S$) in the reforming process and readily poison the nickel-based anode for SOFCs, leading to dramatic reduction in cell performance and operational life.

In the fiscal year of 2009, this project focused on (i) characterizing both the immediate and the slow sulfur poisoning process for state-of-the-art SOFC button cells with an anode-supported structure under various operating conditions, and (ii) investigating the effect of sealant on second-stage poisoning behaviors.

## Approach

Multi-cell testing had been carried out to evaluate both the short-term and the long-term sulfur poisoning behavior for state-of-the-art anode-supported SOFC button cells. We developed (with the help from Pacific Northwest National Laboratory) procedures for making hermetic seals using the G-18 glass sealant in our testing apparatus and started another 3,000-hour test using 12 commercial cells and G-18 glass sealant, hoping to learn more about the behavior of the state-of-the-art cells (anode-supported cells with lanthanum strontium cobalt iron oxide cathodes) using G-18 glass sealant.

## Results

Shown in Figure 1 are the cell voltages for C03 and C04, run in clean hydrogen without exposure to $H_2S$. Shown in Figure 2(a) are the cell voltages for cells C05, C06, C07, and C08 before and after the fuel was switched from clean hydrogen to hydrogen containing 0.8 ppm $H_2S$ (at ~600 hours). As expected, the cell

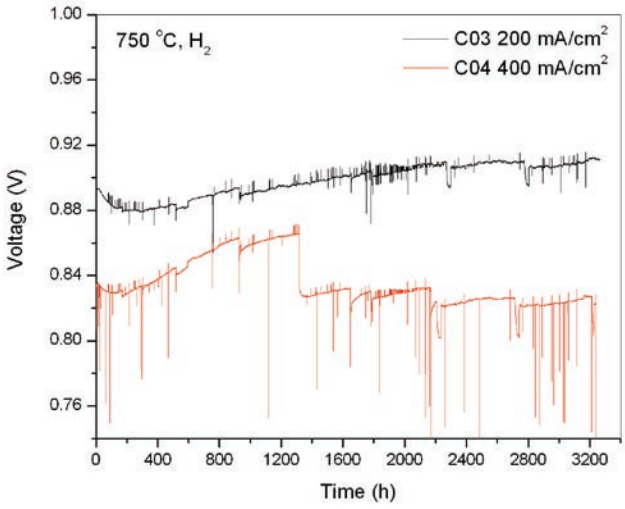


**FIGURE 1.** Typical Performance of the Test Cells without Exposure to $H_2S$

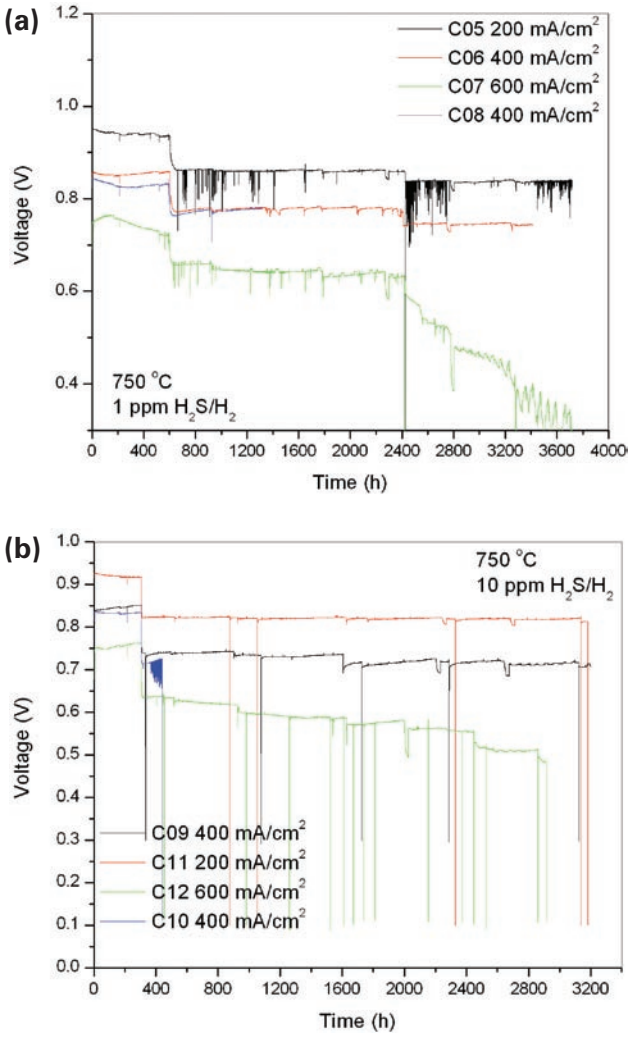


**FIGURE 2.** **(a)** Performance of the cells operated at 200, 400, and 600 mA/cm$^2$ and exposed to 0.8 ppm $H_2S$ after operation in hydrogen for ~ 600 hours. The concentration of $H_2S$ was changed from 0.8 ppm to 1.13 ppm at ~ 2,400 hours (change of gas cylinder); the effect of $H_2S$ concentration is clearly seen. **(b)** Performance of the cells operated at 200, 400, and 600 mA/cm$^2$ and exposed to 10 ppm $H_2S$ after operation in clean hydrogen for ~300 hours (not shown in the figure). It appears that there is no second stage sulfur poisoning effect for the cells operated at 200 and 400 mA/cm$^2$. However, the degradation in performance seems to be significant for the cell operated at 600 mA/cm$^2$, due to either a second stage sulfur poisoning effect of the anode or degradation of the cathode.

voltages further decreased when the concentration of $H_2S$ was changed from 0.8 ppm to 1.13 ppm. Shown in Figure 2(b) are the cell voltages for cells C9, C10, C11, and C12 before and after the fuel was switched from clean hydrogen to hydrogen containing 10 ppm $H_2S$ (at ~300 hours).

Summarized in Figure 3 are the cell voltages before and after initial exposure to $H_2S$. The drop in performance due to the initial exposure to $H_2S$ is similar to previous observations: the relative cell power output

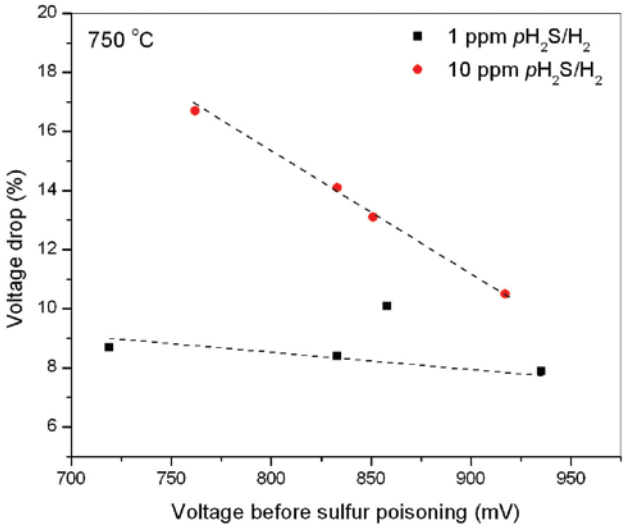


**FIGURE 3.** Cell Voltage Drop upon Initial Exposure to $H_2$ Containing 1 and 10 ppm $H_2S$

drop increased with (1) $H_2S$ concentration and (2) cell current density at high concentration of $H_2S$ (under constant current condition). As shown in Figure 3, the drops in performance are much larger for exposure to ~10 ppm $H_2S$ than to ~0.8 ppm $H_2S$ regardless of electrochemical testing conditions. However, for cells exposed to ~0.8 ppm $H_2S$, the observed relative drop in cell voltage was not sensitive to cell operating current density: -7.9% at 200 mA/cm$^2$, -8.4% (-10.1%) at 400 mA/cm$^2$, and -8.7% at 600 mA/cm$^2$. In contrast, for cells exposed to 10 ppm $H_2S$, the observed relative drop in cell voltage increased with operating current density: -10.5% at 200 mA/cm$^2$ , -13.1% at 400 mA/cm$^2$, and -16.7% at 600 mA/cm$^2$.

Shown in Figures 4(a) and 4(b) are normalized changes in cell voltage (in percentage) after the large initial voltage drop due to switching from $H_2$ to $H_2$ containing $H_2S$. For cells subject to 0.8 ppm $H_2S$, after the initial poisoning effect, the second stage degradation in performance was *not* significant for cells operated at current densities of 200 and 400 mA/cm$^2$. In contrast, the cell operated at 600 mA/cm$^2$ experienced a continued drop in performance during the entire duration of the testing, but the degradation rate seems to be much lower than that observed for the cells sealed using an Aremco sealant under similar testing conditions. However, the cell degraded rapidly when the concentration of $H_2S$ was switched from 0.8 ppm to 1.13 ppm. Third, for the cells exposed to 10 ppm $H_2S$, after the initial performance drop due to sulfur poisoning, the second stage degradation in performance was significant for the cells operated at 600 mA/cm$^2$, but *not* significant for the cells operated at 200 and 400 mA/cm$^2$, similar to that observed for the cells exposed to 1 ppm $H_2S$. The second stage degradation for the cells operated at 600 mA/cm$^2$

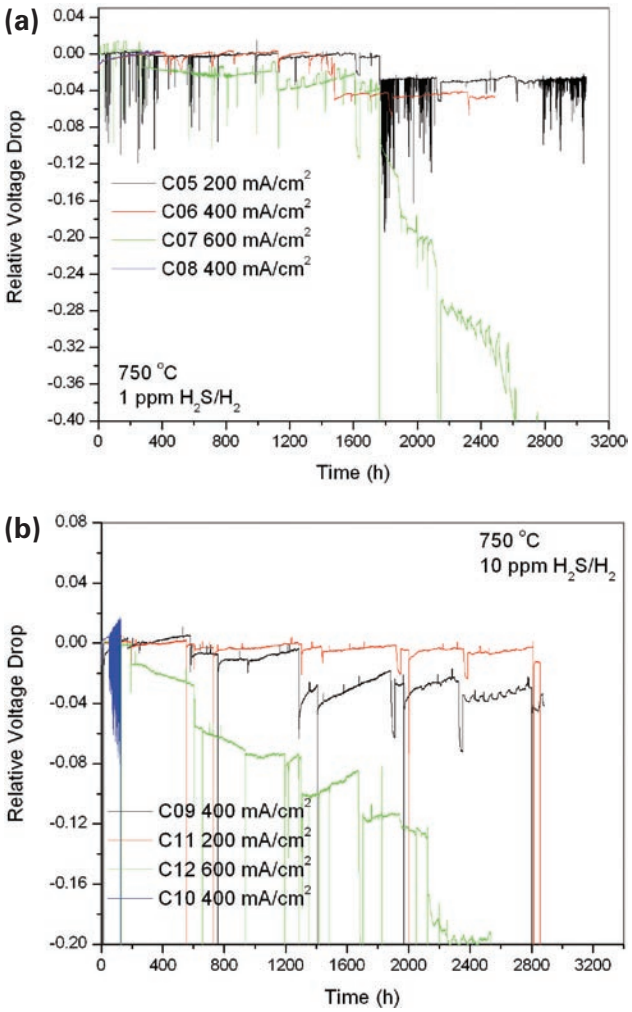


**FIGURE 4.** Normalized voltage changes (in percentage) after the large initial voltage drop due to switching from clean $H_2$ to $H_2$ containing **(a)** 1 ppm and **(b)** 10 ppm $H_2S$. A reading of -0.01 on the vertical axis would be equivalent to 1% voltage drop, corresponding to a second stage degradation due to sulfur poisoning.

(exposed to ~1 and 10 ppm $H_2S$) may be attributed to either a second stage sulfur poisoning or a degradation of cathode performance at a high operating current density.

## Conclusions

Based on the results we have collected, the key conclusions can be summarized as follows. For exposure to low concentrations of $H_2S$ (e.g., 1 ppm in humidified hydrogen), the drop in power output (or drop in voltage at a constant current) due to the *initial* $H_2S$ exposure appears independent of operating conditions (e.g., cell potential). In contrast, for exposure to high concentrations of $H_2S$ (e.g., 10 ppm), the degradation appears to be more severe at a higher operating current density (or lower cell potential). The degradation due to initial $H_2S$ exposure occurs quickly, typically within hours, and performance then remained relatively constant for continuous operation up to ~3,000 hours at 200 and 400 mA/cm$^2$. For cells operated at 600 mA/cm$^2$, however, there appears a continued degradation in performance after the *initial* large drop in performance due to the $H_2S$ exposure, but at a much lower rate. This continued degradation in performance during the long-term operation of the cells may result from a "second stage" sulfur poisoning effect or degradation in performance of the cathode at high current densities.

## FY 2009 Publications/Presentations

**1.** Z. Cheng, J.H. Wang, and M. Liu, "Anodes," Chapter 2, in Solid Oxide Fuel Cells: Materials Properties and Performance (Editors: J.W. Fergus, R. Hui, X.G. Li, D.P. Wilkinson, and J.J. Zhang), CRC Press, p. 73-130, 2008.

**2.** J.H. Wang and M. Liu, "Surface Regeneration of Sulfur-Poisoned Ni Surfaces under SOFC Operation Conditions Predicted by First-Principles Based Thermodynamic Calculations," *Journal of Power Sources*, 176(1), 23-30, 2008.

**3.** S. Choi, J.H. Wang, Z. Cheng, and M. Liu, "Surface Modification of Ni-YSZ Using Niobium Oxide for Sulfur Tolerant Anodes in Solid Oxide Fuel Cells," *Journal of the Electrochemical Society*, 155(5), B449-B454, 2008.

**4.** M. Liu, H. Abernathy, Z. Cheng, and X. Lou, "The Use of Raman Spectroscopy in the Analysis of SOFC Anode Reactions," *Preprints of Symposia - American Chemical Society*, Division of Fuel Chemistry, 2008.

## References

**1.** S. Zha, Z. Cheng, and M. Liu, "Sulfur Poisoning and Regeneration of Ni-Based Anodes in Solid Oxide Fuel Cells," *Journal of the Electrochemical Society,* 154, B201-B06, 2007.

**2.** J.P. Trembly, A.I. Marquez, T.R. Ohrn, and D.J. Bayless, "Effects of Coal Syngas and $H_2S$ on the Performance of Solid Oxide Fuel Cells: Single-Cell Tests," *Journal of Power Sources*, 158, 263-73, 2006.

**3.** E.R. Ray, "Contaminant Effects in Solid Oxide Fuel Cells," in W.J. Hubner (Ed.), *Proceedings of the Third Annual Fuel Cells Contractors Review Meeting*, U.S. Department of Energy, Washington, DC, p. 108-16, 1992.

**4.** C.H. Bartholomew, P.K. Agrawal, and J.R. Katzer, "Sulfur Poisoning of Metals," *Advances in Catalysis*, 31, 153, 1982.

# III.B.2 Coal-Based Fuel Cells

Randall Gemmen (Primary Contact),
Kirk Gerdes, Xingbo Liu, Paul Salvador
National Energy Technology Laboratory
3610 Collins Ferry Road
Morgantown, WV 26507
Phone: (304) 285-4536; Fax: (304) 285-0903
E-mail: Randall.Gemmen@netl.doe.gov

Contract Number: 07-220621

Start Date: October 1, 2007
End Date: September 30, 2008

### FY 2009 Objectives

- Identify cleanup levels for trace contaminant species contained in coal syngas via solid oxide fuel cell (SOFC) performance tests on direct coal syngas and single trace coal species.
- Identify low cost coating methods suitable for applying $(Mn,Co)_3O_4$ spinel protective coatings on low cost stainless steel interconnects.
- Develop the experimental protocols to determine the crystallographic nature of the interfaces and triple phase boundaries in SOFCs, especially in the cathode, as well as to establish a basic understanding over the factors that determine their populations and evolution.

### Accomplishments

Trace Species Effects:

- Deployed and operated a fuel cell test array at a remote gasification site.
- Operated a gas chromatograph-inductively coupled plasma/mass spectrometer system in support of testing at the remote gasification site.
- Completed 500-hour SOFC performance testing on naphthalene and mercury

Interconnect Coatings:

- Successfully deposited Mn/Co alloys onto interconnects by electrodeposition.
- Tests showed stable area specific resistance with a slight increase at 800°C for 1,200 hours.
- On-cell tests substantiate that electrodeposition of Mn/Co spinels can successfully block chromium evaporation, maintain conductivity, and survive thermal cycles.

Crystalographic Analysis:

- Determined processing conditions to generate dense and porous compacts of yttria-stabilized zirconia (YSZ), lanthanum strontium manganate (LSM), YSZ/LSM, using fuel cell materials and processing techniques.
- Optimized the electron back-scattered diffraction (EBSD) collection and processing methods to quantify the microstructure of all compacts and obtain 3-dimensional microstructure of real fuel cells.
- Fully characterized the microstructure of YSZ and LSM as a function of thermal anneals.
- Fully characterized the cathode microstructure from a button cell SOFC.

## Introduction

To achieve the DOE goal of developing 60% efficient coal-based fuel cell systems will require test and evaluation of existing SOFC technology on coal syngas, and examination of novel SOFC fuel cell materials and concepts. The work performed here accomplishes the first objective by studying the impact of trace contaminant species on SOFC performance. Here, SOFC test specimens are evaluated for their voltage degradation that follows from the injection of a specific trace material. The trace contaminate work will allow us to determine levels of trace materials found in coal that are acceptable to SOFC performance and thereby set cleanup targets for gasification technology. The second objective is accomplished by investigating the performance of low cost coating methods, as well as the behavior of electrode microstructure over time. Here, electroplating methods are used to coat SOFC interconnects, and electron back-scattering methods are used to analyze the electrode microstructure. The coating work will allow us to achieve low degradation by protecting the cell against chromium attack and interconnect oxidation. And finally, the crystallographic studies will allow us to quantify any microstructure changes over time and correlate those effects to cell performance changes.

## Approach

Trace Species Effects – Individual coal contaminant tests are performed using laboratory test facilities designed to deliver known amounts of contaminant to the anode of an SOFC button cell. By determining how specific contaminants attack SOFC anode materials

(YSZ and Ni), improved assessments for cleanup targets can be achieved. The direct coal syngas tests are performed using a unique, portable, multi-cell test capability that can be taken to gasification facilities for fuel cell testing. This test rig allows for twelve individual cells to be tested simultaneously thereby allowing for redundant cell testing and improved statistical analysis of the post-run data. Such capability is needed in order to maximize "data through-put" and cost-effectiveness when performing tests on *real world* large-scale gasification technology.

Interconnect Coatings – Electrodeposition of Mn/Co metallic alloys followed by controlled oxidation to the desired spinel phase offers a low-cost alternative method for applying protective interconnect coatings. The main issue of Mn/Co co-deposition is the dramatic difference of deposition potentials of Mn (-1.18 V) and Co (-0.28 V), which makes it challenging to co-deposit these materials. The approach to overcome these challenges is the use of pulse deposition.

Crystalographic Analysis – EBSD can be used to quantify the microstructure of commercially-prepared SOFCs. We are now determining quantitatively the crystallographic nature of the important cathode microstructural features as a function of load (thermal and/or electrical); we will correlate these changes to performance and, ultimately, develop cells having microstructural features that improve performance.

## Results

Trace Species Effects – Testing SOFC performance after exposure to naphthalene and mercury as well as syngas from a coal gasifier has been completed. Naphthalene exposure at 100 ppm and 500 ppm produced voltage degradation rates of 4.0% and 11.0%/1,000 hours, respectively, in spite of a syngas composition that was far from carbon deposition conditions as determined by thermodynamics (3% $C_{10}H_8$). Mercury exposure at 10 ppm produced a degradation rate of 2.2%/1,000 hours (see Figure 1 for the mercury results). Direct coal syngas experiments were conducted by interfacing a mobile SOFC array with a partially cleaned syngas stream derived from coal gasification (Wilsonville Power Systems Development Facility). Initial results showed that the supplied syngas was able to be sufficiently cleaned to prevent generation of secondary phases within the anode. Results to date show that syngas intended for SOFCs must be sufficiently scrubbed of trace material to prevent additional cell degradation, and that such conditioning can be accomplished by available technology.

Interconnect Coatings – Figure 2 shows the cell performance with Mn-Co coated T441 substrates at constant voltage of 0.7 V. In the initial 100 hours, the performance kept increasing due to current treatment.

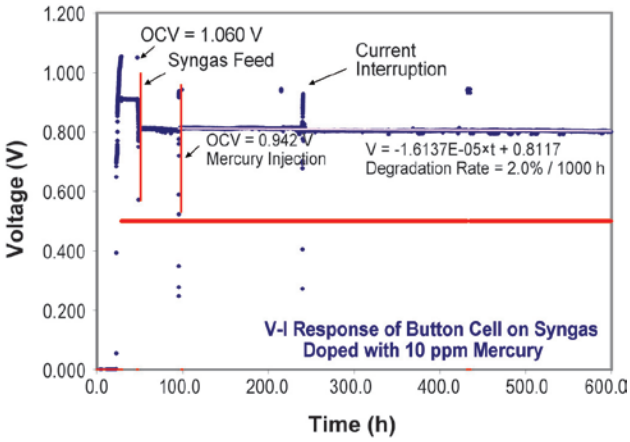


**FIGURE 1.** Cell Performance on Syngas with 10 ppm Mercury

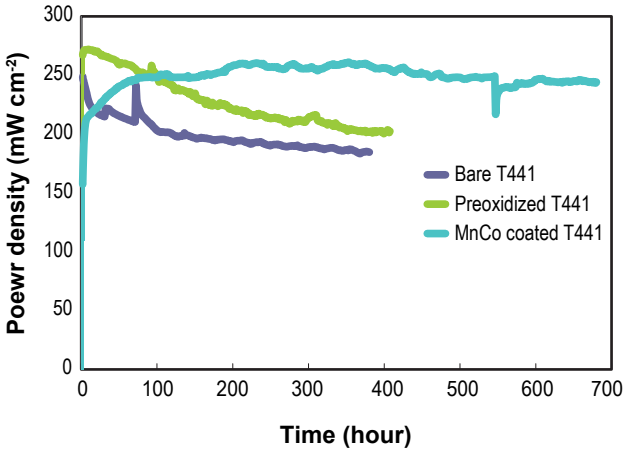


**FIGURE 2.** On-Cell Performance of Electroplated T441 Interconnect Coatings

Stable performance was obtained between 100-180 hours and 440-545 hours. Note the performance improves a little between 180-440 hours. The reason is not totally clear, but may be due to contact improvement. Two thermal cycles were conducted at 545 hours between 800°C to room temperature. The first thermal cycle was done to heat the cell to 800°C in 0.5 hour, the second one was in 2 hours. Each cooling down took 2 hours to room temperature. The performance shows improvement after the thermal cycles, similar to the current treatment effect at the start of the test. It remains stable until 680 hours, which proved that Mn-Co coating can survive severe thermal cycles.

Crystalographic Analysis – Figure 3 shows the distributions of grain boundary normals as multiples of random for all orientations in the standard stereographic triangle (binned in 10° angles). The respective multiples of a random distribution (MRD) spreads are as follow: 0.88-1.15 for the as sintered (AS) sample, 0.84-1.19 for the

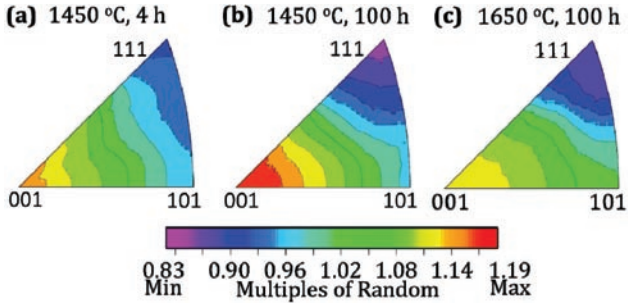


**FIGURE 3.** Grain Boundary Distribution of YSZ Compacts Showing Isotropic Behavior

(AS+) 1,450°C, 100-hour sample, and 0.86-1.12 for the (AS+) 1,650°C/100-hour sample. These distributions are all essentially identical, indicating that the microstructure has reached a steady-state value after the initial sintering step in which the grains grew from 300-500 nm to ≈6 microns. Though each distribution exhibits a weak preference at the (100) pole and a weak suppression at the (111) pole, the values are fairly small and approximating the distribution as random is reasonable. Recent work has shown that the binning procedure in the Orientation Image Microscopy software produces similar distributions when a perfectly random data set is used. Also, the data set was reshuffled to approximate a random set and similar distributions were obtained. All of these results indicate that the SOFC YSZ compacts have very isotropic distributions of grain boundary normals. Similar results are observed for SOFC LSM. Interestingly, these materials are the most uniform observed by the material research group at Carnegie Mellon University.

## Conclusions and Future Directions

Results show that syngas intended for SOFCs must be sufficiently scrubbed of trace material to prevent additional cell degradation, and that technology exists that achieves such performance. Suitability of such cleanup for commercial applications remains to be assessed. Results also showed that cost-effective and environmental friendly processes are available for depositing Mn-Co spinel coatings on SOFC interconnects. And finally, SOFC materials have grain boundaries that are crystalographically isotropic.

Future research will be conducted to repeat the direct coal syngas tests. Also, scale-up of the coating method is needed for practical SOFC stack interconnects. And finally, quantification of SOFC microstructures is needed under electrochemical load to determine basic degradation modes related to microstructure.

## FY 2009 Publications/Presentations

**1.** Junwei Wu, Christopher Johnson, Randall Gemmen, Xingbo Liu*, "The Performance of Solid Oxide Fuel Cells with Mn-Co Electroplated Interconnect as Cathode Current Collector," Accepted by *Journal of Power Sources*, 189 (2009) 1106-1113.

**2.** Yihong Li, Junwei Wu, Christopher Johnson, Randall Gemmen, Scott Mao, Xingbo Liu, "Oxidation Behavior of Metallic Interconnects for SOFC in Coal Syngas," *International Journal of Hydrogen Energy*, 34 (2009) 1489.

**3.** Christopher Johnson, Nina Orlovskaya, Anthony Coratolo, Caleb Cross, Xingbo Liu, Junwei Wu, Randall Gemmen, "The Effect of Coating Crystallization and Substrate Impurities on Magnetron Sputtered Doped $LaCrO_3$ Coatings for Metallic Solid Oxide Fuel Cell Interconnects," *International Journal of Hydrogen Energy*, 34 (2009) 2408.

**4.** Junwei Wu, Christopher Johnson, Yinglu Jiang, Randall Gemmen, Xingbo Liu*, "Pulse Plating of Mn-Co Alloys for SOFC Interconnect Applications," *Electrochimica Acta* (October 2008) 793-800.

**5.** "Microstructural Studies of Solid Oxide Fuel Cell Cathodes by Orientation Imaging Microscopy," The 15th International Conference on Textures of Materials (ICOTOM 15), Pittsburgh, Pennsylvania, June 1–6, 2008 (Poster).

**6.** "Microstructural Studies on Solid Oxide Fuel Cell Cathode Materials," Materials Science and Technology (MS&T) Conference 2008, Pittsburgh, Pennsylvania, October 2008 (Oral).

**7.** "Quantitative Microstructural Analysis of Solid Oxide Fuel Cell Cathode Materials," 2nd International Congress on Ceramics, Verona, Italy, June/July 2008 (Poster).

**8.** "Crystallography of Interfaces and Triple Phase Boundaries in SOFCs from Three Dimensional Microstructure Data," 33rd International Conference & Exposition on Advanced Ceramics and Composites, Daytona Beach, Florida, January 2009.

**9.** "Oxide Thin Films Used to Investigate Chemical Conversion in Photochemistry and Solid Oxide Fuel Cells," Materials Science Division (MSD) Colloquium at Argonne National Laboratories on February 12, 2009.

**10.** "Oxide Thin Films Used to Investigate Chemical Conversion in Photochemistry and Solid Oxide Fuel Cells," Electronic & Magnetic Nanoscale Composite Multifunctional Materials Center at the Ohio State University on March 13, 2009.

**11.** "The Crystallographic Orientation Distribution of Interfaces and Three Phase Boundaries in Solid Oxide Fuel Cell Cathodes," to be submitted as a communication to J. Amer. Ceram. Soc.

**12.** "Quantifying Microstructure of Dense Yttria-Stabilized Zirconia," to be submitted to Int. J. Appl. Ceram. Tech.

# III.B.3 SECA Coal-Based Systems Core Research: Anode Reactions in Coal-Derived Fuels

Olga A. Marina (Primary Contact), Christopher A. Coyle, Edwin C. Thomsen, Danny J. Edwards, Carolyn N. Cramer, Gregory W. Coffey, and Larry R. Pederson
Pacific Northwest National Laboratory
902 Battelle Blvd., PO Box 999
Richland, WA 99352
Phone: (509) 375-2337; Fax: (509) 375-2186
E-mail: olga.marina@pnl.gov

DOE Project Manager: Briggs White
Phone: (304) 285-5437
E-mail: Briggs.White@netl.doe.gov

Subcontractor:
Montana State University, Bozeman, MT

Contract Number: 44036

Start Date: October 1, 2008
End Date: September 30, 2009

### FY 2009 Objectives

- Assess interactions of antimony, arsenic, hydrogen chloride, phosphorus, selenium, and sulfur impurities found in coal gas with the nickel-based solid oxide fuel cell (SOFC) anode with a purpose of establishing maximum permissible concentrations of these impurities without causing unacceptable SOFC degradation rates.
- Determine effect of the electrical potential on the rate of contaminant interactions with the nickel at the active interface.
- Design a method of removing phosphorus impurities from coal gas.

### Accomplishments

- Completed studies of nickel interactions with phosphorus, arsenic, hydrogen chloride, selenium, and sulfur impurities. Phosphorus, antimony and arsenic were found to interact strongly with nickel and result in extensive alteration phase formation, mostly at the fuel inlet, consistent with expectations based on thermodynamic properties. Selenium, sulfur, and hydrogen chloride adsorb on the nickel surface without forming secondary phases and decrease hydrogen and carbon monoxide chemisorption. Selenium and sulfur interactions with nickel were strongly affected by the cell voltage, while the interactions of other impurities with nickel were not. No interactions of phosphorus-, arsenic-, antimony-, selenium-, sulfur-containing species with zirconia were observed.
- Developed a supported fixed bed absorber for arsenic and phosphorus in coal gas.

## Introduction

The coupling of coal gasification with an SOFC is being considered by the United States Department of Energy as a highly efficient means of electricity production [1]. Gasified coal contains high concentrations of hydrogen and carbon monoxide, which can be utilized by an SOFC to produce electricity. Gasified coal also contains many other minor and trace components that could have an impact on SOFC performance. A modeling study by Trembly et al. [2] identified Sb, As, Cd, Hg, Pb, P, and Se as coal gas contaminants that are most likely to affect the performance of an SOFC, some of which are predicted to form secondary bulk phases with Ni. Experimental verification of modeling calculations was identified as a critical need.

The effect of phosphorus, arsenic, antimony, selenium, hydrogen chloride and sulfur impurities in the synthetic coal gas on the SOFC performance was investigated under typical SOFC operation conditions. Testing was performed using both yttria-stabilized zirconia (YSZ) electrolyte-supported and anode-supported button cells. Nickel/YSZ anodes and 20 at% strontium-doped lanthanum manganite (LSM) cathodes were used in both cell configurations. Electrodes were exposed to single and multiple contaminants at concentrations appropriate to their presence in gasified coal, and the cell electrochemical performance was evaluated. Electrolyte-supported cells more quickly responded to the presence of coal gas contaminants, while anode-supported cells were similar in configuration to those being considered for use in planar stacks. In addition to button cells, coupon tests were performed to help identify whether alteration phases are formed from nickel-contaminant reactions, the critical pressure of the contaminant required for formation, and contaminant penetration kinetics. Coupon tests included the use of Ni/YSZ support material in a flow-through and flow-by arrangement to provide information on relative uptake kinetics. Experimental observations with regard to alteration phase formation, distribution, and stability were compared to the results

of thermochemical calculations, necessary to provide a predictive capability for contaminant/anode interactions.

## Approach

The ultimate goal of this project is to establish maximum acceptable concentrations of coal gas contaminants and contaminant combinations that would permit SOFCs to meet long-term standards for degradation. The long-term performance of the anode-supported button cells were evaluated as functions of impurity concentration, temperature, fuel utilization, current density and time of the exposure. Additionally, screening tests with Ni/YSZ coupons were employed in a flow-by and flow-through arrangement. Post-test analyses were conducted with analytical scanning electron microscopy (SEM) and transmission electron microscopy, X-ray diffraction, electron back-scatter diffraction, X-ray photoelectron spectroscopy (XPS), Auger electron spectroscopy (AES), and time-of-flight secondary ion mass spectroscopy (ToF-SIMS) were performed to establish the extent and form of contaminant/anode interactions. Surface analytical probes, Tof-SIMS, AES and XPS, are sufficiently sensitive to reveal sub-monolayer adsorption, including competitive adsorption effects, whereas electron microscopy and diffraction techniques revealed the formation of bulk or surface phases.

## Results

The interaction of 0.5 to 10 ppm phosphorus in synthetic coal gas with the nickel-based anode of SOFCs was studied at 700 to 800°C. Two primary modes of degradation were observed. The most obvious was the formation of a series of nickel phosphide phases, of which $Ni_3P$, $Ni_5P_2$, $Ni_{12}P_5$ and $Ni_2P$ were identified. Phosphorus was essentially completely captured by the anode, forming a sharp boundary between converted and unconverted anode portions. These products partially coalesced into large grains, which eventually affected electronic percolation through the anode support as illustrated in Figure 1. Thermodynamic calculations predict that formation of the most stable nickel phosphide phases is possible at sub-parts per billion concentrations in coal gas at temperatures relevant to fuel cell operation. A second mode of degradation is attributed to surface diffusion of phosphorus to the active anode/electrolyte interface to form an adsorption layer. Direct evidence for the presence of such an adsorption layer on nickel was obtained by surface spectroscopies on fracture surfaces. Further, cell performance losses were observed well before the entire anode was converted to nickel phosphide phases. Impedance spectroscopy revealed that these losses were primarily due to growth in electrodic resistance, whereas large ohmic increases were visible when the entire anode was converted to nickel phosphide phases. The rate

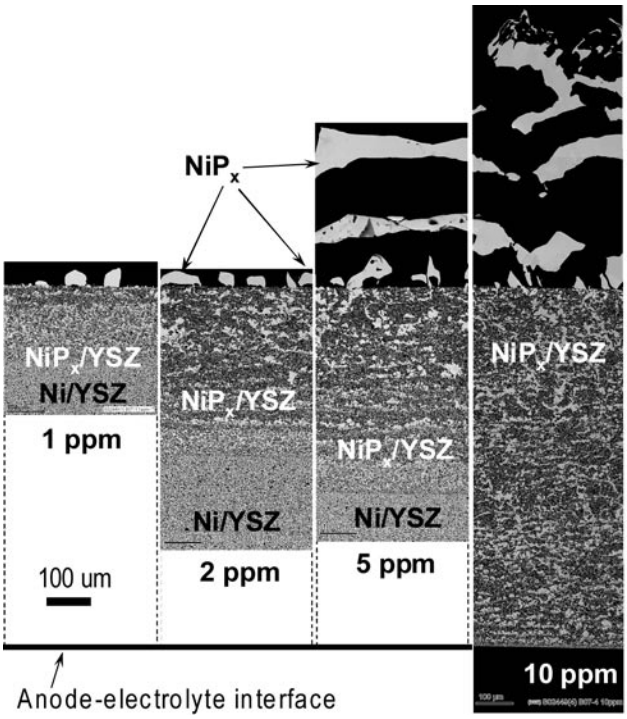


**FIGURE 1.** Cross-sectional SEM images of Ni/YSZ anode support after 990-hour cell test at 700°C in synthetic coal gas with 1, 2, 5, and 10 ppm of phosphine. All of the Ni in Ni/YSZ anode support was converted to $NiP_x$ during test with 10 ppm $PH_3$; not converted Ni/YSZ is seen in images of cells tested with 1, 2 and 5 ppm $PH_3$. Larger agglomerates in the upper part of each cell are $NiP_x$/YSZ. Large $NiP_x$ crystallites on the anode surfaces are either Ni scavenged from the Ni/YSZ, or from the Ni current collector.

of resistance growth for anode-supported cells showed a very low phosphorus concentration dependence, attributed to phosphorus activity control within the anode by nickel phosphide products.

For arsenic a major mode of degradation was loss of electronic percolation, the result of alteration phase formation, grain growth, and inducement of micro-fractures within the affected portions of the anode support. An arsenic concentration of 0.5-10 ppm was found to interact strongly with nickel at 700-800°C, resulting in the formation of nickel-arsenic solid solution, $Ni_5As_2$ and $Ni_{11}As_8$, depending on temperature, arsenic concentration, and reaction time. For anode-supported cells, loss of electrical connectivity in the anode support was the principal mode of degradation, as nickel was converted to nickel arsenide phases that migrated to the surface to form large grains, Figure 2. Cell failure occurred well before the entire anode was converted to nickel arsenide, and followed a reciprocal square root of arsenic partial pressure dependence consistent with a diffusion-based rate-limiting step. Failure occurred more quickly with electrolyte-supported cells, which have a substantially smaller nickel inventory. For these cells, time to failure varied linearly with the

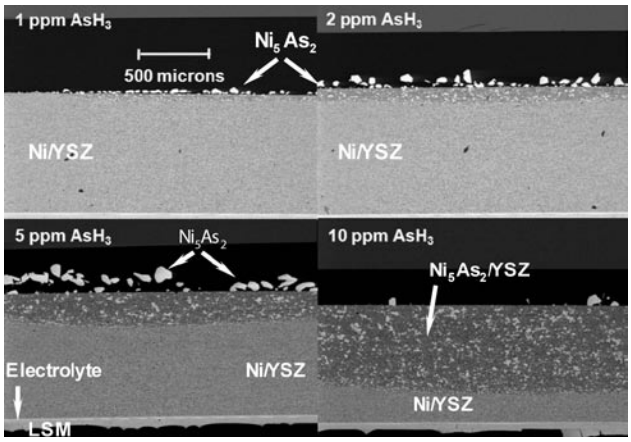


**FIGURE 2.** Cross-sectional SEM images of the four Ni/YSZ anode-supported cells after 480-hour exposure to coal gas containing 1, 2, 5, or 10 ppm of $AsH_3$ at 800°C. Reaction products on the surface and in the upper part of the anode support shown as light features are $Ni_5As_2$. Most of nickel arsenide reaction products spalled off from the surface of the sample exposed to 10 ppm $AsH_3$. Dense YSZ electrolyte and LSM cathode are seen at the very bottom of each image.

reciprocal arsenic concentration. Failure occurred when arsenic reached the anode/electrolyte interface, though agglomeration of nickel reaction products may have also contributed. Tests performed with nickel/zirconia coupons showed that arsenic was completely captured in a narrow band near the fuel gas inlet. Arsenic concentrations of ~10 parts per billion or less are estimated to result in acceptable rates of fuel cell degradation.

The effect of chlorine on the SOFC performance was studied in the temperature range 650-850°C and HCl concentrations of 5-200 ppm. Cell degradation due to HCl exposure occurred relatively fast, and increased with HCl concentration. Cell area specific resistances increased by 10-30% and the power output dropped <10% during ca. 500 hours after exposure to HCl. When HCl was removed from the coal gas, cells recovered rather fast. As determined by impedance spectroscopy, the electrodic resistance increased when the anode was exposed to HCl. The SEM analysis following the test termination revealed no microstructural changes in the nickel/YSZ anode. The mechanism of degradation was attributed to the formation of a chlorine adsorption layer on the surface of nickel.

Cells exposed to 0.5-5 ppm of hydrogen selenide in coal gas in the temperature range 600-800°C modestly decreased in power output (10-20% power output drop at a constant current density of 0.5 A/cm$^2$) to a steady-state level, similar in behavior to cells exposed to hydrogen sulfide. Power loss occurred more slowly for hydrogen selenide exposure. Recovery was similarly slower and less complete for hydrogen selenide exposure. Electrochemical impedance analyses revealed that the loss in cell performance was the result of a decreased electrocatalytic activity of the anode. No nickel selenide bulk phase formation was observed, consistent with predictions based on thermochemical calculations. Low levels of surface-adsorbed selenium were found by XPS. Performance loss was strongly affected by the local oxygen partial pressure (overpotential) at the active interface, Figure 3. Depending on cell potential (current density), larger changes were observed including oscillatory behavior and total irreversible failure. For failed cell microstructural changes at the active anode/electrolyte interface were revealed that potentially contributed to the electrode irreversibility, Figure 4. No electrical potential gradient effect on the rate of phosphorus and arsenic interactions with the Ni/YSZ anode was found.

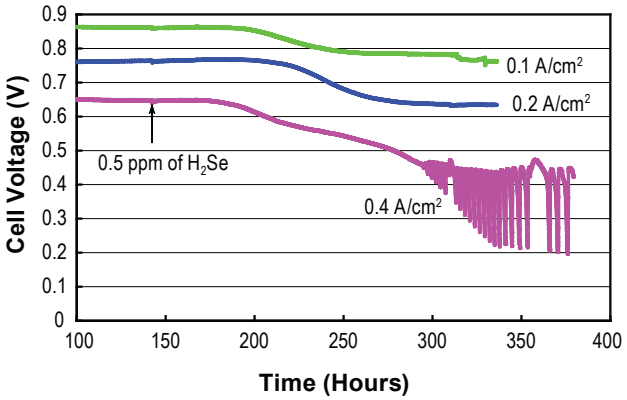


**FIGURE 3.** Cell voltage at a constant current density of 0.1, 0.2, and 0.4 A/cm$^2$ at 700°C after 0.5 ppm $H_2Se$ was added to synthetic coal gas.

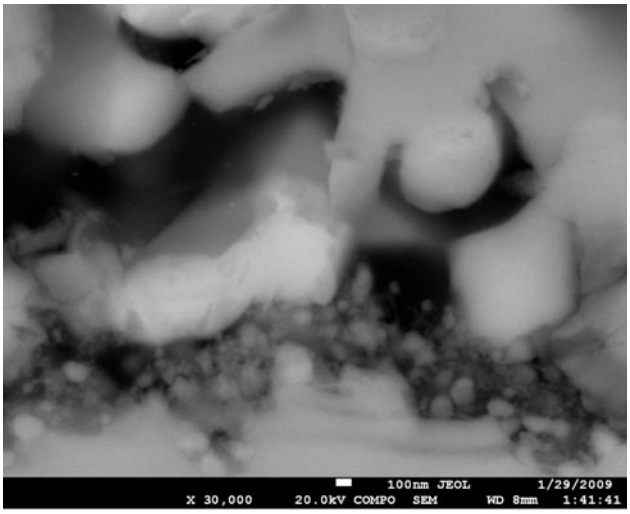


**FIGURE 4.** SEM image of the Ni/YSZ –YSZ interface after 160-hour test at a current density of 0.5 A/cm$^2$ in coal gas with 1 ppm of $H_2Se$ at 700°C.

Effective absorber materials to remove phosphorus and arsenic from coal gas were developed. An important issue with these absorber materials is extensive recrystallization upon exposure to arsenic and phosphorus, leading to excessively high pressure drop in a fixed bed. To overcome these problems, engineered forms of absorber materials, where the active material was limited to a composition of ~5 volume percent, showed promise. No phosphorus breakthrough was observed following 100-hour exposure, and pressure drops remained stable.

## Conclusions and Future Directions

- Exposure of nickel-based SOFC anodes to phosphorus, arsenic, and antimony compounds in coal gas at concentrations from 0.1 to 10 ppm resulted in irreversible performance losses. Arsenic exposure of nickel anodes similarly led to irreversible performance losses, principally attributed to loss of electrical percolation in the anode support associated with secondary phase formation. Degradation in phosphorus is attributed to both a loss of electrical percolation in the outer portion of the anode as well as to an adsorption layer at the active anode/electrolyte interface.
- Exposure of nickel/YSZ to hydrogen sulfide, hydrogen selenide and hydrogen chloride in coal gas, although decreased power output, was largely reversible.
- Other critical coal gas contaminants previously identified will be considered in future tests. Both anode-supported and electrolyte-supported cell configurations will be utilized, the former of which provides information on possible reduction of continuity in the anode support, and the latter of which will allow contaminants to reach the active interface more rapidly. Maximum allowable concentrations of contaminants and combinations of contaminants will be established that would permit SOFC stacks operating on coal gas to meet requirements for long-term degradation.
- Coupon testing will be conducted in actual coal gas and mixed coal/biogas to better understand the kinetics and mechanisms of impurity interactions with the fuel cell anode. These tests will provide information with regard to the distribution of impurity uptake, not possible with button cells, and are needed to validate approaches used in button cell testing in synthetic coal gas containing a small subset of impurities.
- Absorbers for phosphorus and arsenic will be further evaluated to establish both the capacity and kinetics of phosphorus and arsenic absorption by these absorbers.

## Special Recognitions & Awards/Patents Issued

**1.** O.A. Marina and L.R. Pederson, "Composite Solid Oxide Fuel Cell Anode Based on Doped Ceria and Doped Strontium Titanate," U.S. Patent 7,468,218, issued December 23, 2008.

## FY 2009 Publications/Presentations

**1.** O.A. Marina, L.R. Pederson, D.J. Edwards, C.A. Coyle, J.W. Templeton, M.H. Engelhard, and Z. Zhu, "Effect of Coal Gas Contaminants on Solid Oxide Fuel Cell Operation," *ECS Transactions*, 11 (3) (2008) 33.

**2.** C.A. Coyle, O.A. Marina, E.C. Thomsen, D.J. Edwards, C.D. Cramer and L.R. Pederson, "Interactions of Nickel/Zirconia SOFC Anodes with Coal Gas Containing Arsenic," *Journal of Power Sources*, 193 (2009) 730-738.

**3.** B.P. McCarthy, L.R. Pederson, Y.S. Chou, X.D. Zhou, W.A. Surdoval, and L.C. Wilson, "Low-Temperature Sintering of Lanthanum Strontium Manganite-Based Contact Pastes for SOFC," *Journal of Power Sources*, 180 (2008), 294-300.

**4.** B.P. McCarthy, L.R. Pederson, R.E. Williford, and X.D. Zhou, "Low-Temperature Densification of Lanthanum Strontium Manganite ($La_{1-x}Sr_xMnO_{3+\delta}$), x=0.0-0.20," *Journal of the American Ceramic Society* (2009), in print.

**5.** E.C. Thomsen, G.W. Coffey, L.R. Pederson, and O.A. Marina, "Performance of Lanthanum Strontium Manganite Electrodes at High Pressure," *Journal of Power Sources*, 191 (2008) 217-224.

**6.** Z.Q. Yu, S.V.N.T. Kuchibhatla, L.V. Saraf, O.A. Marina, C.M. Wang, M.H. Engelhard, V. Shutthanandan, P. Nachimuthu, and S. Thevuthasan, "Conductivity of Oriented Samaria-Doped Ceria Thin Films Grown by Oxygen-Plasma-Assisted Molecular Beam Epitaxy," *Electrochemical and Solid-State Letters,* 11 (5) (2008), B76-B78.

**7.** Z.Q. Yu, S.V.N.T. Kuchibhatla, M.H. Engelhard, V. Shutthanandan, C.M. Wang, P. Nachimuthu, O.A. Marina, L.V. Saraf, S. Thevuthasan, and S. Seal, "Growth and Structure of Epitaxial $Ce_{0.8}Sm_{0.2}O_{1.9}$ by Oxygen-Plasma-Assisted Molecular Beam Epitaxy," *Journal of Crystal Growth*, 310 (2008) 2450–2456.

**8.** D. Bera, S.V.N.T. Kuchibhatla, S. Azad, L. Saraf, C.M. Wang, V. Shutthanandan, P. Nachimuthu, D.E. McCready, M.H. Engelhard, O.A. Marina, D.R. Baer, S. Seal, and S. Thevuthasan, "Growth and Characterization of Highly Oriented Gadolinia-Doped Ceria (111) Thin Films on Zirconia (111)/Sapphire (0001) Substrates," *Thin Solid Films*, 516 (2008) 6088–6094.

**9.** O.A. Marina, L.R. Pederson, C.A. Coyle, E.C. Thomsen, G.W. Coffey, D.J. Edwards, and M.H. Engelhard, "Effect of Coal Gas Contaminants on Solid Oxide Fuel Cell Operation," Presented at the 213th meeting of the Electrochemical Society, Phoenix, Arizona on May 21, 2008.

**10.** O.A. Marina, L.R. Pederson, C.A. Coyle, E.C. Thomsen, D.J. Edwards, C.D. Nguyen, and G.W. Coffey, "SOFC Interactions with Coal Gas Contaminants," Presented at the 9th Annual SECA Workshop, Pittsburgh, Pennsylvania, August 9, 2008.

**11.** O.A. Marina, L.R. Pederson, E.C. Thomsen, C.A. Coyle, and G.W. Coffey, "Operation of Solid Oxide Fuel Cells on Gasified Coal," Presented at the 214th meeting of the Electrochemical Society, MA2008-02, Honolulu, Hawaii, October 12 – 17, 2008.

**12.** B.P. McCarthy, L.R. Pederson, Y.S. Chou, X.D. Zhou, W.A. Surdoval, and L.C. Wilson, "Low-Temperature Sintering of Lanthanum Strontium Manganite-Based Contact Pastes for SOFCS," Patent application 15855-E.

## References

**1.** J.P. Strakey, SECA, Coal, and FutureGen, 8th Annual SECA Workshop, 2007, http://www.netl.doe.gov/publications/proceedings/07/SECA_Workshop.

**2.** J.P. Trembly, R.S. Gemmen, and D.J. Bayless, *J. Power Sources*, **163**, 986 (2007).

# III.B.4 Investigation of Modified Ni-YSZ-Based Anode for High Impurities Containing Syngas Fuels

Dr. Conghua Wang
TreadStone Technologies, Inc.
201 Washington Road
Princeton, NJ 08540
Phone: (609) 734-3071; Fax: (609) 734-2967
E-mail: cwang@TreadStone-Technologies.com

DOE Project Manager: Joseph Stoffa
Phone: (304) 285-0285
E-mail: Joseph.Stoffa@netl.doe.gov

Contract Number: NT0006343

Start Date: June 2009 (planned)
End Date: May 2010

### FY 2009 Objectives

- Modify the Ni-YSZ anode surface to improve its contaminant tolerance.
- Investigate migration rate of the surface treatment material to the Ni-YSZ substrate, and approaches to mitigate the risk.
- Identify a catalyst to enhance the modified Ni-YSZ anode reaction activity using syngas fuels.

### Accomplishments

- Initiate project work in June 2009.

## Introduction

TreadStone Technologies, Inc. will initiate work to investigate modified Ni-YSZ-based anodes that improve the resistance to impurities contained in syngas fuels from coal-based power plants. Improved power generation technologies will help the nation make more efficient and environmentally responsible use of its abundant domestic coal reserves. Accordingly, advances in solid oxide fuel cell (SOFC) technology are sought for integrated gasification fuel cell (IGFC) systems. IGFC systems are attractive alternatives to current technologies in large-scale stationary applications. SOFCs offer considerable opportunities with respect to $CO_2$ capture (by keeping the fuel and oxidant streams separate) and lower $CO_2$ generation (as a result of higher efficiency). With these advantages, systems containing improved fuel cell technology in combination with heat recovery subsystems and commercial $CO_2$ capture technology can meet DOE goals: efficiency greater than 50% from coal (higher heating value) to electrical power, NOx emissions less than 15 ppm with 0.5 ppm readily achievable, carbon capture greater than 90% with 99% achievable, and a significantly reduced water footprint. Consistent with these goals, the DOE-sponsored Solid State Energy Conversion Alliance will develop commercially viable ($400/kW) SOFC power generation systems by the year 2010. This SOFC technology has potential application in United States Army fuel cell programs such as Army Mobile Power.

## Approach

The primary objective of this project is to demonstrate, using existing proprietary concepts and technology, the feasibility of utilizing high-impurity tolerant SOFC anodes to mitigate the costs of coal gas cleanup. Ni-YSZ anodes will be used because of their wide use, high power density, and long-term stability. They will be modified by providing a barrier layer for improved sulfur tolerance and carbon deposition resistance. To establish the feasibility of this approach, the effects of the barrier layer on the long-term stability of the anode and power density of the cell will be evaluated. TreadStone will identify a high performance catalyst to improve the anode activity, and demonstrate the solutions to minimize long-term performance degradation of the anode.

## Conclusions and Future Directions

This project will be initiated in June 2009.

# III.B.5 Direct Utilization of Coal Syngas in High Temperature Fuel Cells

Prof. Ismail Celik
West Virginia University (WVU)
P.O. Box 6106
Morgantown, WV 26506
Phone: (304) 293-3111 x2325; Fax: (304) 293-6689
E-mail: ismail.celik@mail.wvu.edu

DOE Project Manager: Briggs White
Phone: (304) 285-5437
E-mail: Briggs.White@netl.doe.gov

Contract Number: 46299

Start Date: August 1, 2006
End Date: July 31, 2009

## FY 2009 Objectives

- Characterize the effects of major trace contaminants in coal syngas on solid oxide fuel cell (SOFC) performance.
- Identify the fundamental mechanisms through which these impurities affect performance.
- Develop novel materials to minimize impact of contaminants.
- Propose remedies for adverse effects of contaminants on fuel cell performance.

## Accomplishments

- Assessed the effects of phosphorus in coal syngas on SOFC performance and proposed a possible pathway of P impurity reaction with Ni in the anode.
- Observed nickel migration to the anode surface and into voids during exposure of the anode to 10 ppm phosphine.
- Observed dramatic and irreversible performance loss at a rate of ~0.5–1.5 mV/hr in long-term tests of cells running on syngas containing 10 ppm $PH_3$.
- Measured the degradation rate in SOFCs due to 100 ppm HCl in the fuel stream to be steady at about 0.03 mV/hr for over 300 hrs at 800°C and 0.1 mV/hr for over 100 hrs at 850°C.
- Improved cell fabrication capabilities and achieved open circuit voltage (OCV) values 50-60 mV higher than before by careful optimization of the cell microstructure.
- Developed a new coating for SOFC anodes which was shown to significantly delay the onset of cell degradation due to sulfur impurity and reduce the cell performance loss by 50%.
- Measured the real-time button cell surface temperature as a function of gas composition and current density using a novel in situ test apparatus developed in-house.
- Modeled mass transfer and multiple chemical reactions inside a typical anode pore using Molecular Dynamics simulations.
- Refined the in-house SOFC simulation tools further and conducted several parametric studies on button cell operation.
- Performed equilibrium calculations to deduce the stable forms of impurities under SOFC conditions.
- Developed a phenomenological model to predict the typical degradation pattern due to syngas impurities.

## Introduction

This project is supported under the Department of Energy Experimental Program to Stimulate Competitive Research (EPSCoR), a program designed to enhance the capabilities of EPSCoR states in energy research and economic development through the support of advanced research at academic institutions. Our goal is to establish an internationally recognized, sustainable fuel cell research center for coal-based clean power generation which serves as a technology resource for the emerging fuel cell industry in West Virginia. Our strengths are in applying nano-technology to develop and fabricate materials for advanced coal-based fuel cells; state-of-the-art material characterization and fuel cell testing facilities involving both ex situ and in situ measurement techniques; and modeling fuel cells from atomistic to continuum scales using high performance computing. We have formed a multidisciplinary team of research professionals who have worked together for several years and have strong credentials in their respective areas of expertise. Under the present project, we will develop a laboratory infrastructure, solidify interactive working relationships, and attain national recognition for the work conducted by the center in the area of coal-based clean power generation via fuel cells. Our project will be conducted in collaboration with the National Energy Technology Laboratory and in consultation with other federal laboratories and private industries working on similar topics.

## Approach

The research cluster is based on a multi-scale, multi-disciplinary approach conducted by nine faculty members in four departments at WVU. The work is organized under four integrated projects: 1) anode material development and experimental characterization of fuel cell anodes, 2) sub-micro-scale modeling, 3) multi-scale continuum modeling, and 4) laboratory testing of individual fuel cells and fuel cell systems. The knowledge gained from experiments (Projects 1 and 4) and multi-scale computational models (Projects 2 and 3) will be combined to understand basic mechanisms of cell performance degradation and to formulate preventive remedies, as well as predictive models.

## Results

### Anode Materials Development and Characterization

This task seeks to characterize the behavior of SOFC anodes exposed to simulated coal syngas using a combination of in situ (electrochemical, conductivity, and optical) and ex situ experimental methods (mainly imaging and surface analysis); to fabricate fuel cells with custom anodes; and to systematically explore several anode compositions and double-layered structures.

More tests, characterization and analyses were done on SOFC anodes exposed to $PH_3$ impurity which confirmed previous observations and also revealed further information. The new findings include changes in surface composition (apparent depletion of Zr on the surface of the anode after $PH_3$ exposure and the presence of nickel phosphate instead of usually expected nickel phosphide). The phosphate formation is attributed to conversion of $PH_3$ to $P_2O_3$ in the presence of water in the syngas which was confirmed using equilibrium calculations. A possible pathway of the reaction of the P impurity with Ni in the anode is proposed based on these results. A unique in situ test bench was developed and used to monitor real time button cell surface temperature under different conditions (see Figure 1). The data from these in situ measurements were used for validation of the computational model.

On the cell manufacturing front, research efforts have been mainly focused on the cell performance-structure relationship to optimize single cell output and the stability of anode and electrolyte components for operation with coal-derived syngas. Anode-supported cells with different anode interlayers and electrolyte compositions have been fabricated and tested. Both double-layered yttria-stabilized zirconia (YSZ) (40 µm) electrolyte and scandia-stabilized zirconia (SSZ)/YSZ composite electrolytes have been deposited on the anode support to improve cell stability. NiO content in the anode interlayer is varied between 50~60% and carbon

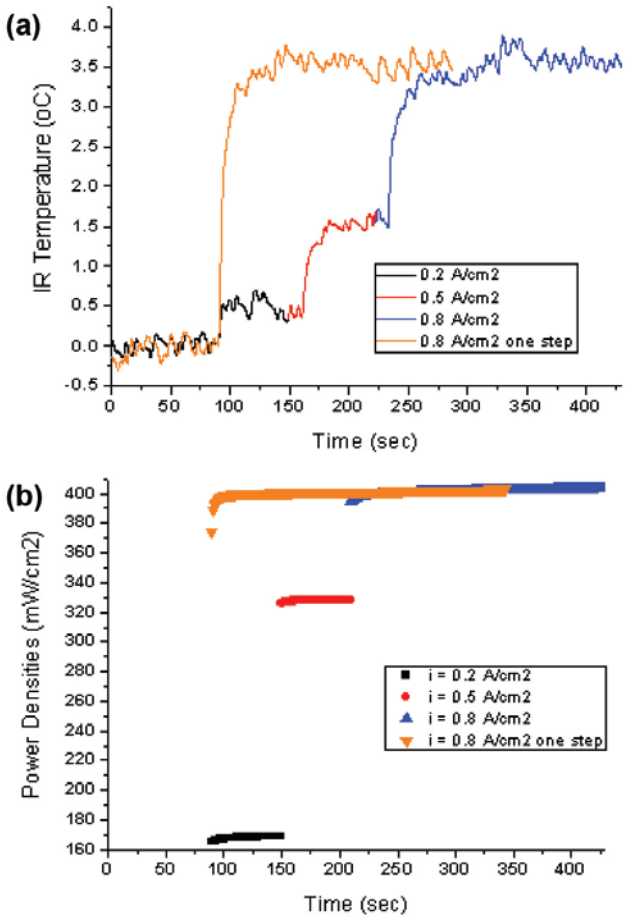


**FIGURE 1.** Simultaneous measurements of optical surface temperature changes of the anode and power density. (a) Surface temperature changes during steps in the current density. (b) Corresponding changes in power densities.

content is varied from 2.5% to 20%. In Figures 2(a) and 2(b), all of the cells with double-layered or composite electrolytes showed OCV values 50~60 mV higher than the previously tested cell with a single-layer YSZ electrolyte. The study also indicated that a higher Ni content in anode interlayer improves electrode kinetics while higher porosity of anode interlayer improves fuel transport at high current density and thus gives rise to higher peak power density. Knowledge gained through the above investigation helped in the design and fabrication of anode-supported cells with an optimized structure of interlayer/electrolyte which showed better performance than commercially-popular MSRI cells both in $H_2$ and coal syngas.

### Sub-Micro Scale Modeling

The objective of this project is to perform simulations for understanding fundamental reaction mechanisms in SOFCs using: 1) quantum mechanical approximations for computing electron configurations

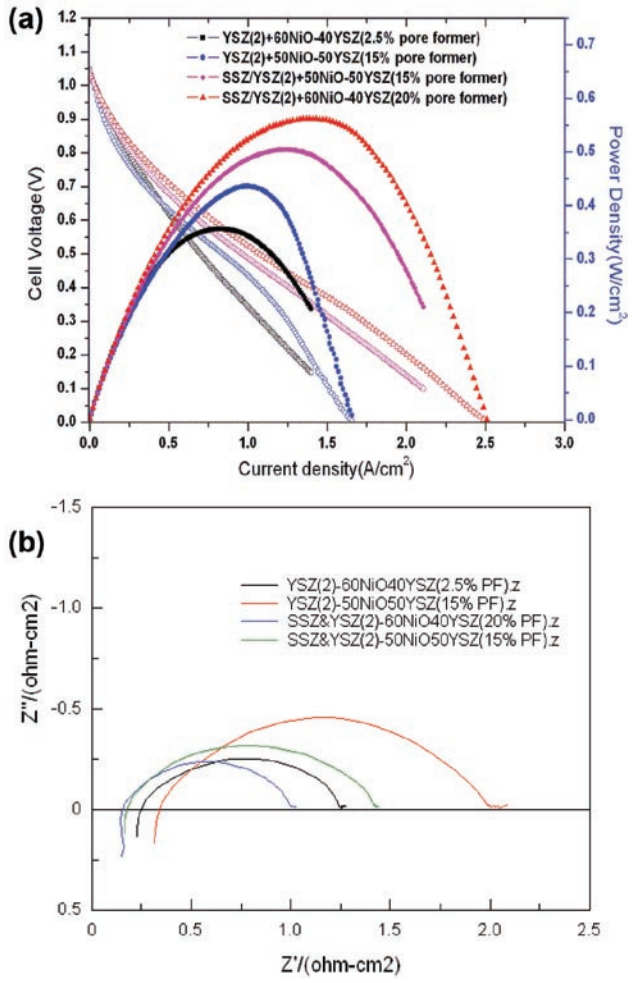


**FIGURE 2.** Effects of preparation compositions on SOFC performance. (a) Polarization and power density plots. (b) Impedance plots measured at open circuit voltage.

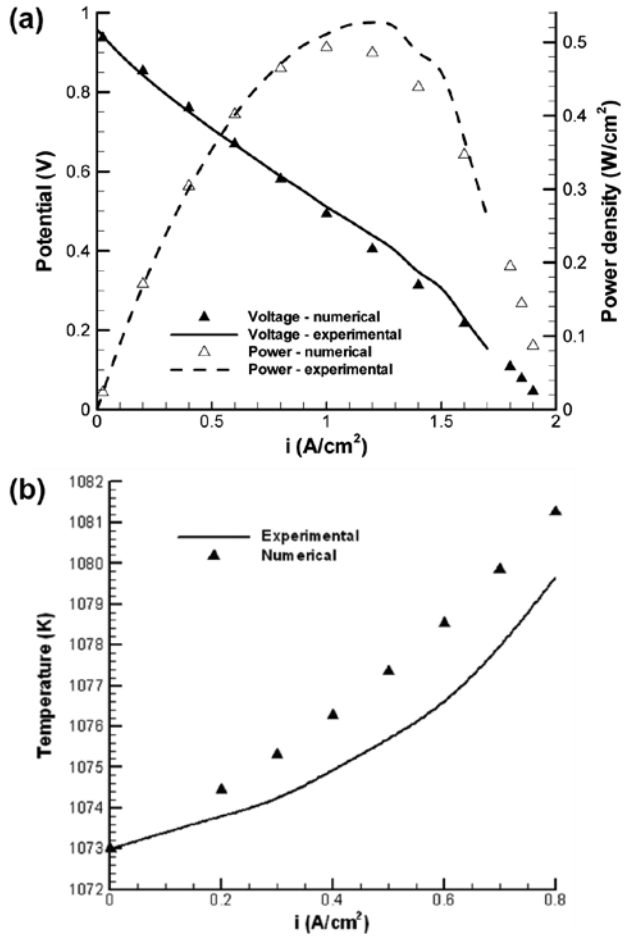


**FIGURE 3.** Comparison of experiments and the continuum-based computational model. (a) Polarization and power density curves (lines) and computational points (symbols). (b) Optical temperature measurements (line) and computational points (symbols).

and inter-atomic forces (density functional theory); and, 2) molecular dynamics simulations based on classical Newtonian mechanics. A molecular dynamics code, ReMoDy, was further refined. To be able to trace the motion and interactions of millions of molecules efficiently, a domain segmentation algorithm was implemented, which enabled reduction of the time of processing interactions from $N^2$ to a near-linear dependence. Initially, a 1 micron cube representing as electrode pore was used to simulate the self diffusion of hydrogen. The diffusion coefficients obtained from ReMoDy are compared to those from published experimental data and from Chapman-Enskog Theory. Using a reaction mechanism consisting of 13 species, 23 gas-phase reactions and 40 surface reactions, reactive molecular dynamics simulations of syngas transport in a micron cube anode pore are performed. A total of 16 million molecules are used in the simulation to assess the production of $H_2O$ molecules at the triple phase boundary and their diffusion against the incoming flow.

## Multi-Scale Continuum Modeling

The objective of this project is to develop a continuum-based computational model to study the transport and reaction of critical species in the cell and a continuum damage mechanics model for predicting long-term structural degradation including effects of coal syngas impurities. Button cells were simulated in parallel to the physical experiments using DREAM SOFC, a multi-dimensional modeling tool developed in-house. The experimental results were used for both calibration of some empirical parameters of the model and for validation of the model (see Figure 3). Several parametric studies were conducted using the model which provided information about $H_2$ and CO oxidation kinetics, methane-reforming kinetics, sources of various over-potentials, etc. A large database of thermochemical properties is compiled for equilibrium calculations to determine the stable forms of impurities under the SOFC conditions. Calculations were performed for P impurity to aid the ongoing experiments.

A new phenomenological one-dimensional (1D) model was formulated to simulate the typical degradation patterns observed for coal syngas contaminants. The model parameters were calibrated to match degradation rates reported in literature. The results closely emulate the characteristic behavior of SOFC anodes exposed to syngas contaminants such as $PH_3$. On the structural modeling front, an alternative anode durability model was developed to incorporate thermo-mechanical as well as fuel gas contaminant effects on the anode microstructure. This model is implemented in finite element analysis and simulations were performed under different conditions.

## Cell and System Laboratory Testing

The aim of this project is to determine mechanisms by which trace contaminants in coal syngas cause degradation. A secondary aim is to develop remedies for the degradation. More long-term tests (170 to 250 hours) of commercial Ni-YSZ anode-supported SOFC cells exposed to syngas with 10 ppm $PH_3$ impurity have been performed. Dramatic and irreversible degradation of cell performance (loss of voltage about 0.5~1.5 mV/hr at constant current, increase in both series and polarization resistance) is assigned to the functional deterioration of the Ni-YSZ anode active layer. When the anode was exposed directly to the syngas mixture (no intervening current collector or metal paste), degradation started immediately upon exposure to 10 ppm $PH_3$.

Scanning electron microscope (SEM) analysis of the top 300 µm on the anode side showed that the microstructure was significantly reconstructed by exposure to $PH_3$ resulting in nickel migration to the anode surface and reduction of the porosity. $Ni_5P_2$ is identified as the major product by X-ray diffraction (XRD). X-ray photoelectron spectroscopy (XPS) data indicated that both phosphide and phosphate were present in the nickel layer on the anode surface, and that phosphate was present in the active layer. In situ Van der Pauw measurements on the anode demonstrated that the resistivity of the anode support was constant during prolonged operation in syngas with and without $PH_3$. The changes in ohmic resistance and the polarization resistance are tentatively assigned to the nickel redistribution, most likely in the active composite layer next to the electrolyte. The polarization resistance increase can also be attributed to the loss of porosity and triple phase boundary length.

Another tolerance test of the Ni-YSZ anode supported cell for 100 ppm HCl has been conducted. Figure 4(a) shows the degradation of the cell voltage at constant current with time using syngas after the addition of 100 ppm HCl at 800°C for 300 hrs and at 850°C for 100 hrs. Figure 4(b) shows the impedance

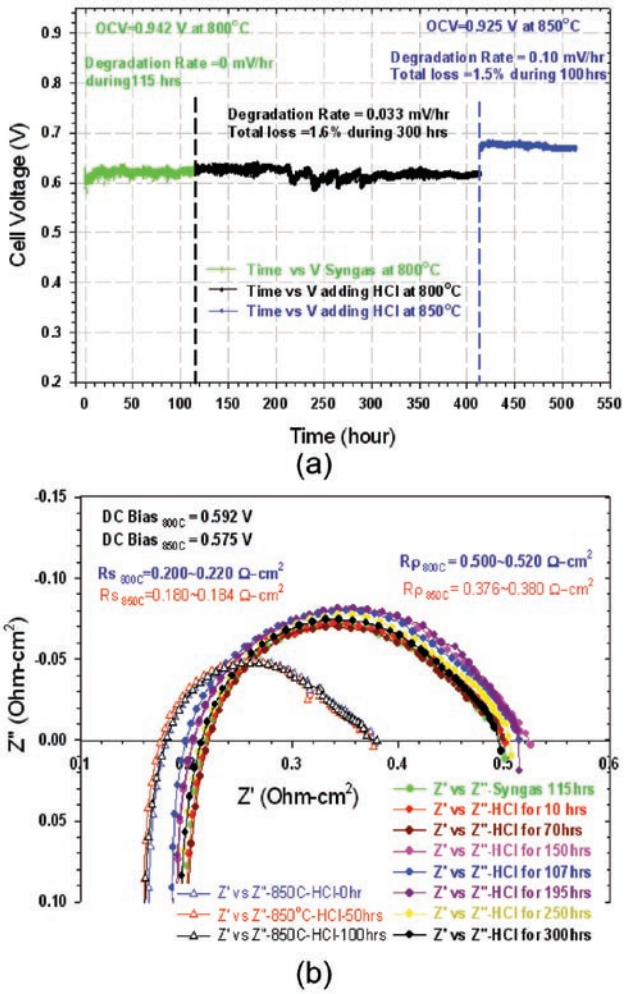


**FIGURE 4.** Degradation of SOFC performance in the presence of 100 ppm HCl. The fuel is wet hydrogen. (a) Voltage loss during constant current operation. (b) Impedance plots at open circuit voltage. Both the series and the polarization resistances barely increase upon exposure to HCl.

spectra whereby both ohmic and polarization resistances barely increase after adding 100 ppm HCl at 800°C for 300 hrs and at 850°C for 100 hrs. However, there is evidence in the literature [1,2] that at higher concentrations and temperatures, significant degradation may occur.

The basic testing protocols for SOFCs have been established. Raman spectroscopy, SEM, energy-dispersive X-ray spectroscopy, XRD and XPS analyses are regularly used in the characterization of cell materials. The Van der Pauw resistivity method has been introduced for in situ cell resistance measurements. The anode pore size and porosity can be measured by mercury porosimetry.

## Conclusions and Future Directions

Substantial progress has been made on all fronts of the project. Degradation experiments were conducted for three different impurities: S, P and Cl. Phosphorous impurity was extensively studied and the modes and mechanisms for the degradation were identified. Unique in situ button cell temperature measurements were accomplished. Cell manufacturing capabilities are further refined and improved cell microstructures were obtained. Parametric studies were conducted using in-house simulation tools and a new phenomenological model was developed to predict SOFC anode degradation.

In the future, tolerance tests will continue for impurities such as S, P, Cd, Cl etc., and the changes occurring at the anode with respect to both microstructure and composition will be investigated. XPS combined with sputtering will be used in post-mortem analysis to resolve some of the questions about the nature of the products formed by the impurities. Out-of-plane surface deformations will be measured at specified time intervals each with a series of increasing applied pressures. The test results will facilitate the understanding of the mechanisms as well as provide quantitative evaluation of the long-term SOFC structural degradation under coal syngas. The infrared temperature measurement technique will be further refined in order to get a precise measurement on the small spot location of the button cell surface during SOFC operation. Analysis similar to that done for the phosphorus impurity will be extended for Cd and Cl. The results will be used to determine the governing factors that lead to degradation of SOFC anodes that are exposed to the impurity-containing syngas. On the cell manufacturing front, future research will focus on optimization of fabrication process for doped ceria coating on the MSRI cell to enhance sulfur tolerance. The three-dimensional (3D) SOFC model will be extended to simulate planar cells operating on coal syngas. The 1D degradation model will be calibrated for all the species with available experimental data. The methodology will then be used as a contaminant transport sub-model in the 3D model. Equilibrium calculations will continue using CANTERA to estimate the most significant forms for other impurities and combinations of impurities. Material parameters for the durability model will be estimated using an in situ experimental setup. The durability model will be applied on planar SOFC anodes to estimate thermo-mechanical and syngas contaminants degradation effect and hence predict its structural service life.

## Special Recognitions & Awards/Patents Issued

**1.** Patent/disclosure: Xingbo Liu, Junwei Wu, Yinglu Jiang, and Christopher Johnson: Novel Electroplating Method to Deposit SOFC Interconnect Coating (filed in 2007).

**2.** Patent/disclosure: N.Q. Wu and M. Zhi: Nanowire/Nanotube Electrodes of Solid Oxide Fuel Cells (filed in 2009).

## FY 2009 Publications/Presentations

**1.** M. Zhi, F.N. Cayan, I. Celik, R. Gemmen, S.R. Pakalapati, and N. Wu, "Temperature and Impurity Concentration Effects on Degradation of Nickel/Yttria-Stabilized Zirconia Anode in $PH_3$-Containing Coal Syngas," submitted to Fuel Cells, January 2009.

**2.** F.N. Cayan, S.R. Pakalapati, F. Elizalde-Blancas, and I. Celik, "On Modeling Multi-Component Diffusion Inside the Porous Anode of Solid Oxide Fuel Cells Using Fick's Model," Journal of Power Sources, accepted March 2009.

**3.** F. Elizalde-Blancas, S.R. Pakalapati, F.N. Cayan, and I.B. Celik, "Numerical Prediction of the Performance of SOFCs Operating on Coal Syngas," submitted to Journal of Fuel Cell Science and Technology, March 2009.

**4.** G. Iqbal, H. Guo, B. Kang, and O.A. Marina, "Durability Prediction of SOFC Anode Material under Thermo-Mechanical and Fuel Gas Contaminants Effects," accepted, The International Journal of Applied Ceramics Technology, January 2009.

**5.** H. Guo, G. Iqbal, and B. Kang, "Development of an In-Situ Surface Deformation and Temperature Measurement Technique for SOFC Button Cell," accepted, The International Journal of Applied Ceramics Technology, January 2009.

**6.** C. Xu, J.W. Zondlo, H.O. Finklea, O. Demircan, M. Gong, and X. Liu, "The Effect of Phosphine in Syngas on Ni-YSZ Anode-Supported Solid Oxide Fuel Cells," accepted, Journal of Power Sources, February 2009.

**7.** O. Demircan, C. Xu, J. Zondlo, and H.O. Finklea, "In-Situ Van der Pauw Measurements of the Ni/YSZ Anode During Exposure to Syngas with Phosphine Contaminant," accepted, Journal Power Sources, March 2009.

**8.** F.N. Cayan, M. Zhi, S.R. Pakalapati, I. Celik, N. Wu, and R. Gemmen, "Effects of Coal Syngas Contaminants on SOFC Anodes: A Review," submitted to 2008 Pittsburgh Coal Conference, September 28 – October 2, 2008.

**9.** M. Gong, X. Liu, and R. Gemmen, "Improving Sulfur-Tolerance of Ni-YSZ Anode in SOFC by Impregnation of Doped Ceria," Proceedings of 213th Electrochemical Society Meeting, Phoenix, Arizona, May 18–22, 2008.

**10.** M. Gong, X. Liu, Y. Jiang, C. Xu, J. Zondlo, C. Johnson, and R. Gemmen, "Anode Supported SOFC Fabricated by Tape Casting and Co-Sintering of Anode and Electrolyte," Proceedings of Materials Science & Technology 2008, Pittsburgh, Pennsylvania, October 5–9, 2008.

**11.** G. Iqbal, H. Guo, and B. Kang, "Structural Degradation Mechanisms of SOFCs Anode and FEA for Long-Term Anode Material Behavior in Coal Syngas Environment," Proceedings of Material Science & Technology 2008, Pittsburgh, Pennsylvania, October 5–9, 2008.

**12.** H. Guo, R. Dastane, G. Iqbal, and B. Kang, "Development of an In-Situ Deformation and Temperature Measurement Technique for SOFC Button Cell under Operation Condition," Proceedings of Material Science & Technology 2008, Pittsburgh, Pennsylvania, October 5–9, 2008.

**13.** G. Iqbal, H. Guo, and B. Kang, "Continuum Degradation Model for SOFCs Anode Material under Coal Syngas and its Implementation in FEA to Predict Long-Term Structure Integrity," Proceedings of the Twenty-Fifth Annual International Pittsburgh Coal Conference, Pittsburgh, Pennsylvania, September 29 – October 2, 2008.

**14.** H. Guo, G. Iqbal, R. Dastane, and B. Kang, "In-Situ Surface Deformation and Temperature Measurement of Button Cell under SOFC Operating Conditions," Proceedings of the Twenty-Fifth Annual International Pittsburgh Coal Conference, Pittsburgh, Pennsylvania, September 29 – October 2, 2008.

**15.** O. Demircan, C. Xu, J. Zondlo, and H.O. Finklea, "The Effect of $PH_3$ Impurity in Coal Syngas on SOFC Performance," Proceedings of the Twenty-Fifth Annual International Pittsburgh Coal Conference, Pittsburgh, Pennsylvania, September 28 – October 2, 2008.

**16.** G. Iqbal, H. Guo, and B. Kang, "Reliability Prediction of SOFCs Anode Material Exposed to Fuel Gas Contaminants: Modeling & Experiment," Proceedings of The Mineral, Metals & Materials Society Conference 2009, San Francisco, California, February 15–19, 2009.

**17.** R. Carreno, A. Smirnov, J. Nanduri, and I. Celik, "Application of Reactive Molecular Dynamics to Simulate Diffusion and Reaction in a Solid Oxide Fuel Cell Pore," Proceedings of Seventh International ASME Conference on Nanochannels, Microchannels and Minichannels, June 22–24, 2009, Pohang, South Korea.

**18.** O. Demircan, J. Zondlo, H.O. Finklea, and C. Xu, "In-Situ Van Der Pauw (VdP) Resistance Measurement on a SOFC Using Syngas with and without Phosphine Impurity," Proceedings of 215th Electrochemical Society Meeting, San Francisco, California, May 24–29, 2009.

## References

**1.** G.N. Krishnan, P. Jayaweera, K. Lau, and A. Sanjurjo, "Effect of Coal Contaminants on Solid Oxide Fuel System Performance and Service Life," Technical Progress Report 3, SRI International, Morgantown, 2006.

**2.** J.P. Trembly, R.S. Gemmen, and D.J. Bayless, "The Effect of Coal Syngas Containing HCl on the Performance of Solid Oxide Fuel Cells: Investigation into the Effect of Operational Temperature and HCl Concentration," Journal of Power Sources 169 (2007) 3347-354.

# III. SECA CORE RESEARCH & DEVELOPMENT

## C. Interconnects and Contact Materials

# III.C.1 Evaluation of a Functional Interconnect System for SOFCs

Matthew D. Bender (Primary Contact) and
James M. Rakowski (Secondary Contact)
ATI Allegheny Ludlum
Technical and Commercial Center
1300 Pacific Avenue
Natrona Heights, PA 15065
Phone: (724) 226-6575; (724) 226-6483
E-mail: mbender@alleghenyludlum.com
jrakowski@alleghenyludlum.com

DOE Project Manager: Robin Ames
Phone: (304) 285-2078
E-mail: Robin.Ames@netl.doe.gov

Contract Number: 42513

Start Date: January 1, 2006
End Date: June 30, 2010

### FY 2009 Objectives

- Evaluate commercially available ferritic stainless steels with coatings applied for oxidation resistance and enhancement of electrical properties.
- Optimize alloy compositions and surface treatments to maximize performance in solid oxide fuel cell (SOFC) environments.
- Demonstrate significant improvement in critical SOFC-related properties for interconnect systems incorporating new or modified alloy compositions and surface modifications.

### Accomplishments

- Long-term oxidation testing was completed in simulated anode and cathode environments at 750-850°C for exposure times as long as 5,000 hours at temperature. Systematic trends in oxidation behavior were related to deliberate variations in composition.
- Area specific resistance (ASR) testing of coated and uncoated alloy plates was completed for exposure times as long as 5,000 hours at temperature. The rate of increase in ASR once the test systems reached steady-state conditions was observed to be as low as 6.5 $m\Omega \cdot cm^2$ for a coated Fe-17Cr alloy and 1.5 $m\Omega \cdot cm^2$ for a coated Fe-26Cr alloy, both with optimized composition.
- Further avenues of development were identified for alloys based on both low chromium and high chromium compositions, leading to the melting of a third generation of SOFC interconnect alloy compositions.
- ATI 441HP[1]™ alloy material has been produced in the form of a 25,000 pound coil meeting commercial specifications at four different thicknesses for Industrial Team members. The material is being supplied for small and full-scale stack production and evaluation.

## Introduction

This project is focused on evaluating the performance of affordable materials integrated into systems for use as SOFC interconnects. Interconnects can be a source of degradation of fuel cell stack performance by the formation and growth of electrically-resistive surface oxide layers. It is critical to control which types of oxides form and to minimize layer growth for an extended period of time.

The reference point for this project is a monolithic ferritic stainless steel; examples include ATI 441HP stainless steel (UNS S44100) and E-BRITE[2]® alloy (UNS S44627). These were chosen for their combination of low cost, general availability, and performance characteristics. Functionality can be added to these basic interconnect materials at the cost of increased complexity. Modifications are aimed at tailoring the relevant properties of a surface to its local environment in the fuel cell and include special processing, surface treatments, and applied coatings.

## Approach

Two methods for increasing metallic interconnect performance are being explored. The first is to incorporate minor but impactful modifications to alloy compositions in what are essentially commercially available materials. A set of six alloy compositions was reduced to practice, based on current state-of-the-art information and the results from Phase I of this project.

The second approach is to alter the surface of the stainless steel by post-fabrication processing to yield long-lasting benefits by removing/sequestering elements (e.g. silicon and/or aluminum) which form resistive interfacial phases. This may be possible by annealing in specific atmospheres followed by chemical cleaning in some cases. Alternatively, an external oxidation-resistant and electrically conductive coating can be

[1] ™ Trademark of ATI Properties, Inc.
[2] ® Registered Trademark of ATI Properties, Inc.

applied to remove the stainless steel surface from direct contact with the SOFC environment.

## Results

A set of six experimental compositions were melted to explore relatively minor modifications to commercially available alloys, notably E-BRITE alloy and ATI 441HP stainless steel, which are iron-chromium ferritic stainless steels alloyed with a small amount of niobium. The significant difference between the two primary groups of alloys is the chromium content. The E-BRITE type alloys contain a high level of chromium (23-26 wt%) while the ATI 441HP alloy and various modifications have lower chromium content (nominally 17 wt%). Table 1 contains a review of the material used for testing in the current study. It is a mix between two commercially available alloys and experimentally melted and processed material (designated as "EXP").

**TABLE 1.** Overview of Test Material (weight percent)

| Alloy | Cr | Nb | Si | Others |
|---|---|---|---|---|
| ATI 441HP alloy | 17.5 | 0.3 | 0.5 | 0.3 Mn, 0.3 Ti |
| E-BRITE alloy | 26 | 0.2 | 0.3 | 1 Mo |
| EXP 580-2 | 17 | 0.3 | 0.05 | 0.1 Ce+La |
| EXP 580-5 | 26 | 0.2 | 0.3 | 1 Mo, 0.3 Mn |
| EXP 580-6 | 17 | 0.3 | 0.15 | 0.3 Mn |
| EXP 580-7 | 17 | 0.3 | 0.05 | 0.3 Mn |
| EXP 580-8 | 23 | 0.3 | 0.15 | 0.3 Mn, 1 Mo |
| EXP 580-9 | 24 | 0.3 | 0.05 | 0.3 Mn, 1 Mo |

Evaluation of this set of test materials took the form of relatively simple gravimetric oxidation testing (weight change measurements) and more complex ASR testing. Oxidation testing was covered extensively in the Fiscal Year 2008 Annual Report. This report will focus on the ASR test results.

ASR testing was carried out on both bare and coated alloy substrates. All coatings were of the cerium-modified manganese cobaltite spinel type developed by researchers at the Pacific Northwest National Laboratory (PNNL) [1]. The coatings were applied at PNNL on small specimens provided by Allegheny Ludlum with an unaltered, non-directional dull finish produced by cold rolling, annealing, and acid pickling.

ASR testing was carried out on both bare and coated alloy substrates. ASR test parameters are typical of those used in the industry – 800°C test temperature, lanthanum strontium manganate ceramic contact layer, and a constant current density of 0.5 A/cm$^2$ of contact area. The test results are summarized in Table 2, with the critical metric being the rate of ASR increase as a function of time, made specific to an interval of 1,000 hours for ease of interpretation. This value was obtained by taking the linear slope as a function of time of each individual ASR curve. After extended exposure times, such curves generally fall into a constant or steady-state region where the value remains constant.

**TABLE 2.** Overview of ASR Test Results

| Sample ID | ASR Evolution Rate (mΩ·cm$^2$/1,000 h) | | Comments |
|---|---|---|---|
| | Bare | Coated | |
| ATI 441HP alloy | 35.4 | | Commercial material (0.4 wt% Si) |
| EXP 580-7 | 33.7 run 1<br>550.9 run 2 | 2.2 | Very low Si (0.05 wt%), divergent test results from identical uncoated samples |
| EXP 580-6 | 25.1 | 6.9 | Moderate Si (0.15 wt%) |
| EXP 580-2 | 47.2 | | Very low Si (0.05 wt%)+ Ce addition |
| E-BRITE alloy | 936.5 | 21.1 | Commercial material (0.3 wt% Si) |
| EXP 580-5 | 38.1 | 1.4 | Standard E-BRITE alloy + 0.3 wt% Mn |
| EXP 580-8 | 17.2 | 7.5 | Fe-23Cr-1Mo-0.3Mn, moderate Si (0.15 wt%), divergent test results from identical coated samples |
| EXP 580-9 | 7.9 | 2.5 | Fe-24Cr-1Mo-0.3Mn, very low Si (0.05 wt%) |

Important findings from the testing are summarized below:

- Commercial E-BRITE alloy exhibited high rates of ASR increase in both the coated and (particularly) in the uncoated tests.
- Minor modifications to the base E-BRITE alloy composition yielded the best long-term performance in the test matrix. EXP 580-5, in particular, exhibited a very low steady-state rate of ASR increase. This is shown graphically in Figure 1. EXP 580-8 and 580-9, which examined variations in chromium content, also exhibited good behavior in the coated condition, with the rate of increase inversely proportional to chromium content, as shown in Figure 2.
- EXP 580-7 exhibited variable behavior, consistent with the variability observed for low chromium, very low silicon alloys in the basic oxidation testing.
- EXP 580-6 exhibited a moderate but significant improvement in performance over standard ATI 441HP alloy in the uncoated condition and exhibited a stable, relatively low rate of ASR increase in the coated condition (Figure 3).

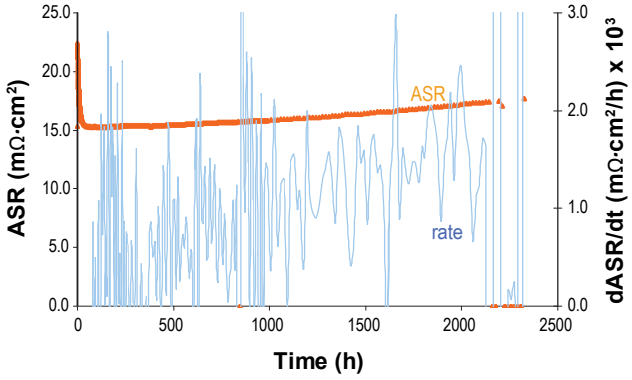


**FIGURE 1.** ASR as a Function of Time and Instantaneous Slope for EXP 580-5, Tested with the PNNL Ce-Modified Manganese Cobaltite Spinel Coating

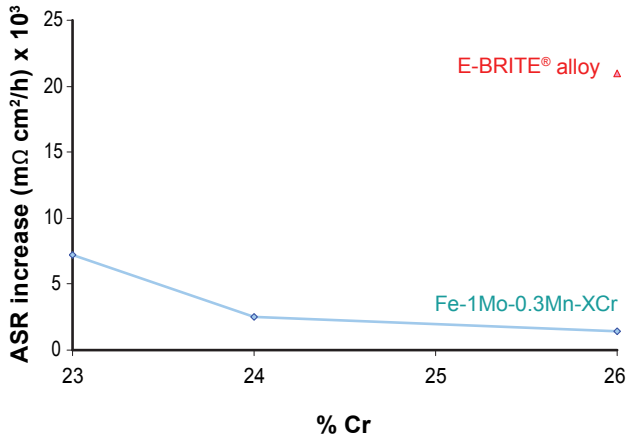


**FIGURE 2.** Rate of ASR Increase with Time as a Function of Cr Content for Fe-xCr-1Mo Alloys, Tested with the PNNL Ce-Modified Manganese Cobaltite Spinel Coating

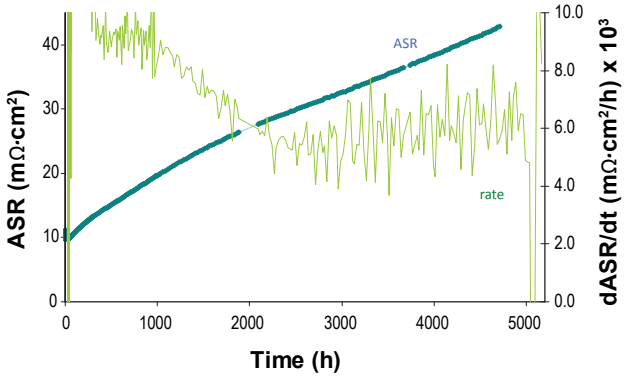


**FIGURE 3.** ASR as a Function of Time and Instantaneous Slope for EXP 580-6, Tested with the PNNL Ce-Modified Manganese Cobaltite Spinel Coating

- Cerium-modified manganese cobaltite spinel coatings was effective in reducing the rate of ASR increase for all the alloys tested.

## Conclusions and Future Directions

- Alloys based on ATI 441HP stainless steel have shown encouraging test results. However, evaluation at the upper end of the SOFC operating temperature range has shown somewhat unpredictable behavior in terms of oxidation resistance and ASR evolution. Analysis indicates that the silicon level may play a role in retarding accelerated oxidation. An experiment to test large numbers of samples from several alloy compositions is underway. This will generate data for a statistical analysis of the potential for breakaway oxidation.
- Compositions based on modifications to the basic ATI 441HP alloy melted for this study have exhibited low observed rates of ASR increase. Specifically, the value determined for a manganese cobaltite spinel-coated Fe-17Cr alloy was 6.9 $m\Omega \cdot cm^2$/1,000 hours after 5,000 hours at 800°C in air. Based on this result, five additional heats of optimized "third generation" low chromium alloys are being melted and processed for testing.
- Compositions based on modifications to the basic E-BRITE alloy tailored for SOFC interconnect applications have exhibited the lowest observed rates of ASR increase in this study. Specifically, the value determined for a manganese cobaltite spinel-coated Fe-26Cr alloy was 1.5 $m\Omega \cdot cm^2$/1,000 hours after 5,000 hours at 800°C in air. This is several orders of magnitude better than the uncoated base composition. Based on this result, two additional heats of optimized "third generation" high chromium alloys are being melted and processed for testing.
- Post-processing techniques on flat-rolled ATI 441HP stainless steel are to be investigated to incrementally reduce the rate of oxidation, which should yield beneficial effects on the electrical properties of the surface.
  - Cold work has been shown to decrease the rate of oxidation. Deformation localized to the surface by grinding and blasting will be investigated, along with the testing of cold worked material produced by temper rolling.
  - Silicon tends to form resistive phases at the scale metal interface during exposure to SOFC operating conditions. A technique has been demonstrated to remove silicon from finished plates. Initial results are promising, and longer-term ASR performance analysis will be carried out.

- A full-size coil of ATI 441HP stainless steel will be provided to Industrial Teams for stack prototyping and manufacturing, with deliveries in full scheduled for the end of 2Q 2009.

## Special Recognitions & Awards/Patents Issued

**1.** U.S. and associated foreign patent applications have been filed by ATI Allegheny Ludlum on higher-Cr content alloy compositions (U.S. patent publication numbers 2006/0286433, 2006/0286432, and 2006/0285993) and on the silicon removal process (U.S. patent publication number 2008/0236710).

## FY 2009 Publications/Presentations

**1.** Quarterly status report for Project 42513, July 2008.

**2.** Quarterly status report for Project 42513, October 2008.

**3.** Quarterly status report for Project 42513, January 2009.

**4.** Quarterly status report for Project 42513, April 2009.

## References

**1.** Zhenguo Yang, Guanguang Xia, Zimin Nie, Joshua Templeton, and Jeffry W. Stevenson, "Ce-Modified $(Mn, Co)_3O_4$ Spinel Coatings on Ferritic Stainless Steels for SOFC Interconnect Applications," *Electrochem. Solid-State Lett*., Volume 11, Issue 8, 2008: B140-B143.

# III.C.2 Effect of SOFC Interconnect-Coating Interactions on Coating Properties and Performance

Jeffrey W. Fergus
Auburn University
Materials Research and Education Center
275 Wilmore Laboratories
Auburn, AL 36849
Phone: (334) 844-3405; Fax: (334) 844-3400
E-mail: jwfergus@eng.auburn.edu

DOE BES Project Manager: Timothy Fitzsimmons
Phone: (301) 903-9830
E-mail: Tim.Fitzsimmons@science.doe.gov

DOE NETL Project Manager: Briggs White
Phone: (304) 285-5437
E-mail: Briggs.White@netl.doe.gov

Contract Number: 46497

Start Date: June 15, 2008
End Date: June 14, 2011

### FY 2009 Objectives

- Determine the chromium solubility in the spinel manganese-cobalt oxide coating material.
- Determine the mechanism of the reaction between chromia and the spinel manganese-cobalt oxide coating material.

### Accomplishments

- Chromium can dissolve in the spinel phase. The maximum chromium content is two chromium atoms per $M_3O_4$ unit, *i.e.*, $(Mn,Co)Cr_2O_4$. Lower chromium contents also form, but with morphologies distinctly different from those of compositions with the maximum chromium content.
- The reaction between chromium and the spinel phase can occur at the regions of solid-solid contact or through vapor-phase transport. The compositions and morphologies are distinctly different, presumably due to a lower chromia activity resulting from a difference in the partial pressure of the chromium-containing gas species.
- The Co/Mn concentration of the reaction layer is related to that of the coating, but the reaction layer typically has a higher Co/Mn ratio indicating that cobalt diffuses more rapidly than manganese through the reaction layer.

## Introduction

The high operating temperature of solid oxide fuel cells (SOFCs), which provides their excellent fuel flexibility, can lead to degradation of individual fuel cell components. One form of degradation is chromium poisoning of the cathode, which results from volatilization of chromium from the chromia scale formed on alloys used for the interconnect. The amount of chromium volatilization, and thus the associated cell poisoning, can be minimized by applying a ceramic coating to the alloy surface. One promising coating material system is the spinel $(Mn,Co)_3O_4$ [1-4], which has been shown to reduce chromium volatilization [5,6].

Although chromium can form a spinel phase with other transition metals, chromium has not been observed in the coating during use in an SOFC [7,8]. However, with time, interaction of the coating with the chromia scale or with other SOFC components can lead to changes in the coating composition, which can affect properties and thus performance. The purpose of this work is to study the interaction between chromia and potential interconnect coating materials to provide information needed to design effective coatings for long-time SOFC operation.

## Approach

The project addresses three aspects of coating properties and performance: i) thermodynamics, ii) transport properties and iii) physical properties. The thermodynamic aspects include phase equilibria, crystal structure stability and chemical activity. The transport properties to be evaluated include conductivity and diffusion rates. The physical properties are those that are important for coating performance, such as the coefficient of thermal expansion. These aspects will be evaluated for the original coating composition and for compositions resulting from interaction of the coating with other fuel cell components by preparing bulk analogues of the compositions expected after the interaction occurs. Characterization of these bulk analogues will provide valuable information for evaluating any changes in the performance after interaction with other components. Finally, the results will be used to identify compositions with potentially improved performance and these promising compositions will be similarly evaluated. This knowledge and understanding will allow coatings to be designed so that the expected compositional changes

during operation increase the conductivity in an amount that offsets the increase in resistance due to growth the chromia scale. In this case, the coating electrical resistance, and thus the associated overpotential, would be constant with time, so fuel cell performance would not degrade during operation.

## Results

The initial focus of the project is on the spinel $(Mn,Co)_3O_4$, which is the most promising coating material identified by Pacific Northwest National Laboratory. In particular, the interaction of this coating with chromia was studied. The initial studies were performed at temperatures higher than those used in SOFCs to accelerate the interaction and overcome kinetic limitations of SOFC operating temperatures.

The surface and cross-section of the as-prepared $Mn_{1.5}Co_{1.5}O_4$ sample are shown in Figure 1a. After reaction with $Cr_2O_3$ at 1,200°C a chromium-rich layer formed on the surface. In the regions in contact with $Cr_2O_3$, the composition of this surface layer reached $Mn_{0.4}Co_{0.6}Cr_2O_4$ and had a faceted morphology as shown in Figure 1b. The regions of the surface that were not in contact with the $Cr_2O_3$ also reacted, but the chromium content was not as high and the faceted microstructure did not form. Rather, as shown in Figure 1c, faster growth appeared to occur at the grain boundary regions. The cross-sectional views in Figure 1 show that a dense layer of similar thickness formed in both cases and these dense regions correspond to the increased chromium content shown in Figure 2. Although the penetration

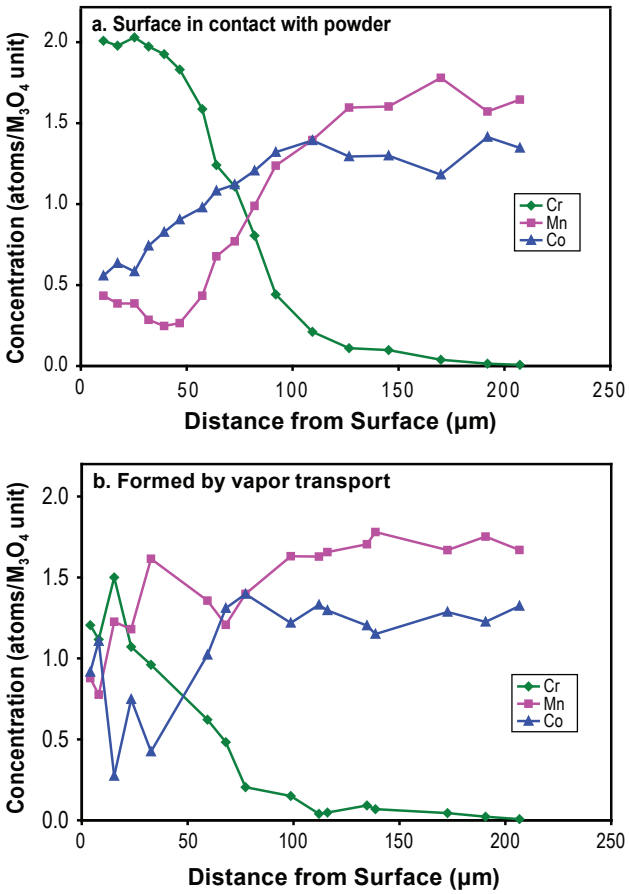


**FIGURE 2.** Composition Profiles through Cross-Section of Reaction Zone as Determined by EDS

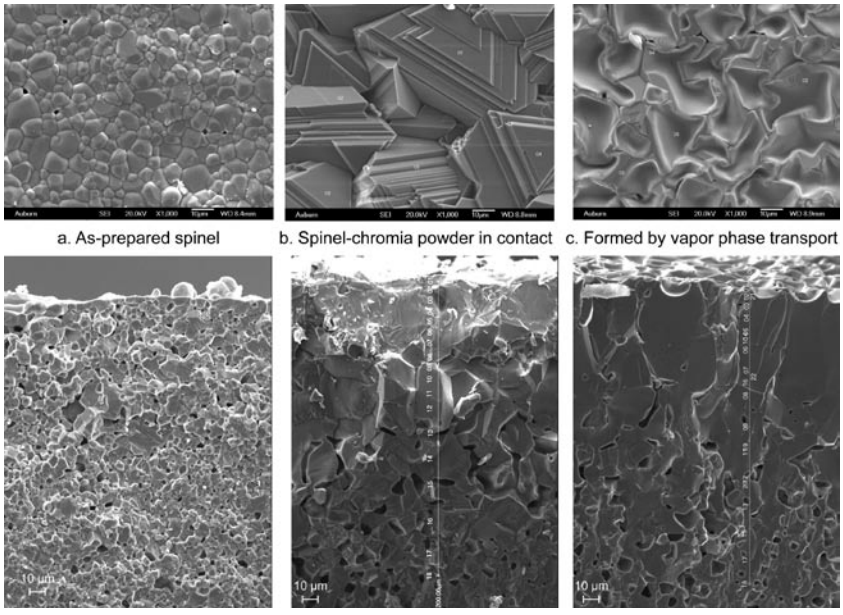


**FIGURE 1.** Scanning electron micrographs of surfaces and cross-sections: a) as-prepared $Mn_{1.5}Co_{1.5}O_4$ and after reaction in air at 1,200°C for 336 hours; b) region in contact with $Cr_2O_3$ powder; c) region not in contact with $Cr_2O_3$ powder.

depth of chromium is similar in both cases, the surface composition is very different. For the regions in contact with chromia, the chromium composition reached a maximum of two chromium per formula unit, *i.e.,* $(Mn,Co)Cr_2O_4$, at which point, presumably, all the manganese and cobalt have a valence of 2+ and the chromium has valence of 3+ to obtain the required average valence of 2.67+. Such a layer did not form in the regions that grew by vapor phase transport and the faceted structure did not form from the vapor phase even after long exposures. It was possible to obtain the maximum chromium content through vapor phase transport by enclosing a $Mn_{1.5}Co_{1.5}O_4$ sample in a $Cr_2O_3$ chamber as shown schematically in Figure 3. The scanning electron

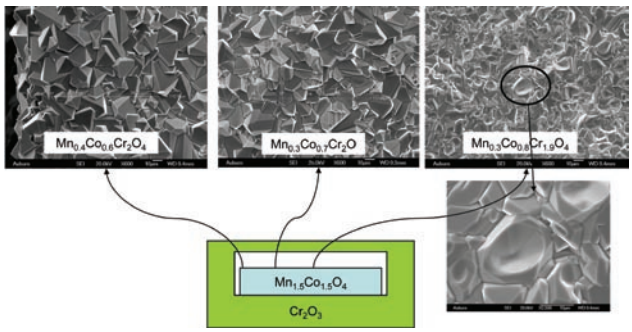


**FIGURE 3.** SEM Micrographs after Reaction in $Cr_2O_3$ Chamber for 72 Hours in Air at 1,200°C

microscope (SEM) images show the transition to the faceted morphology as the chromium content approaches the maximum concentration due to the close proximity of the region to the chamber wall (*i.e.,* the chromium source).

The effect of the Mn/Co ratio was evaluated using samples with three different compositions: $Mn_2CoO_4$, $Mn_{1.5}Co_{1.5}O_4$ and $MnCo_2O_4$. The surface morphologies of the samples after reaction were similar. The only exception was that the amount of porosity for the reaction layer formed by vapor phase transport on the composition with the highest cobalt content, $MnCo_2O_4$, was higher. One possible reason for this difference is that this composition is expected to consist of a two-phase mixture of a spinel phase (lower cobalt) and a rocksalt phase (higher cobalt) at 1,200°C. However, this two-phase microstructure did not appear to affect the reaction layer formed in contact with chromia powder. As shown in Table 1, the Co/Mn ratio in this surface layer increased with increasing cobalt content in the $(Mn,Co)_3O_4$ spinel, but the cobalt content in the surface layer was generally higher than that in the original $(Mn,Co)_3O_4$ spinel.

The surface morphologies of the reaction layer formed at 1,000°C are shown in Figure 4. The

**TABLE 1.** Spinel Compositions as Determined by EDS

| Initial composition | | Surface composition after 72 hours at 1,200°C | | | |
|---|---|---|---|---|---|
| | | Solid-solid contact | | Vapor-phase transport | |
| Formula | Co/Mn | Formula | Co/Mn | Formula | Co/Mn |
| $Mn_2CoO_4$ | 0.5 | $Mn_{0.65}Co_{0.35}Cr_2O_4$ | 0.54 | $Mn_{1.3}Co_{0.85}Cr_{0.85}O_4$ | 0.85 |
| $Mn_{1.5}Co_{1.5}O_4$ | 1.0 | $Mn_{0.40}Co_{0.60}Cr_2O_4$ | 1.5 | $Mn_{0.8}Co_{1.3}Cr_{0.9}O_4$ | 1.6 |
| $MnCo_2O_4$ | 2.0 | $Mn_{0.25}Co_{0.75}Cr_2O_4$ | 3.0 | $Mn_{1.0}Co_{1.45}Cr_{0.55}O_4$ | 1.45 |

EDS - Energy dispersive X-ray spectroscopy

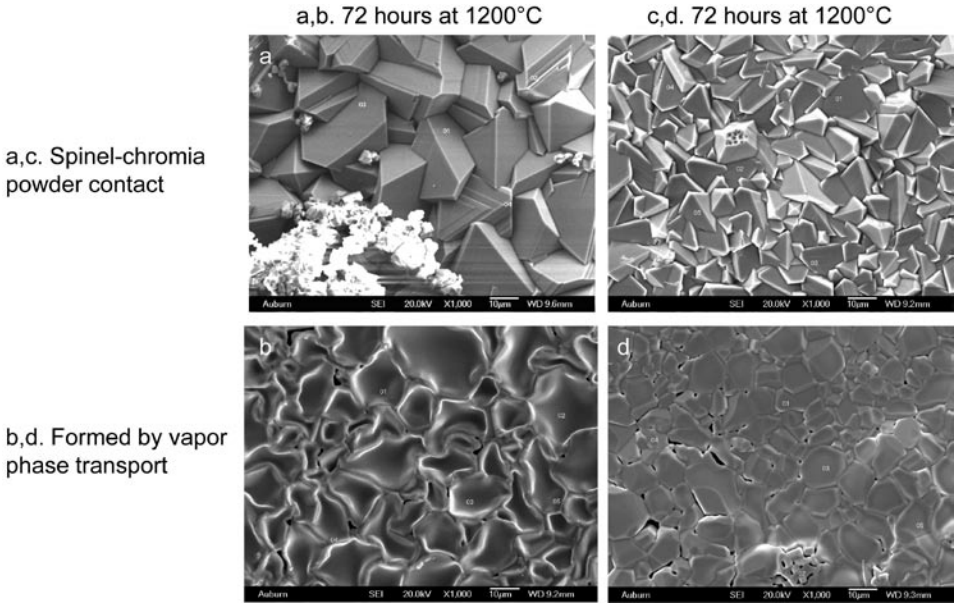


**FIGURE 4.** SEM micrographs of surfaces of reaction products after 72 hours in air at a,b) 1,200°C and c,d) 1,000°C. Figures a/c are regions in contact with chromia powder and figures b/d are regions formed by gas phase transport.

morphology is similar to that formed at 1,200°C except that the features are smaller (*i.e.,* smaller facets, less reaction product at the grain boundary), which is expected for the slower diffusion at the lower temperature.

## Conclusions and Future Directions

The surface morphology and concentration gradients suggest that reaction occurs by outward diffusion of cobalt and manganese through the initial reaction layer formed between chromia and the $(Mn,Co)_3O_4$ spinel phase. During SOFC operation, the formation of $(Mn,Co)Cr_2O_4$ and the diffusion layer at the interface between the alloy oxidation scale and the protective coating would reduce the amount of chromium reaching the coating surface and thus inhibit the associated chromium poisoning of the cathode. However, this reaction layer would be part of the fuel cell circuit, so its presence could affect fuel cell performance. Thus, the compositions, and associated properties, of this reaction layer must be considered in selection of the optimal coating composition for long-time SOFC operation. The following future activities are directed toward providing the information needed to design the optimal coating composition.

The mechanism appears to be similar at 1,000°C and 1,200°C, but lower temperature experiments will be performed to determine if the trend continues to SOFC operating temperatures.

The properties of the reaction layer compositions will be measured, since the reaction layer will become part of the fuel cell circuit. This will include structural and transport properties, such as electrical conductivity.

## FY 2009 Publications/Presentations

**1.** J.W. Fergus, "Alloys and Coatings for Solid Oxide Fuel Cell Interconnects," National Nuclear Energy Agency (BATAN), Serpong, Indonesia, May 19, 2009.

**2.** J.W. Fergus, "SOFC Interconnect Alloys and Coatings," Nanyang Technological University, Singapore, May 22, 2009.

## References

**1.** Y. Larring and T. Norby, "Spinel and Perovskite Functional Layers between Plansee Metallic Interconnect (Cr-5 wt% Fe-1 wt% $Y_2O_3$) and Ceramic $(La_{0.85}Sr_{0.15})_{0.91}MnO_3$ Cathode Materials for Solid Oxide Fuel Cells," *J. Electrochem. Soc.,* **Vol. 147**, 2000, pp. 3251-3256.

**2.** Z. Yang, G.-G. Xia, G.D. Maupin and J.W. Stevenson, "Conductive Protection Layers on Oxidation Resistance Alloys for SOFC Interconnect Applications," *Surf. Coating Tech.,* **Vol. 201**, 2006, pp. 4476-4483.

**3.** M.R. Bateni, P. Wei, X. Deng and A. Petric, "Spinel Coatings for UNS 430 Stainless Steel Interconnects," *Surf. Coating Tech.*, **Vol. 201**, 2007, pp. 4677-4684.

**4.** M.J. Garcia-Vargas, M. Zahid, F. Tietz and A. Aslanides, "Use of SOFC Metallic Interconnect Coated with Spinel Protective Layers Using the APS Technology," *ECS Trans.,* **Vol. 7**, 2007, pp. 2399-2405.

**5.** H. Kurokawa, C.P. Jacobson, L.C. DeJonghe and S.J. Visco, "Chromium Vaporization of Bare and of Coated Iron-Chromium Alloys at 1073 K," *Solid State Ionics,* **Vol. 178**, 2007, pp. 287-296.

**6.** C. Collins, J. Lucas, T.L. Buchanan, M. Kopczyk, A. Kayani, P.E. Gannon, M.C. Deibert, R.J. Smith, D.-S. Choi and V.I. Gorokhovsky, "Chromium Volatility of Coated and Uncoated Steel Interconnects for SOFCs," *Surf. Coating Tech.*, **Vol. 201,** 2006, pp. 4467-4470.

**7.** Z. Yang, G.-G. Xia, H.-H. Li and J.W. Stevenson, "$(Mn,Co)_3O_4$ Spinel Coatings on Ferritic Stainless Steels for SOFC Interconnect Applications," *Int. J. Hydrogen Energy,* **Vol. 32**, 2007, pp. 3648-3654.

**8.** Z. Yang, G. Xia and J.W. Stevenson, "$Mn_{1.5}Co_{1.5}O_4$ Spinel Protection Layers on Ferritic Stainless Steels for SOFC Interconnect Applications," *Electrochem. Solid-State Lett.,* **Vol. 8**, 2005, pp. A168-A170.

# III.C.3 Development of SOFC Interconnects

Zhenguo "Gary" Yang (Primary Contact), Guanguang Xia, Joshua Templeton, and Jeff Stevenson
Pacific Northwest National Laboratory (PNNL)
P.O. Box 999, MS K2-44
Richland, WA 99352
Phone: (509) 375-3756; Fax: (509) 375-2186
E-mail: zgary.yang@pnl.gov

DOE Project Manager: Briggs White
Phone: (304) 285-5437
E-mail: Briggs.White@netl.doe.gov

Contract Number: 40552

Start Date: October 1, 2008
End Date: September 30, 2009

### Objectives

- Develop cost-effective, optimized materials for intermediate temperature solid oxide fuel cell (SOFC) interconnect applications.
- Identify, understand, and mitigate degradation processes in interconnects and at interconnect interfaces.

### Accomplishments

- Evaluated performance of spinel-coated ferritic stainless steel interconnect materials under single and dual atmosphere exposure conditions.
- Optimized composition and processing parameters of Ce-modified MnCo spinel coatings.

## Introduction

In previous work, $(Mn,Co)_3O_4$ (MC) spinels have been systematically investigated and applied as protection layers on a variety of candidate SOFC interconnect steels. In recent years, the primary emphasis has been on the application of spinel coatings to AISI441 ferritic stainless steel, which is being investigated as an interconnect alloy by PNNL in collaboration with Allegheny Technologies and the National Energy Technology Laboratory. AISI441 is prepared via conventional melt metallurgy and is therefore less expensive than other candidate steels, such as Crofer22APU, which utilize vacuum processing to reduce the Si content to very low levels. Additions of Nb and Ti to the 441 tie up residual Si in Laves phase at grain boundaries, eliminating the need for expensive processing. The stability and electrical performance of 441 coated with $Mn_{1.5}Co_{1.5}O_4$ protection layers were previously evaluated in short-term testing (e.g., 500 or 1,000-hour tests). These tests indicated that the spinel protection layers helped minimize the interfacial electrical resistance and mitigate the scale growth beneath the spinel coatings on 441. Subsequently, to improve the observed weak scale adherence of the oxide scale to the 441 substrate, a Ce-modified $Mn_{1.5}Co_{1.5}O_4$ (Ce-MC) spinel coating was developed, which appears to combine the advantages of rare earth (RE) surface treatment or additions, and the MC spinel coating. Short-term evaluations indicated comparable electrical performance of the Ce-modified spinel coating in comparison with the unmodified spinel coating. In addition, however, the Ce-modified coatings significantly improved the scale adherence and overall interconnect surface stability.

## Approach

To supplement the previous short-term evaluations, one year area specific resistance (ASR) tests were carried out to evaluate the long-term performance and structural stability of MC and Ce-modified MC coatings on AISI441. The AISI441 was provided by the manufacturer, Allegheny Technologies Inc. MC and Ce-MC spinel powders were applied to selected alloy coupons using a slurry-based approach, and sintered to form protective coatings. The electrical resistance of bare and coated 441 was measured using a four-probe direct current technique, with Sr-doped lanthanum manganite (LSM) as the contact material. Scanning electron microscopy/energy dispersive spectroscopy (SEM/EDS) analyses were performed after testing.

## Results

Figure 1 shows the ASR of bare 441, MC coated 441, and Ce-MC coated 441. As observed previously in short-term tests, the ASR of the bare 441 increased rapidly to values too high to satisfy SOFC interconnect requirements. Also, it was observed that the ASR jumped discontinuously after power breaks, indicating possible surface instability and spallation. After the test was completed, surface spallation was visually observable on the exposed bare side of the coupon. However, SEM cross-section analysis on the other side of the coupon, which interfaced with the LSM contact material, found no spallation. Instead, the scale grown during the test appeared to be adherent to the 441 substrate. Also, the morphology of the metal/scale

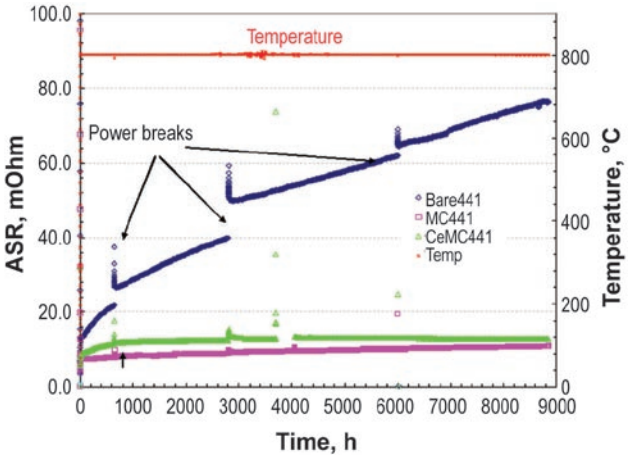


**FIGURE 1.** Area specific resistance of $Mn_{1.5}Co_{1.5}O_4$ (MC) coated and Ce-modified MC coated AISI441, in comparison with that of bare 441. The measurement was carried out at 800°C in air for a duration of ~1 year.

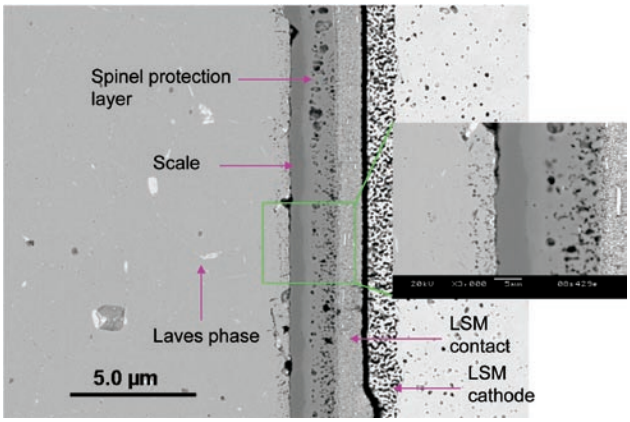


**FIGURE 2.** SEM cross-section images of AISI441 coated with MC protection layer, after one year area specific resistance test at 800°C in air. $La_{0.8}Sr_{0.2}MnO_3$ paste was applied as the contact material between a $La_{0.8}Sr_{0.2}MnO_3$ simulated cathode and the 441 coupon.

interface was quite different from the smooth interface that is often observed on bare 441 after oxidation tests. This is likely due to the presence of La in the LSM contact, which may have modified the scale growth behavior via the abovementioned RE effect. A series of point analyses in the bulk metal near the surface scale indicated consistent Cr% of ~18%, so there was no obvious Cr depletion in the bulk Fr-Cr substrate after the one year test. Laves phase, which appears to tie up residual Si in the matrix, was still present in the metal substrate, both along grain boundaries and inside grains. EDS area analysis on the LSM contact layer indicated a Cr content of ~5% as a result of Cr diffusion from the scale grown on the metal surface.

In contrast to the bare 441, the ASRs of both the MC and Ce-MC coated 441 were low and remained essentially unchanged during the one year test. SEM cross-section analysis on the long-term tested MC coated sample, as shown in Figure 2, indicated a smooth interface between the metal and the scale that was grown beneath the MC protection layer due to the inward diffusion of oxygen across the MC layer. Although no spallation was observed on the MC coated surface, cracks or localized detachment were observed (see the inset in Figure 2). SEM/EDS line scans across the interfaces found no Cr penetration through the MC layer into the LSM contact. This was supported by an area EDS analysis in the LSM contact material that detected no Cr in the LSM contact. The analysis did detect the presence of Co in the LSM contact material, indicating Co-outward migration into the LSM contact. SEM/EDS analyses also found Fe transport through the subscale into the MC layer, stabilizing the cubic spinel structure, but no Fe was detected in the LSM contact material.

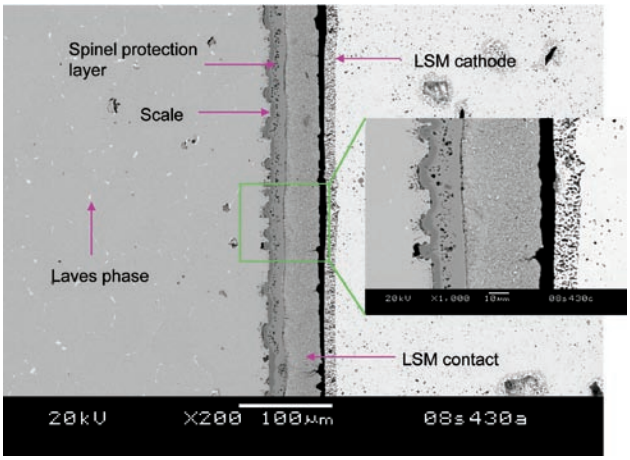


**FIGURE 3.** SEM cross-section images of AISI441 coated with Ce-modified MC protection layer, after one year area specific resistance test at 800°C in air. $La_{0.8}Sr_{0.2}MnO_3$ paste was applied as the contact material between a $La_{0.8}Sr_{0.2}MnO_3$ simulated cathode and the 441 coupon.

SEM cross-section analysis on the Ce-MC coated 441 (Figure 3) revealed a metal/scale interface that differed from that between the metal and the standard MC layer described above. The presence of Ce in the coating appeared to alter the scale growth, leading to a rougher interface with the metal substrate than was observed on the MC-coated 441. The scale also appeared to have improved adherence to the metal substrate. Unlike the MC coated 441, no cracks or localized detachments were observed on the Ce-MC coated 441. SEM/EDS line scan analyses indicated no Cr diffusion through the Ce-MC protection layer after one year. SEM/EDS area analyses also found no Cr in either the Ce-MC layer or the LSM contact material. Similar to the MC coated 441, some Fe was transported

through the scale into the Ce-MC layer, but Fe was not detected in the LSM contact material. Co was also found in the LSM contact material, again indicating some Co migration from the Ce-MC layer into the LSM contact material.

Dispersed Mn-enriched regions were observed within the oxide scale that grew beneath the spinel coating (Figure 4). Electron backscatter diffraction and EDS analyses indicated that those regions were a cubic Cr-Mn spinel phase (also containing Si, Mn, and Fe) embedded in a Ti-doped chromium oxide matrix.

In other coating-related work, studies were performed to optimize the Ce-MC coating processing conditions. The main processing parameters examined were:

1. MnCo powder calcination temperature
2. Powder particle size
3. Type of binder and powder-to-binder ratio
4. Coating drying temperature and rate
5. Reducing gas composition
6. Reduction temperature and time
7. Oxidation temperature

After a series of trials, the preferred conditions for application of MnCo coatings on 441 were identified; these conditions are summarized in Table 1.

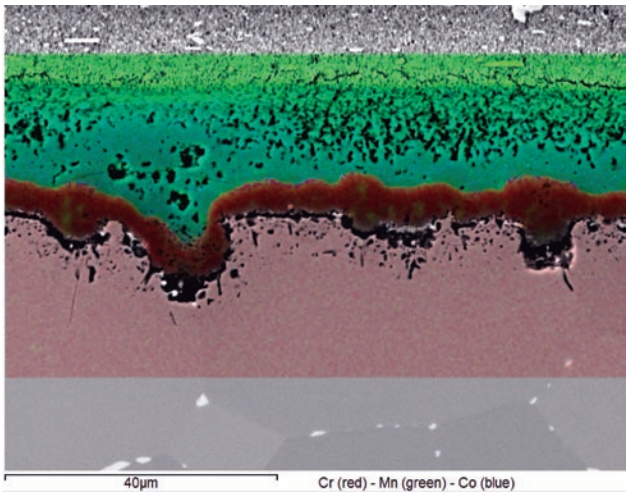


**FIGURE 4.** SEM/EDS cross-section area analysis of AISI441 coated with Ce-modified MC protection layer, after one year area specific resistance test at 800°C in air.

**TABLE 1.** Coating Process Parameters

| Parameters | Value | Comments |
|---|---|---|
| Calcination Temp. | 900°C | key parameter |
| Particle Size | <1 µm | attrition-milled |
| Binder to Powder Ratio | 0.6:1 | may vary with binder type |
| Coating Drying Temp. | <60°C | better results with slow drying |
| Reducing atmosphere | 2.7% $H_2$, wet | gas passing through a water bubbler |
| Reducing Temp. and Time | 850°C, 4 h | at least 650°C |
| Pre-oxidation Temp. | 950°C, 0.5 h | match with sealing temperature |

## Conclusions and Future Directions

The one year ASR tests appear to validate the long-term structural and electrical performance stability of spinel-coated 441. In particular, the Ce-modified MC coatings provided substantially improved electrical performance compared to bare 441, as well as improved scale adherence to the metal substrate. The long-term tests also confirmed the effectiveness of the spinel coatings as a Cr barrier that sealed off Cr and prevented Cr-migration into cathode contact materials. The one year tests also demonstrated the stability of the grain boundary Laves phase, which captures Si from the alloy matrix, and the ferritic structure and microstructure of the alloy matrix. Future directions include development and evaluation of alternative coating compositions, with an emphasis on reducing the Co content, and evaluation of interconnect materials under interconnect exposure conditions relevant to coal-based SOFC systems (i.e., air vs. simulated coal gas).

## FY 2009 Publications/Presentations

**1.** G.G. Xia, Z.G. Yang, J.D. Templeton, X.S. Li, Z.M. Nie, and J.W. Stevenson, "Development of Spinel Protection Layers for Steel-Based SOFC Interconnects," 36th International Conference on Metallurgical Coatings and Thin Films (ICMCTF 2009), San Diego, California, April 27 – May 1, 2009.

**2.** Z.G. Yang, G.G. Xia, J.D. Templeton, Z. Nie, C.M. Wang, X.S. Li, J.W. Stevenson, and P. Singh, "Mixed Conductive Coatings on Metallic Interconnects in SOFCs," 138th Annual TMS Meeting, San Francisco, California, February 15–19, 2009.

**3.** Z. Yang, G.G. Xia, J.D. Templeton, X. Li, Z. Nie, J. Coleman, C. Wang, J.W. Stevenson, and P. Singh, "Advanced SOFC Interconnect Development at PNNL," 33rd International Conference on Advanced Ceramics and Composites, Daytona Beach, Florida, January 18-23, 2009.

**4.** Z.G. Yang, G.G. Xia, X. Li, Z. Nie, C. Wang, J.D. Templeton, J. Coleman and J.W. Stevenson, "Conductive Oxide Coatings on Metallic Components for Applications in High Temperature Electrochemical Energy Systems," 214th Electrochemical Society Meeting, Honolulu, Hawaii, October 14, 2008.

**5.** Z.G. Yang, G.G. Xia, Z. Nie, J.D. Templeton, X.S. Li, C.M. Wang, J.W. Stevenson, and P. Singh, "Durability and Suitability of Fe-Cr-Nb(-Ti) Base Ferritic Steels for SOFC

Interconnect Applications," MS&T 2008 Conference & Exhibition, Pittsburgh, Pennsylvania, October 6–9, 2008.

**6.** Z.G. Yang, G.G. Xia, J.D. Templeton, G.D. Maupin, J.W. Stevenson, P. Singh, and X.D. Zhou, "Development and Investigation of $(Mn,Fe,Co)_3O_4$ Protection Layers on Ferritic Stainless Steels for SOFC Interconnect Applications," MS&T 2008 Conference & Exhibition, Pittsburgh, Pennsylvania, October 6–9, 2008.

# III.C.4 Optimization of Protective Coatings for SOFC Interconnects

Jung-Pyung Choi (Primary Contact),
K. Scott Weil, Jeff Stevenson
Pacific Northwest National Laboratory (PNNL)
P.O. Box 999, K6-28
Richland, WA 99352
Phone: (509) 376-3380; Fax: (509) 375-2186
E-mail: jungpyung.choi@pnl.gov

DOE Project Manager: Briggs White
Phone: (304) 285-5437
E-mail: Briggs.White@netl.doe.gov

Contract Number: 40552

Start Date: October 1, 2008
End Date: September 30, 2009

### Objectives

- To optimize fabrication procedures for $(Mn,Co)_3O_4$ spinel coatings for steel-based interconnects for intermediate temperature solid oxide fuel cell (SOFC) stacks.
- To evaluate and improve the chemical stability and mechanical integrity of interconnect steel/sealing glass interfaces.

### Accomplishments

- Initiated development of an ultrasonic spray process for fabrication of $(Mn,Co)_3O_4$ spinel coatings.
- Continued optimization of alumina coatings for steel-based SOFC interconnects.

## Introduction

Planar SOFC stacks require adequate seals between the interconnects and cells in order to prevent mixing of the oxidant and fuel gases within the stack, and leakage of the gases from the stack. Alkaline earth-containing glasses offer many advantages as sealing materials, but they also exhibit a tendency to form undesirable alkaline earth chromate layers at the glass/interconnect alloy interfaces. Mechanical testing of the seal/joint strengths of sealed glass-alloy coupons has confirmed degradation in seal strength during high temperature exposure to air due to the formation of this interfacial phase. In addition to seal/interconnect interfacial reactions, steel-based interconnects also exhibit surface instability at SOFC operating temperatures; challenges include oxidation, spallation, and reactions with neighboring components, increasing electrical resistance due to continuous oxide scale growth, and chromia-scale evaporation, which may lead to cathode poisoning. To overcome all of these issues, PNNL is developing $(Mn,Co)_3O_4$ spinel (MC) coatings to protect interconnect surfaces exposed to the cathode air stream, and alumina coatings for interconnect sealing surfaces to prevent Cr in the steel from contacting, and subsequently reacting with, alkaline earth constituents (e.g., Ba or Sr) in the glass seal material.

## Approach

PNNL's aluminization process (referred to as reactive air aluminization or RAA) involves spraying a low-viscosity Al powder/polymer binder slurry onto the surfaces of the substrate, drying the coated component at 80ºC in air to drive off the slurry solvent, and heating in air to 700ºC or higher to initiate diffusion of the aluminum into the underlying substrate and formation of a protective alumina scale. The MC spinel coatings are typically prepared from slurries containing spinel powder and an organic binder system. While the aluminization process typically involves only one (oxidizing) heat treatment, two heat treatments (reducing followed by oxidizing) are required to densify the spinel coating. Scale-up of PNNL's spinel and alumina coating techniques is being pursued via development and optimization of application processes based on ultrasonic spray technology.

## Results

### Reactive Air Aluminization

A parametric study of the effects of powder particle size and binder selection on the RAA process was performed. Preliminary testing of the effect of heat treatment on coating adhesion indicated that heat treatment at 700°C resulted in poor coating adhesion while heat treatment at 1,000°C led to good coating adhesion, so the samples in this study were heat-treated in air at 1,000°C for 1 hour. Specific variables evaluated are listed in Table 1.

**TABLE 1.** Variables Tested in the Parametric Study

| Binder Type | Al Powder Particle Size |
|---|---|
| None | 0.1 μm (purity: 97.5%) |
| Isopropanol | 3 μm (purity: 97.5%) |
| Heraeus V-006 | 44 μm (purity: 99.5%) |
| ESL 450 | |

## Binder System Effects

Three separate slurries were prepared, each containing 44 μm Al powder suspended in isopropanol, Heraeus V-006, or ESL 450. Results from coating experiments conducted with these slurries were compared with a baseline case in which no binder was used. It was found that only slurries prepared with the Heraeus or ESL binders resulted in well-adherent coatings displaying uniform surface coverage of the type shown in Figure 1(a). The loose powder and isopropanol slurry coatings yielded virtually no aluminization, as shown in Figure 1(b). The viscosity of the ESL slurry was lower than desired for screen-printing, but was appropriate for ultrasonic spray coating processes. Based on the success with the Hereaus binder-based slurries, subsequent slurry preparations employed only this binder system for screen-printing. It is possible that organic constituents in the binder carburize and/or volatilize at temperatures near or above the melting point of aluminum, thereby delaying excessive oxidation in the powder particles and allowing greater melting and diffusion of aluminum into the substrate to take place.

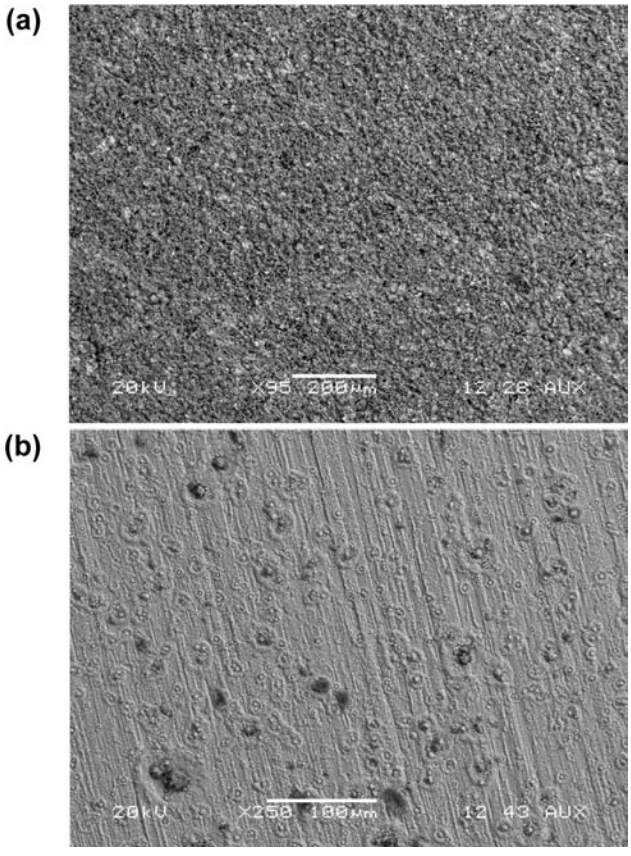


**FIGURE 1.** Surface SEM Micrographs of Crofer Aluminized Using 44 μm Al Powder Slurries Prepared with: (a) Heraeus-V006 Binder and (b) Isopropanol

## Powder Particle Size Effects

The average size of the aluminum powder appears to play a significant role in defining several characteristics of the final coating, including surface roughness and morphology and the extent of aluminum diffusion into the substrate (i.e., depth of the Al diffusion zone). These factors in turn lead to changes in the thermal expansion properties of the substrate, which affect the likelihood of oxide scale spallation and general coating durability under thermal cycling conditions. Fundamentally, powder particle size determines the balance between competing oxidation and diffusion mechanisms that occur during the air heat treatment step. Surface oxidation consumes aluminum within each particle, forming an $Al_2O_3$ scale layer. In general, the larger the powder particle size, the lower the surface area available for particle oxidation to take place and therefore the greater the amount of aluminum available to diffuse into the substrate. Conversely, at very small powder particle sizes, a larger fraction of the aluminum will be consumed via oxidation during heat treatment in air, leaving less molten aluminum to react with and/or diffuse into the substrate alloy.

In addition, based on prior work with molten aluminum seals, it is suspected that there is a minimum particle size at which aluminum diffusion does not take place because a sufficiently strong oxide shell forms on each particle, which encases the molten aluminum within. Above a threshold particle size, the volumetric ratio of oxide and metal is such that the molten aluminum will break through this shell due to high stresses associated with volumetric expansion during melting. The parametric studies are consistent with this trend. Shown in Figures 2(a)-(c) are a series of cross-sectional scanning electron microscope (SEM) micrographs of Crofer22APU aluminized using 44 μm, 3 μm, and 0.1 μm size aluminum powder. It was observed that the extent of aluminum diffusion dropped significantly for each decrease in powder size, to the point that at the 0.1 μm powder size there essentially was no diffusion zone, just a thin alumina scale layer. It was also apparent that powder particle size affected the morphology of the final coated surface. Again, the trend was such that the larger particle size led to higher values of surface roughness, with little roughness being observed for the 0.1 μm powder coatings. However, it should be noted that regardless of the degree of surface roughness, the top scale appeared to be nearly pure aluminum oxide.

Because larger Al powder particles afford a greater amount of aluminum available to diffuse into the substrate, subsequent physical property changes in the substrate alloy are more extensive. While aluminum is a strong ferrite stabilizer (i.e., the crystal structure of the common 400-series stainless steel alloys should remain unchanged when adding aluminum),

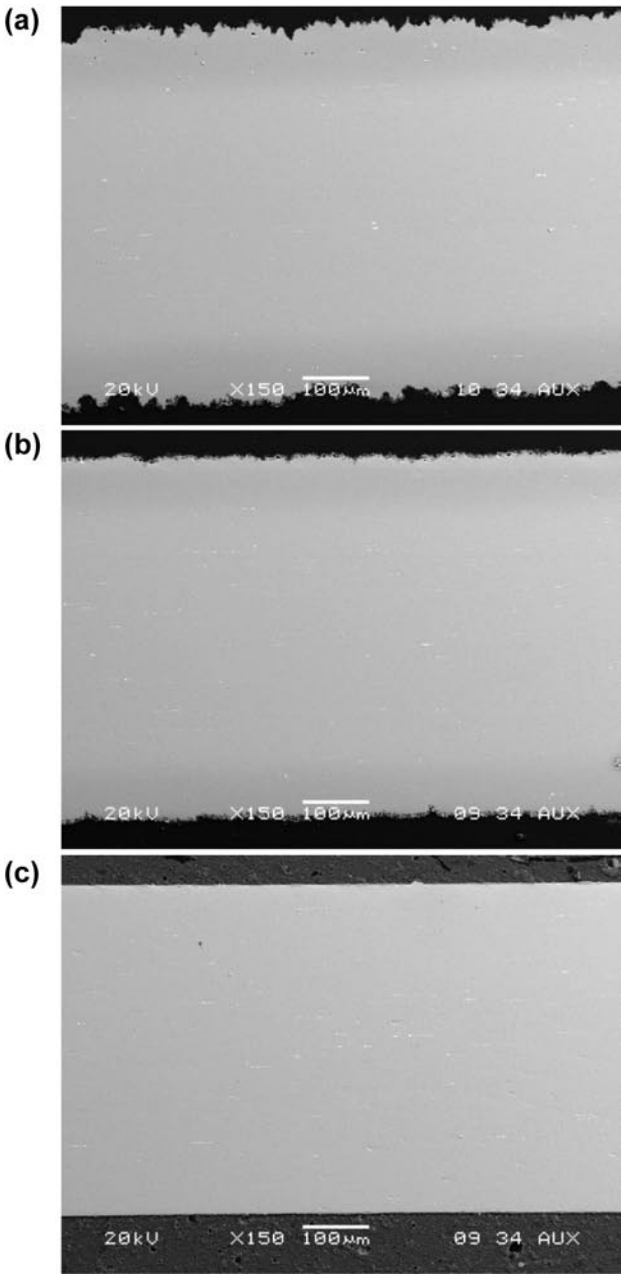


**FIGURE 2.** Cross-Sectional SEM Micrographs of Ferritic Steel Aluminized at 1,000°C for 1 Hour Using Heraeus Binder-Based Slurries Containing Aluminum Powders of the Following Average Size: (a) 44 µm, (b) 3 µm, (c) 0.1 µm

there can be a dramatic increase in the coefficient of thermal expansion. Additionally, intermetallic phases can potentially form. Both changes can lead to possible cracking of material in the aluminized region. Measurements of thermal expansion show that the impact of the aluminization coating can be minimized by employing smaller powder particle sizes and thinner applied coating thicknesses, as seen in Figure 3. The result labeled Crofer II is from a hand printed coating. The other results are from screen-printed coatings.

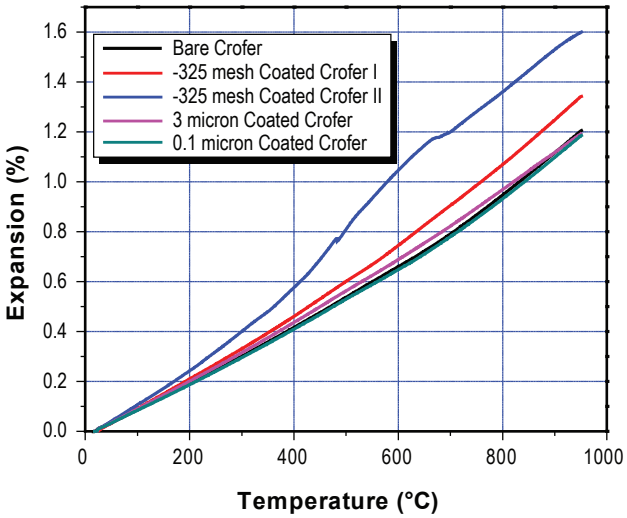


**FIGURE 3.** Plots of Thermal Expansion for Bare and Aluminized Ferritic Steel as a Function of Temperature

Based on results to date, the optimal set of coating parameters for aluminizing ferritic stainless steel components by this process include: 3 µm average Al powder size, Heraeus binder, 1,000°C heat treatment temperature, and ~10 µm applied slurry layer thickness. However, more work, including longer term testing, is needed to verify these parameters and to determine the degree of "robustness" associated with minor deviations from optimal process conditions.

### Ultrasonic Spray Fabrication

In other coatings-related work, intended to allow for scale-up of PNNL's protective coating processes, ultrasonic spray techniques were developed for aluminized coatings and are now being adapted for the application of MC spinel coatings. Unlike previously developed screen-printing fabrication techniques, spray-based processes will allow for application of protective coatings to selected regions of full-size, "shaped" SOFC interconnects, as shown in Figure 4. In preliminary work, MC spinel coatings sprayed onto steel coupons and then subjected to the standard reduction and oxidation heat treatments exhibited higher density than hand-painted reference coatings prepared with the same precursor powder.

## Conclusions and Future Directions

In summary, while uniform $Al_2O_3$ coatings can be formed from aluminum powders with a wide range of sizes, the larger particle sizes afford a measurable Al diffusion zone. This diffusion zone represents a store of aluminum that can be "tapped" during stack operation so that a protective alumina scale inherently reforms if it becomes damaged, for example during thermal

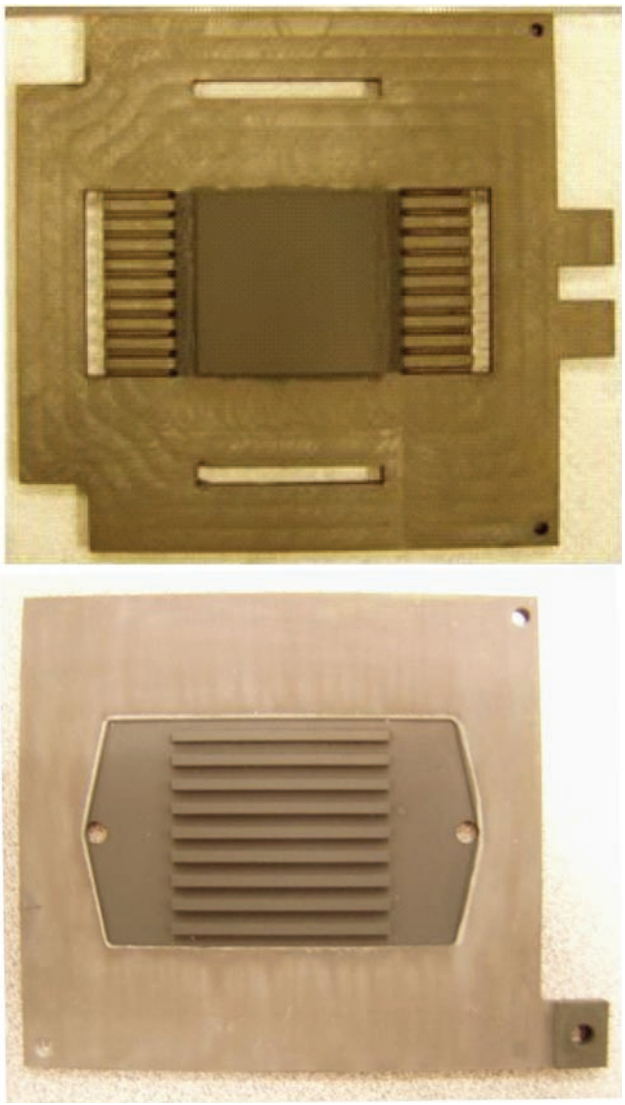

**FIGURE 4.** Spray-Coated, Heat-Treated Steel Interconnect Plates

cycling. On the other hand, too much aluminum can cause intermetallic formation and/or changes in the coefficient of thermal expansion of the substrate's outer layer relative to its core, both of which can lead to crack formation in the scale or sub-scale regions of the coated part.

Co-fabrication techniques for dual alumina/MC spinel coatings onto steel SOFC interconnects are under development, with an emphasis on processes compatible with a single heat treatment in air at 800-1,000ºC. Future directions include development of an improved understanding of the effects of various processing and material parameters on the thickness, microstructure, and composition of both the alumina and spinel coatings. In addition, scale-up of developed processes will be accomplished through optimization of ultrasonic spray-based application methods.

## FY 2009 Publications/Presentations

**1.** J.P. Choi, K.S. Weil, and J.W. Stevenson, "Thermal and Electrical Stability of New Aluminizing Process in Planar SOFC Stacks," 138th Annual TMS Meeting, San Francisco, California, February 15–19, 2009.

**2.** J.P. Choi, K.S. Weil, Y.S. Chou, J.W. Stevenson, Z.G. Yang, G.G. Xia, and P. Singh, "Development of MnCoO Coating with New Aluminizing Process for Planar SOFC Stacks," 138th Annual TMS Meeting, San Francisco, California, February 15–19, 2009.

**3.** J.P. Choi, K.S. Weil, and J.W. Stevenson, "Development of a New Aluminizing Process to Mitigate Chromium Volatility in Planar SOFC Stacks," MS&T 2008 Conference & Exhibition, Pittsburgh, Pennsylvania, October 6–9, 2008.

# III.C.5 Novel Composite Materials for SOFC Cathode-Interconnect Contact

J.H. Zhu (Primary Contact), L.T. Wilkinson, and J.M. Shoulders
Department of Mechanical Engineering
Tennessee Technological University
115 W. 10th St., Box 5014
Cookeville, TN 38505
Phone: (931) 372-3186; Fax: (931) 372-6340
E-mail: jzhu@tntech.edu

DOE Project Manager: Robin Ames
Phone: (304) 285-0978
E-mail: Robin.Ames@netl.doe.gov

Contract Number: 42533

Start Date: August 1, 2005
End Date: July 31, 2009

## Objectives

- Elucidation of the mechanism of Ag evaporation at elevated temperatures.
- Assessment of the effect of various alloying additions on the Ag evaporation rate of Ag.
- Evaluation of the effectiveness of the addition of the perovskite phase on the performance of Ag-based contact materials.
- Demonstration/assessment of performance of the new contact materials in solid oxide fuel cell (SOFC) operating conditions.

## Accomplishments

- The overall area-specific resistances (ASRs) of Ag-$(La_{0.8}Sr_{0.2})MnO_3$ (LSM) were compared to those of Ag-$(La,Sr)(Co,Fe)O_3$ (LSCF), with their differences explained by the sinterability of the perovskite phase in the composites.
- The interaction between the Ag-containing contact materials and the Cr-containing steel interconnects was elucidated, and both $Ag_2CrO_4$ and $AgCrO_2$ have been identified.
- The mechanism responsible for the abnormal oxidation of the ferritic interconnect in contact with the composite contact materials with high amounts of LSM under thermal cycling conditions was proposed.
- The effectiveness as "chromium-getter" was compared for LSCF- and LSM-containing composites with LSCF identified as more effective.

## Introduction

To reduce the electrode/interconnect interfacial resistance in SOFC stacks, electrical contact layers are often applied between the interconnect and electrodes during construction of an SOFC stack by compensating for the corrugations present on their respective surfaces. Some of the major criteria for SOFC contact materials are: 1) sufficiently high electrical conductivity over the SOFC lifetime; 2) chemical stability under high current condition and compatibility with other cell components, especially negligible effects on the formation of protective oxides on interconnect alloy; and 3) reasonable match in coefficient of thermal expansion (CTE) with other cell components. In addition, it is highly desirable for the contact materials to have some damage tolerance (possible self-healing if thermal cycle-induced cracking occurs in the contact layer) and to act as a Cr "sponge" by absorbing the Cr species migrating from the interconnect to the cathode and therefore reducing the Cr "poisoning" of the cathode. Because of the stringent criteria, finding a suitable material for the interconnect-cathode contact is very challenging.

The materials currently under consideration for cathode/interconnect contact application include low melting-point ceramics (such as doped $LaCoO_3$), noble metals (e.g. Ag or Pt), and their composites [1,2]. Pt, Au, and Pd are not desirable for this application because of their high raw material cost. However, Ag is an exception due to its relatively low price. Ag-ceramic composite is one of the very promising candidates for an SOFC contact due to the inherent properties of Ag, such as high chemical stability, high electrical conductivity, high ductility, and relatively low melting point. The perovskite component in the composite is expected to provide a more desirable CTE match and potentially act as a Cr absorbent and/or a barrier for Cr migration to the cathode. One major drawback of Ag as an SOFC interconnect/cathode contact material is its tendency to evaporate at the SOFC operating temperatures, while for the perovskite material thermal cycle-induced cracking and damage accumulation might be an issue.

## Approach

The performance of the composite materials as an interconnect/cathode contact was further evaluated under both isothermal and cyclic exposure conditions using a special testing rig which can host six cells for simultaneous testing. The ASR data of the Ag-LSM amd Ag-LSCF were compared and general trends were assessed.

After thermal exposure was completed, the test cells were mounted, cross-sectioned, and examined with scanning electron microscopy (SEM) attached with an energy-dispersive spectroscopy (EDS). The oxide scales formed on the interconnect alloy after thermal exposure were observed carefully for all the cells. In addition, the phase evolution and morphological features of the microstructure in the contact layer and the cathode were assessed, particularly with regard to Ag migration. Another aspect of interest is the detection of Cr migration throughout the cell during the thermal exposure. EDS analyses of the average chemical composition of the contact layer as well as the porous cathode area were conducted to quantify the Cr content in each layer. This allowed for rough estimate and comparison of the Cr-blocking and absorbing capabilities of each contact material.

## Results

Comparing the ASR performance of the Ag-LSCF and Ag-LSM composite contact materials, we found that the self-healing behavior was much more pronounced in the Ag-LSCF system than in the Ag-LSM system. Overall, the Ag-LSM composite contact materials exhibited higher overall ASRs than those of Ag-LSCF. Furthermore, even with the 90% LSM contact material, an order-of-magnitude drop in both ASR and ASR degradation rate was observed when compared to the 100% LSM contact material. As can be seen in Figure 1, the degradation rate (as determined from the slope of the ASR curve during the final 100 hours at 800°C) of the isothermally-held contact materials was much lower than that of the thermally-cycled contact materials, especially for the materials with greater than 50% ceramic content. It should be noted that some of the ASR degradation rates were negative in the figure, which indicates that the overall ASR was still decreasing during the final 100 hours of testing as a result of the self-healing behavior of the contact material.

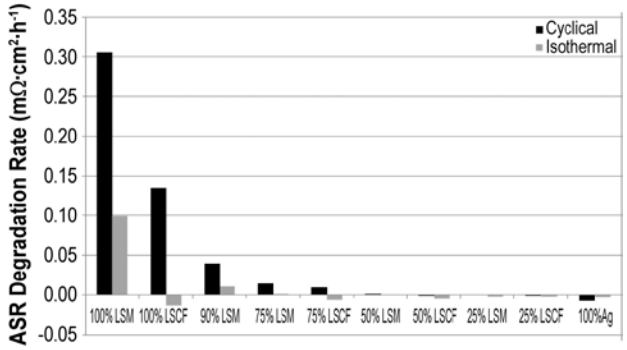


**FIGURE 1.** Comparison of ASR Degradation Rates of the Various Cells under the Isothermal and Cyclical Testing Conditions

It has been reported that for some of the cells under cyclic exposure, a very thick (~60 μm), irregular oxide scale was observed on the surface of the Crofer interconnect on the side in contact with the contact layer, as reported last year. While this phenomenon is most noticeable on the test cells with 100% LSM contact material, the cells with 100% LSCF contact material and many of the Ag-LSM and Ag-LSCF composites also exhibited abnormal oxide scales up to ~25 μm thick. Thermally-induced stresses due to the extreme thermal cycling and the inability of the ceramic contact materials to deform was assumed to have caused cracking in the protective $Cr_2O_3$ layer thermally grown on the interconnect on the cathode side, allowing further oxidation to occur on the exposed interconnect surface. The 100% LSCF contact material was shown to have significant amounts of cracking within the contact layer, while the 100% LSM contact material did not. It is believed that the cracking within the contact layer mitigated the thermal stresses developed during thermal cycling and thus reduced the extent of the cracking in the protective $Cr_2O_3$ scale. Even though Ag has a much higher CTE compared to the perovskite, interconnect, and the cathode, the abnormal oxidation gradually diminished as the Ag content in the composite increased. This can be explained by the fact that Ag is very ductile and could easily deform under stress, which will reduce the thermal stress level and potentially avoid the cracking of the protective $Cr_2O_3$ scale.

Another interesting observation with cross-sectional analysis was made on the Ag-containing contact materials. There appeared to be a substantial amount of Ag migration into the cathode material that occurred during cell testing. Both $AgCrO_2$ and $Ag_2CrO_4$ were formed as a result of the interaction between Ag and Cr in oxidizing environments at elevated temperatures, as shown in Figure 2. It should be noted that the amount of Ag observed in the contact layer and porous cathode after 500-hour exposure at 800°C was so significant that it could not explained by the Ag evaporation from Ag in the composite alone. It is possible that the interaction between Ag and Cr near the interface between the interconnect and contact layer first caused the formation of $AgCrO_2$, which might have a much higher evaporation rate than that of pure Ag, leading the accelerated Ag contamination in the contact layer as well as the porous cathode.

Cr migration was evaluated by quantifying the atomic percentage of Cr in each contact layer and its adjacent cathode layer using SEM/EDS. Figures 3 and 4 show a comparison of the amount of chromium present in cathode and contact layers for cells with different contact materials subjected to isothermal and thermal cycling exposures. The general trend observed in the data was that a higher percentage of perovskite in the composite contact layer resulted in a lower amount

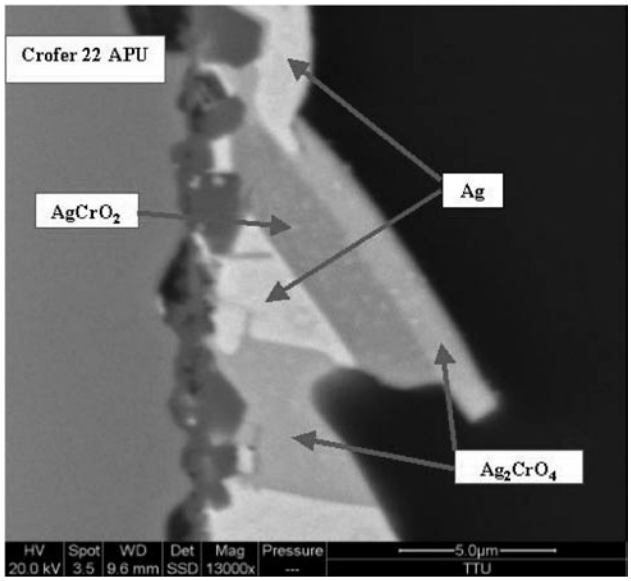


**FIGURE 2.** Cross-Sectional View Showing the Presence of Multiple Ag-Mn-O Phases in the 100% Ag Contact Material after Thermal Cycling for 500 Hours at 800°C

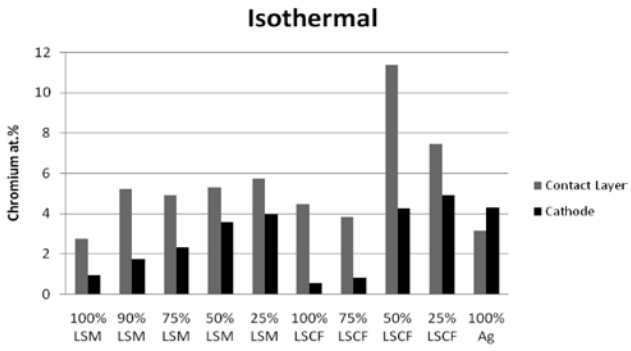


**FIGURE 3.** Chromium Content in the Contact and Cathode Layers of the Cells with Different Contact Materials Isothermally-Exposed to Air for 500 Hours at 800°C

of Cr detected in the contact material and the adjacent cathode layer. Furthermore, higher amounts of Cr are present in the contact layer than in the adjacent cathode layer. For the Ag-LSM composites under cyclical exposure conditions, the amount of Cr present in the contact material was just slightly higher than the amount detected in the adjacent cathode material. This seems to indicate that LSM is not very effective at trapping Cr within the contact material and preventing further spread to the cathode. For the Ag-LSM composites after isothermal testing, there was a noticeably greater amount of Cr present in the contact material than in the LSM cathode. This could be attributed to the reduced amount of thermal stresses and cracking within the contact layer under isothermal conditions, resulting in a less effective pathway for Cr migration into the cathode material.

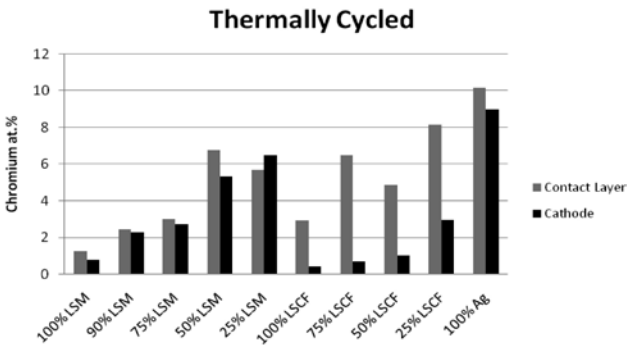


**FIGURE 4.** Chromium Content in the Contact and Cathode Layers of the Cells with Different Contact Materials Cyclically Exposed to Air for 500 Hours at 800°C

For the Ag-LSCF composites, there is a clear disparity in the amount of chromium present in the contact material compared to that in the adjacent LSM cathode material for both isothermally and cyclically tested cells. A substantially higher amount of Cr was detected in the contact material than in the cathode, indicating that LSCF reacts with the migrating Cr species and effectively traps them within the contact layer. The formation of $SrCrO_4$ crystals was widely reported in Co-containing perovskites such as LSC and LSCF following exposure to Cr-containing vapors at elevated temperatures, and it is believed that this reaction is the primary mechanism for Cr capture in the Ag-LSCF composite contact materials. The ability of LSCF to absorb Cr and inhibit it from poisoning the cathode makes it a more desirable candidate for use in contact materials than LSM.

## Conclusions and Future Directions

The following conclusions can be drawn based on this study:

- Both $Ag_2CrO_4$ and $AgCrO_2$ were detected as a result of the interaction between the Ag-containing contact materials and the Cr-containing steel interconnects.
- The abnormal oxidation of the ferritic interconnect in contact with the composite contact materials with high amounts of LSM was due to the thermal stress-induced cracking of the $Cr_2O_3$ scale under thermal cycling conditions.
- LSCF is a more effective "chromium-getter" than LSM due to its ability to absorb Cr in the composite contact layer.

No additional work is planned, as the project is ending this year. However, several questions remain to be answered, including: the Ag evaporation behaviors of $Ag_2CrO_4$ and $AgCrO_2$; the effect of sintering temperature

on the ASR performance of the low-Ag composites; and identification of other potential perovskites or spinels to be used in the composites, etc.

## FY 2009 Publications/Presentations

**1.** "Ag-Perovskite Composite Materials for SOFC Cathode-Interconnect Contact," *J. Electrochem. Soc.*, 156(8), p. B905 (2009).

**2.** Quarterly Report for 3rd quarter 2008, October 2008.

**3.** Quarterly Report for 4th quarter 2008, January 2009.

**4.** Quarterly Report for 1st quarter 2009, April 18, 2009.

## References

**1.** S. Koch and P.V. Hendriksen, *Solid State Ionics*, 168, 1 (2004).

**2.** Z. Yang, G. Xia, P. Singh, and J.W. Stevenson, *J. Power Sources*, 155, 246 (2006).

# III. SECA CORE RESEARCH & DEVELOPMENT

## D. Seals

# III.D.1 Viscous Glass/Composite SOFC Sealants

Scott Misture (Primary Contact), James Shelby
NYS College of Ceramics at Alfred University
2 Pine St., Binns-Merrill Hall
Alfred, NY 14802
Phone: (607) 871-2438; Fax: (607) 871-2354
E-mail: misture@alfred.edu

DOE Project Manager: Joseph Stoffa
Phone: (304) 285-0285
E-mail: Joseph.Stoffa@netl.doe.gov

Contract Number: NT0005177

Start Date: October 1, 2008
End Date: September 30, 2011

### FY 2009 Objectives

- Develop the new viscous glasses and glass/composite sealing materials needed to advance solid oxide fuel cell (SOFC) technologies.
- Improve our fundamental understanding of viscous sealants and their potential for meeting the desired sealing requirements and the nature and magnitude of the limitations of such materials.
- Optimize thermochemical and thermomechanical properties iteratively.

### Accomplishments

- Produced and tested 20 viscous silicate glasses with coefficient of thermal expansion (CTE) values near 12.0 ppm/K with glass transition temperatures as low as 600°C and as high as 830°C.
- Demonstrated that silicate glasses containing $Ga_2O_3$ (10 or 15 mol%) exhibit excellent resistance to crystallization even in fritted form at 850°C for 504 hrs, along with lower viscosity.
- Demonstrated, using 15 candidate germanium silicate glasses, that this glass system also offers promise with reasonable flow behavior at temperatures as low as 850°C.
- Demonstrated that candidate phosphate glass compositions are highly volatile and not applicable.
- Down-selected gallio-silicate and germano-silicate glasses for further study and compositional development.

## Introduction

Large-scale production of SOFC laminate stacks is complicated by difficulties of sealing the stack components using a reliable method that is robust over the lifetime of the device. Candidate sealants should exhibit high CTE values near 12 ppm/K, gas impermeability, minimal interaction with SOFC stack components for 40,000 hours between 600 and 850°C, and a maximum processing temperature of ~950°C [1]. Glass, glass-ceramic, and glass-ceramic composite seals are the best candidates for forming seals due to ease of manufacture and ability to control CTE, viscosity, and sealing temperatures with composition.

Many sealants currently being developed contain large amounts of alkaline earths such as barium or strontium which aids in seal formation below 1,000°C, yet form undesirable crystals when held at temperatures within the SOFC target operating temperature range [2,3]. Some contain undesirable amounts of boron which readily exhibits volatilization in a hydrogen atmosphere at SOFC operating temperatures [4]. The current project centers on developing new viscous oxide glass sealants that will flow at the operating temperature to reduce mechanical stresses between components but maintain the required hermeticity. By using glasses with lower alkaline earth content and reduced alkali content as well, we hope to avoid known reactivity issues. Compositions with gallium and germanium additions to silicate based compositions appear to be promising candidates.

## Approach

Initial candidate glass sealants were researched in the literature. Glass compositions containing low alkali concentrations and exhibiting properties described above were surveyed using the SciGlass® Database to identify initial SOFC sealant compositions. These glasses were melted and screened by measuring thermophysical properties such as CTE, glass transition temperature, viscosity, and crystallization behavior. Quantitative crystallization behavior and weight loss screening studies were performed via heat treatment for 504 hrs. Compositional modifications were used to optimize properties that were undesirable in relation to the target properties.

An iterative approach of screening, down-selection and optimization is in process. Some of the down-selected glasses from the initial matrices were also evaluated for stability in glass composite seals.

Optimized compositions were fritted and mixed with $Al_2O_3$ or 8 mol% yttria-stabilized zirconia (8YSZ) powders to characterize interactions between the glass and substrate materials and properties of the glass-ceramic composite material. Heat treatments of ~500 hrs, followed by extensive characterization, are currently underway.

## Results

The viscosity vs. temperature behavior of the range of glasses studied spans from "applicable at 850°C" to "viscosity too high." The initial viscous glass sealants tested were in the alkali silicate compositional system. Initial viscous candidates contained approximately 20 mol% alkali such as $K_2O$ or $Na_2O$. This high alkali content is undesirable in the fuel cell application, but the glasses provide a reference point for compositional modification. Within the alkali silicate system, we achieved applicable CTE values of 10-12 ppm/K, but the viscosities were too high at the target operating temperature. Weight loss was typically well below 0.4 wt%, but extensive crystallization was evident for the viscous glasses heat treated for 504 hrs at 850°C.

The alkali gallio-silicate system showed lower glass transition and softening temperatures than the alkali silicates. These glasses exhibited excellent resistance to crystallization in both bulk samples and fritted forms. Compositional adjustments with additions of ZnO and SrO have been made to decrease alkali content to 10 mol% while reducing viscosity within SOFC operating temperatures. The additions appear to increase the viscosity fragility and may allow use of the sealants at the target SOFC temperatures.

Glasses with even lower viscosity were discovered in the germanate or germano-silicate compositions. Some compositions with alkali content below 15 mol% exhibited low viscosities for operation below 900°C. These glasses exhibit much more desirable viscosity behavior with less alkali than the viscous sealants in the alkali silicate or gallio-silicate systems described above. Glass transition temperatures were below 630°C and as low as 514°C. Weight loss was typically lower than 0.5 wt%, but crystallization was apparent for the germanate and germano-silicate glasses heat treated for 504 hrs at 850°C. Compositional modifications of the germano-silicate glasses were designed to completely remove alkali and incorporate $B_2O_3$ and alkaline earths while maintaining low sealing temperatures. Five modified compositions have been melted and testing is in progress.

Examples of glasses with good and poor viscosity vs. temperature behavior are shown in Figure 1. We note here several viscosity values for reference. The viscosity of honey at room temperature is ~10 Pa-s, while the "glass softening temperature" is $10^{6.6}$ Pa-s. The viscosity

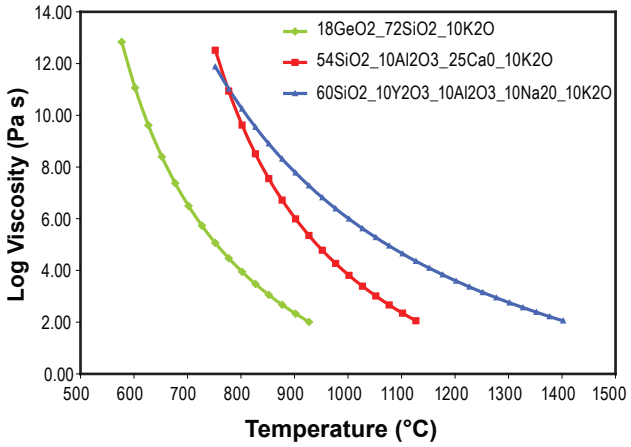


**FIGURE 1.** Approximations of Viscosity versus Temperature Behavior of Selected Glass Candidates

of roofing cement is about $10^{4.4}$ Pa-s. Therefore we note that the examples shown in Figure 1 have viscosity ranging from softer than roofing cement to just barely softening at ~850°C.

In addition to focusing in on several glass compositional regions, we have also demonstrated that several phosphate glasses, which offer excellent flow properties, are not applicable. We noted that some of the phosphates evaporate completely even after only 12 hours at 850°C in air. Therefore, we have eliminated phosphate containing glasses from the study.

## Conclusions and Future Directions

Over the first ~7 months of the project, we have identified two glass systems with promising properties. Galliosilicate glasses are candidates for glass sealants for use in SOFC operation conditions. The glasses exhibit low weight loss at SOFC operating temperatures, excellent resistance to crystallization, and glass transition temperatures that are acceptable if a bit high. Further compositional modifications should allow viscous seal operation at or below 850°C. Germanosilicate glasses exhibit softening temperatures well below 900°C and low glass transition temperatures with low alkali content. Compositional modifications should allow germanium ions to remain stable in a hydrogen atmosphere while maintaining low sealing temperatures with low alkali content.

Future glass composition work will center on statistical compositional design and iterative improvement in the glass properties. Studies of the interactions between the candidate sealants and $Al_2O_3$ and 8YSZ substrates has begun, however, extensive additional testing is needed. The benefits of additions of $Al_2O_3$ or 8YSZ ceramic fibers will also be assessed as the project progresses.

## References

**1.** S.C. Singhal and K. Kendall, High Temperature Solid Oxide Fuel Cells : Fundamentals, Design, and Applications; pp. xvi, 405 p. Elsevier, Oxford; New York, 2003.

**2.** Z. Yang, J.W. Stevenson, and K.D. Meinhardt, "Chemical Interactions of Barium-Calcium-Aluminosilicate-Based Sealing Glasses with Oxidation Resistant Alloys," *Solid State Ionics,* **160** [3-4] 213-25 (2003).

**3.** M. Brochu, B.D. Gauntt, R. Shah, G. Miyake, and R.E. Loehman, "Comparison between Barium and Strontium-Glass Composites for Sealing SOFCs," *Journal of the European Ceramic Society,* **26** [15] 3307-13 (2006).

**4.** A. Flugel, M.D. Dolan, A.K. Varshneya, Y. Zheng, N. Coleman, M. Hall, D. Earl, and S.T. Misture, "Development of an Improved Devitrifiable Fuel Cell Sealing Glass," *Journal of the Electrochemical Society,* **154** [6] B601-B8 (2007).

# III.D.2 Glass Composite to Coated Interconnect Seals for Long-Term Chemical Stability

Niladri Dasgupta (Primary Contact),
Bruce Butler, Erinn Sorge
Materials & Systems Research, Inc. (MSRI)
5395 West 700 South
Salt Lake City, UT 84104
Phone: (801) 706-8273
E-mail: ndasgupta@msrihome.com

DOE Project Manager: Joseph Stoffa
Phone: (304) 285-0285
E-mail: Joseph.Stoffa@netl.doe.gov

Contract Number: 85202

Phase I Start Date: June 30, 2008
Phase I End Date: March 29, 2009

### FY 2009 Objectives

- Optimize the amount of nano-MgO to be added to the Ba-Ca-Al-B silicate (BCAS) glass composition.
- Apply Nb-$LaCrO_3$ coatings on metallic interconnects.
- Test seals against leakage.
- Evaluate sealing potential of the sealant in short solid oxide fuel cell (SOFC) stacks.

### Accomplishments

- It was conclusively demonstrated that it is possible to prevent the deleterious phase hexa-celsian from forming in BCAS glass with the addition of 15 volume percent or more of nano-MgO powder.
- The coefficient of thermal expansion (CTE) of BCAS glass with 15 volume percent nano-MgO is 12.4 x $10^{-6}$/°C and remains nearly unchanged after 900 hours at 800°C.
- A niobium doped $LaCrO_3$ coating was successfully applied to the sealing area of the metallic interconnect by a technique of spraying and curing. It was established that the coating acts as an effective barrier layer against chromium migration and prevents an undesirable reaction between the metallic interconnect and glass-based seal after 675 hours at 800°C.
- Sealing gaskets of glass-MgO composites were fabricated by tape-casting.
- It was conclusively shown by helium leak testing at 800°C that the addition of MgO nanopowder to the BCAS glass significantly enhances the thermal cycling capability of the glass to metal seal.
- It was demonstrated in a five-cell anode-supported SOFC stack that the glass-MgO seals in conjunction with the niobium-doped $LaCrO_3$ coating on the interconnects performs satisfactorily even after thermal cycling.

## Introduction

SOFCs operate in the temperature range 650 to 850°C and typically function under an oxygen partial pressure gradient that develops across the electrolyte. A hermetic seal which prevents the intermingling of the cathode and anode side gases is a critical requirement for planar SOFCs as any leakage leads to reduced system performance, lower power-generation efficiency, poor fuel utilization [1,2] and accelerated degradation of the stack [2]. One popular approach for such seals is to use rigid bonded, specially tailored glass or glass ceramic compositions. The primary challenges in developing such seals are: i) maintaining proper viscosity in the glass, ii) matching the thermal expansion of the material with that of the primary cell components and stabilizing it as a function of time and temperature and iii) controlling their reactivity with metal components. An example of state-of-the-art sealing glass is a BCAS glass developed by the Pacific Northwest National Laboratory [3,4] which has a very good CTE match with other SOFC components after short-term crystallization. However the CTE reduces significantly after ageing at 750°C after 1,000 hours. The glass also reacts in contact with common metallic interconnects which results in the weakening of the seal joint. Recent attempts to remove these impediments by design of the glass composition [5,6] has met with limited success. Loehman [7] demonstrated that the flow, adhesion, thermal expansion and reactivity of borate glasses can be controlled by the selective addition of oxide nanoparticles. Similar results were reported by Nielsen et al. [8] for sodium aluminosilicate glasses using a nano-MgO filler.

Materials & Systems Research Inc. has investigated the effect of adding varying amounts of nano-MgO powder into a BCAS base-glass composition. The changes in phase development on crystallization after 48 hours at 800°C were investigated as a function of nano-MgO addition. The stability of the CTE for MgO added glass was also investigated over a duration of 900 hours at 800°C. A helium leak test was performed

on the glass-MgO seals at 800°C with thermal cycling. A Nb-$LaCrO_3$ spray coating was developed and applied as a barrier layer on the interconnect area in contact with the glass seal. A five-cell SOFC stack was operated for a short duration with glass-MgO sealing gaskets and Nb-$LaCrO_3$ coated interconnects and subjected to thermal cycling.

The addition of appropriate amounts of nano-MgO was found to prevent the formation of the undesirable hexa-celsian phase and to stabilize the CTE over 900 hours at 800°C. The thermal cycling ability of the base glass improved with nano-MgO addition. The Nb-$LaCrO_3$ coating functioned as an effective barrier layer against chromium migration and prevented an undesirable reaction between the metallic interconnect and glass-based seal after 675 hours at 800°C. The performance of the glass-MgO seal and Nb-$LaCrO_3$ coating combination performed satisfactorily in a five-cell SOFC stack even after thermal cycling. The results suggest that the sealing technology developed by MSRI significantly improves the long-term chemical and thermal stability of rigid seals thereby enabling longer duration of stable SOFC operation.

## Approach

The approach followed in this Phase I effort was to select a base glass which is widely known to be compatible with standard SOFC materials and conditions and to eliminate some of its glaring deficiencies by i) adding suitable amounts of nano-MgO and ii) applying a Nb-$LaCrO_3$ coating to part of the metallic interconnect in contact with the seal. While the nano-MgO will modify the thermal expansion of the base glass and stabilize the CTE, the Nb-$LaCrO_3$ coating will prevent chromium migration and interfacial chemical reaction. The Nb was added to the $LaCrO_3$ to make it less conductive to oxygen ions and thereby reduce the formation of oxide scales on the metal surface. Varying amounts of MgO were added and the optimum amount was determined based on wetting experiments, thermal expansion measurements and helium leak tests. The crystalline phases formed at different MgO additions were determined by X-ray diffraction (XRD). The CTE stability was established by thermal expansion measurements on bar samples heat treated at 800°C for 900 hours. The effectiveness of the Nb-$LaCrO_3$ coating in preventing chemical reaction and chromium migration was established by energy dispersive analysis by X-ray (EDAX) and scanning electron microscope (SEM) analysis. Helium leak tests using tape-cast glass-MgO gaskets established the sealing capability and thermal cycling ability of samples with MgO addition in comparison to the base glass. A short stack test was run to test the glass-MgO seals in conjunction with the Nb-$LaCrO_3$ interconnect coatings under actual operating conditions.

## Results

MSRI has demonstrated that the addition of suitable amounts of nano-MgO powder to a base BCAS glass composition can result in prevention of hexa-celsian formation and stabilizing of the CTE. Hexa-celsian progressively converts to monoclinic celsian which has a very low CTE of 2.3 x $10^{-6}$/°C thereby reducing the overall CTE of the material. Our experiments have shown that the addition of nano-MgO progressively reduces the formation of hexa-celsian until at 15 volume percent MgO it is absent. Figure 1 shows the XRD patterns for BCAS glass with additions of nano-MgO. The arrow indicates the position of the diffraction peak corresponding to hexa-celsian. Table 1 shows the comparative CTE values obtained for samples

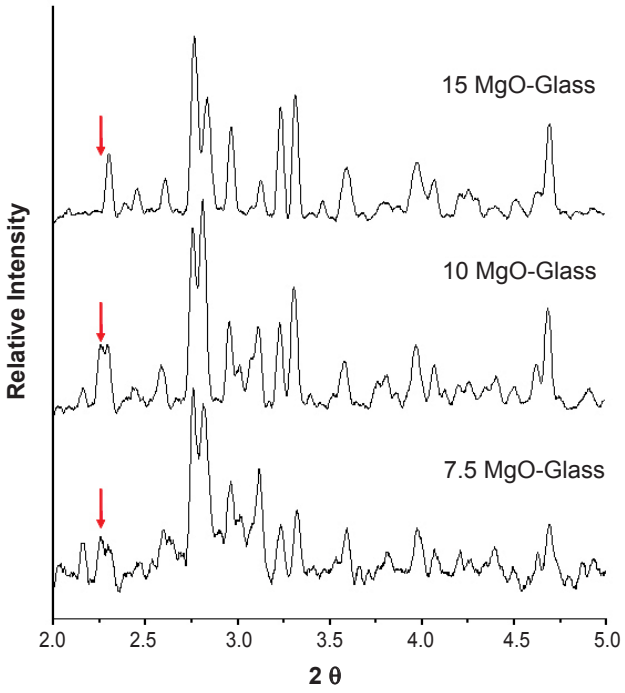


**FIGURE 1.** X-ray Diffraction Patterns for 7.5, 10 and 15 vol% MgO-Glass Compositions Held at 850°C for 30 Minutes Showing the Reduction in the Hexacelsian Phase at 15 vol% MgO

**TABLE 1.** Comparison of CTEs of Glass-MgO Compositions Crystallized for 0.5 and 900 Hours at 800°C

| Composition | Coefficient of thermal expansion (25 to 500°C) | |
|---|---|---|
| | 800°C / 0.5 hr. | 800°C / 900 hrs. |
| BCAS Glass<br>Glass + 5MgO | 11.6 x $10^{-6}$ / °C<br>10.5 x $10^{-6}$ / °C | 10.0 x $10^{-6}$ / °C<br>9.0 x $10^{-6}$ / °C |
| Glass + 10MgO | 11.5 x $10^{-6}$ / °C | 9.0 x $10^{-6}$ / °C |
| Glass + 15MgO | 12.4 x $10^{-6}$ / °C | 12.1 x $10^{-6}$ / °C |

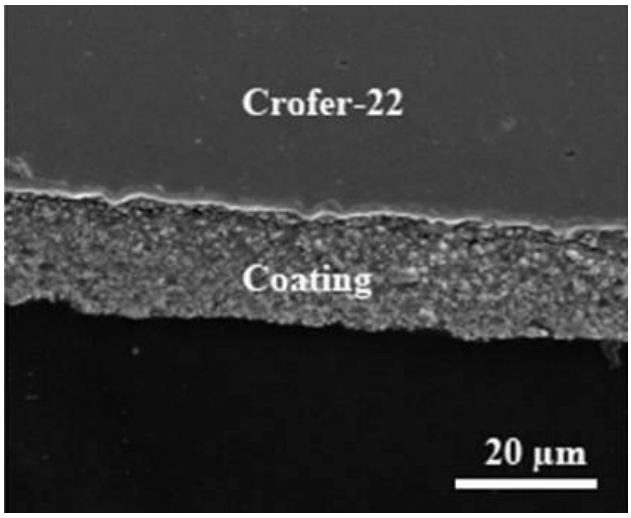


**FIGURE 2.** SEM Micrograph of Crofer-22 Metal Foil Spray-Coated with Nb-$LaCrO_3$

heat treated at 800°C for 0.5 hours and 900 hours, respectively. It is seen in the table that the CTEs for glass with 0%, 5% and 10% MgO show considerable reduction whereas it is minimal for 15% MgO.

A 20 µm coating of Nb-$Cr_2O_3$ was applied on Crofer-22 interconnect foil by a spray coating technique (Figure 2). The coating though not completely dense, prevented chromium migration from the metal into the glass and in effect prevented chemical reaction between the glass and the metal. This was determined by a combination of SEM and EDAX analysis.

The results of the helium leak test at 800°C for pure BCAS glass seals indicate that they perform very well upon initial heating, but do not survive thermal cycling. The glass with the MgO additive performed significantly better with no leak detected upon completion of three thermal cycles. The five-cell stack described earlier behaved in a manner under MSRI's high utilization and steady-state discharge tests which indicates robust sealing. The stack was run under 80/40, 60/60 and 40/40 fuel/air utilizations and discharged under constant current (0.4 A/$cm^2$) conditions for 12 hours, then thermal cycled and discharged for an additional 24 hours under the same conditions.

## Conclusions and Future Directions

Phase I results indicate that with the better long-term stability of the CTE and the right selection of the MgO-glass composition, better adherence and uniform bonding of the MgO containing glass to the interconnect will be obtained. This coupled with the superior chemically inert Nb-$LaCrO_3$ coating on the seal-interconnect interface will result in significantly improved results over BCAS glass or other state-of-the-art glass seals when subjected to long-term SOFC stack tests under thermal cycling.

In further work, MSRI will like to fine tune the composition of the base glass to permit higher additions of nano-MgO, to improve on the Nb-$LaCrO_3$ coating technique so that a dense coating can be obtained and to perform long-term thermal, chemical, mechanical and stack tests for the glass-MgO sealing compositions.

## References

**1.** T. Iwata and Y. Enami, "Analysis of Fuel Utilization Performance of Round Substrates, Planar Solid Oxide Fuel Cells," J. Electrochem. Soc., 145 (1998) 931.

**2.** J. Hartvigsen et al., Ceram. Trans., 65 (1996) 279.

**3.** Z. Yang, J.W. Stevenson and K.D. Meinhardt, "Chemical Interactions of Barium-Calcium-Aluminosilicate-Based Sealing Glasses with Oxidation Resistant Alloys," Solid State Ionics, 160 (2003) 213-225.

**4.** K.D. Meinhardt, J.D. Vienna, T.R. Armstrong and L.R. Pederson, "Glass-Ceramic Material and Method of Making," US Patent No. 6,430,966 (2002).

**5.** R.K. Brow and D.S. Reis, "Designing Sealing Glasses for Solid Oxide Fuel Cells," ASM Materials Solutions Conference and Exposition, Columbus, Ohio, October 18–20, 2004.

**6.** R.N. Singh, "Sealing Technology for Solid Oxide Fuel Cells," Int. J. Appl. Ceram. Technol., 4 (2007) 134-144.

**7.** R. Loehman, "Development of High Performance Seals for Solid Oxide Fuel Cells," SECA Core Technology Program Review, Albany, New York, October 1, 2003.

**8.** K.A. Nielsen, M. Solvang, S.B.L. Nielsen, A.R. Dinesan, D. Beeaff and P.H. Larsen, "Glass Composite Seals for SOFC Application," J. Eur. Cer. Soc., 27 (2007) 1817-1822.

# III. SECA CORE RESEARCH & DEVELOPMENT

## E. Cross-Cutting Materials and Manufacturing

# III.E.1 SOFC Research and Development in Support of SECA

Michael Krumpelt (Primary Contact),
Terry A. Cruse, Brian D. Ingram
Argonne National Laboratory
9700 S. Cass Avenue
Argonne, IL 60439
Phone: (630) 252-8520; Fax: (630) 252-4176
E-mail: krumpelt@cmt.anl.gov

DOE Project Manager: Briggs White
Phone: (304) 285-5437
E-mail: Briggs.White@netl.doe.gov

Contract Number: 49071

Start Date: October 1, 2008
End Date: September 30, 2009

### Objectives

- Explore performance and stability trade-offs in cathode materials.
- Determine work functions of cathode materials.
- Explore seals with high temperature elasticity.

### Accomplishments

- Electronic conductivities and charge transfer resistances were determined for several new manganites and ferrites.
- Improved performance of lanthanum manganite was shown by partially substituting with iron, zinc, or chromium.
- Aluminum, chrome, nickel and zinc were shown to improve the performance of ferrites.
- The stress/strain behavior of a new seal concept has been determined and resilience has been demonstrated.

## Introduction

The economics and durability of solid oxide fuel cells (SOFCs) can be improved by higher power densities of cathodes and more resilience of the seals. The most proven cathode material is the strontium doped lanthanum manganite, but it works best at temperatures near 1,000°C, which are too high for planar cell configurations. Mixed ferrite/cobaltites have higher power densities, but are less durable. In this activity, the fundamentals and trade-offs of cathode performance are explored.

Similarly, currently used seals have limited durability because they cannot conform to changing cell dimensions. To remedy the problem a new concept of engineering resilience into the glass seals is being explored.

## Approach

The performance of SOFC cathodes is determined by many factors: electrical and ionic conductivities, charge transfer, surface area and morphology, etc. Here we attempt to find new compositions that have low work functions and good ionic and electronic conductivities. Work functions will be determined by X-ray photoelectron spectroscopy (XPS), electronic conductivity by 4-probe impedance measurement, charge carrier concentration from Seebeck coefficients, and electrochemical characterization by measuring the area specific resistance (ASR). Compositions are selected by elements with multiple valence states and thermodynamic stability of the oxides.

To engineer resilience into the glassy seals, a structural ceramic component is added to the glass with a compressible core, analogous to a steel reinforced tire.

## Results

The standard cathode material, $La_{.8}Sr_{.2}MnO_3$ (LSM), was modified by substituting some of the manganese with either aluminum, iron, chromium, or zinc. The electronic conductivity of the parent compound and of the four modified materials increased with temperature as expected for semiconductors, but the Seebeck coefficients decreased, indicating that the charge carrier concentration decreased also. A conceivable explanation is that "charge compensation mechanism" controlling the ratio of $Mn^{4+}/Mn^{3+}$ decreases with temperature.

The ASR for the same materials is plotted in Figure 1 as a function of the concentration of the substitute elements. Addition of aluminum, chromium and iron decreased the ASR but zinc had the opposite effect. There appears to be a minimum at 17% substitution. Since all of these compounds crystallize in the form of perovskites, the minimum at 17% signifies that one of the six neighbors of every manganese is replaced by a substitute element. Apparently, the substitute elements affect the Jahn-Teller distortion of the manganese.

Lanthanum ferrites of the general composition $La_{.8}Sr_{.2}FeO_3$ (LSF) are known to be better cathodes than

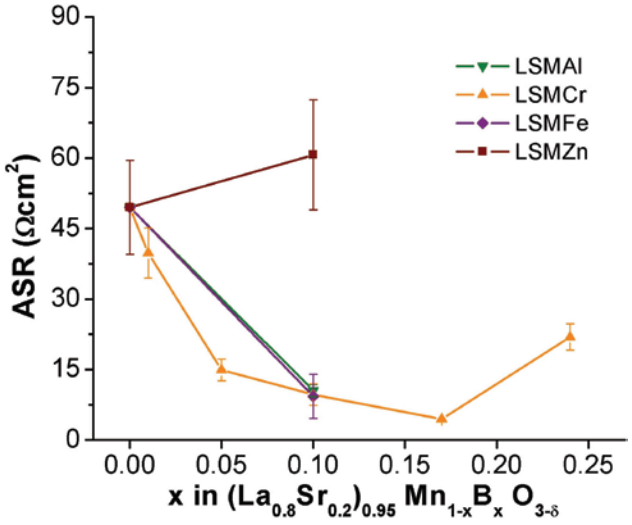


**FIGURE 1.** Area Specific Resistances of Modified LSM

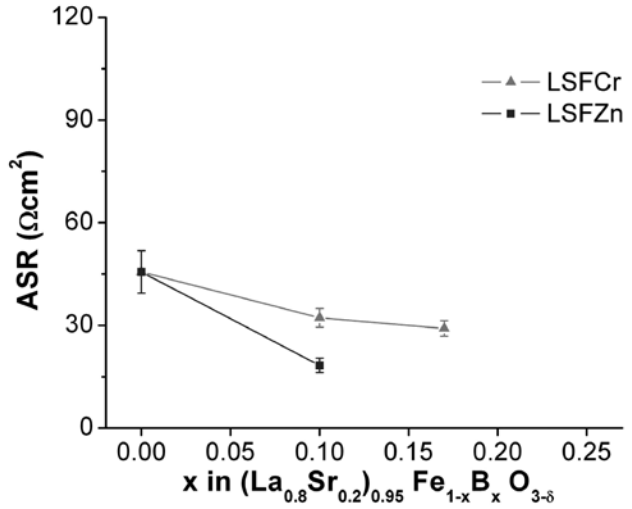


**FIGURE 2.** Area Specific Resistances of Modified LSF

the manganites but are also less stable. Substitution of some of the iron with nickel decreases the ASR further as shown in Figure 2, but longer term testing of the substituted materials revealed a not unexpected reactivity with the zirconia electrolyte. Substitution with zinc is beneficial too and more stable.

To further correlate the electrochemical performance of the cathode compositions, efforts are underway to measure the work functions using XPS. An existing spectrometer had to be modified for the planned activities and will soon be available.

Our novel seal design consists of a "Swiss role" made of a glass and a ceramic with a hollow core, as shown in Figure 3. To test the compressibility, seals with different hollow core diameters were mechanically

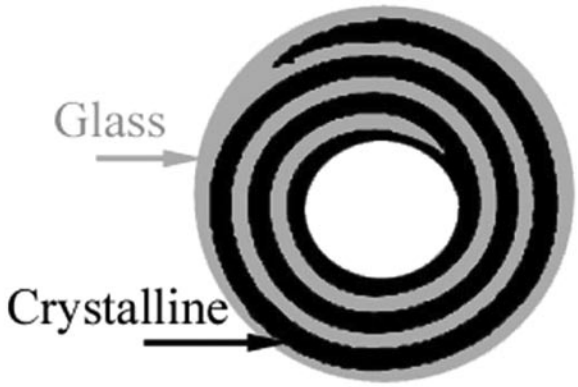


**FIGURE 3.** Conceptual Seal Geometry

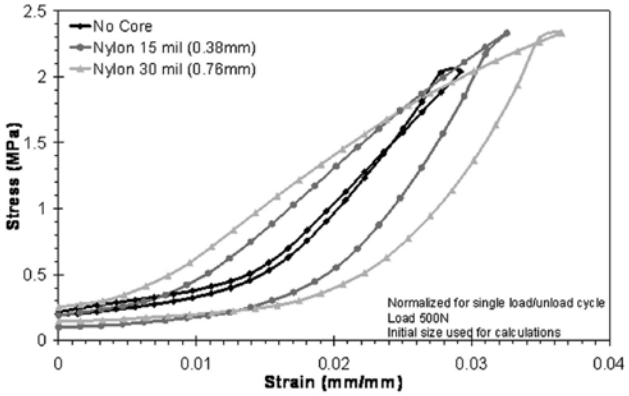


**FIGURE 4.** Stress/Strain Relation of a Swiss Role Glass/Ceramic Seal

tested at elevated temperature. Mechanical cycling demonstrated that this seal design can withstand elastic deformations of at least 3% as shown in Figure 4. Depending on the type of glass, this new seal concept can be tailored to different ranges of temperature and can be self-healing.

## Conclusions and Future Directions

It is apparent that the performance of the manganite cathodes is not limited by charge carrier concentrations but by the charge compensation mechanism of the manganese. Substitution of certain transition elements seems to affect this mechanism.

Replacing the cobalt in lanthanum ferrites with nickel or zinc has been shown to yield good ASRs. The cobalt substituted ferrite is known to require a ceria interlayer between cathode and electrolyte to prevent formation of a resistive layer. In the present work, no such layer was used and one of the materials was stable but the nickel-based one was not. To address this issue, the stoichiometry will be changed to improve the thermodynamic stability.

Efforts to measure the work functions of cathodes have just begun and will continue.

The new seal concept has been demonstrated to possess the anticipated spring-back characteristics. More work is needed to identify glass compositions that have the right glass transition temperatures and viscosity. Actual seal tests will begin shortly. If successful, transfer of this promising technology to the industrial teams will be initiated.

## FY 2009 Presentations

**1.** B.J. Ingram, T.A. Cruse, and M. Krumpelt, "Bulk and Surface Electronic Properties of B-site Substituted LSM Cathodes for SOFC Applications," American Ceramic Soc. 32nd International Conference, Daytona, 2009.

**2.** T.A. Cruse, S. Wang, G. Chen, B.J. Ingram, P.A. Salvador, and M. Krumpelt, "Examination of Chromium's Effects on a LSM/YSZ Solid Oxide Fuel Cell Cathode," American Ceramic Society 32nd International Conference & Exposition on Advanced Ceramics and Composites, 2008.

**3.** S. Wang, P.A. Salvador, T.A. Cruse, and M. Krumpelt, "Investigation of Chromium Contamination in SOFC Cathodes Using Transmission Electron Microscopy," American Ceramic Society 32nd International Conference & Exposition on Advanced Ceramics and Composites, 2008.

**4.** T.A. Cruse, M. Krumpelt, B.J. Ingram, G. Chen, S. Wang, P.A. Salvador, "Effects of Cell Operating Conditions on Degradation by Chromium," TMS 1327th Annual Meeting & Exhibition, 2008.

# III.E.2 Reliability and Durability of Materials and Components for Solid Oxide Fuel Cells

Edgar Lara-Curzio (Primary Contact), Yanli Wang, Rosa Trejo, Amit Shyam, Jianming Bai, Tom Watkins, Wallace Porter
Oak Ridge National Laboratory
1 Bethel Valley Rd.
Oak Ridge, TN 37831-6062
Phone: (865) 574-1749; Fax: (865) 574-4913
E-mail: laracurzioe@ornl.gov

DOE Project Manager: Travis Shultz
Phone: (304) 285-1370
E-mail: Travis.Shultz@netl.doe.gov

Contract Number: FEAA066

Start Date: October 1, 2008
End Date: September 30, 2009

### FY 2009 Objectives

- Support the Solid State Energy Conversional Alliance (SECA) industrial teams in the development of reliable and durable solid oxide fuel cells (SOFCs).
- Support the SECA Core Technology Program (CTP) modeling efforts by establishing material property databases.
- Establish failure criteria for SOFC materials and components.
- Characterize and develop sealing concepts.

### Accomplishments

- Used in situ synchrotron X-ray diffraction (XRD) to monitor phase evolution of the oxide scale on ferritic stainless steel interconnects.
- Evaluated in situ the growth stresses and residual stresses developed in the oxide scale of ferritic stainless steel interconnects.
- Successfully characterized the microstructural changes in glass seals after 865 hours of aging at 800°C in air and in a gas mixture of steam+$H_2$+$N_2$.

## Introduction

Growth and residual stresses are often responsible for the delamination of the oxide scale that forms on metallic interconnects when these are subjected to thermal cycling. This report presents results from experiments designed to monitor the growth of the oxide scale as well as the growth stresses and residual stresses associated with the oxidation of 441 stainless steel (AL441). These findings will support ongoing efforts to develop models to predict the service life of SOFCs and provide critical information to ensure the design of durable and reliable SOFCs.

Another key aspect of SOFC design is sealing. Seal materials must be capable of a service life of more than 40,000 hours in a high temperature reactive environment (moist reducing and/or oxidizing conditions) while in contact with other cell and interconnect materials.

During the reporting period a methodology was established to expose glasses to relevant SOFC environments to assess the effects of temperature and time of exposure on their chemical composition, microstructure and physical and mechanical properties.

Results are presented from the characterization of a barium alkali silicate glass[1] after aging in air or under a gas mixture of steam+$H_2$+$N_2$ at 800°C. The wetting and chemical interaction of the glass with 8 mol% yttria-stabilized zirconia (8YSZ) and alumina was also investigated. The results from this study are providing insight into the mechanisms responsible for the degradation of glass seal and in turn, strategies to overcome these limitations.

## Approach

Test specimens were prepared from AL441 sheets for in situ oxide growth and residual stress measurements. Synchrotron XRD techniques were used to perform the measurements. The high intensity of the monochromatic synchrotron X-ray beam (~$10^{12}$ photons/s) allows the detection of minor phases. In addition, the state of residual stresses in the oxide scale of two test specimens with different surface roughness that had been pre-oxidized at 800°C for 600 hours[2] was determined between room temperature and 800°C.

Digital videography, XRD, scanning electron microscopy (SEM), differential scanning calorimetry (DSC), thermomechanical analyses (TMA), resonant ultrasound spectroscopy (RUS), neutron activation analysis (NAA), and inductively-coupled plasma (ICP) were utilized to characterize the microstructure,

[1] SCN-1, SEM-COM Company, Toledo, OH 43623
[2] Test specimens provided by the SECA-CTP team at Pacific Northwest National Laboratory

**TABLE 1.** Glass Chemical Composition Measured by ICP-OES and NAA (wt%)

| | Al | B | Ca | Fe | K | Mg | Na | Ti | Zn | Zr | Li | B |
|---|---|---|---|---|---|---|---|---|---|---|---|---|
| ICP-OES | 1.43 | 7.08 | 2.29 | 0.15 | 7.97 | 0.36 | 5.19 | 0.31 | 0.01 | 0.01 | 0.01 | 0.01 |
| NAA | 2.21 ±0.30 | 7.16 ±0.60 | 1.94 | — | 6.86 ±0.52 | 0.68 ±0.15 | 5.71 ±0.72 | — | — | — | — | — |

composition and physical and mechanical properties of glasses. Exposure tests were performed in a tubular furnace with environmental control in air or gas mixture of steam+$H_2$+$N_2$ at 800°C. The study includes chemical composition analysis using ICP-optical emission spectroscopy (OES) and NAA (Table 1), contact angle measurement at 850°C, glass transition temperature evaluation using DSC and TMA, elastic modulus evaluation using RUS, thermal expansion behavior using TMA, phase identification using XRD and microstructural analysis using SEM. All tests were performed on 8YSZ and alumina substrates.

## Results

### Part I. Growth of Oxide Scale on AL441 and the Residual Stresses

At 800°C a layer of chromium oxide (chromia) appeared within ~10 minutes upon exposure of the 441 stainless steel test specimens to air. Additional Bragg peaks associated with the formation of manganese chromite appeared after approximately 2 hours of exposure (Figure 1). Previous characterization of these oxide scales revealed that they have a layered structure with a layer of manganese chromite on top of chromia layer [1]. When the manganese chromite outer layer forms, the diffusion of oxygen needed to grow the inner chromia phase is limited, and therefore its growth is slowed. Similarly the growth of the manganese chromite phase requires the diffusion of Mn and Cr atoms through the chromia layer. These arguments are consistent with the parabolic growth mechanism suggested by Galerie et al. [2].

The growth stresses in chromia, determined in situ by XRD techniques, were found to be compressive at the beginning of the oxidation process and then became slightly tensile after ~1,000 minutes of exposure to air. The stresses leveled at ~0.06 GPa after 48 hours of exposure (Figure 2a). The compressive residual stress

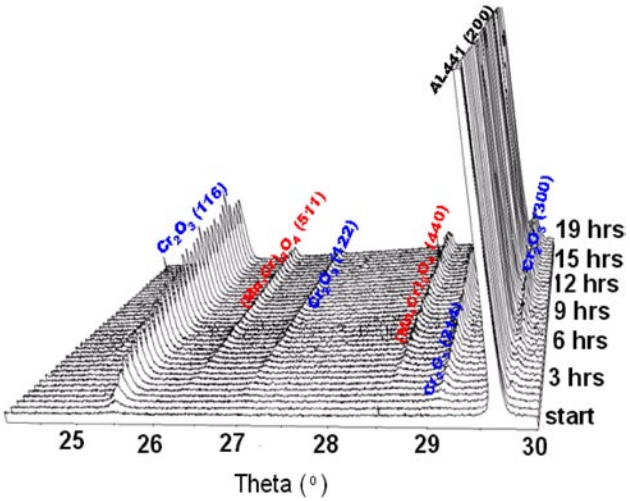


**FIGURE 1.** In Situ Synchrotron XRD Spectra of the Oxide Scale on AL441 at 800°C

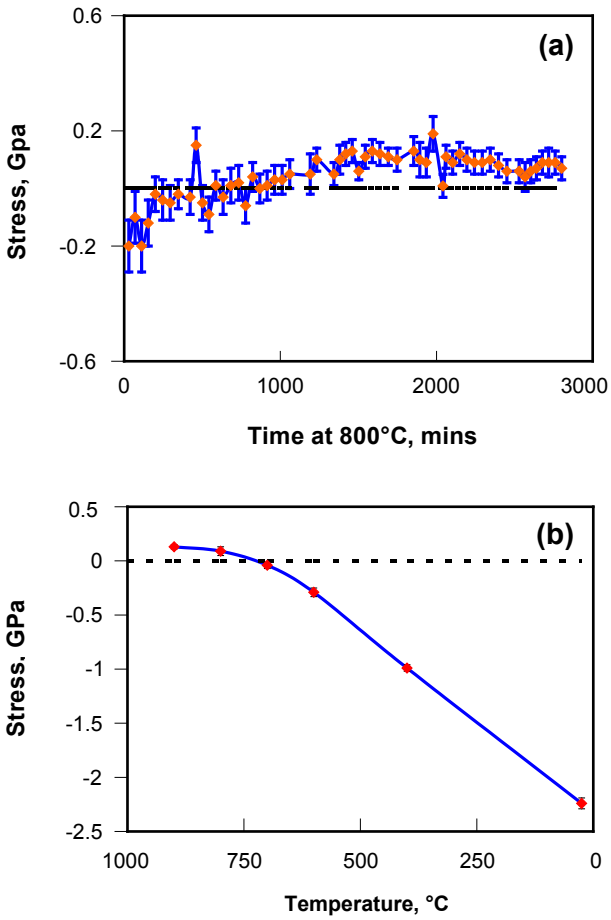


**FIGURE 2.** In Situ Stress Measurements in the Chromia for AL441 with (a) the Growth Stresses at 800°C and (b) Residual Stresses in the Chromia Layer during Cooling

in the chromia layer increased in magnitude linearly as temperature decreased (Figure 2b).

The residual stress in the chromia layer of test specimen PRE-C (with smoother metal surface) was equibiaxial with a magnitude of -1.78±0.04 GPa, whereas the residual stress in the chromia layer of test specimen PRE-D (with rougher metal surface) was -1.53±0.09 GPa (Table 2). After the room temperature measurements, these two pre-oxidized test specimens were heated up in air at a rate of 10°C/min up to 800°C and held at 800°C for 10 hours. At 800°C, the stresses for both samples became tensile. Upon cooling to room temperature, the residual stress in the chromia layer of test specimen PRE-C was found to recover but with a slight drop in magnitude. However, the residual stress in the chromia layer of test specimen PRE-D was found to be completely relaxed after the thermal cycle. These results suggest that finer surface finish results in oxide scale with smaller residual stresses and improved adhesion of the oxide scale to the metal substrate.

**TABLE 2.** Summary of Residual Stress Measurements for Pre-Oxidized Test Specimens

| Sample ID | Substrate surface roughness, $R_a$, $\mu$m | As–oxidized, GPa | At the end of 10 hours holding at 800°C, GPa | After cooling down to RT, GPa |
|---|---|---|---|---|
| PRE-C | 0.08 | -1.78±0.04 | 0.10±0.02 | -1.69±0.04 |
| PRE-D | 0.63 | -1.53±0.09 | 0.07±0.03 | 0.09±0.04 |

RT – room temperature

## Part II. Characterization of Barium Alkali Silicate Glass

DSC was used to determine the glass transition temperature of as-received glass powders. DSC tests were performed following the procedures outlined in ASTM test method E1356 [3]. The programmed heating and cooling rate was 20°C/min. The average glass transition temperature (represented by the mid point) was found to be 533°C. These results are summarized in Table 3.

**TABLE 3.** Glass Transition Temperature (°C) Analyzed by DSC

| Cycle | Onset | Midpoint | Inflection | End |
|---|---|---|---|---|
| Heating 1 | 513.8 | 535.1 | 548.7 | 556.4 |
| Cooling 1 | 493.6 | 529.2 | 546.8 | 564.9 |
| Heating 2 | 525.7 | 539.8 | 550.5 | 553.9 |
| Cooling 2 | 464.7 | 509.3 | 522.5 | 553.9 |
| Average | 499.5 ±26.7 | 528.4 ±13.4 | 542.1 ±13.2 | 557.3 ±5.2 |

The thermal expansion coefficient and the glass transition temperature were determined by TMA. The tests were performed with three different levels of applied compressive contact load, i.e., 0.1 N, 0.05 N and 0.01 N. The linear coefficient of thermal expansion for as-sintered test specimens was found to be between 9.4 and 11 ppm/K for the temperature range between 100°C and 400°C. It was also found that the amount and rate of axial contraction (with the consequent lateral expansion) for temperatures greater than the glass transition temperature increased with increasing axial load. The glass transition temperature (represented by the onset temperature) determined by TMA was found to be in the range between 468°C and 494°C. The changes of the glass transition temperature were insignificant after aging 856 hours in air or steam+$H_2$+$N_2$.

Morphological changes of glass beads were obtained using digital imaging techniques as a function of time while sintering at 850°C on alumina and 8YSZ substrates. Values of contact angles were determined by analyzing digital images of the glass bead. The glass was found to flow, due in part to gravitational forces (assuming the surface energy of the substrate-glass bead interface and the glass itself do not change as a function of time), resulting in a decrease in the magnitude of the contact angle as illustrated by the results in Figure 3. The contact angle decreased from an average of ~92° to ~25° after 168 hours without reaching an asymptotic value.

The elastic properties of the glass were determined as a function of temperature using RUS. The elastic modulus was found to be 51.9±0.06 GPa at room temperature. The elastic modulus decreased as temperature increased and finally reached 49.8±0.08 GPa at 400°C.

For the as-sintered and the aged test specimens, all the glass beads remained attached to the 8YSZ substrate, whereas all the glass beads on alumina substrate

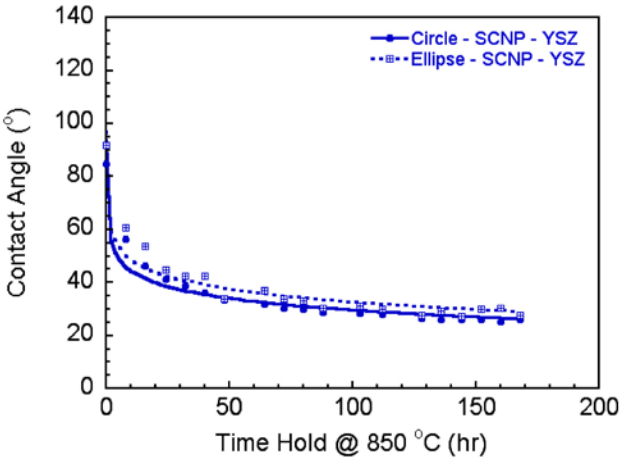


**FIGURE 3.** Evolution of Contact Angle of Glass on 8YSZ Substrate at 850°C in Air

became detached except one that had been exposed for 850 hours in air. The coefficient of thermal expansion mismatch between the glass and the substrates are responsible for the detachment. The as-sintered glass was found to be amorphous. However, after aging 100 hours in air or in the steam+$H_2$+$N_2$ gas mixture, crystalline phases were formed (shown from the cross-section images in Figure 4 for aging in air and Figure 5 for aging in gas mixture). The concentration of the crystalline phase, $KAlSi_3O_8$, which was identified by XRD, was found to increase with increasing aging time. The glass exhibited chemical interaction with the alumina substrate, forming an interfacial phase (Figures 4 and 5), and this phase was also found to be $KAlSi_3O_8$. No interfacial phases were found between the glass and the 8YSZ substrate. The difference in the microstructure between the two aging environment was insignificant.

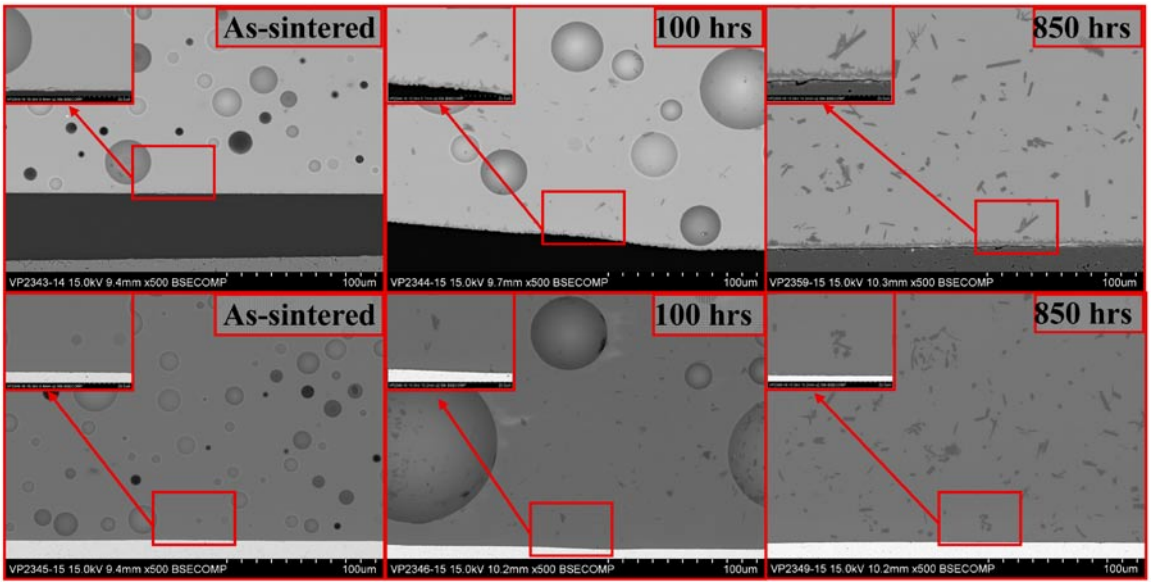


**FIGURE 4.** Cross-section scanning electron micrographs of glass test specimens after exposure to air. Top row for alumina substrate and bottom row for 8YSZ substrate.

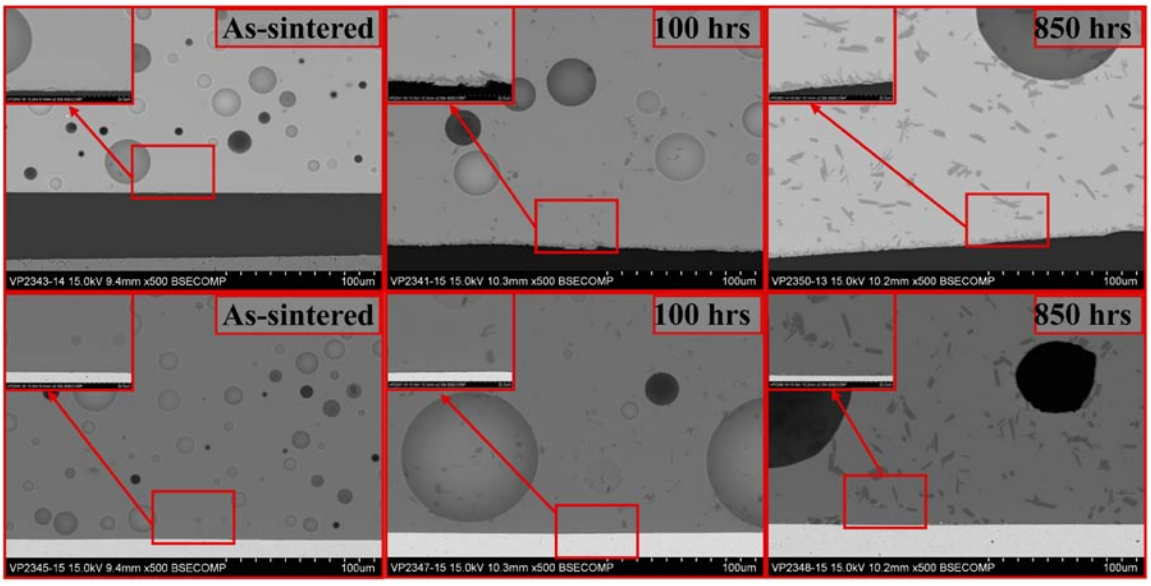


**FIGURE 5.** Cross-section scanning electron micrographs of glass test specimens after exposure to steam+$H_2$+$N_2$. Top row for alumina substrate and bottom row for 8YSZ substrate.

## Conclusions and Future Directions

Chromia was formed on AL441 within 10 minutes and manganese chromite started to form after 2 hours of exposure in air at 800°C. In situ growth stresses in the chromia layer were successfully measured and found to be initially compressive and became tensile as oxidation progressed. Upon cooling down to room temperature residual stresses become compressive. The residual stress at room temperature was caused by the thermal expansion mismatch between the oxide scale and the metal substrate. After one thermal cycle, the residual stresses for the sample with rougher initial surface finish dropped to near zero, but appeared to be reversible for the sample with finer surface finish. The stress relaxation is associated with oxide scale delamination. Work is in progress to compare these results when a $Mn_{1.5}Co_{1.5}O_4$ protective coating layer is applied onto the metal substrate prior to oxidation.

A barium alkali silicate glass was characterized using various advanced characterization techniques. It was found that the crystalline phase $KAlSi_3O_8$ was formed in the glass after aging in air or in a gas mixture of steam+$H_2$+$N_2$, and that the concentration of the crystalline phase increased with aging time. The glass was found to interact with alumina substrate but it did not interact with the 8YSZ substrate. The effect of longer aging time (tens of thousands of hours), on microstructure, glass transition temperature and chemical composition is being investigated.

## FY 2009 Publications/Presentations

**1.** Quarterly Report for 1st quarter fiscal year 2009, January 2009.

**2.** Y. Wang, B. Armstrong, R. Trejo, J. Bai, T. Watkins, and E. Lara-Curzio, "Mechanical Properties of Cathode-Interconnect Interfaces in Planar SOFCs," ICACC, 2009.

**3.** Quarterly Report for 2nd quarter fiscal year 2009, April 2009.

**4.** "Characterization of a Barium Silicate Glass," ORNL Technical Report TM-SECA-02-09.

## References

**1.** DOE Office of Fossil Energy Fuel Cell Program Annual Report for fiscal year 2008, July 2008.

**2.** A. Galerie, F. Toscan, M. Dupeux, J. Mougin, G. Lucazeau, C. Valot, A.-M. Huntz, and L. Antoni, Materials Research, 7(1)2004, 81-88.

**3.** ASTM E 1356-08, Standard Test Method for Assignment of the Glass Transition Temperatures by Differential Scanning Calorimetry, ASTM International, West Conshohocken 19428-2959.

# III.E.3 Development and Implementation of Stack Fixture Tests

Yeong-Shyung "Matt" Chou (Primary Contact), Jung-Pyung Choi, Jeff Stevenson
Pacific Northwest National Laboratory (PNNL)
K2-44, P.O. Box 999
Richland, WA 99354
Phone: (509) 943-5233; Fax: (509) 375-2186
E-mail: yeong-shyung.chou@pnl.gov

DOE Project Manager: Briggs White
Phone: (304) 285-5437
E-mail: Briggs.White@netl.doe.gov

Contract Number: 40552

Start Date: October 1, 2008
End Date: September 30, 2009

### Objectives

- Develop a solid oxide fuel cell (SOFC) stack test fixture for use by PNNL and other Solid State Energy Conversion Alliance (SECA) Core Technology Program (CTP) participants.
- Implement the test fixture in evaluation/validation of new materials, processes, and design concepts developed by PNNL and other SECA CTP participants.

### Accomplishments

- Optimized 1st generation stack test fixture on behalf of SECA CTP.
- Evaluated performance of refractory glass seals and protective interconnect coatings in stack fixture tests.

## Introduction

PNNL and other SECA CTP participants use a wide range of materials characterization techniques (X-ray diffraction [XRD], scanning electron microscopy [SEM], energy dispersive spectroscopy [EDS], transmission electron microscopy, X-ray photoelectron spectroscopy [XPS], thermal gravimetric analysis, differential scanning calorimetry, particle size analysis, electrical conductivity, single and dual atmosphere oxidation, etc.) and sub-stack multiple component tests (e.g., "button" cell testing, area specific resistance testing of interconnect/cathode/cathode structures, and leak testing of cell/seal/interconnect structures) to evaluate the performance of newly developed materials, fabrication processes, and design concepts. In recent years, PNNL has developed and implemented a "stack" test fixture intended to evaluate/validate cell and stack component performance under realistic stack conditions. It is anticipated that results from these stack fixture tests will help to bridge the gap between typical CTP tests and the full-scale cells and stacks under development by the SECA industrial teams, and thus facilitate technology transfer from the CTP to those teams.

## Approach

The test fixture, which is based on a 50 mm x 50 mm cell, includes a cell frame component as well as anode and cathode plates simulating the anode and cathode faces of an SOFC interconnect. As a result, the fixture allows for the simultaneous testing of cell-to-frame and stack perimeter seals, anode and cathode contact materials, interconnect materials (including coatings), and cell constituents (cathode, electrolyte, anode). Most components of the modified test fixture (cell frames, anode and cathode plates, contact pastes, and seals) are fabricated at PNNL. Stack fixtures are assembled and then sealed and tested in test stands consisting of a furnace, heat exchangers, gas handling system with mass flow controllers, and electrical characterization units. Electrochemical performance of the cells is measured under isothermal and/or thermal cyclic conditions. Once the tests are complete, the fixtures are disassembled and their components are analyzed by appropriate characterization techniques such as optical and electron microscopy, EDS, XRD, XPS, etc. Results from the tests are compared to results obtained from testing of individual components and sub-stack structures to assess intrinsic stability and inter-component reactions, and their effects on performance under stack operating conditions.

## Results

The fixture design approach has been iterative in nature, with results from previous fixture tests helping to identify further design changes required to optimize fixture performance. The 1st generation fixture went through several modifications leading up to a final design designated as Version 3 (Gen1.V3). Computer-aided design drawings of the steel components of the Gen1.V3 fixture are shown schematically in Figure 1.

The Gen1.V3 fixture was used for evaluation of candidate coatings, i.e., aluminization and Ce-modified MnCo spinel coatings on AISI441 steel parts at 800ºC. These tests used a double-seal concept (with refractory sealing glass and hybrid mica seals adjacent

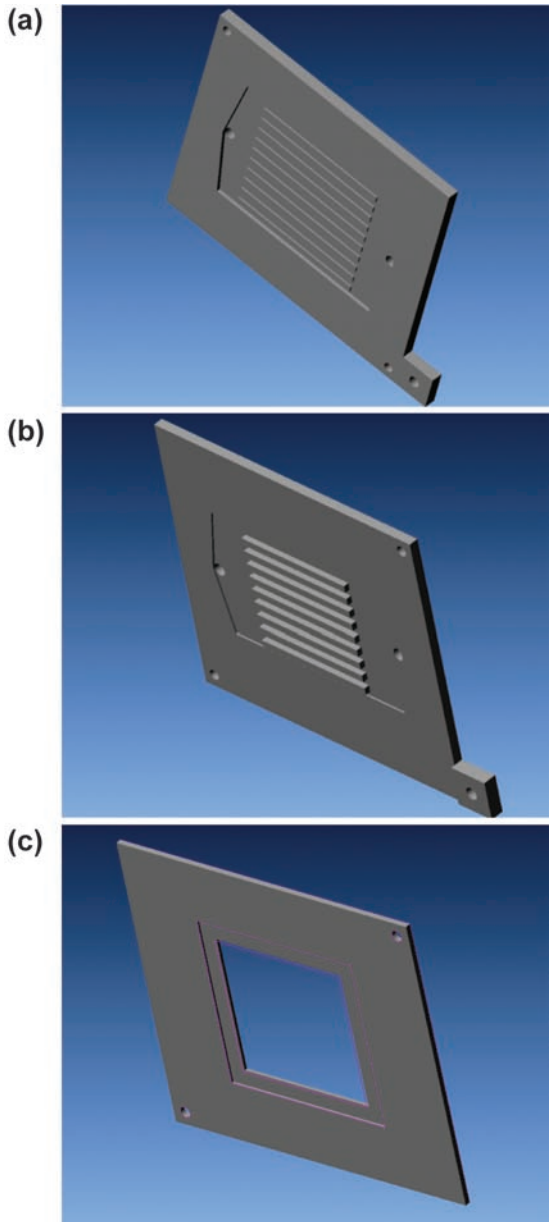


**FIGURE 1.** 1st Generation,Version 3 Single-Cell Stack Test Fixture Components: (a) Anode Interconnect Plate, (b) Cathode Interconnect Plate and (c) Cell Frame Plate

to each other) for the perimeter seals, and refractory sealing glass for the cell-to-frame seals. The cell was a commercial Ni/yttria-stabilized zirconia (YSZ) anode-supported cell with Sr-doped lanthanum manganite (LSM)/YSZ cathode (H.C. Starck, type ASC-3). LSM was the cathode side contact material, and Ni mesh and NiO contact paste were the anode side contact materials. The electrochemical performance in terms of power density vs. time for one of these tests (#24) is shown in Figure 2. Another duplicate test (cell test #26) exhibited similar performance and stability.

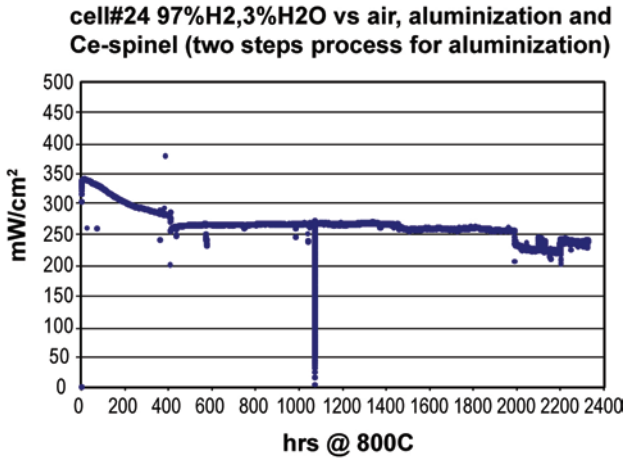


**FIGURE 2.** Stability Test of Cell #24 at 800°C and 0.7 V Using 97% $H_2$, 3% $H_2O$ vs. Air

Cell test #24 exhibited an initial open circuit voltage (OCV) of 1.095 V at 800°C using 97% $H_2$/3% $H_2O$ vs. air. During operation at 0.7 V, the cell showed a typical conditioning behavior, with power density increasing from ~303 mW/cm$^2$ (t=0 hr) to ~340 mW/cm$^2$ (t~7 hr). The cell performance then decreased rapidly during the first ~200 hr, and more slowly during the following ~200 hr. At t ~400 hr, the cell was accidentally shorted electrically, which resulted in a sudden drop in power density. The cell exhibited almost no degradation for the following ~1,000 hr. The cell was then cooled down to ~200°C to refill the water in the room temperature gas humidifier, and then heated back up to 800°C and tested again at 0.7 V. There was a small loss of power after this thermal cycle. The test was then continued till t=2,325 hr, at which point the OCV was ~1.0 V. At t=~2,000 to ~2,200 hr, there was a grounding problem which caused large fluctuations in the data. The impedance spectrum was also recorded at different time intervals, showing results consistent with the power versus time plots. The ohmic part showed almost identical values over the time tested, suggesting the Ce-spinel coating was effective in minimizing oxide scale growth. During post-test analysis, the cause of the reduction in OCV (to ~1.0 V) was determined to be the result of a failure of the welded joint of the ¼" Inconel600 tubing and the Inconel600 fuel heat-exchanger. This conclusion is also consistent with the visual observation of the cell-to-frame seal (Figure 3). Close inspection of the sealing area showed a homogeneous whitish color, suggesting hermetic sealing, which should lead to high OCV. In previous cell tests, a brownish color was sometimes observed at localized seal leakage sites, where increased local oxygen partial pressure had caused the AISI441 to oxidize.

One of the goals of cell test #24 was to evaluate the stability of two protective interconnect coatings,

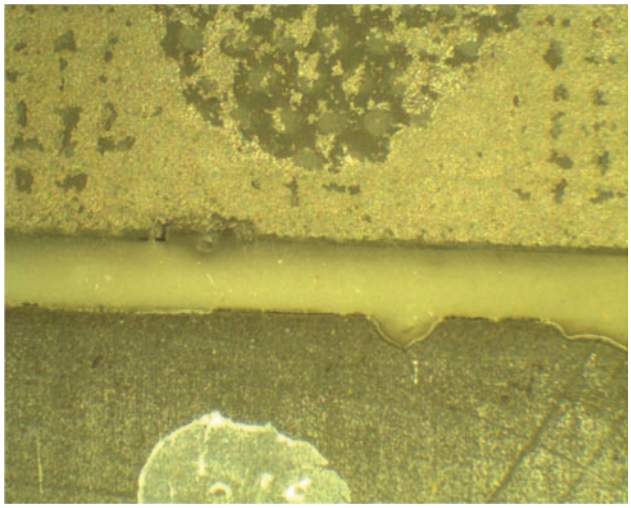

**FIGURE 3.** Post-Test Analysis of Cell #24 after 2,325 hr Testing at 800°C and 0.7 V: Sealing Area of the Cell-to-Frame Assembly

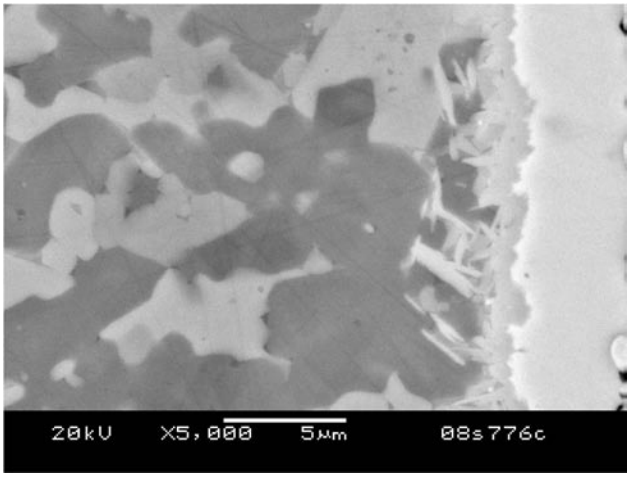


**FIGURE 4.** SEM Image of Sealing Glass/YSZ Electrolyte Interfacial Microstructure (near Fuel Side)

i.e., aluminization at the sealing areas, and Ce-modified spinel coating on exposed surfaces. Both coatings were intended to minimize the diffusion and volatilization of Cr from the AISI441 interconnect plates. The characterization of Cr stabilization was first conducted at the cathode outer surface. Area chemical analysis by SEM/EDS showed no substantial difference between two randomly selected locations, and no Cr was detected either in the area scans or in spot scans. In addition to the top surface, a cross-section was also examined to characterize/identify Cr though the whole cathode thickness. Again, no Cr was detected across the cathode thickness, although it should be noted that EDS is not particularly sensitive to small elemental concentrations. Examinations for Cr were also conducted near the Ce-modified spinel-coated AISI441. A small amount of Cr (~0.9%) was detected within the dense spinel coating and near the coating/LSM interface. Away from the interface, no Cr was detected in the contact material, suggesting that the Ce-modified spinel coating was effective in mitigating Cr diffusion from the AISI441 interconnect into the cathode.

The refractory glass/aluminized AISI441 and refractory glass/YSZ electrolyte interfaces of cell test #24 were also characterized. In previous glass seal development work, the refractory sealing glass showed minimal change in phase assemblage and coefficient of thermal expansion (CTE) after 1,000 hr of ageing in air or reducing environment. Testing of the glass in cell test #24 for 2,325 hr provided an opportunity to investigate the seal behavior for a longer period of time under realistic stack conditions. Some reaction between YSZ and the refractory sealing glass was apparent, as shown in Figure 4; note the fine "needles" formed along the interface near the fuel side of the seal. The glass/YSZ interface near the air side of the seal showed no such features. SEM/EDS analysis indicated that the needle-like particles contained an appreciable amount of Zr, indicating reaction of the glass with the YSZ electrolyte, likely during the initial cell-to-frame sealing process. Note that the cell was sealed into the cell frame at 950°C for 2 hr prior to the final fixture assembly heat treatment (930°C for 2 hr). Note that the presence of Zr-rich needles was limited to the glass/YSZ interfacial region. The high concentration of Zr suggests the formation of $BaZrO_3$ or $SrZrO_3$,which is thermodynamically favored to form at 950°C from $ZrO_2$ and BaO or SrO.

Regarding the chemical compatibility of the sealing glass with aluminized AISI441, no evidence of $SrCrO_4$ formation was observed at the glass/aluminized metal interface. For uncoated ferritic stainless steel, $BaCrO_4$ or $SrCrO_4$ is often observed at the glass/metal interface, which can greatly degrade the mechanical strength due to its very large CTE mismatch. A Cr-rich band of 6-8 microns thickness was observed at the interface, but no $BaCrO_4$ or $SrCrO_4$ grains were observed. Outside this Cr-rich band, a typical devitrified glass microstructure was observed, although it was also apparent that some Al had diffused into the glass to a depth of ~20 microns.

## Conclusions and Future Directions

Design modifications to the CTP stack test fixture led to improved performance and stability. Stack fixture tests indicated satisfactory performance of refractory glass seals, aluminization of steel interconnects, and spinel coatings on steel interconnects. Future directions will include modification and optimization of a second generation fixture based on thinner steel stock than was used for the first generation fixture, and continued evaluation/validation of new materials, processes, and design concepts developed by PNNL and other participants in the SECA CTP.

## FY 2009 Publications/Presentations

**1.** Y.S. Chou, J.D. Templeton, G.D. Maupin, J.P. Choi, J.W. Stevenson, and P. Singh, "Novel Concept of "Double Seal" for Planar Solid Oxide Fuel Cell Stacks," 33rd International Conference on Advanced Ceramics and Composites, Daytona Beach, Florida, January 18–23, 2009.

**2.** Y.S. Chou, J.W. Stevenson, G.G. Xia, J.D. Templeton, G.D. Maupin, J.W. Templeton, P. Singh, and X.D. Zhou, "SOFC Materials Evaluation in a Standard Stack Test Fixture," MS&T 2008 Conference & Exhibition, Pittsburgh, Pennsylvania, October 6–9, 2008.

# III.E.4 Novel Low Temperature Solid State Fuel Cells

Jian Liu, Greg Collins, Patrick Nash, and Chonglin Chen (Primary Contact)
Department of Physics and Astronomy
University of Texas at San Antonio
One UTSA Circle
San Antonio, TX 78249-1644
Phone: (210) 458-6427; Fax: (210) 458-4919
E-mail: cl.chen@utsa.edu

DOE Project Manager: Patricia Rawls
Phone: (412) 386-5882
E-mail: Patricia.Rawls@netl.doe.gov

Contract Number: 43063

Start Date: December 16, 2006
End Date: December 15, 2009

### FY 2009 Objectives

- Develop an intermediate temperature (550-700°C) electrolyte material that is capable of ionic conduction comparable to present high temperature materials (>850°C).
- Combine electrolyte with specific cathode and anode materials that work in unison to achieve a more efficient, longer lasting solid oxide fuel cell (SOFC).
- Fabricate and test cathode/electrolyte half-cells as well as whole-cells to optimize the cell function.

### Accomplishments

- New cathode material candidate, lanthanum barium cobalt oxide (LBCO), has been deposited epitaxially on selected substrates with characterization showing excellent conductivity.
- Multilayered cathode/electrolyte half-cells have been constructed with cathode material $PrBaCo_2O_{5+x}$ (PBCO) and multi-layered electrolyte $Gd:CeO_2$ (GCO) (Gd:Ce=0.25) and yttrium (mole 8%) stabilized zirconia (YSZ) on $LaAlO_3$(001) substrate in various thicknesses and ratios.
- Anode supported whole-cells constructed using tape-cast NiO/YSZ as the anode, multilayered GCO/YSZ as the electrolyte and PBCO as the cathode using the data from the half cells to optimize the GCO/YSZ ratio has begun.
- Intermediate temperature (575-650°C) peak cell power realized with further characterization and optimization of whole-cell structures on-going.

## Introduction

In current SOFCs, the functionality of the electrolyte and cathode are the limiting factors. The optimum characteristics for the electrolyte are high ionic conductivity at low temperature combined with electronic insulation. For the cathode, it should have mixed ionic and electronic conductivity along with the catalytic properties necessary for oxidation at the surface and transport of the oxygen ions to the cathode/electrolyte interface. YSZ, in bulk form, is a good ionic conductor with very good electronic insulating properties, however, this material is only ionically conductive at high temperatures. Lower temperature electrolytic materials have a high amount of electronic conductivity, leading to current leakage and voltage loss through the cell. This problem necessitates a compromise between these traits when using bulk materials in SOFC applications.

GCO is a material that offers excellent intermediate temperature ionic conduction but is also an electronic conductor. YSZ is an electronic insulator and, while in bulk form, requires a high temperature for ionic conduction, however, it has been found that when in ultra-thin (~10 nm) form, it will conduct up to 150 times that of the bulk form at lower temperatures. The combination of these materials in a multilayered thin film construction can offer high ionic with low electronic conduction at low to medium temperatures.

## Approach

The mixed conductive material GCO and the ionic conductive/electronic insulator YSZ will be used to form multilayered structures in various ratios. The goal of this research is to utilize the specific qualities of each material and tailor the interface transport characteristics (by altering the strain, oxygen content, etc, of the thin films) to create a multilayered structure that has superior electrolytic properties. Construction of these structures will be accomplished through pulsed laser deposition (PLD) methods. Testing and characterization will be accomplished with X-ray diffraction (XRD) (for crystallographic information), tunneling electron microscopy (for surface morphology), impedance spectroscopy and alternating current resistance measurements (for half-cell transport and electrochemical information) and precision current/voltage curve measurements (to measure whole-cell performance).

The use of PLD methods to produce thin films allows the control of material orientation, composition, domain size, crystallinity, stress/strain, etc, to a high degree of precision for many materials. Thus, the use of this method will allow the construction of multilayered structures with many differing properties so that a careful study of these materials in non-bulk form can be made. This will include the manipulation of interface properties, which have the greatest effect on transport properties, so that optimization of its effect might be realized. The application of this structure using different methods, such as molecular beam epitaxy and, more importantly, sputtering techniques, will also be explored since these methods will not only provide more information, sputtering methods are more suitable for industry production methods.

## Results

Double perovskite LBCO thin films were grown on (001) $LaAlO_3$ (LAO) single crystal substrates by using PLD. Microstructure characterizations from X-ray diffraction and electron microscopy (Figure 1) indicate that the films are cationic ordering and highly a-axis oriented with cube-on-cube epitaxy. Transport property measurements indicate that the films have typical semiconductor behavior with a novel phase transition and hysteresis phenomena at 540 K. The chemical dynamic studies reveal that the resistance of the film changes drastically with the change of redox environment, i.e., the magnitude of resistance changes, $\Delta R=10^2 \Leftrightarrow 10^6\ \Omega$, is found within a short response time (~700 ms). These phenomena suggest that the as-grown $LaBaCo_2O_{5+\delta}$ film have extraordinary sensitivity to reducing-oxidizing environment and an exceedingly fast surface exchange rate.

For the impedance study of the symmetric cell (Figure 2), cathode material PBCO and multi-layered electrolyte GCO/YSZ were deposited on the $LaAlO_3$(001) substrate (GCO:YSZ=15:1 x 4). X-ray diffraction shows that PBCO (100)-type reflections together with the corresponding reflections from the LAO substrate appear, indicating that the as-grown PBCO films, both of bottom and top electrode, are a-axis aligned. The GCO:YSZ multilayer which were grown directly on top of the PBCO shows only the (00*l*) reflections of GCO indicating that the GCO film has its c-axis aligned normal to the substrate surface. The (111)-type reflections of GCO which appeared on the GCO:YSZ on (001) MgO completely vanished.

The temperature dependence of the resistance of the half-cell (Figure 3) was analyzed in different environments. The resistance is much higher in nitrogen

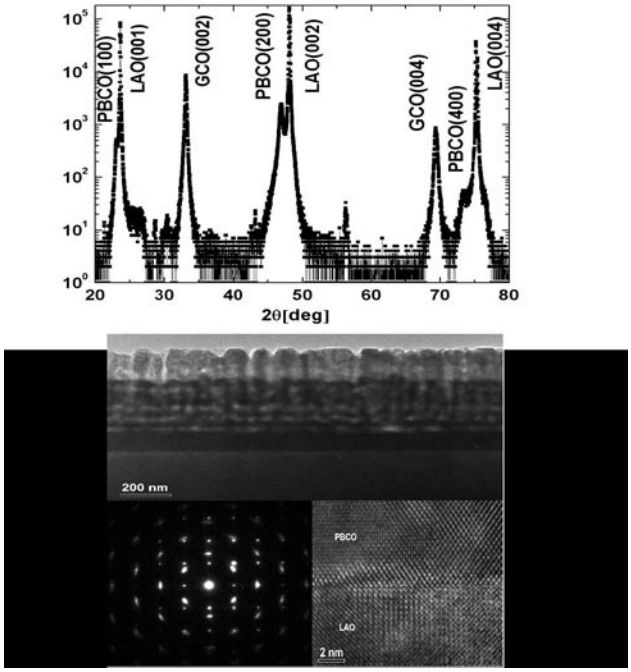


**FIGURE 1.** (top) XRD Analysis, (middle) Transmission Electron Microscope (TEM) Side View, (left/bottom) Selected Area Diffraction, (right/bottom) High Resolution TEM

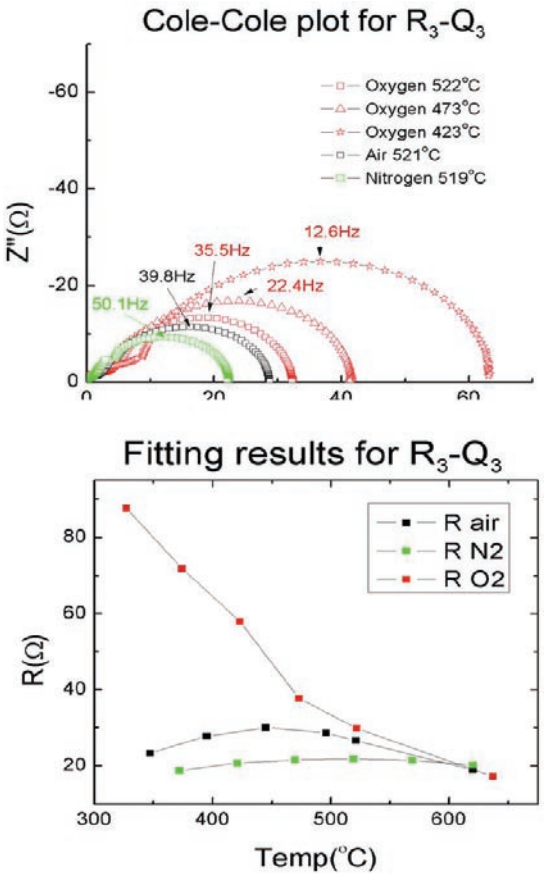


**FIGURE 2.** (top) Cole-Cole Plot, (bottom) Cathode Resistance as a Function of Temperature

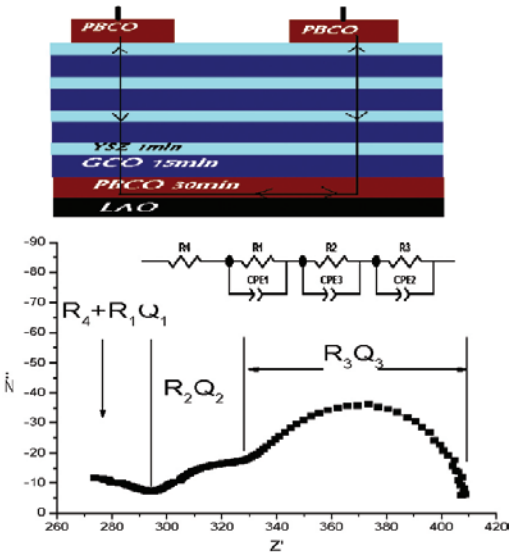


**FIGURE 3.** (top) Symmetric Cell Diagram, (bottom) Impedance Plot of Half-Cell

which is consistent with the previous results of both PBCO and YSZ/GCO. At a higher temperature range the resistance in air is lower than in oxygen and it is reversed at low temperature. The activation energy of the whole cell is also calculated from the linear fitting of the results and varies between 0.17 eV~0.24 eV according to different atmospheres. While the value is very close to our previous result of PBCO on LAO the activation energy change still follows the results of YSZ/GCO on MgO: i.e., $E_a(O_2)<E_a(N_2)<E_a(Air)$. The impedance study of the symmetric cell was carried out at the temperature range of 400°C to ~710°C in pure oxygen air and pure nitrogen. The data was fitted with a circuit based on three Z ARCs that is a common model for the impedance spectra of composite electrodes. $R_3$ is believed to associate with the main cathodic process, namely absorption and dissociation of oxygen molecules on the surface of the electrode (PBCO). At a fixed temperature, the resistance of $R_3$ is decreased with lower oxygen partial pressure indicating enhanced ionic conductivity induced by the increase of oxygen vacancies at the electrode surface.

Applying these findings to whole-cell construction we have constructed anode-supported cells and begun characterization and modification of electrolyte layer/ ratio composition in order to maximize the ionic transport (i.e. maximize cell power) in the intermediate temperature range. The anode material used, a NiO/YSZ cermet with pore formers, is a 50/50 mixture of NiO and YSZ. It is well known that the nickel in this material is catalytic with hydrocarbon fuels causing a separation of the hydrocarbon into useful $H_2$ and CO with the side-effect of a pore-clogging layer of carbon being adsorbed on the anode structure, eventually resulting in cell failure.

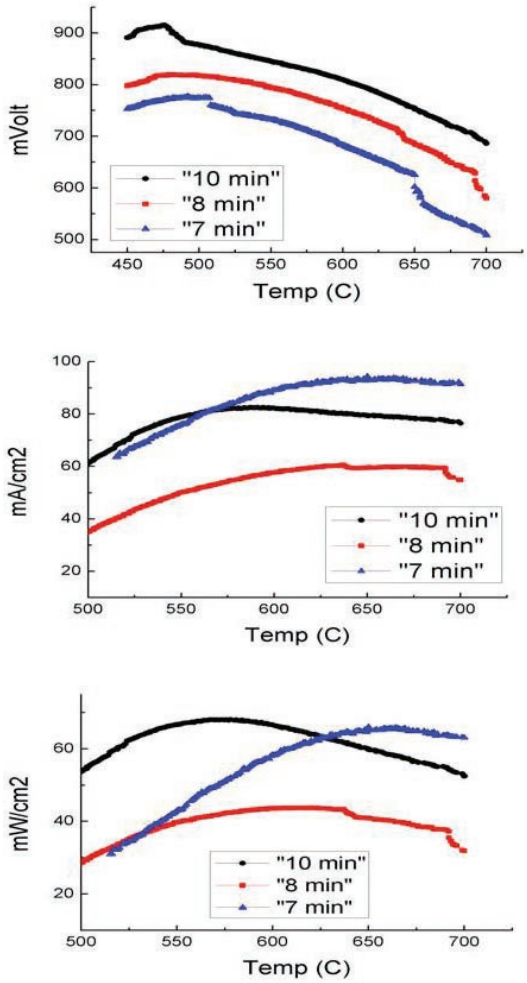


**FIGURE 4.** Measurements of Whole-Cell Output in 4% $H_2$/96% $N_2$ at 300 SCC/Minute Flow Rate: (top) mVolts, (middle) mAmpere/cm$^2$, (bottom) mWatt/cm$^2$

Our test gas is a 96/4 mixture of $N_2$ and $H_2$, respectively, so that while our current output will be considerably less than pure $H_2$, it will not suffer from an anode-based efficiency decay, making our electrolyte material and its composition the dependent variable. We have been able to produce a current of up to 95 mA/cm$^2$ with an average of approximately 65 mA/cm$^2$. Calculations of the cell voltage with the Nernst equation gives a voltage of approximately 1.15 volts. Our maximum voltage of approximately 0.91 V indicates current leakage in the cell. This problem is partially due to the inherent porosity of the anode material and that it has a large amount of surface roughness adversely affecting the insulating property of the YSZ layer. With these shortcomings, positive results are still seen (Figure 4). While the current peaks between 625°C and 650°C, the voltage reaches a maximum at a lower temperature of around 500°C, resulting in a peak power being realized between 575-625°C.

## Conclusions and Future Directions

- The cathode performance of LBCO will be systematically studied with the half-cell and full-cell setup using impedance spectroscopy. The size effect of $La^{3+}$ and $Pr^{3+}$ on the electrode properties will be subjected to detailed research.
- Conduct long-term testing to determine longevity problems: thermal degradation, reduction of the $GdCeO_2$ (indicating leakage of the YSZ insulating layer), etc.
- Improve our anode fabrication technique thereby eliminating uncertainty in our results.
- Conduct tests in a higher $H_2$ content if possible.
- Carry out further characterization of yttrium barium cerium oxide as an anode material as preliminary results are promising.

## Special Recognitions & Awards/Patents Issued

**1.** C.L. Chen, J. Liu, G. Collins, "2008.024.UTSA: Multilayered YSZ/GCO structure for intermediate temperature fuel cell applications," patent disclosure.

## FY 2009 Publications/Presentations

**1.** X.M. Xu, J. Liu, Z. Yuan, J. Weaver, C.L. Chen, Y.R. Li, N. Shi, and H.J. Gao, "Single Crystalline Highly Epitaxial Pt Thin Films on (001) $SrTiO_3$," Appl. Phys. Lett., **92** (2008) 102102.

**2.** Y. Lin and C.L. Chen, "Interface Effects on Highly Epitaxial Ferroelectric Thin Films," J. Mat. Res. (in press).

**3.** J.C. Jiang, C.L. Chen, Y. Lin, J. Horwitz, A.J. Jacobson, and E.I. Meletis, "Effects of Substrate Surface Local Structures on Properties and Interface Structures of Epitaxial Oxide Thin Films," Thin Solid Films (in press).

**4.** X.N. Jiang, S. Wang, G. Kim, J. Liu, M. Liu, W.Q. Gong, C.L. Chen, and A.J. Jacobson, "Oxygen Exchange Kinetics of Epitaxial $PrBaCo_2O_{5+\delta}$ and $LaBaCo_2O_{5+\delta}$ Thin Films," MRS Proceedings (2008).

**5.** J. Liu, X. M. Xu, G. Collins, Z. Yuan, J. Weaver, C.L. Chen*, G.T. Kim, A.J. Jacobson, "Strain Effects on Oxygen Transport Property in Highly Ionic Conductive $PrBaCo_2O_5$ Thin Films," Solid State Ionics (submitted).

**6.** J. Liu, M. Liu, G. Collins, C.L. Chen, X.N. Jiang, W.Q. Gong, A.J. Jacobson, J. He, J.C. Jiang, and E.I. Meletis, "Epitaxial Nature and Transport Properties in Double Perovskite $LaBaCo_2O_{5.5+\delta}$ Thin Films," J. Mat. Chem. (submitted).

**7.** J. Liu, G. Collins, M. Liu, C.L. Chen*, Q.Y. Zhang, and C. Dong, "Highly Epitaxial $LaBaCo_2O_{5+\delta}$ Thin Films – A Promised New Candidate for Developing High Temperature/Highly Sensitive Chemical Sensors with Critical and Reducing Environments," J. Am. Chem. Soc. (submitted).

# III. SECA CORE RESEARCH & DEVELOPMENT

## F. Fuel Processing

# III.F.1 Reformer for Conversion of Diesel Fuel into CO and Hydrogen

Michael V. Mundschau (Primary Contact), David A. Gribble, Jr., Paul N. Plassmeyer and Lee M. Henton
Eltron Research and Development Inc.
4600 Nautilus Court South
Boulder, CO 80301-3241
Phone: (303) 530-0263; Fax: (303) 530-0264
E-mail: mmundschau@eltronresearch.com

DOE Project Manager: Joseph Stoffa
Phone: (304) 285-0285
E-mail: Joseph.Stoffa@netl.doe.gov

Contract Number: 84394

Start Date: August 8, 2008
End Date: August 7, 2009

## FY 2009 Objectives

- Design a reformer for converting commercial diesel fuel with a maximum of 15 parts per million by mass sulfur into a mixture of $H_2$ and CO.
- Demonstrate self-cleaning reactor walls that prevent deposition of carbonaceous residues and plugging of reformers by effusing air through the walls.
- Develop perovskite catalysts for dry partial oxidation of diesel fuel that are sulfur tolerant, stable near 950°C, resist deactivation by sintering and contain vacancies for enhancing mobility of oxygen anions allowing rapid oxidation of hydrocarbons and inhibition of deposition of carbon.

## Accomplishments

- Distilled commercial diesel fuel; collecting 20% by mass of the most volatile components. Showed that the volatile fraction could be relatively easily re-vaporized and reformed by dry catalytic partial oxidation - eliminating steam and more complex fuel injectors and mixers. Nearly 90% of the carbon in the volatile fraction was converted into the desired CO, and about 75% of the hydrogen into $H_2$, with minimum deposition of carbon or naphthelene and no soot in the exhaust.
- Produced CO and $H_2$ by dry catalytic partial oxidation from volatile components of commercial diesel fuel that may have application in the regeneration of NOx traps used in pollution control of diesel engines.

## Introduction

Dry catalytic partial oxidation of diesel fuel into $H_2$ and CO has potential applications for operation of solid oxide fuel cells and for regeneration of NOx traps used in pollution control of diesel exhaust. Reforming of diesel fuel into synthesis gas is also a first step in the production of pure hydrogen for proton exchange membrane fuel cells after water-gas shift and impurity removal using hydrogen transport membranes [1,2].

Dry partial oxidation of diesel fuel has a number of unique issues not encountered in the reforming of volatile fuels, fuels with higher H/C or O/C atomic ratios, or in steam reforming. Much effort in this research has been expended in understanding the fundamental science required for diesel fuel reforming. The major findings are summarized as follows.

The H/C atomic ratio in the fuel, along with the quantity of oxygen in the system, dictates the thermodynamic equilibrium temperature required to favor production of $H_2$ and CO over $H_2O$ and $CO_2$ and to completely suppress formation of elemental carbon that can deactivate catalysts and plug reformers. Combustion analysis of commercial diesel fuel containing <15 ppmw sulfur, indicates H/C atomic ratios ranging from 1.87:1 to 1.78:1. To eliminate deposition of even single monolayers of carbon that might deactivate catalysts, calculations predict that catalysts must operate above about 950°C, assuming a stoichiometry of one mole of atomic oxygen for each mole of carbon in the fuel to form CO [3]. Temperatures required for partial oxidation of diesel fuel are considerably higher than that required for partial oxidation of methane with an atomic ratio of H/C of 4:1, or for steam and autothermal reforming of hydrocarbons where $H_2O$ increases both H/C and O/C atomic ratios in the system.

The extreme temperatures required for dry partial oxidation of diesel fuel rule out most conventional high surface area, supported metallic catalysts that sinter and lose surface area and activity or that might be pyrophoric upon cycling between reducing conditions and exposure to air. For this high temperature application, refractory oxides with the perovskite crystal structure were selected [3]. The perovskites are designed to be electron conducting for the difficult reduction step: $O_2 + 4e^- = 2O^{2-}$ and are designed with oxygen-anion vacancies to enhance oxygen mobility and attack of adsorbed carbon from beneath. The perovskites have proven to be quite effective in suppressing deposition of carbon in catalyst beds [3]. Surface area is limited to about 1 $m^2 \cdot g^{-1}$, but at these extreme temperatures gas-

phase diffusion of large molecules is expected to be rate limiting rather than surface kinetics, and no great effort has been expended or deemed necessary to improve catalyst surface area.

Iron-based perovskites of general formula, $La_{1-x}(Ca,Sr)_xFeO_{3-\delta}$, have shown the best activity and stability of the base metal perovskites tested. Under appropriate thermodynamic conditions, Fe, Co and Ru, the three catalysts used in Fischer-Tropsch synthesis, catalyze the reverse reactions, converting *n*-alkanes into synthesis gas. Of the base metals, iron and cobalt best resist poisoning by sulfur at levels of 15 ppmw in diesel fuel [3]. Iridium, platinum and rhodium are the most sulfur-tolerant catalysts, based upon instability of their bulk sulfides at elevated temperatures [3], and Pt-Rh wire gauze operated near 1,000°C is sulfur-tolerant and thermally stable. The elements, Pt, Rh, Ru, Co and Fe are predicted to have catalytic activity for opening aromatic rings. However, the ability of iron in the perovskites tested to date to reform naphthalene is less than desired.

Thermodynamic and kinetic analysis indicates that elemental carbon is the preferred product in the fuel heating zone between 200-600°C [3]. Long-chain *n*-alkanes, such as *n*-hexadecane (cetane), are the least stable hydrocarbons in diesel fuel, cracking to form free radicals at autoignition temperatures near 205°C, well below the boiling point of 286.5°C. Carbon will deposit from long-chain ($>C_{12}$) *n*-alkanes well below their boiling points if heated above fuel cracking temperatures under oxygen lean conditions unless appropriate precautions are taken. Aromatic compounds such as naphthalene and benzene are the most stable molecules in the fuel, vaporizing well below their autoignition temperatures at 526°C and 562°C, respectively. Under oxygen-lean conditions, hydrocarbon free radicals react with high probability with other hydrocarbons, initiating radical polymerization and formation of tar and other carbonaceous residues. Because temperatures below about 950°C favor formation of graphite and soot, radical chain propagation in the heating zone leading to deep oxidation but also release of heat accelerating nucleation and growth of soot, must be suppressed.

## Approach

Figure 1 shows schematically the laboratory porous membrane reactor. The fuel line and air brought in at the top are kept just below 200°C to minimize cracking of fuel and formation of tar. About 10% of the air required for partial oxidation is brought in with the fuel at the top through a porous baffle of yttria-stabilized zirconia fiber, stated by the manufacturer (Zircar Zirconia) to be 76% porous, which also acts as an infrared shield for the fuel line. It is desired that the oxygen in the cooler air react with hydrocarbon free radicals as they form in the gas phase of the heating zone between 205-562°C to produce easier-to-reform, small, oxygenated molecules that are very rapidly swept to the reformer hot zone operated above 950°C. Heat released by formation of the oxygenated compounds is partially absorbed by cooler air effusing through the walls of porous zirconia-toughed-alumina, stated by the manufacturer, Refractron, to be 40% porous. Inner walls in the heating zone are kept carbon-free by high local partial pressures of oxygen near the inner walls. Radical chains leading to polymerization and tar or to deep oxidation in the heating zone are terminated, in part, by the proximity of the walls of the relatively narrow porous tube (22-mm) and surfaces within the pores. It is also desired that air be effused throughout the length of the porous walls enclosing the bed of perovskite to produce a more uniform temperature distribution throughout the catalyst bed and to avoid hot spots at the entrance of the bed, which would be the case if all of the air and fuel were mixed before the entrance of the bed. Mobile lattice oxygen in the perovskite catalyst acts as a reservoir for oxygen in oxygen-lean regions, and the vacancy-rich perovskites act as sinks for excess oxygen in oxygen-rich regions.

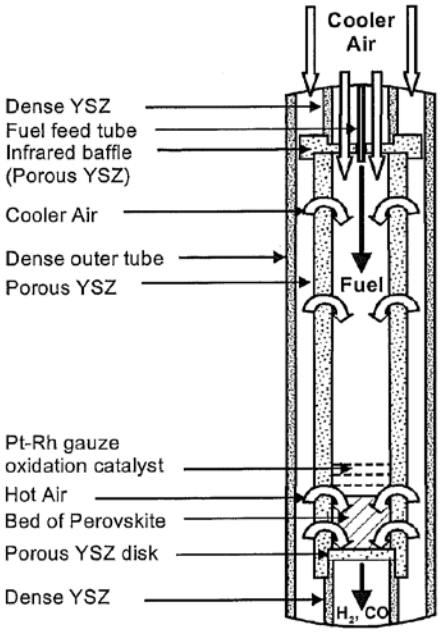


**FIGURE 1.** Schematic of a porous membrane reactor for reforming diesel fuel into synthesis gas. Cooler air (<200°C) is fed through walls of a narrow porous ceramic tube to suppress deposition of carbon on inner walls and to react with free radicals formed in the gas phase of the reformer heating zone. Pre-heated hot air (~900°C) is fed through porous walls to partial oxidation catalysts in the lower reformer hot zone.

## Results

To circumvent need for complex and expensive liquid-fuel injectors and air mixers, diesel fuel was distilled below 200°C, and 20% by mass of the most

volatile components were collected into a reservoir. The distillate from the reservoir was relatively easily re-vaporized just below 200°C and entered the reformer in the gas phase. Figure 2 shows percent yields of carbon and hydrogen from dry partial oxidation of the distillate. Catalysts were very stable over the 72 h period tested. Nearly 90% of the carbon in the distillate was converted into the desired CO and about 75% of the hydrogen into molecular hydrogen. Very slight deposition of carbon occurred on the inner walls in the 2 cm above the catalyst, but exhaust and traps had no soot and negligible naphthalene. The catalyst was free of carbon. To suppress carbon, quantity of air was about 20% above that required for partial oxidation, and this produced the $CO_2$ and $H_2O$ seen. Methane slip was evident, implying that the system was not brought to equilibrium or that methane formed in the cooler exhaust. Figure 3 plots the data as mole % (= volume %) of products in the reformate, that also contains 58 mol% $N_2$. Levels of CO and $H_2$ would be more than sufficient to regenerate NOx traps used in pollution control for diesel engines.

Figure 4 shows results for dry partial oxidation of full commercial diesel fuel (<15 ppmw S). Yields of desired CO and $H_2$ were less than that of the volatile distillate, and slight decay in yield was seen over 72 h. Tar appeared on the outer surface of the fuel nozzle and more carbon appeared deposited on

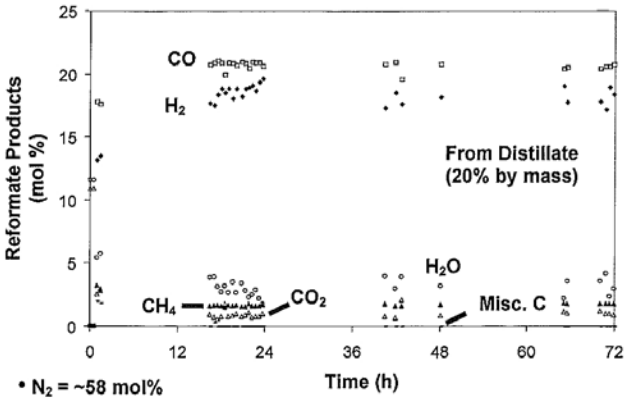


**FIGURE 3.** Reformate products as mole % (= volume %) from dry partial oxidation of the most volatile components distilled from diesel fuel. On-board reforming of components vaporized from diesel fuel may have application in regeneration of NOx traps used in pollution control of diesel exhaust.

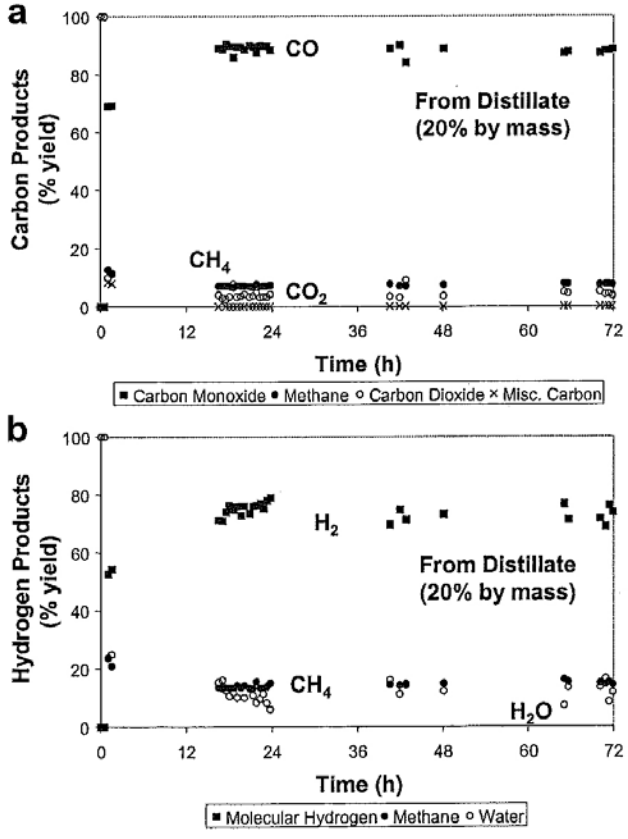


**FIGURE 2.** Percent yields of products containing (a) carbon and (b) hydrogen by dry partial oxidation of volatile compounds distilled from diesel fuel. Nearly 90% of the carbon in a distillate containing 20% by mass of the diesel fuel is converted into CO and 75% into molecular hydrogen.

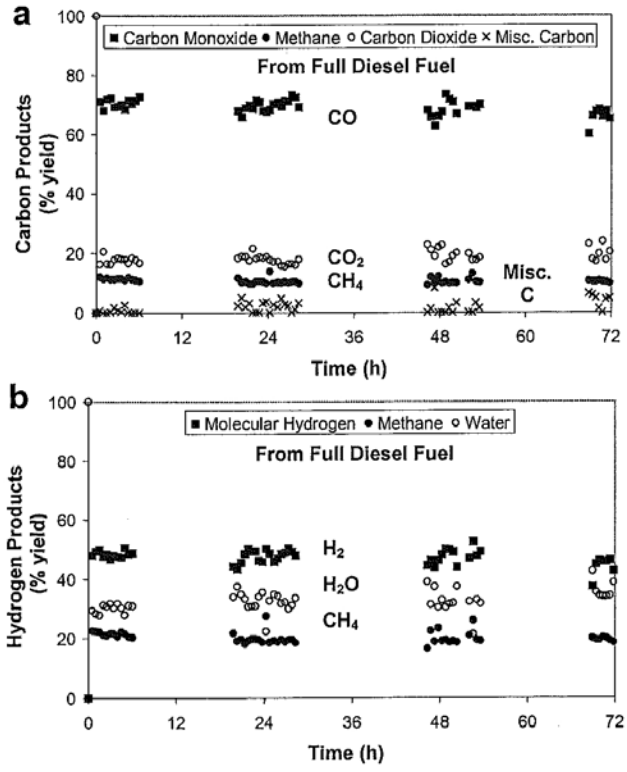


**FIGURE 4.** Percent yields of products containing (a) carbon and (b) hydrogen by dry partial oxidation of full commercial diesel fuel containing <15 ppmw sulfur. Although exhaust is soot-free, considerable naphthalene escapes through the catalyst bed, and yields of desired products are lower relative to reforming of the most volatile compounds distilled from diesel fuel.

inner walls, although there was no immediate danger of plugging the system. No soot was seen in the exhaust traps. However, considerable naphthalene was seen crystallized onto cooler exhaust lines and in the exhaust trap, implying inadequate catalyst activity for decomposition of naphthalene or formation of naphthalene in the system.

## Conclusions and Future Directions

- Considerable work remains to produce a practical reformer for fuel cells. Sulfur even at levels of 15 ppmw in "ultra-low sulfur diesel" in the reformate is likely to poison nickel-based catalysts in solid oxide fuel cells. Parasitic power consumption for fuel injection, air flow and external heating of air fed to catalysts will need to be greatly reduced if efficient fuel cell systems are to be fabricated. Cost of all components will need to be greatly reduced.
- Narrow, self-cleaning walls of porous ceramic show promise for suppressing deposition of carbon in the critical diesel fuel heating zones but will require considerable effort to produce practical, cost-effective, devices.
- Perovskite catalysts, especially those containing iron, show promise as sulfur-tolerant, dry partial-oxidation catalysts for diesel fuel but will require further development.
- Dry partial oxidation of volatile components distilled from diesel fuel at temperatures below a modest 200°C might find immediate application for regeneration of NOx traps.

## Special Recognitions & Awards/Patents Issued

**1.** Michael V. Mundschau, *Catalytic Membrane Reactor and Method for Production of Synthesis Gas,* United States Patent Application Publication: US 2008/0169449 A1, July 17, 2008.

## FY 2009 Publications/Presentations

**1.** Michael V. Mundschau, David A. Gribble, Jr., Paul N. Plassmeyer, Lee M. Henton, and Nicholas R. Jentzsch, "Dry Catalytic Partial Oxidation of Diesel-Fuel Distillates into Syngas," *Fuel,* submitted.

**2.** Michael V. Mundschau, David A. Gribble, Jr., Paul N. Plassmeyer, Lee M. Henton, and Nicholas R. Jentzsch, "Dry Catalytic Partial Oxidation of Diesel-Fuel Distillates into Syngas," *Proc. 2009 AIChE Spring National Meeting,* April 26-30, 2009, Tampa, Florida.

**3.** M.V. Mundschau, David A. Gribble, Jr., Paul N. Plassmeyer, Lee M. Henton, and Nicholas R. Jentzsch, "Dry Catalytic Partial Oxidation of Diesel-Fuel Distillates into Syngas," Presentation 145639 at the AIChE Spring National Meeting, April 26-30, 2009, Tampa, Florida.

**4.** Michael V. Mundschau, David A. Gribble, Jr., Lee M. Henton, Nicholas R. Jentzsch, and Paul N. Plassmeyer, "Reforming Diesel-Fuel Distillates with Membrane Reactors," *Asia-Pacific Journal of Chemical Engineering*, DOI: 10.1002/apj.367.

## References

**1.** M.V. Mundschau, Hydrogen Separation Using Dense Composite Membranes: Part 1 Fundamentals, in: Inorganic Membranes for Energy and Environmental Applications, A. C. Bose, Editor (Springer, New York, 2009) pp. 125-153, DOI: 10.1007/978-0387-34526-0_8.

**2.** M.V. Mundschau, X. Xie, and C.R. Evenson IV, Superpermeable Hydrogen Transport Membranes, in: Nonporous Inorganic Membranes, A.F. Sammells and M.V. Mundschau, Editors (Wiley-VCH, Weinheim, 2006) pp. 107-138.

**3.** M.V. Mundschau, Christopher G. Burk and David A. Gribble, Jr., "Diesel Fuel Reforming Using Catalytic Membrane Reactors," *Catal. Today* 136 (2008), 190-205, DOI: 10.1016/j.cattod.2008.02.003, and references therein.

# III.F.2 Structured Oxide-Based Reforming Catalyst Development

David A. Berry (Primary Contact) and
Dushyant Shekhawat
U. S. Department of Energy
National Energy Technology Laboratory (NETL)
3610 Collins Ferry Road
Morgantown, WV 26507-0880
Phone: (304) 285-4430; Fax: (304) 285-0943
E-mail: David.Berry@netl.doe.gov

Contractors:
- Daniel Haynes, RDS Inc., Morgantown, WV
- Mark Smith, REM Engineering Services, PLLC, Morgantown, WV
- J.J. Spivey, Louisiana State University, Baton Rouge, LA

Contract Number: 07-220611

Start Date: October 1, 2008
End Date: September 30, 2009

## FY 2009 Objectives

- Conduct research and development (R&D) towards development of a viable hydrocarbon reformer that is suitable for commercially-representative fuel cell applications (e.g., diesel auxiliary power units).
- Examine effect of oxygen-conducting supports catalyst performance.
- Demonstrate long-term performance stability of oxide powder catalyst on oxygen-conducting support for diesel fuel reforming.
- Identify support structure for depositing active catalyst phase and oxygen-conducting material for scaled-up reforming tests.

## Accomplishments

- Prepared numerous oxide catalyst powders on oxygen-conducting supports; performed catalyst characterization by X-ray diffraction, inductively coupled plasma, Brunauer, Emmett, Teller surface area analysis, temperature programmed reduction/temperature programmed oxidation (TPO), extended X-ray absorption fine structure, X-ray absorption near edge structure; and evaluated activity and selectivity under several modes of reforming.
- Determined catalyst formulation and support composition for oxidative steam reforming (OSR) of diesel fuel; successful 1,000-hr diesel reforming test completed.
- Collaborated with industrial partners to evaluate catalyst viability.
- Patent application filed for pyrochlore catalyst materials.

## Introduction

The development of solid oxide fuel cell technology has been a priority of the Department of Energy. The significance of this technology is demonstrated by the DOE's sponsoring of R&D for a variety of applications. Moving this technology forward in a rapid manner has necessitated the use of current infrastructure fuels (coal, diesel, natural gas, etc.). These fuels can be reformed into a hydrogen-rich synthesis gas for use in transportation fuel cell applications. A promising example of such an application is auxiliary power units for commercial diesel trucks.

Catalytic partial oxidation (POX) of liquid hydrocarbons is viewed as an attractive option for reforming due to its inherent simplicity that avoids the need for water addition, water management or extraneous heat exchangers, and/or other costly components. POX catalysts typically consist of Ni or Group-VIII noble metals incorporated onto various high surface area oxide substrates such as $\gamma$-$Al_2O_3$, $SiO_2$, and more recently, mixed metal oxides. Carbon formation and deactivation by sulfur are key challenges for POX catalysts. It has been shown that catalyst poisoning by sulfur and/or carbon is a structure sensitive reaction, and is influenced by the cluster size of the active metal. Larger metal clusters have a much stronger interaction with carbon and sulfur than smaller, well-dispersed metal particles [1–3]. This problem becomes worse at the high reforming temperatures of POX, because conventional supported metals tend to sinter and agglomerate into even larger particles.

## Approach

Approaches to develop a hydrocarbon reforming catalyst and minimize deactivation from sulfur and aromatic contaminants during reforming have included 1) using oxygen-conducting supports [4-6], and 2) substituting active metal particles into thermally stable oxide structures, such as perovskites, $ABO_3$ [4-9], pyrochlores, $A_2B_2O_7$ [10-13], and hexaaluminates, $AAl_{12}O_{19}$ [4, 14, 15]. Although these approaches have demonstrated some improvement, deactivation still occurs rapidly under partial oxidation conditions. However, combining these approaches by supporting

thermally stable oxides on oxygen-conducting supports has led to a synergistic effect in the partial oxidation of liquid hydrocarbons containing sulfur and aromatic species [16].

Studying this combined approach was divided into two efforts. The first was improvement of the previously developed Rh-substituted pyrochlore powder catalyst by varying the A- and B-site dopants to obtain desired surface properties, activity, and selectivity. The second was the study of several oxygen-conducting support compositions, and varying levels of substituted oxide catalysts. Both studies utilized POX of a surrogate diesel fuel, tetradecane (TD). The experiments involved three steps. First, the POX of TD was performed for 1-2 hrs to establish baseline activity and selectivity of the catalyst. Next, the feed was switched to TD + 50 ppmw sulfur as dibenzothiophene (DBT) + 5 wt% 1-methylnaphthalene (MN) for 2 hrs to observe the effect of sulfur and aromatic species. Finally, the feed was switched back to TD for 1-2 hrs to examine activity recovery. After each experiment, carbon deposition was measured by TPO.

Another option for mitigating carbon formation on reforming catalyst surfaces is through the addition of water to the feed stream. For transportation applications, this is highly undesirable if supplemental water is stored; however, recycling a portion of the fuel cell exhaust could supply enough water to extend the life of the catalyst sufficiently without the need for water storage. The amount of water would not necessarily need to be in quantities for pure autothermal conditions, but rather, some extent of OSR, where the majority of the fuel conversion would remain POX and the water would be used primarily to convert strongly adsorbed coke precursor species on the catalyst surface. These ratios of water and oxygen could also be adjusted to meet the specifications of the desired application.

The final stage of the development was preparing a catalyst in a form that would be more representative and usable in a commercial application. The form selected was a coated alumina monolith. Collaborating with commercial catalyst manufacturers to produce and validate a sufficiently active material has led to the production of a monolith coated with both an oxygen-conducting material, and the active catalyst phase developed by NETL. The monoliths were tested under POX and OSR of pump diesel and on a biodiesel fuel.

## Results

**1000-hr Oxidative Steam Reforming of Diesel:** The catalyst powder selected for the long-term catalyst demonstration was a Rh-substituted pyrochlore. The active phase was supported onto zirconium-doped ceria (ZDC), an oxygen-conducting support. The fuel used for the test was pump diesel from a local fuel station. The testing conditions can be seen in Table 1.

**TABLE 1.** Experimental Conditions for 1,000-hr OSR Demonstration

| Reaction Conditions | |
|---|---|
| Overall O/C ratio | 1.5 |
| O/C from air | 1.0 |
| S/C ratio | 0.5 |
| GHSV (scc $gcat^{-1}$ $h^{-1}$) | 25,000 |
| Bed Temperature (°C) | 900 |
| Catalyst Bed (g) | 9.6 |
| Pressure (MPa) | 0.23 |

O/C – oxygen to carbon ratio
S/C – steam to carbon ration
GSHV – gas hourly space velocity

The results of the 1,000-hr run are presented in Figure 1. The testing demonstrated surprisingly stable, near-equilibrium performance throughout the entire 1,000-hr test. It also demonstrated impressively low single-digit ppm production levels of >C1 hydrocarbons (the species that could potentially degrade a fuel cell). This is very significant in light of recent fuel cell testing that indicates degradation of fuel cell performance can occur upon exposure of concentrations in the 10s of ppm of certain higher hydrocarbon species like ethylene.

An additional result to notice from this run is the catalyst's ability to recover after a system upset. Between Day 6 and 8, the pump supplying the water to the reactor malfunctioned. For approximately 20 hrs, the catalyst was exposed to severely oxygen-deficient conditions without complete deactivation. Further, the catalyst performance returned to pre-upset levels when the water pump was restarted. These results demonstrated a level of stability that surpassed the team's expectations.

**Biodiesel Fuel Testing:** To prepare for an upcoming demonstration of an integrated reformer/fuel cell operation on biodiesel, additional parametric catalyst

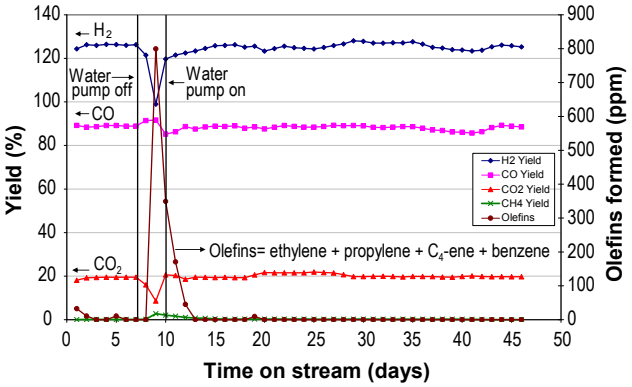


**FIGURE 1.** Results from 1,000-hr Reforming Test on Pump Diesel with NETL Catalyst

powder studies were conducted. The biodiesel fuel was initially characterized and tested in a series of baseline reforming experiments for both POX and OSR modes. The POX experiments examined the effect of varying the O/C ratio from 1.0 to 1.3. The OSR tests looked at the use of both air and steam as oxidizing species. An O/C of 1.0 from air was used and the S/C ratio was varied for an overall atomic O/C ratio range of 1.0 to 1.5. Finally, the biodiesel was tested for 24 hrs under partial oxidation conditions on the NETL 1,000-hr catalyst formulation for comparison to the diesel reforming experiments. The product gas compositions for this run are presented Figure 2. The biodiesel yielded near equilibrium gas compositions for 24 hrs under POX conditions (more severe than OSR) with no deactivation of the catalyst.

**Catalyst Monolith Development:** The next step in the development was to apply the catalyst and support formulations used for the 1,000-hr test to a structured material (i.e., monolith, foam, pellet). The catalyst structure selected was an alumina monolith coated with the ZDC oxygen-conducting support and pyrochlore catalyst phases. The monoliths were prepared by Nextech, and a photograph of one of these monoliths is shown in Figure 3. Though difficult to see, the channels of the tubes shown have been coated first with a layer of ZDC, and second by a layer of the NETL Rh-doped pyrochlore catalyst.

A series of short-term qualification tests on monolithic catalysts with diesel fuel were conducted to evaluate catalyst-coating procedures. The monolith piece was located in the center of an externally-heated reactor with an inside thermocouple touching the bottom of the monolith and a surface thermocouple on the reactor tube. Runs were conducted under both POX and OSR conditions at 900°C, and space velocity of 25,000-50,000 $hr^{-1}$. Diesel fuel used in this study was obtained from a local gas station.

The POX test results for the first monolith catalysts prepared by Nextech are presented in Figure 4. $H_2$ and CO compositions in the effluent were slightly decreased over the first two hours of the run before plateau at steady-state values. However, $CH_4$ and $CO_2$ yields increased as the catalyst performance goes down. This monolith (C10003-12.3) contained 0.6951 gram of pyrochlore material, which contained 2 wt% substituted Rh metal in it.

OSR runs were also conducted on the monolith. Flow rates used for these runs were 0.065 cc/min diesel fuel, 0.036 cc/min water, 215 sccm air, and 355 sccm $N_2$. The reaction temperature was 900°C, the O/C ratio was 1.0, and the S/C ratio was 0.5 (an O/C of 1.2 was used for the first 30 mins of run to make sure there was enough oxidant in the reactor). There was some oscillation in the results attributed to the water injection

**FIGURE 3.** Alumina Monolith Coated with NETL Reforming Catalyst, Prepared by Nextech

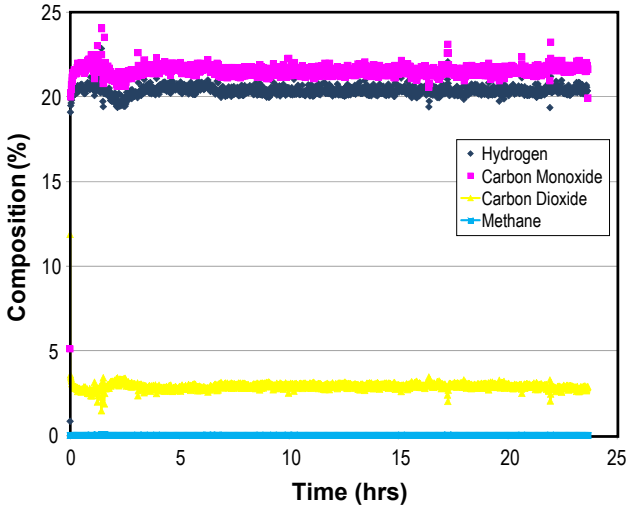


**FIGURE 2.** Partial Oxidation of Biodiesel with NETL Catalyst

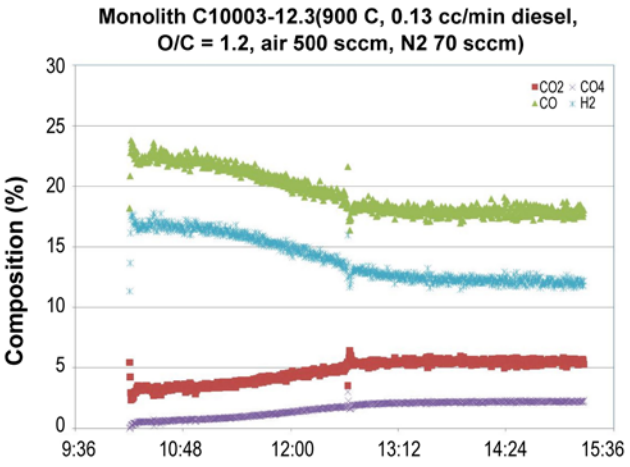


**FIGURE 4.** Results of POX Reforming Test in Catalyst Screening Unit for Monolith Catalysts Prepared by Nextech

problem in the system. $H_2$ and CO compositions in the reactor effluent were stabilized right after the extra air from the system was reduced after 30 mins into the run. Results for this run can be seen in Figure 5.

**Demonstration Tests:** Two near-term demonstration tests of note to be conducted with the NETL reforming catalyst are planned. The first, as mentioned previously, involves the use of a biodiesel fuel, which will be reformed through a monolithic catalyst (Figure 6) housed within NETL's fuel processing unit (FPU) shown in Figure 7. The reformate from the reformer will be fed directly to a solid oxide fuel cell to demonstrate an integrated reformer-fuel cell operation.

The second near-term demonstration test involves evaluating the use of the NETL catalyst with the Precision Combustion Incorporated (PCI) reforming technology. PCI employs the use of a patented catalyst structure, microlith, which consists of catalyst coated screens (Figure 8) that are contained within a reformer vessel. Testing is being planned for FY 2010.

## Conclusions and Future Directions

The successful completion of a 1,000-hr diesel reforming test on a powder pyrochlore catalyst developed by NETL over an oxygen-conducting support demonstrates that the catalyst and support compositions selected have significant potential in a commercial reforming application. Transforming this powder catalyst into a commercially viable form is the next major step to the development of a final product. Commercial catalyst producing partners have developed an alumina monolith structure coated with both the oxygen-conducting support and the active pyrochlore phase. NETL has validated the performance of the precursor materials, and preliminary testing of the monoliths have shown very promising results under the OSR conditions used for the 1,000-hr test.

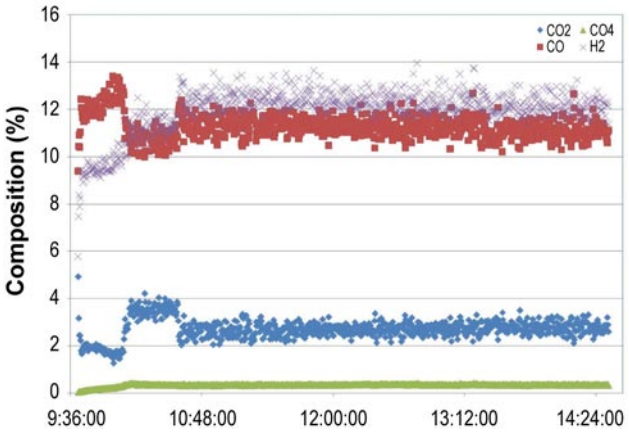


**FIGURE 5.** Results of OSR Test in Catalyst Screening Unit for Monolith Catalysts Prepared by Nextech

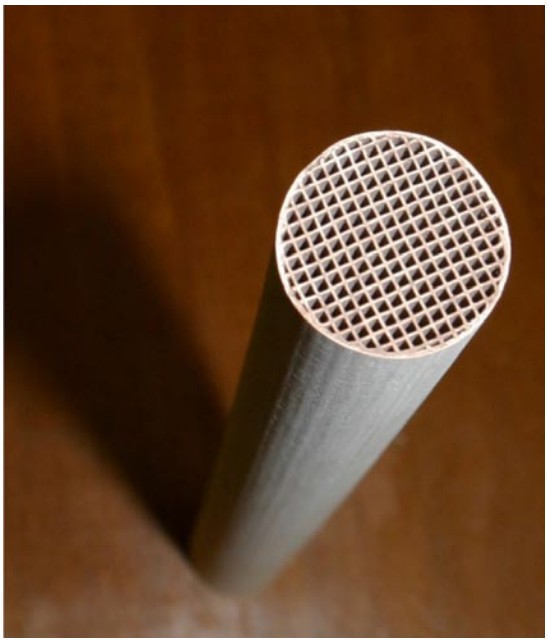

**FIGURE 6.** Alumina Monolith Coated with NETL Reforming Catalyst, Prepared by Nextech

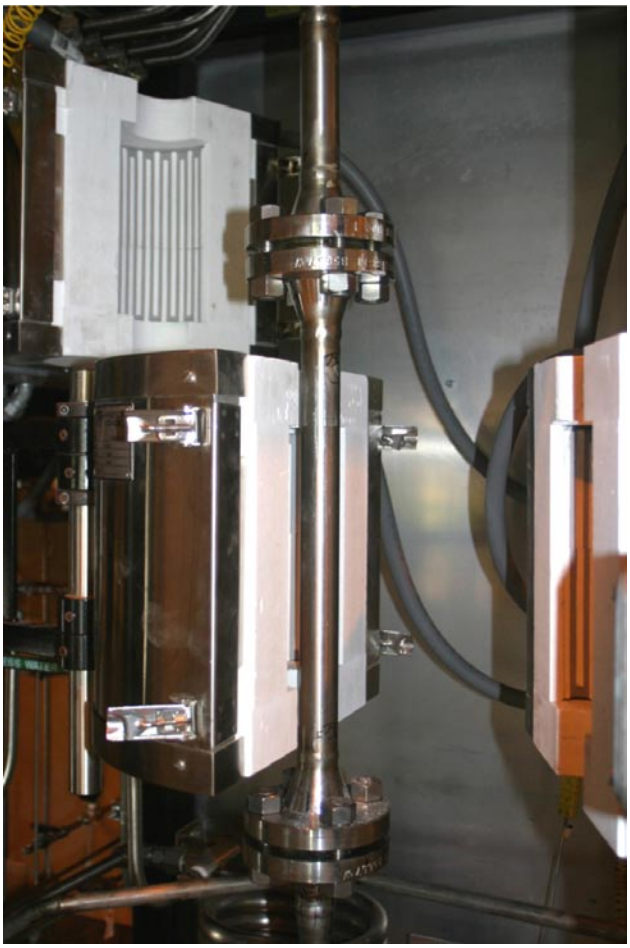

**FIGURE 7.** Photograph of NETL Fuel Processing Unit (FPU)

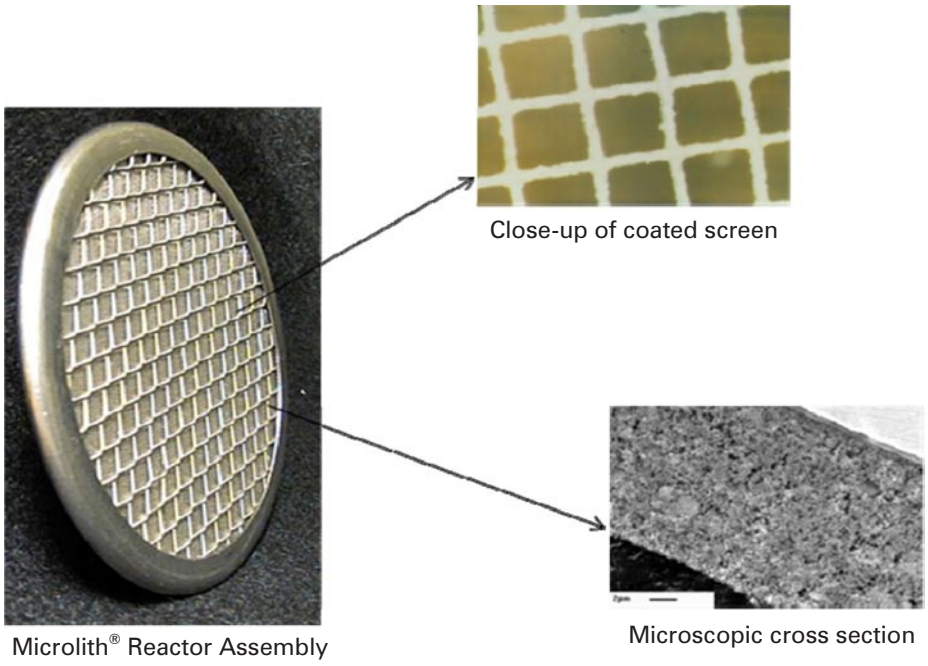


**FIGURE 8.** PCI Patented Microlith Reactor Technology

Future work will focus on optimizing the catalyst/coating formulation throughout the reaction zone and applying it to commercially-representative coated catalyst structures. Evaluation and technology transfer of the catalyst system to catalyst, fuel processing and fuel cell/system developers will be pursued to support NETL's Fuel Cell program.

## Special Recognitions & Awards/Patents Issued

**1.** D.A. Berry, D. Shekhawat, D. Haynes, J.J. Spivey (LSU), and M.W. Smith, "Pyrochlore-type Catalysts for the Reforming of Hydrocarbon Fuels," Patent Application Filed (2009).

**2.** NETL Organized American Institute of Chemical Engineers Conference Symposium, *2009 Spring National Meeting – Topical B: Advanced Fossil Energy Utilization.*

## FY 2009 Publications/Presentations

**1.** M.W. Smith, D.A. Berry, D. Shekhawat, D. Haynes, and J.J. Spivey, "Effect of Oxide Catalysts and Oxygen-conducting Supports on Partial Oxidation of Liquid Hydrocarbons," *237th National Meeting and Exposition*, American Chemical Society, Salt Lake City, Utah, March 23–26, 2009.

**2.** M.W. Smith, D.A. Berry, D. Shekhawat, D.J. Haynes, and J.J. Spivey, "Effect of Catalyst Layer Formation and Character on Partial Oxidation of Liquid Hydrocarbons in the Presence of Oxygen-conducting Supports," *2009 Spring National Meeting*, American Institute of Chemical Engineers, Tampa, Florida, April 26–30, 2009.

**3.** D.J. Haynes, D.A. Berry, D. Shekhawat, M.W. Smith, and J.J. Spivey, "Catalytic Partial Oxidation of a Surrogate Diesel Fuel Mixture Using Pyrochlores: Effect of Reforming Metal," *2009 Spring National Meeting*, American Institute of Chemical Engineers, Tampa, Florida, April 26–30, 2009.

**4.** D. Haynes, D.A. Berry, D. Shekhawat, M.W. Smith, and J.J. Spivey, "Catalytic Partial Oxidation of n-Tetradecane over Rh Substituted Pyrochlores: Effect of A-site Substitution," *21st North American Meeting*, North American Catalysis Society, San Francisco, California, June 2009.

**5.** M.W. Smith, D.A. Berry, D. Shekhawat, D. Haynes, and J.J. Spivey, "Reforming Liquid Hydrocarbons with Ni-substituted Barium Hexaaluminates: Effect of Oxygen-conducting Support," *21st North American Meeting*, North American Catalysis Society, San Francisco, California, June 2009.

**6.** J.J. Spivey, A. Campos, D.A. Berry, D. Shekhawat, D.J. Haynes, and M.W. Smith, "Substituted Pyrochlores: New Catalytic Materials for Reforming of Liquid Fuels," *23rd International Materials Research Conference,* Cancun, Mexico, August 16-20, 2009.

**7.** J.J. Spivey, D.A. Berry, D. Shekhawat, M.W. Smith, and D.J. Haynes, "Reducing the Deactivation of Ni-metal During the Catalytic Partial Oxidation of a Surrogate Diesel Fuel Mixture," *International Symposium on Catalyst Deactivation*, Delft, The Netherlands, October 25-28, 2009.

**8.** M.W. Smith, D.A. Berry, D. Shekhawat, D. Haynes, and J.J. Spivey, "Partial Oxidation of Liquid Hydrocarbons in the Presence of Oxygen-conducting Supports for Solid Oxide Fuel Cells: Effect of Catalyst Layer Deposition," *Fuel* (Accepted).

## References


**1.** B.J. Wuensch, K.W. Eberman, C. Heremans, E.M. Ku, P. Onnerud, E.M.E. Yeo, S.M. Haile, J.K. Stalick, and J.D. Jorgensen, Solid State Ionics 129 (2000) 111.

**2.** K.V.G. Kutty, C.K. Mathews, T.N. Rao, and U.V. Varadaraju, Solid State Ionics 80 (1995) 99.

**3.** P. Erri, P. Dinka, and A. Varma, Chem. Eng. Sci. 61 (2006) 5328. J. Barbier and P.J. Marecot, Catal.102 (1986) 21.

**4.** D. Shekhawat, et al., "Catalytic Partial Oxidation of n-Tetradecane in the Presence of Sulfur or Polynuclear Aromatics: Effects of Support and Metal," Applied Catalysis A: General, 2006. 311: p. 8-16.

**5.** H. He and J.M. Hill, "Carbon Deposition on Ni/YSZ Composites Exposed to Humidified Methane," Applied Catalysis A: General, 2007. 317(2): p. 284-292.

**6.** M. Salazar, et al., "Catalytic Partial Oxidation of Methane over Pt/Ceria-Doped Catalysts: Effect of Ionic Conductivity," Applied Catalysis A: General, 2006. 310: p. 54-60.

**7.** P. Erri, P. Dinka, and A. Varma, "Novel Perovskite-Based Catalysts for Autothermal JP-8 Fuel Reforming," Chemical Engineering Science, 2006. 61(16): p. 5328-5333.

**8.** A. Qi, et al., "La-Ce-Ni-O Monolithic Perovskite Catalysts Potential for Gasoline Autothermal Reforming System," Applied Catalysis A: General, 2005. 281(1-2): p. 233-246.

**9.** T. Hayakawa, et al., "$CO_2$ Reforming of $CH_4$ over Ni/Perovskite Catalysts Prepared by Solid Phase Crystallization Method," Applied Catalysis A: General, 1999. 183(2): p. 273-285.

**10.** D.J. Haynes, et al., "Catalytic Partial Oxidation of n-Tetradecane Using Rh and Sr Substituted Pyrochlores: Effects of Sulfur," Catalysis Today, 2009. 145(1-2): p. 121-126.

**11.** D.J. Haynes, et al., "Catalytic Partial Oxidation of n-Tetradecane Using Pyrochlores: Effect of Rh and Sr Substitution," Catalysis Today, 2008. 136(3-4): p. 206-213.

**12.** D.J. Haynes, et al., "Catalytic Partial Oxidation of a Diesel Surrogate Fuel Using an Ru-Substituted Pyrochlore," Catalysis Today. In press, corrected proof.

**13.** J. Cheng, et al., "Catalytic Combustion of Methane over $La_2TM_{0.3}Zr_{1.7}O_{7-[delta]}$ (TM = Mn, Fe, and Co) Pyrochlore Oxides," Catalysis Communications, 2009. 10(8): p. 1170-1173.

**14.** T.H. Gardner, et al., "Effect of Nickel Hexaaluminate Mirror Cation on Structure-Sensitive Reactions during n-Tetradecane Partial Oxidation," Applied Catalysis A: General, 2007. 323: p. 1-8.

**15.** H. Zhu, et al., "Catalytic Partial Oxidation of Methane Using RhSr- and Ni-Substituted Hexaaluminates," Proceedings of the Combustion Institute, 2007. 31(2): p. 1965-1972.

**16.** M.W. Smith, D.A. Berry, D. Shekhawat, D.J. Haynes, and J.J Spivey, "Effect of Oxide Catalysts and Oxygen-Conducting Supports on Partial Oxidation of Liquid Hydrocarbons," in 237th National Meeting and Exposition. 2009, American Chemical Society: Salt Lake City, Utah.

# III.F.3 Novel Water-Neutral Diesel Fuel Processor and Sulfur Trap

Subir Roychoudhury (Primary Contact), Christian Junaedi, and Dennis Walsh
Precision Combustion, Inc. (PCI)
410 Sackett Point Rd.
North Haven, CT 06473
Phone: (203) 287-3700 ext. 267; Fax: (203) 287-3710
E-mail: sroychoudhury@precision-combustion.com

DOE Project Manager: Joseph Stoffa
Phone: (304) 285-0285
E-mail: Joseph.Stoffa@netl.doe.gov

Contract Number: 84674

Start Date: August 15, 2008
End Date: August 14, 2010

## FY 2009 Objectives

- Experimentally demonstrate feasibility of reformer operation under a water neutral condition via water recovery through condensation or recycle approaches.
- Compare different catalyst options and evaluate their performance to determine the optimal catalyst for water neutral operation.
- Further develop and optimize the low pressure drop fuel injector/nozzle to permit stable steady-state operation, cold start-up, and 5:1 turndown ratio. Map autothermal reforming (ATR) performance with the low pressure drop nozzle and show coking avoidance with complete fuel conversion to C1 products and >80% reforming efficiency.

## Accomplishments

Within the nine-month period of this 2-year Phase II project, the feasibility of the proposed approaches has been demonstrated. In the next few months, more rigorous tests will be performed to confirm these preliminary results.

- **Developed system design for water neutral operation:** ASPEN modeling and simulation studies were conducted to determine the heat and mass balance requirements, overall system efficiency, and expected product composition for water neutral operation.
- **Demonstrated the feasibility of a recycle approach for water neutrality:** Preliminary tests have been completed to demonstrate the viability of using an anode recycle approach for water recovery and water neutrality on a Microlith®-based fuel reformer with Tier II diesel fuel. Stable reformer operation was achieved. The reformate gas composition obtained experimentally was in good agreement with that obtained via ASPEN analysis.
- **Further developed and optimized low pressure drop nozzle:** Further refinement of the nozzle design is ongoing. The optimized nozzle design has shown lower pressure drop and is expected to allow stable operation throughout the operating range without compromising catalyst performance.

## Introduction

Key barriers for the Solid State Energy Conversion Alliance industrial teams are the lack of a compact and economical diesel fuel processor capable of operating with long-term stability under a water neutral condition (i.e., very low steam to carbon ratios) while being resistant to coke formation and sulfur poisoning. Fuel preparation for these reformers also remains problematic primarily due to the lack of good mixing at low air pressure drop and resultant reactor non-uniformities leading to coke formation, among other things.

In previous work, PCI has identified the viability to operate a Microlith® diesel reformer at low steam-to-carbon ratios as to permit water neutral operation. The reformer was operated for more than 1,000 hours using low sulfur fuel without performance degradation, coking, and sulfur poisoning. Additionally, PCI has developed and demonstrated a low air pressure drop fuel injector with uniform mixing of fuel, air, and steam that enabled stable reformer operation without coke formation. In this Phase II project, PCI proposes to build on Phase I success to develop a novel compact and efficient integrated Microlith® diesel fuel processor for water neutral operation using feasible water recovery approaches. Additionally, further refinement of the low air pressure drop fuel injector will be performed to enable cold start-up and 5:1 turndown ratio while maintaining stable steady-state performance. This system and balance-of-plant simplification will allow for cost optimization to meet commercially viable targets for the entire auxiliary power unit (APU) fuel cell system.

## Approach

Reformer operation under water neutral or waterless condition by avoiding the need for external water addition is a significant requirement for practical portable systems. Moreover, lower water usage can lead to faster start-up times, as less water needs to

be vaporized at start-up. The reduction/elimination of water usage, however, can result in higher peak temperatures within the reactor/catalyst bed and can increase the production of higher hydrocarbons, particularly olefins, in the reformate stream. The former can compromise catalyst durability while the latter increases the likelihood of coking in the fuel cell stacks. It is important, therefore, to demonstrate long-term reformer operation at a water neutral condition using feasible water recovery approaches without performance degradation and coking.

The proposed concept to be refined and demonstrated in this project builds upon PCI's Microlith® reforming technology which employs a mesh-based, short contact time catalyst as an integrated component of a novel reformer system involving fuel injector, reactor, steam generator, and sulfur trap. PCI's existing 5 $kW_{th}$ system size is approximately 5 liters and weighs about 5 kg. This reactor starts up in partial oxidation mode and then transitions to ATR mode upon introduction of steam, operating at low steam-to-carbon ratios. It uses a limited amount of water that can be recovered from the system exhaust and permits efficient fuel reformation without performance degradation and coke formation. Since the reformer is operated at very low steam-to-carbon ratios, sulfur compounds are readily adsorbed in a downstream desulfurizer bed. Appropriate thermal integration of the reformer, SOFC, water recovery unit, and other balance-of-plant components in the APU system is also necessary to maximize the overall system efficiency.

## Results

The Phase II project started in fall 2008, and within the nine-month period of this 2-year project, several tests have been performed to demonstrate the feasibility of reformer operation under a water neutral condition. Additionally, preliminary tests have been completed to evaluate the viability of oxygen-blown ATR operation and to examine a new low pressure drop fuel injector. In the next few months, more rigorous tests will be performed to confirm these preliminary results.

### System Design Development via ASPEN for Water Neutral Operation

ASPEN modeling and simulation studies were conducted to determine the heat and mass balance requirements, overall system efficiency, and expected product composition for the reformer-anode gas recycle (AGR) configuration. The approach sought to avoid the need to supply water from an external source. The model was run for a variety of conditions spanning target internal oxygen-to-carbon (O/C) ratios and steam-to-carbon (S/C) ratios as well as AGR-air mixture inlet temperatures.

Evaluation of system efficiencies requires additional work, but initial findings suggest that the water-neutral reformer operation with direct mixing AGR configuration may give a similar efficiency to that of other alternatives. The comparative simplicity of the recycle approach may provide a more attractive solution.

### Reformer Operation with Anode Recycle Gas for Water Neutrality

PCI has modified an existing test rig to enable testing of a Microlith® fuel reformer coupled with anode recycle gas split stream. With the modified test rig, a surrogate gas mixture simulating anode recycle gas, consisting of steam, $H_2$, CO, $CO_2$, and $N_2$, at a controlled temperature and flowrate can be introduced. A reformer was fabricated and installed within the reactor housing and test rig.

In this study, the performance of PCI's reformer when operating with an AGR split stream to provide the required steam was examined. The tests were performed to demonstrate the feasibility of operating an integrated reformer and solid oxide fuel cell system with anode recycle gas for water-neutral operation. Based on the ASPEN modeling efforts described above, two AGR cases were examined by performing ATR operations at two different sets of O/C ratio and S/C ratio. A surrogate gas mixture that simulates the desired AGR composition was prepared and pre-mixed with air prior to entering the ATR reactor. The reactor was started under dry catalytic partial oxidation condition (i.e., waterless operation) by flowing Tier II diesel fuel and air, and then it transitioned to an ATR mode by introducing the AGR mixture consisting of $H_2O$ along with $H_2$, CO, and inerts. The temperature profile recorded during the preliminary tests showed minimal temperature fluctuations. A slip stream was taken from the outlet of the reformer for gas chromatograph analysis to measure the reformate gas composition. The experimental data showed that, in spite of a few differences in the operating conditions with the ones used in ASPEN analysis, the reformate gas composition obtained experimentally was in acceptable agreement with that obtained via thermodynamic analysis. The next step will be to perform additional tests at different conditions (i.e., O/C and S/C ratios) to characterize the reformer and to optimize the operating conditions such that the reformer can give complete fuel conversion and high reforming efficiency with no catalyst degradation over long-term operation.

### Development of a Low Pressure Drop Fuel Injector

A crucial challenge for on-board fuel reforming applications is the use of low pressure drop fuel injector/mixer for fuel, air, and steam introduction prior to entering the reactor. This will significantly reduce

the parasitic losses associated with pumping, and will increase the overall system efficiency. A prototype low pressure drop fuel injector is currently being further refined and optimized.

## Conclusions and Future Directions

The feasibility of operating a Microlith® diesel fuel reformer under water neutral condition using anode recycle gas as a water recovery approach was demonstrated. The test results showed that stable reformer operation was achieved, and <20 $ppm_v$ of coke precursors (e.g., ethane, ethylene) were measured in the reformate stream during these proof-of-concept tests. Additionally, ASPEN modeling and simulation studies were carried out to determine the heat and mass balance requirements, overall system efficiency, and expected product composition for the reformer-AGR configuration. The reformate gas composition obtained experimentally was in good agreement with that obtained via ASPEN thermodynamic analysis. This demonstrates the potential of a water-neutral system concept utilizing anode recycle approach. In the next few months, more rigorous tests will be performed to confirm these preliminary results.

Further refinement of the nozzle design is currently ongoing. The optimized nozzle design is expected to allow for cold start-up without compromising catalyst performance.

## FY 2009 Publications/Presentations

1. AIChE 2009 Spring Meeting in Tampa, Florida.
2. Abstract submitted for Fuel Cell Seminar in 2009.

# III. SECA CORE RESEARCH & DEVELOPMENT

## G. Power Electronics

# III.G.1 A Low-Cost Soft-Switched DC-DC Converter for Solid Oxide Fuel Cells

Jason Lai (Primary Contact), Sung-Yeul Park, Rae-Young Kim, and Hide Miwa
Virginia Polytechnic Institute and State University (VT)
302 Whittemore Hall
Blacksburg, VA 24061-0111
Phone: (540) 231-4741; Fax: (540) 231-3362
E-mail: laijs@vt.edu

DOE Project Manager: Maria Reidpath
Phone: (304) 285-4140
E-mail: Maria.Reidpath@netl.doe.gov

Subcontractors:
- Electric Power Research Institute, Knoxville, TN
- Southern California Edison, Los Angeles, CA

Contract Number: 41567

Start Date: October 1, 2002
End Date: July 31, 2008

## FY 2009 Objectives

- Develop a low-cost high-efficiency direct current (DC)-DC converter for solid oxide fuel cell (SOFC) applications in automotive auxiliary power units.
- Develop power management control strategies and demonstrate the ability to interface with SOFC controllers for battery charging.
- Test a high-efficiency DC-DC converter with a Delphi SOFC for 12 V vehicle battery charging.
- Test dynamic response of the DC-DC converter and SOFC under load transient conditions.

## Accomplishments

- Developed a low-cost multiphase DC-DC converter for SOFC applications in automotive auxiliary power units.
- Demonstrated compatibility of a DC-DC converter interfacing with a Delphi SOFC simulator and actual fuel cell controllers.
- Demonstrated 98% peak efficiency of the DC-DC converter and high efficiency operation over a wide load range.
- Demonstrated stable operation of the DC-DC converter and SOFC under dynamic load changes.

## Introduction

VT has developed high efficiency DC-DC converters for low-voltage fuel cells for the Solid State Energy Conversion Alliance (SECA) Core Technology Program. The original VT 6-phase DC-DC converter (V6) was designed for a 20 to 50 V input and 400 V output for a typical DC-alternating current (AC) inverter that can output 220 V AC power. However, the SOFC developed by Delphi is aimed at automotive applications, which has a similar fuel cell voltage range, from 35 V to 63 V, but the output is for 12 V vehicle battery and associated DC loads. Therefore, some modifications are needed for the V6 DC-DC converter to work with the Delphi SOFC.

The major modification is to change the 6-phase output to 3-phase output to reduce the number of inductors, and then to replace the transformer with the inductor to serve as a step-down converter. Furthermore, a new interface board needs to be designed and built so the new converter can communicate with the Delphi SOFC controller. The interface board takes frequency command signals from Delphi SOFC control signals and converts them to internal voltage and current commands for the DC-DC converter control.

Major efforts include to:

(1) Modify existing V6 DC-DC converter to change from nominal 400 V to 13.8 V output
(2) Design and build an interface board for communication
(3) Test the new converter with VT SOFC simulator
(4) Test the new converter with Delphi SOFC simulator
(5) Test the new converter with Delphi SOFC
(6) Final reporting

Basic specifications of the converter are listed as follows:

(1) Input: 35 V to 63 V with 36 V as nominal
(2) Output: 13 V to 16 V with 13.8 V as nominal
(3) Power: 3 kW
(4) Efficiency: >96%
(5) Cooling: Forced air cooling
(6) Size: Standard rack mount unit 5.25” high × 19” wide × 16” deep
(7) Interface: 20 to 900 Hz frequency for 0 to 200 A current setting

The first test was performed with the Delphi SOFC controller but running with a DC power supply as the source. The test essentially mimics the actual SOFC test condition. After rigorous tests with a high voltage level (60 V) and high current level (200 A) using the power supply as the source and final calibration of the controller parameters, the DC-DC converter was proven working very well under both steady-state and dynamic conditions. The current ramp can also be precisely controlled. From no-load to full-load, test results showed a voltage regulation of ±0.01 V for the 13.8 V output range and a current regulation of ±1 A for the 200 A output range. Efficiency was consistently higher than 97% for the load above 1 kW conditions. No significant temperature rise or hot spot was observed after the test. The temperature of key power components remains lower than human body temperature after a full load test. With the confidence of the converter performance, the converter was then tested with the actual SOFC. The entire converter test with the SOFC was very smooth, and the performance agreed with the test results obtained from fuel cell simulators.

## Approach

Figure 1 shows the circuit diagram and photograph of the modified three-phase (V3) DC-DC converter designed for the Delphi SOFC. The power circuit is simplified from six phases to three phases, so the number of output inductors remains at three. The three phases are operated 120° apart; therefore, the original programmed phase sequence in the V6 converter does not need to be changed. The input voltage is higher than the original design level, so the devices need to be changed to a higher voltage rated metal oxide semiconductor field effect transistor (MOSFET). The new device is rated at 75 V, which should be sufficient to handle the 63 V input. Notice that the bottom side MOSFET switches of the 3-phase bridge are paralleled with Schottky diodes to reduce the switching loss. The buck converter requires only a diode for the bottom side. However, a typical diode has a fixed voltage drop of 0.7 V at light load conditions, which accounts for 2% conduction loss. Even with a Schottky diode, the voltage drop is about 0.4 V at light load conditions. Under the rated load condition, a Schottky diode will see at least a 0.7 V drop. With an additional upper MOSFET switch conduction voltage drop, switching loss, inductor loss, capacitor loss, and parasitic losses, the theoretical maximum efficiency will be less than 95%. Therefore, we propose to use a power MOSFET as the bottom switch to operate under synchronous rectification mode, while keeping the Schottky diode to reduce the switching loss under light load conditions, so the efficiency remains high over the entire load range. The calculated efficiency is higher than 97% in most load conditions.

The interface between the SOFC and DC-DC converter involves power and control and communication. The power connections include input and output terminals. We added two DC contactors to help start-up control for both input and output connections. The input contactor cannot be turned on without the output connected to a 12 V battery, while the output connector cannot be turned on when the converter output and battery voltage difference is too high. A high voltage difference tends to spark over the contacts of the DC contactor and damage the mechanical contacts. If the converter output voltage is less than the battery voltage, turning on the contactor can also damage the power MOSFET because the circuit functions like a boost converter that produces excessive voltage and can damage the power devices.

For the control and communication interface, the design options can be digital or analog. Digital interface is less sensitive to noise interference but requires additional conversion. Analog interface is simple, but the signal can be easily corrupted by the noise. Therefore, our choice is a more reliable digital interface, which should be compatible with the Delphi fuel cell controller's 20 Hz to 900 Hz. For the current control or current limit, this frequency range represents 0 to 200 A. For the voltage control, the frequency range can

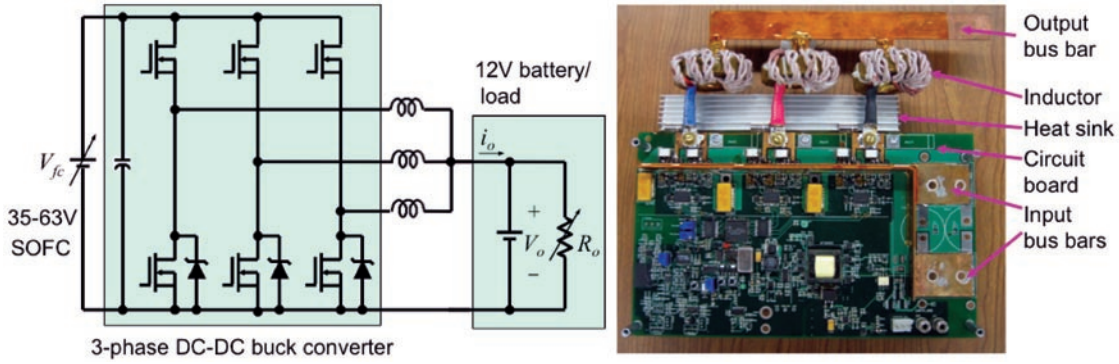


**FIGURE 1.** Circuit Diagram and Photograph of a 3-Phase DC-DC Converter for Auxiliary Power Units

be specified to cover the battery voltage state-of-charge range, typically from 11 V to 16 V.

## Results

Before testing with an actual SOFC, the converter was tested with both the VT and Delphi fuel cell simulator. Test points include some high-voltage, low-current points and some low-voltage, high-current points to simulate actual SOFC operating points. Figure 2 shows efficiency evaluation results for the voltage range of 60 V down to 35 V and output current from 5 A up to 200 A. The efficiency is generally higher under heavier load conditions. For the first point with a load less than 250 W, the efficiency is only 70%. At 500 W, the efficiency quickly moves to 90%, and at 1 kW, the efficiency reaches 97%. There are two unusual efficiency points that indicate an efficiency of >99% between 1 kW and 1.5 kW range, which could be measurement error. As a comparison, we added three points measured with the VT fuel cell simulator; the efficiency is around 97%. As the load increases to full load (3 kW) range, the efficiency stays around 97.5%, which is consistent with what has been measured in the VT lab. This result confirms that the proposed approach with a synchronous rectification operated power MOSFET in parallel with a Schottky diode can break the theoretical efficiency limit of 95% when only a Schottky diode is used.

After the converter was tested with the SOFC simulator, it was moved to the fuel cell test stand. Figure 3 shows a photograph of the test setup with the VT DC-DC converter and the Delphi SOFC. The fuel cell output is monitored and controlled by setting a set of fuel cell parameters. The load contains a 12 V battery pack and a programmable electronic load. The entire test condition is the same as that under the SOFC simulator test, except that the source voltage and available current are dependent on the SOFC condition. For every test point, the SOFC parameters need to be adjusted to match the output.

Three efficiency points were tested to compare with the results obtained from the SOFC simulator test. Figure 4 shows the efficiency and fuel cell output voltage as a function of the output power. The first point starts at about the 600 W condition, and the efficiency is about 95%. This is slightly better than the one obtained from the fuel cell simulator test (94.5%) because its voltage is lower. The second point runs at about the 900 W condition, and the efficiency is about 97%, which agrees the test result obtained from the simulator test very well. The third point is measured at about 1.3 kW, and the efficiency reaches 98.5%. This agrees with the results obtained from the Delphi fuel cell simulator, but is more than 1% higher than the one measured with the VT fuel cell simulator. It appears that the instrumentation tends to favor output power between the 1 and 1.5 kW

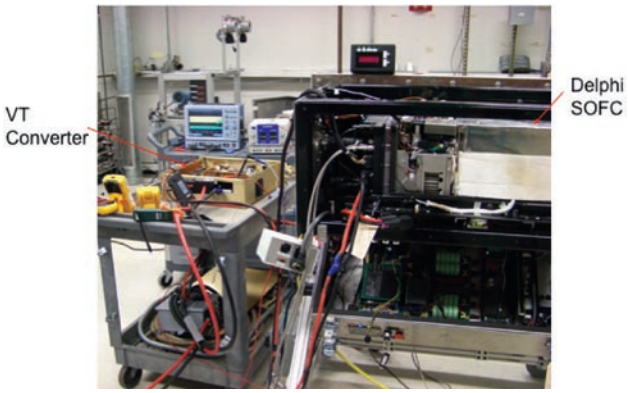


**FIGURE 3.** Photograph Showing Setup of the VT DC-DC Converter Tested with the Delphi SOFC

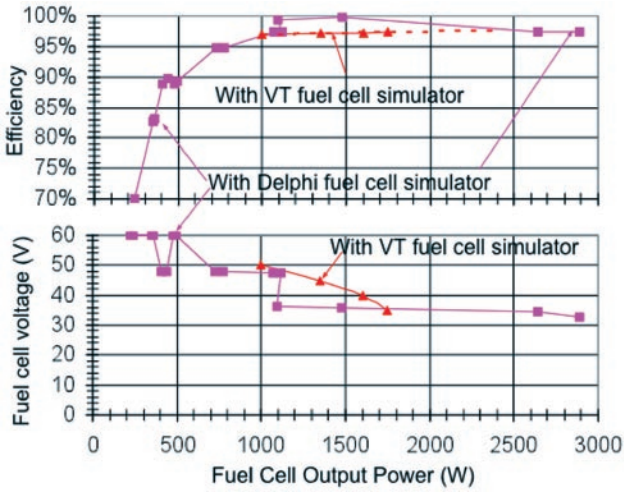


**FIGURE 2.** Efficiency Test Results with SOFC Simulators

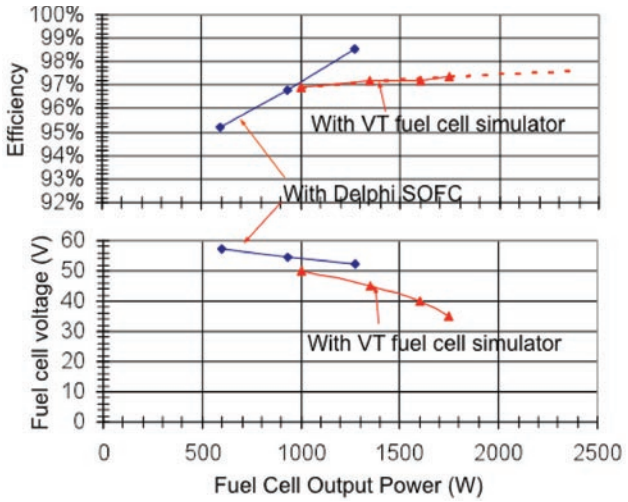


**FIGURE 4.** Efficiency Evaluation Results with the Delphi SOFC

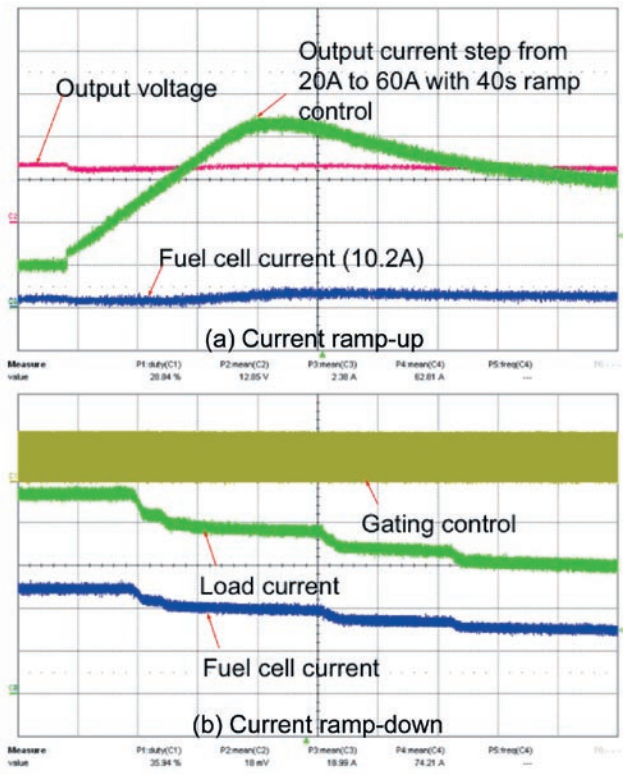


**FIGURE 5.** SOFC Output Current Responses under Dynamic Load Current Ramp-up (a) and Ramp-down (b) Control

range. Nevertheless, the VT converter has demonstrated a superior efficiency under both SOFC and SOFC simulator test conditions.

The fuel cell power availability depends on various factors. With temperature as the dominant factor, the fuel cell output current ramp needs to be slowed down with proper control. Although the previous fuel cell simulator tests indicated that the VT converter has a fast current loop control, and the current ramp can be achieved within 10s of milli-seconds, the actual fuel cell output ramp needs to be controlled in 10s of seconds. Figure 5(a) shows test results using the Delphi SOFC controller to obtain the current ramp control of 40 A/40 s rise rate. Figure 5(b) shows voltage and current waveforms under a load dump from 95 A to 60 A. The load dump process was performed continuously with several steps, and the scope time scale was changed to 1 s/div to capture the current waveforms. Again, the fuel cell and load currents smoothly reduce and follow the command precisely.

## Conclusions and Future Directions

The entire test with the VT DC-DC converter operating under the Delphi SOFC controller was very smooth and successful. The VT DC-DC converter communicates with the Delphi SOFC controller very well with current control scale well calibrated. Major test items are summarized as follows:

- Tested voltage range: 32 to 60 V
- Test current range: 0 to 203 A
- Voltage regulation from the 0 to 3 kW test condition is within 0.01 V.
- Current regulation from the 0 to 200 A test condition is within 1 A.
- Efficiency exceeds 97% at loads higher than 1 kW and peaks at 97.5% at the 3 kW full load condition.
- Dynamic load step and load dump follow the command rate precisely and operate smoothly.

Some of the test conditions are actually tougher than the original specification. For example, the low-end tested voltage of 32 V is lower than the original specified 35 V. The highest current tested was 203 A, which is higher than the specified 200 A. The DC-DC converter ran robustly even after the failure of the mechanical contactor. The efficiency exceeds the SECA goal of 97%. Multiple-phase interleaving operation design was proved to be reliable and ripple free at the output, which is desirable for the battery charging. The efficiency numbers are consistent throughout all the tests in the VT Future Energy Electronics Center and Delphi test stand. Overall this is a very successful collaboration project between the SECA Core Technology Team and Industrial Team.

## Patent

**1.** Jih-Sheng Lai, "Multiphase soft switched DC/DC converter and active control technique for fuel cell ripple current elimination," U.S. Patent #7,518,886, April 2009.

## FY 2009 Publications/Presentations

**1.** S.-Y. Park, C.-L. Chen, and J.-S. Lai, "A Wide Range Active and Reactive Power Flow Controller for a Solid Oxide Fuel Cell Power Conditioning System," *IEEE Trans. on Power Electronics,* November 2008, pp. 2703–2709.

**2.** S.-Y. Park, C.-L. Chen, J.-S. Lai, and S.R. Moon, "Admittance Compensation in Current Loop Control for a Grid-Tie LCL Fuel Cell Inverter," *IEEE Trans. on Power Electronics,* July 2008, pp. 1716 – 1723.

**3.** J.-L. Chen, Jih-Sheng Lai, Y. Wang, S.-Y. Park, and H. Miwa, "Design and Control for LCL-Based Inverters with Both Grid-Tie and Standalone Parallel Operations," in *Conf. Rec. of IEEE IAS, Edmongton*, Alberta, Canada, October 2008.

**4.** S.-Y. Park, C.-L. Chen, and J.-S. Lai, "A Wide Range Active and Reactive Power Flow Controller for a Solid Oxide Fuel Cell Power Conditioning System," in *Proc. of IEEE APEC*, Austin, Texas, February 2008, pp. 952-958.

# III. SECA CORE RESEARCH & DEVELOPMENT

## H. Modeling and Simulation

# III.H.1 SOFC Design Basis Development Project

Anthony Amato
American Society of Mechanical Engineers (ASME)
Three Park Avenue
New York, NY 10016-5990
Phone: (212) 591-7003; Fax: (212) 591-7196
E-mail: amatoa@asme.org

DOE Project Manager: Travis Shultz
Phone: (304) 285-1370
E-mail: Travis.Shultz@netl.doe.gov

Contract Number: 41817

Start Date: December 8, 2008
End Date: November 14, 2009

### FY 2009 Objectives

- Develop a peer-reviewed guide which contains recommended design practices and associated modeling and analysis procedures developed within the Solid State Energy Conversion Alliance (SECA) Core Technology Program for solid oxide fuel cells (SOFCs). Facilitate development of cost-effective, reliable SOFC designs.

### Accomplishments

- Results and methodologies developed within the SECA Core Technology Program were incorporated into the design guide.
- The final design guide draft was completed, including review and editing of complete document by ASME consultants.
- The complete design guide has been released to the National Energy Technology Laboratory (NETL) for peer review by SOFC developers.

## Introduction

In 1999, the United States (U.S.) Department of Energy established SECA to accelerate development of affordable SOFCs. Participants in the program include independent industrial teams, tasked with producing state-of-the-art SOFC systems, and Core Technology Teams, charged with addressing key technology barriers and transferring their research results to the industrial teams. As part of this technology transfer process, NETL teamed with ASME to produce a Solid Oxide Design Basis, a document that would collect research results as well as best-practice analytical procedures and experimental methods from Core Technology Program participants, particularly the national laboratories, in order to make them readily available to the industrial teams and other U.S. SOFC developers.

The objective of the guide is to provide recommended design practices and associated modeling and analysis procedures, to be used by U.S. designers and fabricators of SOFCs, to optimize the design of durable and reliable SOFCs. The guide is based on past successful usage of modeling tools to improve SOFC designs as well as advances in the state of knowledge. It describes suggested analytical procedures developed by the SECA Core Technology Program to model electrochemical and thermo-mechanical performance of SOFCs as well as how these tools and other simulation tools can be used in designing a structurally-reliable and durable SOFC stack. The recommended modeling procedures contained in the guide attempt to account for the variability in material properties and design parameters of the essential elements in the SOFC structure. These modeling procedures address the coupled electrochemical and thermo-mechanical nature of SOFCs by quantifying the electrochemistry activities and the associated thermal-mechanical behaviors of various SOFC components for different design configurations. The guide is intended to facilitate development of cost-effective, reliable, SOFC designs.

The guide is intended to provide design criteria for routine use and not necessarily to provide specific criteria for infrequently encountered problems that might occur in the full range of SOFC design. Because many of the topics addressed are still under intensive research and development, the document is also intended to serve as a repository for state-of-the-art knowledge and experience gained in SOFC designs.

## Approach

A team was assembled comprising technology leads for the Core Technology efforts at Pacific Northwest National Laboratory and Oak Ridge National Laboratory, a subject matter expert with industry experience and experts on standards development from ASME. Relevant research completed by the national laboratories and industry was identified for incorporation into the document. Based on this research, recommended design practices and procedures were developed.

The document structure was designed for ease of access to relevant information and for ease of updating. The main document body contains general principles, methods and approaches, with detailed results and data

located in appendixes. As new research is conducted and incorporated, the appendixes can be updated appropriately with minimal changes required to the main body of the guide.

An ASME code writing expert was engaged to compile the various research reports and data into standards-type format and language. The draft document was provided for peer review by a group of SOFC subject matter experts from industry and national laboratories.

## Results

A complete draft of the SOFC design guide has been completed. The guide's structure and topics covered are indicated in Table 1. The draft has been submitted to NETL, from where it will be forwarded to SOFC developers for peer review.

The completed guide outlines a systematic process for SOFC stack design. It contains guidelines that provide a methodology for evaluation and optimization of SOFC reliability, focusing on failure mechanisms associated with the thermo-mechanical properties and state of the SOFC. The guide also contains newly developed content, including materials, component and operational sensitivity analysis to guide SOFC redesign and optimization, as well as derived safety factors for component design.

## Conclusions and Future Directions

The SOFC design guide is undergoing peer review by SOFC developers. The guide will be appropriately edited in response to this review and released as a completed document.

Many of the topics addressed herein are under on-going research and development and therefore the SOFC design basis development guide will be regularly updated so that it contains state-of-the-art knowledge and experience gained in SOFC designs. A plan and schedule for revision and updating will be developed. Future updates of the guide will incorporate coverage of additional topics, including SOFC performance degradation with time and response to transients.

**TABLE 1.** SOFC Design Basis Development Guide Elements

| Element | Description |
|---|---|
| Forward | |
| Acknowledgments | |
| Acronyms and Abbreviations | |
| Introduction & Background | |
| Scope & Assumptions | Stationary, Base-loaded systems<br>Design for initial operation<br>SOFC stack only<br>Manufacturing methods and tolerances |
| SOFC Requirements | Stack power output<br>Stack operating voltage<br>Fuel and oxidant flows<br>Weight and Volume<br>Electrical load profile |
| Materials and Material Properties | SOFC Components commonly used<br>Electrolyte<br>Anode<br>Cathode<br>Interconnect<br>Seal<br>Material Properties<br>Structural<br>Thermal<br>Electrical<br>Interfacial Material Properties |
| SOFC Electrochemistry | Fuel Cell Electrochemical Reactions<br>Current-Voltage Relation<br>Pressurization |
| Analysis Procedures & Tools | Physical Phenomena Being Modeled<br>Modeling and Analysis Tools<br>Thermal-Fluid-Electrochemical Analysis<br>Thermal-Structural Analysis |
| Design/Failure Criteria | Bulk Failure<br>Discrete Fracture<br>Delamination<br>Loss of Contact |
| Evaluation & Redesign | Component Design Modifications and Sensitivities<br>Operational Design Modifications and Sensitivities<br>Materials Design Modifications and Sensitivities<br>Redesign |
| References | |
| Appendices | |

# III.H.2 Solid Oxide Fuel Cell Design Guide

M.A. Khaleel (Primary Contact), B.J. Koeppel, K.P. Recknagle, E.V. Stephens, X. Sun, B.N. Nguyen, E. Lara-Curzio, A. Shyam, Y. Wang, J. Powers, R. Swayne, B. White, T. Shultz, and W. Surdoval
Pacific Northwest National Laboratory (PNNL)
902 Battelle Blvd.
Richland, WA 99352
Phone: (509) 375-2438; Fax: (509) 375-4392
E-mail: moe.khaleel@pnl.gov

DOE Project Manager: Briggs White
Phone: (304) 285-5437
E-mail: Briggs.White@netl.doe.gov

Contract Number: 40552

Start Date: October 1, 2008
End Date: September 30, 2009

### FY 2009 Objectives

- Provide recommended practices and associated modeling and analysis procedures for use by Solid State Energy Conversion Alliance (SECA) affiliated stack designers and fabricators.
- Provide recommended practices for design of durable and reliable solid oxide fuel cell (SOFC) stacks.
- Serve as a repository for state-of-the-art knowledge and experience gained in SOFC designs.

### Accomplishments

Completed the first version of the SOFC fuel cell design document that provides SOFC designers with guidance on the design, analysis, material data needs, and redesign options for planar stacks.

## Introduction

In 1999, the United States Department of Energy, along with industrial teams and groups from the scientific community, established the Solid State Energy Conversion Alliance to accelerate development of affordable SOFCs. This guide was created to provide recommended design practices and associated modeling and analysis procedures to be used by SECA affiliated designers and fabricators of SOFCs to optimize the design of durable and reliable fuel cells.

This guide is based on past successful use of modeling tools to improve SOFC designs as well as advances in the state of knowledge. It describes suggested analytical procedures developed by the SECA Core Technology Program to model electrochemical and thermomechanical performance of SOFCs and how simulation tools can be used in designing a structurally reliable SOFC stack. The recommended modeling procedures presented in this guide attempt to account for the variability in material properties and design parameters of the essential elements in the SOFC structure. These modeling procedures capture the coupled physical phenomena of SOFCs by quantifying the electrochemistry activities and the associated thermomechanical behaviors of various SOFC components for different design configurations. This guide is intended to facilitate development of cost-effective, reliable, SOFC designs and is intended to serve as a repository for state-of-the-art knowledge and experience gained in SOFC designs as research and development continues.

## Approach

The technical approach taken here was to create a document that mirrors PNNL's stack design work flow. The guide is structured according to a design process work flow beginning with key inputs such as system requirements and material property data before beginning the iterative design process. The work flow of the document (and of the design process) can be grouped into two parts: 1) the development of the design envelope (the upper row of elements in Figure 1); and 2) the iterative design process loop in which convergence to a working design may be achieved (the lower loop of elements in Figure 1). High level descriptions are provided in the main body of the document with technical details listed in the appendices. Since many of the topics addressed by this guide are still under intensive research and development, this document will be a living document and revised as warranted.

## Results

### The Design Envelope

Any design process must begin with a variety of inputs. The SOFC needs to be designed to meet numerous requirements, both of performance and operating conditions. The SOFC stack is a multi-component system containing many different materials that must be compatible and stable. It is also fundamentally an electrochemical device, and the

thermomechanical state of the stack strongly depends on the electrochemical performance. By establishing the system requirements such as total power, power density, stack volume, gas flow and pressure drop and identifying material sets with acceptable properties and electrochemical performance, etc., all of these inputs come together to define the working design envelope.

The work flow of the document begins with the upper row of elements in Figure 1. These key inputs are steps in the work flow diagram that also correspond to the respective chapter within the guide. The scope and assumptions for the design must be established in order to determine what analyses need to be done to validate a design. A set of limiting assumptions relevant to the analyses described in this guide include the following: 1) the user of this guide is assumed to have a basic knowledge in fuel cell design, operation and material selection; 2) analyses are limited to stationery systems; 3) focus is on planar SOFCs; 4) the SOFC is designed for steady-state operating conditions; and 5) analytical models consider only nominal component dimensions.

Chapter 2 discusses the scope and assumptions of the design guide document. The requirements that most strongly influence SOFC design are discussed in Chapter 3 such as determining the stack size and operation characteristics to obtain the desired electrical power; and the specifications of the fuel and oxidant flows such as inlet and outlet temperatures, pressures, compositions, and fuel and air utilization. Chapter 4 discusses commonly used materials for SOFC components and key materials properties needed. It also discusses the solid material properties required and the models to which they apply. Details and descriptions of methods used to determine material properties for many SOFC materials currently used are provided in the appendix. Chapter 5 provides background and a summary of how the electrochemical performance model is assembled for the various reactions that occur in an operating SOFC and used for analysis of the stack.

## The Iterative Design Process

The second part of the work flow in the design guide is the iterative design process, as shown in the lower loop of Figure 1. After an initial design is prepared, it must be analyzed to establish the thermomechanical state of the SOFC stack. Once the stack has been modeled, its state must be compared to a set of design and failure criteria to establish whether the design is successful. If the design results exceed the failure criteria specified (e.g., the local stress in a cell exceeds the failure stress, causing cracking), then the design must be modified. Any changes implemented, whether it be geometrical, operational, or material, must be evaluated and the design process repeated. Again, these steps in the work flow diagram also correspond to the respective chapter within the guide.

Chapter 6 describes the various analysis tools needed and the physics required to sufficiently model the stack. It also provides insight regarding issues to be aware of during model setup; key elements required to provide good thermal management; how to implement custom material property data into the models; and a discussion on PNNL-developed SOFC modeling procedures that have been implemented

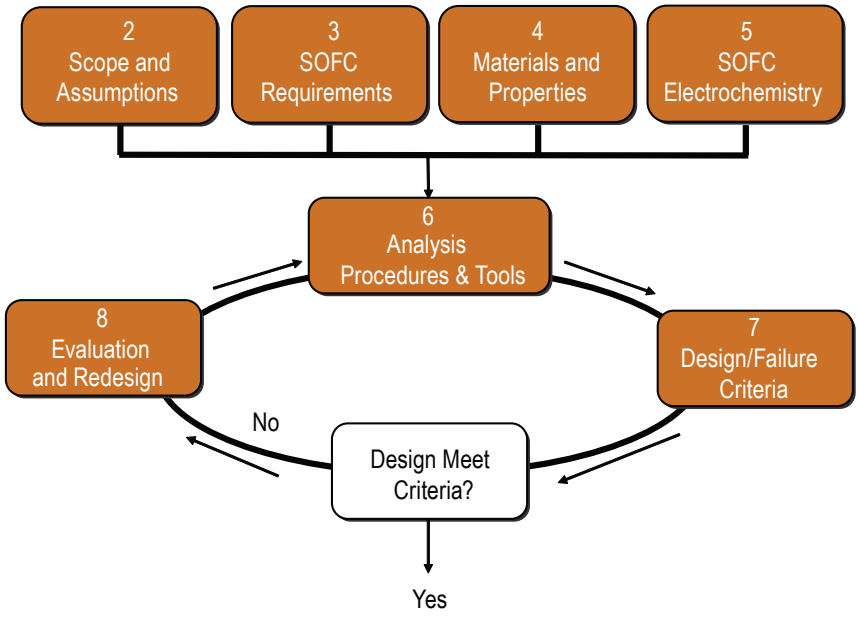


**FIGURE 1.** The Work Flow Diagram for the Developed SOFC Design and Analysis Guidance Document

into commercially available modeling tools. Chapter 7 describes failure criteria and provides guidelines for safety factors to be used in SOFC design. The analysis tools in Chapter 6 and the failure criteria in Chapter 7 provide methods to evaluate the SOFC design as described in Chapter 8. Chapter 8 also provides guidelines for improving the design showing relationships and sensitivities between design parameters and the resulting thermomechanical state of the SOFC.

## Conclusions and Future Directions

During this year, PNNL in collaboration with the National Energy Technology Laboratory, Oak Ridge National Laboratory, and the American Society of Mechanical Engineers Codes and Standards Technology LLC have developed a design guidance document that provides SECA affiliated designers and fabricators with recommended design practices and associated modeling and analysis procedures to optimize the design of durable and reliable planar SOFCs. The guide is structured according to a design process work flow beginning with key inputs such as system requirements and material property data before beginning the iterative design process.

Future direction of this document includes a peer review as directed by the DOE project manager and release of this initial version design guide document.

# III.H.3 Interconnect Life Prediction

Xin Sun (Primary Contact), Wenning Liu, Elizabeth Stephens and Mohammad A. Khaleel
Pacific Northwest National Laboratory
902 Battelle Blvd.
Richland, WA 99352
Phone: (509) 372-6489; Fax: (509) 372-6099
E-mail: xin.sun@pnl.gov

DOE Project Manager: Briggs White
Phone: (304) 285-5437
E-mail: Briggs.White@netl.doe.gov

Contract Number: 40552

Start Date: October 1, 2008
End Date: September 30, 2009

### Objectives

- Ensure long-term structural integrity of metallic interconnect (IC).
- Provide optimized spinel coating thickness to meet Solid State Energy Conversion Alliance (SECA) life requirements.

### Accomplishments

- Predict IC life/durability for various IC candidates by comparing predicted interfacial stress during cool down with interfacial strength.
- Examine effects of surface modifications on oxide adhesion strength and tendency for spallation.

## Introduction

The oxidation reaction of the metallic ICs in SOFC working environments is unavoidable. The oxidation reaction can be slowed but not completely stopped by the application of protective coatings. The appearance and growth of the oxide scale will cause growth stress in the oxide scale. In addition, the coefficient of thermal expansion (CTE) mismatch between the oxide and the substrate creates stresses in the scale and on the scale/substrate interface during cooling, leading to possible scale delamination and spallation.

The interfacial strength between the oxide scale and the substrate is crucial to the reliability and durability of the metallic IC in SOFC operating environments. The goal of this task is to develop an integrated experimental/analytical methodology for quantifying the interfacial strength between the oxide scale and the different metallic IC candidates, therefore being able to predict the life of various IC candidates under the typical SOFC operating conditions. Furthermore, this integrated approach can also be used to quantify the effects of different surface finishes, coating layer thicknesses as well as different coating materials such that optimized coating thickness as well as surface condition for the IC candidates can be developed to satisfy SECA life requirements.

## Approach

The following technical approaches have been taken in Fiscal Year 2009 to meet the overall project goals:

- Integrated analytical/experimental approach in quantifying interfacial adhesion strength and in predicting coated and uncoated IC life during stack cooling.
- Experimental/analytical approach in examining the effects of various substrate surface finishes on the adhesion strength between oxide and substrate during isothermal cooling.
- Optimize substrate and coating thickness to meet SECA 40,000-hour life requirement.

## Results

### Effect of Spinel Coating Thickness and Oxide-Scale Growth on Predicted Cooling Induced Interfacial Stresses for SS441

The influence of the thickness of the protective spinel coating layer on the interfacial stresses is studied for SS441 using finite element analyses. Three different spinel coating thicknesses and four different oxide-scale thicknesses have been considered. The detailed results are summarized in a separate topical report. Table 1 tabulates the predicted maximum interfacial stress upon cooling for the different cases considered. It is found that for the same oxide-scale thickness, the cooling-induced interfacial stresses only slightly increase with coating thickness. This is because of the subtle CTE differences among the tri-layers (i.e., oxide scale, substrate, and coating). As expected, the interfacial stresses at both interfaces increase with the increase of oxide-scale thickness. Based on the previously quantified strength of 886 MPa for the interface between the oxide-scale and the spinel coating, results predicted in Table 1 indicate that the interfaces between the scale and the spinel coating are safe during cooling for all the cases considered (green column). On the other

**TABLE 1.** Predicted Maximum Cooling-Induced Interfacial Shear Stresses for Different Coating and Oxide-Scale Thickness

| Coating | Coating: 10 um SS441: 1.6mm | | Coating: 25 um SS441: 1.6mm | | Coating: 50 um SS441: 1.6mm | |
|---|---|---|---|---|---|---|
| Scale thickness | Scale/441 | Scale/Coat | Scale/441 | Scale/Coat | Scale/441 | Scale/Coat |
| 2 um | 441 MPa | 322 MPa | 443 MPa | 325 MPa | 444 MPa | 326 MPa |
| 5 um | 487 MPa | 350 MPa | 491 MPa | 361 MPa | 492 MPa | 365 MPa |
| 10 um | 489 MPa | 360 MPa | 518 MPa | 361 MPa | 503 MPa | 374 MPa |
| 15 um | 485 MPa | 345 MPa | 527 MPa | 359 MPa | 527 MPa | 382 MPa |

hand, higher cooling induced interfacial stresses are consistently predicted at the interfaces between the scale and SS441. Comparing these stresses with the strength quantified for that interface, i.e., 320 MPa, it is found that cooling induced spallation will occur at that interface, even for SS441 with the thinnest oxide-scale (red column). Possible methods of improving the life of coated SS441 were also examined. It should be noted that these cooling induced stresses are predicted for SS441 with substrate thickness of 1.5 mm, and the highest shear stress is predicted at the edges of the samples. Our prior work has shown that reducing the substrate thickness can effectively reduce the cooling induced interfacial stresses. In addition, the interfacial adhesion strength between the oxide scale and the substrate can also be improved through Ce-doped spinel coatings as well as other methods of substrate surface modifications. Collaborations with the materials development team in this area are currently underway.

## Effects of Surface Quality on Oxide Adhesion upon Cooling and Indentation

In order to examine the effects of surface roughness on oxide scale adhesion of SS441, seven 2" x 1" 441SS substrate specimens were fabricated where half of each sample was taped off to allow fine polishing of the neighboring surface and to leave the taped surface in the as-received condition. A one micron diamond paste was used in the final polishing step of the polished surface. Figure 1(a) is a representative image of the non-oxidized specimens. Surface roughness measurements were performed and the measured $R_a$ value averaged approximately 0.02 for the polished surfaces and approximately 0.30 for the non-polished surfaces as received. Three specimens were oxidized for 900 hours at 850°C then furnace cooled to room temperature.

Upon removal of the oxidized specimens from the furnace, spalling of the oxide scale was observed on one of the specimens with surfaces left in the as-received condition. The oxide scale remained intact on the polished surfaces of all specimens. Figure 1(b) is an image of one of the oxidized specimens after removal from the furnace. The furnace cooling results therefore

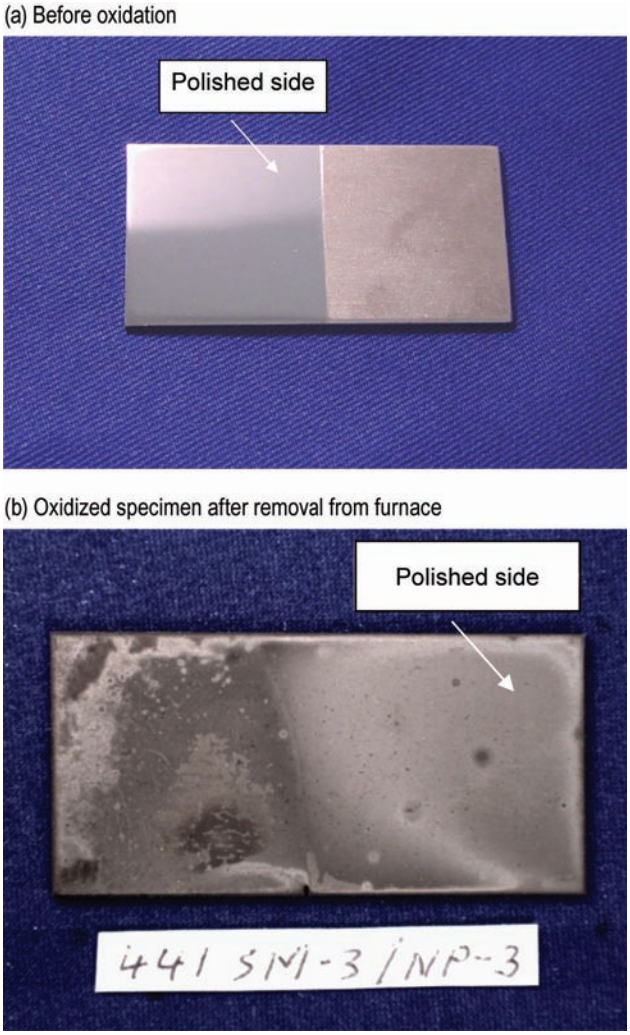


**FIGURE 1.** Representative Images in Studying the Effects of Surface Roughness

indicate that a smoother than as-received surface can reduce the probability for scale spallation during cooling.

Indentation tests utilizing a 1/16" ball indenter were performed on the three oxidized specimens. Analysis of the region around the indentations showed good scale adhesion in the polished regions with two catastrophic spallations observed on one of the polished surfaces.

Spallation occurred at 75 kgf. The non-polished adhesion results were mixed with one surface completely spalling prior to indentation (NP-3), one surface not spalling even with indentation (NP-1), and one surface spalling in three indented locations (NP-2). Spallation occurred at 100 kgf for these specimens. It is believed that the surface modification may not have been uniform and the standard deviation determined from the surface roughness measurements of the as-received 441 material reveals the presence of some localized defect. During indentation testing, if the indenter is applied directly on a defect, localized stress concentrations will lead to spallation.

### Effects of Shot Peening on Oxide Adhesion upon Cooling for SS441

It is well established that shot peening roughens a surface. However, the effects of shot peening on the oxide adhesion to substrate during cooling is not well established. To investigate and quantify this effect, eighteen 2" x 1" 441 SS samples were shot-peened utilizing stainless steel shots and standard automotive shot peening processing parameters. A representative image of a shot-peened specimen is shown in Figure 2(a). Shot peening of the surface created an average $R_a$ surface roughness of 2.7 um with a compressive residual stress of 230 MPa at a depth of 125 um.

(a) Shot peened sample before oxidation

(b) Oxidized shot peened sample after removal from furnace

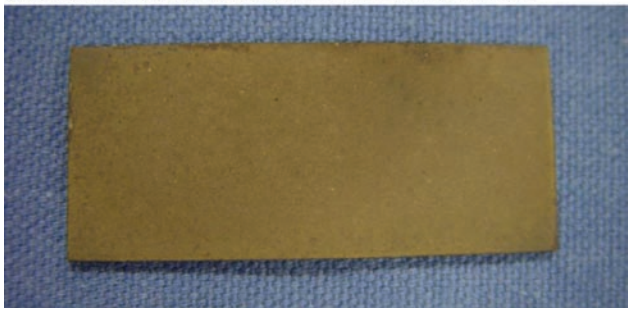

**FIGURE 2.** Representative Images in Studying the Effects of Shot Peening

Uncoated shot-peened specimen substrates were then oxidized at 850ºC in atmosphere for 600, 900, and 1,200 hours, two specimens for each condition. To date, the 600-hour specimens have completed oxidizing. A representative image of the oxidized sample upon furnace removal is shown in Figure 2(b).

It should be noted that neither of the sample surfaces nor the edges spalled during the cooling phase. Comparing these results with the ones shown in Figure 1(b), it is clear that shot peening not only influences the adhesion strength between the oxide and the substrate, it also reduces the interfacial shear stress at the sample edges during cooling, which is the driving force for edge spallation. Further work in quantifying these effects is underway and results will be presented later.

## Conclusions and Future Directions

During FY 2009, our work in predicting and extending coated interconnect life has focused on the effects of surface finish on the adhesion strength and driving forces for spallation during cooling. Several conclusions can be made based on the experimental and modeling work to date:

- Reducing the substrate thickness can effectively reduce the cooling induced interfacial shear stresses.
- As-received SS441 has high tendency for oxide scale spallation during cooling. Polishing the surface to $R_a$ of 0.02 reduces the tendency for scale spallation.
- Surface modification through mechanical shot peening also dramatically reduces the tendency for oxide scale spallation during cooling.

Our future work in the interconnect life prediction and improvement will continue in the following areas:

- Quantify the adhesion strength improvement and delamination driving force reduction with different methods of surface modifications.
- Life prediction for Ce-MC spinel coated SS441 with various surface qualities.
- Continue to work with IC materials development team in optimizing the coating and substrate thickness in achieving SECA life requirements.

## FY 2009 Selected Publications/Presentations

**1.** W.N. Liu, X. Sun, and M.A. Khaleel, 2008, "Effect of Interconnect Creep on Long-Term Performance of SOFC of One Cell Stacks," In *32nd International Conference & Exposition on Advanced Ceramics and Composites,* vol. 29, no. 5, pp. 53-63. American Ceramic Society, Daytona Beach, Florida.

**2.** W.N. Liu, X. Sun, and M.A. Khaleel, 2008, "Effects of Creep Behaviors of Glass Ceramic Seal and Ferritic Stainless Steel Interconnect on Solid Oxide Fuel Cell Stacks," In *International Plasticity Symposium*. PNNL-SA-63755, Pacific Northwest National Laboratory, Richland, Washington.

**3.** W.N. Liu, X. Sun, and M.A. Khaleel, 2009, "Quantifying the Interfacial Strength of Oxide Scale and SS 441 Substrate Used in SOFC," In *MT&S 2009*. PNNL-SA-66651, Pacific Northwest National Laboratory, Richland, Washington.

**4.** X. Sun, A.M. Tartakovsky, and M.A. Khaleel, 2009, "Probabilistic Based Design Methodology for Solid Oxide Fuel Cell Stacks," *Journal of Fuel Cell Science and Technology 6(2)*: Art. No. 021004.

**5.** X. Sun, W.N. Liu, E.V. Stephens, and M.A. Khaleel, 2008, "Determination of Interfacial Adhesion Strength between Oxide Scale and Substrate for Metallic SOFC Interconnects," *Journal of Power Sources* 176(1):167-174. doi:10.1016/j.jpowsour.2007.10.027.

**6.** W.N. Liu, X. Sun, E.V. Stephens, and M.A. Khaleel, 2009, "Life Prediction of Coated and Uncoated Metallic Interconnect for Solid Oxide Fuel Cell Applications," *Journal of Power Sources* 189(2):1044-1050.

**7.** W.N. Liu, X. Sun, and M.A. Khaleel, 2009, "Global Failure Criteria for Positive/Electrolyte/Negative Structure of Planar Solid Oxide Fuel Cell," *Journal of Power Sources*. [In Press].

# III.H.4 Optimization of Load Path and Contact Paste

Brian J. Koeppel (Primary Contact), Wenning Liu, Elizabeth V. Stephens, Kyoo Sil Choi, Kurt P Recknagle, and Moe A. Khaleel
Pacific Northwest National Laboratory (PNNL)
902 Battelle Blvd.
Richland, WA 99352
Phone: (509) 372-6816; Fax: (509) 375-6736
E-mail: brian.koeppel@pnl.gov

DOE Project Manager: Briggs White
Phone: (304) 285-5437
E-mail: Briggs.White@netl.doe.gov

Contract Number: 40552

Start Date: October 1, 2008
End Date: September 30, 2009

## FY 2009 Objectives

- Utilize finite element analysis (FEA) stack models to evaluate the effect of contact layers on mechanical load path development through planar stacks and to reduce stresses in seal and cell layers.
- Develop a continuum constitutive model to evaluate volumetric material changes during stack processing events such as contact paste densification and seal devitrification.
- Obtain necessary material properties for contact paste constitutive models and strength dependence of porous ceramics.
- Evaluate the effect of stack assembly and densification behaviors on the stack load path and stresses at operating and shutdown conditions.
- Optimize load path and stresses by modifications to geometry and assembly conditions.

## Accomplishments

- Demonstrated benefits of the contact paste layer serving as a structural interface to distribute mechanical loads from the cell to the interconnect such that perimeter seal load requirements are reduced.
- Developed a continuum viscous sintering model to evaluate densification strains and residual stresses of contact materials during low temperature constrained sintering within the stack.
- Implemented the continuum viscous sintering constitutive model in MSC MARC for the evaluation of time dependent densification behavior of contact pastes.
- Demonstrated the benefits of contact paste densification in the proposed Solid State Energy Conversion Alliance (SECA) test cell geometry for reducing perimeter seal loads at operating and shutdown conditions.

## Introduction

The planar solid oxide fuel cell (SOFC) stack performance depends on reliable uniform contact to carry the electrical current between the series-connected cells. On the cathode side, the contact layer must survive the oxidizing environment to maintain a durable bond between the ceramic electrode and the metallic interconnect. Stable but expensive noble metals have been used for contact pastes, but less expensive alternatives are being investigated including ceramics using novel lower temperature processing [1,2]. Here the contact layer is often completed during stack assembly, so processing temperatures are limited for this joint when a metallic interconnect is used. Ceramic contact pastes are desirable due to compatibility with the cathode and good oxidation resistance, but densification of the contact paste layer during assembly will result in volumetric changes that create residual stresses in the stack. To date, densification and other similar material behaviors during stack fabrication have not been typically included in thermal-stress analyses of SOFCs. An understanding of these densification effects on the load distribution and stresses in the stack during assembly is necessary to quantify the mechanical reliability of the contact layer. Furthermore, if the structural ability of the contact layer can be improved sufficiently to carry and distribute the thermal mismatch loads between the cell and interconnect (Figure 1), mechanical reliability of the entire cell and seal layers can also be improved. Specifically, transmitting load to the ductile metallic interconnect can beneficially reduce the transmitted load through the cell perimeter seal. Numerical modeling can be used to evaluate these contact layer residual stresses in addition to the typically evaluated thermal-mechanical stresses. The results of these modeling analyses will help stack designers reduce high stresses in the stack so that structural failures are prevented and high stack mechanical reliability is achieved to meet program technical targets.

## Approach

The technical approach taken here was to utilize PNNL's existing SOFC modeling tools, or when needed, to develop the necessary model enhancements for eventual migration into these tools. The existing single cell FEA model in MSC MARC for the first generation SECA test cell was used as the baseline stack geometry for all evaluations. This FEA model was first used in parametric studies to evaluate the average stresses (i.e. loads) and local stresses on seal and cell components as a function of the cathode contact paste and interconnect properties. Next, constitutive models were researched in the literature and evaluated for implementation to capture the mechanical effects of contact paste densification. Based on a literature review, the continuum viscous sintering model [3] was selected as state-of-the-art and suitable for simulating volumetric material changes due to densification in the 3-dimensional (3D) stack modeling framework. This phenomenological constitutive model is a general nonlinear-viscous continuum model based on plastic deformation of porous materials. The model computes the inelastic strain rates as a function of grain size, relative density, mechanical properties, stress, and temperature. The model can capture the enhanced sintering behavior that occurs under applied stress and the influence of the mechanical constraint by the material layers being joined. Material properties, including their dependence on porosity, were taken from the literature and experiments for development of the constitutive model in a spreadsheet initially. The model was then implemented in MARC through user defined subroutines using an explicit integration approach. Using the test cell geometry, the results considering contact layer densification on stack load path and stresses were compared with the previous results which did not include densification effects. This model would then be ready for subsequent parametric evaluations to optimize the load path and minimize stresses in the critical components.

## Results

### Load Path

In general, the load carrying capacity of the cathode contact layer was found to be advantageous for reducing the transmitted loads on the cell perimeter seal (Figure 1) under operating environments of SOFCs, but the amount of reduction depends upon the relative stiffness values of the cell, interconnect, porous media, and support structures. Comparison of a fully bonded interface to a frictionless sliding interface resulted in 30-50% less transmitted load through the perimeter seal, with the greater reductions due to stiffer contact/media/interconnect structures. It was also demonstrated that thicker interconnect plates (evaluated for the range of 0.5-1.5 mm) could also reduce perimeter seal loads by 6-13% under operating conditions. When creep of the ferritic steel interconnect was considered, the transmitted seal loads depended on the interconnect thickness. Stresses in the seal were higher for thinner interconnects but lower for thicker interconnects at the operating temperature. These results demonstrate that the mechanical contribution of the contact layer can be substantial and warrant design consideration.

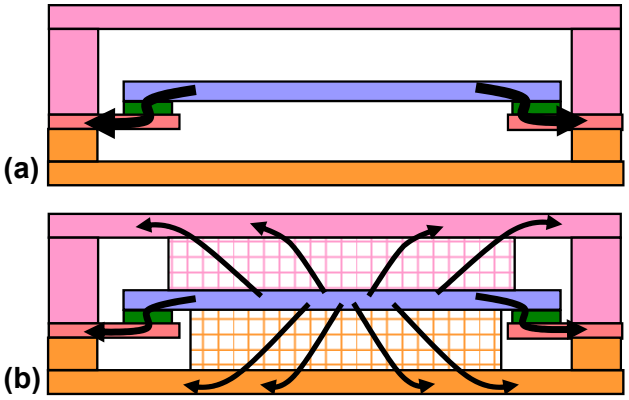


**FIGURE 1.** Cross-Sectional Schematic of Load Path from the Cell to the Interconnect and Perimeter Seal a) without and b) with Load Distribution through the Contact Paste Layers

### Densification Model

The basic constitutive law [3] assuming a linear-viscous incompressible material is given by

$$\sigma_{ij} = 2\eta_o\left[\varphi\dot{\varepsilon}_{ij} + \left(\Psi - \frac{1}{3}\varphi\right)\dot{e}_{kk}\delta_{ij}\right] + P_L\delta_{ij}$$

where $\sigma_{ij}$ is the stress, $\dot{\varepsilon}_{ij}$ is the inelastic strain rate, $\eta_o$ is the shear modulus of the porous skeleton, $\dot{e}_{kk}$ is the first invariant of the strain rate tensor corresponding to the volumetric change, $P_L$ is the sintering stress, $\delta_{ij}$ is the Kronecker delta, and $\varphi$ and $\Psi$ are relations that provide the dependence of the shear and bulk moduli on the porosity, respectively. The constitutive model was implemented in both a spreadsheet and the MARC FEA code through user-defined subroutines (primarily CRPLAW for the inelastic strain rate computation, HOOKLW for porous material properties, ANEXP for thermal strains, and other subroutines for tracking and viewing of state variables representing the material relative density and grain size). Parameters determining the rate constants were obtained by comparison with experimental sintering rate data, while porous material relations and elastic properties were obtained from the literature. Qualitatively, the FEA model properly captured the enhanced sintering rates that occur under compressive loading and compared well with the spreadsheet implementation (Figure 2).

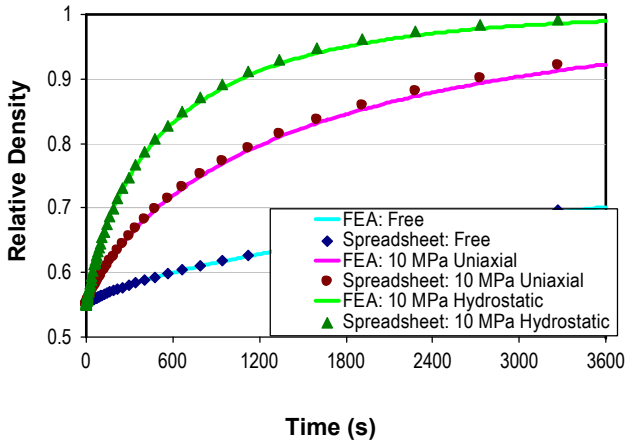


**FIGURE 2.** Comparison of the Spreadsheet and FEA Results for Relative Density Evolution during Free, Pressure-Assisted, and Isostatic Sintering

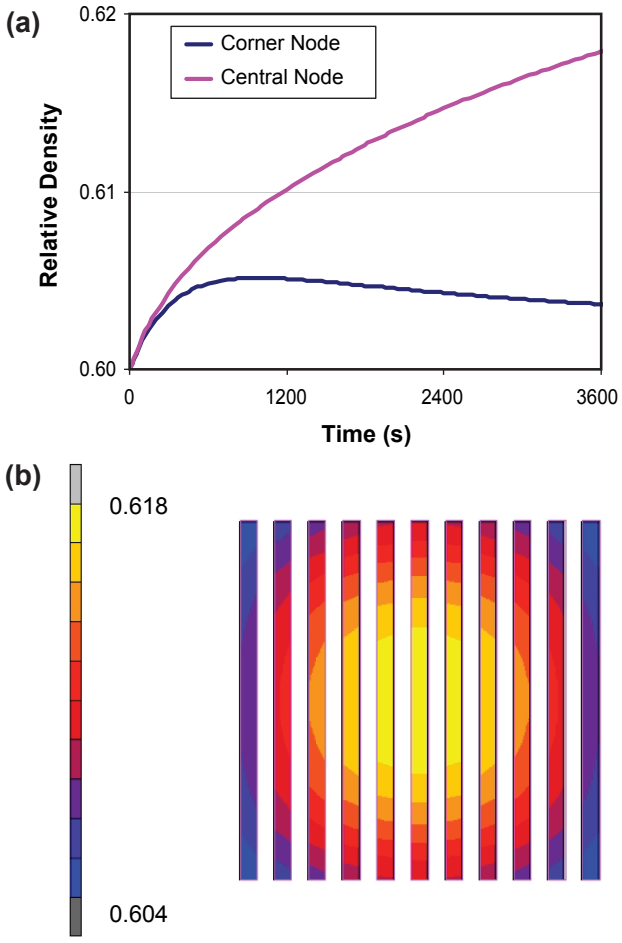


**FIGURE 3.** Results for the Relative Density of the Cathode Contact Paste under the Interconnect Ribs a) at Two Locations during Densification and b) after Processing

### Effects of Densification

The load path studies were repeated for the same stack geometry using the densification model for a hypothetical processing condition of 1.0 hour at 900°C before reducing the temperature to the operating condition temperatures. It was observed that densification of the cathode paste layer was not uniform across the active area ribs. The center of the stack had higher compression due to the stack preload and sintered better than the corner regions which began to experience tension due to the overall volumetric changes (Figure 3a). The center sintered from a relative density of 60% to 62% while the corner was almost unchanged, which indicates that a higher strength bond is expected at the center of the preloaded stack (Figure 3b). Due to the inherent constraint by the joined interconnect rib and cathode, out-of-plane strains are approximately 50X greater than the in-plane strains (this is expected and similar to behavior of the high density electrolyte formation during co-firing). In comparison to the case with no densification, it was found that the paste stresses at operating temperature increased slightly but were still less than the experimentally measured tensile strengths of 1-14 MPa. The in-plane shear loads on the perimeter seal were beneficially reduced 3-10% depending on the rib orientation, while the out-of-plane compressive load (critical to preventing seal delamination) improved 35-65%. Stresses on the cell remained largely unchanged. For the room temperature shutdown condition, the noted beneficial trends were similar although the perimeter seal's out-of-plane load would still be tensile overall.

## Conclusions and Future Directions

During this year, the 3D continuum densification model was evaluated, implemented, and utilized to study load path and contact layer behavior in a prototypical planar cell. Structural benefits to the load path and perimeter seal stresses were realized, but the preload distribution was observed to be important for densification to proceed. Future activities will focus on exercising the developed model for other materials and parametric studies to improve stack reliability:

- Perform parametric studies to identify sensitivities of the load path to processing temperature, paste densification properties, and component thicknesses. Optimize the load path and stresses for operation and shutdown conditions.
- Extend the model to consider volumetric changes in other components during fabrication (e.g., seal devitrification, anode reduction) and evaluate effects on contact formation, load path, and residual stresses.
- Evaluate the mechanical reliability of stack assembly and interconnection through simultaneous refractory glass seal devitrification and low-temperature cathode contact densification.

- Adapt the explicit FEA scheme to an implicit algorithm to speed computations and permit evaluations with better mesh resolution.

## References

**1.** B.P. McCarthy et al., "Enhanced Shrinkage of Lanthanum Strontium Manganite ($La_{0.90}Sr_{0.10}MnO_{3+\delta}$) Resulting from Thermal and Oxygen Partial Pressure Cycling," *Journal of the American Ceramic Society* **90** [10] 3255-3262 (2007).

**2.** B.P. McCarthy et al., "Low-Temperature Sintering of Lanthanum Strontium Manganite-Based Contact Pastes for SOFCs," *Journal of Power Sources* **180**, 294-300 (2008).

**3.** E.U. Olevsky, "Theory of Sintering: From Discrete to Continuum," *Materials Science and Engineering* **R23**, 41-100 (1998).

# III.H.5 SOFC Modeling and Simulation Tools

Mohammad A. Khaleel (Primary Contact), Xin Sun, Wenning Liu, Elizabeth Stephens, Kurt RecknagleBrian Koeppel, and Kevin Lai
Pacific Northwest National Laboratory (PNNL)
902 Battelle Blvd.
Richland, WA 99352
Phone: (509) 375-2438; Fax: (509) 375-4392
E-mail: moe.khaleel@pnl.gov

DOE Project Manager: Briggs White
Phone: (304) 285-5437
E-mail: Briggs.White@netl.doe.gov

Contract Number: 40552

Start Date: October 1, 2008
End Date: September 30, 2009

## FY 2009 Objectives

- Develop and validate multi-physics (MP) modeling tools to simulate solid oxide fuel cell (SOFC) stack performance.
- Utilize computational techniques for the optimization of modular SOFC stack and system designs with mitigation of performance degradation.
- Disseminate/transfer modeling tools to Solid State Energy Conversion Alliance (SECA) industry teams and Core Technology Program (CTP) members.

## Accomplishments

- Developed a modeling capability to examine densification and strength of cathode contact materials enabling the evaluation of densification strains in contact materials and prediction of residual stress induced by the sintering process.
- Developed a model to include creep of SOFC materials and to examine the effect on stress distribution with the stack components.
- Enhanced the PNNL-developed modeling tool SOFC-MP with improved calculation speed by incorporation of an algebraic multi-grid (AMG) solver, removal of previous memory limitations, and strategic code restructuring.
- Developed an improved SOFC stack modeling capability that enables simulation of the enhanced electrochemical performance and altered methane reforming that results from pressurized operation.
- Performed a numerical study of the effect of operating at pressures ranging from 1 to 10 atmospheres on the thermal and electrical performance of a generic 20 x 20 cm stack to optimize the thermal performance and electrical power.
- Performed simulations of SOFC anodes with discrete microstructure to determine the inter-particle stresses created by volume expansion due to the conversion of nickel to nickel-oxide within the porous anode material.
- Developed a stack calculator that quickly solves the 2-dimensional temperature distribution in a vertical plane through the stack center, and is suitable for incorporation into a system level model.
- Continued to promote and support the use of SOFC-MP and Mentat-FC software packages with industry teams and CTP university researchers for modeling and development of SOFC stacks.
- Developed an integrated modeling/experimental framework to predict the life of SOFC interconnect (IC) materials with and without spinel coatings.
- Investigated the effect of oxide growth and metallic IC surface quality on interfacial strength of oxide scale and substrate. Reported the interfacial strength at the different interfaces in the spinel coating/oxide scale/metallic substrate tri-layer systems.

## Introduction

In order to efficiently develop and optimize planar SOFC stacks to meet technical performance targets, it is desirable to perform numerical experiments on the effects of geometry, material properties, operational parameters, and thermal-mechanical loading. The computations with representative baseline designs, validated by experimental data, have been used to develop better understanding of the stack behavior while avoiding costly and time-consuming experiments. In order to model the coupled physics associated with an SOFC stack, the simulation tool SOFC-MP was developed. This modeling tool combines the versatility of a commercial multi-physics code and a validated electrochemistry calculation routine to predict the gas flow distributions, current distribution, temperature field, and power output for stack-level simulations. The fundamental building blocks of the modeling and simulation tools are electrochemical models, heat and mass transfer simulations, computational mechanics, and experimental data.

The modeling tools were then used to evaluate challenging issues anticipated for cell scale-up.

A systematic methodology was developed for quantifying the thermal and electrical performance improvements available with pressurized operation. For SOFC cathode contact materials and stack development, a sintering model was developed to explore/optimize the load distribution within the stack as a function of cathode contact densification and strength. The modeling tools developed were also used in studying current material development and degradation challenges. The mechanical durability of the surface scale present on metallic interconnects was evaluated for its ability to resist scale growth-induced spallation. The developed design methodology and stack analytical procedures have been documented in a design guide for distribution within the SECA program.

## Approach

The following technical approach has been taken in the modeling task to meet program goals:

- Maintain, enhance, and provide guidance for the integrated modeling tools developed under the SECA CTP for evaluating fuel cell stack design concepts by the industry teams.
- Explore scale-up related topics such as enhanced cooling and performance boosting strategies.
- Investigate the effects of materials degradation on cell performance and life.
- Investigate the effects of cell geometric design, material property distributions, and operating conditions on SOFC reliability.
- Perform material experiments for property data essential to constitutive and numerical model development.

## Results

### Enhancement and Performance Improvement of Modeling Tools

The PNNL-developed modeling tools were greatly enhanced during the past year. The modeling tools and techniques played a greater role in continued support of SOFC technology development for the SECA industry and university team members:

- The SOFC-MP solver was also given improved calculation speed by incorporation of an AMG solver, the removal of previous memory limitations, and a strategic code restructuring update. Table 1 shows an example of the computer time needed to perform similar fuel cell stack simulations was shortened by roughly a factor of seven.
- Developed a stack calculator that quickly solves the 2-dimensional temperature distribution in a vertical plane through the stack center. Figure 1 shows results from the simulation of a 24-cell, co-flow stack model and temperature profiles from inlet to outlet along various cells within the stack. These predicted temperatures can provide valuable input for a system level or controls model.
- The SOFC-MP modeling tools have been enhanced by the inclusion of a sub-model to characterize material creep behavior of SOFC materials and the effects that creep has on stress distribution and relaxation, and the ability of a component to maintain its intended form.

**TABLE 1.** Compute Time for an AMG Solved 7-Cell Stack Simulation Was Less Than Half That of a Pre-AMG Solver 6-Cell Stack Simulation

| Compute Method | Compute time, minutes | Cells in Stack/ Compute nodes | Iterations to converged solution | Minutes/ (iteration-node) |
|---|---|---|---|---|
| Pre-AMG | 360 | 6 / 76,000 | 200 | 2.37E-5 |
| AMG | 18 | 7 / 88,000 | 60 | 3.41E-6 |

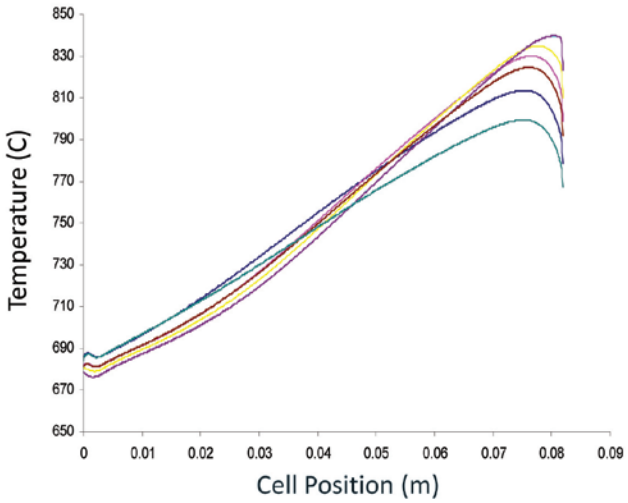


**FIGURE 1.** Temperature Profiles from Inlet to Outlet along Various Cells within a 24-Cell, Co-Flow Stack as Predicted by the Fast Running, 2-Dimensional, Stack Modeling Tool

### Modeling for Issues Related to Scale-Up

The desire to use SOFC stacks in megawatt-scale power applications using coal-based fuels provided motivation to study scale-up of cell dimensions. Larger cells are expected to have greater challenges with thermal management due to temperatures that increase as the heat removal paths lengthen with increasing cell size. Stack designers must optimize the heat removal by conduction, convection, and radiation. Further improvement of the thermal condition involves removing additional heat from the stack, and/or decreasing the heat load by improving the electrical efficiency of the fuel cell. Additional heat removal can be achieved

by operating the stack on methane enriched coal gas, and improved electrical efficiency can be achieved by operating the stack at elevated pressures. The following activities were performed to evaluate the effect of both on-cell reforming of methane and pressurized operation:

- The SOFC simulation capability was expanded with the development of a model to characterize the enhanced electrochemical performance due to pressurization. This model also considers the effect of pressurization on methane reforming resulting in a tool that is able to simulate the coupled effects of reforming and electrochemistry.
- The modeling tool was then exercised in a numerical study of the effect of operating at pressures ranging from 1 to 10 atmospheres on the thermal and electrical performance of a generic 20 x 20 cm stack, methane reforming case to optimize the thermal performance and electrical power. The simulations showed that electrical performance (power) increased monotonically with increasing operating pressure, the thermal performance was improved for pressures above 2.5 atmospheres, and the optimal performance was realized when operated at 10 atmospheres, a pressure at which the thermal and electrical performance was improved by more than 10%. Figure 2 presents temperature profiles along the anode flow channel for the operating pressures simulated and show decreasing maximum temperature and decreasing difference between maximum and minimum temperatures for operating pressure greater than 2.5 atmospheres.

### Modeling of Material Mechanical Behavior and Experiments

The integrated experimental/modeling method was applied to examine and improve the cathode contact materials such that the contact can provide additional adhesive strength within the stack to improve the mechanical load path and assist the glass-ceramic seals at maintaining hermeticity. Contact paste sintering experiments and test cell experiments performed to examine cathode contact materials provided input for material behavior models and stack simulations:

- A sintering/densification model was developed, based on experimental data, to examine densification and strength of cathode contact materials. The enhanced modeling capability enables the evaluation of densification strains in contact materials and the ability to predict the residual stress induced by the sintering process. Structural analysis can now include these physics which affect the distribution of mechanical load within the stack and can be used to assist with stack and materials design.

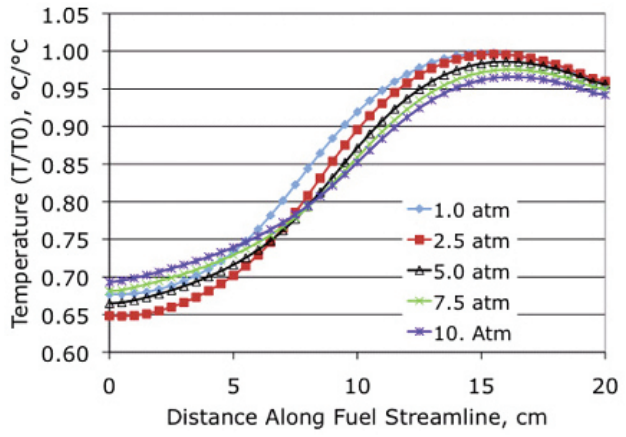


**FIGURE 2.** Temperature Profiles along Anode Flow Channel for Various Operating Pressures

### Modeling of Discrete Microstructures for the Electrodes

The anode is a porous material consisting of nickel (Ni) and and yttria-stabilized zirconia, and works in a primarily reducing environment. If the nickel is oxidized the phase conversion to nickel-oxide causes a volumetric increase which can induce stress in the microstructure. If enough of the nickel present in the anode is converted to oxide the stress may be enough to lead to failure of the anode or the anode/electrolyte interface.

- Parametric simulations of an SOFC anode with discrete microstructure were performed to determine the inter-particle stresses created by volume expansion due to the conversion of nickel to nickel-oxide within the porous anode material. The anode microstructure was determined by scanning electron microscop imaging and recreated in a finite element model. Figure 3 shows the distribution of von Mises stress due to the nickel to nickel-oxide conversion near the anode-electrolyte interface. It is important that the stack would be operated in a manner to avoid this condition because this level of stress in the anode microstructure would be large enough to cause a crack to initiate and propagate leading to failure of the anode.

## Conclusions and Future Directions

During Fiscal Year 2009, the modeling tools were improved and expanded with additional capabilities developed to address scale-up, strength, and durability issues. Future modeling activities will continue to focus on these issues together with work on reliability, degradation, and time-dependent response:

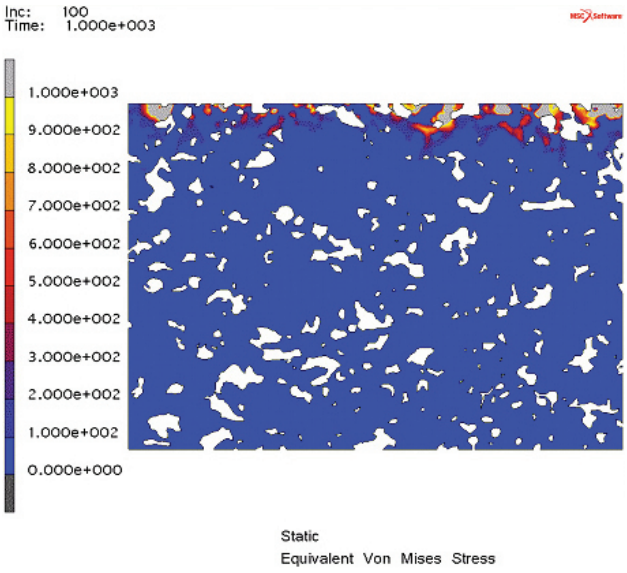


**FIGURE 3.** Stress Distribution in the Anode Microstructure Due to Volume Expansion Caused by Nickel Metal Being Converted to Nickel-Oxide near the Anode-Electrolyte Interface (top)

- Continue to improve the modeling tools to meet the needs of the SECA program. Continue to promote the usage of the tools by the industry and academic teams.
- Continue to add improved material models and numerical procedures to the modeling tools for simulation of time-dependent mechanical response and reliability.
- Continue modeling work on ferritic stainless steel interconnects to meet SECA target on stack life.
- Develop modeling tools to examine secondary reactions that can take place within the cell electrodes and have detrimental effects on structural and electrochemical performance.
- Evaluate thermal management needs and reliability of seal/cell structures during cell scale-up.
- Continue to support development of a robust test cell design.
- Evaluate the mechanical requirements for successful fabrication using refractory glass sealants and low-temperature sintering of cathode contact materials for reliable interconnection during operation and shutdown.

## FY 2009 Selected Publications/Presentations

**1.** K.P. Recknagle and M.A. Khaleel, "Modeling of Pressurized Electrochemistry and Steam-Methane Reforming in Solid Oxide Fuel Cells and the Effects on Thermal and Electrical Stack Performance," PNNL Topical Report 18338, Pacific Northwest National Laboratory, Richland, Washington, March 2009.

**2.** W.N. Liu, X. Sun, and M.A. Khaleel, "Effect of Interconnect Creep on Long-Term Performance of SOFC of One Cell Stacks," in 32nd International Conference & Exposition on Advanced Ceramics and Composites, vol. 29, no. 5, pp. 53-63. American Ceramic Society, Daytona Beach, Florida, 2008.

**3.** W.N. Liu, X. Sun, and M.A. Khaleel, "Effects of Creep Behaviors of Glass Ceramic Seal and Ferritic Stainless Steel Interconnect on Solid Oxide Fuel Cell Stacks," in International Plasticity Symposium, PNNL-SA-63755. Pacific Northwest National Laboratory, Richland, Washington, 2008.

# III.H.6 High Efficiency Coal Gasification-Based SOFC Power Plants

Professor Scott Samuelsen
Advanced Power and Energy Program (APEP)
University of California
Irvine, CA 92697-3550
Phone: (949) 824-7302 x120; Fax: (949) 824-7423
E-mail: gss@uci.edu

DOE Project Manager: Travis Shultz
Phone: (304) 285-1370
E-mail: Travis.Shultz@netl.doe.gov

Subcontractors:
- James D. Powers, Santa Monica, CA
- David M. Francuz, Rancho Santa Margarita, CA

Contract Number: 41817

Start Date: July 13, 2007
End Date: October 31, 2009

## FY 2009 Objectives

- Develop a portable, stand-alone planar solid oxide fuel cell (SOFC) performance model that can be used to support systems studies with a large number of user-adjustable parameters associated with material properties and cell/stack geometry, enabling users to tailor the model to fit details of their systems or to optimize fuel cell design.
- Identify and evaluate coal gasification-based SOFC power plant concepts for large-scale central power plant applications, consistent with the Office of Fossil Energy's Fuel Cell Systems goals, targeting 60% efficiency (coal higher heating value [HHV]) while incorporating capability to isolate 90% of carbon from coal for sequestration. Develop rough order of magnitude cost estimates for the integrated gasification fuel cell (IGFC) plants to evaluate the economic feasibility and guide design optimization.
- Produce position papers that assess benefits and synergies of fuel cells in coal-fueled central generation plants and possibly include: amenability to carbon capture/sequestration, pollutant emissions, water usage, efficiency and cost of electricity, in a format suitable for a variety of public uses.

## Accomplishments

- A planar SOFC model capable of evaluating various overpotential mechanisms (activation, ohmic and diffusion) and physically resolving the internal current density, flow compositions and temperature profiles in a SOFC has been developed. The model can be applied to a set of defined geometries (co-, counter- or cross-flow configuration, with one or two dimensions resolved) with various material properties and input flows including those with high methane-content syngas.
- Sensitivity analyses have identified model parameters to represent modern SOFC performance. The model has been advanced by: (1) close communication and cooperation with the Pacific Northwest National Laboratory (PNNL) SOFC modeling group to employ PNNL methane reformation kinetics, providing an alternative to the previous methane reformation parameters of Achenbach [1], and (2) explicitly accounting for the temperature of interconnects, which is important for simulating modern SOFC that use metallic interconnects with thermal conductivities that are much larger than ceramic materials.
- The developed SOFC model has been translated into FORTRAN code to take advantage of superior efficiency in scientific calculations and intrinsic compatibility with Aspen Plus® (FORTRAN is the default programming language of Aspen Plus® [2]).
- The SOFC model has been extensively verified against established literature models (e.g., International Energy Agency Benchmark [3], and Imperial College [4]), in-house SOFC models (e.g., Simulink® model previously developed by APEP [5]), and the SOFC-MP model developed by PNNL. The results predicted by the APEP model agree satisfactorily with these models demonstrating the credibility of the newly developed model.
- The importance of using a dimensional SOFC model in IGFC systems analyses to capture internal temperature other operating condition distributions has been peer-reviewed and presented at an international conference.
- IGFC systems employing catalytic hydro-gasification and pressurized SOFC are very promising for achieving 60% thermal efficiency. Such IGFC systems have been conceptually designed and optimized in Aspen Plus®.
- A paper describing the SOFC model has been published and presented in the American Society of Mechanical Engineers 7th International Fuel Cell Science, Engineering & Technology Conference and a draft paper presenting analysis of an IGFC system employing hydro-gasification and capable of achieve 60% thermal efficiency has been submitted to DOE for technical review.

## Introduction

Deployment of SOFC technology in coal-based power plants is essential to realizing ultra high thermal efficiencies, on the order of 60% (HHV basis), while enabling $CO_2$ sequestration. Previous conceptual analyses of SOFC-based power plants indicate that it may be possible to achieve an improved combination of efficiency, emissions, and specific power output, which can reduce the power generation equipment cost on a $/kW basis. Thus, a need exists to perform detailed systems analyses of advanced SOFC-based power plant designs to identify the best opportunities worthy of support by the U.S. DOE for their development. A detailed SOFC model is also required to support the systems analyses. The University of California, Irvine APEP is part of a Research and Development Solutions team contracted to supply the required resources and lead the technical effort to develop the necessary models, perform the systems analyses, reports and papers on high efficiency coal gasification-based SOFC power plants.

## Approach

**SOFC Model:** A stand-alone executable finite volume SOFC model that is transferable and executable without any special software requirements is under development. This model includes flexibility to accept various user inputs to produce steady-state operating results based upon sound and rigorous analysis of expected future SOFC performance. Overall model requirements and specifications include cell geometry (e.g., length, width, flow channels), cell configuration (e.g., co-flow, counter-flow, cross-flow), stack geometry and size, extent of internal reforming, electrochemical loss terms (e.g., exchange current density, cell resistance), heat losses, oxidant properties (e.g., species composition), oxidant inlet thermodynamic conditions (e.g., temperature, pressure), fuel properties (e.g., species composition), fuel inlet thermodynamic conditions (e.g., temperature, pressure), fuel utilization, and operating pressure. The solution approach iterates between two modules: the "Species Conservation" module that accounts for chemical (methane reformation and water gas shift) and electrochemical (oxidation of $H_2$) reactions and calculates the chemical species profiles and current distribution, and the "Energy Conservation" module that calculates heat transfer, the temperature distribution and heat loss terms.

**Systems Analysis:** IGFC design concepts are developed from a variety of sources, including previous work conducted by APEP, literature, discussions with the National Energy Technology Laboratory and brainstorming sessions. Special consideration is given to capturing synergies between the SOFC and the gasification systems that are not found in traditional IGCC designs. Design schemes that violate practical constraints imposed by the presence of the SOFC are disqualified. A 2020 deployment date is assumed for selection of the technologies. Design concepts that have potential for achieving 60% efficiency, 90% $CO_2$ separation, competitive installed plant cost, acceptable reliability, and low risk associated with SOFC requirements and other advanced technologies required are identified. IGFC system simulation models are then set up in Aspen Plus® integrated with the SOFC model to develop overall IGFC system performance estimates. Sensitivity analyses are conducted to quantify impacts of plant configuration on performance. Rough order of magnitude capital, operating and maintenance cost estimates are then developed to arrive at an indicative cost of electricity assuming the target cost for the system power block of $700/kW (installed cost and year 2007 dollars basis) and an SOFC stack life of 40,000 hours.

**Position Papers:** Position papers are generated that outline benefits and synergies, emanating from literature, the above analyses and prior research conducted by APEP on fuel cell use in coal-based power plants. The papers are structured to meet a variety of audiences representing stakeholders engaged in environmentally-sensitive coal utilization technologies for power generation. The primary foci of the papers are to add to the technical analysis literature and to educate the public regarding the potential, synergies and advantages of IGFC systems.

## Results

**SOFC Model:** The developed model was verified against the finite difference model developed by Aguiar [4] at Imperial College showing that the two models agree well with each other. Figure 1 shows a comparison of the internal temperature profile predictions made by the two models for a counter-flow SOFC. Both models capture the temperature peak associated with operation on methane-containing syngas. In this case, the APEP model predicted an internal peak temperature of 1,135 K, which is slightly lower than the Imperial College model prediction. The APEP model has also been compared with the SOFC-MP model of PNNL. A detailed comparison matrix was developed to address the effects of on-cell reformation (0 to 80%), air utilization (14 to 30%), cell dimensions (10 cm vs. 30 cm long), etc. The APEP and PNNL models produced comparable results for identical operating conditions. For cases using methane-containing syngas, the APEP model predicted slightly higher peak temperature (~5-10 K) than the PNNL model.

Spatially resolved predictions of performance are required because SOFC inlet/outlet temperatures no

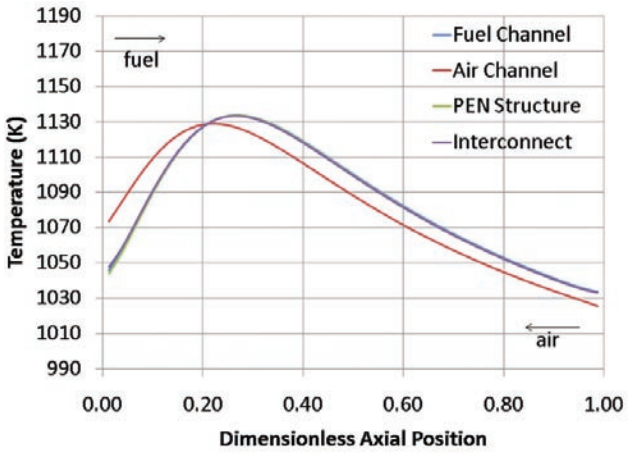


(a) APEP model results

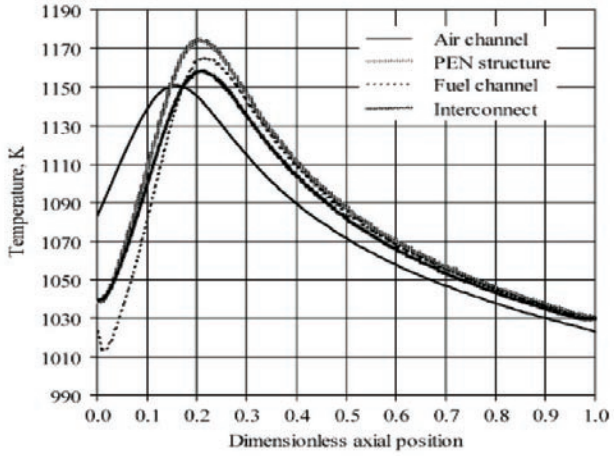


(b) IC model results

**FIGURE 1.** Comparison of APEP model results with Imperial College model results. Internal temperature profiles of a SOFC operating on syngas containing 28.0% $CH_4$ and 12.3% $H_2$ (mole fraction), both cells have ~0.5 A/cm$^2$ current density, with $U_f$ = 75% and $U_a$ = 12%.

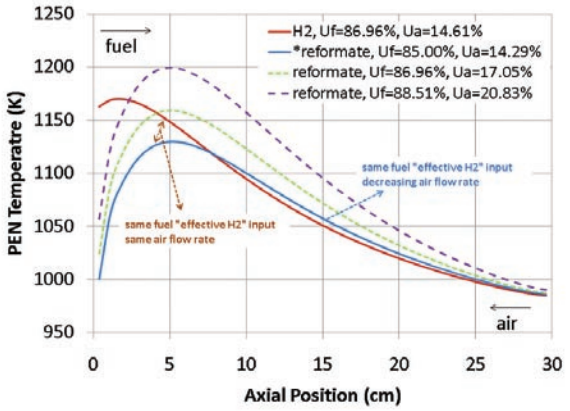


(a) Counter-flow operation of SOFC with fuels containing same equivalent $H_2$ input

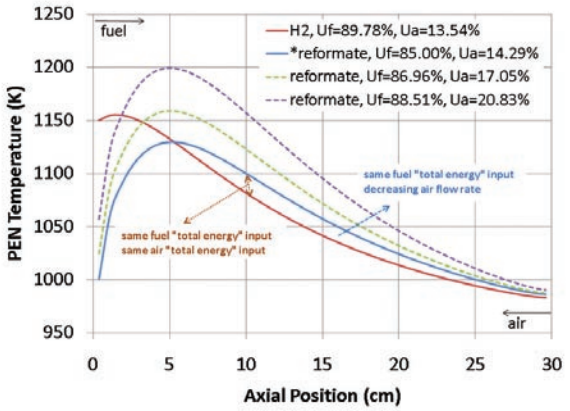


(b) Counter-flow operation of SOFC with fuels containing same total energy

**FIGURE 2.** Conceptual Test Results Demonstrating the Benefits and Limitations of Methane Containing Syngas in SOFC Thermal Management

longer represent the peak temperature in difference, which makes 0-dimensional (0-D) thermodynamic model predictions insufficient for detailed IGFC system analysis. Temperature peaks can be more serious for high performance SOFCs where reaction kinetics are fast. A conceptual test of the benefit and limitations of methane containing syngas has been accomplished. Two plots are shown in Figure 2. Figure 2(a) shows temperature distributions of an SOFC operating on fuels containing the same equivalent $H_2$ input, but different amounts of methane (0 vs. 17%). These results show that only a 4% increase in air utilization can be achieved for the same SOFC temperature difference using the cooling of a 17% methane-containing syngas in a counter-flow configuration. Figure 2(b) similarly indicates that air utilization cannot be increased as substantially as a 0-D thermodynamic model would suggest for the same total energy input. Figure 3 presents representative temperature and current density distributions from the quasi-3-dimensional (3-D) APEP model for a cross-flow SOFC configuration.

**Systems Analysis:** Figures 4a and 4b show the overall block flow diagrams for promising IGFC plant concepts, one for a near atmospheric pressure SOFC and the other for an elevated operating pressure SOFC. In both case, the raw syngas rich in $CH_4$ after cleanup is humidified and then supplied to the reactor/expander topping cycle where additional methane is formed and the gases heated up by the exothermic methanation reaction are expanded through a turbine to recover power. The advantage with the reactor/expander topping cycle are two-fold: (1) it increases the temperature of the inlet to the expander to increase the power developed by the expander, and (2) the increase in $CH_4$ content of the syngas is beneficial for chemically recuperating the heat generated within the SOFC system. The $CH_4$-rich gas is then supplied to the SOFC system which includes a pre-reformer where a

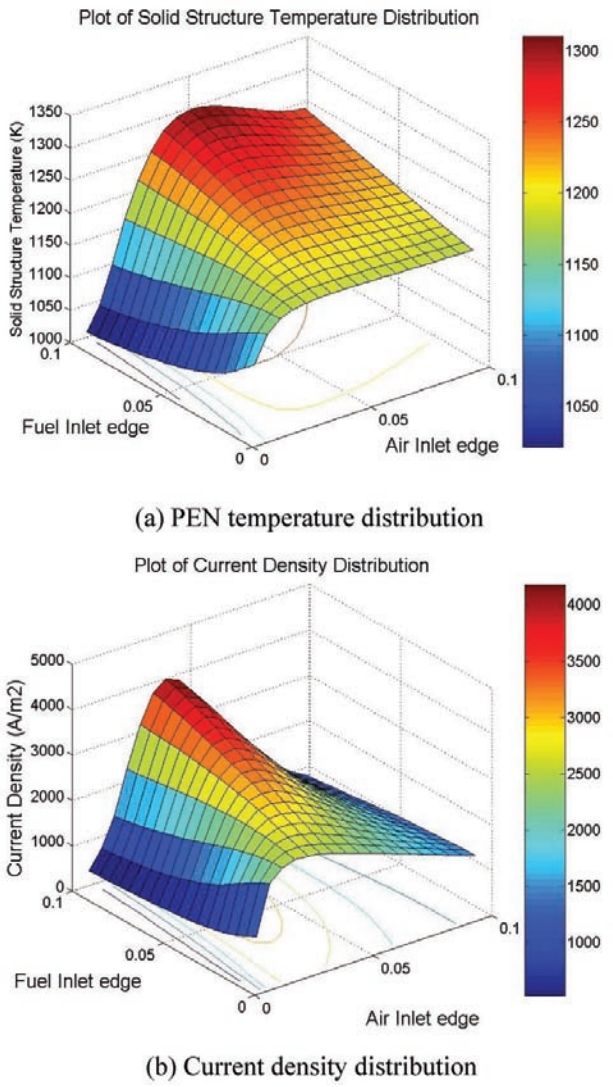


**FIGURE 3.** Sample Results of the APEP Model Extended to Quasi-3-D for a Cross-Flow Configuration

portion of the $CH_4$ is reformed to chemically recuperate the sensible heat contained in the anode exhaust gas. The $H_2$ demand of hydrogasification is met partially by supply of syngas from the $O_2$ blown section of the gasifier and partially by the recycle of the anode exhaust gas after $CO_2$ separation. The IGFC plant with the pressurized SOFC (at 10 atm) generates power at a net efficiency of 60.8% on a coal HHV basis. The IGFC configured with an SOFC operating near atmospheric pressure has a net thermal efficiency of 53.9% on a coal HHV basis, about 7 percentage points lower which corresponds to an increase of about 13% in heat rate over the pressurized SOFC case.

**Position Papers:** A large number of the benefits of IGFCs have been identified with supporting data and analysis at both the system and cell level. These include efficiency, $CO_2$ emissions, $NO_x$ and other criteria pollutants, water demand, scalability, methane conversion capability, and capital cost advantages. A peer-reviewed technical publication was completed that touches upon these features and describes the SOFC model in detail. A second technical paper has been drafted documenting the IGFC plant configurations and the resulting overall performance simulated in Aspen Plus® for the following two cases:

- IGFC with a catalytic hydrogasifier and a hybrid fuel cell-gas turbine power block, and SOFC operating pressure of 10 atm, with an efficiency of 60.8% (coal HHV basis).
- IGFC with a catalytic hydrogasifier and a near atmospheric pressure fuel cell power block with an efficiency of 53.9% (coal HHV basis).

## Conclusions and Future Directions

- The developed SOFC model has been extensively verified and tested using established "well-regarded" models and the results generated by the model have been closely reviewed and accepted by peer researchers. Experimental data that can be used to validate the developed model would be very precious to the whole SOFC community, but accurately measuring SOFC internal temperature distribution is very challenging and beyond the scope of current project.
- APEP is working with DOE to acquire experimental data for model validation from a Solid State Energy Conversion Alliance industry team.
- Some innovative approaches, such as cascading fuel cell stacks and separate reformation channels, are promising for mitigating the challenge of temperature spikes in counter-flow methane containing syngas SOFCs and employing the potential advantages of endothermic methane reformation to reduce parasitic cooling air usage. The model can be extended to incorporate capabilities to analyze such configurations.
- Power plants utilizing high rank bituminous coals with a net thermal efficiency as high as 60% while separating 90% of the carbon as $CO_2$ may be configured. The two critical technologies required for such power plants are the high pressure catalytic hydrogasifier and the SOFC stack. The remainder of the power plant may be configured with subsystems that have been commercially proven in similar services.
- Sensitivity analyses will be completed to quantify impacts of IGFC plant configuration on performance. Rough order of magnitude capital, operating and maintenance cost estimates will be developed in order to arrive at an indicative cost of electricity.

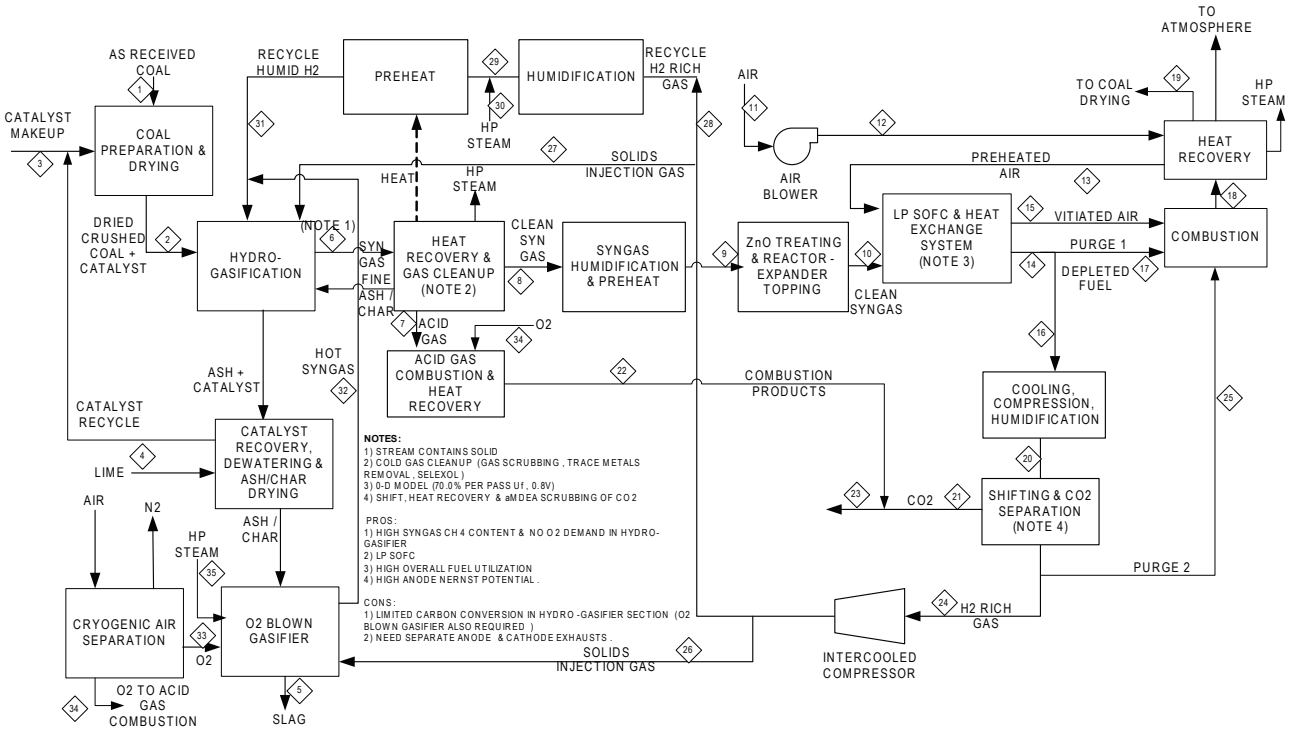


**FIGURE 4A.** Overall Block Flow Diagram – Catalytic Hydrogasifier IGFC – Low Pressure SOFC

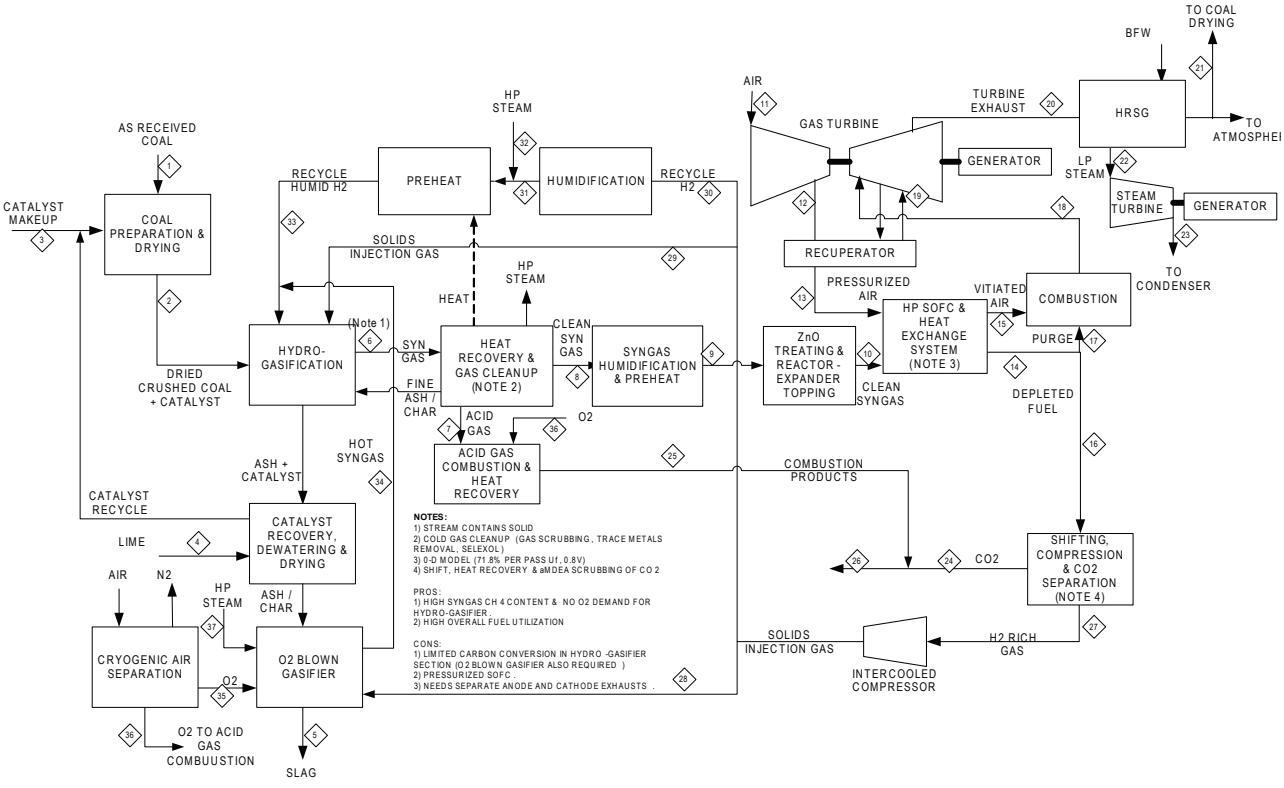


**FIGURE 4B.** Overall Block Flow Diagram – Catalytic Hydrogasifier IGFC – Pressurized SOFC

- APEP is drafting several additional technical papers on coal-based fuel cell systems that highlight the key benefits and realistic targets and capabilities of IGFC systems. White papers and fact sheets are being drafted to highlight the benefits of IGFC systems.

## FY 2009 Publications/Presentations

**1.** National Energy Technology Laboratory, SOFC Modeling Meeting presentation, Morgantown, West Virginia, August 26–27, 2008.

**2.** 1st Bimonthly Progress Report dated July 30, 2008 covering the period June – July 2008.

**3.** 2nd Bimonthly Progress Report dated September 30, 2008 covering the period August – September 2008.

**4.** 3rd Bimonthly Progress Report dated November 28, 2008 covering the period October – November 2008.

**5.** 4th Bimonthly Progress Report dated January 30, 2009 covering the period December 2008 – January 2009.

**6.** International Colloquium on Environmentally Preferred Advanced Generation (ICEPAG) presentation, Newport Beach, California, February 11, 2009.

**7.** 5th Bimonthly Progress Report dated March 30, 2009 covering the period February – March 2009.

**8.** Pacific Northwest National Laboratory (PNNL) modeling meeting presentation, Richmond, Washington, April 8, 2009.

**9.** 6th Bimonthly Progress Report dated May 29, 2009 covering the period April – May 2009.

**10.** M. Li, J. Powers, and J. Brouwer, "A Finite Volume SOFC Model for Coal-Based IGFC Systems Analysis," ASME Paper Number FuelCell2009-85247, May, 2009.

**11.** 7th International ASME Fuel Cell Science, Engineering and Technology Conference presentation, Newport Beach, California, June 9, 2009.

## References

**1.** E. Achenbach and E. Riensche, "Methane/Steam Reforming Kinetics for Solid Oxide Fuel Cells," *Journal of Power Sources*, 52:283-288, 1994.

**2.** Aspen Technology, "Aspen Plus User Models, Version Number: 2006," 2006.

**3.** E. Achenbach, "SOFC Stack Modeling, Final Report of Activity A2, Annex II: Modeling and Evaluation of Advanced Solid Oxide Fuel Cells," *International Energy Agency Program on R, D&D on Advanced Fuel Cells*, Jüelich, Germany, 1996.

**4.** P. Aguiar, et al., "Anode-Supported Intermediate Temperature Direct Internal Reforming Solid Oxide Fuel Cell. I: Model-Based Steady-State Performance," *Journal of Power Sources*, 138:120-136, 2004.

**5.** R.A. Roberts, et al., "Dynamic Simulation of Carbonate Fuel Cell-Gas Turbine Hybrid Systems," *Journal of Engineering for Gas Turbines and Power*, 128:294-301, 2006.

# III. SECA CORE RESEARCH & DEVELOPMENT

## I. Balance of Plant

# III.I.1 Hybrid Ceramic/Metallic Recuperator for SOFC Generator

Mr. Anthony F. Litka (Primary Contact),
Norm Bessette
Acumentrics Corporation
20 Southwest Park
Westwood, MA 02090
Phone: (800) 332-0277; Fax: (781) 461-1261
E-mail: tlitka@acumentrics.com

DOE Project Manager: Robin Ames
Phone: (304) 285-0978
E-mail: Robin.Ames@netl.doe.gov

Subcontractor:
Blasch Precision Ceramics, Albany, NY

Contract Number: 84590

Start Date: June 28, 2006
End Date: August 7, 2009

### Objectives

- Enable the use of inexpensive metallic alloys in a solid oxide fuel cell (SOFC) exhaust recuperator through the use of a ceramic heat exchange section in the high temperature region.
- Design and develop methods to mechanically integrate the ceramic and metallic sections into a recuperator assembly.
- Evaluate and characterize the performance of a hybrid ceramic/metallic recuperator under typical SOFC operating conditions.
- Demonstrate the performance and durability of the hybrid recuperator through both long-term steady-state and thermal cycle testing.

### Accomplishments

- Completed the detailed design of a cross flow ceramic/counter flow metallic hybrid recuperator.
- Designed and manufactured molds to produce cross flow ceramic monoliths with two different specific heat transfer areas.
- Manufactured prototype ceramic parts.
- Completed assembly of prototype 1 kW hybrid recuperators.
- Conducted performance testing of 1 kW hybrid recuperators utilizing two different ceramic cores and two different metallic section configurations.

## Introduction

Acumentrics Corporation is focused on the development of efficient, reliable, and low-cost SOFC generators for the residential and commercial markets. A key component of the SOFC generator is the heat exchanger, or recuperator, which preheats the incoming cathode air using available heat in the exhaust stream. Typical exhaust temperatures of an SOFC generator are in the range of 800 to 1,000°C and a recuperator effectiveness of >80% is required for high overall generator electrical efficiency.

While the use of full metallic recuperators requires expensive high-alloy metals for oxidation resistance, these operating temperatures are well within the capabilities of lower cost ceramic and refractory materials. The goal of this project is the development of a "hybrid" recuperator which utilizes ceramic and metallic materials to achieve the recuperator design goals of high effectiveness, low pressure drop, low cost and compact size. The hybrid configuration takes advantage of the high temperature, low fouling capability of the ceramic section, while enabling the use of lower grade metallic alloys in the medium-to-low temperature regions.

## Approach

Work has focused on the design and construction of a high temperature, high effectiveness recuperator using a cast ceramic monolith technology in conjunction with a counter flow metallic recuperator. The design goal is for the high temperature ceramic section to reduce the exhaust side temperature sufficiently so that lower grade, lower cost, metals can be utilized in the metallic section. Figure 1 illustrates the design concept: a cross flow ceramic core is added to the air side outlet of a metallic recuperator. This core is encased in a metallic housing which directs the exhaust flow from the stack to the core exhaust passages and then directs the exhaust leaving the core to the inlet of the metallic recuperator. Expandable insulation is used to seal the core to the metallic casing preventing leakage from air to exhaust chambers. This configuration eliminates the need for complex plenums and allows for differential expansion of the heat exchange components through the use of flexible high temperature ceramic gaskets similar to that used on catalytic converters and the linear arrangement of the metallic and ceramic cores.

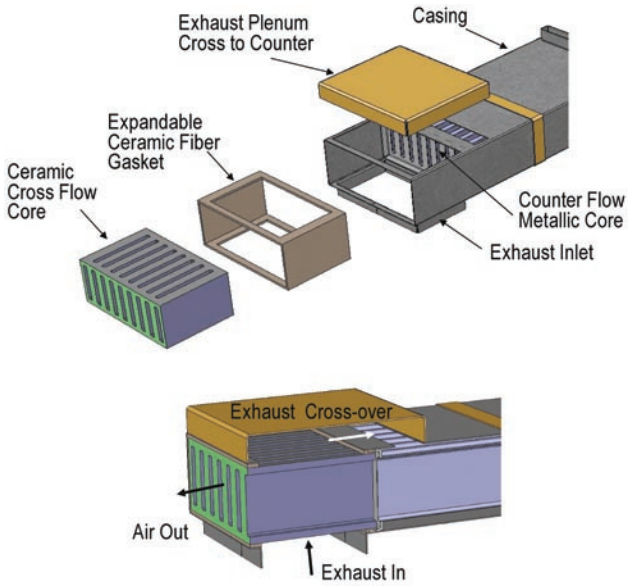


**FIGURE 1.** Hybrid Recuperator Assembly

## Results

Acumentrics has worked closely with Blasch Precision Ceramics to design and manufacture a single-pass cross-flow ceramic core, made of silicon carbide. A mold was manufactured to permit manufacture of ceramic cores using Blasch's proprietary forming method capable of producing net shape ceramic parts with relatively thin walls. Initial cores were made having a flow passage width of 6.3 mm. Further refinements in the core mold and the manufacturing process allowed for a decrease in the passage width to 3.2 mm, resulting in an increase in the heat transfer area of the monolith core by a factor of 1.75 with the same core volume. Figure 2 shows both ceramic heat exchanger cores. Performance testing was conducted with both cores and Figure 3 provides a comparison of the results with air and exhaust flow rates of 130 slpm.

Testing was also conducted using two different metallic sections: a brazed, finned core technology and a folded sheet technology. The folded sheet configuration is projected to have a lower volume cost. Table 1 gives the recuperator effectiveness of the folded sheet metallic section alone and with the combined ceramic and metallic sections utilizing the 6.3 mm flow channel core.

Duration and thermal cycle testing was conducted on the hybrid recuperator. After 1,000 hours of operation and multiple cycles from ambient to operating temperature, both cores were structurally sound without cracks or defects. Inspection also revealed that the ceramic core sealing was intact without significant leakage from the air to exhaust sides of the unit. Figure 4 shows the 6.3 mm passage core after 1,000 hours of testing.

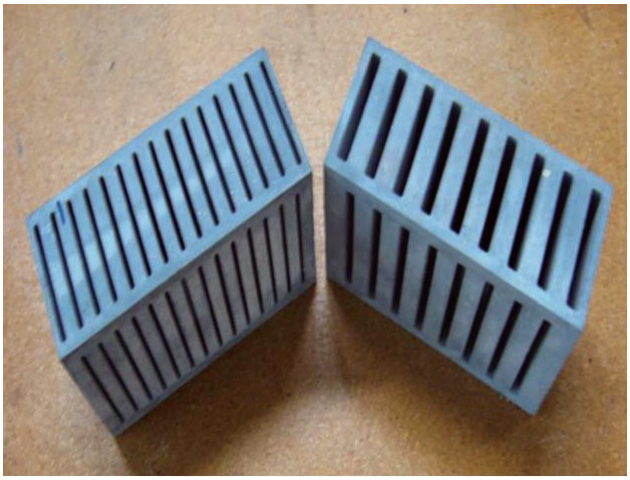

**FIGURE 2.** 6.3 mm and 3.2 mm Flow Passage Ceramic Monoliths

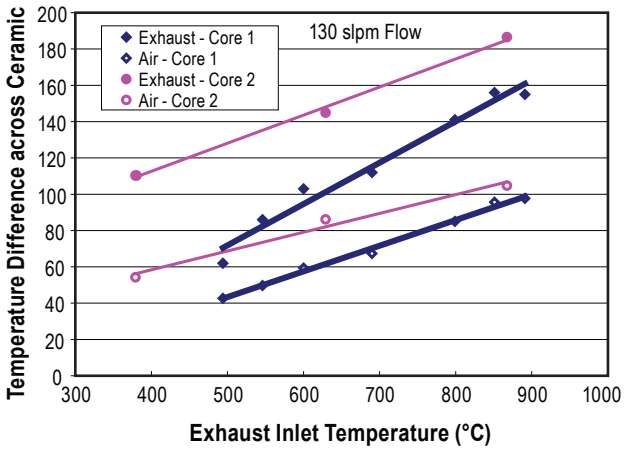


**FIGURE 3.** Air and Exhaust Temperatures across Ceramic Cores

**TABLE 1.** Folded Sheet Recuperator Effectiveness

| Air Flow | Overall Effectiveness | |
|---|---|---|
| slpm | Metallic | Hybrid |
| 100 | 0.710 | 0.787 |
| 200 | 0.705 | 0.816 |
| 300 | 0.698 | 0.780 |

## Conclusions and Future Directions

Acumentrics Corporation, in conjunction with Blasch Precision Ceramics, has successfully integrated a cross flow ceramic monolith with a counter flow metallic recuperator and obtained greater than 80% effectiveness. A design has been developed which provides for a straightforward attachment of the ceramic monolith

**FIGURE 4.** 6.3 mm Ceramic Core after 1,000 Hours of Operation

into the metallic section housing without the need for complex and expensive seals and plenums.

Future work will include additional performance and long duration testing of the hybrid recuperator along with evaluation of techniques to increase the heat transfer performance of the ceramic monolith. The following is a summary of future technical objectives:

- Conduct performance testing of the ceramic monoliths independent of the low temperature metallic section.
- Evaluate ceramic component manufacturing techniques to optimize the ceramic core heat transfer rates and increase the specific surface area.
- Conduct integrated fuel cell stack testing with the hybrid recuperator.
- Evaluate scale-up of the heat exchanger geometry to larger generator sizes.
- Evaluate a foil design counter flow metallic section which has the potential to further reduce the recuperator cost.
- Evaluate recuperator designs which are compatible with a “replaceable” fuel cell bundle stack configuration.

# III.I.2 Anode and Cathode Blower Systems for SOFC

Dr. Mark C. Johnson
Phoenix Analysis & Design Technologies
7755 S. Research Dr., Suite 110
Tempe, AZ 85284
Phone: (480) 813-4884; Fax: (480) 813-4807
E-mail: mark.johnson@padtinc.com

DOE Project Manager: Maria Reidpath
Phone: (304) 285-5432
E-mail: Maria.Reidpath@netl.doe.gov

Contract Number: 84209

Start Date: June 7, 2005
End Date: August 6, 2009 (project is now complete)

### FY 2009 Objectives

- Develop large multi-stage blower that can pump anode gas at 500°C (hot anode recycle blower [HARB]). This unit will serve up to 500 kW power plants as part of FutureGen.
- Develop multi-stage blower that can pump warm anode or cathode gas up to 100°C (small multi-stage [SMS] blower). This unit will serve up to 50 kW power plants.
- Verify bearing/seal selection and design.
- Integrate and evaluate controller/motor.
- Develop low-cost integrated assembly to provide required performance and offer low cost in high volume.
- Prototype the unit for testing in a solid oxide fuel cell (SOFC) system.

### Accomplishments

- Multi-stage blower aerodynamic technology now optimized for HARB and SMS blowers. Provisional patent has been filed.
- Developed two bearing rigs and initiated endurance testing. Goal is 40,000 hours of life. A novel bearing system has been developed and has demonstrated superior life in a 5,000-hour endurance test.
- Complete prototype build and test of HARB with capability to service up to a 500 kW SOFC system. Performance testing and short endurance testing are now complete.

## Introduction

The thrust of this research and development effort was to develop technology that serves the SOFC industry and help developers in this industry to succeed. The starting point for success rests with understanding the needs of the companies involved and this was been done through substantial discussions with these companies and the development of specifications with them. These discussions have lead to two distinct designs – the HARB, which will serve hot anode gas requirements in FutureGen demonstration units, and the SMS blower which will serve warm anode and cathode gas requirements for SOFC and other fuel cell industries.

The challenge in this project was to develop blowers that can satisfy very difficult performance specifications and operate in harsh environments, while also providing low-cost solutions. Therefore, the focus of this project was to develop an innovative multi-stage blower approach that is low cost and high performing. At this point, the project is complete and we have seen mixed results from the effort. The HARB was found to have higher costs than were hoped for due to the fabrications costs with nickel-based sheet metal. We found that even with very simple sheet metal components, the fabrication costs were large. The SMS blower was found to have exceptionally good performance and good opportunity for low cost. This is because the SMS blower is made from aluminum sheet metal and is not only inexpensive but easy to work with. The SMS pumphead technology is suitable for retrofitting off-the-shelf Ametek blowers.

## Approach

The approach used to develop these technologies emphasized design iterations with a reduction to working prototypes in rapid succession. Because of the complexities involved, side testing was used extensively. Side testing implies a test of some subsystem, or even a component, to insure suitability. Finite element analysis was used liberally whenever detailed analysis could provide insight into design tradeoffs.

## Results

There are two major collections of results for this work. First, the development of the SMS pumphead has lead to significant improvements in performance as compared to other off-the-shelf-technologies. Second, the working prototype of the HARB was delivered to a customer for testing in a power plant.

## SMS Results

SMS performance development (Figure 1) was done by purchasing an off-the-shelf Amatek blower unit and stripping the aerodynamic components off the blower and replacing those components with stereolithography-based designs. In order to ensure a low-cost result, we restricted ourselves to work with simple materials and manufacturing techniques. This resulted in simple stamp-and-stake impellers and static structures that are amenable to low-cost, high-volume production. Estimated costs in volume are approximately $3 per stage. Our final designs allow for retrofitting of Amatek blowers (a practical solution for the industry until volumes are larger) with performance numbers that are much better than off-the-shelf solutions.

We iterated through 11 different pumphead designs and simultaneously developed our two-dimensional tools and data reduction tools to help us optimize the performance. The result is a very high-performance solution with a design system that allows us to design new pumpheads (within this manufacturing paradigm) based on custom specifications.

Table 1 illustrates the results of our work.

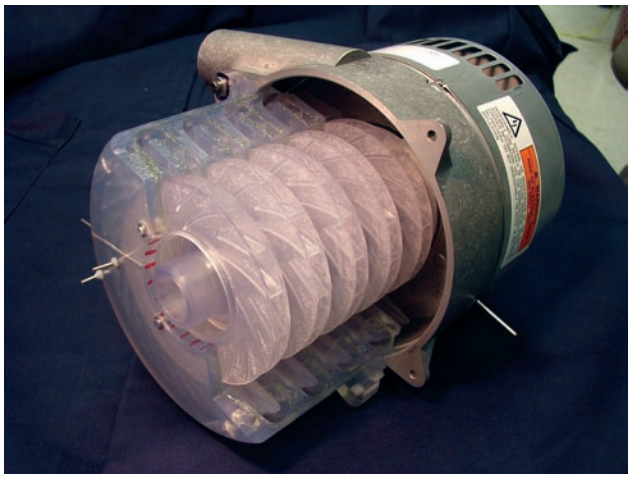

**FIGURE 1.** SMS Aerodynamic Development System

**TABLE 1.** Description of Development Iterations for Low, Medium and High Specific Speed Designs

| | Low Specific Speed Designs | Medium Specific Speed Designs | High Specific Speed Designs |
|---|---|---|---|
| Number of Iterations | 6 | 3 | 2 |
| Peak Efficiencies | ~ 68% | ~ 70% | ~ 75% |

A picture of a low specific speed, 3-stage prototype, based upon this work is shown in Figure 2.

## HARB Results

One important outcome of the present work is the fabrication and testing of HARB and delivery of that blower to a SOFC developer. This development began as a very small blower with application in the original SECA specification for an approximately 10 kW small power plant. However, about halfway through the development, the SECA requirements shifted to the FutureGen program which needed a much larger blower more on the level of 1 MW. Based on this, we shifted to a larger design that can service from as low as 20 kW up to about 500 kW. Figure 3 shows the final prototype on test in our high-temperature test rig.

**FIGURE 2.** SMS Prototype

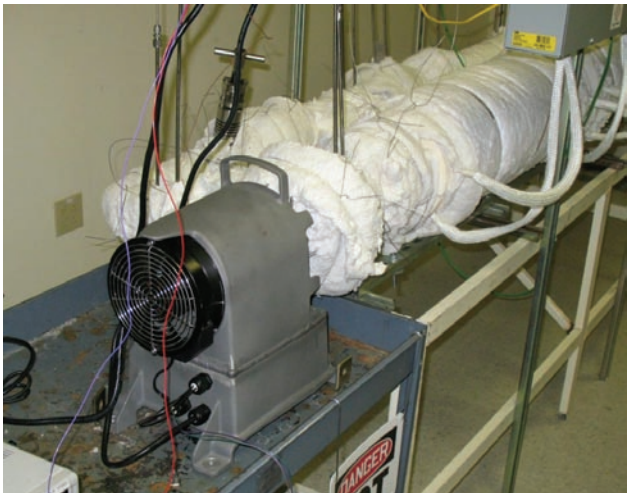

**FIGURE 3.** PADT HARB Prototype with 4-stage Pumphead

Table 2 highlights the strengths and weaknesses of this final prototype.

**TABLE 2.** Strengths and Weaknesses of the HARB Prototype

| Strength/ Weakness | Discussion |
|---|---|
| Strength: Flexible pumphead design | The pumphead has multiple stages made from stamped sheet metal. We can vary the number, size, and blading in these designs to accommodate various specifications |
| Strength: Low weight | The final design weighs about 70 lbm which is fairly low compared to competitive blowers that would come out of the heat treat industry. The blower is much smaller also. |
| Strength: Pumphead Efficiency | Because we can employ the pumphead designs that were developed in the SMS project, we should be able to provide high efficiencies compared to off-the-shelf solutions. However, this first prototype was built for such a small system (20 kW) that it has a fairly low efficiency. |
| Weakness: Cost | One of the main thrusts in this effort was to develop a low-cost approach to anode recycle. However, the costs for this unit were higher than expected. There are several reasons for this. First is volume – the industry is not ready for high volumes so cost is high. Second, the cost associated with sheet metal fabrication, especially nickel-based alloys, is expensive. Third, the size of the blower is much larger than initially expected due to the change in specification. |
| Weakness: Limited Pressure Rise | Our design employs grease-for-life ball bearings which were used to provide a low-cost solution. However, they also create a limitation on the rotational speed and this then limits the amount of pressure rise that can be obtained efficiently from a given stage. In the end, even with four stages, it is difficult to get the pressure rise that SOFC developers want. Still, off-the-shelf blowers available from the heat treat industry are only single stage devices and they too would not be able to easily reach the pressure rise needed. |
| Weakness: Durability | We designed this blower to run at modest speed (up to ~15,000 RPM). However, the large blowers from the heat treat industry run at very slow RPM and therefore will have longer bearing life. |

## Conclusions and Future Directions

The SMS work we have done so far has lead us to the conclusion that the SMS technology is very strong and offers a solid value proposition for small power plants that need only warm gas delivery. It truly offers the potential for excellent performance and very low cost in high volumes. We are seeking groups that want to license or implement this technology in their systems.

However, the HARB is not in as good a position. First, the FutureGen-sized power plants have significant development required before they reach a sizeable market. Even then, the volumes will be low for some time to come – which means low sales for the HARB. Therefore, there is no ready market for the HARB. Additionally, competition from conventional heat treating blowers will be significant. The heat treating blowers have supporting volume from another industry (heat treating) and also run at low speed which offers good durability. Therefore, we see that HARB as serving in a research role for some time and it is not likely to reach significant commercial revenues.

Future work will focus on finding high volume applications for SMS like designs.

## FY 2009 Publications/Presentations

**1.** We have filed a provisional patent on our multi-stage aerodynamic technology.

# III.I.3 Foil Gas Bearing Supported High-Speed Centrifugal Anode Gas Recycle Blower

Giri Agrawal (Primary Contact), Bill Buckley, Dennis Burr, Ali Shakil
R&D Dynamics Corporation
15 Barber Pond Rd.
Bloomfield, CT 06002
Phone: (860) 726-1204; Fax: (860) 726-1206
E-mail: agragiri@rddynamics.com
Web Site: www.rddynamics.com

DOE Project Manager: Robin Ames
Phone: (304) 285-0978
E-mail: Robin.Ames@netl.doe.gov

Contract Number: 84210

Start Date: June 27, 2005
End Date: August 6, 2009

### FY 2009 Objectives

- Improve the blower design and eliminate the leakage of anode gas at high temperature up to 850°C.
- Manufacture the parts and test the blower up to 850°C. Previously the blower was tested to 718°C.

### Accomplishments

R&D Dynamics has made significant progress in developing a high temperature anode gas recycle blower for solid oxide fuel cell (SOFC) systems. A foil gas bearing supported high speed centrifugal anode gas recycle blower (FBS-AGRB) was previously developed and tested successfully up to 718°C inlet temperature.

The blower testing results had been very encouraging and demonstrated the viability of the technology; however, some improvements were required in order for the blower to reach the inlet temperature goal of 850°C. The required improvements made during fiscal year 2009 were as follows:

- Analyzed and optimized design.
- Upgraded blower materials to achieve 850°C.
- Designed and manufactured motor capable of handling high temperature.
- Improved sealing design to eliminate anode gas leakage at high temperature.
- Manufactured parts.
- Blower was assembled and is ready for testing.

## Introduction

The goal of the Solid State Energy Conversion Alliance (SECA) is to develop commercially-viable ($400/kW) 3 to 10 kW SOFC systems by the year 2010. SOFC power generation systems are attractive alternatives to current technologies in diverse stationary, mobile, and military applications. SOFC systems are very efficient, from 40 to 60 percent in small systems and up to 85 percent in larger co-generation applications. The electrochemical conversion in an SOFC takes place at a lower temperature (650 to 850°C) than combustion-based technologies, resulting in decreased emissions – particularly nitrogen oxides, sulfur oxides, and particulate matter. These systems all offer fuel flexibility, as they are compatible with conventional fuels such as hydrogen, coal, natural gas, gasoline, or diesel. Despite these advantages, advances in balance of plant component design must be developed before the SECA program goal can be realized.

SOFC systems that incorporate some recycling of the anode exhaust gas, which is mixed with incoming fresh fuel prior to entering the pre-reformer, have a higher efficiency and offer the potential for lower overall system cost. An anode gas recycling blower is an attractive solution to perform this task.

## Approach

R&D Dynamics focused on the design and development of a FBS-AGRB to achieve the goals set by SECA members. An innovative, cost-reduced, compact, high-temperature, high-speed centrifugal blower was designed, built and tested in Phase II. The unit was tested in a closed loop using a heat furnace. Due to limitation on materials, leakage at high temperature and motor design, the unit testing was limited up to 718°C.

In order to reach the goal of making economically viable and efficient SOFC systems, the FBS-AGRB has been redesigned and parts have been manufactured to meet the requirements of SOFC systems because of its potential for:

- Low-cost using simple design and material.
- High temperature capability (>850°C) using foil gas bearings, advanced high temperature magnets for the permanent magnet (PM) motor.
- Highest blower efficiency via high speed centrifugal impeller, foil gas bearings, PM motor and sensor-less controller.

- Contamination-free using oil-free foil gas bearings.
- High reliability requires no maintenance.
- Compactness and light weight.

## Results

The FBS-AGRB has been designed for an inlet temperature of 600 to 850°C, atmospheric pressure, pressure rise of 4-10 inches of water, and a flow of 100 standard liters per minute (slpm), which is nominally composed of 46 slpm $H_2O$, 27 slpm $CO_2$, 20 slpm $H_2$ and 7 slpm CO. Overall efficiency exceeds 40% under the aforementioned operating conditions. The unit has a variable speed control with a flow turn down ratio of 5 to 2. The blower unit will have a design life of >40,000 hours, with a 100% duty cycle and 10,000-hour maintenance interval. The unit will be able to tolerate at least 30 thermal cycles between operating and room temperatures over its design life.

Design points for the FBS-AGRB are as follows:

| | |
|---|---|
| Shaft Speed | 98,000 rpm |
| Pressure Ratio | 1.025 |
| Pressure Rise | 25.4 cm of water (10 inches of water) |
| Inlet Pressure | 1.01 bar (14.69 psia) |
| Outlet Pressure | 1.08 bar (15.06 psia) |
| Inlet Temperature | 850°C (1,562°F) |
| Outlet Temperature | 857.3°C (1,575.2°F) |
| Gas Constant | 0.369 J/kg°C (68.64 ft-lbf/lbm R) |
| Specific Heat Ratio | 1.274 |
| Mass Flow | 1.54 g/s (0.204 lbm/min) |
| Volume Flow | 100 slpm |
| Impeller Isentropic Power | 15.6 Watt |

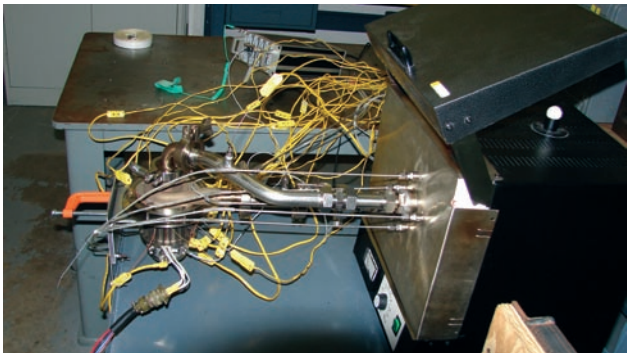

**FIGURE 1.** FBS-AGRB Test Rig

Figure 1 shows the recently modified blower mounted on a closed-loop furnace rig. Figure 2 shows a thermal map of the blower tested in Phase II. Figure 3 shows the manufactured blower assembly. Figure 4 shows the manufactured shaft assembly.

Key technologies were incorporated into the blower design including state-of-the-art aerodynamics, foil gas bearings, PM motor using advanced high-temperature magnets, innovative fan design with fins mounted on the shaft assembly, thermal choke to separate the hot side from the cold side and sensor-less controller. Design analysis included performance prediction maps, preliminary design, finite element analysis including thermal, vibration and stress, computational fluid dynamic analysis, rotor dynamics analysis, cooling flow analysis, detailed design and drawings. Tests performed on AGRB components were load deflection on journal and thrust bearings, back electromotive force testing on the motor rotor and stator, etc. A furnace will be used to heat up the gas to 850°C for elevated temperature testing of FBS-AGRB. The blower is being readied for testing.

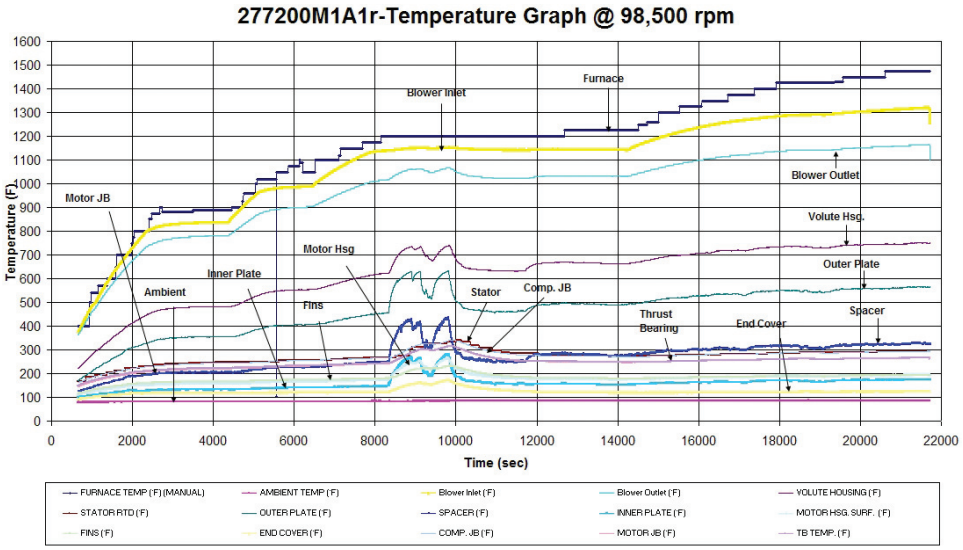


**FIGURE 2.** Thermal Map from FBS-AGRB Testing

Fi**GURE 3.** View of the Manufactured FBS-AGRB Prototype Unit

**FIGURE 4.** View of the Manufactured Shaft Assembly

## Conclusions and Future Directions

- Modified blower technologies were proven by extensive design and analysis.
- A prototype unit has been designed and built which is ready for testing.
- The high-temperature blower design evolved to be a successful design which can achieve SECA goals.

Future work to be performed is as follows:

- Test blower at high temperature conditions.
- Demonstrate blower to SECA members.
- Test blower at SECA member's fuel cell systems.

## Special Recognitions & Awards/Patents Issued

**1.** "Foil Gas Bearing Supported High Temperature Centrifugal Blower & Method for Cooling Thereof," Patent filed on October 2, 2008.

**2.** 2009 R&D 100 Award Application submitted.

## FY 2009 Publications/Presentations

**1.** "Project Review Presentation," March 6, 2009, DOE National Energy Technology Laboratory, Morgantown, West Virginia.

# III.I.4 Foil-Bearing Supported High-Speed Centrifugal Cathode Air Blower (Low-Cost Cathode Blower)

Giri Agrawal (Primary Contact), Bill Buckley, Dennis Burr, Sam Rajendran
R&D Dynamics Corporation
15 Barber Pond Road
Bloomfield, CT 06002
Phone: (860) 726-1204; Fax: (860) 726-1206
E-mail: agragiri@rddynamics.com
Web Site: www.rddynamics.com

DOE Project Manager: Robin Ames
Phone: (304) 285-0978
E-mail: Robin.Ames@netl.doe.gov

Contract Number: 84616

Start Date: June 28, 2006
End Date: August 14, 2010

### FY 2009 Objective

Develop a low-cost cathode air blower meeting all the technical requirements of Solid State Energy Conversion Alliance (SECA) members for 3 to 10 kW solid oxide fuel cell (SOFC) systems. The manufacturing cost target for the blower is $100 per unit based upon a production volume of 50,000 units/year.

### Accomplishments

- A low-cost cathode blower (LCCB) with only 16 parts was designed. A cost model targeting $100 was developed and feasibility of the project was achieved.
- Detailed design of the blower was completed.
- Detailed drawings are being prepared for manufacturing of the blower.
- A low-cost controller was developed and tested.

## Introduction

The goal of SECA is to develop commercially-viable ($400/kW) 3 to 10 kW SOFC systems by the year 2010. SOFC power generation systems are attractive alternatives to current technologies in diverse stationary, mobile, and military applications. SOFC systems are very efficient, from 40 to 60 percent in small systems and up to 85 percent in larger co-generation applications. The electrochemical conversion in an SOFC takes place at a lower temperature (650 to 850°C) than combustion-based technologies, resulting in decreased emissions – particularly nitrogen oxides, sulfur oxides, and particulate matter. These systems all offer fuel flexibility, as they are compatible with conventional fuels such as hydrogen, coal, natural gas, gasoline, or diesel. Despite these advantages, advances in balance of plant component design must be developed before the SECA program goal can be realized.

SOFC systems require blowers to provide motive force to incoming atmospheric air, in order to overcome the pressure drop in the various valves and heat exchangers, and in the fuel cell stack. The energy required to drive this component is typically one of the largest parasitic loads for the SOFC system; consequently, high blower efficiency is paramount to high system efficiency. Furthermore, blower reliability is critical to ensure safe long-term system operation.

## Approach

- In Phase I, an LCCB was conceived and designed. A process using DFMA® (Design for Manufacturing and Assembly) techniques was developed for reducing manufactured cost of the LCCB to $100 per unit, based upon a production volume of 50,000 units per year.
- In Phase II, a detailed design of the blower was completed and a prototype blower is planned to be tested in an actual fuel cell system in the year 2010.
- Phase III will start the commercialization phase of the project.

## Results

An existing fuel processor blower developed at R&D Dynamics Corporation was used as a baseline to develop and cost-reduce the blower during Phase I. A split housing design was invented and the parts count was reduced from a total number of 113 parts for the existing blower using a DFMA® tool to a part count of 16 for the LCCB. Figure 1 shows the concept of the LCCB. The LCCB estimated cost is $105.11 at a production rate of 50,000 units per year.

Detailed aerodynamic design, motor design, controller design, bearing design and mechanical design were completed. Computational fluid dynamics and finite element analysis done on the blower design are shown in Figures 2 and 3.

A low-cost controller was developed. A low-cost direct current (DC)-DC converter for the controller was

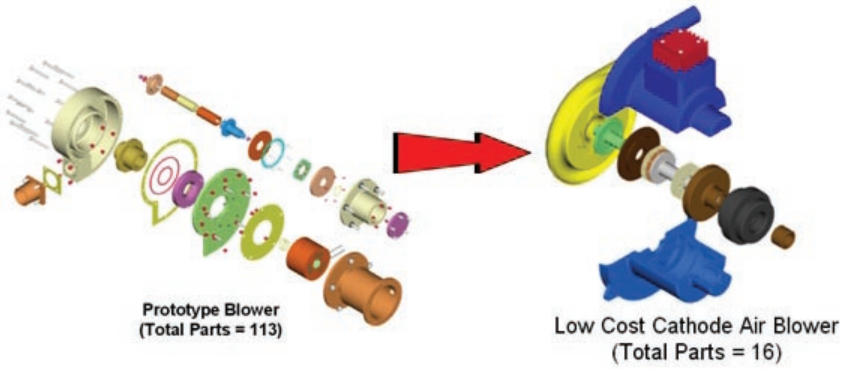


**FIGURE 1.** Low-Cost Blower Concept

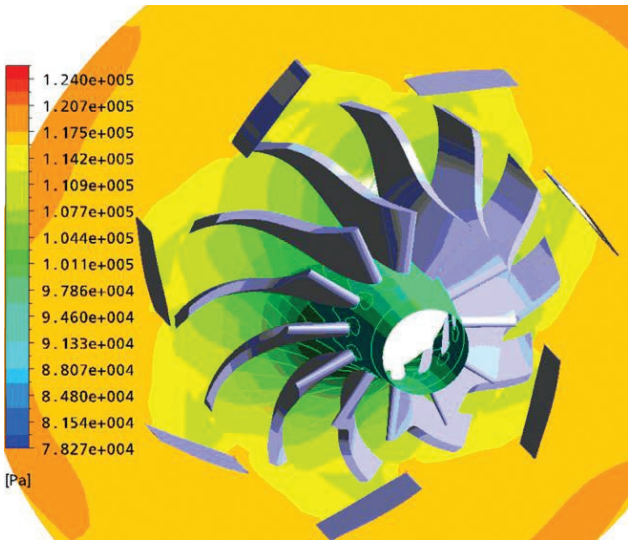


**FIGURE 2.** Aerodynamic Analysis

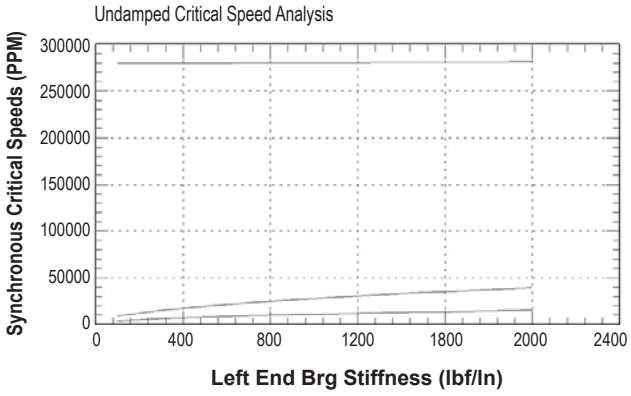


**FIGURE 3.** Critical Speed Analysis

developed. A low-cost commercial insulator gate bipolar transistor was identified for the design. The controller is a high-price part. By developing a low-cost controller in this power range the blower price is reduced significantly. The low-cost controller is being developed in-house at R&D Dynamics and is being extensively tested at different load conditions using existing blowers of similar power range. Figure 4 shows testing of the low-cost controller.

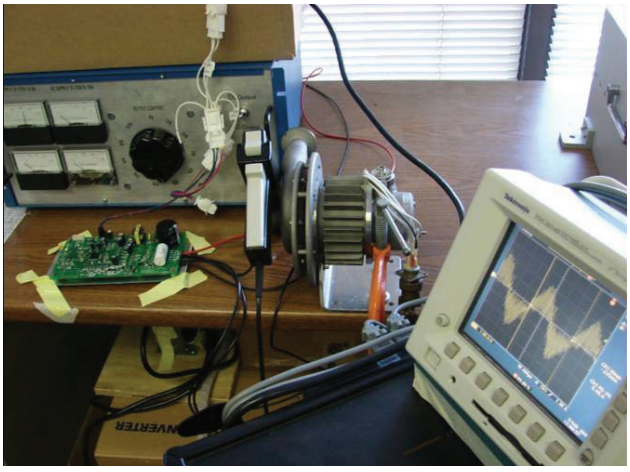

**FIGURE 4.** Low-Cost Controller Testing

## Technical Summary

The technical summary of the blower design is as follows:

| | |
|---|---|
| Blower Type | Centrifugal |
| Mechanical Speed | 80,500 rpm |
| Weight | 1.45 kg (3.2 lbm) |
| Bearings | Foil Gas Bearings |
| Motor Type | Permanent Magnet Motor |
| Controller Type | Sensorless Controller |
| Input Electric Power | 769 watt |
| Overall Efficiency | 61.6% |
| Total Blower Cost | $105.11 [@ 50,000 units/year] |
| Life | >40,000 hrs |

## Conclusions and Future Directions

Phase I research work was highly successful and proved the feasibility of the project. Phase II work has been progressing well and all the milestones are achieved as planned. A prototype blower is planned to be tested in a fuel cell system in the year 2010.

## FY 2009 Publications/Presentations

**1.** "Project Review Presentation," March 6, 2009, DOE National Energy Technology Laboratory, Morgantown, West Virginia.

# III.I.5 Foil Gas Bearing Supported High-Temperature Cathode Recycle Blower (for Large Megawatt Size SOFC Power Plants)

Giri Agrawal (Primary Contact), Bill Buckley, Dennis Burr, Sam Rajendran
R&D Dynamics Corporation
15 Barber Pond Road
Bloomfield, CT 06002
Phone: (860) 726-1204; Fax: (860) 726-1206
E-mail: agragiri@rddynamics.com
Web Site: www.rddynamics.com

DOE Project Manager: Robin Ames
Phone: (304) 285-0978
E-mail: Robin.Ames@netl.doe.gov

Contract Number: 85020

Start Date: June 30, 2008
End Date: March 29, 2009

### FY 2009 Objective

Design and prove the feasibility of efficient, reliable, low-cost and oil-free high temperature cathode recycle and anode recycle blowers for large megawatt size solid oxide fuel cell (SOFC) power plants.

### Accomplishments

- A high-temperature cathode recycle blower has been designed.
- The blower was designed such that it can be used dually also as a high-temperature anode recycle blower.
- Breadboard testing was conducted to prove feasibility of a 6-inch diameter journal bearing to be used for the recycle blowers.
- Feasibility of the project was achieved by design, analysis and breadboard testing.

## Introduction

Fossil fuels are projected to remain the mainstay of energy consumption well into the 21st century. As the nation strives to reduce its reliance on imported energy sources, the DOE's Office of Fossil Energy supports research and development to help ensure that new technologies and methodologies will be in place to promote the efficient and environmentally sound use of America's abundant fossil fuels.

The Solid State Energy Conversion Alliance (SECA) goal is to develop and design a SOFC capable of manufacture at $400/kW. Concurrently, SECA large-size systems will scale and integrate SECA SOFC technology for delivery to 5 MWe proof-of-concept plants to be tested in 2012. Development of large (greater than 100 MWe) SOFC power blocks will enable affordable, efficient and environmentally friendly electrical power from coal.

SOFC-based power block configurations for large central generation applications could benefit from recycling a portion of the high-temperature (e.g., 800-850°C) cathode or anode gas effluent back to the system in order to improve the overall plant efficiency. The most important considerations for high-temperature blowers required for recycling are:

- Reliability, which is critical to ensure safe long-term system operation.
- Free of oil or grease contamination of process gas.
- Low cost.

Currently there is no high-temperature blower available in the market that can meet these requirements.

## Approach

- During Phase I, the feasibility of the project was successfully proven by performing design and analysis of the blower. An optimized 6-inch foil bearing design suitable for this high-temperature blower application was tested.
- In Phase II, detailed design of the blower will be carried out and detailed drawings will be made for manufacturing. The blower will be manufactured, assembled and tested as a cathode recycle blower. Modifications for using as anode recycle blower will be made and the unit will be tested again as an anode recycle blower. The blower design will be optimized and cost-reduced using a DFMA® (Design for Manufacturing and Assembly) model.
- In Phase III, the blower will be tested in an actual SOFC system and will be commercialized and produced in quantities.

## Results

The high-temperature cathode recycle blower is an innovative high-temperature design where the hot-fan side is separated from the motor. It was determined that with small modifications the cathode recycle blower

design could also be used as a high-temperature anode recycle blower. Hence it would have dual use.

The hot-fan side takes in the recycle gas and raises the pressure using an axial fan. The rotating assembly of the blower is supported on high-reliability, foil-gas bearings. The blower is driven by an induction motor and controlled by a sensorless controller.

A 6-inch journal bearing was tested up to design speed proving the feasibility. Figure 1 shows the aerodynamic design of the blower impellers. Figure 2 shows finite element analysis stress of the fan rotating assembly. The test rig is shown in Figure 3.

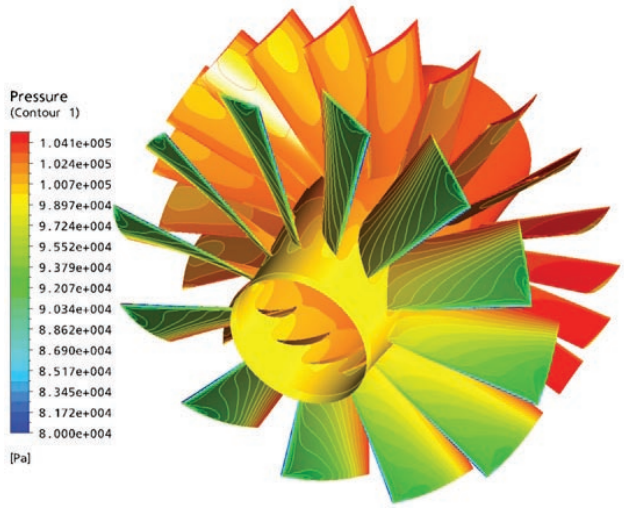


**FIGURE 1.** Aerodynamic Analysis

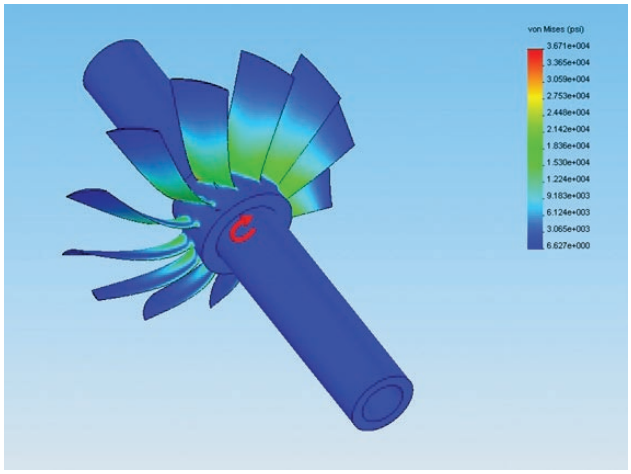


**FIGURE 2.** Fan Rotating Assembly Finite Element Stress Analysis

The blower design has following features:

- High temperature capable (up to 850°C)
- Highly reliable
- Highly energy efficient
- Low life cycle cost
- Oil free
- Maintenance free
- Higher design life (>40,000 hrs)
- Lower noise (<70 dBa)
- Easily scalable
- Turn down ratio up to 5:1

## Technical Requirements of Cathode Blower

Through discussion with DOE and SECA members, a nominal specification for design of the blower was chosen to prove out the feasibility of the project in Phase I. The specifications are as follows:

| | |
|---|---|
| Process Gas | Air |
| Inlet Gas Temperature | 800°C |
| Inlet Pressure | 15.6 psia |
| Pressure Rise | 12” of water |
| Required Flow | 20,000 SCFM |
| Turn Down Ratio | 2:1 |
| Design Life | >40,000 hours |
| Maintenance Interval | 10,000 hours |

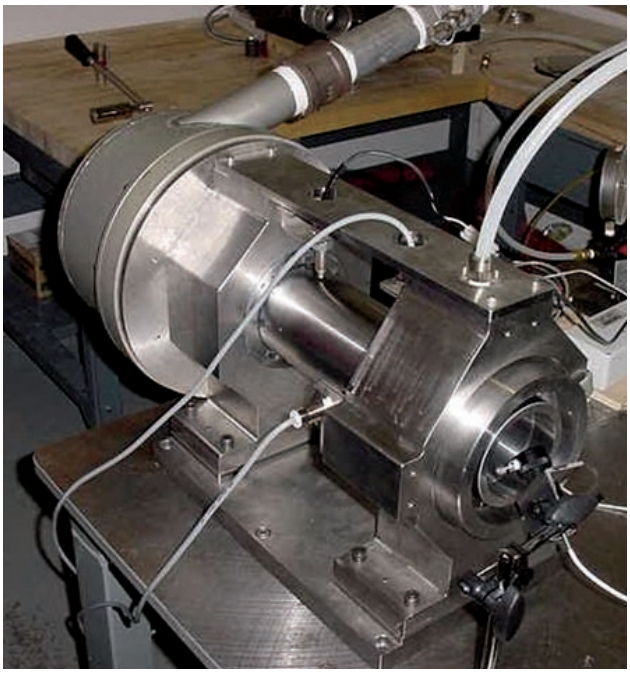

**FIGURE 3.** Journal Bearing Test Rig

### Technical Summary

The blower is sized and designed from the nominal specifications; the technical summary of the design is as follows:

| | |
|---|---|
| Blower Type | Axial |
| Fan Diameter | 28.6 inches |
| Mechanical Speed | 9,244 rpm |
| Bearing Type | Foil Gas Bearings |
| Motor Type | Induction Motor |
| Controller Type | Sensorless Controller |
| Overall Dimension | 11 ft x 8 ft x 4 ft |
| Weight | 6,436 lbs |
| Life | >100,000 hrs |

## Conclusions and Future Directions

Phase I research work was highly successful in meeting all the requirements of SECA members and proved the feasibility of the project. Phase I work opened venues for further development to manufacture the designed blower and test successfully to commercialize the technology for large SOFC power plants, which will be done in the Phase II stage of this project.

## FY 2009 Publications/Presentations

**1.** "Project Review Presentation," March 6, 2009, DOE National Energy Technology Laboratory, Morgantown, West Virginia.

# IV. INNOVATIVE CONCEPTS

# IV.1 Novel Fuel Cells for Coal-Based Systems

Dr. Thomas Tao
CellTech Power, LLC
131 Flanders Road
Westborough, MA 01581
Phone: (508) 898-2223 x34; Fax: (508) 898-2690
E-mail: Tao@celltechpower.com

DOE Project Manager: Joseph Stoffa
Phone: (304) 285-0285
E-mail: Joseph.Stoffa@netl.doe.gov

Contract Number: NT0004111

Start Date: October 1, 2008
End Date: June 1, 2009

### FY 2009 Objectives

- Quantify the fate of coal contaminants in tin at electrochemical looping (ECL) operating conditions.
- Measure impurities remaining after reacting coal and tin oxide.
- Spike a significant quantity of coal contaminants known to be harmful to cell components into an operating liquid tin fuel cell.
- Operate spiked cell and compare results to typical liquid tin anode fuel cell performance.

### Accomplishments

- Successfully developed a small-scale reactor to simulate reaction between selected coal and fuel cell anode tin.
- Developed an experimental apparatus and test procedure to evaluate coal reaction with tin oxide.
- Conducted five coal/tin reactor tests to determine the fate of coal impurities.
- Conducted electrochemical impurity testing using a sub-scale (6 watt) liquid tin anode fuel cell spiked with 1,600 ppm of the five elements contained in coal which were predicted to detrimental to the yttria-stabilized zirconia (YSZ) electrolyte. The post mortem analysis was split into three distinct sections as follows:
  - Optical inspection of the electrolyte and other cell components for damage;
  - Scanning electron microscope and energy dispersive X-ray analysis of the electrolyte-tin interface; and,
  - Glow discharge mass spectrometry (GDMS) analysis of tin samples from the top and bottom of the cell.

## Introduction

ECL is a new approach to direct power generation from coal or biomass based on the liquid tin anode solid oxide fuel cell (LTA-SOFC). The LTA-SOFC is closely related to SOFC technology, using the same cathode and yttria electrolyte materials while replacing the conventional nickel anode with liquid tin. In the ECL configuration, a separate coal-tin reactor feeds the LTA-SOFC, allowing the *direct* (no reformer or gasifier) conversion of carbonaceous fuels and is projected to obtain over 60% efficiency using coal, with 95% or better $CO_2$ capture. This configuration also creates the opportunity to separate coal ash, impurities and $CO_2$ prior to power generation.

The purpose of this project is to conduct an initial evaluation of the behavior of coal contaminants in the presence of molten tin and to provide experimental validation of the concept of using a coal-tin reactor as a purification step to eliminate impurities which may harm the fuel cell. Testing of the LTA-SOFC with common coal contaminants spiked into the tin anode demonstrated that at high concentrations (1,600 ppm), performance degradation can be observed. Experiments simulating the coal-tin reactor verified that the molten tin provides good separation of ash and gaseous reaction components. Chemical analysis of the tin following reaction verified that nearly all of the coal contaminants of concern are not present in the tin following reaction, providing an expectation that a pure liquid tin stream can be fed from the coal-tin reactor to the fuel cell.

## Approach

To assess the potential impact of coal contaminants on the LTA-SOFC, a Gen 3.1 LTA-SOFC was constructed with tin spiked with a high level of contaminants. The contamination level for V, Cr, and As was 400 ppm and the level for Mo and Nb was 200 ppm. The fuel cell was operated on hydrogen under load to evaluate degradation differences from normal (not spiked) LTA-SOFC cells.

To assess the cleaning capability of the coal-tin reactor in the ECL configuration, coal and tin oxide were reacted in an experimental set-up designed to emulate a coal-tin reactor. The resulting tin product was

subjected to highly sensitive GDMS chemical analysis to assess the amount of contamination remaining in the tin. The details of the experimental setup are shown in Figure 1.

## Results

The measured LTA-SOFC cell voltage under load vs. time is shown in Figure 2. The spiked cell was loaded to 4.2 amp and operated for 420 hours. Results for unspiked cells operating on hydrogen and JP-8 are shown for comparison.

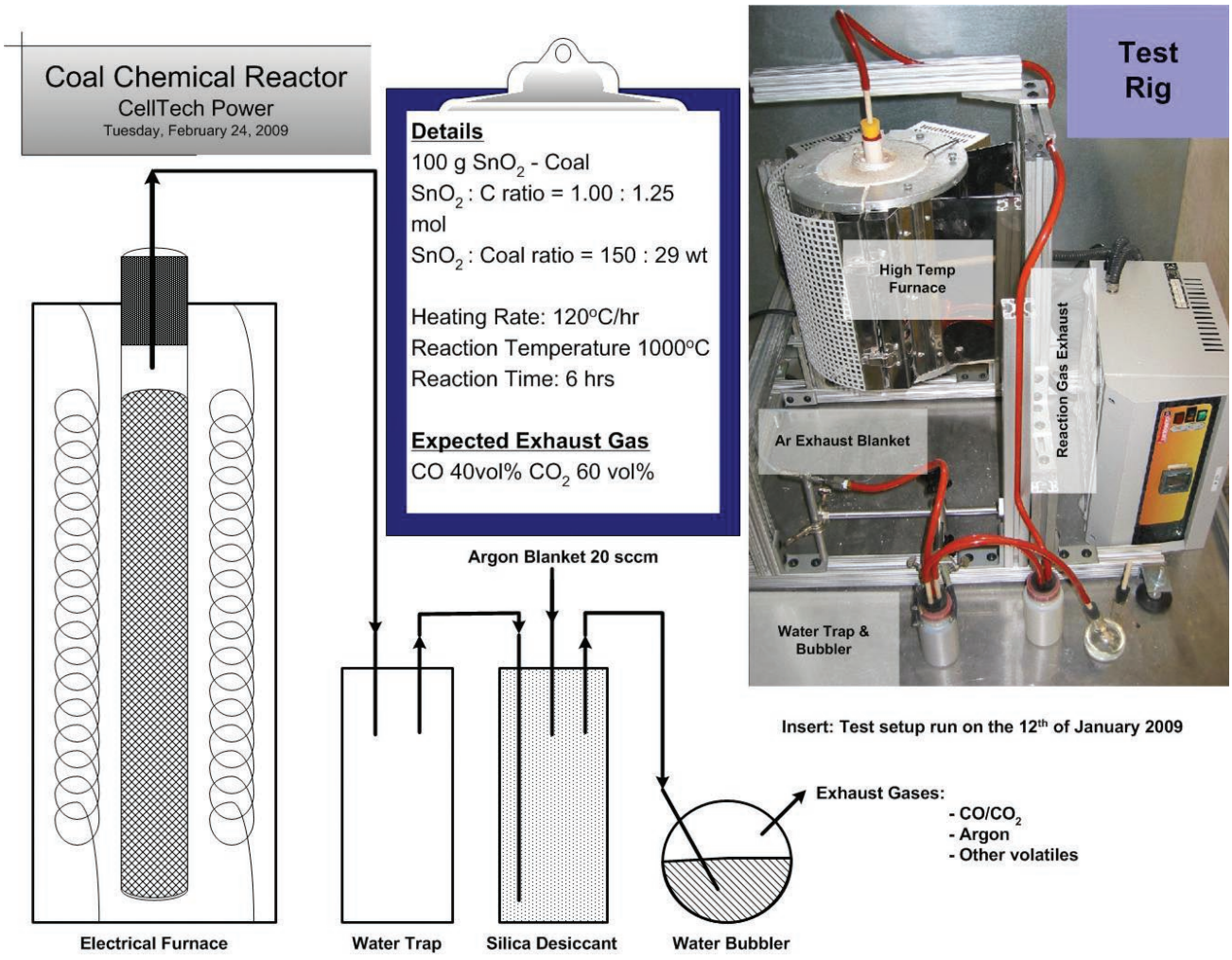


**FIGURE 1.** Experimental Test Setup for the Chemical Reactor That Operates at 1,000°C to Separate the Pre-Charged Mixture of Coal and Tin Dioxide into Tin and Slag with a Vented Gas

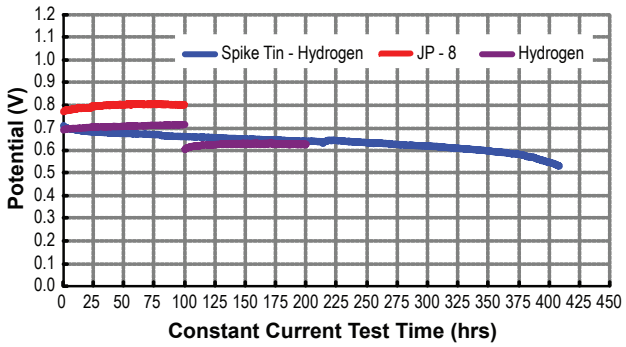


**FIGURE 2.** The spiked tin cell potential at constant 4.2 amps. As comparison, regular Gen 3.1 cells ran on JP-8 and hydrogen at various currents show no cell voltage degradation.

Results of the GDMS chemical analysis of tin following reaction between coal and tin oxide are shown in Table 1.

## Conclusions and Future Directions

This work illustrates that high concentrations of some coal contaminants (Mo, V, Nb, etc) in direct contact with the electrolyte caused irreversible damage to YSZ. The GDMS data and thermodynamic analyses indicate fundamental trends about the fate of coal impurities in molten tin under conditions where the tin-coal reactor was projected to operate. It was observed that molten tin indeed was able to provide a media for separation, purification or even elimination of harmful elements/impurities found in coal under certain conditions that were similar to the tin-coal reactor. Data from the tin reactor tests indicate the technical feasibility of using the LTA-SOFC as a potential candidate for direct coal conversion. This will overcome a key risk item related to coal impurity contamination and by providing a subsequent risk mitigation strategy.

Future work is planned to more systematically assess the impact of individual contaminant species on fuel cell components. This work should also include:

- Evaluate and improve LTA-SOFC component durability, sealing and current collector durability under coal-tin conditions.
- Design, and build test stands for chemistry, electrochemistry and longevity evaluations.
- Evaluate the fuel properties for a range of coals representing the majority of United States coal use.

**TABLE 1.** GDMS analysis of tin sample (sample S5) from coal-tin oxide reactor. Their most common oxide valance, Nernst Potential of oxidation, etc. are also listed – only those elements with potential less than 0.9 V found in tin samples.

| Element | S5 Concentration (ppm wt) | Oxide, valance at highest or stable | Nernst Potential @1.000C | Coulombic Energy CE |
|---|---|---|---|---|
| Ag | 1.1 | 1 | -0.24 | 0.16 |
| Se | < 0.01 | 6 | -0.2 | 2.57 |
| Rh | < 0.005 | 3 | 0.06 | 0.81 |
| As | 8.8 | 5 | 0.34 | 1.96 |
| Cu | 29 | 1 | 0.39 | 0.23 |
| Bi | 13 | 3 | 0.4 | 0.52 |
| Pb | 150 | 2 | 0.49 | 0.3 |
| Te | < 0.1 | 2 | 0.56 | |
| Ni | 2.9 | 2 | 0.65 | 0.52 |
| Sb | 400 | 3 | 0.66 | 0.71 |
| Cd | < 0.05 | 2 | 0.67 | 0.38 |
| Co | 0.28 | 2 | 0.75 | 0.55 |
| S | 23 | 4 | 0.75 | 1.95 |
| Sn | Matrix | 4 | 0.82 | 1.04 |
| Fe | 51 | 3 | 0.85 | 0.98 |
| Ge | < 0.01 | 4 | 0.87 | 1.36 |
| In | 58 | 3 | 0.89 | 0.67 |
| W | < 0.01 | 6 | 0.9 | 1.8 |
| Mo | < 0.01 | 4 | 0.93 | 1.11 |
| P | < 0.01 | 5 | 0.93 | 2.37 |
| K | < 0.01 | 1 | 1.01 | 0.13 |
| Cr | < 0.005 | 4 | 1.07 | 1.31 |
| V | < 0.001 | 5 | 1.07 | 1.67 |
| Mn | < 0.005 | 3 | 1.09 | 0.93 |
| Zn | < 0.01 | 2 | 1.1 | 0.49 |
| Ga | < 0.005 | 3 | 1.16 | 0.87 |
| Na | < 0.01 | 1 | 1.27 | 0.18 |
| Nb | < 0.005 | 5 | 1.4 | 1.41 |
| Ta | < 5 | 5 | 1.55 | 1.41 |
| U | < 0.005 | 6 | 1.55 | 1.48 |
| Si | < 0.01 | 4 | 1.77 | 1.8 |
| Ti | < 0.005 | 4 | 1.85 | 1.18 |
| Al | < 0.05 | 3 | 2.2 | 1 |
| Zr | < 0.005 | 4 | 2.22 | 1 |
| Li | < 0.005 | 1 | 2.23 | 0.24 |
| Mg | < 0.01 | 2 | 2.39 | 0.47 |
| Sr | < 0.005 | 2 | 2.4 | 0.31 |
| Be | < 0.005 | 2 | 2.51 | 0.8 |
| Ca | < 0.01 | 2 | 2.6 | 0.36 |
| Sc | < 0.001 | 3 | 2.65 | 0.72 |
| Y | < 0.005 | 3 | 2.66 | 0.6 |
| Tl | 0.04 | 3 | <0.9 | 0.61 |

## FY 2009 Publications/Presentations

**1.** Contract Quarterly Progress Report #1, dated January 28, 2009.

**2.** Contract Quarterly Progress Report #2, dated May 7, 2009.

**3.** W. McPhee, T. Tao et al., "Direct Conversion of Coal and Bio-Mass into Electricity at High Efficiencies Using a Liquid Tin Anode Fuel Cell," 2008 Fuel Cell Seminar, November 2008, Phoenix, Arizona.

# IV.2 Liquid Tin Anode Direct Coal Fuel Cell

Dr. Thomas Tao
CellTech Power, LLC
131 Flanders Road
Westborough, MA 01581
Phone: (508) 898-2223 x34; Fax: (508) 898-2690
E-mail: Tao@celltechpower.com

DOE Project Manager: Joseph Stoffa
Phone: (304) 285-0285
E-mail: Joseph.Stoffa@netl.doe.gov

Contract Number: 85006

Start Date: June 30, 2008
End Date: March 29, 2009

## FY 2009 Objectives

- Development of a baseline electrochemical looping (ECL) system concept.
- Analysis and preliminary design of a liquid tin anode solid oxide fuel cell (LTA-SOFC) cell for ECL application.
- ECL system performance analysis.
- Identification of risk areas for ECL development.
- Creation of an ECL commercialization development plan.

## Accomplishments

- Conceptual plant design with tin-coal reactor separates coal oxidation from electrochemical reaction. Near 100% fuel utilization.
- Developed three designs for 1 kW single cell that meet performance requirements.
- Thermodynamic analysis projects 61% higher heating value efficiency for direct coal powerplant.
- Cost analysis projects capital expenditure of $1,888/kw, slightly higher than integrated gasification fuel cell.
- Cell development risk items identified. Major concern is for material longevity. Proposed mitigating action is durability testing/material development.
- Development plan leverages early commercial markets for LTA to assist in development of ECL technology.

## Introduction

Coal plays a vital role in the power economies of major countries and biomass is a key fuel for sustainable power generation in the future. Improved generation efficiency can increase the economic viability and improve the environmental responsiveness of these fuels but efficient generation options are limited, particularly for applications where carbon capture and sequestration is desired. ECL[1] is a new concept for direct generation of power from a variety of fuels including coal and biomass. Direct conversion is more efficient. ECL combines multiple processes, reducing inefficiency and lowering capital cost compared to other advanced baseload technologies (Figure 1). For instance, there is no oxygen plant or gasifier required. The enabling technology for ECL is a new type of fuel cell that uses a liquid tin anode. Liquid tin fuel cell technology has been demonstrated in small scale and commercialization for small power applications provides an important link to commercialization of large scale generation technologies. A plan of action to accelerate ECL development includes further work on key risk items - durability, demonstration of a bench-scale system and scale-up of the enabling technology components. The commercialization path incorporates early revenue from markets such as portable power and distributed generation, providing near-term reliability improvement while reducing the time and risk associated with development of baseload applications.

[1] The electrochemical aspect refers to the highly efficient production of power without combustion while the looping concept refers to the shuttling or "looping" of oxygen by the liquid tin anode.

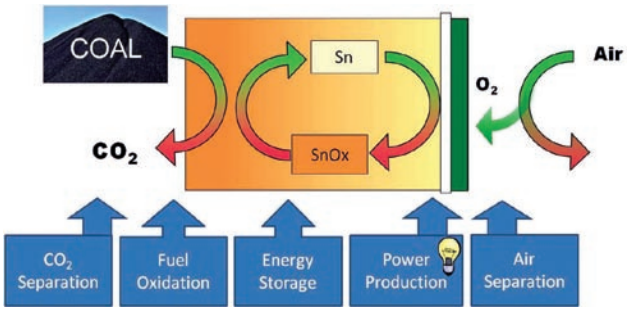


**FIGURE 1.** Electrochemical looping utilizes the liquid tin anode fuel cell to make power directly from coal. It eliminates multiple process steps and allows the capture of $CO_2$.

## Approach

1. CellTech Power developed the baseline system diagram for a direct coal LTA system in conjunction with Jan Thijssen, a consultant to the project. Attributes for this systems concept include:
   - Provides a means for feeding coal directly into the tin anode by using a tin-coal reactor (TCR). Introduction of a separate reactor also allowed for separation of ash, slag and contaminants.
   - Maximization of fuel utilization by recirculating fuel to the TCR after stripping of $CO_2$.
   - Use of conventional technology for cooling, cleaning and heat recovery.
2. Several geometries were evaluated during the Phase I cell design effort to provide multiple options to mitigate the risk of cell scale-up. Three very different cell geometries were considered.
   - Tubular cell design
   - Flat tube (elliptical) design
   - Design similar to Siemens HPD cell
3. The baseline flowsheet developed was used as the basis for plant-level performance and cost estimates. In order to make the results of the system performance analysis consistent with DOE's analyses of other coal-based systems, the detailed system analysis for LTA Direct Coal was conducted by Jan Thijssen, a consultant who has conducted similar assessments of other power generation technology on behalf of the National Energy Technology Laboratory.
4. The risk identification process described here focuses on the two technical areas which are the subject of these combined programs:
   - Scalability to MW power plant – 1,000 W single-cell design and
   - Coal impurities and their impacts on electrolyte ytrria-stabilized zirconia.
5. CellTech developed a stage-gate plan for direct coal development. Several validation and risk reduction programs have already been completed with most of the results discussed in Tasks 1-4.

## Results

- 1 kW Cell Preliminary Design Results: Tubular Cell (Figure 2)
- 1 kW Cell Preliminary Design Results: Flat Tube Elliptical Design (Figure 3)
- System Analysis Results: Projected System Performance (Figure 4)

## Conclusions and Future Directions

The ECL systems analysis has demonstrated the potential for LTA-SOFC technology to be used in coal power generation systems to achieve unprecedented efficiency while enabling carbon capture. Conceptual

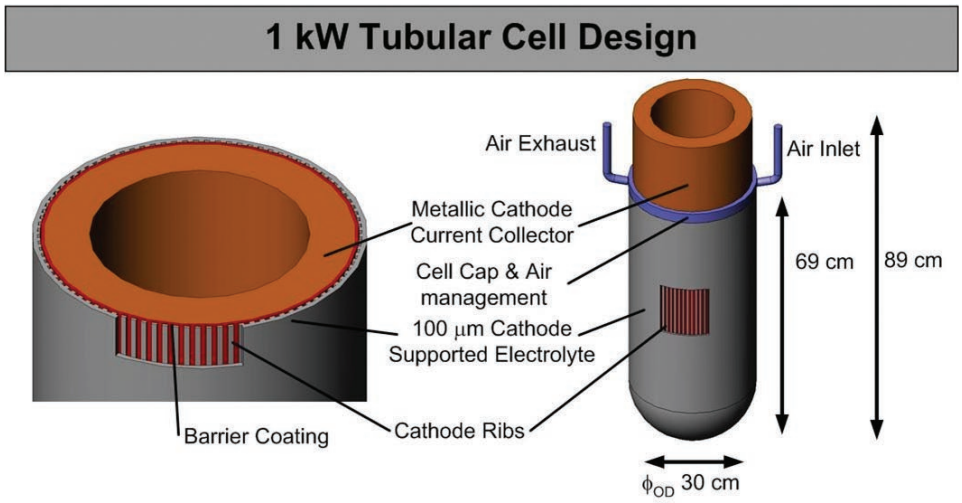


**FIGURE 2.** The tubular LTA-SOFC cell design for a 1 kW single cell is derived from CellTech's Gen 3.1 Direct JP- 8 cell design.

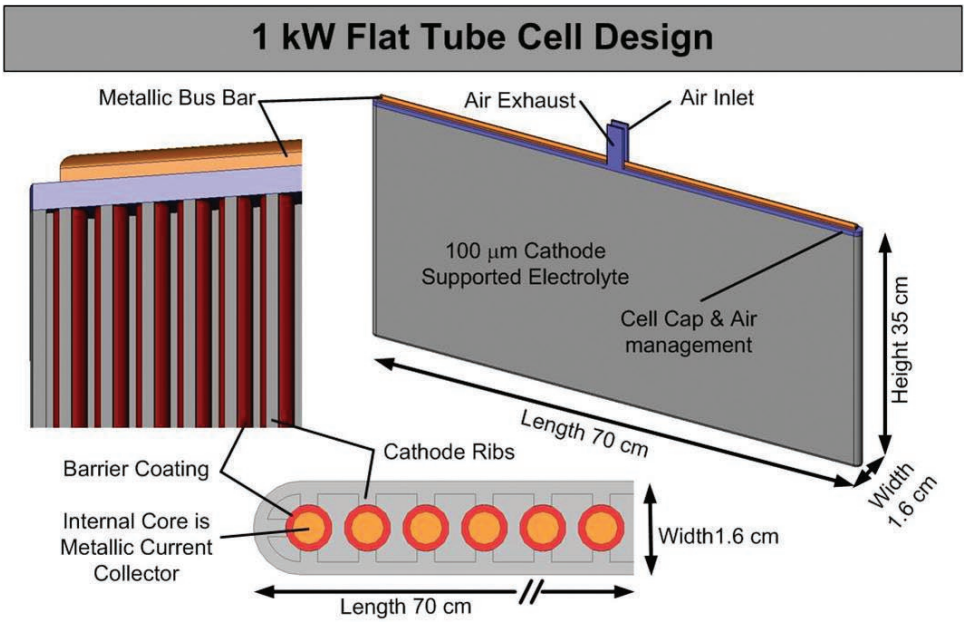


**FIGURE 3.** The flat tube concept meets cell resistance targets and has improved manufacturability characteristics.

| Projected System Performance | | |
|---|---|---|
| Fuel Cell Stack | Maximum O Content (mass/mass) | 0.1% |
| | Cathode Stoichiometry | 1.22 |
| | Stack Temperature | 1000°C |
| | Air Inlet Temperature | 500°C |
| | Cell Voltage | 0.69 V |
| | Fuel Cell Gross Power | 250 MW |
| TCR | Coal/O (mass/mass) | 0.51 kg/kg |
| | Anode Recycle | 75% |
| | Temperature Drop | 26.5°C |
| BoP | Steam Cycle Efficiency | 40% |
| | Steam Cycle Power | 45 MW |
| System | Parasitic Load | 13 MW |
| | Exhaust Temperature | 180°C |
| | System Efficiency (HHV Basis) | 63.0% |
| | Carbon Emissions | 29 g/kWh |

**FIGURE 4.** ECL system performance projections estimate 61% to 63% efficiency with carbon capture.

design feasibility for LTA-SOFC cell scale-up has been established. Risk areas have been identified and a development plan established to address the risks and exploit the commercial potential of ECL.

Future planned work includes the development of LTA cell technology to address the key issue of durability in a coal environment. The method of identifying durability issues is through long-term testing of single cells. In order to accomplish this testing, test stands are required which can reliably maintain test conditions over the duration of testing. Also, more information is required regarding the behavior of impurities likely to be present in tin, in order to establish the level of contaminant spiking of elements of interest. This impurity data will be obtained by analysis and test. Cell testing with single component spiking will allow the identification of specific contaminants which cause degradation and allow evaluation of degradation mechanisms. Finally, the durability data and failure mechanism knowledge will be used to propose materials and flowsheet changes to minimize durability impacts. These changes can also be evaluated on the test stands constructed during Phase II.

## FY 2009 Publications/Presentations

**1.** W. McPhee, T. Tao et al., "Direct Conversion of Coal and Bio-Mass into Electricity at High Efficiencies Using a Liquid Tin Anode Fuel Cell," 2008 Fuel Cell Seminar, November 2008, Phoenix, Arizona.

# IV.3 Validation of Novel Planar Cell Design for MW-Scale SOFC Power Systems

Michael J. Day, Ph.D. (Primary Contact), Robin Kimbrell, Lora Thrun, and Scott Swartz
NexTech Materials, Ltd.
404 Enterprise Drive
Lewis Center, OH 43035
Phone: (614) 842-6606; Fax: (614) 842-6607
E-mail: m.day@nextechmaterials.com

DOE Project Manager: Briggs White
Phone: (304) 285-5437
E-mail: Briggs.White@netl.doe.gov

Subcontractor:
Professor Mark Walter
Ohio State University, Columbus, OH

Contract Number: NT0004113

Start Date: October 1, 2008
End Date: September 30, 2011

## FY 2009 Objectives

The overall goal of this project is to validate the performance, robustness, cost and scalability of a novel electrolyte-supported planar cell design, termed the *FlexCell*, for use in coal-based solid oxide fuel cell (SOFC) power systems. Specific objectives of the Phase I project include:

- Demonstrate that high performance can be achieved in *FlexCells* made with yttrium-stabilized zirconia (YSZ), instead of scandium-stabilized zirconia (ScSZ) as the electrolyte material. This objective will be met by achieving a power density of at least 300 mW/cm$^2$ at 800ºC (>0.7 volts and 70 percent fuel utilization) with diluted hydrogen as the fuel.
- Demonstrate that *FlexCells* have sufficient mechanical robustness for SOFC applications. This objective will be met by through finite element analyses of the *FlexCell* architecture at Ohio State University.
- Demonstrate potential of achieving stack manufacturing cost of less than $100/kW using *FlexCells*. This objective will be met by performing a comprehensive manufacturing and cost analysis and confirming that cell costs will be less than $50/kW at full-scale production (250 MW/year).

## Accomplishments

- Successfully fabricated YSZ-based *FlexCells* with varying membrane thicknesses (total cell area of 100 cm$^2$ and active area of 28 cm$^2$).
- Evaluated the effect of membrane geometry on single-cell SOFC performance, and achieved area-specific power densities ranging from 438 to 599 mW/cm$^2$ at 800°C (0.7 volts and 70 percent fuel utilization) with diluted hydrogen as the fuel (exceeding the performance target).
- Established a finite element analysis model of mechanical robustness that will be applied to the design of large-area (500-cm$^2$ area) *FlexCells* that will be fabricated and tested in Phase II (Ohio State).

## Introduction

This Solid State Energy Conversion Alliance (SECA) Core Technology project is aimed at advancing planar SOFC technology for coal-based, megawatt-scale power generation systems. It is anticipated that such systems will be comprised of a multitude of SOFC stack modules to achieve targeted power outputs. In order to increase the power output per stack module (and reduce the number of modules in the system), planar SOFC cells with large areas will be required. NexTech Materials has established a novel electrolyte-supported planar cell design, termed the *FlexCell*, which offers intrinsic scalability to large areas, as well as other important performance attributes. The *FlexCell* is based on a patent-pending, electrolyte-supported planar membrane. As shown in Figure 1, the *FlexCell* is a two-layer structure comprising a thin electrolyte membrane layer that is mechanically supported by a "honeycomb" mesh layer of electrolyte material. With the *FlexCell*, 60 to 80 percent of the electrolyte membrane within the active area is thin (less than 40 microns), and the periphery of the cell is dense.

NexTech established its *FlexCell* membrane design using ScSZ as the electrolyte material. Although ScSZ offers an excellent combination of high oxygen ion conductivity and high mechanical strength, its cost is expected to be prohibitive for large-scale power generation systems. Thus, the focus of work on this project is on fabrication and testing of *FlexCell* membranes made with lower-cost YSZ as the electrolyte material. Phase I of this project focuses on validating

manufacturability and performance capabilities of YSZ-based *FlexCells* under conditions expected for coal-based SOFC systems. Specific tasks include fabrication of 100-$cm^2$ area *FlexCells*, testing of these *FlexCells* under application-specific conditions, finite element analysis of mechanical robustness of *FlexCell* membranes, and manufacturing cost analysis. Phase II of this project will be aimed at fabrication and testing of large-area *FlexCells* (nominally 500 $cm^2$), and validation of the cost model established in Phase I.

## Approach

The YSZ electrolyte composition selected for work in this project is the partially stabilized composition with 3 mol% $Y_2O_3$ (YSZ-3). The ionic conductivity of YSZ-3 is approximately half that of the fully stabilized composition (8 mol% $Y_2O_3$ or YSZ-8), but YSZ-3 has four times the mechanical strength compared to YSZ-8. Commercially sourced YSZ-3 powder was used to prepare green tape, from which *FlexCell* membranes were prepared using NexTech's standard procedures. NexTech's proprietary anode and cathode layers then are applied in separate deposition/sintering steps, with the anode applied to the support (corrugated) face of the *FlexCell* membrane and the cathode applied to the non-corrugated face. Successfully fabricated *FlexCells* are subjected to SOFC performance testing following NexTech's existing single-cell testing methods. The manifolds for these tests are made a high-chrome alloy (Crofer 22 APU), and sealing force is provided by the weight of the top manifold (and by the top of the clamshell furnace that houses the test fixture). The active cell area for these tests is 28 $cm^2$, as defined by the area of the current collector meshes. Finite element analysis work on this project is being performed at Ohio State University (Professor Mark Walter). Manufacturing cost analyses are being performed using costing principles established by SECA.

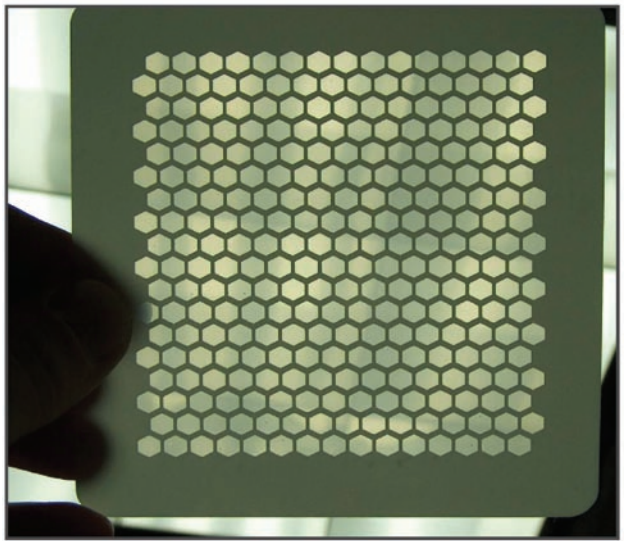

**FIGURE 1.** Example of a *FlexCell* Membrane

## Results

YSZ-based *FlexCells* have been successfully fabricated. The primary geometric variables that can be modified in the *FlexCell* are thickness of the support layer, thickness of the membrane layer, and the percentage of unsupported (thin) membrane within the active cell area. The focus of *FlexCell* fabrication work to date in the project has been on changing thicknesses of the support and membrane layers and evaluating the impact of geometry on performance. NexTech demonstrated the fabrication of YSZbased *FlexCells* with thin support and membrane layers (see Figure 2), which enables high performance to be achieved.

Two types of SOFC performance tests were performed on *FlexCells* with 28-$cm^2$ active areas. In the first set of tests, current-voltage (I-V) data were collected

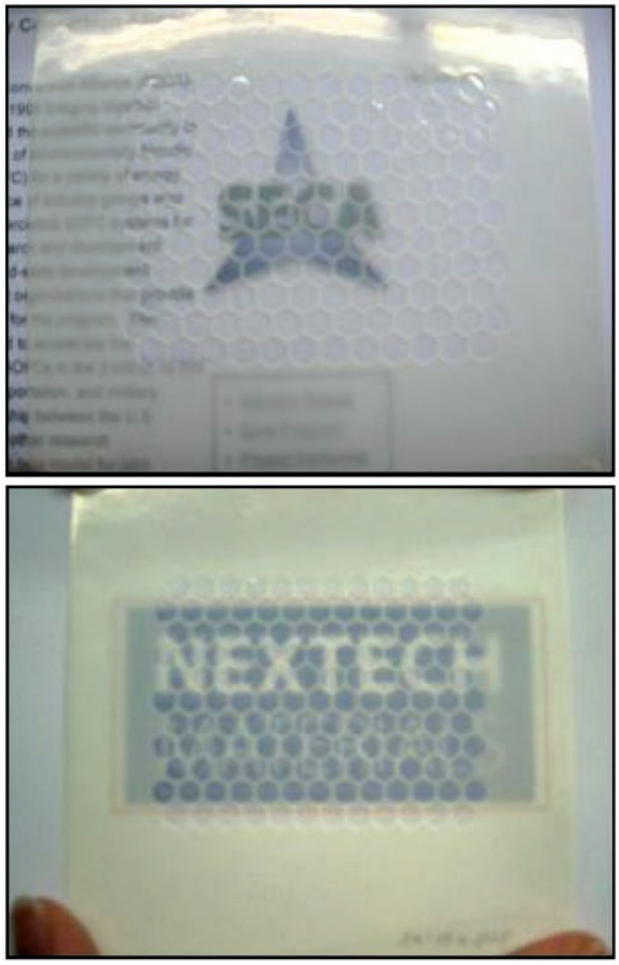


**FIGURE 2.** Photographs of Thin YSZ-based *FlexCells,* Indicating High Translucency

with constant fuel and air flow rates of 450 sccm $H_2$ and 1,500 sccm air. Under these conditions, cells are tested at low fuel utilization, which allows intrinsic performance characteristics to be assessed and area-specific resistance (ASR) values to be calculated. In the second set of tests, I-V data (pole curves) were recorded under conditions of constant fuel utilization (50 to 80 percent) at different temperatures (700 to 850°C), with diluted hydrogen (50% $H_2$, 50% $N_2$) as the fuel. Results are summarized below:

- ASR values (calculated from 0.8 to 0.6 volts, with $H_2$ fuel at low utilization) ranged from 0.373 to 0.524 Ω-cm$^2$ at 800°C, and decreased as constituent layer thicknesses of the *FlexCell* were reduced. Under these conditions, area-specific power densities at 0.7 volts ranged from 438 to 599 mW/cm$^2$ at 800°C, and decreased as constituent layer thicknesses of the *FlexCell* were reduced. For the highest performing *FlexCell*, ASR values were 0.550, 0.373 and 0.281 Ω-cm$^2$, and power densities were 428, 599 and 778 mW/cm$^2$, at temperatures of 750, 800 and 850°C, respectively.
- Data obtained from constant utilization pole curve tests also were consistent with *FlexCell* membrane geometry and confirmed the intrinsic attributes of the *FlexCell* architecture. Power density values at 800°C, 70 percent fuel utilization and 0.7 volts ranged from 333 to 475 mW/cm$^2$, again increasing with decreasing membrane thickness. Very tight spreads of pole curves were obtained over the range of 50 and 80 percent fuel utilization (see Figure 3). These data illustrate the fact that thin anode layers that are intrinsic to the *FlexCell* lead to reduced gas diffusion limitations (i.e., fuel in and steam out). When tested at 800°C with 70% fuel utilization, the highest performing YSZ-based *FlexCell* achieved power densities of 287 and 475 mW/cm$^2$ at 0.8 and 0.7 volts, respectively (see Figure 4), which far exceeds the original performance milestone targets for this project.

NexTech is collaborating with Ohio State University to measure material properties and generate predictive models of the mechanical robustness of *FlexCells*. Simulations have been conducted both on the small, repeating unit scale as well as the large scale. Figure 5 is a schematic of the *FlexCell* active area with honeycomb (hexagonal) mesh layer. Each rectangle shown in the center of Figure 5 is a unit cell that can be repeated vertically and horizontally. With appropriate boundary conditions, the stresses, strains, and displacements in the unit cell are representative of the entire area. Figure 6 depicts equivalent stress contours for a unit cell. The frame (mesh) around the hexagonal center portion provides the necessary mechanical strength. The geometry of the repeating unit has been varied

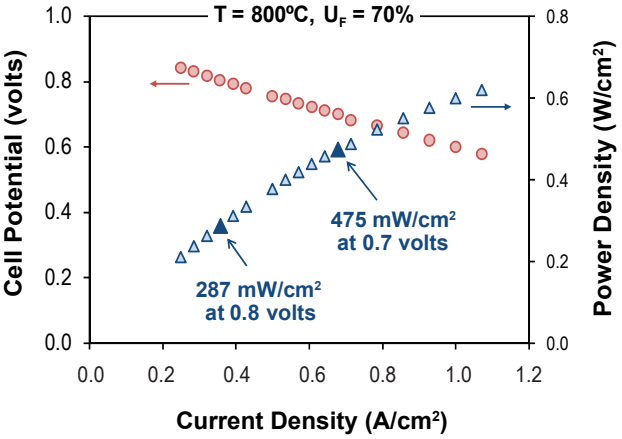


**FIGURE 4.** Constant Stoichiometry Pole Curve Data Obtained at 800°C with 70% Fuel Utilization for the YSZ-based *FlexCell* with Ultra-Thin Support and Membrane Layers

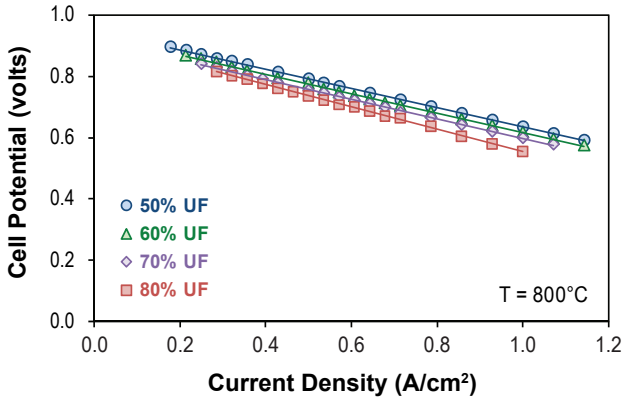


**FIGURE 3.** Pole Curves Obtained at 800°C with Different Fuel Utilizations (UF) for the YSZ-based *FlexCell* with Ultra-Thin Support and Membrane Layers

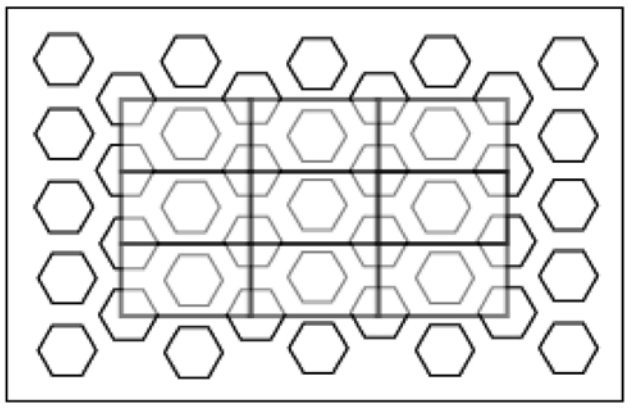

**FIGURE 5.** Illustration of the Repeating Unit Cell Used in Conjunction with Periodic Boundary Conditions to Approximate Large Area Membranes

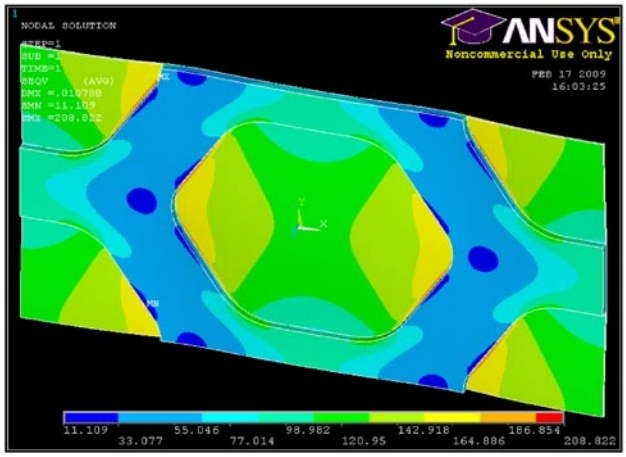


**FIGURE 6.** Contour Map Showing Equivalent Stresses Associated with Uniform Stretching of the Unit Cell

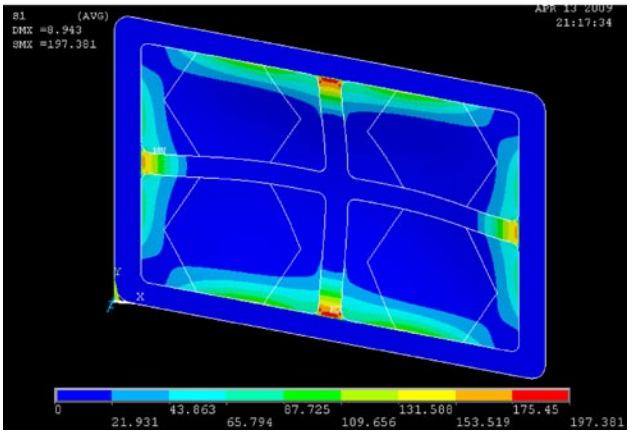


**FIGURE 7.** Principle stress contours for a large-area electrolyte membrane with vertical and horizontal support ribs. The loading profile is uniform pressure on the entire membrane with the outer frame area being fully constrained.

to simulate different active areas, including those with circular support mesh cutouts and different size supports.

The large area finite element simulations with shell elements have been developed during the current reporting period. To qualify the approach, simple cantilever beams were simulated with solid brick elements and with shell elements and results from both simulations were compared to theory. Simple beams simulated with shell elements with spatially varying properties and thicknesses were also found to behave well. The active areas within the frame and outside the ribs are composed of the different hexagonally and circularly thinned geometries simulated with the unit cells described earlier. Thus effective materials properties for active areas are obtained from the unit cell simulations. Current simulations of large area membranes are being undertaken with the intent to determine how much internal support is necessary for actual applications. Figure 7 shows one membrane with both vertical and horizontal support ribs. Other geometries under investigation have no ribs or different rib thicknesses.

## Conclusions and Future Directions

To date in this project, NexTech has successfully demonstrated the fabrication of *FlexCell* membranes made with YSZ as the electrolyte material. Anode and cathode layers were applied and promising single-cell SOFC test results were obtained. By reducing thicknesses of the constituent layers of the *FlexCell* membrane, SOFC performance data was obtained that is identical to those achieved with thicker *FlexCells* made with ScSZ electrolyte material (and state-of-the-art anode supported cells). Finite element analysis modeling of the *FlexCell* architecture has been initiated at Ohio State with the aim of optimizing mechanical robustness of large-area *FlexCells*. Additional work on the project includes the following:

- Additional work will be performed to assess the effects of *FlexCell* geometry on SOFC performance.
- Long-term testing will be conducted on simulated coal gas with the goal of demonstrating stable performance over a minimum of 1,000 hours of testing.
- The manufacture of *FlexCells* will be scaled up to 500-cm$^2$ areas, and these large area *FlexCells* will be subjected to single-cell and long-term SOFC testing.
- Mechanical robustness work at Ohio State University will continue with a primary focus on extending the finite element analysis model to full-scale *FlexCell* membranes. Validation tests will be designed and performed to refine the model and suggest membrane architectures for FlexCell manufacturing work at NexTech.
- A manufacturing cost analysis will be completed, with the goal of demonstrating that *FlexCell* manufacturing costs of less than $50/kW are achievable at a production scale of 250 MW per year.

## FY 2009 Publications/Presentations

1. Quarterly Status Report # 1 (January 31, 2009).
2. Quarterly Status Report #2 (April 30, 2009).
3. Interim Review Meeting Presentation (February 24, 2009).
4. Interim Review Meeting Presentation (June 22, 2009).

# V. ADVANCED RESEARCH

# V.1 Proton Conducting Solid Oxide Fuel Cell

S. (Elango) Elangovan (Primary Contact),
J. Hartvigsen, F. Zhao
Ceramatec, Inc.
2425 South 900 West
Salt Lake City, UT 84119-1517
Phone: (801) 978-2162; Fax: (801) 972-1925
E-mail: Elango@ceramatec.com

DOE Project Manager: Joseph Stoffa
Phone: (304) 285-0285
E-mail: Joseph.Stoffa@netl.doe.gov

Contract Number: 84595

Start Date: August 8, 2007
End Date: August 7, 2009

## FY 2009 Objectives

- Identify dopant type and concentration in a perovskite host to achieve high proton conductivity and high protonic transference number under solid oxide fuel cell (SOFC) operating conditions.
- Evaluate a ceramic composite approach to provide resistance to reactivity towards $CO_2$ and $H_2O$.
- Evaluate electrode materials using symmetric cells and full cells in button cell configuration.
- Test button cells using selected perovskite compositions.
- Test short stacks of nominal 100 Watts.

## Approach

- Select an appropriate B-site dopant in a perovskite matrix by evaluating protonic conductivity and transference number in SOFC relevant atmospheres.
- Investigate the effect of adding a second phase to the stability of compositions in syngas.
- Evaluate a range of perovskite compositions as potential low temperature cathodes for conductivity, thermal expansion, and reactivity with proton conducting membranes.
- Evaluate the best combination of electrolyte and electrodes using symmetric cells and full cells.
- Develop tape casting techniques to fabricate 10x10 cm cells.
- Test short stacks in hydrogen and natural gas reformate at 700-800°C.

## Accomplishments

- Dopant type was identified to achieve a high protonic conductivity of $1x10^{-2}$ to $3x10^{-2}$ S/cm at 800°C to 900°C.
- Addition of doped ceria was found to improve stability of $BaCeO_3$ in the presence of syngas ($H_2O + CO_2$).
- High ionic transference number was demonstrated as indicated by open circuit voltage (OCV) in button cells.
- A proton transference number of 0.7 was estimated at 800°C.
- Potential for high efficiency operation using a proton conductor based SOFC relative to oxygen conductor based SOFC was shown.
- Electrode evaluation was completed using thick electrolyte discs.
- Tape cast process was developed to enable fabrication of thin electrolytes.
- Anode supported cells were shown to exhibit high performance characteristics.
- Stable cell performance demonstrated with high $CO_2$ containing fuel compositions.

## Future Directions

Evaluation of stack performance using syngas fuel.

## Introduction

One of the prime attractions of fuel cells is the possibility of realizing energy conversion efficiencies much higher than possible with the thermal cycle systems. The basis of this difference is that thermal cycle system efficiencies are bounded by Carnot cycle thermodynamics, whereas fuel cell efficiencies are determined by chemical equilibrium thermodynamics and non-equilibrium force-flux relationships that govern charge, mass, momentum and energy transport. Materials have been developed which function as high temperature solid electrolytes in fuel cell applications. Two of the most widely considered materials are yttria doped $ZrO_2$ (YSZ) which transports oxygen ions and gadolinium doped $BaCeO_3$ which transports protons [1].

The thermodynamic difference between proton and oxygen ion cells is manifest in reversible potential variation with reactant utilization as a function of product water location. Excess air flow, used to remove

the heat generated by cell operation, results in a lower water concentration in the cathode stream of a proton cell than in the anode stream of an $O^{2-}$ cell.

Reversible potential variation with fuel utilization is shown for both proton and oxygen ion cells in Figure 1. The proton cell has a substantially higher reversible potential across the full range of fuel utilization. An interesting observation is that steam ratios greater than stoichiometric (S/C=2) increase the high utilization potential of a proton cell while oxygen ion cell potentials are uniformly higher with sub-stoichiometric steam ratios. This is due to the use of carbon monoxide via the shift reaction. The oxygen ion cell generates water in the anode stream so inlet compositions can be water deficit (high potential) and still have sufficient water to drive the shift reaction as utilization increases. The proton cell, on the other hand, must have sufficient or even excess water at the inlet to drive the shift reaction at high utilizations. However, water in the anode stream does not directly enter in the calculation of proton cell potentials and thus has little effect on the potential until higher utilizations where shift-produced hydrogen is important. Thus, high temperature proton conductors have a thermodynamic advantage over oxygen ion conductors.

Comparable electrolyte ionic conductivities are required to take practical advantage of the thermodynamic benefit. Applications driven by maximizing efficiency at the expense of power density would favor proton cells. Thus, the opportunity for very high efficiency operation is one of the primary motivating factors for investigating proton conducting SOFCs (P-SOFC). The challenges that have been encountered in P-SOFC systems are discussed below.

### Proton Conductivity

As mentioned earlier, the differences in electrolyte ionic conductivity may be greater than differences in driving force and must be included in any comparison of an operating cell at a fixed current density. In general the protonic conductivity of commonly known perovskite materials such as doped $SrCeO_3$ and $BaCeO_3$ are considerably lower than the oxygen ion conductivity of YSZ. The proton conductivity ranges from $5x10^{-3}$ to $2x10^{-2}$ S/cm at 800°C [2-6]. While the high end of this range is comparable to the oxygen conductivity of 8-YSZ, the perovskite materials also possess some level of oxygen ion conductivity and electronic conductivity at various temperatures. Thus, the protonic transference number varies as a function of temperature. While the doped $BaCeO_3$ composition functions as an effective electrolyte, an increase in hydrogen conductivity is preferable to fully exploit the benefit of high efficiency with high power density.

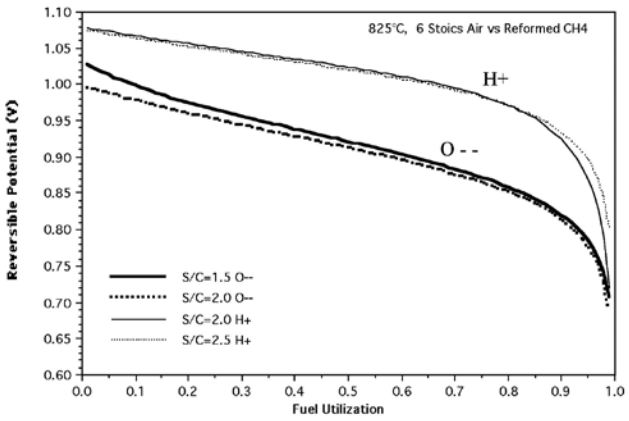


**FIGURE 1.** Comparison of Reversible Cell Potential

### Stability

One of the biggest technical challenges lies in maintaining the chemical stability of the perovskite in the presence of $CO_2$ and moisture, both are present in a typical hydrocarbon fuel. Numerous studies have confirmed the instability of the perovskite compositions.

It has been shown [7] that partial replacement of the B-site dopant with Zr completely eliminates this reaction. A similar improvement in stability in moist conditions was also reported with Zr substitution [8]. However, the stability improvement is at the expense of protonic conductivity. The proton conductivity was found to decrease monotonically with increasing Zr content [9-11].

Thus, what is required for successful development of a P-SOFC is an electrolyte material that has high proton conductivity to achieve a low area specific resistance, high protonic transference number relative to oxygen transference number to realize high efficiency, and stability in $CO_2$ and $H_2O$ without compromising protonic conductivity for cell operation using practical hydrocarbon fuels.

## Approach

Perovskite compositions that are known to exhibit protonic conductivity were evaluated for dopant study. The B-site dopants, typcially rare earth metals, have been shown to increase the proton conductivity of perovskites such as $BaCeO_3$. Several dopants and dopant levels were screened to identify compositions that have high conductivity and stability. Selected compositions were evaluated in button cell tests.

As the reaction product of the pervoskite material when exposed to $CO_2$ and $H_2O$ is ceria, a composite of perovskite-ceria was evaluated for stability in syngas.

## Results

A variety of B-site dopants were evaluated for their effect in total ionic conductivity and proton transference number. Protonic conductivity as high as 0.015 S/cm at 700°C and 0.02 to 0.03 S/cm at 800°C was measured. In addtion, the estimated protonic transference number ranged from 0.6 to 0.7 at 800°C, while the total ionic transference number was around 0.9.

Selected compositions, baseline and composite perovskites, were also exposed to syngas at 900°C. Comparison of powder X-ray diffraction patterns showed a significant reduction in the $BaCeO_3$ for for the composite relative to the baseline material as shown in Figure 2. As the target cell operating temperature is 700°C, various ratios of ceria-perovskite composites were exposed to syngas at 700°C. It was shown (Figure 3) that even 10 vol% addition of ceria provides a significant improvement to the stability.

Button cell tests with 500 µm thick doped $BaCeO_3$ pellets were conducted. The cell performance was somewhat low. Post-test examination showed poor anode bonding to the electrolyte. However, comparison of proton and oxygen conducting electrolyte fuel gas potential as a function of cell current density, as measured by independent reference electrodes, showed the high efficiency potential for the proton SOFCs. This is shown in Figure 4.

Comparison of the reference voltage trace provides several interesting points.

- First, at open circuit the proton OCV is lower than that of oxygen OCV. This again is a confirmation of pure ionic conduction of zirconia electrolyte providing near theoretical Nernst potential. The lower OCV of the proton cell is indication of the ionic transference number, $t_{ion}$ being less than one, in this case about 0.96.

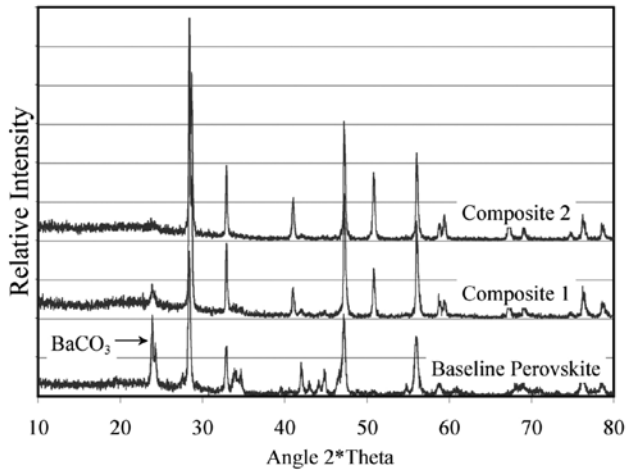


**FIGURE 2.** Comparsion of Sintered Density with and without the Addition of a Sintering Aid

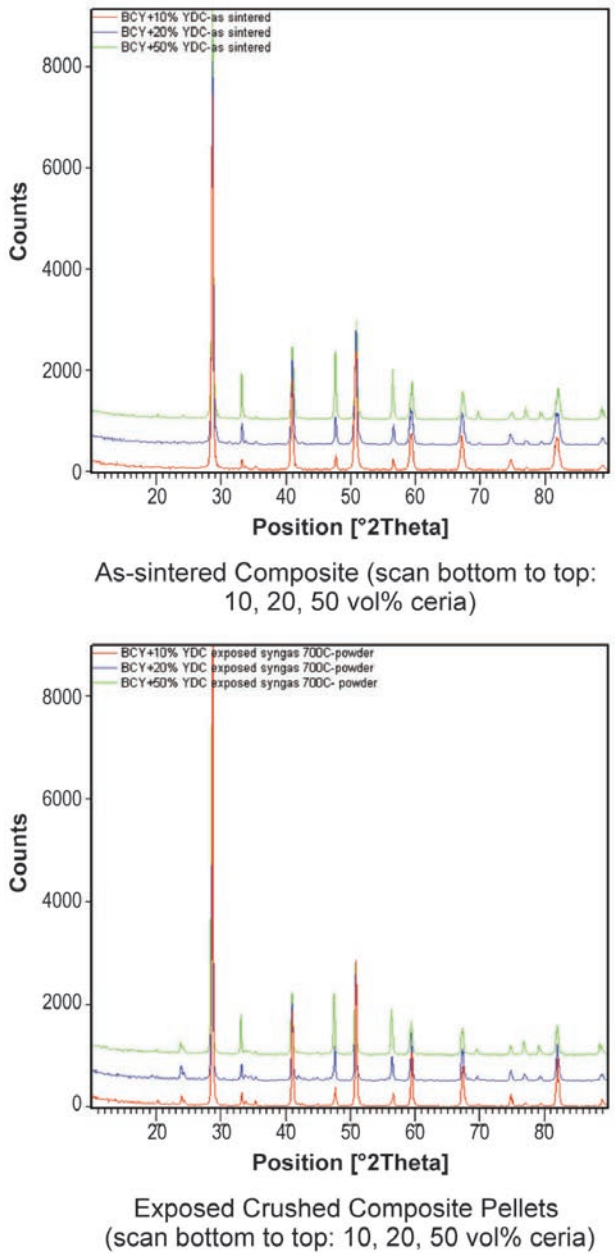


**FIGURE 3.** Powder X-ray Diffraction Patterns of 900°C Syngas Exposed Baseline and 50 vol% Ceria – Perovskite Composite

- As a function of utilization however, the driving potential of the oxygen cell drops more steeply than the proton cell again confirming the benefit of proton cell in maintaining higher driving force.
- Because of $t_{ion}$ being less than 1, the true benefit of a proton cell does not manifest until the cell reaches much higher utilization. The driving potential in this case will cross over at about 10 to 15% fuel utilization. It is theoretically possible to achieve very high utilization at higher operating voltage with a proton cell.

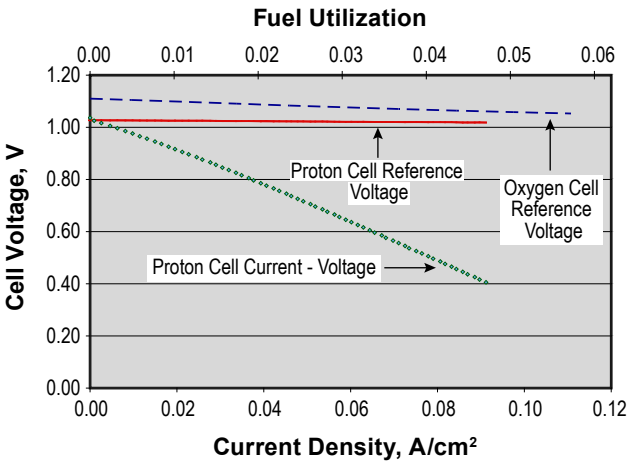


**FIGURE 4.** Comparison between Proton SOFC and Oxygen SOFC: Fuel Potential as a Function of Fuel Utilization

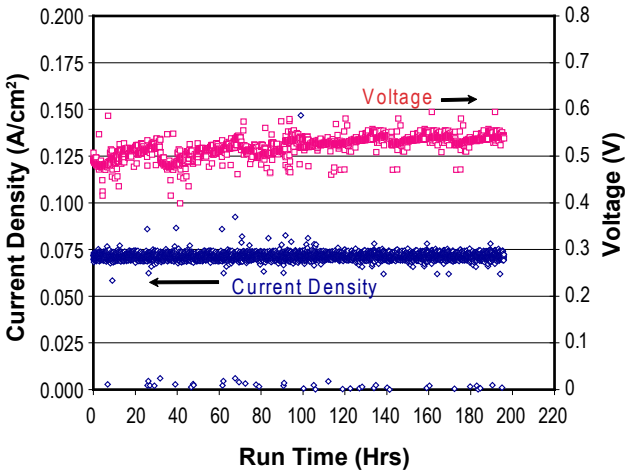


**FIGURE 6.** Stability of P-SOFC Cell at 700°C in High Concentration of $CO_2$ Containing Fuel (90% $CO_2$ – 10% Humidifed $H_2$)

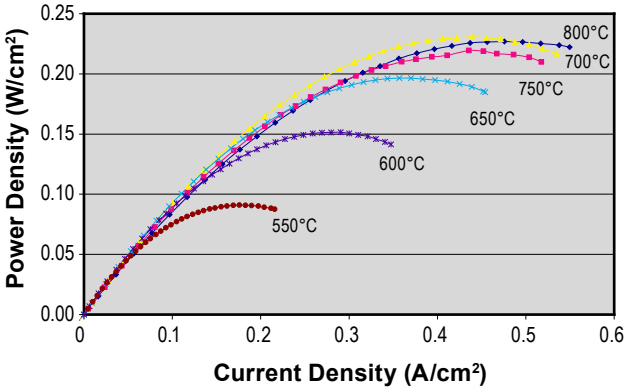


**FIGURE 5.** Anode Supported Cell Performance in Humidified Hydrogen Fuel

In order to improve performance through better anode adhesion and thinner electrolyte, an anode supported cell was tested. The cell test results are shown in Figure 5. The cell was also tested using very dilute hyrogen and high $CO_2$ fuel (90% $CO_2$, 10% humidified hydrogen) to evaluate performance at simulated high utilization condition. Very stable cell performance was observed as shown in Figure 6.

## Conclusions and Future Directions

The project results reconfirm the high efficieny potential for P-SOFCs. By proper B-site doping, very high proton conductivity, comparable to that of the oxygen ion conductivity of YSZ, can be achieved to enable high performance cell operation. Stability in syngas can be achieved by using a composite electrolyte. The inherent mixed ionic conductivity in the $BaCeO_3$ type of material limits the efficiency benefit to some extent depending on the operating conditions. When the cell is operated at high utlization, significantly higher electrochemical efficiency can be realized compared to an oxygen ion conductor based SOFC.

## References

**1.** H. Iwahara, T. Hibino, and M. Yamada, Proc. 3rd International Symposium on Solid Oxide Fuel Cells, p. 137, Singhal and Iwahara eds., Honolulu, Hawaii, 1993.

**2.** H. Iwahara, T. Esaka, H. Uchida, and N. Maeda, Solid State Ionics 3/4, 359 (1981).

**3.** H. Iwahara, H. Uchida, and N. Maeda, J. Power Sources 7, 193 (1982).

**4.** H. Iwahara, H. Uchida, and I. Yamasaki, Int. J. Hydrogen Energy 12, 73 (1987).

**5.** H. Iwahara, Solid State Ionics 28–30, 573 (1988).

**6.** N. Bonanos, K.S. Knight, and B. Ellis, Solid State Ionics 79 (1995) 61.

**7.** T.R. Armstrong et al., "Stability of Perovskite Hydrogen Separation Membranes," AR Materials Conference, Baltimore, Maryland, April 2003.

**8.** N. Taniguchi et al., "Endurance Against Moisture for Protonic Conductors of Perovskite-Type Ceramics and Preparation of Practical Conductors," Solid State Ionics 145, 349–355 (2001).

**9.** K.H. Ryu and S.M. Haile, "Chemical Stability and Proton Conductivity of Doped Perovskite Oxides in the $BaCeO_3$-$BaZrO_3$ System," Solid State Ionics 125 (1999) 355-367.

**10.** K. Katahira, Y. Kohchi, T. Shimura, and H. Iwahara, "Protonic Conduction in Zr-Substituted $BaCeO_3$," Solid State Ionics, 138, 91-98 (2000).

**11.** S. Wienströer and H.-D. Wiemhöfer, "Investigation of the Influence of Zirconium Substitution on the Properties of Neodymium-Doped Barium Cerates," Solid State Ionics 101-103, 1113-1117 (1997).

# V.2 SECA Coal-Based Systems Core Research – Montana State University

Lee H. Spangler (Primary Contact),
Richard Smith, Yves Idzerda, Hugo Schmidt,
Hashem Nehrir, Steven Shaw, Stephen Sofie,
Max Deibert, Paul Gannon, Hongwei Gao
Montana State University
207 Montana Hall
Bozeman, MT 59717-2460
Phone: (406) 994-4399; Fax: (406) 994-2893
E-mail: spangler@montana.edu

DOE Project Manager: Paul Tortora
Phone: (304) 285-0906
E-mail: Paul.Tortora@netl.doe.gov

Contract Number: 44036

Start Date: June 3, 2002
End Date: September 30, 2009

## FY 2009 Objectives

- Investigate corrosion behavior of coated and uncoated steel solid oxide fuel cell (SOFC) interconnects (ICs).
- Develop testing facilities for high temperature exposures to controlled atmospheres.
- Develop improved SOFC-IC coating compositions and deposition approaches.
- Investigate corrosion behavior of coated and uncoated steel SOFC-IC materials.
- Calculate gas flow, tortuosity, and V(i) for SOFCs.
- Prepare and test proton-conducting SOFCs and hydrogen separation membranes.
- Identify new dopant additions to lower liquidus temperature as a replacement for silicon in copper-based, noble metal free, braze system.
- Develop and test new high temperature rupture fixture to characterize seal performance in stack relevance pressure loading.
- Identify effects of sulfur poisoning on chemically anchored/strengthened nickel-based electrodes.
- Evaluate preparation of engineered porosity in metal SOFC supports.
- Identify the effects of NiO dopants on the sintering performance, ionic conductivity, and mechanical properties of sintered yttria-stabilized zirconia (YSZ) electrolytes.
- Investigate electrically induced degradation of SOFCs:
  - Collected initial evidence connecting electrical environment to microstructural degradation.
  - Check if degradation evident at terminals can be reversed at temperature.
  - Conduct further experiments to narrow mechanistic explanations for what is being observed.
- Characterization of Siemens 5 kW stack:
  - Commissioning, instrumentation and initial tests.
  - Stack identification using ripple current.
  - Active ripple cancellation and identification using test signal.
- Evaluate SOFC for combined–heat-and-power (CHP) operation in a real-world application.
- Demonstrate and quantify advantages of SOFC-CHP power plant over conventional heat and power delivery.
- Investigate the duty ratio loss of the phase-shift controlled direct current (DC)/DC converter with interleaved and non-interleaved transformers.

## Accomplishments

- Designed, constructed and operated SOFC-IC experimental systems, including thermal cycling and dual atmosphere corrosion at 800°C in moist air and moist hydrogen.
- Observed and reported substantial differences in SOFC-IC corrosion behavior depending upon environmental exposure and thermal history.
- Demonstrated physical vapor deposition (PVD) coatings on ferritic steels with excellent corrosion-resistance, high electronic conductivity, cathode compatibility and negligible Cr volatility.
- Prepared several types of coatings on steel IC coupons and characterized corrosion behavior and Cr volatility using ion beam analysis.
- Included laminar flow in gas flow equations for calculating tortuosity, gas pressure changes across the anode, and resulting effect on concentration polarization.
- Rearranged V(i) expression to clearly identify how each cell construction parameter and operating condition affects the V(i) curve.
- Analyzed and optimized glycine-nitrate synthesis of barium zirconium cerium yttrium oxide (BZCY) electrolyte material.
- Determined effect of LiF sintering aid on sintering times and temperatures required for BZCY electrolyte materials.
- Used infrared imaging furnace as alternate sintering method for electrolytes.

- Performed in situ X-ray diffraction (XRD) and micro-Raman spectroscopy of BZCY electrolyte materials at high temperatures in various atmospheres.
- Constructed and tested SOFCs with proton-conducting electrolytes.
- Identified Mg additive as a method for decreasing the liquidus temperature in copper based brazes and finished the design and fabrication of two SOFC braze fixtures developed for shear based stack relevant testing.
- Completed setup and preliminary testing for new contaminant test fixture for long duration unattended operation under hydrogen sulfide for evaluating degradation mechanisms and sulfur tolerance strategies.
- Characterized the sintering behavior of NiO doped YSZ as well the ionic conduction and mechanical characteristics of tape cast electrolytes.
- Successfully processed and microstructurally characterized stainless steel graded pore SOFC supports.
- A demonstration of electrically induced degradation and recovery of an SOFC button cell was completed.
- Measurements and excitation of Siemens stack were used to demonstrate in situ impedance spectroscopy and time-domain model identification on a stack delivering power to the grid. This was done using both exogenous excitation and the ripple introduced by power electronics.
- Custom power electronics were connected to the Siemens stack and used to demonstrate in situ characterization in a multi-source scenario.
- Building on our 5-kW SOFC dynamic model, we have previously developed a 1-MW SOFC stationary power plant. We have evaluated the capabilities and limitations of the plant in CHP applications through a series of simulation studies for the system.
- We have evaluated SOFC-CHP energy delivery characteristics in a real-world residential community application for the purpose of demonstrating SOFC-CHP system scalability.
- Use interleaved and non-interleaved transformers in the same phase-shift controlled DC/DC converter and test the duty ratio loss of the converter.

## Introduction

**High Temperature Corrosion and Corrosion Protection**

Ferritic stainless steels (FSSs) are employed in many high temperature applications in advanced coal-based energy conversion systems, including ICs in planar SOFC stacks. During high temperature operation in oxidizing environments, thermally grown oxide (TGO) scales form and grow on FSS surfaces. TGO scales protect the underlying FSS from further oxidation; however, continued growth (governed by ion transport through the TGO) eventually results in scale spallation, exposing the bare steel surface to environmental attack and introducing the spalled TGO into the service environment. Other deleterious effects of growing TGO scales include volatility, e.g., $CrO_3$ or $CrO_2(OH)_2$ from chromia-based TGO scales, and increased area specific resistance (ASR). Coatings are being developed to protect against oxidation, serving as a barrier against inward and outward ion transport, while providing low and stable ASR values.

**Interconnects and Cr Volatility**

The requirements of low cost and high temperature corrosion resistance for bipolar IC plates in SOFC stacks has directed attention to the use of steel plates with coatings to slow oxidation rates, and to act as diffusion barriers for the Cr species diffusing from the interior of the steel plate to the surface, slowing the degradation process. We have developed a relatively quick, quantitative procedure using Rutherford backscattering spectroscopy to measure the time evolution of various elemental vaporization rates.

**Interrelations of Gas Flow and Tortuosity in Electrodes with SOFC V(i) Curves**

The model calculations for gas flow and tortuosity are intertwined with the V(i) calculations, because fuel, exhaust, and oxidant flow rates are directly proportional to electrolyte current.

**Preparation and Characterization of Proton-conducting SOFCs and their Component Materials**

These materials must be stable in atmospheres containing syngas components, and must have desirable gas flow and electrical conduction properties.

**Noble Metal Free, Active Metal Brazing for SOFC Sealing Application**

Traditional approaches to SOFC sealing have been focused on compliant and/or rigid glass or glass/ceramic seals; however, the metallic braze seal may yield

a more robust, chemically bound, and true hermetic seal. While a key goal for cost-effective implementation is the elimination of noble metals, additional concerns with metallic seals include: the use of inert/vacuum environments, the potential shorting of the cell due to the electrical conductivity of braze, oxidation resistance of non-noble metal base materials, metal/ceramic bonding, and substantial thermal expansion mismatch.

**Engineered Metal SOFC Supports**

While concentration polarization is not a primary development task for standard operation of SOFC stacks with anode cell supports in the range of 500 um, the development of metal supported cells can utilize thicker porous metal supports that can be substantially restrictive to fuel flow and byproduct release. The engineering of pore structures in sintered metal substrates can provide a means of improving performance and implementation of this robust SOFC concept. Results indicate that metal powder precursors can be utilized with ceramic processing routes to establish aligned pore channels in planar stainless steel supports suitable for SOFC fabrication.

**Coal Gas Contaminant Study**

One disadvantage of using currently available fuels is their naturally occurring, or artificially added, contaminants content such as hydrogen sulfide ($H_2S$), which is known to have detrimental effects on SOFC performance. Prior results from this task have established that $H_2S$ promotes nickel migration and can compromise the percolating nickel network in nickel/ceramic anodes, thereby destroying their electrical conductivity. Prior results have also established that aluminum titanate dopants introduced into the NiO/YSZ anode facilitate chemical bonding between the Ni and YSZ network thus imparting substantial improvement in mechanical properties of the anodes. This chemical anchoring of the nickel network to the YSZ network has promise to stabilize the anode from accelerated coarsening induced from $H_2S$ exposure.

**Enhanced YSZ Sintering and Conductivity via Low Level NiO Dopants**

The success of co-sintering of SOFCs and mitigation of chemical interactions is strongly driven by the necessity of high sintering temperature required to densify YSZ electrolytes. While the use of nano-particulate is effective at lowering sintering temperature, the use of nano-particulate in powder dispersion processes is problematic at best. The results indicate that NiO at 1 mol% or less is highly effective in densifying micro-sized YSZ ceramics at temperature less than 100°C without allowing co-sintering at ≤1,300°C. The effects of the dopant on mechanical properties and ionic conductivity will also be evaluated.

**Electrically-Induced Degradation and SOFC Stack Characterization**

The emphasis of this project is to explore the rich opportunities for control and characterization at the electrical terminals of SOFC devices. We have two threads in this work. The first involves individual planar SOFC button cells that can be kept under tightly controlled conditions and analyzed destructively after test. In addition, we have a 5 kW Siemens tubular stack, configured to deliver power to the grid, that allows the development and testing of larger-scale electronics and controls.

**SOFC System Integration Modeling**

SOFCs show significant potential for hybrid operations. Hybrid SOFC applications encompass combined-cycle (CC) systems and CHP systems. In both categories, high temperature SOFC exhaust gases are utilized for further energy extraction. Conventional CC systems are most commonly seen in gas turbine (GT) applications, where the unutilized turbine exhaust heat is recovered in a heat recovery steam generator (HRSG). This steam then drives a secondary turbine-generator for additional electricity production. It has been shown that SOFC operation in CC mode, such as SOFC-GT systems, is an attractive application. SOFC-CHP systems, also known as cogeneration systems, do not typically generate additional electricity, but instead take advantage of SOFC exhaust gas streams for uses such as residential/commercial heating or process steam generation. Drawing upon our experience on efficiency evaluation of SOFC in CC operation mode, we are investigating the operation of SOFCs in SOFC-CHP mode in a real-world residential application and intend to investigate the SOFC-HRSG operation mode.

**Power Electronic Design Considerations for Fuel Cell Systems**

The transformer in a phase-shift controlled DC/DC converter, if built without interleave between the primary and secondary winding, will have lower cost but higher leakage inductance. Though the low cost of a non-interleaved transformer is preferable, the high leakage inductance may cause unacceptable duty ratio loss. Therefore, tests need to be done to evaluate the duty ratio loss of a non-interleaved transformer and an interleaved transformer.

## Approach

**High Temperature Corrosion and Corrosion Protection**

High temperature corrosion behavior and ASR of coated and uncoated FSSs is investigated as a function of exposure to SOFC-IC environments. Coatings are

deposited by conventional screen printing, electroplating, magnetron sputtering and electron beam PVD, and compared with those from advanced filtered arc-assisted PVD. High temperature exposures are carried-out using custom furnace systems. Surface analysis is performed using state-of-the-art microscopy and spectroscopy techniques, which are available through Montana State University's (MSU's) Image and Chemical Analysis Laboratory.

**Interconnects and Cr Volatility**

Using magnetron sputtering, novel SOFC-IC coatings of TiCrAlYO and Al-doped CoMnO were developed and evaluated.

**Interrelations of Gas Flow and Tortuosity in Electrodes with SOFC V(i) Curves**

The model for these interrelations was improved to include laminar flow and to identify easily which construction and operating parameters most need improvement to enhance performance.

**Preparation and Characterization of Proton-Conducting SOFCs and their Component Materials**

The glycine-nitrate process was analyzed and improved, and also the solid state reaction was employed. LiF sintering aid was used, and its effects on sintering time and temperature, and on stability in $CO_2$ atmosphere, were studied. Sintering was performed also in an infrared imaging furnace. Stability of various BZCY electrolyte compositions in $CO_2$ atmosphere at various temperatures was examined by in situ XRD and micro-Raman scattering. Fuel cells with various proton-conducting BZCY compositions prepared with LiF sintering aid and with several cathode compositions were tested for their V(i) characteristics at various temperatures.

**Noble Metal Free, Active Metal Brazing for SOFC Sealing Application**

Axial rupture tests of SOFC seals does not accurately represent the stress state that seals are subjected to SOFC stack environments. While prior studies indicate exceptional bond strength at room temperature and substantial loss of strength at 700°C, a new test fixture is being designed to test the seal in shear mode of failure as opposed to a purely tensile load. Further, thermodynamic simulations of binary phase diagrams has indicated that magnesium metal as an additive to quaternary braze system will provide a liquidus temperature close to 1,000°C in a similar manner that the silicon provided, thus allowing the effective removal of potentially deleterious silicon. Brazes will be synthesized with varying Mg concentration and characterized by thermal analysis and ultimately braze rupture tests.

**Engineered Metal SOFC Supports**

Utilizing previously developed freeze-based tape cast processing metallic substrates will be fabricated by powder metallurgy methods to attain graded, aligned pore channels to serve as optimized metal supports for SOFCs. Particle size and solids loading of 440SS powders will be evaluated as a function of casting bed temperature. Planar 440SS supports will be sintered under vacuum, inert, and/or reducing atmospheres to facilitate chemical bonding of metallic particles. These engineered metal supports will be evaluated by electron microscopy and ultimately mechanical testing prior to proof of concept cell fabrication.

**Coal Gas Contaminant Study**

Utilizing standard MSU fabricated electrolyte-supported cells as a baseline, sulfur degradation tests are being performed on traditional Ni/YSZ as well as the new anode blends consisting of Ni/YSZ and 5% aluminum titanate. The performance of the anodes with and without the anchoring additives will be evaluated as a function of electrochemical degradation under $H_2S$ introduced into the fuel stream. Further, post mortem scanning electron microscopy (SEM) analysis will be performed for observation of microstructural changes within the nickel metal catalyst network. Additionally, X-ray absorption spectroscopy analysis as done previously to identify sulfur degradation mechanisms will be performed to attain further evidence of the proposed degradation mechanism.

**Enhanced SZ Sintering and Conductivity via Low Level NiO Dopants**

Experiments with 0 to 1 mol% NiO doping have been performed by uniaxial pressing to evaluate the effects of NiO on the densification of YSZ. The net shrinkage, onset of densification, rate of densification, and density have been characterized using both 3YSZ and 8YSZ micro powder obtained from Tosoh. Tape cast YSZ substrates were also prepared for mechanical properties testing to ascertain the effect of the dopant on bending strength. Further, the ionic conductivity was evaluated by electrochemical impedance spectroscopy to identify the initial effects of the doping strategy.

**Electrically Induced Degradation**

Commercially available, InDEC button cells are used for individual cell testing. These are mounted in our standard testing fixture, heated to 750°C, and supplied with humified hydrogen and oxygen. Each experiment consists of one or more degradation and recovery phases. During degradation, the cell is constrained to a fixed voltage, to within parasitic resistance. For recovery, the cell is open circuit. Periodic current/voltage ( I/V) curve sweeps are

performed to assess the electrical condition of the cell during both degradation and recovery. The hypothesis is that high current density leads to localized nickel oxidation in the anode, resulting in a depletion of active triple phase boundary sites. Under open circuit conditions, we speculate that the nickel is reduced and cell performance recovers.

### SOFC Stack Characterization

Whole stack testing was done using a modified Siemens 5-kW stack. This stack features extra current and voltage sensors, and an externally accessible connector leading directly to the stack terminals. External loads can be attached via this connector, in addition to the inverter system delivering power to the grid. We characterized this stack in operation by measuring and analyzing the response of the stack to the power electronic ripple, the stack response to an external load comprised of laboratory instrumentation, and the response to a modular, multi-source power electronic system.

### SOFC System Integration Modeling

We built the scale-up model of an SOFC plant to 1-MW level using our 5-kW SOFC dynamic model. Using the hot exhaust from the SOFC stacks, we are evaluating scale residential applications of the 1-MW plant in CHP mode.

### Power Electronic Design Considerations for Fuel Cell Systems

We used an interleaved and a non-interleaved transformer in the same phase-shift controlled DC/DC converter and tested the duty ratio loss of the converter.

## Results

### High Temperature Corrosion and Corrosion Protection

Marked differences in corrosion behaviors were observed among SOFC-IC steels/coatings:

- Dual atmosphere exposures ($H_2$/Air) accelerate air-side corrosion compared with air-only exposures. This effect appears more pronounced in FSS alloyed with Nb.
- FSSs which are pre-oxidized in 800°C air prior to coating exhibit improved corrosion resistance compared with coated steels without pre-oxidation. Pre-oxidation has also been observed to inhibit outward Fe transport into coatings.

### Interconnects and Cr Volatility

Numerous coatings were prepared and tested for corrosion resistance. A manuscript describing the performance of TiCrAlY oxide appeared in print (see publications).

### Interrelations of Gas Flow and Tortuosity in Electrodes with SOFC V(i) Curves

Laminar flow effects are only near the 1% level in typical anode structures. The difference in performance for $H_2$ and CO fuels can be accounted for by the much slower CO mean speed, without needing to assume that Ni in the anode is a better catalyst for $H_2$ than for CO reaction. For a typical anode-supported SOFC design, [1] for $H_2$ fuel the performance benefits of increasing pressure or decreasing tortuosity soon meet the law of diminishing returns, whereas for CO fuel there is much more room for improvement.

### Preparation and Characterization of Proton-Conducting SOFCs and their Component Materials

Glycine/nitrate ratios near and above stoichiometric 5/9 ratio yield the optimal single phase in $Ba(Zr_{0.7}Ce_{0.1}Y_{0.2})O_{2.9}$ powders. LiF sintering aid gave dramatic reduction in needed sintering time and temperature. Nuclear reaction analysis showed that no Li and little F remain after sintering. The in situ XRD and micro-Raman results show that $Ba(Zr_{0.8-x}Ce_xY_{0.2})O_{2.9}$ ceramics with $x \leq 0.2$ are promising candidates for proton-conducting applications in a $CO_2$-containing environment. Results for electrolyte-supported BZCY SOFCs are shown in Figure 1. A clear need for better ceramic cathode materials to replace expensive Pt is evident.

### Noble Metal Free, Active Metal Brazing for SOFC Sealing Application

Magnesium metal additions to the copper braze system has shown a reduction in liquidus temperature. The concentration of Mg, however, is shown to be less than predicted by thermodynamic analysis to achieve ~1,023°C liquidus of the silicon modified braze. Preliminary brazing tests indicate a sufficient chemical bond to the YSZ. Two new rupture braze fixtures have been fabricated with 440SS to test the high temperature performance of the copper-based brazes in shear loading. Room temperature tests with the new braze fixture show no failure of the braze joints up to 10 bar (the maximum pressure capability of the system).

### Engineered Metal SOFC Supports

Microstructrually engineered planar metallic substrates, up to 5 mm thick, have successfully been fabricated through freeze casting techniques. The levels of directed gas flow and open porosity can be tailored to far exceed that of traditional metal frits and sponges allowing for SOFC specific targeted development.

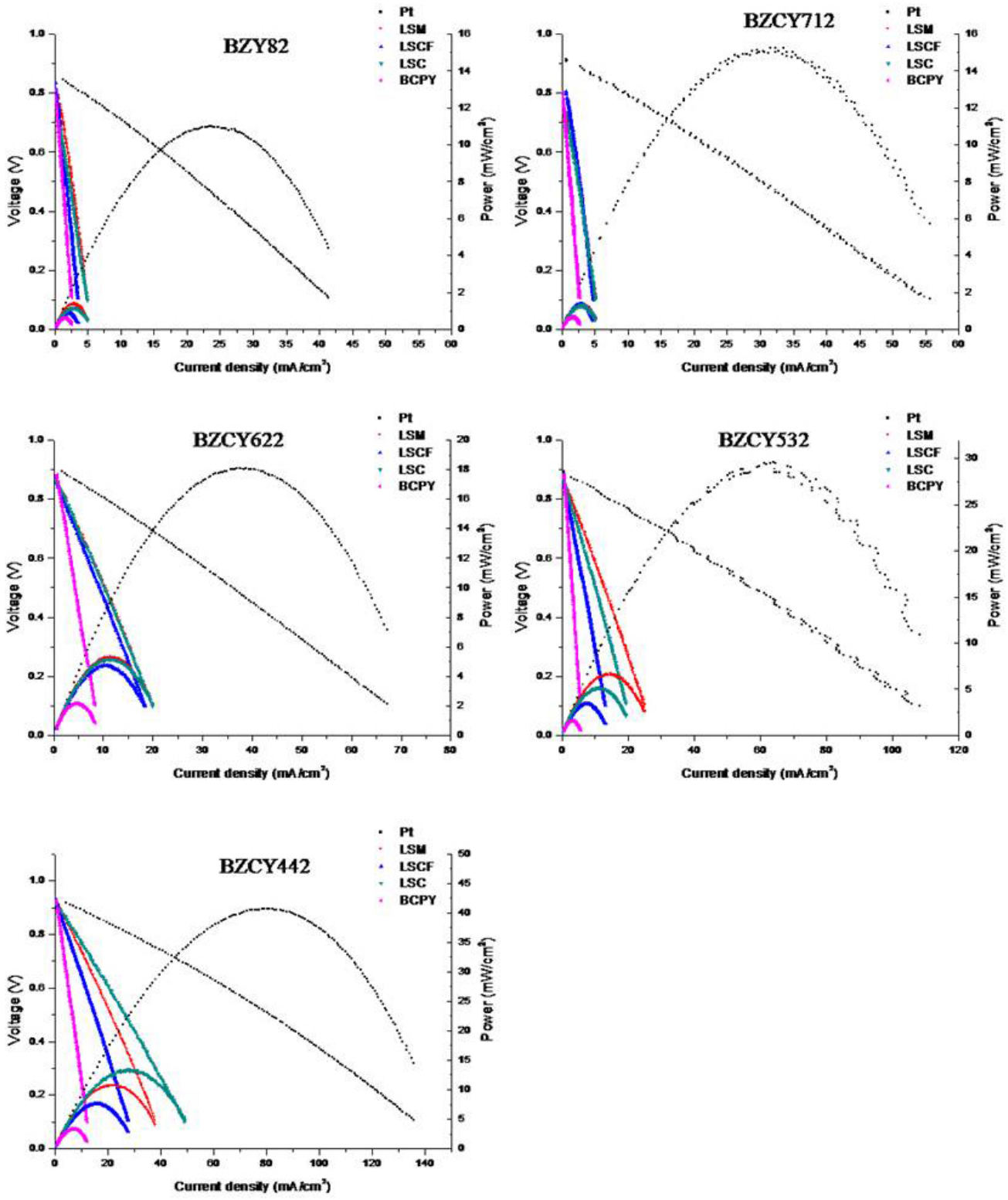


**FIGURE 1.** Cell Performances with Different Cathode Materials at 800°C

### Coal Gas Contaminant Study

The coal gas contaminant text fixture has been relocated and modified for long duration testing with fuel contaminants.

### Enhanced YSZ Sintering and Conductivity via Low Level NiO Dopants

Nickel oxide at 1 mol% is shown to dramatically improve the densification and strength of YSZ ceramics at 1,300°C, which yielded open porosity in the undoped specimens. The performance of the NiO dopants is shown in Figure 2. The grain boundary (GB) ionic conductivity was shown to increase slightly with the NiO dopant and a change from intergranular to transgranular fracture was observed for the doped specimens, suggesting improved GB strength.

### Electrically Induced Degradation

Figure 3 shows sample results from cell #14, an InDec 52 mm anode-supported YSZ/lanthanum strontium manganite cell. The plot shows Thevenin equivalent voltage and resistance parameters as a function of time, as determined by analysis of periodic measurement of I/V curves. The green line indicates one standard deviation error bars, as determined by bootstrap. The overall trend in this case is toward degraded performance, although the graph shows that the cell degrades in electrical performance and recovers. Preliminary SEM results show that this cell showed essentially no mechanical degradation.

### SOFC Stack Characterization

We were able to successfully identify parametric and non-parameteric models of a Siemens 5-kW stack, on-line. One result is shown in Figure 4, which is a whole-stack impedance spectroscopy plot, incorporating multiple sources of excitation. The data above the axis is primarily from external excitation, during operation, using a sine wave and active load. The clustered data

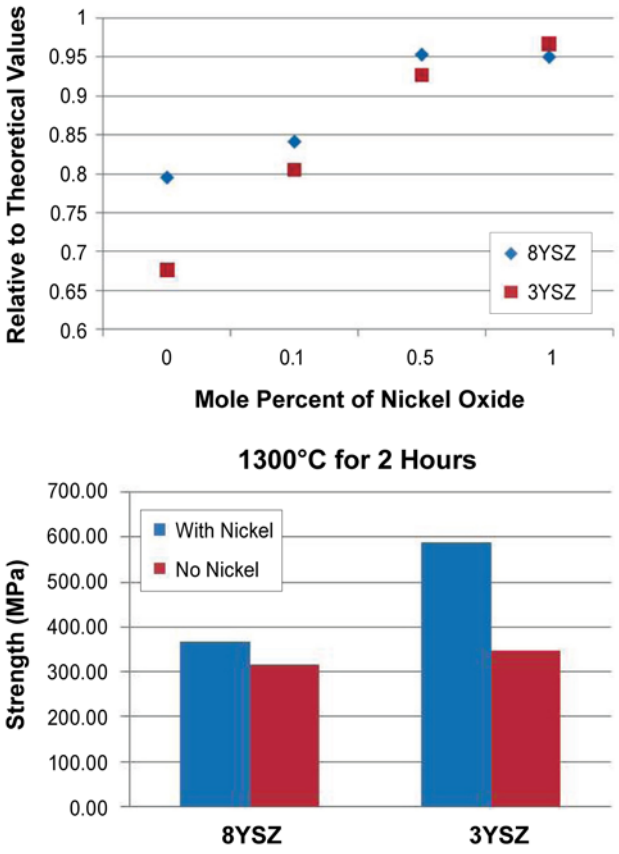


**FIGURE 2.** Density and Bending Strength of 3YSZ/8YSZ Ceramics Doped with 1 mol% NiO

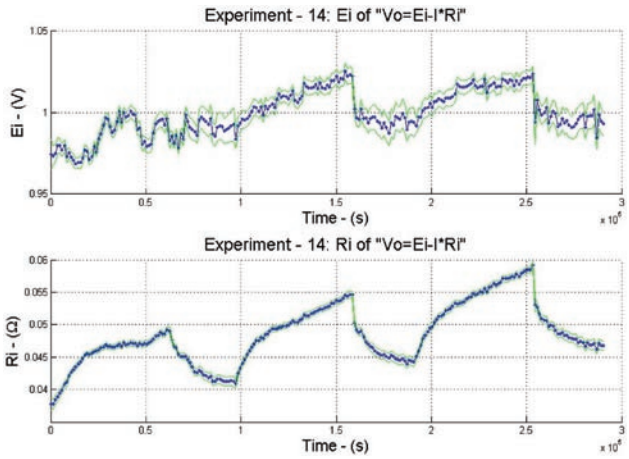


**FIGURE 3.** Parameters of cell as a function of time for three degradation/recover cycles. Green lines represent one standard deviation error bars, as determined by bootstrap.

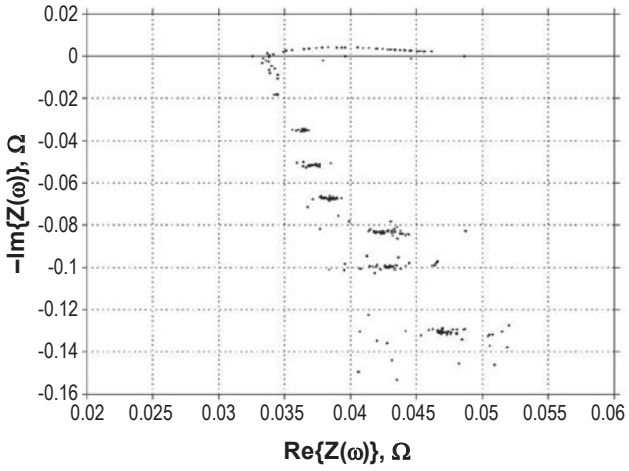


**FIGURE 4.** Whole-stack, in situ impedance spectroscopy result combining exogenous excitation and power electronic ripple for Siemens 5-kW stack. Note increasing variance and inductive dominance at high frequency.

showing inductive behavior is from the ripple current. The clusters result from the localization of excitation at the Fourier series of the ripple. The increasing variance is the result of the decrease in persistence of excitation as the frequency increases. We have also collected data showing the long-term degradation of our stack over the last year.

**SOFC System Integration Modeling**

We have obtained the dynamic performance (electrical characteristics) of the 1-MW SOFC power plant model, as well as its output heat. We have used the power plant in CHP mode to provide electricity and hot water to a residential neighborhood and are in the process of evaluating the amount of $CO_2$ emission reduction compared to using the electricity generated by conventional coal-fired power plants to provide electricity and hot water for the residential neighborhood.

**Power Electronic Design Considerations for Fuel Cell Systems**

We found the converter had almost 25% more duty ratio loss if a non-interleaved transformer is used.

## Conclusions and Future Directions

**High Temperature Corrosion and Corrosion Protection**

Corrosion behavior of FSSs with and without coatings is a strong function of environmental exposure and thermal history. Dual atmosphere and thermally-cycled exposures lead to anomalous corrosion, as compared with single atmosphere and isothermal exposures. Pre-oxidation, prior to depositing protective coatings significantly inhibits metal ion transport from the FSS through the coating. Mechanisms responsible for the observed behaviors are under investigation.

Future work will also include development of furnace systems capable of simulating exposures to high-carbon activity and other impurity-laden gases, in addition to calcium magnesium alumino-silicates and other condensed-phase corrodants. These systems will be used in investigations of metal dusting and other phenomena related to coal-based energy conversion systems.

**Interconnects and Cr Volatility**

Additional coated coupons are currently under test. Effort will continue towards assembly of test apparatus to make direct comparison of volatility measurements using our Rutherford backscattering spectroscopy procedures and conventional transpiration techniques.

**Interrelations of Gas Flow and Tortuosity in Electrodes with SOFC V(i) Curves**

Detailed modeling of gas flow, tortuosity, and V(i) characteristics has been shown to be valuable for YSZ oxygen-conducting electrolyte SOFCs, and similar modeling is off to a good start for proton-conducting SOFCs.

**Preparation and Characterization of Proton-conducting SOFCs and their Component Materials**

We are routinely making and testing such SOFCs, trying to overcome the major challenges of having both high electrolyte conductivity and resistance to degradation by syngas components such as $CO_2$, and of finding a suitable inexpensive cathode material. The infrared imaging furnace sintering method shows promise for improving properties of BZY electrolytes (BCZY without cerium), and the process is still being optimized.

**Noble Metal Free, Active Metal Brazing for SOFC Sealing Application**

Copper-based brazes show strong viability for SOFC seals and have shown to be readily modified for specific SOFC geometries and processing restrictions. The use of Mg and liquidus reducer will require the optimization of Ti and Al for braze effectiveness.

**Engineered Metal SOFC Supports**

Freeze cast processing is shown to be effective in fabricating metal SOFC supports with engineering microstructures. Finer 440SS powders have recently been received for which metal supports will be fabricated for proof of concept metal supported cell fabrication and testing.

**Coal Gas Contaminant Study**

Fabrication and testing of baseline MSU electrolyte-supported cells is complete and tests are underway with standard and modified anode blends under $H_2S$ streams to ascertain the extent of sulfur tolerance in the new anodes.

**Enhanced YSZ Sintering and Conductivity via Low Level NiO Dopants**

NiO additions to the YSZ clearly improve the sintering characteristics of YSZ and are ideal for SOFC fabrication and co-sintering approaches. A publication is being prepared to detail the results of this study. Cell fabricated with and without the electrolyte dopants will be prepared to contrast electrochemical performance.

**Electrically Induced Degradation and SOFC Stack Characterization**

There are significant opportunities at the electrical terminals for both characterization and control of SOFC materials. In semi-commercial stacks, we have demonstrated the ability to do system identification, impedance spectroscopy, and degradation analysis as the stack operates, under normal conditions, at the electrical terminals. A significant outstanding question is whether power electronic ripple serves to mask underlying phenomena, similar to dither signals in non-linear control systems. In button cells, we have demonstrated the ability to degrade both electrical terminal performance and micro-structure at the electrical terminals. Initial results suggest that the electrical degradation is reversible under some conditions, and the associated mechanical degradation may also be avoidable. Controls and power electronics at the terminals of future fuel cell systems may take these observations into account, increasing the number of degrees of freedom available to improve the performance and lifecycle of fuel cell systems.

**SOFC System Integration Modeling**

The results obtained indicate that fuel cell technologies coupled with CC components can boost their cost effectiveness and ultimately aid in the pursuit of the Solid State Energy Conversion Alliance's goal to minimize environmental consequences of fossil fuel use in energy generation. Our work on efficiency evaluation for SOFC-CC/CHP operation (described above) makes up the foundation of this task.

Future tasks include the completion of the application of the 1-MW SOFC power plant model to provide electricity and hot water to a residential neighborhood and evaluate the amount of $CO_2$ emission reduction compared to using electricity generated from coal-fired power plants for the above purposes. Another future direction is to investigate the HRSG applications of the 1-MW SOFC power plant and analyze its energy extraction benefits.

**Power Electronic Design Considerations for Fuel Cell Systems**

An interleaved transformer is a better choice than a non-interleaved transformer though the transformer has higher cost.

## Special Recognitions & Awards/Patents Issued

**1.** Professor Stephen Sofie received for a second consecutive year the MSU Mechanical & Industrial Engineering Outstanding Teacher Award. Dr. Sofie's teaching/mentoring is heavily founded in SOFC research.

## FY 2009 Publications/Presentations

**1.** C. Macauley, P.E. Gannon, M.C. Deibert and P. White, "The Influence of Pre-Treatment on the Oxidation Behavior of Co Coated SOFC Interconnects," Int. J. of Hydrogen Energy, Submitted April 2009.

**2.** A. Balland, P. Gannon, M. Deibert, S. Chevalier, G. Caboche and S. Fontana, "Investigation of $La_2O_3$ and/or $(Co,Mn)_3O_4$ Deposits on Crofer22APU for the SOFC Interconnect Application," Surface and Coatings Technology, In Press.

**3.** P.E. Gannon and P. White, "Oxidation of Ferritic Steels Subjected to Simulated SOFC Interconnect Environments," Proceedings of the Electrochemical Society Meeting, Honolulu, Hawaii, November 2008.

**4.** P.E. Gannon, P. Piccardo, S. Fontana, R. Amendola, S. Chevalier and G. Caboche, "Interconnect Materials for Next-Generation Solid Oxide Fuel Cells," Journal of Applied Electrochemistry, In Press.

**5.** P.E. Gannon, S. Sofie, M.C. Deibert, R.J. Smith and V.I. Gorokhovsky, "Thin Film YSZ Coatings on Functionally Graded Freeze Cast Anode Supports," Journal of Applied Electrochemistry, In Press.

**6.** "Oxidation of Ferritic Steels Subjected to Simulated SOFC Interconnect Environments," Invited Presentation, The Electrochemical Society Meeting, Honolulu, Hawaii, November 2008.

**7.** "Ferritic Steel Interconnects for SOFC Systems; Corrosion and Protection," Invited Presentation, TMS 2009, San Francisco, California, February 2009.

**8.** H. Chen, J.A. Lucas, W. Priyantha, M. Kopczyk, R.J. Smith, K. Lund, C. Key, M. Finsterbusch, P.E. Gannon, M. Deibert, V.I. Gorokhovsky, V. Shutthanandan, P. Nachimuthu, "Thermal Stability and Oxidation Resistance of TiCrAlYO Coatings on SS430 for Solid Oxide Fuel Cell Interconnect Applications," Surface and Coatings Technology, 202 (2008) 4820-4824.

**9.** P. Gannon, S. Sofie, M. Deibert, R.J. Smith, V. Gorokhovsky, "Thin Film YSZ Coatings on Functionally Graded Freeze Cast NiO/YSZ SOFC Anode Supports," J. Appl. Electrochem., 39 (2009) 497–502.

**10.** A. Kayani, K.J. Wickey, M.I. Nandasiri, A. Moore, E. Garratt, S. AlFaify, X. Gao, R.J. Smith, T.L. Buchanan, W. Priyantha, M. Kopczyk, P.E. Gannon, V.I. Gorokhovsky, "High Temperature Thermal Stability and Oxidation Resistance of Magnetron-Sputtered Homogenious CrAlON Coatings on 430 Steel," AIP Conf. Proceedings, 1099 (2009) 303.

**11.** V.H. Schmidt, R.R. Chien, and L.M. Lediaev, "Laminar Flow and Total Pressure Effects in Solid Oxide Fuel Cell Electrode Pores and Their Effects on Voltage-Current Characteristics," accepted for publication in Proceedings of the 33rd International Conference and Exposition on Advanced Ceramics and Composites, Daytona Beach, Florida, January 18-23, 2009. Talk presented by V.H. Schmidt.

**12.** R.R. Chien, V.H. Schmidt, S.-C. Lee, C.-C. Huang, and S.P. Tu, "Glycine-Nitrate Synthesis and Characterization of $Ba(Zr_{0.8-x}Ce_xY_{0.2})O_{2.9}$," accepted for publication in Proceedings of the 33rd International Conference and Exposition on Advanced Ceramics and Composites, Daytona Beach, Florida, January 18–23, 2009.

**13.** C.-S. Tu, S.C. Lee, C.-C. Huang, R.R. Chien, V.H. Schmidt, and C.-L. Tsai, "In Situ X-ray Diffraction and Raman Spectroscopy of LiF-Added $Ba(Zr_{0.7}Ce_{0.1}Y_{0.2})O_{2.9}$ Ceramics," accepted for publication in Proceedings of the 33rd International Conference and Exposition on Advanced Ceramics and Composites, Daytona Beach, Florida, January 18–23, 2009.

**14.** C.-S. Tu, R.R. Chien, V.H. Schmidt, S.-C. Lee, C.-C. Huang, and C.-L. Tsai, "Thermal Stability of $Ba(Zr_{0.8-x}Ce_xY_{0.2})O_{2.9}$ Ceramics in Carbon Dioxide," Journal of Applied Physics, Vol. 105, 103504 (2009).

**15.** V.H. Schmidt and L.M. Lediaev, "Pressure and Gas Concentration Effects on Voltage vs. Current Characteristics of a Solid State Fuel Cell and Electrolyzer," Advances in Solid Oxide Fuel Cells IV, Wiley, Hoboken, New Jersey, 2009, pp. 105-115.

**16.** C.-S. Tu, R.R. Chien, S.-C. Lee, C.-L. Tsai, V.H. Schmidt, A. Keith, S.A. Hall, and N.P. Santorsola, "In-situ Temperature-Dependent X-ray Diffraction Study of $Ba(Zr_{0.8-x}Ce_xY_{0.2})O_{3-\delta}$ Ceramics," Advances in Solid Oxide Fuel Cells IV, Wiley, Hoboken, New Jersey, 2009, pp. 117-123.

**17.** V.H. Schmidt and C.-L. Tsai, "Anode-Pore Tortuosity in Solid Oxide Fuel Cells Found from Gas and Current Flow Rates," Journal of Power Sources, Vol. 180, 253-264 (2008).

**18.** V.H. Schmidt, "Dynamic First-Principles Molecular-Scale Model for Solid Oxide Fuel Cells," Electrochemical Society Transactions, Vol. 6, Issue 21, Design of Electrode Structures, 11-24 (2008).

**19.** R.R. Chien, C.-S. Tu, V. H. Schmidt, C.-C. Huang, and S.-C. Lee, "Synthesis and Characterization of Nano-Sized Proton-Conducting $Ba(Zr_{0.8-x}Ce_xY_{0.2})O_{2.9}$ Ceramic Powders," Journal of Power Sources, submitted May 14, 2009.

**20.** C.-S. Tu, C.C. Huang, S.C. Lee, R.R. Chien, V.H. Schmidt, C.L. Tsai, "Effect of Lithium Fluoride on Thermal Stability of Proton-Conducting $Ba(Zr_{0.8-x}Ce_xY_{0.2})O_{2.9}$ Ceramics," Solid State Ionics, submitted May 31, 2009.

**21.** V.H. Schmidt, R.R. Chien, and L.M. Lediaev, "Laminar Flow and Total Pressure Effects in Solid Oxide Fuel Cell Electrode Pores," 33rd International Conference on Advanced Ceramics and Composites, Daytona Beach, Florida, January 18-23, 2009. Talk presented by V.H. Schmidt.

**22.** C.-L. Tsai and V.H. Schmidt, "$Ba(Zr_{0.8-x}Ce_xY_{0.2})O_{3-\delta}$ Proton Conductors as Electrolytes for Solid Oxide Fuel Cells," 33rd International Conference on Advanced Ceramics and Composites, Daytona Beach, Florida, January 18–23, 2009. Poster presented by C.-L. Tsai.

**23.** R.R. Chien, V.H. Schmidt, S.-C. Lee, C.-C. Huang, and C.-S. Tu, "Glycine-Nitrate Synthesis and Characterization of $Ba(Zr_{0.8-x}Ce_xY_{0.2})O_{2.9}$," 33rd International Conference on Advanced Ceramics and Composites, Daytona Beach, Florida, January 18-23, 2009. Poster presented by V.H. Schmidt.

**24.** C.-S. Tu, S.C. Lee, C.-C. Huang, R.R. Chien, C.-L. Tsai, and V.H. Schmidt, "In-situ X-ray Diffraction and Raman Spectroscopy of LiF-Added $Ba(Zr_{0.8-x}Ce_xY_{0.2})O_{2.9}$ Ceramics," 33rd International Conference on Advanced Ceramics and Composites, Daytona Beach, Florida, January 18–23, 2009. Poster presented by C.-S. Tu.

**25.** P. Burr, C.-L. Tsai, R. Callahan, R.J. Smith, and V.H. Schmidt, "Effects of Lithium Fluoride on the Conductivity of SOFC Electrolytes," 33rd International Conference on Advanced Ceramics and Composites, Daytona Beach, Florida, January 18–23, 2009. Poster presented by P. Burr.

**26.** C.-S. Tu, "Thermal Stability in $CO_2$ and Phase Transformation of Proton Conducting BZCY Ceramics by In Situ X-ray Diffraction and Raman Light Scattering," MSU Physics Department Solid Oxide Fuel Cell Seminar, February 4, 2009.

**27.** V.H. Schmidt and L.M. Lediaev, "Pressure and Gas Concentration Effects on Voltage vs. Current Characteristics of a Solid Oxide Fuel Cell and Electrolyzer," Poster #404 presented by L.M. Lediaev at MSU Graduate Recruitment Weekend, March 6, 2009.

**28.** L.M. Lediaev, R.R. Chien, and V.H. Schmidt, "Pressure and Gas Concentration Effects on Voltage vs. Current Characteristics of a Solid Oxide Fuel Cell and Electrolyzer," Poster presented by L.M. Lediaev at MSU Student Research Celebration, April 14, 2009.

**29.** C. L. Tsai and V.H. Schmidt, "$Ba(Zr_{0.8-x}Ce_xY_{0.2})O_{3-\delta}$ Proton Conductors as Electrolytes for Solid Oxide Fuel Cells," Poster #410 presented by C.-L. Tsai at MSU Graduate Recruitment Weekend, March 6, 2009.

**30.** S. Rane, V.H. Schmidt, and C.-L. Tsai, "Compatibility Test of Cathode Materials and Electrolyte for Solid Oxide Fuel Cells," Poster presented by S. Rane at MSU Student Research Celebration, April 14, 2009.

**31.** C.M. Colson, M.H. Nehrir, M.D. Deibert, M.R. Amin, and C. Wang, "Efficiency Evaluation of Solid-Oxide Fuel Cells in Combined-Cycle Operation," ASME Journal of Fuel Cell Science and Technology, Vol. 6, May 2009.

**32.** M. Hashem Nehrir and Caisheng Wang, Modeling and Control of Fuel Cells: Distributed Generation Applications, IEEE Press-Wiley, 2009.

**33.** D. Ator and S.W. Sofie, "Robust Copper Braze for the Hermetic Sealing of Planar Solid Oxide Fuel Cells," J. Mat. Science, submission returned for correction.

**34.** A. Lussier, S.W. Sofie, J. Dvorak, Y.U. Idzerda, "Hydrogen Sulfide Induced Nickel Depletion of SOFC Anodes," Proceedings of FuelCell2008 Sixth International Fuel Cell Science, Engineering and Technology Conference, In Press.

**35.** P.E. Gannon, S.W. Sofie, M.C. Deibert, R.J. Smith and V.I. Gorokhovsky, "Thin Film YSZ Coatings on Functionally Graded Freeze Cast Anode Supports," J. of Applied Electrochem., 39, 4, 497-502, April 2009.

**36.** S.W. Sofie, P. Gannon and Vladimir Gorokhovsky, "Silver-Chromium Oxide Interactions in SOFC Environments," J. Power Sources, 191, 2, 465-472, June 2009.

**37.** A. Lussier, S.W. Sofie, J. Dvorak, Y.U. Idzerda, "Mechanism for SOFC Anode Degradation from Hydrogen Sulfide Exposure," International Journal of Hydrogen Energy, 33, July 2008, 3945.

**38.** S.W. Sofie and D.R. Taylor, "Controlled Thermal Expansion Anode Compositions with Improved Strength for Use in Anode Supported SOFC's," Ceramic Engineering and Science Proceedings, v 28, n 4, Advances in Solid Oxide Fuel Cells III - A Collection of Papers Presented at the 31st International Conference on Advanced Ceramics and Composites, 215-223 (2008).

**39.** S.W. Sofie and J.M. Buscher, "Copper Based Braze for Robust Sealing of Planar Solid Oxide Fuel Cells," Ceramic Engineering and Science Proceedings, v 28, n 4, Advances in Solid Oxide Fuel Cells III - A Collection of Papers Presented at the 31st International Conference on Advanced Ceramics and Composites, 335-342 (2008).

**40.** S.W. Sofie, "Structural Characterization and Fluid Flow Behavior of Aqueous Freeze Cast Porous Substrates," Presented at the International Conference on Advanced Ceramics, Daytona Beach, Florida, January 2009.

**41.** C. Law and S.W. Sofie, "Increased Thermal Stability of Infiltrated Nickel Anode Catalysts on YSZ Scaffolds by Chemical Anchoring Techniques," Materials Science and Technology 2008 Conference and Exhibition, Pittsburgh, Pennsylvania, October 2008.

**42.** P. Gentile and S.W. Sofie, "High Performance Interleaved Electrolyte Supported Solid Oxide Fuel Cell," Materials Science and Technology 2008 Conference and Exhibition, Pittsburgh, Pennsylvania, October 2008.

**43.** K. Sternberg and H. Gao, "A New DC/DC Converter for Solid Oxide Fuel Cell Powered Residential Systems," in the Proceedings of 2008 the IEEE Industrial Electronics Society Annual Meeting, Page(s): 2273-2277, Orlando, Florida, November 2008.

## References

**1.** Y. Jiang and A.V. Virkar, Journal of the Electrochemical Society, Vol. 150, A942-A951 (2003).

# V.3 Oxide Contaminant Removal in Liquid Tin Anode Fuel Cells by Direct Reduction with Coal

Paul E. King (Primary Contact) and
William O'Connor
National Energy Technology Laboratory
Process Development Division
1450 Queen Ave. SW
Albany, OR 97321
Phone: (541) 967-5948; Fax: (541) 967-5958
E-mail: Paul.King@netl.doe.gov

Contract Number: 08-220696

Start Date: October 1, 2007
End Date: September 30, 2008

### FY 2009 Objectives

This project investigates the in situ reduction of the tin oxides through the addition of carbon to the cell. The goal is to determine whether coal can be utilized as a reductant and how to sequester contaminants introduced by the coal in the tin oxide reduction process.

### Accomplishments

Preliminary evaluation of the reduction efficiency indicated that the reduction tests had a better than 95% reduction efficiency.

## Introduction

The National Energy Technology Laboratory (NETL) Fuel Cell Program has identified tin (Sn) as a possible material to support concurrent electrochemistry and fossil fuel utilization. In this concept, liquid tin provides a 'fuel' for the electrochemical step. The process utilizes coal introduced into the liquid tin to convert the tin oxides back to tin at the same rate that the 'fuel' is consumed. This project investigates the in situ reduction of the tin oxides through the addition of carbon to the cell. The ultimate goal is to develop a tin reduction cell utilized to recycle tin oxide into tin without further contaminating the fuel cell and to determine whether coal can be utilized as a reductant directly as well as how to sequester contaminants introduced by the coal in the tin oxide reduction process. To this end, NETL has performed a number of tin oxide reduction tests in an effort to determine a reduction efficiency at operating conditions for the cell. Although the work is in its preliminary stage, results indicate a reduction efficiency of greater then 95%.

## Approach

In order to test the theory that the carbon from coal can be successfully utilized as a direct reductant of the tin oxide, a test matrix evaluating direct reduction of tin oxide was completed by mid-May 2009. The test matrix was designed to investigate three reductant materials at three stoichiometric carbon levels and three temperatures. Reductants included two coals acquired from the Penn State Coal Bank, DECS-26 Wyodak Seam Coal (Wyoming), DECS-34 Pittsburgh Seam Coal (Pennsylvania), and metallurgical coke. A high purity tin oxide sample was acquired from Universal Photonics, with a typical chemical analysis of 99.7% $SnO_2$ (78.65% as Sn) and 0.02% Fe. Chemical analyses for the major constituents and trace elements were acquired for all three reductants and the tin oxide sample from CONSOL Energy Inc., R&D.

Preparation of the samples followed the following procedures: The coal samples were rod milled wet at 50% solids for 30 min, then dried at 105°C to prepare a finely divided material. The metallurgical coke was supplied at minus 200 mesh (75 microns). The tin oxide had a listed particle size of >99% minus 325 mesh (43 microns). However, it had an affinity to agglomerate, thus its effective particle size was greater. All of the final feed materials under-went Tyler screen size analysis to determine effective particle size. Figure 1 provides a typical view of the reactants.

The carbon addition to the tin oxide was based on the chemistry of the tin oxide, fixed carbon content


**FIGURE 1.** Typical Reactants and Feed Mixture after Blending

of the reductant, and the following stoichiometric reduction equations:

$$SnO_2 + 2C \Rightarrow Sn + 2CO$$
$$SnO_2 + 2CO \Rightarrow Sn + 2CO_2$$

Three theoretical carbon additions were investigated: 100% (1 mole carbon/mole $SnO_2$); 115%; and 130% stoichiometric. The materials were blended for approximately 10 minutes in a multi-speed bench-top Hobart blender, weighed out into 100 g allotments, and sealed in plastic bags prior to their addition to the crucible. The vessels used for the reduction tests were 100 $cm^3$ high-alumina crucibles, fitted with high-alumina lids which were drilled to provide inlet and outlet holes. The empty crucibles were purged with 99.9% argon gas for ~1 min at a flow rate of 1,000 $cm^3$/min. Following the Ar purge, the lids were removed and the crucibles were loaded with the 100 g feed mixture. The lids were then replaced, and the loaded crucible was re-purged for ~30 sec at the same Ar flow rate. The Ar purge was intended to provide an inert atmosphere above the bed of material and prevent oxidation of the carbon reductant with air. The crucibles were laid out in a 3x3 grid, with each row representing one reductant at the three carbon levels.

A Harrop SiC element furnace (Figures 2 and 3) with a nominal 1 $ft^3$ hearth was used for the reduction tests. The furnace was ramped up to temperature and allowed to stabilize prior to loading the nine crucibles onto the hearth. A thermocouple was placed within one of the crucibles, into the bed of feed material, to monitor bed temperature. Once the targeted bed temperature was reached, a 1 hour soak was conducted, followed by removal of all the crucibles at temperature. This methodology was used to rapidly cool the molten tin in an effort to prevent re-oxidation.

Direct reduction tests were conducted at 800°C, 1,000°C, and 1,200°C. Original plans to conduct a test at 1,400°C were aborted due to temperature limitations of the furnace. Because bed temperature was used as the control temperature, rather than furnace temperature, a significant thermal gradient was encountered, likely due to the position of the crucibles at the base of the hearth and the crucibles themselves. For example, it was necessary to set the furnace temperature set point at 1,430°C to achieve a bed temperature of 1,200°C. Thus, the 1,400°C bed temperature tests were not possible, because they would have required a furnace temperature exceeding the furnace rating. However, this is not considered problematic, based on the cursory results of the 1,000 and 1,200°C tests.

Furnace and crucible temperatures were recorded for each of the runs, with typical temperature curves included in Figure 4. The major endotherm in the crucible temperature marks the insertion of the thermocouple into the bed material. The opening and closing of the furnace door are clearly defined by the endotherms in the furnace temperature plot.


**FIGURE 2.** Harrop Furnace

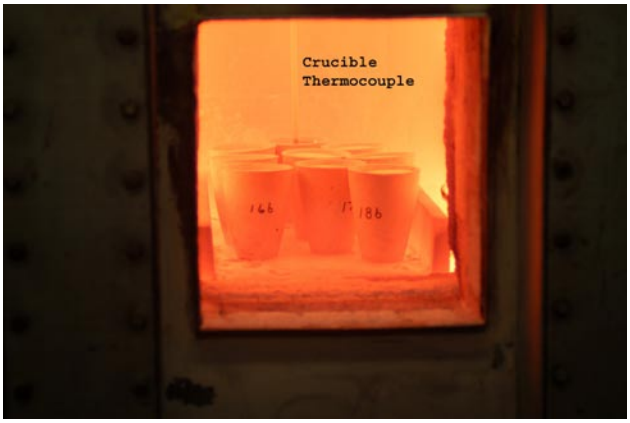


**FIGURE 3.** Crucibles on Furnace Hearth Plate

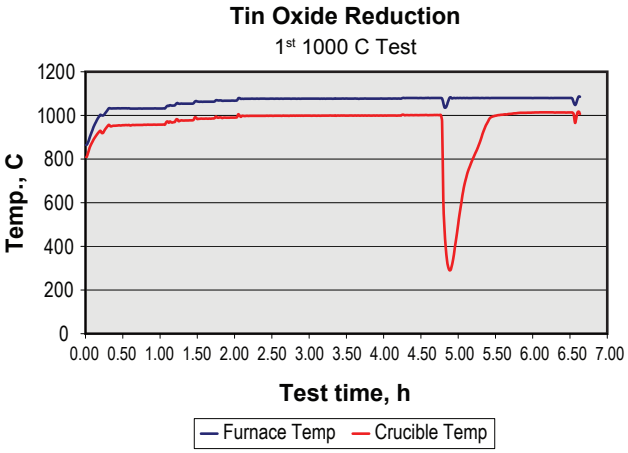


**FIGURE 4.** Temperature Plots for 1,000°C Reduction Test

## Results

Recovery of the products from the crucibles is currently underway, but material balance results were used for one of the runs to present some cursory results here as an example (Table 1). In most cases, effective separation was achieved, and a competent metal button was produced. However, in some instances the metal product is better defined as a sintered material, which may be an indication of re-oxidation of the reduced tin. These sintered samples appear to occur where the slag seal was either incomplete or breached at some time during the test. Analyses will determine the chemical composition of the products, while X-ray diffraction analyses will determine phase composition of the slags or oxide products.

**TABLE 1.** Recoveries to the Metal Button, Based on Material Balance Data from the First 1,000°C Direct Reduction Test

| Reductant | Carbon Theory | Recovery, pct |
|---|---|---|
| Pittsburgh Seam | 100% | 95.9 |
| | 115% | 98.1 |
| | 130% | 93.7 |
| Wyodak Seam | 100% | 90.2 |
| | 115% | 94.4 |
| | 130% | 94.1 |
| Metallurgical Coke | 100% | 73.0 |
| | 115% | 80.1 |
| | 130% | 82.6 |


**FIGURE 5.** Typical Reduction Products

Typical products from the reduction tests are depicted in Figure 5. In this case, a well defined metal button was produced, and two distinct (at least by color) slag samples were collected. The gray slag was collected by simply inverting the crucible and lightly tapping it with a hammer. The green slag was fused to the top of the metal button, and was collected by grinding the slag onto the button while both were still within the crucible. The slag was then removed by inversion of the crucible. The metal button was recovered by breaking the crucible away from the button, once the slag materials had been recovered.

## Conclusions and Future Directions

Preliminary evaluation of the reduction efficiency indicated that the reduction tests had a better than 95% reduction efficiency. There was a fine separation between the metallic tin and any remaining tin oxide after reduction indicating that a close-coupled reduction process is a viable means of recycling the tin in the tin anode fuel cell. Further testing will be aimed at gauging the overall reduction efficiency as a function of time and environment. An analysis of the tramp elements that remain after reduction is underway and will be reported in as they are received. Once the technique is fully validated, a reduction cell will be designed that can easily be coupled to the liquid tin anode fuel cell. This system should include the ability to introduce the coke and remove any slags formed during reduction.

# V.4 Testing and Evaluation of Solid Oxide Fuel Cells in Extreme Conditions

A. Alan Burke (Primary Contact),
Louis G. Carreiro
Naval Undersea Warfare Center (NUWC),
Division Newport (DIVNPT)
1176 Howell Street, Bldg. 1302/1
Newport, RI 02841
Phone: (401) 832-6675; Fax: (401) 832-6202
E-mail: Adrian.Burke@navy.mil

DOE Project Manager: Travis Shultz
Phone: (304) 285-1370
E-mail: Travis.Shultz@netl.doe.gov

Subcontractors:
Versa Power Systems, Littleton, CO
Delphi Corporation, Troy, MI

Contract Number: 43247

Start Date: July 23, 2008
End Date: July 22, 2009

### FY 2009 Objectives

- Examine solid oxide fuel cell (SOFC) performance under extreme conditions (pure oxygen and reformate) for the benefit to future coal gasification plants as well as NUWC's unmanned, undersea vehicles (UUVs).
- Provide independent testing and evaluation of SOFC stacks being developed under the DOE's Solid State Energy Conversion Alliance (SECA) program.

### Accomplishments

- Performed system level demonstration using a 30-cell Delphi stack, steam reformer, carbon dioxide scrubber, anode recycle blower, and stoichiometric oxygen control. Using feeds of only pure oxygen and S-8 fuel (synthetic diesel fuel from Syntroleum), showed over 75% fuel utilization, 95% oxygen utilization, over 1 kilowatt power, and over 50% efficiency based on lower heating value (LHV) S-8.
- Used Pacific Northwest National Laboratory (PNNL) model for Delphi SOFC stack to predict maximum current draw under UUV operating conditions to avoid damaging the interconnect from high-temperature excursions.
- Redesigned and fabricated separate $CO_2$ scrubber and steam reformer reactors in order to perform longer and more frequent system demonstrations.
- Procured 28-cell stack from Versa Power Systems for testing under pure oxygen and proof-of-concept system demonstrations.

## Introduction

The United States (U.S.) Navy is targeting next generation energy storage systems that can be deployed in UUVs. SOFCs are being studied because they can use hydrocarbon fuels with minimal fuel processing. Diesel or logistics-type fuels may allow for fast refueling between missions and higher energy storage than state-of-the-art batteries. The U.S. DOE is interested in spin-off applications for SOFCs such as undersea vehicles or other military settings because these are potential early-entry markets that can help establish the industrial base for mass production and lower cost. Evaluation and testing of SOFC stacks under extreme conditions is useful in evaluating the robustness and durability of the technology and its suitability to certain novel integrated gasification fuel cell systems.

## Approach

A novel UUV system design is being investigated which involves anode gas recycle and high-temperature carbon dioxide sorption to achieve both high fuel utilization and efficiency, as well as a means for driving the steam reformer. On the cathode side, pure oxygen is fed into the stack under stoichiometric control. Stoichiometric oxygen control refers to "dead-ending" a flow of oxygen that is proportional to the current being drawn from the SOFC stack (100% $O_2$ utilization). A concern of using stoichiometric oxygen control is the inability to actively cool the SOFC via excess cathode gas flow. A semi-empirical model developed at PNNL is being used in conjunction with data collected at NUWC/DIVNPT to help determine operational limits and proper insulation for the stack in this type of system.

While a proof-of-concept system demonstration was conducted in 2007 with a 30-cell Delphi Corporation stack, the run time was limited by $CO_2$ sorbent lifetime. One aspect of this year's efforts focused on redesign of the sorbent reactor to allow for easier regeneration and/or replacement if necessary so that longer duration system tests are possible. Another aspect was to test a Versa Power Systems stack under pure oxygen. The newly designed sorbent system will be tested with a Versa Power Systems stack to achieve both of these goals.

## Results

An integrated SOFC system, consisting of a 30-cell Delphi SOFC stack, InnovaTek fuel processor, R&D Dynamics high-temperature recycle blower, TDA Research carbon dioxide scrubber and balance-of-plant components, was tested with synthetic diesel fuel (S-8 from Syntroleum) and pure oxygen. The system employed a unique high-temperature recycle of SOFC anode exhaust to increase system efficiency and fuel utilization. A picture of the experimental set-up is shown in Figure 1. Note that the cylindrical reactor in Figure 1 was the integrated steam reformer/$CO_2$ scrubber delivered under InnovaTek's Navy Small Business Innovative Research Contract #N00014-06-C-0057.

The stack was initially started on hydrogen cylinder gas to generate steam for the steam reformer. Once a steady reformate was being produced, the anode loop was closed and the stack was run with only pure oxygen and S-8 fuel fed into the system. Figure 2 shows the current-voltage (IV) plot of the stack during this transition from cylinder gas to closed-loop operation. Over 1 kilowatt power was generated with over 50% efficiency based on the LHV of the S-8 fuel being pumped into the system. At the system level, 75% S-8 utilization and 95% oxygen utilization were attained. Over 8 hours of steady operation were conducted before the $CO_2$ sorbent bed became fully consumed and carbon levels were too high to continue safely operating the system. The potential for carbon deposition was a concern at this point.

To complement the experimental effort, modeling of the stack was conducted to gain insight into the temperature and current gradients across the cells. A semi-empirical SOFC stack model is being developed by PNNL to estimate temperature and current density profiles throughout a Delphi stack. NUWC has been using this model to determine operational limits for

**FIGURE 1.** Experimental Set-up for 30-Cell Delphi Stack with System Components

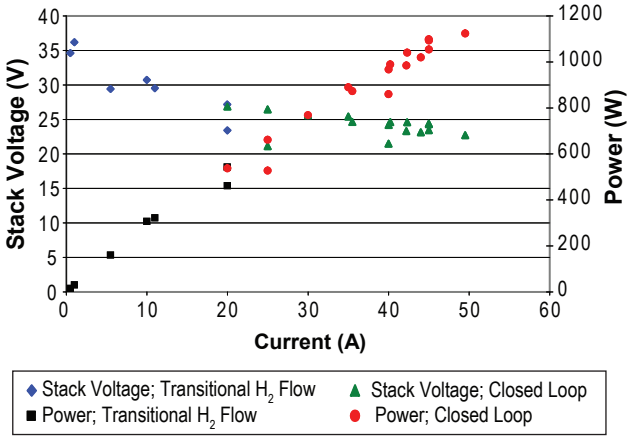


**FIGURE 2.** IV plot of 30-cell Delphi stack during transition from cylinder gas to closed-loop, anode recycle operation. Power exceeded 1 kilowatt at 50 amps.

a Delphi stack under UUV operating conditions (i.e., stoichiometric oxygen control and reformate). Because ferritic steel interconnects are used in Delphi's stack, the maximum temperature in the stack must be below 800°C in order to minimize interconnect degradation and the associated resistance gains. Preliminary studies indicate that the maximum allowable current through Delphi's Gen III, 30-cell stack is 50 amps. The composition of gas at the anode inlet was 39.5% $H_2$, 2.3% CO, 2.1% $CO_2$, 5% $CH_4$, and 51.2% $H_2O$ at a flow of 31.7 slpm and temperature of 700°C. Cathode flow was 5 slpm pure $O_2$.

Pertaining to future system demonstrations, the $CO_2$ scrubber reactor and steam reformer reactor have now been separated to facilitate temperature control and replacement of sorbent or catalyst material as required. The integrated steam reformer/$CO_2$ scrubber has been replaced because 100% sorbent regeneration proved to be difficult and replacement of the sorbent would require cutting apart the integrated reactor, rendering it unusable. A picture of the new set-up is shown is Figure 3. While this set-up is a departure from the integrated system that will ultimately be required for the UUV, this will allow more flexible and cost-effective laboratory demonstrations to evaluate prototyped components.

## Conclusions and Future Directions

The SOFC stack tested in this study utilized pure oxygen as a cathode feed and S-8 reformate as the fuel. Overall performance showed that greater than 1 kilowatt power was generated with over 50% efficiency based on the LHV of the S-8 fuel being pumped into the system. At the system level, 75% S-8 utilization and 95% oxygen utilization were attained. The use of pure oxygen enhances SOFC performance, but it also

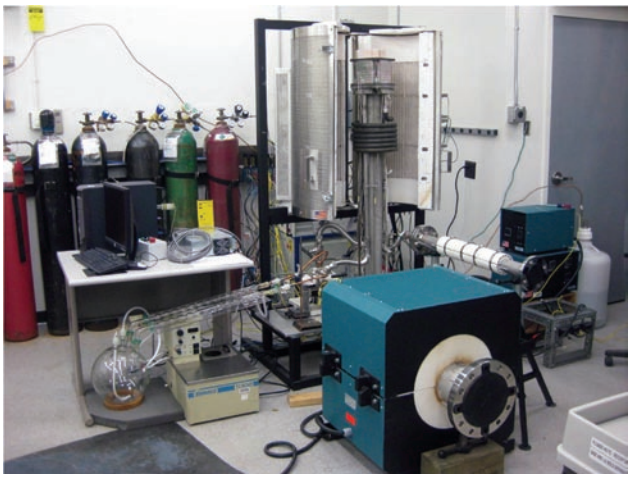

**FIGURE 3.** Experimental Set-up for New $CO_2$ Scrubber and Steam Reformer Reactors

presents challenges. Approximately 10% efficiency gains were shown with pure oxygen versus air, but long-term exposure of stack components to oxygen may prove detrimental as degradation may be accelerated in a pure oxygen atmosphere. Lifetime testing of a pure oxygen fuel cell for stationary power will need to be conducted in order to ascertain the extent of degradation versus air-based stacks.

## FY 2009 Publications/Presentations

**1.** Louis G. Carreiro and A. Alan Burke, "Solid Oxide Fuel Cell System for Air-Independent Applications," Presentation at the Materials Research Society, Fall Meeting, December 1-5, 2008, Boston, Massachusetts.

# VI. Acronyms and Abbreviations

| | |
|---|---|
| ° | Degree |
| °C | Degrees Celsius |
| Δ | Change, delta |
| ~ | Approximately |
| ≈ | Equals approximately |
| > | Greater than |
| ≥ | Greater than or equal to |
| ” | Inch(s) |
| ≤ | Less than or equal to |
| < | Less than |
| # | Number |
| % | Percent |
| ® | Registered trademark |
| µl | Microliter(s) |
| µm | Micrometer(s), micron(s) |
| Ω | Ohm(s) |
| Ω/cm$^2$ | Ohm(s) per square centimeter |
| Ω-cm$^2$ | Ohm(s) - square centimeter(s) |
| $ | U.S. Dollars |
| 0-D | Zero dimensional |
| 2D | Two dimensional |
| 2Q | Second quarter |
| 3D | Three dimensional |
| 3YSZ | Three mol% yttria-stabilized zirconia |
| 441 | A ferritic stainless steel |
| 8YSZ, 8-YSZ | Eight mol% yttria-stabilized zirconia |
| A | Ampere, amp |
| Å | Angstrom |
| $ABO_3$ | Perovskite type materials |
| ac, AC | Alternating current |
| A/cm$^2$ | Amp(s) per square centimeter |
| AES | Auger electron spectroscopy |
| AFM | Atomic force microscopy |
| Ag | Silver |
| $AgCrO_2$ | Silver chromium dioxide |
| $Ag_2CrO_2$ | Silver chromium tetroxide |
| AGR | Anode gas recycle |
| AGRB | Anode gas recycle blower |
| AIChE | American Institute of Chemical Engineers |
| AISI | American Iron and Steel Institute |
| AISI441 | A ferritic stainless steel |
| Al | Aluminum |
| AL | Alabama |
| $Al_2O_3$ | Alumina, aluminum oxide, sapphire |
| AMG | Algebraic mullet-grid |
| ANEXP | A user-defined subroutine in the MARC model |
| ANL | Argonne National Laboratory |
| APEC | Applied Power Electronics Conference |
| APEP | Advanced Power and Energy Program |
| Appl. | Applied |
| APS | Advanced Photon Source |
| APU | Auxiliary power unit |
| Ar | Argon |
| Arb, arb. | Arbitrary |
| As | Arsenic |
| AS | As sintered |
| ASC | Anode-support cell |
| $AsH_3$ | Arsine |
| ASME | American Society of Mechanical Engineers |
| ASPEN | Modeling software, computer code for process analysis |
| ASR | Area specific resistance |
| ASTM | ASTM International, originally known as the American Society for Testing and Materials |
| ATR | Autothermal reforming |
| a.u. | Arbitrary unit |
| AZ | Arizona |
| B | Boron |
| $B_2O_3$ | Boron (III) oxide |
| Ba | Barium |
| $BaCeO_3$ | Barium cerate |
| BaO | Barium oxide |
| $BaZrO_3$ | Barium zirconiate |
| BCAS | Barium-Calcium-Aluminum-Boron silicate |
| Bi | Bismuth |
| Bldg. | Building |
| BOP | Balance of plant |
| BSCF | Barium strontium cobalt ferrite ($BaSrCoFeO_3$) |
| BZCY | Barium zirconium cerium yttrium oxide |
| C | Carbon |
| C | Celsius |
| Ca | Calcium |
| CA | California |

| | |
|---|---|
| CANTERA | An open source kinetics code |
| CBS | Coal-based systems |
| CC | Combined cycle |
| cc/min | Cubic centimeter(s) per minute |
| Cd | Cadmium |
| Ce | Cerium |
| Ce-MC | Ce-modified manganese-cobalt spinel |
| $CeO_2$ | Ceric oxide |
| Ceram. | Ceramics |
| $CH_4$ | Methane |
| chem. | Chemistry |
| CHP | Combined heat and power |
| Cl | Chlorine |
| cm | Centimeter(s) |
| $cm^{-1}$ | reciprocal centimeter(s) (an energy unit) |
| $cm^2$ | Square centimeter(s) |
| cm/s | Centimeter(s) per second |
| CMU | Carnegie Mellon University |
| Co | Cobalt |
| CO | Carbon monoxide |
| CO | Colorado |
| $CO_2$ | Carbon dioxide |
| $Co_3O_4$ | Cobalt oxide |
| CPOX | Catalytic partial oxidation |
| Cr | Chromium |
| $Cr_2O_3$ | Chromic oxide |
| CRC | Chemical Rubber Company |
| $CrO_2$ | Chromium dioxide |
| CRPLAW | A user-defined subroutine in the MARC model |
| CT | Connecticut |
| CTE | Coefficient of thermal expansion |
| CTP | Core Technology Program |
| d | Distance |
| D | Diffusion coefficient |
| dBA | Decibel(s), A-weighted |
| DBT | Dibenzothiophene |
| DC, dc | Direct current |
| DC | District of Columbia |
| DC | Doped ceria |
| DC-DC, (DC)/DC | Direct current to direct current |
| DFMA | Design for Manufacturing and Assembly |
| DOE | U.S. Department of Energy |
| DPS | Delphi Power Systems |
| Dr. | Doctor |
| DREAM SOFC | A multi-dimensional modeling tool |
| DSC | Differential scanning calorimetry |
| DSO | $DyScO_3$ |
| Dy | Dysprosium |
| E&MB | Energy and mass balances |
| EBSD | Electron back-scatter diffraction |
| ECL | Electrochemical looping |
| ECR | Electrical conductivity relaxation |
| ECS | The Electrochemical Society |
| EDAX | Energy dispersive analysis by x-ray |
| EDS | Energy dispersive spectroscopy |
| EELS | Electron energy loss spectroscopy |
| e.g. | exempli gratia, for example |
| EIS | Electrochemical impedance spectroscopy |
| EPSCOR | Experimental Program to Stimulate Competitive Research |
| ESL | Electroscience Laboratories |
| et al. | et alii, and others |
| etc. | et cetera, and so on |
| Eur. | European |
| eV | Electron volt(s) |
| FBS-AGRB | Foil gas bearing supported anode gas recycle blower |
| FCE | FuelCell Energy, Inc. |
| Fe | Iron |
| $Fe_2O_3$ | Iron oxide |
| FEA | Finite element analyses |
| FeCrAlY | Iron chromium aluminum yttrium |
| FIB | Focused ion beam |
| FL | Florida |
| FORTRAN | A computer programming language |
| FPS | Fuel processing system |
| FPU | Fuel processing unit |
| FSS | Ferritic stainless steel |
| ft | Foot (feet) |
| $ft^3$ | Cubic foot (feet) |
| ft-lbf | Foot-pound force per pound mass |
| FY | Fiscal year |
| FY | Fluorescence yield |
| g | Gram(s) |
| Ga | Gallium |
| GA | Georgia |
| $Ga_2O_3$ | Gallium oxide |
| GCO | Gadolinium doped ceric oxide |
| GCO/YSZ | Gadolinium doped ceric oxide/yttria-stabilized zirconia |
| Gd | Gadolinium |
| GdC, GDC | Gadolinia-doped ceria |

| | |
|---|---|
| GDMS | Glow discharge mass spectrometry |
| GE | General Electric |
| Gen | Generation |
| Gen1.V3 | Version 3 of first generation fixture design |
| GHSV | Gas hourly space velocity |
| g/kWh | Grams per kilowatt hour |
| GPa | Gigapascal(s) |
| GT | Gas turbine |
| h | Hour(s) |
| $H_2$ | Diatomic hydrogen |
| $H_2O$ | Water |
| $H_2S$ | Hydrogen sulfide |
| $H_2Se$ | Hydrogen selenide |
| HARB | Hot anode recirculation blower |
| H/C | Hydrogen to carbon |
| HCl | Hydrogen chloride |
| Hg | Mercury |
| HHV | Higher heating value |
| HI | Hawaii |
| HOOKLW | A user-defined subroutine in the MARC model |
| HP | High pressure |
| HPD | High power density |
| hr | Hour(s) |
| hrs. | Hours |
| HRSG | Heat recovery steam generator |
| HRTEM | High resolution transmission electron microscopy |
| Hz | Hertz |
| I | Current |
| I&C | Instrumentation and controls |
| IAS | Industry Applications Society |
| IC | Interconnect |
| ICACC | International Conference and Exhibition on Advanced Ceramics and Composites |
| ICP | Inductively-coupled plasma |
| ICP-OES | Inductively-coupled plasma–optical emission spectroscopy |
| i.e. | id est, that is |
| IEEE | Institute of Electrical and Electronics Engineering |
| IGFC | Integrated gasification fuel cell |
| IGSOFC | Integrated gasification solid oxide fuel cell |
| IL | Illinois |
| Inc. | Incorporated |
| Ind | Independent |
| Int'l | International |
| IP | Integrated-planar |
| IP-SOFC | Integrated-planar solid oxide fuel cell |
| IR | Infrared |
| ISBN | International Standard Book Number |
| ITM | Ion transport membrane |
| IV, I-V | Current-voltage |
| J | Joule(s) |
| J. | Journal |
| $J/cm^2$ | Joule(s) per square centimeter |
| J/Kg | Joule(s) per kilogram |
| JP-8 | Jet Propellant 8, a jet fuel |
| k | Surface exchange coefficient |
| K | Kelvin |
| K | Potassium |
| $K_2O$ | Potassium oxide |
| keV | Kilo electron volt(s) |
| kg | Kilogram(s) |
| KPS | Kelvin probe spectroscopy |
| kW | Kilowatt(s) |
| kWe | Kilowatt(s) electric |
| L | Liter(s) |
| La | Lanthanum |
| LA | Louisiana |
| $LaCrO_3$ | Lanthanum chromite |
| $LaMnO_3$ | Lanthanum manganite |
| LaO | Lanthanum oxide |
| LAO | Lanthanum aluminum oxide |
| LBCO | Lanthanum barium cobalt oxide |
| lbm | Pound mass |
| LBNL | Lawrence Berkeley National Laboratory |
| LCCB | Low-cost cathode blower |
| LDA | Local-density-approximation |
| LEED | Low energy electron diffraction |
| Lett. | Letter |
| LHV | Lower heating value |
| Li | Lithium |
| LLC | Limited Liability Company |
| LNF | Lanthanum nickel ferrite |
| LNO | Lanthanum nickel oxide |
| LSC | Lanthanum strontium cobaltite, lanthanum strontium cobalt oxide |
| LSCF | Lanthanum strontium cobalt ferrite, lanthanum strontium cobalt iron oxide |
| LSF | Lanthanum strontium ferrite |

| | |
|---|---|
| LSM | Lanthanum strontium manganite, strontium doped lanthanum manganite, lanthanum strontium manganese oxide |
| LTA | Liquid tin anode |
| LTA-SOFC | Liquid tin anode solid oxide fuel cell |
| m | Meter(s) |
| MA | Massachusetts |
| mA | Milliampere(s) |
| $mA/cm^2$ | Milliampere(s) per square centimeter |
| MARC | A fuel cell stack computer model |
| MARC-SECA | A solid oxide fuel cell stack computer model |
| mbar | Millibar(s) |
| MCO | Manganese-cobalt spinel $(MnCo)_3O_4$ |
| MDU | Module Demonstration Unit |
| Mg | Magnesium |
| MgO | Magnesium oxide |
| MI | Michigan |
| MIEC | Mixed ionic-electronic conductor |
| min | Minute(s) |
| MIT | Massachusetts Institute of Technology |
| mm | Millimeter(s) |
| Mn | Manganese |
| MN | Methylnaphthalene |
| MnCo | Manganese cobalt |
| MnO | Manganese oxide |
| $MnO_2$ | Manganese dioxide |
| $MnO_3$ | Manganate |
| $MnO_6$ | Manganese hexoxide |
| Mo | Molybdenum |
| mΩ | Milli-ohm(s) |
| $m\Omega \cdot cm^2$ | Milli-ohm square centimeter(s) |
| mOhm | Milli-ohm(s) |
| mol | Mole(s) |
| mol% | Mole percent |
| MOSFET | Metal-oxide-semiconductor field effect transistor |
| MP | Multi-physics |
| MPa | Megapascal(s) |
| MRD | Multiples of a random distribution |
| MRS | Materials Research Society |
| ms | Millisecond(s) |
| MS | Mail stop |
| MS&T | Materials Science and Technology |
| MSC MARC | A fuel cell stack model |
| MSRI | Materials and Systems Research, Inc. |
| MSU | Montana State University |
| MT | Montana |
| mTorr | Millitorr(s) |
| mV | Millivolt(s) |
| mV/hr | Millivolt(s) per hour |
| MW | Megawatt(s) |
| mW | Milliwatt(s) |
| $mW/cm^2$ | Milliwatt(s) per square centimeter |
| MWe | Megawatt(s) electric |
| N | Newton |
| N | Nitrogen |
| $N_2$ | Diatomic nitrogen |
| nA | Nanoampere(s) |
| Na | Sodium |
| NAA | Neutron activation analysis |
| $Na_2O$ | Sodium oxide |
| Nb | Niobium |
| Nd | Neodymium |
| NETL | National Energy Technology Laboratory |
| NG | Natural gas |
| NGO | $NdGaO_3$ |
| Ni | Nickel |
| $Ni_2P$ | Nickel phosphide |
| $Ni_3P$ | Nickel phosphide |
| $Ni_5P_2$ | Nickel phosphide |
| $Ni_{12}P_5$ | Nickel phosphide |
| NiO | Nickel oxide |
| $NiO_3$ | Nickel oxide |
| NiO-YSZ | Nickel oxide-yttria-stabilized zirconia |
| NiS | Nickel sulfide |
| $NiS_2$ | Nickel sulfide |
| Ni-YSZ, Ni/YSZ | Nickel-yttria-stabilized zirconia |
| NJ | New Jersey |
| nm | Nanometer(s) |
| no. | Number |
| NOC | Normal operating conditions |
| NOx | Oxides of nitrogen |
| NP | Non polished |
| NUWC | Naval Undersea Warfare Center |
| NUWC/DIVNPT | Naval Undersea Warfare Center Division Newport |
| NV | Nevada |
| NW | Northwest |
| NY | New York |
| O | Oxygen |
| $O_2$ | Diatomic oxygen |

| | |
|---|---|
| $O_3$ | Ozone |
| O/C | Oxygen to carbon ratio |
| OCV | Open circuit voltage |
| OH | Ohio |
| OR | Oregon |
| OR | Oxygen reduction |
| OSR | Oxidative steam reforming |
| p. | Page |
| P | Phosphorus |
| P | Pressure |
| $P_2NO$, $Pr_2NiO_4$ | Praseodymium nickelate |
| $P_2O_3$ | Phosphoric oxide |
| PA | Pennsylvania |
| Pa-s | Pascal-second(s) |
| Pb | Lead |
| PBCO | $PrBaCo_2O_{5+x}$, Praseodymium barium cobalt oxide |
| PCI | Precision Combustion Inc. |
| PCM | Piezoelectric crystal microbalance |
| PCS | Power control system |
| pct | Percent |
| $PH_3$ | Phosphine |
| Phys. | Physics |
| PLD | Pulsed laser deposition |
| PLLC | Professional Limited Liability Company |
| PNNL | Pacific Northwest National Laboratory |
| PO | Post office |
| $pO_2$ | Partial pressure of oxygen |
| POC | Proof-of-concept |
| POX | Partial oxidation |
| pp. | Pages |
| ppm | Part(s) per million |
| ppm/K | Part(s) per million per degree Kelvin |
| ppmv, $ppm_v$ | Part(s) per million by volume |
| ppmw | Part(s) per million by weight |
| Pr | Praseodymium |
| $Pr_2NiO_4$ | Praseodymium nickelate |
| P-SOFC | Proton conducting solid oxide fuel cell |
| Pt | Platinum |
| PVD | Physical vapor deposition |
| R | Resistance |
| R&D | Research and development |
| $R_a$ | Surface roughness |
| RAA | Reactive air aluminization |
| Rd. | Road |
| Ref. | Reference |
| ReMoDy | A molecular dynamics code for computing reactive gas mixtures |
| Rev. | Review |
| Rh | Rhodium |
| ROI | Region of interest |
| RPM | Revolution(s) per minute |
| RRFCS | Rolls Royce Fuel Cell Systems |
| RT | Room temperature |
| RUS | Resonant ultrasound spectroscopy |
| s | Second(s) |
| S | Sulfur |
| S-8 | A synthetic diesel fuel |
| SAED | Select area electron diffraction |
| Sb | Antimony |
| Sc | Scandium |
| S/C | Steam to carbon |
| scc $gcat^{-1}$ $h^{-1}$ | Standard cubic centimeter(s) per gram catalyst per hour |
| sccm | Standard cubic centimeter(s) per minute |
| Sci. | Science |
| ScSZ | Scandium-stabilized zirconia |
| SDC | Scandia-doped ceria |
| SDC | Samarium-doped ceria |
| Se | Selenium |
| sec | Second(s) |
| SECA | Solid State Energy Conversion Alliance |
| SEM | Scanning electron microscopy |
| SEM/EDS | Scanning electron microscopy/energy dispersive spectroscopy |
| SERS | Surface-enhanced Raman spectroscopy |
| SFC | Stationary Fuel Cell Division of Siemens Energy, Inc. |
| Si | Silicon |
| SiC | Silicon carbide |
| SIMS | Secondary ion mass spectrometry |
| $SiO_2$ | Silicon dioxide |
| slpm | Standard liter(s) per minute |
| Sm | Samarium |
| SMS | Small multi-stage |
| Sn | Tin |
| $SnO_2$ | Tin oxide |
| $SnO_x$ | Oxides of tin |
| Soc. | Society |
| SOFC | Solid oxide fuel cell |
| SOFC/GT | Solid oxide fuel cell/gas turbine |
| SOFC-MP | Solid oxide fuel cell multi physics |
| Sol. | Solid |

| | |
|---|---|
| SPU 1 | A natural gas and diesel SOFC powerplant |
| Sr | Strontium |
| $SrCrO_4$ | Strontium chromium tetroxide |
| SrO | Strontium oxide |
| $SrMnO_3$ | Strontium manganate |
| $SrTiO_3$ | Strontium titanate |
| $SrZrO_3$ | Strontium zirconiate |
| SS | Stainless steel |
| SSC | Strontium samarium cobalt oxide |
| SSZ | Scandia stabilized zirconia |
| St | State |
| St. | Street |
| STEM | Scanning transmission electron microscopy |
| STM | Scanning tunneling microscopy |
| STO | $SrTiO_3$ |
| STS | Scanning tunneling spectroscopy |
| Surf. | Surface |
| t | Time |
| T | Temperature |
| TCR | Tin-coal reactor |
| TCs | Thermal cycling tests |
| TD | Tetradecane |
| TEM | Transmission electron microscopy or tunneling electron microscopy |
| Temp | Temperature |
| TEY | Total electron yield |
| Ti | Titanium |
| TiCrAlY | Titanium chromium aluminum yttrium |
| TMA | Thermomechanical analysis |
| TMS | The Metallurgical Society |
| TN | Tennessee |
| ToF-SIMS | Time-of-flight secondary ion mass spectroscopy |
| TPO | Temperature programmed oxidation |
| TSC | Tape casting–Screen printing–Co-firing |
| TX | Texas |
| UF, $U_F$ | Fuel utilization |
| UHV | Ultra-high vacuum |
| um | Micrometer(s) |
| UNLV | University of Nevada, Las Vegas |
| UNS | Unified Numbering System |
| US, U.S. | United States |
| USD | United States Dollar |
| UT | Utah |
| UTC | United Technologies Company |
| UTRC | United Technologies Research Center |
| UTSA | University of Texas at San Antonio |
| UUV | Unmanned undersea vehicle |
| V | Volt(s) |
| V | Vanadium |
| V6 | Six-phase DC-DC converter |
| VA | Virginia |
| VDC | Volt direct current |
| V-I | Volt-current |
| V(i) | Terminal voltage vs. current density |
| Vol. | Volume |
| vol% | Volume percent |
| VPS | Versa Power Systems |
| VT | Virginia Polytechnic Institute |
| W | Watt(s) |
| WA | Washington |
| $W/cm^2$ | Watt(s) per square centimeter |
| wt., Wt. | Weight |
| wt.%, wt% | Weight percent |
| WV | West Virginia |
| WVU | West Virginia University |
| XANES | X-ray absorption near edge spectroscopy |
| XAS | X-ray adsorption spectroscopy |
| XES | X-ray emission spectroscopy |
| XPS | X-ray photoelectron spectroscopy |
| XRD | X-Ray diffraction |
| XRF | X-ray fluorescence |
| Y | Yttrium |
| $Y_2O_3$ | Yttrium oxide (yttria) |
| YDC | Yttria-doped ceria |
| YSZ | Yttria-stabilized zirconia |
| Z | Impedance |
| ZDC | Zirconium-doped ceria |
| Zn | Zinc |
| ZnO | Zinc oxide |
| Zr | Zirconium |
| $ZrO_2$ | Zirconium dioxide (zirconia) |

# VII. Primary Contact Index

# VIII. Organization Index

# IX. Contract Number Index

# X. Index of Previous Projects

### Projects Discontinued Since the FY 2008 Annual Report

| Contract Number | Performer | Project Topic |
|---|---|---|
| 05690 | American Society of Mechanical Engineers | SOFC Design Basis Development Project (project transferred to RDS41817.3130105-036) |
| 08-220692 | National Energy Technology Laboratory | Materials Development for the Solid Oxide Fuel Cell Environment |
| 41572 | Georgia Institute of Technology | Functionally Graded Cathodes for Solid Oxide Fuel Cells |
| 42221 | Missouri University of Science & Technology | Thermochemically Stable Sealing Materials for Solid Oxide Fuel Cells |
| 42223 | Tennessee Technological University | Development of Low-Cr Fe-Ni-Based Alloys for Intermediate Temperature SOFC Interconnect Application |
| 42225 | Arcomac Surface Engineering, LLC | Oxidation Resistant, Cr Retaining, Electrically Conductive Coatings on Metallic Alloys for SOFC Interconnects |
| 42227 | University of Cincinnati | Innovative Seals for Solid Oxide Fuel Cells (SOFCs) |
| 42229 | Delavan d.b.a. Goodrich Turbine Fuel Technologies | An Innovative Injection and Mixing System for Diesel Fuel Reforming |
| 42471 | Ceramatec, Inc. | Intermediate Temperature Solid Oxide Fuel Cell Development |
| 42516 | University of Michigan | Carbon Tolerant Steam Reforming and SOFC Anode Catalysts |
| 42527 | Ohio University | Combined Theoretical and Experimental Investigation and Design of $H_2S$ Tolerant Anode for Solid Oxide Fuel Cells |
| 42614 | GE Global Research | Solid Oxide Fuel Cell Coal-Based Power Systems |
| 42623 | University of Utah | A High Temperature Electrochemical Energy Storage System Based on Sodium Beta Alumina Solid Electrolyte (BASE) |
| 42627 | SRI International | Effect of Coal Contaminants on Solid Oxide Fuel Cell System Performance and Service Life |
| 44036 | University of Florida | SECA Coal-Based Systems Core Research - University of Florida |
| 49071 | Massachusetts Institute of Technology | Local Electronic Structure and Surface Chemistry of SOFC Cathodes |
| 68250 | Sandia National Laboratories | Reliable Seals for Solid Oxide Fuel Cells |
| 84662 | Aspen Products Group, Inc. | Waterless 5 kWe Diesel Reformer |
| 84663 | Ceramatec, Inc. | SOFC Integrated Multi-Mode Diesel Reformer |
| 84673 | Lynntech, Inc. | Low Cost, Compact Plasma Fuel Reformer for APUs |
| 84881 | NexTech Materials Ltd. | Intermediate Temperature Solid Oxide Fuel Cell Cathode Enhancement through Infiltration Fabrication Techniques |

## Projects Discontinued Since the FY 2007 Annual Report

| Contract Number | Performer | Project Topic |
|---|---|---|
| 41838 | Acumentrics Corporation | Development of a Low Cost 10 kW Tubular SOFC Power System |
| 41245 | GE Global Research | Solid State Energy Conversion Alliance (SECA) Solid Oxide Fuel Cell Program |
| 42175 | University of Missouri-Rolla | Resilient Sealing Materials for Solid Oxide Fuel Cells |
| 41247 | Siemens Power Generation | Small-Scale Low Cost Solid Oxide Fuel Cell Power Systems |
| 42220 | University of Utah | Electrically Conductive, Corrosion-Resistant Coatings through Defect Chemistry for Metallic Interconnects |
| 42741 | Virginia Polytechnic Institute and State University | Digital Manufacturing of Gradient Meshed SOFC Sealing Composites with Self-Healing Capabilities |
| 84611 | Mesta Electronics Inc. | DC-AC Inverter with Reactive-Power-Management Functionality |
| 84616 | R&D Dynamics Corporation | Foil-Bearing Supported High-Speed Centrifugal Cathode Air Blower |
| 84624 | TIAX LLC | Low-Cost, High-Temperature Recuperators for SOFC Fabricated from Titanium Aluminum Carbide ($Ti_2AlC$) |
| 83795 | TDA Research, Inc. | Sorbents for Desulfurization of Natural Gas and LPG |
| 84608 | Materials and Systems Research, Inc. | A Thin Film, Anode-Supported Solid Oxide Fuel Cell Based on High Temperature Proton Conducting Membrane for Operation at 400 to 700°C |
| 86280 | Materials and Systems Research, Inc. | A High Temperature (400 to 650°C) Secondary Storage Battery Based on Liquid Sodium and Potassium Anodes |
| 86140 | FuelCell Energy, Inc. | Advanced Control Modules for Hybrid Fuel Cell/Gas Turbine Power Plants |
| 86283 | NexTech Materials, Ltd. | Component Manufacturing and Optimization of Protonic SOFCs |
| 41244 | Cummins Power Generation | 10 kW Solid Oxide Fuel Cell Power System Commercialization |
| 42184 | University at Albany – SUNY | Feasibility of a SOFC Stack Integrated Optical Chemical Sensor |
| 42624 | Massachusetts Institute of Technology | Photo-Activated Low Temperature, Micro Fuel Cell Power Source |
| 42625 | Northwest University | High Temperature Fuel Cells for Co-Generation of Chemicals and Electricity |
| 42626 | United Technologies Research Center | Techno-Economic Feasibility of Highly Efficient Cost Effective Thermoelectric-SOFC Hybrid Power Generation Systems |

## Projects Discontinued Since the FY 2006 Annual Report

| Contract Number | Performer | Project Topic |
|---|---|---|
| FEAA067 | Oak Ridge National Laboratory | Power Electronics for Solid Oxide Fuel Cells |
| FWP49100 | Argonne National Laboratory | Technology Development in Support of SECA |
| 34139 | Siemens Power Generation | High Temperature Solid Oxide Fuel Cell Development |
| 40798 | FuelCell Energy, Inc. | Direct Fuel Cell/Turbine Power Plant |
| 41562 | University of Florida | Determination of Electrochemical Performance and Thermo-Mechanical-Chemical Stability of SOFCs from Defect Modeling |
| 41566 | University of Washington | Advanced Measurement and Modeling Techniques for Improved SOFC Cathodes |
| 41569 | Ceramatec, Inc. | Metal Interconnect for Solid Oxide Fuel Cell Power Systems |
| 41571 | Georgia Institute of Technology | An Integrated Approach to Modeling and Mitigating SOFC Failure |
| 41574 | [1]University of Illinois at Chicago<br>[2]Ceramatec Inc.<br>[3]Virginia Polytechnic Institute and State University<br>[4]Oak Ridge National Laboratory<br>[5]Pacific Northwest National Laboratory | An Investigation of Resolve the Interaction between Fuel Cell, Power Conditioning System and Application Load |
| 41575 | NexTech Materials, Ltd. | Continuous Process for Low-Cost, High-Quality YSZ Powder |
| 41578 | University of Pittsburgh | Fundamental Studies of the Durability of Materials for Interconnects in Solid Oxide Fuel Cells |
| 41915 | Southern University and A&M College | Dense Membranes for Anode Supported All-Perovskite IT-SOFCs |
| 41959 | University of Florida | Electrocatalytically Active High Surface Area Cathodes for Low Temperature SOFCs |
| 41960 | University of Houston | New Cathode Materials for Intermediate Temperature Solid Oxide Fuel Cells |
| 42222 | Chevron Energy Research and Technology Company | Development of Ni-Based Sulfur-Resistant Catalyst for Diesel Reforming |
| 42228 | Connecticut Global Fuel Cell Center University of Connecticut | Low-Cost Integrated Composite Seal for SOFC: Materials and Design Methodologies |
| 42514 | Franklin Fuel Cells, Inc. | Novel Cathodes Prepared by Impregnation Procedures |
| 42515 | Georgia Institute of Technology Center for Innovative Fuel Cell and Battery Technologies | Quantitative Characterization of Chromium Poisoning of Cathode Activity |
| 42517 | University of Michigan | Desulfurization of High-Sulfur Jet Fuels by Adsorption and Ultrasound-Assisted Sorbent Regeneration |
| 73138 | Ceramatec, Inc. | Advanced Net-Shape Insulation for Solid Oxide Fuel Cells |
| 83528 | NexTech Materials, Ltd. | Highly Textured Glass Composite Seals for Intermediate-Temperature SOFCs |
| 84387 | FuelCell Energy, Inc. | Diesel Plasma Reformer |
| 84212 | Spinworks, LLC | Low-Cost/High-Temperature Heat Exchanger for SOFCs Using Near-Net-Shape Ceramic Powder Forming Process |

## Projects Discontinued Since the FY 2005 Annual Report

| Contract Number | Performer | Project Topic |
|---|---|---|
| FE09 | Los Alamos National Laboratory | Diesel Reforming for Solid Oxide Fuel Cell Auxiliary Power Units |
| 40779 | General Electric | SOFC Hybrid System for Distributed Power Generation |
| 41539 | Boston University | Materials System for Intermediate-Temperature SOFC |
| 41602 | University of Utah | Active Cathodes for Super-High Power Density SOFC Through Space Change Effects |
| 41631 | California Institute of Technology | Enhanced Power Stability for Proton-Conducting Solid Oxide Fuel Cells |
| 41801 | Virginia Polytechnic Institute and State University | Modeling and Design for a Direct Carbon Fuel Cell with Entrained Fuel and Oxidizer |
| 41803 | University of Akron | Carbon-based Fuel Cell |
| 41804 | Duke University | Carbon Ionic Conductors for Use in Novel Carbon-Ion Fuel Cells |
| 83212 | Ceramatec, Inc. | Lanthanum Gallate Electrolyte Based Intermediate-Temperature Solid Oxide Fuel Cell Development |

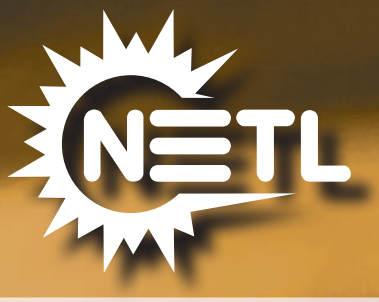


**National Energy Technology Laboratory**

1450 Queen Avenue SW
Albany, OR 97321-2198
541-967-5892

3610 Collins Ferry Road
P.O. Box 880
Morgantown, WV 26507-0880
304-285-4764

626 Cochrans Mill Road
P.O. Box 10940
Pittsburgh, PA 15236-0940
412-386-4687

Wayne A. Surdoval
Technology Manager, Fuel Cells
412-386-6002
wayne.surdoval@netl.doe.gov

Visit the NETL website at:
www.netl.doe.gov

Customer Service:
1-800-553-7681


DOE/NETL-2009-1379 October 2009